The University Of Sheffield.

The Identification and Characterisation of Novel Suppressors of DNA Replication Stress

Charlotte Elizabeth Tripp

Department of Oncology and Metabolism

Thesis submitted to the University of Sheffield in December 2017 for the degree of Doctor of Philosophy

Declaration:

I hereby declare that all work presented within this thesis has not been previously submitted for any academic award at this or any other institution. All work submitted is my own, unless otherwise stated, and has not been plagiarised.

Charlotte Tripp

Acknowledgements

I would like to take this opportunity to thank everybody who has made this work possible.

Firstly, I would like to thank my primary supervisor Dr. Spencer Collis for his continued advice, support and feedback throughout my time in Sheffield. Under his supervision, I have gained numerous skills, without which my progression as a researcher would not have be possible. I would also like to thank my secondary supervisors, Dr. Helen Bryant and Professor Alastair Goldman, for their contributions, questions and comments which greatly helped in the completion of this project.

Secondly, I would like to thank all within the Collis and the Bryant labs, past and present, as well as the rest of the Academic Unit of Molecular Oncology. Without your camaraderie and support there is no way that I would have made it this far. I would like to particularly thank Dr. Katie Myers for her continued patience and advice and Mr. Anil Ganesh, without whom I probably would still be carrying out my qPCR analysis of CCDC15. Without the encouragement of Caroline, Clair and Natasha I would not have made it through this last three years, thank you all for the friendship, support and most of all, the cake!

I also would like to thank the staff of the Sheffield RNAi Screening Facility, particularly Dr. Steve Brown, for their help during the development of the high throughput screen. Your continued optimism and advice, despite all the setbacks, helped me to keep moving forward.

Last but by no means least I would like to thank all my friends and family outside of the lab who have always been there for me. I would specifically like to thank Tom for all his continuous support and my parents who have always believed in me even when I did not, for this I am eternally grateful. To everybody else who has helped me through all the exams, tears and ordeals throughout my academic career, I will never forget your kindness.

Abstract

Replication stress is present in cancers cells at higher than normal levels due to the increased proliferation caused by oncogene activation. This results in elevated levels of phosphorylated RPA2 (pRPA2) and DNA damage, which can ultimately result in genetic instability. By inhibiting suppressors of replication stress, it may be possible to target this cancer-specific phenotype to selectively kill tumour cells. Attempts were therefore made to develop a high throughput whole genome RNAi screen to detect increased endogenous levels of pRPA2 foci formation following gene knockdown, however, this proved unsuccessful. As a contingency measure a selected panel of kinases, identified as putative replication stress suppressors and potential druggable targets, were assessed for their ability to induce pRPA2 foci following gene knockdown. This approach identified several hits, which were then evaluated for their ability to preferentially kill cells lacking p53 signalling or overexpressing several clinically relevant oncogenes (Cyclin E, H-RAS and MYC-N). They were also assessed for their ability to potentiate the effects of the replication stress inducing drugs Gemcitabine and 5-Flurouracil as well as the PARP inhibitor Olaparib.

In addition, the putative DNA damage repair factor CCDC15, which has been hypothesised to act in the resolution of replication impeding lesions, was also investigated as a potential replication stress suppressor. However, it does not appear to modulate DNA replication stress as its loss does not induce pRPA2 and the formation of DNA damage following its knockdown is independent of entry into S phase. Interestingly, depletion of CCDC15 sensitised certain cell lines to the effects of DNA crosslinking agents. Furthermore, knockdown of CCDC15 also slightly increased the formation of endogenous FANCD2 foci, but not in cells treated with DNA crosslinking agents. However, CCDC15-depleted cells exhibited delayed formation and resolution of RAD51 foci following DNA damage, which were not due to perturbations in cell cycle progression. Although CCDC15 appears to have little effect on the cell cycle distribution of cycling cells, its loss potentially delays re-entry into the cycle of cells paused in G1 phase.

Abbreviations

5-FU	5-Flurouracil
53BP1	p53-binding Protein 1
8-oxo-dG	8-oxo-deoxyguanosine
9-1-1	RAD9-HUS1-RAD1
ABC	ATP Binding Cassette
AD	Activation Domain
AP	Apurinic Site
APC	Anaphase Promoting Complex
AT	Ataxia-telangiectasia
ATM	Ataxia-telangiectasia Mutated
ATR	Ataxia-telangiectasia Mutated and RAD3 Related
BCNU	Bis-chloroethylnitrosurea
BER	Base Excision Repair
BIR	Break Induced Repair
BPDE	Benzo(a)pyrene Dioleoxide
BSA	Bovine Serum Albumin
CAK	CDK Activating Kinase
CCDC15	Coiled-coil Domain Containing 15
CDK	Cyclin Dependent Kinase
CFS	Common Fragile Sites
Chk1	Checkpoint Kinase 1
Chk2	Checkpoint Kinase 2
CIN	Chromosomal Instability
CKI	CDK Inhibitory Subunits
CML	Chronic Myelogenous Leukaemia
CPD	Cyclobutane Pyrimidine Dimers
CSA	Cockayne Syndrome Protein A
CSB	Cockayne Syndrome Protein B

DDK	DBF4 Dependent Kinase
DDR	DNA Damage Response
dHJ	Double Holliday Junction
DMEM	Dulbecco's Modified Eagle Medium
DMSO	Dimethyl Sulfoxide
DNA	Deoxyribonucleic Acid
DNA-PK	DNA-dependent Protein Kinase
DNA-PKcs	DNA-dependent Protein Kinase Catalytic Subunit
dNTP	Deoxyribonucleotide
DSB	Double Strand Break
DSBR	Double Strand Break Repair
DTT	1,4-dithiothreitol
EDTA	Editic Acid
FA	Fanconi Anaemia
FCS	Foetal Calf Serum
FRT	Flippase Recognition Target
FUCCI	Fluorescence Ubiquitination Cell Cycle Indicator
G1 Phase	Growth 1 Phase
G2 Phase	Growth 2 Phase
GBM	Glioblastoma Multiforme
ggNER	Global Genome Nucleotide Excision Repair
GSEA	Gene Set Enrichment Analysis
HCl	Hydrochloric Acid
HR	Homologous Recombination
hTERT	Human Telomerase Reverse Transcriptase
HU	Hydroxyurea
ICL	Interstrand Crosslink
IF	Immunofluorescence
IP	Immunoprecipitation
IR	Ionising Radiation
Lig III	Ligase III

M Phase	Mitotic Phase
MCM	Minichromosome Maintenance Complex
MDR1	Multi-drug Resistance Protein 1
MEF	Mouse Embryonic Fibroblast
MGMT	O^6-methylguanine Methyltransferase
MIN	Microsatellite Instability
MIRA-1	Mutant p53 Reactivation and Induction of Rapid Apoptosis
MMC	Mitomycin C
MMEJ	Microhomology Mediated End Joining
MMR	Mismatch Repair
MRN	Mre11-RAD50-Nbs1
MTT	(3-(4,5-dimethylthiazol-2-yl)-2,5-diphenyltetrazolium bromide)
NaOH	Sodium Hydroxide
NER	Nucleotide Excision Repair
NHEJ	Non-homologous End Joining
OD	Optical Density
OIS	Oncogene-induced Senescence
ORC	Origin Recognition Complex
PARP	Poly (ADP-ribose) polymerase
PBS	Phosphate Buffered Saline
PCC	Pearson Correlation Coefficient
PCNA	Proliferating Cell Nuclear Antigen
PCR	Polymerase Chain Reaction
PFA	Paraformaldehyde
PI	Propidium Iodide
PI3K	Phosphatidylinositol 3-kinase
PIKK	Phosphatidylinositol 3-kinase like kinase
PIPES	1,4-Piperazinediethanesulfonic acid
PJS	Peutz Jeghers Syndrome
Plk1	Polo-like Kinase 1
PMVK	Phosphomevalonate Kinase

Pol α	DNA Polymerase α
Pol β	DNA Polymerase β
Pol δ	DNA Polymerase δ
Pol ε	DNA Polymerase ε
Pol ζ	DNA Polymerase ζ
Pol η	DNA Polymerase η
Pol θ	DNA Polymerase θ
Pol ι	DNA Polymerase ι
Pol κ	DNA Polymerase κ
Pol λ	DNA Polymerase λ
Pol μ	DNA Polymerase μ
pRb	Retinoblastoma
pre-IC	Pre-initiation Complex
pre-RC	Pre-replication Complex
pRPA	Phosphorylated Replication Protein A
PTEN	Phosphatase and Tensin Homolog
PTN-α	Pifithrin-α
qPCR	Reverse-transcription Polymerase Chain Reaction
RFC	Replication Factor C
RITA	Reactivation of p53 and Induction of Tumour Cell Apoptosis
RNA	Ribonucleic Acid
RNA Pol II	RNA Polymerase II
rNTP	Ribonucleotide
ROS	Reactive Oxygen Species
RPA	Replication Protein A
RRA	Robust Rank Aggregation
RRM1	Ribonucleotide Reductase Catalytic Subunit M1
RSS	Restart Score
S Phase	Synthesis Phase
SAM	S-adenosylmethianine

SDS	Sodium Dodecyl Sulphate
SDSA	Synthesis Dependent Strand Annealing
SMARCAL1	SWI/SNF Related, Matrix Associated, Actin Dependent Regulator Of Chromatin, Subfamily A Like 1
SNRK	Sucrose Non-fermenting Related Kinase
SRSF	Sheffield RNAi Screening Facility
SSA	Single Strand Annealing
ssDNA	Single Stranded DNA
TC-NER	Transcription Coupled Nucleotide Excision Repair
TCGA	The Cancer Genome Atlas
Tet	Tetracycline
TLR	Traffic Light Reporter
TLS	Translesion Synthesis
TTD	Trichothiodystrophy
USD	Unscheduled DNA Synthesis
UV	Ultraviolet
WT	Wild Type
XP	Xeroderma Pigmentosum
XPV	Xeroderma Pigmentosum Variant
YFP	Yellow Fluorescent Protein
γH2AX	Phosphorylated H2AX (Serine 139)

Table of Contents

ABSTRACT 7

ABBREVIATIONS 9

TABLE OF CONTENTS 15

CHAPTER ONE: INTRODUCTION 17

Table of Figures 18

1.1 The Importance of Genome Stability 19

1.2 Maintenance of Genome Stability 20

1.3 Deregulation of Genome Maintenance Mechanisms in Cancer 44

1.4 Targeting Maintenance Mechanisms to Treat Cancer 48

CHAPTER TWO: MATERIALS AND METHODS 61

Table of Figures 62

2.1 Materials 63

2.2 Methods 76

CHAPTER THREE: PHOSPHO-RPA2 RNAI SCREEN DEVELOPMENT 91

Table of Figures 92

3.1 Introduction 94

3.2 Replication Stress Suppressor Knockdown 95

3.3 Phospho-RPA2 Antibody Selection 96

3.4 Phospho-RPA2 Replication Stress Detection in a Cell Line Panel 104

3.5 High Throughput Phospho-RPA2 Replication Stress Detection 108

3.6 Alternative Methods of Detecting Replication Stress 133

3.7 Discussion 140

CHAPTER FOUR: PHOSPHO-RPA2 TARGETED SCREEN 151

Table of Figures 152

4.1 Introduction 153

4.2 Phospho-RPA2 Staining Optimisation in U2OS Cells 154

4.3 Phospho-RPA2 Targeted Screen 156

4.4 Hit Validation and Further Kinase Selection 159

4.5 Further Investigation of the Sensitisation to p53 Loss 166

4.6 SNRK-mediated Lethality to Oncogene Induced Replication Stress 172

4.7 SNRK-mediated Sensitisation to Replication Stress Causing Chemotherapies 178

4.8 Discussion 180

CHAPTER FIVE: CHARACTERISATION OF CCDC15 DEFICIENT CELLS 189

Table of Figures 190

5.1 Introduction 192

5.2 Validation of Gene Set Enrichment Analysis 194

5.3 DNA Damage Response Phenotype 201

5.4 Discussion 228

CHAPTER SIX: CCDC15 LOCALISATION AND INTERACTION STUDIES 237

TABLE OF FIGURES 238
6.1 INTRODUCTION 239
6.2 CCDC15 CLONING AND STABLE CELL LINE GENERATION 240
6.3 CCDC15 SUBCELLULAR LOCALISATION 249
6.4 CCDC15 INTERACTION STUDIES 253
6.5 DISCUSSION 256

CHAPTER SEVEN: CONCLUSIONS 261

7.1 IDENTIFICATION OF REPLICATION STRESS SUPPRESSORS 262
7.2 CHARACTERISATION OF CCDC15 264

BIBLIOGRAPHY 269

APPENDICES 305

APPENDIX 1 TARGETED SCREEN SIRNA SEQUENCES 306
APPENDIX 2 HIGH THROUGHPUT SCREEN DEVELOPMENT 309
APPENDIX 3 TARGETED SCREEN HIT SELECTION 310
APPENDIX 4 TARGETED SCREEN STATISTICS 312

Chapter One:
Introduction

TABLE OF FIGURES 18

1.1 THE IMPORTANCE OF GENOME STABILITY 19

1.1.1 CANCER 19

1.2 MAINTENANCE OF GENOME STABILITY 20

1.2.1 CELL CYCLE CONTROL 20

1.2.2 DNA REPLICATION 24

1.2.3 DNA DAMAGE RESPONSE 29

1.2.3.1 SOURCES OF DNA DAMAGE 29

1.2.3.2 PI3K LIKE KINASES 30

1.2.3.3 CHECKPOINT ACTIVATION 33

1.2.3.4 DNA REPAIR MECHANISMS 36

1.3 DEREGULATION OF GENOME MAINTENANCE MECHANISMS IN CANCER 44

1.3.1 CANCER PREDISPOSITION 44

1.3.2 SPORADIC CANCERS 45

1.4 TARGETING MAINTENANCE MECHANISMS TO TREAT CANCER 48

1.4.1 CONVENTIONAL THERAPY 48

1.4.2 MOLECULAR TARGETING 50

1.4.2.1 TARGETING REPLICATION STRESS RESPONSE 55

1.4.2.2 IDENTIFICATION OF NOVEL REPLICATION STRESS RESPONSE GENES AS POTENTIAL FUTURE ANTI-CANCER TARGETS 58

Table of Figures

Figure 1.2.1.1 Cell Cycle Control Mechanisms. 22
Figure 1.2.2.1 Licensed origin of replication. 24
Figure 1.2.2.2 Pre-initiation Complex. 25
Figure 1.2.2.3 Active DNA replication fork. 26
Figure 1.2.2.4 Stalled DNA replication fork. 27
Figure 1.2.3.2.1 ATR signalling at a stalled replication fork. 32
Figure 1.2.3.3.1 G1/S checkpoint activation. 33
Figure 1.2.3.3.2 Intra-S phase checkpoint activation. 34
Figure 1.2.3.3.3 G2/M checkpoint activation. 35
Figure 1.2.3.3.4 Mitotic spindle checkpoint activation. 35
Figure 1.2.3.4.1 Base excision repair. 37
Figure 1.2.3.4.2 Nucleotide Excision Repair. 38
Figure 1.2.3.4.3 Double strand break repair. 40
Figure 1.2.3.4.4 Interstrand crosslink repair by the Fanconi Anaemia pathway. 42
Figure 1.3.2.1 Oncogene induced DNA damage model of cancer development. 47
Figure 1.4.2.1.1 Targeting the Replication Stress Response. 56

1.1 The Importance of Genome Stability

The fundamental challenge that all cells face is the accurate replication of their DNA and the precise division into two identical progenies. If this is not carried out correctly, the genomes of the daughter cells differ from that of their parent, which can result in genomic instability (Shen, 2011). This instability can be divided into two main classes: chromosomal instability (CIN), where the structure and/or number of chromosomes is altered, or microsatellite instability (MIN), where the repeat sequences present at microsatellites are expanded or contracted (Negrini et al, 2010).

Genomic instability can have positive consequences, such as the generation of evolutionary advantageous mutations, however it is most commonly associated with pathological conditions and ageing (Aguilera & Gomez-Gonzalez, 2008; Vijg & Suh, 2013). Tissue samples from patients with a variety of neurological disorders display instability at repeated sequences which is not observed in control samples (Haeusler et al, 2016). It is also associated with a number of premature ageing syndromes, many of whose symptoms include predisposition to the development of cancer (Burhans & Weinberger, 2007).

1.1.1 Cancer

Cancer is not a single disease but a compendium of hundreds of disorders that can arise from almost any tissue or cell type within the body. Globally it is a major issue; in 2012 alone it resulted in 8.2 million deaths and this is predicted to increase to 13 million by 2030. This extrapolation may be an underestimate of the future cancer burden as the adoption of lifestyles with associated cancer risks is rising internationally (American Cancer Society, 2015). Whilst the cancer survival rate has doubled in the United Kingdom in the last 40 years, only 50% of patients achieve a 10 year survival post-diagnosis (Cancer Research UK, 2017). No single universal strategy can be employed to reduce its incidence as there is a marked change in the prevalence of cancer types between economically developed and developing countries (American Cancer Society, 2015). The impact of cancer is not limited to the human cost, it also poses major financial implications. Therapy costs are rising and as more patients survive for longer, the duration of treatment is increasing (Yabroff et al, 2011). The loss of productivity due to the illness and the drain on patient income also appreciably contribute to the economic consequences of the disease (American Cancer Society, 2015).

Despite the fact that there are tremendous levels of diversity in the effects and characteristics of individual cancer types, they are mostly believed to share a common developmental pathway. All are thought to evolve through the continued acquisition of mutations, some of which confer a survival advantage upon individual cells. These 'driver' mutations are selected for during tumorigenesis, resulting in the clonal expansion of the cells containing them (Martincorena et al; Stratton et al, 2009). Tumours are heterogeneous, as they contain several of these populations, each with their own mutational profile (Greaves & Maley, 2012). Many of these driver mutations are associated with characteristics that are believed to be shared between most cancers, which are referred to as "hallmarks". The initial six hallmarks were defined as: the ability to sustain proliferative signalling, the evasion of growth suppression, the resistance of cell death

signals, replicative immortality, the induction of angiogenesis and the activation of invasion and ensuing metastasis. It was suggested that cancerous cells acquire a succession of these capabilities during their development which allows the progression from premalignant lesions into fully formed tumours (Hanahan & Weinberg, 2000). A review of this system eleven years later suggested the addition of two additional hallmarks, the reprogramming of cancer cell metabolism and the evasion of the immune system. It also included two characteristics that were considered to promote cancer development: inflammation and genomic instability (Hanahan & Weinberg, 2011).

Faithful replication of DNA is essential for the prevention of tumorigenesis as almost all cancers arise through genomic alterations (Martincorena et al; Stratton et al, 2009). A complex network of genome maintenance mechanisms has evolved to counteract these modifications but these can be disrupted during the development of cancer. The resultant mutations fuel the development of the tumours into more malignant lesions as they induce further genome instability.

1.2 Maintenance of Genome Stability

1.2.1 Cell Cycle Control

The cell cycle temporally controls the growth and division of eukaryotic cells. This complex molecular pathway ensures that the stages of cell division occur in the correct order as later events depend upon the completion of those that occur earlier in the cycle. In this way, cells can ensure that their genomes are being passed on without alteration (Nurse, 2000).

The cycle is divided into four distinct phases: an initial growth phase (G1), the synthesis (S) phase of new DNA, a second growth phase (G2) and the division into two daughter cells by mitosis (M phase). The two growth phases make up a large proportion of the cell cycle and are required to give the cells additional time to propagate and to prepare for the events of S phase or M phase. Progression through the cell cycle is controlled by members of the Cyclin dependent kinase (CDK) family of enzymes, predominantly CDK1 and CDK2 (Morgan, 1997). The activation of the CDKs requires the binding of Cyclins and post-translational modification by the CDK activating kinase (CAK) and CDC25 family of phosphatases (Pavletich, 1999).

The Cyclins are a distinct family of proteins whose expression fluctuates throughout the cell cycle. The sequence similarity between these dissimilar proteins is conserved to the 'Cyclin box', a region required for their binding to CDKs (Morgan, 1997). This binding partially activates CDKs by inducing conformational changes in their substrate binding site. In the absence of Cyclin binding, CDKs' T-loop obstructs their catalytic cleft, whilst in the presence of Cyclins it is relocated to allow access to the binding site (Pavletich, 1999). This re-arrangement exposes Threonine 160 (T160), or equivalent, which requires phosphorylation by CAK for the full activation of the kinase (Morgan, 1997) and moves the PSTAIRE helix into the binding site. This helix contains Glutamic Acid 51 (E51) which is required for substrate catalysis (Pavletich, 1999).

The phosphorylation of T160 by CAK increases CDK activity up to 300-fold compared to Cyclin binding alone. It results in the stabilisation of Cyclin binding and further changes to the conformation of the T-loop and catalytic cleft (Morgan, 1997). In mammalian cells, CAK has been identified as CDK7 and its binding partner Cyclin H (Fisher & Morgan, 1994).

CDKs are also phosphorylated at Tyrosine 15 (Y15) and Threonine 14 (T14) by Wee1 and Myt 1 respectively. This has been extensively studied with respect to CDK1, where these modifications result in the obstruction of the substrate binding site and reduce the enzyme's affinity for ATP. In the case of CDK2, Y15 phosphorylation does not completely abrogate the enzyme's ATPase activity (Welburn et al, 2007). The CDC25 family of phosphatases dephosphorylates T14 and Y15 resulting in activation of the CDK/Cyclin complexes (Perry & Kornbluth, 2007).

CDK inhibitory subunits (CKIs) also play a role in the regulation of CDK activity. In mammals two families, Cip and INK4, are present and act in a tissue specific manner to control cell cycle progression. The Cip family (p21, p27 and p57) inhibits CDK2 and CDK4/6 (Blain et al, 1997) by inserting a helix into the ATP binding site and changing the conformation of the catalytic cleft of CDKs (Pavletich, 1999). The INK4 family (p15, p16, p18 and p19) inhibit CDK4/6 alone and in complex with the D Cyclins (Blain et al, 1997) by binding adjacent to the catalytic cleft which disrupts the cyclin and ATP binding sites (Pavletich, 1999).

As alluded to earlier, the expression of the Cyclins oscillates throughout the cell cycle and certain members of the family are associated with each phase: the D Cyclins are active in G1, Cyclins E and A are active in S and Cyclins A and B play a role in the onset of mitosis (Murray, 2004).

In G1, intracellular and environmental conditions regulate whether cells enter a new cell cycle (Lukas et al, 1996). Mitogenic signalling is required for the initiation and maintenance of G1 progression until the 'restriction point' where growth factors are no longer required for the advancement of the cell cycle (Blagosklonny & Pardee, 2002). The mitogenic signalling pathways, including those mediated by membrane Tyrosine kinases, estrogen and G-coupled protein receptors, result in the transcription of the D Cyclins. They also prevents their phosphorylation at Threonine 286 (Fig.1.2.1.1), which targets these proteins for ubiquitin mediated proteasomal degradation (Blagosklonny & Pardee, 2002). The Cyclin D/CDK4/6 complex phosphorylates retinoblastoma (pRb) which prevents its inhibition of the activity of the E2F family of transcription factors (Lukas et al, 1996; Lundberg & Weinberg, 1998). These proteins stimulate the transcription of genes essential for the progression of S phase, including proteins required for DNA synthesis (Blagosklonny & Pardee, 2002) and Cyclin E (Hwang & Clurman, 2005) (Fig. 1.2.1.1). The D Cyclins are degraded at the G1/S boundary as their presence is inhibitory to DNA replication (Fukami-Kobayashi & Mitsui, 1999).

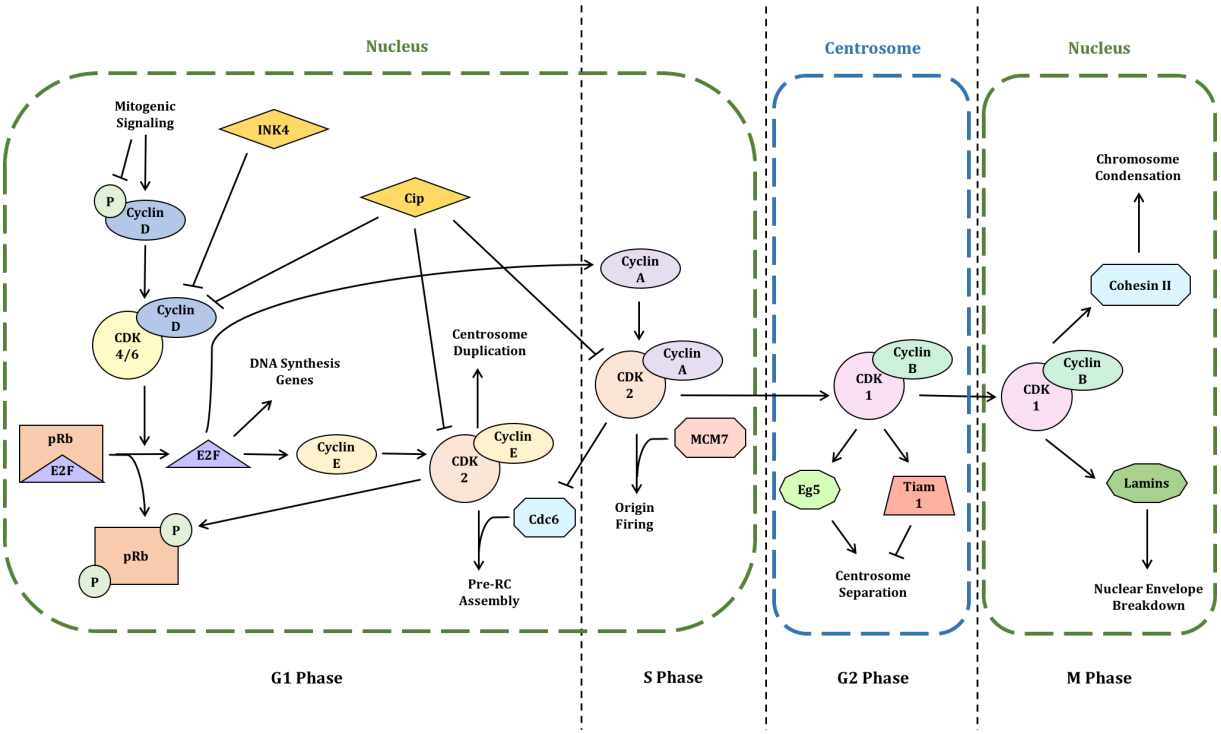

Figure 1.2.1.1 Cell Cycle Control Mechanisms.

Mitogenic signalling triggers the upregulation of Cyclin D expression and inhibits its phosphorylation. Cyclin D binds to CDK4/6 which results in the phosphorylation of pRb and the release of E2F. The INK4 CDK inhibitors repress the action of CDK4/6 to prevent spurious cell cycle entry. The release of E2F elicits the upregulation of several genes required for DNA synthesis including Cyclin E. This Cyclin binds to CDK2 resulting in centrosome duplication and the assembly of the pre-replication complex (pre-RC) by associating with Cdc6. Cyclin E/CDK2 also phosphorylates pRb resulting in an increase in free E2F and the upregulation of Cyclin A. This second binding partner of CDK2 triggers origin firing by interacting with MCM 7 and inhibits the re-formation of the pre-RC by phosphorylating Cdc6. It results in the activation of Cyclin B/CDK1 at the centrosomes. The Cip family of CDK inhibitors inhibit both CDK4/6 and CDK2 to control progression through the cell cycle. The Cyclin B/CDK1 complex is responsible for the initiation of centrosome separation. In M phase it migrates to the nucleus where it subsequently phosphorylates the cohesin II complex and lamins, which results in chromosome cohesion and nuclear envelope breakdown respectively.

Cyclin E binds to CDK2 and activation of this complex terminates the growth factor dependent phase of the cell cycle (Blagosklonny & Pardee, 2002). It primes the cell for later events as its interaction with Cdc6 stimulates the formation of the pre-replication complex (Coverley et al, 2002) and it is required for the duplication of centrosomes (Hinchcliffe et al, 1999) (Fig. 1.2.1.1). It further activates E2F by phosphorylating pRb which upregulates the expression of Cyclin A (Lundberg & Weinberg, 1998; Schulze et al, 1995). Cyclin E is degraded as S phase progresses via a ubiquitin ligase dependent pathway requiring Fbw7 to prevent hyper-proliferation (Siu et al, 2012).

Cyclin A, the second binding partner of CDK2, has biphasic activity which is regulated by its expression level. The complex is initially formed at the onset of S phase with a surge of further activation in early G2 (De Boer et al, 2008). In S phase, Cyclin A/CDK interacts with MCM 7 to initiate replication at licensed origins (Chibazakura et al, 2011; Coverley et al, 2002) and phosphorylates Cdc6 to prevent further licensing to ensure the DNA is only

replicated once (Coverley et al, 2002). In late G2, it has been demonstrated to control progression into M phase by the activation of Cyclin B/CDK1 in both the nucleus and at the centrosomes (De Boer et al, 2008) (Fig. 1.2.1.1).

The activation of Cyclin B/CDK1 begins in late G2 at the centrosomes and its activity steadily rises throughout the remainder of G2 until the onset of mitosis where it spikes rapidly (Lindqvist et al, 2007). It promotes the separation of the centrosomes though the destabilisation of interphase astral microtubules and primes several substrates for phosphorylation by Polo-like kinase 1 (Plk1). One such substrate is Eg5, a kinesin with microtubule sliding activity, which is required for centrosome separation. It also phosphorylates Tiam1 which antagonizes the activity of Eg5 to limits the extent of separation (Whalley et al, 2015). Cyclin B contains a cytoplasmic retention signal which becomes phosphorylated in prophase to allow re-location of the complex to the nucleus (Li et al, 1997). Once within the nucleus, it phosphorylates the cohesin II complex to promote chromosome condensation (Abe et al, 2011) and the nuclear lamins and lamin associated proteins to induce nuclear envelope breakdown (Alvarez-Fernandez & Malumbres, 2014) (Fig. 1.2.1.1).

The mitotic Cyclins A and B are degraded by the anaphase promoting complex (APC) bound to Cdc20 (Zachariae et al, 1998). If Cyclin B cannot be degraded, cells fail to progress through the Metaphase to Anaphase transition and so cannot exit mitosis (Chang et al, 2003). The activity of the APC persists after cell division to allow the cells to prepare for the next cell cycle via its binding to the Cdh1 regulatory subunit (Zachariae et al, 1998).

It is also possible for a cell to exit the cell cycle and enter a non-proliferating resting phase (G0) transitorily or permanently. Transient cell cycle exit, or quiescence, can be reversed which is crucial for post-natal tissue repair and regeneration (Terzi et al, 2016). Cells can be triggered to enter this state by a number of factors, including loss of adhesion or contact inhibition, and is thought to mainly be controlled by the balance of active pRB or E2F. These cells actively maintain this non-proliferative state as they express suppressors of differentiation, apoptosis (Yao, 2014), cell cycle progression and mitogenic signalling (Fukada et al, 2007). Cells experiencing high levels of certain stresses, such as replication stress, can be forced to enter a permanently non-replicating state. In this senescent state, proliferation is actively prevented and in the case of replicative senescence this is achieved by a prolonged DNA damage response (Bartkova et al, 2006).

1.2.2 DNA Replication

In every cell cycle, the entire genome must be precisely replicated once to ensure the maintenance of genomic stability. If errors occur during this process, they would be passed onto the cells progeny and could result in deleterious mutations. Therefore, several mechanisms are employed to ensure DNA is replicated accurately. Due to these maintenance systems, somatic cells incorporate mutations at a rate of approximately 1.2 $x10^{-8}$ per base pair (Milholland et al, 2017).

To ensure that DNA is only replicated once per cell cycle, replication origins must be licensed before replication initiation can occur. This system was first determined in cell-free *Xenopus* egg extracts which demonstrated that cells needed to exit metaphase before replication could occur again (Blow & Laskey, 1988). The replication factor responsible for the licensing of DNA was identified as the mini-chromosome-maintenance (MCM) ring complex (MCM 2-7) which is assembled on chromatin following metaphase exit and displaced after origin firing (Chong et al, 1995). This complex acts as part of the DNA helicase to unwind the duplex DNA for replication (Ishimi, 1997).

The loading of MCM 2-7 onto the DNA requires the assembly of the pre-replication complex (pre-RC), which consist of the origin recognition complex (ORC), Cdc6 and Cdt1 (Nishitani & Lygerou, 2002). The ORC initially binds to DNA replication origins throughout G1 (Rowles et al, 1996) where it recruits Cdc6 (Coleman et al, 1996) and subsequently Cdt1 to the complex (Tsuyama et al, 2005) (Fig. 1.2.2.1). It has recently been demonstrated that MCM 3 initially binds to the pre-RC, closely followed by MCM 4, 6 and 7. This induces a conformation change in the complex which allows DNA to enter the ring between MCM 2 and 5 (Zhai et al, 2017).

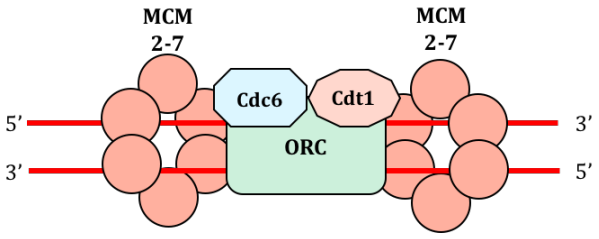

Figure 1.2.2.1 Licensed origin of replication.
The ORC complex binds to origins of replication throughout G1. This subsequently recruits Cdc6 and Cdt1 to form the pre-replication complex which is required for the loading of MCM 2-7 DNA helicase.

This loading can only occur when CDK4/6, CDK2 and CDK1 levels are low (Bendris et al, 2011) which prevents the re-licensing of origins throughout the cell cycle. Once MCM 2-7 is loaded onto the DNA, the pre-RC components are not required to maintain this binding and so are degraded in a cell cycle dependent manner (Blow & Hodgson, 2002). ORC is phosphorylated by the CDKs in late G1 and remains so until exit from metaphase when CDK1 activity is abolished. Cdc6 is also phosphorylated which results in its ubiquitin-mediated proteolysis (Nguyen et al, 2001). It is the inactivation of Cdt1 that appears most influential in the downregulation of licensing (Blow & Gillespie, 2008) as it is degraded in a cell cycle dependent manner (Li et al, 2003) and inhibited by geminin binding from the onset of S phase to metaphase exit (Arias & Walter, 2005; Li & Blow, 2005).

At the initiation of S phase, the pre-RCs are converted into pre-initiation complexes (pre-IC) through the activation of the DNA helicase (Fragkos et al, 2015). It is during this period that Cdc6 and Cdt1 dissociate from the origins. The MCM 2-7 helicase must associate with both Cdc45 and GINS to allow the initiation of DNA replication (Moyer et al, 2006) as these molecules increase its ATPase activity and affinity for DNA (Ilves et al, 2010). The binding of Cdc45 relies upon the phosphorylation of the MCM complex by the DBF4 dependent kinase (DDK) (Heller et al, 2011) and its association with TopBP1 and Treslin in a CDK2 dependent manner (Kumagai et al, 2010). In contrast, Cyclin A/CDK2 activity is also required for the recruitment of GINS to the complex (Heller et al, 2011). Its activity also results in the binding of MCM 10 (Douglas & Diffley, 2016), TopBP1 and RECQL4 to MCM 2-7, all of which are required to maintain the stability of the helicase (Im et al, 2009) and for efficient replication of DNA (Tanaka et al, 2013).

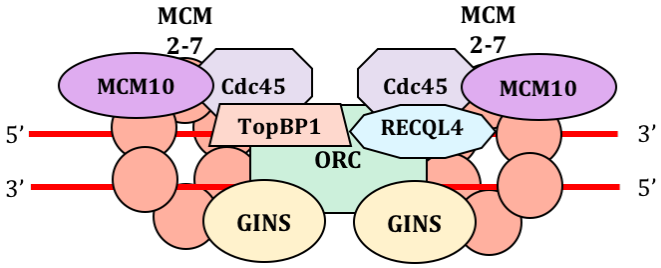

Figure 1.2.2.2 Pre-initiation Complex.
Activation of the MCM 2-7 helicase requires the binding of both Cdc45 and GINS. Its stability and efficiency are maintained by the subsequent binding of MCM 10, TopBP1 and RECQL4.

The replicative DNA polymerases, Pol α primase, Pol ε and Pol δ are recruited to the pre-IC at the onset of S phase. Pol ε recruitment requires the signalling of Cyclin A/CDK2, whilst MCM 10 and DNA unwinding are essential for the binding of Pol α and Pol δ (Heller et al, 2011). Alongside, these polymerases, several other factors are essential for the formation of the replisome. The DNA binding protein RPA is recruited to the single stranded DNA (ssDNA) generated by the activity of the DNA helicase. Its binding is essential to protect the ssDNA from degradation and prevent the formation of secondary structures that could block replication (MacNeill et al, 2012). The proliferating cell nuclear antigen complex (PCNA) is also required for efficient DNA replication as it fastens the polymerases to the DNA to allow rapid replication (Kelman, 1997) and is loaded onto DNA by replication factor C (RFC) (Bowman et al, 2006).

Replication occurs bi-directionally away from the replication origin, with the DNA polymerase travelling from 5' to 3' (Zheng & Shen, 2011). To facilitate replication, the DNA must be primed by a primase, a DNA dependent RNA polymerase, which creates a short RNA primer bound to the template strand (Fien et al, 2004). In eukaryotic cells, the primase is located within the Pol α primase complex (Kilkenny et al, 2013), whose DNA polymerase domain extends the primer with deoxyribonucleotides (dNTPs) (Fien et al, 2004). The RCF loads PCNA onto the primed DNA which displaces Pol α primase and facilitates the switch to Pol ε on the leading strand and Pol δ on the lagging strand (Kunkel & Burgers, 2008; Maga et al, 2000; Pursell et al, 2007; Zheng & Shen, 2011). Synthesis on the leading strand is a continuous reaction (Kunkel & Burgers, 2008) whilst lagging strand synthesis requires repeated priming events by Pol α primase. Pol δ carries on the synthesis from these primers, generating approximately 200 nucleotide long Okazaki

fragments (Zheng & Shen, 2011). This displaces the downstream primer resulting in a 5' DNA flap which is subsequently removed by the combined action of FEN1 and Dna2 (Bae et al, 2001) before the fragments can be joined into a continuous strand by ligation (Zheng & Shen, 2011).

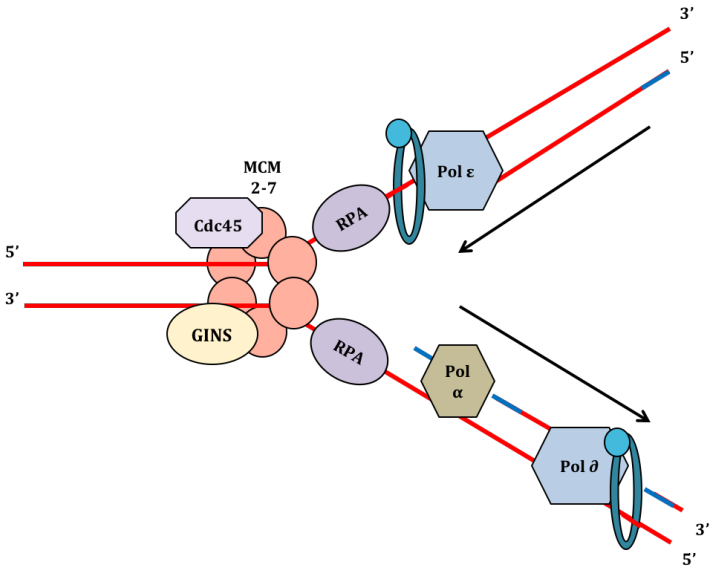

Figure 1.2.2.3 Active DNA replication fork.

MCM 2-7 in complex with Cdc45 and GINS acts as the replicative helicase and unwinds duplex DNA (red) to produce single stranded DNA. This is bound to by RPA to prevent degradation and secondary structure formation. The primase of DNA polymerase α (Pol α) initiates DNA replication by synthesising RNA primers (blue). The RCF-PCNA complex (blue ring) facilitates polymerase switching to Pol ε on the leading strand and Pol δ on the lagging strand. Black arrows represent direction of DNA Polymerase.

DNA polymerases select bases for incorporation into the nascent DNA strand according to Watson-Crick base pairing (Tanaka et al, 2010). Mutations of conserved residues in yeast (Li et al, 2005; Niimi et al, 2004; Venkatesan et al, 2006) and human (Tanaka et al, 2010) DNA polymerases α and δ resulted in increased mutation rates due to a decreased ability to discriminate mismatches. As well as the ability to select the correct bases for insertion, Pol ε and Pol δ exhibit 3'-5' exonuclease proofreading activity that allows them to remove mispaired bases (Kunkel, 1988). This proofreading capacity increases the fidelity of the enzymes approximately 100-fold (Reha-Krantz, 2010) and is required for the proper maturation of Okazaki fragments (Garg et al, 2004).

Any DNA mismatches that remain are removed by mismatch repair (MMR) (Iyer et al, 2006) with the most common sub-pathway dependent on the activity of MutSα and MutLα (Kunkel & Erie, 2015). MutSα, comprised of Msh2 and Msh6, binds DNA mismatches and ATP to form a clamp that can slide along DNA (Lee et al, 2014). It interacts with MutLα (Mlh1 and Pms2) whose activation by PCNA results in the nicking of the nascent DNA strand (Kadyrov et al, 2006). These nicks can facilitate strand displacement synthesis, where Pol δ or Pol ε incorporate the correct base (Tran et al, 1999), before the DNA is ligated (Kunkel & Erie, 2015).

1.2.2.1 DNA Replication Stress

The rate at which DNA replication occurs affects its fidelity as when it is slowed or halts completely, ssDNA accumulates within the nucleus, which is subsequently bound by RPA. This phenomenon is referred to as DNA replication stress and most commonly occurs when the replicative helicase becomes uncoupled from the DNA polymerase (Fig. 1.2.2.4). A number of circumstances can trigger DNA replication stress including the depletion of molecules essential for the completion of DNA replication, such as dNTPs or RPA, or the presence of DNA lesions that physically arrest polymerase progression (Zeman & Cimprich, 2014). Gene transcription can also pose a significant threat to the accurate completion of DNA replication as it can result in the formation of DNA secondary structures or DNA:RNA hybrids (R-loops) that cannot be bypassed by the DNA polymerases. As the transcription machinery traverses along the DNA in a similar fashion to the replisome, this can likewise form a barrier to the completion of DNA replication (Barlow & Nussenzweig, 2014).

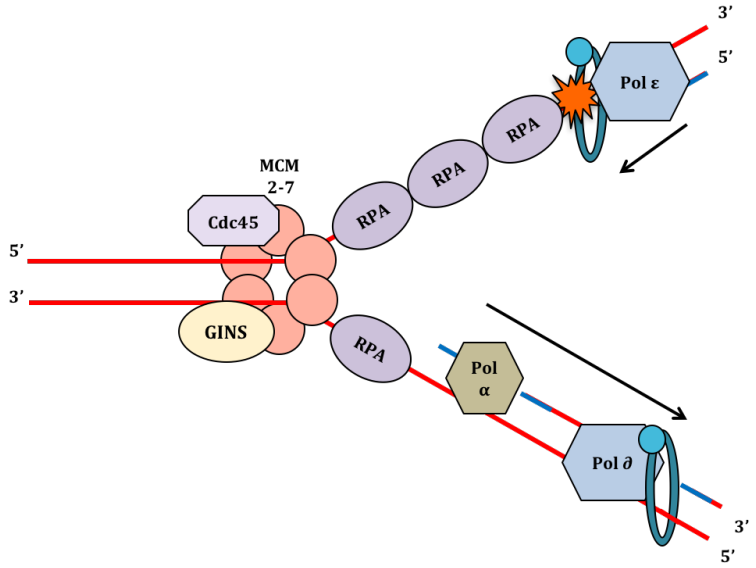

Figure 1.2.2.1.1 Stalled DNA replication fork.

The replicative helicase (MCM 2-7 in complex with Cdc45 and GINS) can become uncoupled from the replicative polymerase due to polymerase blocking structures (orange star). The helicase continues unwinding the DNA resulting in the formation of single stranded DNA that is subsequently bound by RPA.

When a replication fork stalls, DNA synthesis can be restarted once the source of the stress has been removed. If this is not possible, there are also several ways in which cells can restart replication whilst the stress is still present (Zeman & Cimprich, 2014).

This includes the restart of replication downstream of the blockage through the activation of dormant origins or the re-priming of the DNA. During G1, more origins will be licensed than will be required to replicate the genome and these remaining origins lie dormant in an unperturbed cell cycle. However, when replication is impeded, they can be activated to allow the completion of DNA replication before M phase (Ge et al, 2007; Woodward et al, 2006). Physical blockage of polymerase progression is thought to be more problematic when it occurs on the leading strand as synthesis of this strand requires continuous DNA

replication. In contrast these lesions are well tolerated when they occur on the lagging strand as the lesions can be bypassed by re-priming (Yeeles et al, 2013). However, it has been suggested that re-priming can also occur on the leading strand following UV irradiation (Bianchi et al, 2013; Elvers et al, 2011) and requires the activity of the primase and alternative DNA polymerase PrimPol (Bianchi et al, 2013; García-Gómez et al, 2013; Mourón et al, 2013). This process results in a single stranded gap in the DNA, which is subsequently repaired (Berti & Vindigni, 2016).

Replication re-start can also involve remodelling or reversal of the stalled replication fork. The actions of several DNA helicases, including BLM, WRN and SWI/SNF related, Matrix Associated, actin dependent Regulator of Chromatin, Subfamily A Like 1 (SMARCAL1), have been implicated in remodelling (Berti & Vindigni, 2016; Petermann & Helleday, 2010). Cells lacking these enzymes display reduced or inefficient restart of DNA replication following fork stalling (Ciccia et al, 2009; Davies et al, 2007; Sidorova et al, 2008). Replication fork reversal occurs when conditions are sub-optimal (Neelsen & Lopes, 2015) and involves the remodelling of the fork into a four-way 'chicken-foot' (Berti & Vindigni, 2016) or Holliday junction (Yoon et al, 2004). During this process, the two newly synthesised strands anneal and a number of helicases, DNA translocases and recombinases have been implicated in this process, including RAD51 (Berti & Vindigni, 2016). These reversed forks can be restarted in a RECQ1-Poly (ADP-ribose) polymerase-1 (PARP-1) dependent (Berti et al, 2013) or a Dna2 dependent manner (Thangavel et al, 2015). Remodelled or reversed forks can also be restarted by recombination which results in the bypass of the blockage. The loading of RAD51 required for this process is facilitated by phosphatase and tensin homolog (PTEN) (He et al, 2015) and requires DNA end resection. This is carried out by Mre11 which is recruited to stalled forks by PARP-1 (Bryant et al, 2009) where it interacts with both BLM and WRN (Petermann & Helleday, 2010). XRCC3, a facilitator of RAD51 filament formation, is also required for this form of restart.

The prolonged stalling of a replication fork can result in the formation of a DSB through the collapse of the fork (Berti & Vindigni, 2016). This has been linked to the dissociation of the replisome from the DNA (Tercero & Diffley, 2001), however more recent evidence suggests that the replisome remains intact but is in an inactive state or is displaced rather than completely broken down (De Piccoli et al, 2012).

1.2.3 DNA Damage Response

As well as counteracting the incorporation of errors that occur during DNA replication, cells also must contend with DNA damage arising from endogenous and exogenous sources. To negate its effects, they have evolved a complex network of DNA damage response mechanism to neutralise the various types of DNA lesions that they encounter.

1.2.3.1 Sources of DNA Damage

The formation of DNA damage resulting from endogenous sources occurs at an elevated frequency compared to damage arising due to external mutagens. The most common source of endogenous damage is reactive oxygen species (ROS) which arise through normal cellular metabolism and during immune responses. They can result in the oxidation of DNA bases, single strand breaks (SSB) or DSB (De Bont & van Larebeke, 2004). Activated neutrophils have been demonstrated to induce 8-oxo-deoxyguanosine (8-oxo-dG) in an antioxidant repressible manner (Shen et al, 2000) and chronic inflammatory diseases of the liver, such as hepatitis, have a significant correlation with oxidative DNA damage (Shimoda et al, 1994). The oxidation of thymine results in the formation of 5-Hydroxymethyluracil, whose repair can result in DSB and subsequent apoptosis (Rogstad et al, 2002).

As well as oxidation, DNA bases can also be deaminated, alkylated or cleaved from the DNA backbone (depurination) (De Bont & van Larebeke, 2004). Cytosine can be deaminated to form uracil, which is removed from the genome by the uracil-DNA glycosylase, resulting in an abasic site. Its homolog 5-methycytosine is also deaminated to form thymidine resulting in a mismatched GT pair which is repaired by MMR (Lindahl, 1993). This mutation is frequently observed in the p53 genes of human cancerous cells (Rideout et al, 1990). Whilst the alkylation of some bases results in mismatches, others do not affect base pairing but result in the generation of mutagenic apurinic (AP) sites (De Bont & van Larebeke, 2004). S-adenosylmethianine (SAM) is an important endogenous DNA alkylating agent as it can induce 3-methyladenine and O^6-guanine adducts enzymatically which can result in mutagenesis (Rydberg & Lindahl, 1982). DNA bases can become depurinated through the hydrolysis of the N-glycosidic bond resulting in the formation of AP sites, which are susceptible to further damage (An et al, 2014). Bases can be targeted for depurination by modifications, such as those induced by the estrogen 3,4-quinones (Stack et al, 1996).

Environmental mutagens are capable of inducing several types of DNA lesions via a number of mechanisms. Oxidative damage can also arise through exogenous sources such as ultraviolet (UV) or ionizing radiation (IR) (Cooke et al, 2003). UV can induce the formation of singlet oxygen, a type of ROS, which can induce the formation of 8-oxo-dG (Douki et al, 1999) whilst IR absorption by intracellular water can result in the formation of free radicals that can damage DNA (Azzam et al, 2012). As well as the induction of oxidative damage, UV and IR can additionally cause direct damage to DNA independent of ROS. The absorption of UVB (280 – 320nm) photons by DNA bases induces the formation dimeric photoproducts including cyclobutane pyrimidine dimers (CPD) (Douki et al, 1999), which have been implicated in skin cancer carcinogenesis (Burren et al, 1998). IR is

likewise directly absorbed by DNA, which can result in the generation of SSB or DSB when two SSB occur in close proximity on opposite strands. DSB are considered one of the most detrimental DNA lesion as if they are not repaired they can result in mutation or the induction of apoptosis (Mahaney et al, 2009).

Adducts can also form which covalently link two nucleotide residues; this can occur within the same strand (intrastrand) or between the two strands (interstrand). Intrastrand crosslinks are commonly formed by UV (Douki et al, 1999) but can easily be removed by the nucleotide excision repair (NER) pathway (Huang & Li, 2013). However, the interstrand crosslinks (ICLs) pose more of a threat to genome stability as they prevent the separation of the DNA strands which halts DNA replication and gene transcription (Huang & Li, 2013). These lesions can be induced by bifunctional alkylating agents, platinum compounds and the antibiotic Mitomycin C (MMC).

Figure: types of DNA damage and the pathways that repair them

1.2.3.2 PI3K Like Kinases

The phosphatidylinositol 3-kinase (PI3K) like kinase (PIKK) family are serine/threonine kinases whose kinase domain exhibits a high degree of homology with PI3K. Its six members co-ordinate a range of cellular processes with three in particular playing crucial roles within the DNA damage response. Ataxia-telangiectasia mutated (ATM), ATM and Rad3 related (ATR) and DNA-dependent protein kinase (DNA-PK) function to transmit and amplify DNA damage signals to elicit the correct cellular response (Falck et al, 2005; Rivera-Calzada et al, 2015). ATM and ATR both halt the cell cycle in response to DNA damage whilst DNA-PK facilitates the repair of DSBs (Ashley et al, 2014). However, these kinase are to have complementary roles and all three kinases have been demonstrated to phosphorylate the histone H2AX in response to DSBs (Paull et al, 2000), which acts as a global DNA damage marker. All three are localised to DNA damage by a similar mechanism that relies upon recruitment by a damage sensor. For ATM this is the Mre11-Rad50-Nbs1 (MRN) complex, ATR its binding partner ATRIP and DNA-PK the Ku70-Ku80 heterodimer. A conserved region in the C-terminus of Nsb1, ATRIP and Ku80 is required for their interaction with their respective PIKK (Falck et al, 2005).

The Ku70-Ku80 heterodimer binds to the free ends of DNA (Blier et al, 1993) and recruits the catalytic subunits of DNA-PK (DNA-PKcs) to the sites of DSB (Gell & Jackson, 1999). They subsequently *trans*-autophosphorylate at multiple sites resulting in kinase activation and phosphorylation of the proteins that mediate the non-homologous end joining (NHEJ) of DSBs (discussed below) (Goodwin & Knudsen, 2014). DNA-PK also plays a role in the replication stress response as cells expressing mutant forms of this protein fail to arrest replication following the induction of stress (Liu et al, 2012).

ATM is rapidly autophosphorylated at Serine 1981 (Bakkenist & Kastan, 2003), Serine 367 and Serine 1893 (Kozlov et al, 2006) in response to DSB. This autophosphorylation is required to convert the enzyme from an inactive dimer to a functional monomer (Bakkenist & Kastan, 2003) and for ATM's association with chromatin (Berkovich et al, 2007). As well as recruiting ATM to the sites of DSB via Nbs1 (Falck et al, 2005), the MRN

complex is required for its stable association with DNA (Lee & Paull, 2005) and its substrates, p53 and checkpoint kinase 2 (Chk2) (Lee & Paull, 2004). It functions in the G1/S checkpoint (discussed below) and is also required for the localisation of MRN and WRN at stalled replication forks (Ammazzalorso et al, 2010; Trenz et al, 2006). ATM is thought to be the primary kinase responsible for the phosphorylation of the histone H2AX at Serine 139 (γH2AX) in response to DSBs (Burma et al, 2001; Sharma et al, 2012a).

ATR signalling is essential for the preservation of the genome as its basal activity maintains replication fork stability throughout S phase (Cimprich & Cortez, 2008) and is fully activated in response to replication stress (Vidal-Eychenié et al, 2013). As mentioned previously, this phenomenon results in the formation of long tracts of ssDNA that is subsequently bound by RPA, a heterotrimeric protein.

RPA2 (RPA32) is phosphorylated throughout the cell cycle at a number of residues within its N-terminus. Two residues, Serine 23 (S23) and Serine 29 (S29) are phosphorylated by the CDKs during the progression of an unperturbed cell cycle (Fang & Newport, 1993) and in response to genotoxic stress (Zernik-Kobak et al, 1997). Mutation of these sites deregulates cell cycle progression, the replication stress response and results in persistent DNA damage (Anantha et al, 2007). This stress-induced modification promotes further phosphorylation of the N-terminus at a number of sites: Serine 4/8 (S4/8), Serine 12, Serine 13, Serine 14, Threonine 21 (T21) and Serine 33 (S33). It has been proposed that phosphorylation of S23 and S29 by CDK and subsequent phosphorylation of S33 are required before further modification can take place (Anantha et al, 2007), although this may be an over simplification. Efforts have been made to determine the PIKKs that phosphorylate these remaining sites, but the data is contradictory, most likely due to the variety of genotoxic agents and lack of specificity of the PIKK inhibitors used in these studies. It is also thought that there may be a high degree of redundancy within the system which further complicates matters (Liu et al, 2012). Most evidence suggests that ATR and DNA-PK are responsible for RPA2 phosphorylation in response to replication stress (Anantha et al, 2007; Ashley et al, 2014; Liu et al, 2012; Vassin et al, 2009; Vidal-Eychenié et al, 2013) with ATR phosphorylating T21 (Olson et al, 2006) and S33, whilst DNA-PK phosphorylates S4/8 (Maréchal & Zou, 2014). Phosphorylation of these sites is essential for the response to DNA replication stress as mutants demonstrate impaired recovery (Liu et al, 2012; Vassin et al, 2009).

ATR is recruited to DNA via its binding partner ATRIP (Falck et al, 2005) which recognises and binds to ssDNA bound phosphorylated RPA (Zou & Elledge, 2003). A RAD17 containing complex is localised to ssDNA by Pol α primase and loads the RAD9-HUS1-RAD1 (9-1-1) complex onto RPA coated ssDNA 3' overhangs (Ellison & Stillman, 2003; You et al, 2002). TopBP1 binds to RAD9 and activates ATR via its activation domain (AD) allowing for the phosphorylation of ATR's substrates (Delacroix et al, 2007; Lee et al, 2007a) (Fig. 1.2.3.2.1).

ATR's most notable substrate is checkpoint kinase 1 (Chk1) which it phosphorylates at Serine 317 (S317) (Zhao & Piwnica-Worms, 2001) and Serine 345 (S345) (Liu et al, 2000). S317 phosphorylation is found only in stressed cells whilst there is evidence that S345 is

also required for mitosis in unperturbed cell cycles (Wilsker et al, 2008). Chk1 autophosphorylates Serine 296 (S296) in a S317/S345 dependent manner (Okita et al, 2012) which is thought to be required for the DNA damage response (Wilsker et al, 2008). Its phosphorylation allows it to dissociate from the chromatin (Smits et al, 2006) and transmit the damage signals throughout the nucleus (Sørensen & Syljuåsen, 2012). This halts the cell cycle at the Intra-S, G2/M and spindle checkpoints (discussed below). It also suppresses the activation of late firing origins in favour of allowing the continuation of replication at stalled forks once replication stress has been resolved (Ge & Blow, 2010). There is also evidence that Chk1 and the checkpoint mediator Claspin control replication fork progression in unstressed cells (Petermann et al, 2008; Petermann et al, 2010). Claspin is required for stress induced Chk1 phosphorylation but its role in unperturbed cell cycles is independent from that function (Scorah & McGowan, 2009). Chk1 phosphorylates the recombinase RAD51 in response to replication stress to facilitate the repair of DSBs which persist in Chk1 mutant cells (Sørensen et al, 2005).

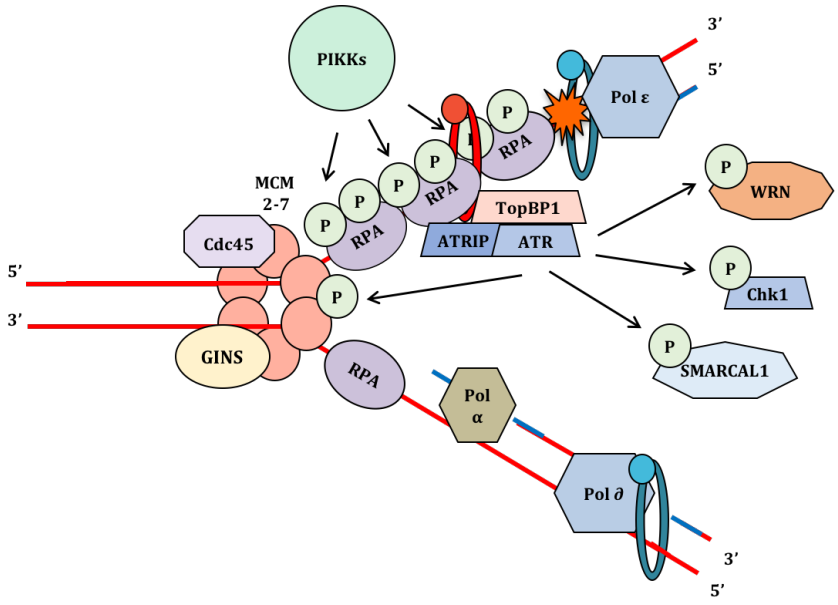

Figure 1.2.3.2.1 ATR signalling at a stalled replication fork.

The single stranded DNA generated in replication stressed cells is bound by RPA which is subsequently phosphorylated by the PIKKs. This recruits ATR via its interacting protein ATRIP and enables the loading of the RAD9-HUS1-RAD1 (9-1-1) complex (red ring). TopBP1 binds to RAD9 which localises it to stalled replication forks where it activates ATR. Once activated, ATR can phosphorylate its substrates, most notably Chk1, but these also include SMARCAL1, WRN and MCM2.

In the absence of ATR signalling, stalled replication forks collapse resulting in the formation of DSBs, although this mechanism is inadequately understood. One way in which ATR maintains stalled fork stability is by the regulation of SMARCAL1. If left unchecked, SMARCAL1 activity results in aberrant resection of stalled forks but if its activity is correctly controlled it can promote fork restart (Couch et al, 2013). Phosphorylation of WRN by ATR is required for its co-localisation with RPA at stalled forks and suppression of DSB formation (Ammazzalorso et al, 2010). It also phosphorylates MCM 2 at stalled replication forks which results in the recruitment of Plk1.

This kinase acts to locally lift the suppression of replication by Chk1 and allow the firing of dormant origins to ensure that replication is completed (Trenz et al, 2008).

1.2.3.3 Checkpoint Activation

Built into the cell cycle are several surveillance mechanisms that ensure certain aspects have been completed properly before the cell can continue onto the next phase. These 'checkpoints' monitor the entry into S phase, the fidelity of DNA replication, the commitment to cell division, and the proper segregation of the chromosomes during metaphase. If any of these events have not been completed, or if a cell's DNA is damaged, cell cycle progress is halted to allow the rectification of these issues (Barnum & O'Connell, 2014; Murray, 1994).

The G1/S transition marks entry into a new cell cycle and beyond this point the cell is committed to DNA replication and cell division. The checkpoint that operates at this boundary is controlled by ATM and its downstream targets Chk2 and p53. It is believed that the activation of the G1/S checkpoint occurs in two phases in response to DSBs: a rapid transient activation of Chk2 and a slower more sustained activation of p53 (Fig. 1.2.3.3.1) (Bartek & Lukas, 2001). Chk2 is phosphorylated at Threonine 68 by ATM in response to DSB (Lee & Paull, 2004; Ward et al, 2001). It subsequently phosphorylates the CDC25A phosphatase at Serine 123 resulting in its ubiquitination which targets the protein for proteasomal degradation (Mailand et al, 2000). This prevents the activation of Cyclin E/CDK2 by dephosphorylation and the consequent transition into S phase. This inhibition is thought to occur within 30 minutes of DSB formation and lasts for several hours (Deckbar et al, 2010).

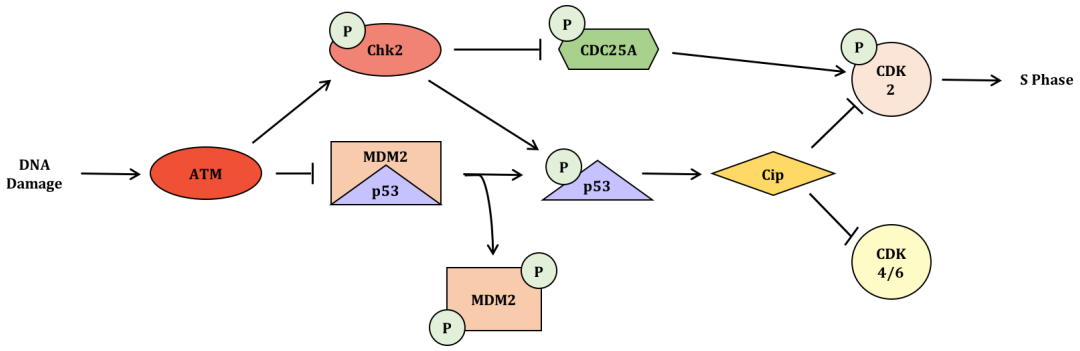

Figure 1.2.3.3.1 G1/S checkpoint activation.

DNA damage triggers the activation of ATM resulting in the phosphorylation of Chk2, MDM2 and p53. Phosphorylated Chk2 subsequently phosphorylates CDC25A which prevents it from removing the inhibitory phosphate from CDK2. MDM2 and p53 phosphorylation result in the stabilisation of p53 and the transcription of p21 (Cip). This protein inhibits CDK2 and CDK4 to prevent entry into S phase.

The tumour suppressing transcription factor p53 is negatively regulated by the ubiquitin E3 ligase MDM2 (Cheng et al, 2011). Phosphorylation of MDM2 by ATM disrupts its conformation which is thought to prevent its binding to p53 (Cheng et al, 2011; Khosravi et al, 1999) which enhances the stability of the transcription factor (Deckbar et al, 2010). ATM and Chk2 also phosphorylate p53, at Serine 15 and Serine 20 respectively (Cheng et al, 2011; Khosravi et al, 1999), which is thought to enhance the stability of the protein and increases its DNA binding efficiency (Deckbar et al, 2010). This allows p53 to induce the

transcription of its target genes, including the CDK inhibitor p21, which inhibits both CDK4 and CDK2 to prevent S phase entry (He et al, 2005). As this checkpoint response is transcription dependent it is activated slowly but the effects last longer than those induced by CDC25A inhibition (Deckbar et al, 2010).

In response to replication stress, an ATR and Chk1 mediated Intra-S phase checkpoint is triggered. As in the G1/S checkpoint, CDC25A plays a key role in the halting of S phase progression. It is phosphorylated by Chk1 which increases the rate of its ubiquitin dependent proteasomal degradation and so prevents the activation of Cyclin A/CDK2 (Uto et al, 2004). Whether Chk2 acts in the Intra-S checkpoint is controversial (Falck et al, 2001; Uto et al, 2004), although contrasting data may be due to the types of damage used to stimulate cell cycle arrest within these studies.

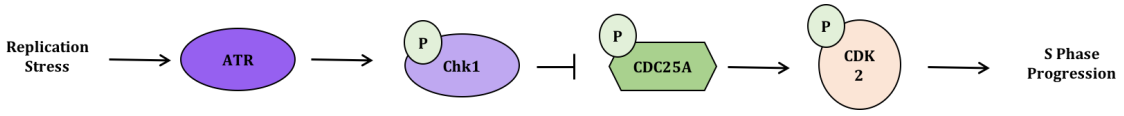

Figure 1.2.3.3.2 Intra-S phase checkpoint activation.
ATR is activated in response to DNA replication stress. This allows for the phosphorylation of its downstream target Chk1 which subsequently phosphorylates CDC25A. This inhibits its phosphatase activity and prevents the activation of CDK2 and the progression of S phase.

The G2/M checkpoint prevents cells with un-replicated or damaged DNA from entering into mitosis as this would have highly detrimental effects on genome stability. ATM and ATR activate Chk2 and Chk1 respectively which both phosphorylate CDC25B/C. This stimulates their binding by the 14-3-3 proteins (Peng et al, 1997) which results in their sequestration in the cytoplasm and prevents their activation of Cyclin B/CDK1 (Brunet et al, 2002). Wee1 is a Chk1 substrate whose phosphorylation results in its stabilisation and increased inhibition of CDKs by phosphorylation (Dai & Grant, 2010). ATM and Chk2 phosphorylate MDM2 and p53, as described previously, which results in the transcription of the 14-3-3σ and GADD45α proteins (Löbrich & Jeggo, 2007). The 14-3-3σ isoform sequesters Cyclin B/CDK1 in the cytoplasm (Chan et al, 1999) and Gadd45α also reduces nuclear Cyclin B levels. (Fig. 1.2.3.3.3) (Bulavin et al, 2001; Reinhardt et al, 2007).

During metaphase the chromosomes align along the equator of the cell and attach to the mitotic spindle. Once this has been completed the cells progress into anaphase where the chromosomes are pulled to the opposite poles of the cell. A checkpoint exists at this transition and is activated when the microtubules of the spindle fail to properly attach to the kinetochores formed at the centromeres of the chromosomes (Musacchio, 2015). Proper attachment generates equal tension across the chromosome (Rieder et al, 1995) and in the absence of tension BUB1 and BUBR1/MAD3 are recruited (Taylor et al, 2001). A complete lack of spindle attachment results in the additional localisation of MAD1 and MAD2 at the kinetochore (Waters et al, 1998). BUBR1 recruitment requires the catalytic activity of Aurora kinase B, which is itself phosphorylated by Chk1 in response to spindle defects (Zachos et al, 2007). The MAD and BUB proteins function to inhibit the APC, responsible for the degradation of cyclins and the onset of anaphase. This complex is regulated by two subunits, Cdh1 and Cdc20, the later of which is required for anaphase

progression (Hwang et al, 1998). It is bound by MAD2, BUBR1/MAD3 and BUB3, referred to collectively as the mitotic checkpoint complex, which regulates the complexing of unbound MAD2 with Cdc20 to prevent its interaction with the APC (Fig. 1.2.3.3.4) (Sudakin et al, 2001).

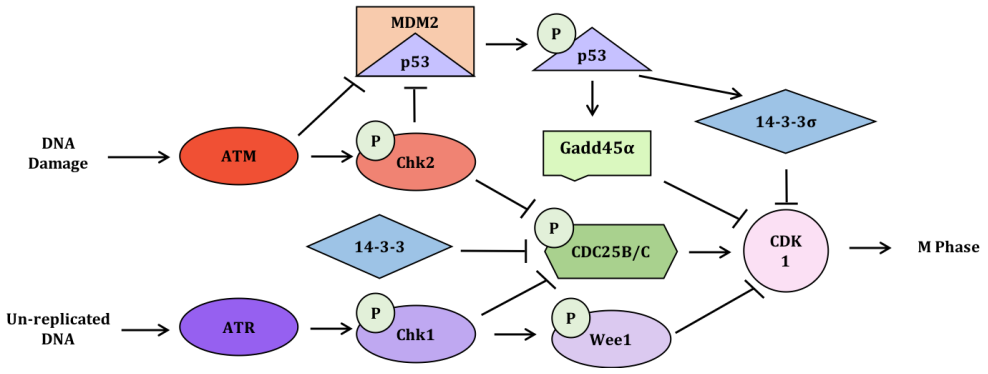

Figure 1.2.3.3.3 G2/M checkpoint activation.

DNA damage and un-replicated DNA activate ATM and ATR respectively. ATM phosphorylates Chk2, MDM2 and p53. Chk2 phosphorylates both p53 and CDC25B/C which inhibits its dephosphorylation of CDK1. Stabilised p53 results in the transcription of 14-3-3σ and Gadd45α which inhibit the activity of CDK1. ATR phosphorylates Chk1 which in turn inactivates CDC25B/C and stimulates the inhibition of CDK1 by Wee1. The 14-3-3 proteins also inhibit the activities of CDC25B/C.

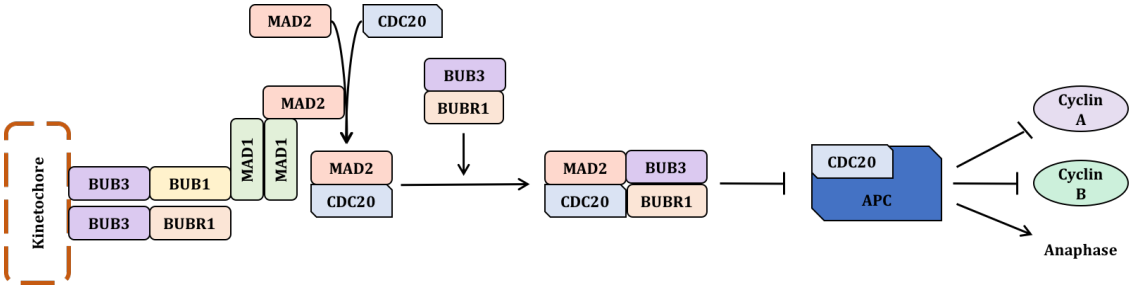

Figure 1.2.3.3.4 Mitotic spindle checkpoint activation.

BUB1, BUBR1, BUB3, MAD1 and MAD2 bind to kinetochores of chromosomes that are not properly attached to the mitotic spindle. This complex allows for the biding of soluble MAD2 to CDC20, a regulatory subunit of the APC. This facilitates the subsequent binding of BUBR1 and BUB3 which aid in the prevention of APC activation. This averts the degradation of Cyclins A and B and the onset of anaphase. Adapted from London & Biggins (2014).

If mitosis is unsuccessful cells can undergo mitotic catastrophe. This is thought to be triggered by premature mitotic entry, abnormal completion or failure to complete division (Ianzini & Mackey, 1997; Kroemer et al, 2009; Vakifahmetoglu et al, 2008). It is predicted to play a role in genomic maintenance by eliminating cells with missegregated chromosomes by forcing them irreversibly into apoptosis, necrosis or senescence (Vitale et al, 2011). Cells can undergo apoptosis or necrosis during an aberrant mitosis or they can enter a new cell cycle with missegregated chromosomes, which is referred to as mitotic slippage (Raab et al, 2015), where they are subsequently forced to die in G1 or enter a senescent state. The mechanisms that dictate the fate of the cells following an anomalous mitosis are currently unclear (Mc Gee, 2015).

1.2.3.4 DNA Repair Mechanisms

As a wide variety of lesions affect DNA, cells have evolved numerous repair mechanisms, each designed to rectify a specific subset of genomic injuries. These range from single enzymes, that directly rectify the damage, to complex multistep pathways involving diverse classes of proteins and specific enzymatic functions.

Certain base modifications can be reversed by direct modification by single enzymes. Three classes of these enzymes have been identified: photolyases, O^6 alkylguanine DNA alkyltransferases and AlkB dioxygenases which reverse UV photoproducts, O-alkylated and N-alkylated bases respectively (Yi & He, 2014). An example of these enzymes is O^6-methylguanine methyltransferase (MGMT) which transfers the alkyl group from O^6 on guanine to a cysteine within its active site. This restores the structure of the base whilst inactivating the enzyme and targeting it for degradation (Pegg, 2000). Whilst crucial for genome maintenance, these enzymes only rectify a small proportion of such DNA lesions (Yi & He, 2014) and more complicated alterations require repair by the multistep base excision repair (BER) and nucleotide excision repair (NER) pathways.

BER amends DNA base modifications that result in little distortion of the DNA helix structure such as oxidation, deamination and alkylation (Krokan & Bjørås, 2013). The first step of the pathway is the removal of the damaged base by DNA glycosylases to form an abasic site (Jin et al, 2013) with the glycosylase that carries out the reaction depending upon the type of lesion being removed (Krokan & Bjørås, 2013). These sites are converted to SSB by APE-1, the major AP-endonuclease in mammals (Tell et al, 2009). The process in then completed by the short- or long-patch pathways depending upon the number of nucleotides that require replacing (Jung‐Suk & Demple, 2006). In short-patch BER, a single nucleotide is excised from the DNA (Dianov et al, 1992) and the AP site is cleaved by APE-1. The gap is then filled by DNA Polymerase β (Pol β) (Podlutsky et al, 2001) and the remaining nicks are ligated by DNA ligase III and XRCC1 (Cappelli et al, 1997). PARP-1 is involved in the repair of SSB and has been demonstrated to prevent the accumulation of these lesions during BER (Parsons et al, 2005). It facilitates the efficient recruitment of Pol β and XRCC1 by PARylation following its binding to the SSB generated by APE-1 (Horton et al, 2014). Long-patch BER generates a gap of between 2 – 10 nucleotides (Krokan & Bjørås, 2013) and requires factors not involved in short-patch repair. The filling of the gap is most likely initiated by Pol β but is completed by the replicative polymerases (Podlutsky et al, 2001). FEN-1 is required to remove the resultant DNA flap (Pascucci et al, 1999) and as DNA Ligase III and XRCC1 are not required for long-patch repair, it is believed Ligase I ligates the remaining nicks (Fig. 1.2.3.4.1) (Sleeth et al, 2004).

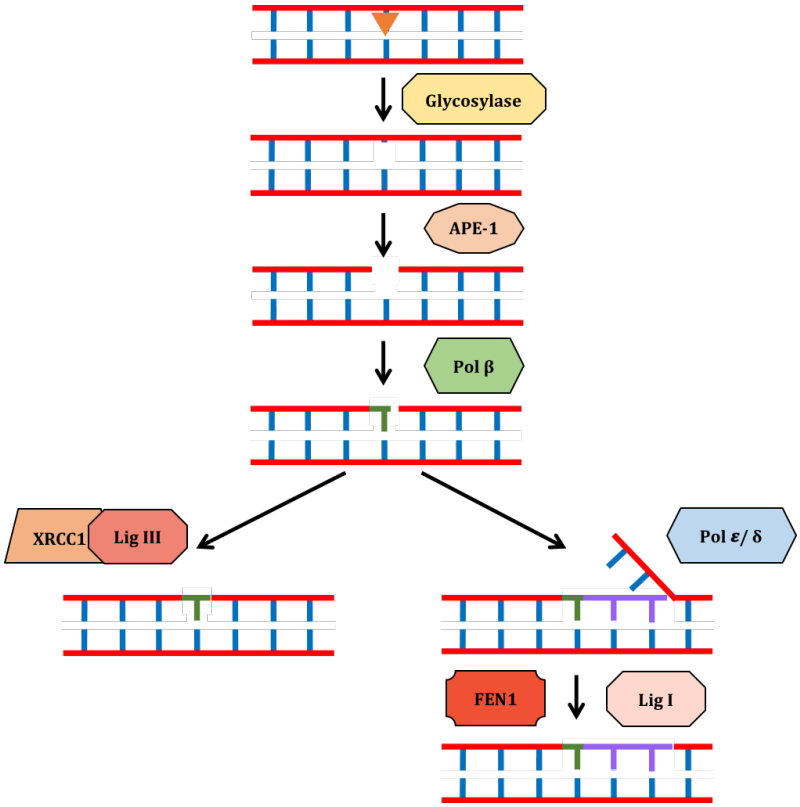

Figure 1.2.3.4.1 Base excision repair.

Base excision repair removes modified bases (orange triangle) from DNA. The pathway is initiated by DNA glycosylases that excise the damaged base resulting in an abasic site which is cleaved by APE-1 forming a single strand break. The filling of this gap is then initiated by DNA Polymerase β (Pol β) (green strand). In the case of short patch repair the remaining nick is ligated by XRCC1 and Ligase (Lig) III. For long-patch repair, the replicative DNA polymerases (Pol ε/δ) continue the strand (purple) started by Pol β resulting in the generation of a DNA flap which is removed by FEN1 with the DNA nick being ligated by Lig I.

In contrast, base alterations that result in the distortion of the DNA helix activate the NER pathway, where a 25 – 30 nucleotide stretch surrounding the damaged base is excised and the resultant break is repaired by gap filling (Marteijn et al, 2009). NER has two sub-pathways that are triggered by different stimuli: global genome NER (ggNER), which occurs when the double helix's structure has been altered (Trego & Turchi, 2006), and transcription coupled repair (TC-NER), which is activated when the lesion halts transcription (Marteijn et al, 2009). In ggNER, the DNA damage is initially recognised by XPC which continuously scans the genome for helix altering lesions (Petruseva et al, 2014). This induces the local opening of the DNA duplex which facilitates the binding of further NER factors (Sugasawa et al, 1998). In TC-NER, the damage is recognised indirectly as it is the pausing of RNA Polymerase II (RNA Pol II) that triggers its activation (Marteijn et al, 2009). Cockayne syndrome protein B (CSB) (Fousteri et al, 2006), UV-stimulated scaffold protein A (UVSSA) and ubiquitin-specific-processing protease 7 (USP7) transiently interact with RNA Pol II (Schwertman et al, 2012) as it elongates the mRNA. Its stalling increases the binding affinity of CSB allowing for the formation of the CSA/CSB complex (Fousteri et al, 2006) which is responsible for the backtracking of the polymerase

(Sigurdsson et al, 2010). This leaves the DNA unwound and accessible for further repair factors (Fig. 1.2.3.4.2).

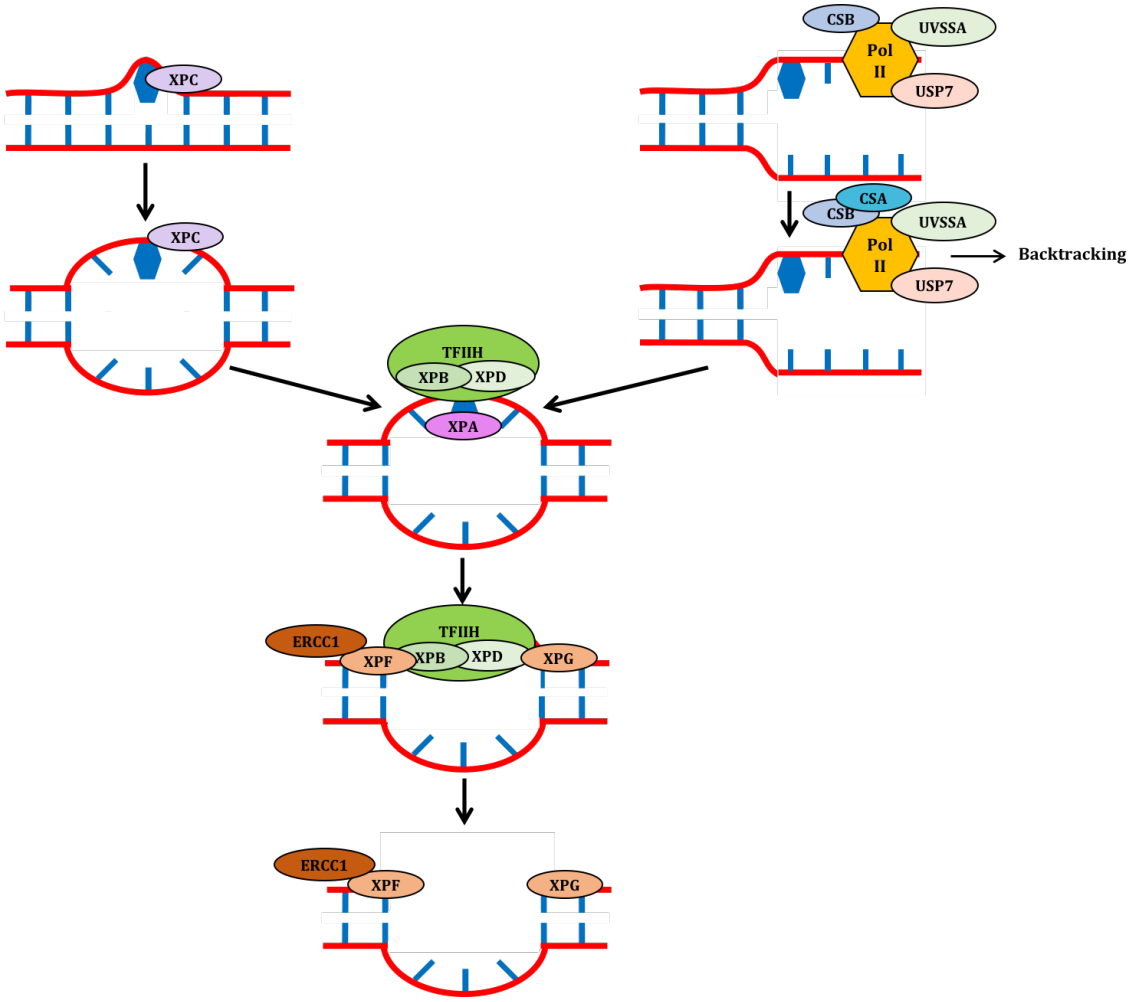

Figure 1.2.3.4.2 Nucleotide Excision Repair.

Nucleotide excision repair (NER) removes modified bases that distort the structure of the DNA helix (blue hexagon). Global genome NER (left hand pathway) occurs when modified bases are detected by XPC. The binding of this protein to DNA induces local opening which allows for the binding of further NER factors. In transcription coupled repair (right hand pathway) lesions that prevent RNA Polymerase II (Pol II) from progressing result in the binding of CSB, UVSSA and USP7. CSB is subsequently bound by CSA and this complex results in the backtracking of the polymerase which facilitates the binding of further NER components. Once the DNA is opened, it is bound to by the TFIIH complex, containing the XPB and XPD helicases, which further open the DNA (not depicted). This facilitates the binding of XPG and the XPF/ERCC1 complex which act as the 3' and the 5' endonucleases respectively. These proteins incise the DNA to remove the strand containing the altered base. Adapted from Martenijn et al, (2014).

In both sub-pathways of NER, the opening of the DNA results in the recruitment of the TFIIH complex (Tapias et al, 2004) comprising the XPB and XPD DNA helicases, p62, p54, p44, p34, p8, GTF2H3 and CAK. XPB binds to chromatin bound XPC (Araújo et al, 2001) which induces the further unwinding of the DNA duplex for approximately 27 nucleotides to the 5' and 5 nucleotides to the 3' of the damaged base (Petruseva et al, 2014). The damaged base within the resultant DNA bubble is identified by XPA in complex with RPA (Buschta-Hedayat et al, 1999). XPG then binds to the 3' end of the bubble, through its

interaction with TFIIH (Zotter et al, 2006), and acts as the 3' endonuclease (Graf et al, 2011). XPF in complex with ERCC1 incises the DNA at the ssDNA/dsDNA junction to the 5' of the damaged base (Fig.1.2.3.4.2) (Tsodikov et al, 2007). Once the DNA has been excised, PCNA is recruited which facilitates the loading of DNA Pol ε and subsequent ligation by DNA Ligase I in replicating cells. In non-replicating cells, Pol δ, or Pol κ fill the gap and DNA Ligase III ligates the nick (Marteijn et al, 2014).

As well as modification to the DNA bases, the phosphodiester backbone can be cleaved resulting in strand breaks. DSBs are highly genotoxic lesions which pose a significant threat to the stability of the genome if they are not repaired correctly. The method of repair depends upon which phase of the cell cycle the damage occurs in. When a second copy of the genome is present, during the S or G2 phases, the break is preferentially repaired by homologous recombination (HR) as this requires the sister chromatid to act as a template for accurate repair. However, this cannot occur when there is only one copy of the genome present during G1 phase and so cells rely on NHEJ or microhomolgy mediated end joining (MMEJ) which are more likely to introduce errors into the genome (Hoeijmakers, 2001; Kent et al, 2015)(summarised in Fig. 1.2.3.4.3).

As mentioned previously, the Ku70-Ku80 heterodimer binds to DSBs and recruits the DNA-PKcs to facilitate NHEJ. The endonuclease Artemis is also recruited by the Ku heterodimer and is activated by DNA-PK (Goodarzi et al, 2006). To facilitate DSB repair by this pathway, the overhanging DNA strands are resected to reveal regions of microhomology. Artemis can resect both 3' and 5' overhangs once it has been activated (Chang et al, 2017; Ma et al, 2002) and it is believed to be the primary nucleases that acts in NHEJ, although roles for MRN, WRN and FEN1 have also been suggested (Pannunzio et al, 2014). If the DNA overhangs have phosphates at their 3' end or lack them at their 5' end these are removed or replaced respectively by polynucleotide kinase to allow their processing (Bernstein et al, 2005). The main polymerases that act in NHEJ are DNA Polymerase μ (Pol μ) and Polymerase λ (Pol λ) (Bebenek et al, 2014; Moon et al, 2014) which interact with Ku70-Ku80 at DSBs (Ma et al, 2004) and incorporate nucleotides in a template independent manner (McElhinny et al, 2005). The nicks that remain following repair synthesis are ligated by DNA Ligase IV (Lieber, 2010). This is thought to be stimulated by XRCC4 and XPF which form a complex to stabilise DNA and allow ligation (Chang et al, 2017; Grawunder et al, 1997).

MMEJ represents a distinct DSB repair pathway as it operates independently of the activity of Ku70-Ku80 and Ligase IV (Bennardo et al, 2008). Like NHEJ it relies upon resection to reveal microhomologies which are utilised to align the DNA. However, this pathway is more error-prone than NHEJ as it promotes rearrangements and deletions within the genome. In human cells this process relies upon DNA Polymerase θ (Pol θ) which uses the opposite overhang of the DSB as a template to stabilise the DNA and repairs the break by strand displacement synthesis (Kent et al, 2015).

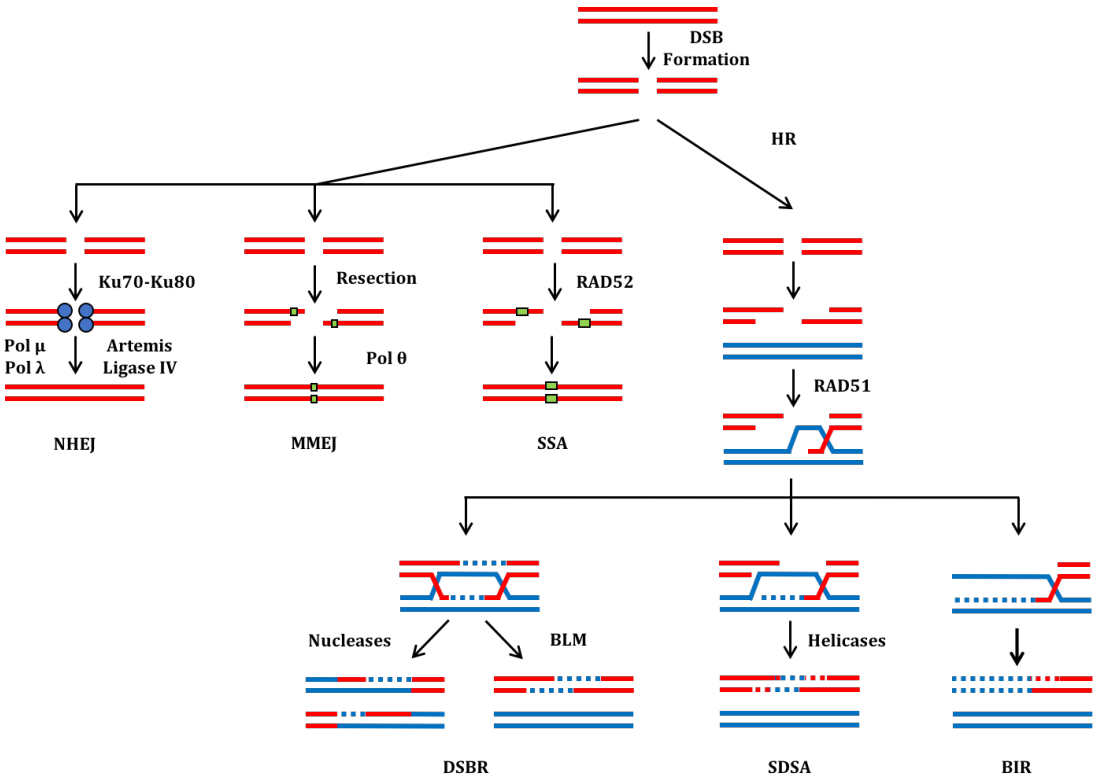

Figure 1.2.3.4.3 Double strand break repair.

Double strand breaks (DBS) can be repaired by several different pathways. When there is no second copy of the genome present the break can be repaired by non-homologous end joining (NHEJ) which requires Ku70-Ku80, the endonuclease Artemis, DNA Polymerases μ and λ (Pol μ and Pol λ) and Ligase IV. Alternatively, the break can be repaired by Ku independent microhomology mediated end joining (MMEJ) which requires small regions of homology (green squares) between the broken strands and Polymerase θ (Pol θ). If during the resection of the DSBs ends larger regions of homology are uncovered, it can be repaired by single strand annealing (SSA) which depends upon RAD52. If a second copy of the genome is present, the break can be repaired by homologous recombination (HR), which results in the RAD51 dependent formation of a D-loop. Once this has occurred, the resolution of the break can occur by three sub-pathways. In DSB repair (DSBR) a double Holliday junction is formed which can either by resolved by nucleases, which results in crossovers, or dissolved by BLM. In synthesis dependent strand annealing (SDSA), helicases displace the D-loop to prevent crossover formation. Break-induced replication (BIR) occurs when one strand of the DSB has been lost completely and relies upon the intact chromosome to replicate the lost DNA.

HR requires the sister chromatid to act as a template for the precise repair of DSBs. In the initial stage, referred to as pre-synapsis, MRN and CtIP initiate the resection of the DSB (Nicolette et al, 2010; Zhu et al, 2008). This facilitates the formation of a 3' overhang by two redundant pathways involving Exo1 or DNA2 acting in concert with BLM, TOP3 and RMI1 (Gravel et al, 2008; Zhu et al, 2008). During the initial resection of the DSB, if regions of homology are revealed, the two strands can anneal with each other in a RAD52 dependent fashion to repair the break, in a process referred to as single strand annealing (SSA) (Bhargava et al, 2016). The RAD51 recombinase competes with RPA (Sugawara et al, 2003) to bind to the ssDNA 3' overhangs (Sung & Robberson, 1995) which is facilitated by the recombination mediators BRCA2 and PALB2 (Filippo et al, 2006). This binding forms the pre-synaptic filament by stretching the ssDNA which is critical for the homology

search (Chen et al, 2008) once it has invaded the sister chromatid. The homologous sequences enable the formation of a D-loop (Krejci et al, 2012) where the 3' of the invading strand acts as the primer for repair synthesis (Bartosova & Krejci, 2014).

Once the D-loop has been formed, several different scenarios can occur that result in the restoration of the DNA; these include classical DSB repair (DSBR), synthesis dependent strand annealing (SDSA) and break-induced replication (BIR). In DSBR the second strand of the DSB is captured and stabilised by RAD52 to form a double Holliday junction (dHJ) through DNA synthesis (Bartosova & Krejci, 2014; Szostak et al, 1983). This can be resolved by nucleases, which can result in crossovers, or dissolved by BLM , where no crossing over occurs (Wu & Hickson, 2003). There is evidence that this pathway may be repressed during the resolution of DSBs as RAD51 suppresses the formation of dHJs (Wu et al, 2008). In SDSA, dHJs are not formed as the D-loop is displaced by helicases. The invading strand re-anneals with the second strand of the DSB where the remaining gaps are filled and the continuous strands are re-formed by ligation (McMahill et al, 2007; Nassif et al, 1994). BIR occurs when the second end of the DSB is lost (Heyer et al, 2010) and can result in the loss of heterozygosity and gross chromosomal rearrangements. The D-loop is converted into a pseudo replication fork (Bartosova & Krejci, 2014) and synthesis occurs along the intact chromosome. This nascent strand is then subsequently used to reform the second strand of the broken chromosome (Lydeard et al, 2007).

DNA interstrand crosslinks (ICLs) are a major threat to the stability of the genome as they disrupt replication and transcription (Huang & Li, 2013) as well as promoting chromosomal breaks and rearrangements. In higher eukaryotes, the Fanconi Anaemia (FA) pathway is required for the removal of these lesions through the coordination of NER, HR and translesion synthesis (TLS) (Moldovan & Andrea, 2009). The method of ICL repair employed by the cell is thought to be dependent upon the stage of the cell cycle it is in. In G1 it is thought that ICL repair is carried out by NER as the levels of unhooking observed correlate with the intensity of helix distortion induced by the lesion (Smeaton et al, 2008). In S phase and G2, FAAP24 and FANCM working in concert recognise DNA damage. When replication forks approach ICLs they stall and FANCM can promote their conversion into four-way "chicken-foot" junctions to promote their stabilisation by HR or bypass by TLS (Gari et al, 2008).

FANCM and FAAP24 recruit the rest of the core FA complex to the ICL (Ciccia et al, 2007). This complex, containing FANCA, FANCB, FANCC, FANCE, FANCF, FANCG, FANCL and FANCM alongside FAAP20, FAAP24 and FAAP100, acts as an E3 ubiquitin ligase. It is responsible for the monoubiquitination of FANCD2 and FANCI which results in their chromatin localisation and the formation of damage repair foci that contain BRCA2/FANCD1 and RAD51/FANCR (Garcia-Higuera et al, 2001; Smogorzewska et al, 2007; Wang et al, 2004a). Ubiquitinated FANCD2 recruits several nucleases to ICLs (Deans & West, 2011; Kim & D'Andrea, 2012). This includes FAN1, which cleaves nicked or branched structures and is a 5' flap endonuclease (Smogorzewska et al, 2010) so could cleave DNA adjacent to stalled replication forks. The loss of certain other nucleases, such as ERCC1, XPF/ERCC4/FANCQ, Slx4/FANCP and MUS81, sensitises cells to crosslinking

agents (Ciccia et al, 2008; Svendsen et al, 2009). As all these enzymes specifically cut at 3' flap structures, they could incise at the other side of the ICL to FAN1 and complete the 'unhooking' of the DNA. The ICL can then by bypassed by the TLS polymerases REV1 or Pol ζ, formed of the REV3L catalytic subunit and REV7/FANCV regulatory subunit. Any resultant DSB are repaired by HR, mediated by RAD51/FANCR, BRCA2/FANCD1, PALB2/FANCN and BRIP1/FANCJ (Deans & West, 2011; Klein Douwel et al, 2014) (Fig. 1.2.3.4.4). It is possible that NER may also play a role in removing the crosslink following TLS (Deans & West, 2011).

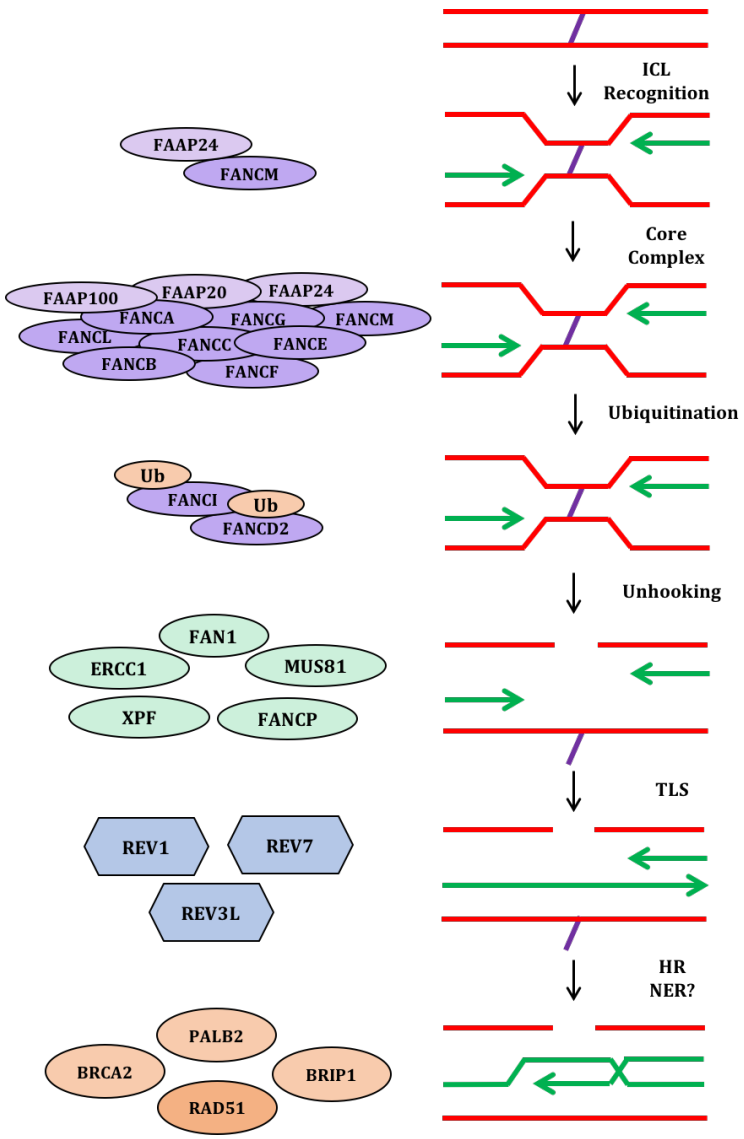

Figure 1.2.3.4.4 Interstrand crosslink repair by the Fanconi Anaemia pathway.

Interstrand cross links (ICL-purple) link the two strands of a DNA helix and prevent them from separating during replication and gene transcription. When two replication forks (green arrows) converge on a ICL, they stall and the ICL is recognised by FANCM and FAAP24. This results in the recruitment of the FA core complex (FANCA/B/C/E/F/G/L and FAAP20/100) which monoubiquitinates FANCD2 and FANCI. These proteins recruit nucleases such as FAN1, MUS81, ERCC1, XPF and FANCP to incise the DNA and unhook the ICL. The lesion can then be bypassed by the translesion synthesis polymerases REV1, REV7 or REV3L and it is possible that the ICL is removed by nucleotide excision repair (NER). The double strand break in the opposite strand is then repaired by homologous recombination (HR) mediated by RAD51, BRCA2, PALB2 and BRIP1.

Translesion synthesis (TLS) is a damage tolerance pathway that allows for the bypass of DNA lesions when they cannot be repaired or the relevant repair pathways are overcome by the level of damage present (Izhar et al, 2013). The replicative polymerases (δ and ε) do not efficiently bypass DNA lesions therefore a number of other polymerases are employed to carry out this function. Whilst several alternative polymerases are capable of bypassing lesions and are involved in DNA repair, the Y family DNA polymerases, Pol η, Pol κ, Pol ι and REV1 (Sale et al, 2012) alongside the B family Pol ζ (Waters et al, 2009), specifically function to bypass a variety of DNA lesions. In contrast to the replicative polymerases, these enzymes have low processivity which prevents them from replicating long strand of DNA (Vaisman & Woodgate, 2017). They also have lower fidelity due to their lack of 3'-5 exonucleolytic proofreading and their flexible active sites, which allow for the processing of bulky DNA lesions (Kim & D'Andrea, 2012; Perlow-Poehnelt et al, 2004).

PCNA is ubiquitinated at stalled DNA replication forks by RAD18 stimulated by RPA and results in the recruitment of the TLS polymerases (Davies et al, 2008). As well as recruiting the polymerases, PCNA stimulates their activity by acting as a processivity factor (Masuda et al, 2015). Whilst REV1 does possess TLS capabilities, it is believed to function mainly as a scaffold protein where it acts as an adaptor between the other TLS polymerases and the PCNA sliding clamp (Guo et al, 2003; Guo et al, 2006; Ross et al, 2005; Waters et al, 2009). The remaining TLS polymerases each function to mitigate the deleterious consequences of a specific set of DNA lesions. Pol η is required for the error-free bypass of CPD following UV irradiation and its loss results in the variant form of cancer susceptibility syndrome Xeroderma Pigmentosum (Kannouche et al, 2003). It is also required for the bypass of crosslinks induced by Cisplatin (Alt et al, 2007). In contrast, Pol κ is required for the efficient bypass of bulky lesions induced by benzo(a)pyrene dioleoxide (BPDE) (Suzuki et al, 2002) and its loss results in reduced levels of NER (Tomoo & Alan, 2006). The remaining Y family polymerase, Pol ι can carry out error prone TLS across a number of substrates (Stallons & McGregor, 2010) including UV damaged DNA (Wang et al, 2007). It is also believed to act in BER as it can partially compensate for the loss of Pol β (Bebenek et al, 2001). Pol ζ is thought to be involved in both HR and crosslink repair (Gan et al, 2008; Sharma et al, 2012b). It has also been implicated in the mutagenic process that results from several carcinogens including UV and BPDE (Diaz et al, 2003).

1.3 Deregulation of Genome Maintenance Mechanisms in Cancer

Despite the extensive efforts that cells employ to prevent or minimise the occurrence of genomic alteration, mutations still arise. Whilst some are relatively harmless, other disruptions can result in deleterious consequences such as genomic instability and cancerous transformation. Genome instability is found in both hereditary and sporadic cancers and in both cases this is linked to the deregulation of genome maintenance mechanisms. Instability can occur in the form small scale changes to the genome, such as MIN or in more substantial alterations in the structure and number of chromosomes present (CIN). MIN is thought to arise through the failure by MMR to rectifying replication slippage at the microsatellite sequences interspersed throughout the genome (Yao & Dai, 2014). It can result in a hypermutator phenotype which aids in cancerous transformation (Boland & Goel, 2010) and is more commonly found in hereditary cancers but can also occur in some sporadic tumours. In contrast, CIN is found in the majority of human tumours and arises through the mis-segregation of chromosomes during mitosis. If chromosome segregation is not carefully regulated, daughter cells can be produced with the incorrect number of chromosomes and abnormal chromosome structures (Yao & Dai, 2014). Such mis-segregation can arise from a number of sources, including incompletion of DNA replication or repair (Burrell et al, 2013). Genomic instability can also arise through changes that do not affect the sequence or abundance of DNA sequences. Changes in the epigenetic regulation of gene expression have also been implicated in the malignant phenotype. Changes in the methylation status of the promoters of genes involved in cell cycle regulation and DNA repair have been demonstrated to contribute to genomic instability (Baylin & Ohm, 2006; Jin & Robertson, 2013). Modification of histones likewise plays a role in the regulation of DNA repair and gene transcription so it is logical that alterations in their abundance would similarly affect genomic instability (Ferguson et al, 2015).

1.3.1 Cancer Predisposition

Between 5 - 10% of the global cancer burden can be accounted for by hereditary cancers (Guan et al, 2015). These cancers arise in individuals who carry germline mutations in genes involved in the cell cycle checkpoints or the repair of DNA, typically tumour suppressors (Negrini et al, 2010). Usually, the mutation only affects one allele of the gene whilst the other remains functional. However, this functional allele can be lost in somatic cells (loss of heterozygosity) which can result in the onset of cancer progression as is described in the Knudson two-hit hypothesis of cancer development (Paige, 2003). As it only requires the mutation of one allele to result in the onset of cancer, individuals harbouring these mutations tend to develop cancer earlier than those suffering from sporadic cancers (Brandt et al, 2008). These mutations can result in a mutator phenotype, allowing for the generation of further mutations and those that provide a growth advantage to the cells are selected for. Through a continuous sequence of mutation and selection, the tumour evolves and progresses into a more malignant lesion (Martincorena et al; Negrini et al, 2010).

Over 200 cancer susceptibility syndromes have been reported, and although many are rare and some only result in benign disease, they still account for a considerable proportion of the global cancer burden (Nagy et al, 2004). The mutation of ATM results in Ataxia-telangiectasia (AT), an autosomal dominant neurodegenerative condition. As well as neurodegeneration, AT patients are predisposed to tumour formation, acutely IR sensitive (Taylor et al, 1975), display chromosomal instability, age prematurely and have decreased life expectancy (Savitsky et al, 1995). Approximately 25% of AT sufferers will develop cancer within their lifetime, usually leukaemia or lymphoma, which reflects the role of ATM in the maturation of the immune system (McKinnon, 2004). ATR hypomorphic mutations result in Seckel syndrome, a rarely occurring autosomal recessive dwarfism syndrome. Like AT it causes premature aging however, it does not predispose patients to cancer, although patients tend to die young and so may not have the chance to develop tumours (Murga et al, 2009).

Inherited mutations in several DNA repair genes have also been linked to cancer predisposition syndromes. Xeroderma pigmentosum (XP) patients lack the ability to effectively repair UV damage and so are highly susceptible to skin malignancies (Kleijer et al, 2008). This syndrome can arise through the mutation of 7 genes involved in NER, XPA-XPG, and the variant form (XPV) arises through loss of Pol η function (Lehmann et al, 2011) Similarly, Fanconi Anaemia patients are sensitive to DNA crosslinks and are predisposed to acute myeloid leukaemia, squamous cell carcinomas and bone marrow failure through the mutation of FA pathway genes (Dong et al, 2015). Currently there are 22 genes reported in the FA Mutation Database that are known to result in FA and FA-like cancer susceptibility syndromes (Auerbach & Smogorzewska, 2017). As discussed above, failure of the MMR genes to prevent replication slippage can result in MIN, the rarer form of genomic instability. Mutations in the MMR genes MLH1 and MSH2 result in a mutator phenotype that drives the development of Lynch syndrome (also referred to as hereditary nonpolyposis colon cancer; HNPCC), whose tumours are characterised by MIN. Mutations in other MMR genes have also been identified but these cause less severe phenotypes (Fishel et al, 1993; Nagy et al, 2004).

1.3.2 Sporadic Cancers

Historically, it was assumed that sporadic cancers would have a similar origin to hereditary cancers, with the mutation of checkpoint and DNA repair genes driving the onset of genomic instability. This mutator hypothesis predicted that these genes became mutated in precancerous lesions resulting in an increased mutation rate and subsequent acquisition of further mutations (Hanahan & Weinberg, 2011). However, high throughput screening studies revealed that DNA repair genes are infrequently mutated in sporadic cancers, and that genomic instability is present before the mutation of cell cycle checkpoint genes (Bartkova et al, 2005; Gorgoulis et al, 2005). It is now believed that oncogenes are the earliest and most frequent class of genes mutated in the majority of sporadic cancers, as implied in the oncogene-induced DNA damage model (Halazonetis et al, 2008; Martincorena et al; Negrini et al, 2010).Unlike the tumour suppressors, whose

mutation results in the predisposition to hereditary cancers, mutation of only one allele of an oncogene would be sufficient to induce oncogenic transformation.

Oncogene activation or overexpression results in the induction of replication stress through the deregulation of oncogene firing and DNA synthesis. Overexpression of several oncogenes including Cyclin E, MYC and RAS results in increased firing of replication origins (Hills & Diffley, 2014) and in the case of Cyclin E this has been demonstrated to deplete the cellular levels of dNTPs resulting in impaired progression of replication forks (Jones et al, 2013). Similarly, the upregulation of E2F1 results in the deregulation of replication initiation and the over-replication of DNA via the overexpression of the licensing factors Cdc6 and Cdt1 (Karakaidos et al, 2004). Cyclin E and RAS overexpression have also been implicated in the re-replication of DNA (Bartkova et al, 2005; Di Micco et al, 2006).

Cells experiencing replication stress preferentially form DSBs at common fragile sites (CFS), which are particularly susceptible to DNA breakage. Even under conditions of mild replication stress that do not trigger cell cycle arrest, these regions exhibit DNA strand breaks (Durkin & Glover, 2007). They are considered difficult to replicate, possibly due to their AT rich nature allowing for the formation of DNA secondary structures (Mishmar et al, 1998) and interference of the transcription machinery (Helmrich et al, 2013). However, it is thought that the scarcity of active replication origins in these regions is the most likely cause of their fragility. This would force forks to have to travel long distances to complete replication and there would be no dormant origins present to rescue a stalled fork (Le Tallec et al, 2011; Zeman & Cimprich, 2014). In premalignant lesions, chromosomal breaks preferentially occur at CFS in the absence of gross CIN, suggesting that it is replication stress that is causing the DSB to occur in this early stage of cancer development (Gorgoulis et al, 2005). It has also been confirmed that replication stress is present in these premalignant lesions through the study of replication fork stalling within these cells (Bartkova et al, 2006). It is hypothesised that the HR machinery may become overwhelmed by the DSB resulting from oncogene-induced replication stress, preventing their error-free repair (Gudjonsson et al, 2012; Jones & Jallepalli, 2012). Indeed, it has been demonstrated that the error prone repair of DSBs by NHEJ, MMEJ and BIR can result in CIN, supporting the role that replication stress plays in the induction of genomic instability (Costantino et al, 2014; Lee et al, 2007b).

During the progression of cancer from a premalignant lesion to a malignant tumour, the genomes of cancer cells become more unstable (Gorgoulis et al, 2005). In premalignant cells, the DNA damage response is active and capable of inducing the cessation of cell cycle progression and entry into senescence or apoptosis (Bartkova et al, 2006; Di Micco et al, 2006; Gorgoulis et al, 2005; Halazonetis et al, 2008). The activation of oncogenes initiates increased levels of DNA replication resulting in replication stress and subsequent activation of the DNA damage response. This triggers entry into a state of oncogene-induced senescence (OIS) in a replication dependent manner (Di Micco et al, 2006). In the later stages of cancer progression, DNA damage does not result in entry into senescence or the induction of apoptosis (Gorgoulis et al, 2005). It has been demonstrated that

mutations in Chk2 or the inhibition of ATM signalling both suppress the induction of OIS resulting in more malignant forms of cancer (Bartkova et al, 2006) and that p53 loss results in the failure to induce apoptosis (Gorgoulis et al, 2005). It was therefore proposed that the DNA damage response and cell cycle checkpoints act as an initial barrier to carcinogenesis (Bartkova et al, 2006; Gorgoulis et al, 2005; Halazonetis et al, 2008). Late stage cells display instability at known tumour suppressor loci (Gorgoulis et al, 2005) and p53 is the most commonly mutated gene in human cancers (Negrini et al, 2010), therefore, it is thought that the DNA damage response must be abrogated to overcome the tumorigenesis barrier and allow cancer progression (Halazonetis et al, 2008) (Fig. 1.3.2.1).

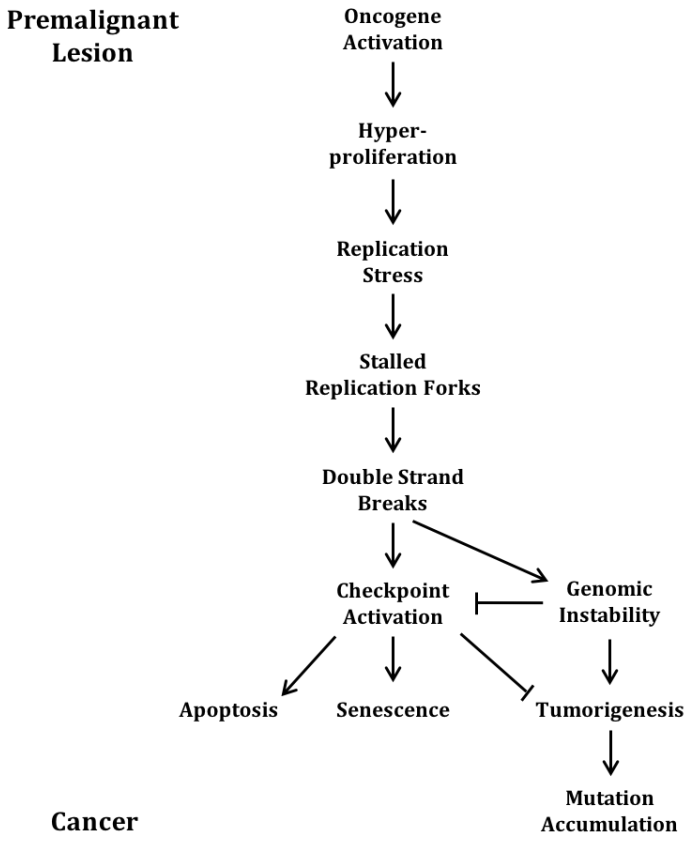

Figure 1.3.2.1 Oncogene induced DNA damage model of cancer development.
Oncogene activation results in hyper-proliferation and subsequent DNA replication stress. The impaired replication forks collapse to form double strand breaks (DSBs) which trigger activation of the DNA damage checkpoint and ensuing apoptosis or senescence which acts as a barrier to tumorigenesis. The genomic instability that can result from the error-prone repair of DSBs allows for the acquisition of mutations and those that inhibit checkpoint activation will be selected for. Once the checkpoint has been inactivated, the cells can progress to the later stages of cancer development by accumulating further mutations.

The error-prone repair of DSBs can result in CIN and therefore allow for the acquisition of the mutations that allow tumour cells to circumvent OIS. It is believed that cancer cells only display mutated checkpoint and DNA damage repair genes once this barrier has been bypassed (Negrini et al, 2010). Clonal populations arise within the tumour, each with its own mutational profile, resulting in a heterogeneous population of cells (Caswell & Swanton, 2017). Alterations in the selective pressures acting on the tumours, such as chemotherapy treatment, can select for mutations that allow the tumour to survive (McGranahan & Swanton, 2015). It has been established that tumours displaying CIN have increased levels of drug resistance compared to CIN negative tumours (Lee et al, 2011).

1.4 Targeting Maintenance Mechanisms to Treat Cancer

As cancer develops from a patient's own cells, the only way that tumour cells can be differentiated from the surrounding normal tissues is through their malignant phenotype. Traditionally, cancer therapies exploited the ability of the majority of cancers to rapidly proliferate, however, this approach has many limitations including the detrimental degradation of normal tissues. Therefore, a new paradigm in cancer therapy has been established where efforts are being made to develop treatments that target cancer cells more specifically at a molecular level.

1.4.1 Conventional Therapy

Historically, cancer treatment strategies have been limited to surgery and DNA damaging agents, including radiotherapy and chemotherapeutics. Whilst surgery can be successful at locally controlling cancer within the patient, this treatment methodology has several limitations. Its efficacy relies on removing all the cancerous cells from the patient and as it is difficult to differentiate between cancerous and normal tissues, some tumour cells can be left behind following the procedure. Surgery is not capable of treating metastatic disease and as cancer is a systemic disease the efficacy of surgery alone has been called into question (Benjamin, 2014).

The efficacy of radiotherapy is due to the ability of IR to induce DNA damage, with up to 40 DSBs induced per gray of exposure, as well as a multitude of SSBs and other DNA lesions (McGrath & Williams, 1966). More recently, it has also been discovered that radiotherapy may stimulate the immune system to aid in the destruction of tumours (Gotwals et al, 2017). Although advances in medical imaging and techniques for delivering radiotherapy have increased its efficacy and reduced the damage to surrounding normal tissues, as with surgery, it is only capable of local control of cancer and is not always a curative regime (Baumann et al, 2016).

As cancer became better understood, and the important role metastasis plays in patient outcome became apparent, it was made clear that systemically acting agents were required for its the effective treatment (Chabner & Roberts, 2005). As a consequence of this, chemotherapeutic interventions have become the corner stone of cancer treatment (Lord & Ashworth, 2012). Since the 1940s and the use of nitrogen mustard for the treatment of lymphatic tumours (Gilman & Philips, 1946), agents that preferentially kill tumour cells have been used to treat cancer.

The majority of these drugs interfere with the cells ability to successfully replicate their DNA and so can target cells that divide rapidly, such as tumour cells, whilst leaving terminally differentiated cells intact. These include several classes of chemotherapeutics incorporating alkylating agents, crosslinking agents, topoisomerase inhibitors and antimetabolites. Exogenous DNA alkylating agents are currently used in the clinic to treat a number of malignancies. One example is Temozolomide, which induces the formation of O^6-methylguanine and is presently used as part of the standard treatment regimen for glioblastoma multiforme (GBM). ICLs pose a major threat to genome stability and can be induced by several agents including the antibiotic Mitomycin C and the platinum based

compounds. The later class contains Cisplatin which is also capable of introducing intrastrand links (Dasari & Tchounwou, 2014). Topoisomerases introduce transient strand breaks which relax supercoiled DNA to allow for the unimpeded progression of replication forks. When these enzymes are inhibited by agents such as Irinotecan and Etoposide, the DNA strands cannot separate or the induced breaks cannot be ligated and persist, both of which are highly toxic to cells (Strumberg et al, 2000). Antimetabolites mimic molecules that are found intracellularly to disrupt cellular metabolism by several mechanisms. Gemcitabine, a deoxycytidine analogue, can incorporate into DNA triggering strand termination (Mini et al, 2006; Plunkett et al, 1995) and inhibit ribonucleotide reductase resulting in the depletion of the dNTP pool (Mini et al, 2006). The uracil analogue 5-Fluorouracil (5-FU) can also disrupt the composition of dNTP pools via the inhibition of thymidylate synthase. Furthermore, it can misincoporate into DNA which poses a threat to DNA polymerase progression (Longley et al, 2003).

Chemotherapeutics can also target other stages of the cell cycle to induce the killing of rapidly proliferating cells. Spindle poisons are able to perturb mitosis by disrupting the dynamics of microtubule formation and de-polymerisation both of which prevent the successful completion of cell division. The vinca alkaloids prevent tubulin polymerisation (Chabner & Roberts, 2005) whilst the taxanes, including Paclitaxel, prevent the breakdown of microtubules (Gligorov & Lotz, 2004).

Whilst chemotherapies have proved effective agents for targeting rapidly dividing tumour cells, there are a number of drawbacks associated with their use. High proliferation rates are not unique to tumour cells, they are also displayed by some normal tissues including the intestinal epithelium and hair follicle cells. As a result of this, one of their most considerable limitations is the adverse side effects resulting from the destruction of normal tissues. They can affect the nervous system resulting in peripheral neuropathy resulting in shooting pains, changes in sensory perception and weakness. The pathogenesis of this condition is poorly understood despite it affecting 68% of patients to some extent within their first month of treatment (Addington & Freimer, 2016). Treatment can also result in myelosuppression (suppression of the bone marrow) which is a major dose limiting side effect of certain chemotherapies, particularly alkylating agents, as they can result in neutropenia (Wang et al, 2006). Another drawback that stems from their targeting of rapidly dividing cells is the development of slowly-proliferating or quiescent populations of cancer cells that are no longer sensitive to the initial drug (indolent cancer). With the rapidly dividing cells removed, these populations face little competition and survive within the patient resulting in relapsed disease (Shah & Schwartz, 2001).

Chemotherapeutic treatment can result in the acquisition of molecular mechanisms of resistance. Once mechanism which cancer cells employ is to increase the efflux of the drug from the cell, which prevents them from having their desired effect. They can achieve this by upregulating their cell membrane transporters, such as multi-drug resistance protein 1 (MDR1/P-glycoprotein), an ATP binding cassette (ABC) transporter that is overexpressed in a number of cancers and can be upregulated by chemotherapeutic treatment (Thomas &

Coley, 2003). Alteration of cellular metabolism can affect how drugs are processed within the cell which can prevent their activation, as has been observed in uveal melanoma resistant to MMC (Gravells et al, 2011). Deregulation of apoptosis through p53 mutation is likewise thought to contribute to drug resistance. The tumour microenvironment also plays a critical role in the response of tumour cells to cancer therapy as some animal models have shown differing responses to certain drugs when the tumour cells are injected ectopically or in metastatic sites (McMillin et al, 2013). Additionally, the inherent DNA repair capacity of the cancer cells can mitigate the effects of these DNA damaging therapies. For instance, high levels of MGMT expression in malignant astrocytomas treated with the alkylating agent bis-chloroethylnitrosurea (BCNU) resulted in lower median survival than patients with low expression (Jaeckle et al, 1998). TLS is another key damage repair pathway that can confer resistance to chemotherapies as they can bypass the lesions induced as demonstrated by Pol η which can replicate across the crosslinks produced by Cisplatin treatment (Alt et al, 2007).

More recently, classical chemotherapies have been used to target genome maintenance defects within tumour cells. DNA crosslinking agents, such as the platinum salts, have preferentially been used to treat cancers displaying defects in HR and NER, including familial breast cancers (Turner et al, 2004) and ERCC1 negative non-small cell lung cancer (Lord & Ashworth, 2012). Alkylating agents have also shown promising results in patients with epigenetically silenced MGMT (Weller et al, 2010).

1.4.2 Molecular Targeting

The latest paradigm in cancer drug discovery is the rational design of compounds that will specifically target molecules implicated in the growth, development and survival of tumours. The selection of appropriate target molecules relies heavily on a detailed knowledge of the molecular changes that occur during cancer development and their prevalence in cancer patients. It is predicted that this new class of drugs should preferentially kill cancer cells, rather than normal tissues, as they target them more specifically than classic chemotherapies and therefore should have reduced adverse side effects (Sawyers, 2004).

One approach to the selection of cancer specific targets is to identify molecules that are only found within cancerous cells. These include the oncogenic fusion genes, which were first discovered in haematological cancers and more recently in solid tumours. These genes are produced by the chromosomal rearrangements associated with CIN positive cancers. A prime example of these genes is the BCR-ABL1 kinase, found in chronic myelogenous leukaemia (CML) patients (Ben-Neriah et al, 1986) which regulates malignant transformation in this cancer (Deininger et al, 2000). An inhibitor of this protein, Inmatinib, has been developed and it proved to induce remission in patients so was successfully licensed for CML treatment (Druker et al, 2001). Another drug, Crizotinib, an inhibitor of the ALK tyrosine kinase, has been approved for the treatment of non-small cell lung cancer positive for ALK rearrangements. It has also entered clinical trials for the treatment of this cancer with rearrangements of an additional tyrosine kinase ROS1

(Davies & Doebele, 2013). However, not all cancers are positive for fusion genes so other methods of specifically targeting cancer cells have been developed.

An alternative strategy is to identify molecules that are essential for the survival of transformed cells but their loss can be tolerated in normal tissues. Many cancers become dependent upon the activation or overexpression of certain 'driver' oncogenes for the preservation of their malignant phenotype and their survival. This phenomenon is referred to as 'oncogene-addiction' (Sharma & Settleman, 2007) and it was proposed that the inhibition of these oncogenes could result in positive therapeutic outcomes. This was observed in MYC-driven osteogenic sarcoma mouse models, where MYC inactivation resulted in the differentiation of the tumour cells into mature bone and prolonged tumour regression (Jain et al, 2002). It has also been exploited clinically to treat several cancers with varying success. As mentioned previously, inhibition of the BCR-ABL1 oncogene in CML results in tumour regression (Druker et al, 2001) as the malignant phenotype is dependent on its expression (Deininger et al, 2000). In contrast, when the HER2 inhibitor Herceptin was administered to breast cancer patients with overexpression of this driver oncogene, only 30% of patients responded to the therapy (Valabrega et al, 2007). It has subsequently been demonstrated that downregulation of PTEN conferred Herceptin resistance (Berns et al, 2007) indicating that the inhibition of a driver oncogene is not necessarily a successful therapy in all cases.

Another promising approach is to identify synthetic lethal relationships within tumour cells. This concept states that if two genes are in a synthetic lethal relationship, the concurrent loss of both genes is not compatible with cell viability, however, the loss of either gene alone could be tolerated. It was therefore predicted that single agent therapies could be developed for targets that were in synthetic lethal relationships with cancer associated mutations (Kaelin Jr, 2005).

One such target identified by this method is PARP1 which has been demonstrated to be in a synthetic lethal relationship with mutations that impair HR. Inhibition of this enzyme in cells with suboptimal HR due to BRCA1, BRCA2, XRCC2 or XRCC3 mutations was cytotoxic (Bryant et al, 2005; Farmer et al, 2005). This was also observed in cells where BRCA2 was disrupted by siRNA transfection. When BRCA2 deficient V-C8 and VC-8 cells that had been complemented with wild type BRCA2 were treated with the same doses of PARP inhibitors, the deficient cells were much more sensitive suggesting that the effects of PARP inhibition are specific to HR deficient cells (Bryant et al, 2005). As mentioned previously, this enzyme is required for the repair of SSBs and its inhibition results in their persistence within the genome. Replication forks stall at these break sites and potentially result in the formation of DSBs. In HR-proficient cells, the stalled replication forks and DSBs would be rescued and repaired respectively by HR. However, in the absence of this pathway, these lesions would persist or be repaired by error-prone pathways which can result in genomic instability (Bryant et al, 2005; Farmer et al, 2005). This work lead to the development of the PARP inhibitor Olaparib which was approved in the UK in 2015 for treatment of ovarian cancer patients with BRCA1 and BRCA2 mutations (Cancer Research UK, 2015).

More recently, RNAi screening approaches have been utilised to identify genes in synthetic lethal relationships with cancer-associated mutations. A genome wide shRNA screen in K-RAS mutant cells measured the levels of the shRNAs present by microarray hybridisation to identify those that prevented cell proliferation. This was also carried out in an isogenic corrected cell line and comparison of the two data sets allowed the identification of genes with apparent synthetic lethality with K-RAS overexpression. This demonstrated that K-RAS activated cells are sensitive to perturbations in, mitosis and particularly, the inhibition of Plk1 (Luo et al, 2009). A whole genome siRNA screen has also been carried out in REV3 deficient cancer cells to identify genes that decreased cell viability. It identified RRM1, the large subunit of ribonucleotide reductase, an enzyme required for nucleotide synthesis, which is also inhibited by hydroxyurea (HU). Treatment with this drug increased the levels of ssDNA formed in REV3 deficient cells suggesting a role for this gene in the replication stress response (Kotov et al, 2014).

It has been suggested that targeted therapies could be used to sensitise cells to DNA damaging agents rather than as single agent therapies. One potential benefit of this approach is that it may reduce the concentrations of these conventional therapies required for effective treatment, as they are commonly administered at their maximum tolerated dose. This may reduce some of their adverse side effects and increase the quality of life for cancer patients. It was hypothesised that chemotherapies could be paired with inhibitors of the repair pathways that remove their cytotoxic lesions to prevent their resolution and reduce levels of resistance. This approach was trialled in GBM models where MGMT was inhibited by O^6-benzylguanine to prevent the removal of O^6-methylguanine induced by Temozolomide treatment. Whilst this approach proved effective in pre-clinical models it did not restore Temozolomide sensitivity in patients that demonstrated resistance to this therapy and results in numerous adverse events (Quinn et al, 2009).

As well as being used as a single agent to target HR deficient cells, PARP inhibitors have also been examined as agents that potentiate chemo- and radiotherapy. The loss of the MMR pathway results in resistance to several chemotherapeutic agents, most likely through an increased tolerance for damaged bases within the DNA (Liu et al, 1996). One such agent is Temozolomide, the tolerance of which is thought to be accentuated by BER therefore the PARP inhibitor AG14361 was tested in combination with Temozolomide. This combination enhanced the cytotoxicity of Temozolomide in MMR proficient cells but the effect was more pronounced in cells with MMR deficiency. PARP inhibition did not sensitise MMR deficient cells to Cisplatin treatment (Curtin et al, 2004), however, combination of Olaparib and Cisplatin results in synergism in BRCA2 deficient cells (Evers et al, 2008). Inhibition of PARP also slows the repair of damage induced by the topoisomerase I poison Camptothecin, as PARP is required for the removal of the adducts induced by this therapy (Smith et al, 2005). This combination has been shown to be most effective in cells with compromised NER due to loss of XFP/ERCC1 as this represents a compensatory mechanism for the repair of Camptothecin induced damage (Zhang et al, 2011). The loss of PARP has also been shown to radiosensitise actively replicating cells

(Banasik et al, 1992) most likely through the collision of replication forks with the SSB that accumulate following PARP inhibition (Saleh-Gohari et al, 2005).

NER plays a crucial role in removing bulky DNA adducts to maintain genome stability, however, it also has a considerable affect upon the efficacy of certain DNA damaging therapeutics. A such, efforts have been made to identify molecules capable of modulating the interaction between ERCC1 and XPF as the downregulation of these proteins sensitises cells to Cisplatin treatment (Arora et al, 2010). The molecule F06/NERI02 was identified in an *in silico* screen as an inhibitor of this interaction and has been demonstrated to sensitise cells to both Cisplatin and MMC treatment (Gavande et al, 2016). Inhibitors of XPA, the protein required for the identification of the adducts have also been identified by *in silico* screens and several have been validated by DNA binding assays (Neher et al, 2010). However, the use of these compounds as cancer therapies is currently still in question as they have not been studied extensively *in vivo* (Gavande et al, 2016).

NHEJ is thought to account for up to 85% of the repair of DSBs induced by radiotherapy (Shibata et al, 2011). Inhibition of DNA-PKcs by the non-specific PIKK inhibitor Wortmaninn and specific DNA-PK inhibitors slows the repair of DSBs and enhances the effects of IR and the topoisomerase II poison Etoposide (Curtin, 2013). The specific inhibitor NU7441 increased the delay in tumour growth induced by Etoposide in colon cancer xenografts (Zhao et al, 2006), sensitised B-cell chronic lymphocytic leukaemia to topoisomerase II poisons (Elliott et al, 2011) and increased the sensitivity of several breast cancer cells lines to both ionising radiation and Doxorubicin (Ciszewski et al, 2014). Some efforts have also been made to inhibit NHEJ by disrupting the processing of the DSB ends. Inhibition of the phosphatase activity of polynucleotide kinase by A12B4C3, resulted in the radiosensitisation of both breast and lung cancer cells, although this inhibitor lacks the potency for clinical assessment (Freschauf et al, 2009). Similarly, inhibitors of Ligase IV have been developed which result in the accrual of DSBs within the genome and subsequent cytotoxicity (Srivastava et al, 2012).

Modulation of the cell cycle checkpoints by targeted therapies could also sensitise cancer cells to DNA damaging agents as they would not be able to halt progression to allow for the damage to be repaired. Potentially, this could result in increased accumulation of DNA damage, disruption of DNA replication and failure of mitosis all of which can result in cell killing. ATM is mutated in AT cells which are characterised by genomic instability and are highly sensitive to the effects of IR (Taylor et al, 1975). This sparked interest in the potential of ATM inhibitors to potentiate radiotherapy and DSB inducing chemotherapies. One of the earliest inhibitors studied was caffeine, which also inhibits ATR, and sensitises cells to a number of genotoxic agents but IR in particular (Sarkaria et al, 1999). These effects were even more pronounced in p53 deficient cells suggesting that ATM inhibitors may specifically target cancerous cells (Powell et al, 1995). The first potent selective ATM inhibitor KU55933 prominently sensitised cells to both IR and DSB inducing chemicals (Hickson et al, 2004) which lead to the development of KU60019 a more potent radiosensitiser (Golding et al, 2009). This compound was shown to radiosensitise glioma xenografts (Biddlestone-Thorpe et al, 2013) whilst having little effect on the viability of

terminally differentiated astrocytes (Golding et al, 2012) and significantly increased survival in mouse models (Biddlestone-Thorpe et al, 2013). Loss of ATM function has also been found to be particularly detrimental in cells with deficiency of the FA pathway. ATM was found to be constitutively activated in FA deficient mice and a double knockout of ATM and FANCG was found to be inviable. Pancreatic cell lines lacking FANCG or FANCC were found to be sensitive to ATM inhibition when compared to isogenic corrected cell lines again suggesting that ATM inhibitors could be used to specifically target FA deficient tumour cells (Kennedy et al, 2007). However, despite this evidence, concerns remain that ATM inhibitors will broadly affect all cells resulting in normal tissue toxicity.

Conversely, p53 can be activated to induce sensitivity of cancer cells to conventional therapies or it can be inhibited to prevent DNA damage to normal surrounding tissues. Reactivation of p53 and induction of tumour cell apoptosis (RITA) binds to p53 which activates it and suppresses the growth of tumours by inducing apoptosis (Issaeva et al, 2004). It achieves this by repressing the upregulation of anti-apoptotic factors and the downregulation of oncogenic signalling (Grinkevich et al, 2009). Mutant p53 reactivation and induction of rapid apoptosis (MIRA-1) restores the function of mutant p53 and therefore may render resistant cancer cells susceptible to killing by DNA damaging therapies. It is capable of restoring p53's DNA binding capacity and allowing for the transcription of its target genes (Bykov et al, 2002; Bykov et al, 2005). Agents that inhibit p53, such as Pifithrin-α (PTN-α), have been utilised to protect normal cells form the adverse side effects associated with conventional cancer treatments. PTN-α has been demonstrated to protects cells and mice from genotoxic insults (Gudkov & Komarova, 2005; Komarov et al, 1999) and decrease the expression of p53 target genes (Culmsee et al, 2001).

The rational for the inhibition of the Intra-S and G2/M checkpoints is that a large proportion of cancer cells lack functional p53 signalling. This abolishes the functionality of the G1/S checkpoint and so the cells rely on the remaining checkpoints to prevent the accumulation of inviable levels of DNA damage. Inhibition of these checkpoints should therefore preferentially kill cells lacking an active G1/S checkpoint but have limited effects on normal surrounding tissues (Blasina et al, 2008). The inhibition of these checkpoints will be described below when discussing the targeting of the replication stress response (1.4.2.1).

As mentioned previously, spindle poisons have been classically used to treat cancers by the induction of mitotic arrest and cell death. However, these agents lack specificity towards cancer cells and so efforts have been made to develop more specific antimitotic agents. Cancer cells frequently display amplified levels of the Aurora kinases (Malumbres & de Castro, 2014) and their inhibition has been demonstrated to be detrimental to cancer cell survival. Several Aurora inhibitors are undergoing clinical trials including the Aurora A inhibitor, Alisertib. It induces defects in the formation of the spindle and chromosome alignment resulting in the induction of apoptosis or mitotic slippage. It has proved effective in a broad range of both solid and haematological cancers, although the explanation for sensitivity remains unclear (Niu et al, 2015). Inhibitors of Plk1 are also

under investigation for antitumor effects. This protein is overexpressed in a number of cancers and its inhibition preferentially results in the elimination of cancerous cells which impedes tumour growth in mouse models (Guan et al, 2005).

Like conventional chemotherapeutic agents, molecular targeting therapies are not without their limitations. Cancer cells can be intrinsically resistant to a targeted therapy due to the levels of expression of certain damage repair pathways. An example of this is NHEJ defective ovarian cancers which are innately resistant to the PARP inhibitor Rucaparib (McCormick et al, 2017). Due to the selective pressures induced by treatment, cancer cells can acquire resistance to these therapies by several mechanisms. They can mutate the target of the drug to prevent its binding which has been observed in non small-cell lung cancers treated with the ATP competitive EGFR inhibitor Gefitinib. Point mutations in the receptor prevented the binding of the drug but did not affect its affinity for ATP allowing it to continue functioning (Kobayashi et al, 2005). Cells can also reactivate pathways downstream of the drug's target to maintain signalling in the presence of the drug as mutations in BRAF have been shown to confer resistance to EGFR inhibitors in lung cancers (Ohashi et al, 2012). Likewise, cells can activate pathways that act in parallel to those affected by the drug to maintain signalling. This has been identified in non small-cell lung cancer patients who have developed resistance to EGFR therapy by overexpressing MET to upregulate PI3K signalling (Cappuzzo et al, 2009). Finally, where therapies rely on intrinsic mutations in the cancerous cells to have their effect, further mutation of these genes can render the therapies ineffective. The prolonged use of the PARP inhibitor Olaparib is associated with the development of resistance. In a subset of BRCA2 negative tumours, this has been demonstrated to be due to secondary mutations which restore the expression of BRCA2 and so mitigate the effects of the drug (Barber et al, 2013).

1.4.2.1 Targeting Replication Stress Response

As discussed previously, premalignant lesions and tumour cells display higher than normal levels of replication stress due to the chronic activation of oncogenes. It has therefore been suggested that this differential in stress levels can be targeted to specifically kill cancerous cells. It is hypothesised that by further increasing replication stress levels by modulating the response to this phenomenon, cancer cells would be forced over a threshold of stress and into crisis. Normal cells, with their lower basal stress levels, would remain below this threshold and retain their viability. As the earlies stages of tumorigenesis display heightened replication stress, this approach may eliminate oncogene expressing or tumour suppressor deficient cells before they have a chance to develop to malignancy and so may be able to prevent the development of tumours.

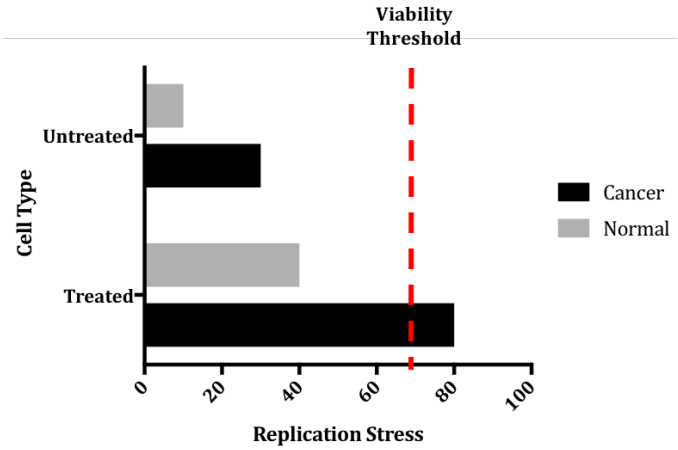

Figure 1.4.2.1.1 Targeting the Replication Stress Response.
Cancerous cells contain higher levels of replication stress then normal cells. It is thought that by inhibiting the replication stress response, cancer cells will be driven over a threshold level of stress beyond which they cannot remain viable. In contrast the normal cells should remain below this threshold and survive.

Several classes of genes have already been classified as suppressors of cellular levels of replication stress. These include the Intra-S checkpoint genes, primarily ATR, Chk1 and Wee1, which modulate the cellular response to impeded DNA replication. Genes involved in the synthesis and maintenance of dNTPs are also considered replication stress suppressors as a lack of nucleotides or an imbalance in the nucleotide pool can result in the stalling of replication forks (Bester et al, 2011). The ssDNA binding protein RPA is also key player in the response to replication stress and a lack of this protein can result in genomic instability (Glanzer et al, 2014). Certain DNA damage repair factors also suppress the build up of replication stress through the resolution of replication fork impeding lesions. Factors involved in RNA processing that facilitate efficient gene transcription also prevent the accumulation of replication stress. When these genes are absent the likelihood of replication-transcription collisions increases which results in higher levels of stalled replication forks. These factors, alongside helicases, prevent the formation of DNA:RNA hybrids such as R-loops which impede replication fork progression and therefore are essential for the suppression of replication stress (Aguilera & Gomez-Gonzalez, 2008; Zeman & Cimprich, 2014).

As discussed previously, inhibition of the cell cycle checkpoints by targeted therapies has been investigated as a technique to potentiate the effects of conventional cancer therapies. Particular attention has been given to inhibitors that abrogate the Intra-S and G2/M checkpoint as loss of these is predicted to preferentially eliminate cells lacking p53.

Inhibition of ATR has been found to be in a synthetic lethal relationship with the activation of certain oncogenes or loss of tumour suppressors. As previously discussed, the activation of oncogenes result in hyper-proliferation and the induction of DNA replication stress. ATR co-ordinates the cellular response to this phenomenon which cancer cells require to prevent the accumulation of inviable levels of DNA damage. Inhibition of ATR has been shown to be especially detrimental in cells lacking p53 and that this is most likely due to the increased rates of replication seen in these cells (Kwok et al, 2016; Murga et al, 2009). Overexpression of Cyclin E in mouse embryonic fibroblasts (MEFs) induces increased levels of replication stress, which is further exacerbated by the inhibition of ATR but not that of PI3K or mTOR. These effects were aggravated further by the loss of p53 which results in apoptosis (Toledo et al, 2011). Cell death is induced independently of p53 in cells experiencing replication stress (Myers et al, 2009; Sidi et al, 2008), so its loss does

not prevent cancerous cells from entering apoptosis. The loss of functional ATR via hypomorphic mutation has also been shown to increase genomic instability and induce cell death in cells expressing oncogenic RAS mutants (H-RAS^{G12V} and K-RAS^{G12D}) (Gilad et al, 2010). The loss of ATR signalling is also potentiated by mutations in several DNA damage repair pathways. Defects in HR mediated repair due to loss of ATM, BRCA2 or XRCC3 and BER due to loss of XRCC1 resulted in increased killing by the ATR inhibitor VE-821 when compared to isogenic matched cells with competent DNA repair. Increases in DNA-PKcs expression also result in the induction of greater cell killing following ATR inhibition due to the amplified levels of replication stress observed within these cells (Middleton et al, 2015). Two ATR inhibitors, VX-970 (Vertex) and AZD6738 (AstraZeneca) are currently in clinical trials: VX-970 in combination with a number of conventional chemotherapeutics, the PARP inhibitor Velaparib and radiotherapy whilst AZD6738 is being trialled as a single agent as well as in combination with both conventional chemotherapy and radiotherapy (Rundle et al, 2017).

Chk1 inhibition has been extensively studied to modulate the cells response to DNA replication stress. Knockdown of Chk1 by siRNA was demonstrated to result in the abrogation of the G2/M checkpoint and increased the cytotoxicity of nucleoside analogues and topoisomerase poisons as well as IR (Carrassa et al, 2004; Ganzinelli et al, 2008). The first Chk1 inhibitor, UCN01, was capable of abrogating G2/M arrest through targeting Chk1 but also inhibited a number of other kinases. A range of more specific Chk1 inhibitors have since been developed that vary in their potency. These inhibitors generally prevent cell cycle arrest and potentiate DNA damaging therapies, especially those that induce DNA replication stress (Chen et al, 2012). Accumulated evidence suggest that Chk1 inhibitors may be viable as single agents in cells overexpressing c-MYC. These cells overexpress Chk1, which is directly induced by c-MYC, and inhibition of Chk1 resulted in DNA damage accumulation and subsequent apoptosis. These effects were not observed in cells that did not overexpress this oncogene (Ferrao et al, 2012; Höglund et al, 2011). Chk1 inhibitors have been demonstrated to potentiate the effects of Gemcitabine in several cell lines, including pancreatic cells (Azorsa et al, 2009; Matthews et al, 2007; Parsels et al, 2009). This combination using the Chk1 inhibitor AZD7762 resulted in increased γ-H2AX foci formation whilst either treatment alone did not, suggesting that the stalled replication forks resulting from Gemcitabine treatment collapsed in the absence of Chk1 triggering a DNA damage response (McNeely et al, 2010). This inhibitor has also been shown to potentiate the effects of Irinotecan (Zabludoff et al, 2008) and IR particularly in p53 deficient cell lines (Mitchell et al, 2010b). It has been demonstrated to potentiate the cytotoxic effects of Olaparib in breast cancer and pancreatic cancer cell lines (Mitchell et al, 2010a). Similar to PARP inhibitors, cells with defective NHEJ appear to be resistant to the effects of Chk1 inhibition. However, downregulation of HR and ICL repair appears to sensitise cells to inhibition of Chk1, which can be achieved through the inhibition of mTOR (Massey et al, 2016). Several Chk1 inhibitors have been previously entered into clinical trials, including AZD7762, but many were halted due to dose limiting toxicities particularly of the haematological system (Chen et al, 2012). Three Chk1 inhibitors are currently in clinical trials: LY2606368/Prexasertib (Eli Lily), MK8776 (Merck and Co.) and

SRA737 (Sierra Oncology Inc.). All three are being trialled as single agents as well as in combination with conventional chemotherapies (Rundle et al, 2017).

An alternate strategy is to inhibit Wee1 whose knockdown prevents G2/M arrest in a similar fashion to the loss of Chk1, and sensitises cells to the effects of DNA damaging agents (Wang et al, 2004b). Its inhibition results in the activation of CDK1 and premature entry into mitosis even before replication can be completed (Aarts et al, 2012). It also increases the activity of CDK2 causing an increase in DNA initiation events which exhausts the cellular supply of nucleotides and results in fork stalling and subsequent collapse to DSBs (Beck et al, 2012). The first potent and selective Wee1 inhibitor MK-1775 (Merck and Co.) has been shown to preferentially sensitise p53 deficient cells to DNA damaging agents including Gemcitabine, 5-FU, Carboplatin and Cisplatin (Hirai et al, 2010; Hirai et al, 2009; Rajeshkumar et al, 2011). It has been clinically evaluated as a combination therapy with these drugs in several Phase I clinical trials which have produced promising results and it is also under investigation as a single agent. It is also undergoing two Phase II trials evaluating its use in combination with Carboplatin in p53 deficient ovarian and cervical cancers (Do et al, 2013).

1.4.2.2 Identification of Novel Replication Stress Response Genes as Potential Future Anti-cancer Targets

In previous studies, RNAi screening approaches have been utilised to identify novel factors involved in the maintenance of genome stability. Two genome wide screens identified genes whose knockdown resulted in increased DNA damage by monitoring levels of γH2AX (Paulsen et al, 2009). In the Paulsen screen, several networks were identified that regulated genome maintenance including cell cycle checkpoints, DNA repair genes, nuclear pores and mRNA processing. They also identified a role for Charcot-Marie-Tooth syndrome genes in the maintenance of the genome. Further study of a number of the novel genome maintenance factors identified in the Collis screen, including Cep131 (Staples et al, 2012), CCDC13 (Staples et al, 2014), MRNIP/C5orf45 (Staples et al, 2016), EBLN1 (Myers et al, 2016) and CDK18 (Barone et al, 2016), have revealed roles for these proteins in maintenance of genome stability. An additional RNAi screen aimed to identify genome maintenance factors by monitoring the phosphorylation of the ATM substrate KAP1 to indicate the activation of a DNA damage response. Hits from this initial screen were then validated by examining γH2AX foci formation. This screen identified SMARCAL1 as a genome maintenance factor and subsequent work demonstrated that it acts at stalled replication forks to prevent the formation of replication stress associated DNA damage. Cells lacking this protein were also shown to display increased levels of phosphorylated RPA and sensitivity to the replication stress inducing agents HU, Aphidicolin and Camptothecin (Bansbach et al, 2009).

Several screening projects have also set out to directly identify novel replication stress response genes. A HU sensitivity screen, which utilised Dharmacon's druggable genome library, identified CDK9 as a replication stress response gene by assessing cell number following gene knockdown (Yu et al, 2010). Further study of this protein revealed that its loss increased DNA damage signalling and prevented recovery from replication stress.

CDK9 in complex with Cyclin K amasses on chromatin following replication stress where it is thought to prevent the formation of excess ssDNA, potentially through its interaction with ATR. A similar study was carried out to identify genes whose loss sensitised cells to the effects of Gemcitabine using an RNAi library of nuclear genes and assessing cell viability following knockdown. They identified NEK9, whose knockdown resulted in DNA damage accumulation, RPA foci formation and impeded the activity of Chk1 in response to replication stress (Smith et al, 2015). Kavanaugh *et al.* carried out a screen to identify proteins whose loss impaired replication restart following the induction of replication stress. Cells were stained with BrdU to assess endogenous levels of DNA replication and subsequently treated with HU for 24 hours. This was then removed and the cells were labelled with EdU to determine ongoing DNA replication and stained with γH2AX antibodies to measure levels of DNA damage. Any gene whose loss affected endogenous replication stress levels, and therefore resulted in low BrdU incorporation, were discounted from this study. The ratio of γH2AX to EdU intensity was calculated for the remaining genes to determine how they affected restart following HU treatment. Cells with impaired restart contained low levels of EdU and high levels of γH2AX and were considered replication stress response genes. This included genes involved in DNA replication and repair, RNA transcription and processing and protein ubiquitination (Kavanaugh et al, 2015).

1.4.2.3 Aims and Hypothesis

As genome wide RNAi screens have been demonstrated to be a successful method for the detection of genome maintenance factors, it was decided to develop an siRNA screen with the intention of identifying novel suppressors of replication stress. Working under the hypothesis that as yet unidentified regulators of replication stress exist within the genome and that their knockdown would increase levels of RPA2 phosphorylation, attempts were made to optimise a high throughput immunofluorescence based screening assay. No screen had previously been developed that utilised immunofluorescence alone and solely quantified the endogenous levels of replication stress. However, when this proved unfeasible the assay was repurposed as a smaller scale targeted screen. This screen aimed to identifying genes whose loss increased phosphorylation of RPA2 from a list of kinases that had been demonstrated to affect replication restart in the Kavanaugh screen. This approach successfully identified hits that were assessed for their ability to sensitise cells to p53 deficiency, oncogene overexpression and replication stress inducing therapies.

During the optimisation of the replication stress suppressor screens, efforts were also made to characterise the prospective replication stress regulating gene CCDC15. This gene had been identified as a prospective genome maintenance factor in the Collis γH2AX screen and bioinformatic analysis had predicted it was involved in the repair of replication impeding lesions. It was therefore hypothesised that it may act as a novel suppressor of replication stress. The objective of this investigation was to characterise the phenotype of CCDC15 deficient cells with regards to the DNA damage and replication stress response. Tagged versions of this protein were also generated to assess its subcellular localisation

(YFP) and to assess potential interactions with DNA damage repair proteins by immunoprecipitation and mass spectrometry approaches.

Chapter Two:
Materials and Methods

TABLE OF FIGURES 62

2.1 MATERIALS 63

2.1.1 STANDARD EQUIPMENT AND CONSUMABLES 63

2.1.2 REAGENTS 65

2.1.2.1 CELL LINES 68

2.1.2.2 siRNAs 71

2.1.2.3 PRIMARY ANTIBODIES 72

2.1.2.4 SECONDARY ANTIBODIES 72

2.1.2.5 PRIMERS AND PROBES 73

2.1.2.6 VECTORS 74

2.1.2.7 SOFTWARE 74

2.1.3 STANDARD SOLUTIONS 74

2.2 METHODS 76

2.2.1 MAMMALIAN CELL BIOLOGY 76

2.2.1.1 PASSAGING CELLS 76

2.2.1.2 siRNA TRANSFECTION 76

2.2.1.3 CHEMOTHERAPY AND SMALL MOLECULE DRUG TREATMENTS 76

2.2.1.4 IMMUNOFLUORESCENCE 77

2.2.1.5 MTT COLORIMETRIC ASSAY 78

2.2.1.6 CLONOGENIC SURVIVAL ASSAY 78

2.2.1.7. ALKALINE COMET ASSAY 79

2.2.1.8 PROPIDIUM IODIDE FLOW CYTOMETRY 80

2.2.1.9 CELL SYNCHRONISATION 80

2.2.1.10 MICRO-IRRADIATION INDUCED LOCALISATION OF DNA DAMAGE 80

2.2.2 MOLECULAR BIOLOGY 81

2.2.2.1 WESTERN BLOTTING 81

2.2.2.2 RNA EXTRACTION 82

2.2.2.3 REVERSE TRANSCRIPTION 83

2.2.2.4 REVERSE-TRANSCRIPTION PCR (qPCR) 83

2.2.2.5 POLYMERASE CHAIN REACTION (PCR) 84

2.2.2.6 AGAROSE GEL ELECTROPHORESIS 85

2.2.2.7 BACTERIAL TRANSFORMATION AND PLASMID ISOLATION 85

2.2.2.8 STABLE CELL LINE GENERATION BY GATEWAY CLONING 86

2.2.2.9 IMMUNOPRECIPITATION 88

Table of Figures

Figure 2.2.1.7.1 RPE-1 Clonogenic Survival Assay Plates. 79
Figure 2.2.2.1.1 Standard Curve Generated from BSA Titration. 81
Figure 2.2.2.14.1 Gateway Cloning of CCDC15 87

2.1 Materials

2.1.1 Standard Equipment and Consumables

Airstream ESCO Class II BSC
Applied Biosystems 3730 DNA Analyser
Applied Biosystems 7900 Real-Time PCR
BD FACSCalibur™
BD Plastipak™ 10ml Syringe
Bio-Rad mini-PROTEAN Tetra Cell
Bio-Rad S1000 Thermal Cycler
Biosphere® Filter Tips 0.1-10µl, 2-20µl, 2-100µl, 100-1000µl
BioTek Elx405 Select CW Plate Washer
Cellstar ® Cell Culture Dishes 100x20mm
Corning 50ml Reagent Reservoir
Costar 24 Well Tissue Culture Treated Plates
Costar 96 Well Tissue Culture Treated Plates
CytoOne Multiwell Plate, 6 well
Eppendorf Centrifuge 5430
Eppendorf Centrifuge 5810 R
Eppendorf Centrifuge S415 R
Epson Expression 1680 Pro Scanner
Fisher Scientific FB15-12 TopMix
Fisher Scientific MH-214 Analytical Balance
Fisher Scientific SG-607 Analytical Balance
FisherBrand™ 5ml, 10ml and 25ml Disposable Serological Pipettes
Fisherbrand™ Electric Pipet Controller
FisherBrand™ Midi Plus Horizontal Gel System
FisherBrand™ Syringe Filter PES 0.2µm sterile
Fujifilm Fuji Medical X-ray Film Super RX
GE NanoVue Plus
Gilson P10, P20, P200 Multichannel Pipettes
Gilson P2, P10, P20, P200 and P1000 Pipettes
Grant JB Aqua 18 Plus
Ibidi µ-Dish 53mm High
Konica Mibolta SRX101A
Labnet 311DS Shaking Incubator
Life Technologies Countess II
Microplate 384 well PP PCR with skirt, Greiner Bio-one
Millex Filter Unit 33mm
MJ Research PTC-200 Peltier Thermal Cycler
Molecular Devices ImageXpress Micro High Content Microscope
Nanodrop ND 1000 Spectrophotometer
Nikon Eclipse TE200 Inverted Microscope

Olympus IX81 Motorised Microscope
Perkin Elmer UltraView VoX Spinning Disk Confocal
Perkin Elmer ViewPlate-384 Black, Optically Clear Bottom, Tissue Culture Treated
PlateLoc Velocity 11
Sanyo MCO-19AIC (UV)
Sarstedt Cell Scraper 25cm
Sarstedt P200, P1000 Pipette Tips
SLS 15ml/50ml polypropylene tubes
Star Lab 8-strip PCR Tubes, 0.2ml & Caps
StarSeal Advanced Polyolefin Film
Sterilin Universal Tubes
Stuart® Mini Gyro-rocker
Stuart® Rotator SB3
Syngene U:GENIUS
Techne Dri-Block® DB-2D
Thermo Megafuge 40
Thermo Multidrop 384
Thermo Multiskan FC
Thermo Nunc™ EasYFlask™ 25cm^2 Nunclon™ Delta Surface
Thermo Nunc™ EasYFlask™ 75cm^2 Nunclon™ Delta Surface
Thermo Scientific Multidrop Combi
Thermo Scientific Nuclon™ Delta Surface, 6 well plate
ThermoScientific Sterilin Single Use Plastic Petri Dishes
UV Transilluminator, UVP Incoporated
UVP CX-200 UV Crosslinker
VWR 13mm Microscope Cover Glasses
Walker Safety Cabinet Class II MSC (Model TDA-2G)
Welch 2515C-75 REV A
XCell SureLock™ Mini-Cell Electrophoresis System

2.1.2 Reagents

1,4-dithiothreitol (DTT): Sigma DTT-RO

1,4-Piperazinediethanesulfonic acid (PIPES): Sigma, P6757

3X FLAG® Peptide: Sigma, F4799

5-Flurouracil: Sigma, F6627

AccuPrime™ DNA Polymerase: ThermoFisher, 12346068

AccuPrime™ GC Rich DNA Polymerase: ThermoFisher, 12337016

Acetic Acid, Glacial: Fisher Scientific, A38-212

Acetone: Fisher Scientific, A18P-4

Agar Granulated: Melford, GM1002

Agarose Gel Loading Dye 6X: Fisher Scientific, RO611

Ampicillin: Melford, A0104

ANTI-FLAG® M2 Affinity Gel: Sigma, A2220

Benzonase Nuclease: Novagen, 70664-3

BioRad Protein Assay Dye Reagent Concentrate: BioRad, 500-0006

BioScript: BioLine, BIO-27036

Blasticydin: InvivoGen, ant-bl-1

Bovine Serum Albumin (BSA): Sigma, A2153

BrdU: Sigma, B5002

Bromophenol Blue: Sigma, B10126

Calcium Chloride: Sigma 499609

Cisplatin: Sigma, P4394

CometAssay® Kit (25 x 2 well slides): Trevigen 4250-050-K

DAPI: Life Technologies, D1306

DH5α™ Competent Cells: ThermoFisher, 18265017

DharmaFECT 1: GE Healthcare, T-2001-01

Dimethyl Sulfoxide (DMSO): Fisher Chemical, D/4120/PB08

Dulbecco's Modified Eagle Medium (DMEM): Lonza, BE12-604F

Edetic Acid (EDTA): Sigma, 1233508

Ethanol: Fisher Scientific, AC615090010

Ethidium Bromide: Sigma, 160359

Fetal Calf Serum: Lonza, BE12-60F4

G418: Sigma, G8168-10ML

Gateway® BP Clonase® II Enzyme Mix: ThermoFisher. 11789020

Gateway® LR Clonase® II Enzyme Mix: ThermoFisher. 11791043

Gemcitabine Hydrochloride: Sigma, G6423

Glycerol: Sigma, G5516

Hi-Res, Low Melt AGAROSE: GeneFlow, AG LM2-100gm

High-Capacity RNA-to-cDNA™ Kit: ThermoFisher, 4387406

Hoechst 33342 Trihydrochloride, Trihydrate: Life Technologies, H3570

Hydrochloric Acid (HCl) 37%: Fisher Sceintific A144-500LB

Hydroxyurea (HU): Sigma, H8627

Hyperladder 1: SLS, BIO-33053
Hyrgromycin: Sigma, 10843555001
Immu-Mount: Thermo Scientific, 99-904-02
Isopropanol: Fisher Scientific, A416-4
Kanamycin: Melford, K0126
KOD Hot Start DNA Polymerase: Sigma, 71086-3
KU55933: Generon, SK-KU55933
LB Agar: Melford, GL1706
LB Broth: Miller Large Granules: Fisher, 1289-1650
Lipo 2000: ThermoFisher,11668019
Lipofectamine RNAiMAX Transfection Reagent: Life Technologies, 13778030
Magnesium Chloride: Sigma, M8266
Marvel Milk Powder
Methanol: Fisher Scientific, A452SK-4
Methylene Blue: Sigma Aldrich, M9140
Mitomycin C (MMC): Sigma, M0503
MTT (3-(4,5-dimethylthiazol-2-yl)-2,5-diphenyltetrazolium bromide): Sigma, M2128
NuPAGE® LDS Sample Buffer (4X): ThermoFisher, NP007
NuPAGE® MOPS SDS Running Buffer (20X): ThermoFisher, NP001
NuPAGE® Transfer Buffer (20X): ThermoFisher NP0006
NuPAGE™ 4-12% Bis-Tris Protein Gels, 1.5mm, 10 well: ThermoFisher, NP0335BOX
NuPAGE™ 4-12% Bis-Tris Protein Gels, 1.5mm, 15 well: ThermoFisher, NP0336BOX
Olaparib: Generon, A10111
Oxoid PBS tablet: Thermo Scientific, Cat. No. BR0014
Paraformaldehyde (PFA) solution 4% in PBS: Sanat Cruz, SC-281692
PerfectPure RNA Cultured Cell Kit: 5 Prime, 2302340
Phosphatase Inhibitor: Sigma, P5726
PIB: Sigma, P2714
Pierce ECL Western Blotting Substrate: Thermo Scientific, 32106
Pifithrin-α (PFT-α) HBr: Tocris, 1267
Platinum™ Hot Start PCR Mastermix (2X): ThermoFisher, 13000012
Potassium Chloride: Sigma, P9333
Propidium Iodide: Sigma, P4170
Protran Nitrocellulose Membrane: VWR, 732-4016
Puromycin: Fisher, VXA1113803
QAIshredder (50): Qiagen, 79654
Qiagen Oligotex Direct mRNA Mini Kit: Qiagen, 72022
Qiagen Rneasy Mini Kit: Qiagen 74104
QIAprep Spin Miniprep Kit: Qiagen, 27104
QIAquick Gel Extraction Kit (50): Qiagen, 28704
QIAquick PCR Purification Kit: Qiagen, 28104,
RNaseA: Sigma, R6513

Roscovitine: Generon, 1950-5

RPMI 1640 with L-Glutamine: Lonza, BE12-702F

RT² First Strand Kit: Qiagen, 330401

SeeBluePlus2 Prestained Standard: ThermoFisher, LC5925

Sodium Chloride: Sigma, S7653

Sodium Citrate: Sigma, 1613859

Sodium Dodecyl Sulphate (SDS): Sigma, L3771-500G

Sodium Hydroxide (NaOH) Pellets: Sigma, 1.06462 EMD

Sucrose: Sigma, S7903

SYBR® Gold Nucleic Acid Gel Stain (10,000X Concentrate in DMSO): ThermoFisher, S11494

TaqMan Reverse Transcription Reagents: Thermo Scientific, N8080234

TaqMan Universal PCR Master Mix No AmpErase UNG: ThermoFisher, 4324018

Tet System Approved FBS: Clontech, 631106

Tetracyclin: Sigma, 87128

Tris Base: Sigma, TRIS-RO

Tris Hydrochloride: Sigma 10812846001

Triton™ X-100: Sigma, X100 SIGMA-ALDRICH

Trypsin (0.5g/l trypsin, 0.2g/l versene (EDTA)): Lonza, 17-161E

TWEEN® 20: Sigma, P1379

Visualiser™ Western Blot Detection Kit: Fisher Scientific, 10553414

Zeocin: Melford, Z0186

β-Mercaptoethanol: Fisher, M/P200/05

2.1.2.1 Cell Lines

Cell Line	Origin	Supplier	Split Ratio	Plating Densities (cells/well)	Transfection Time (Hours)
HCT116	Colorectal Carcinoma	ATCC	1:10 twice weekly	200 000 (6well)	48/72
				20 000 (24 well)	48/72
				750* (96 well)	48
				1000* (384 well)	48/72
HCT116 p53 Null	Colorectal Carcinoma (Hygromycin and Neomycin Resistance genes in place of p53)	Meuth Lab	1:10 twice weekly	200 000 (6 well)	48
				20 000 (24 well)	48
				750* (96 well)	48
HCT116 H-RAS	Colorectal Carcinoma (H-RAS in pCAG-Flox)	ATCC (plasmid from Meuth lab)	1:10 twice weekly	750 (96 well)	48
				200 000 (6 well)	48
HEK 293 FLP	Embryonic Kidney (FRT site)	Thermo Fisher	1:15 twice weekly	3 000 000 (14cm dish)	N/A
				1 500 000 (10cm dish)	N/A
				350 000 (6 well)	N/A
HeLa	Cervix Epithelia	ATCC	1:10 twice weekly	150 000 (6 well)	48/72/96
				30 000 (24 well)	48/72
				1000 (96 well)	72
HeLa EGFP-RPA2	Cervix Epithelia (C-terminal EGFP-RPA2)	Boulton Lab	1:10 twice weekly	30 000 (24 well)	72
HeLa FLP	Cervix Epithelia (FRT site)	ATCC (FRT site incoportaed in Boulton Lab)	1:10 twice weekly	1 000 000 (10cm dish)	N/A
				300 000 (6 well)	N/A
IMR-32	Neuroblastoma Abdominal Metastasis	ATCC	1:10 twice weekly	200 000 (6 well)	48
				1500 (96 well)	48
MRC-5	Foetal Lung Fibroblast	ATCC	1:10 twice weekly	150 000 (6 well)	48
				1000 (96 well)	48

MRC-5 H-RAS	Foetal Lung Fibroblast (H-RAS in pCAG-Flox)	ATCC (plasmid from Meuth lab	1:10 twice weekly	150 000 (6 well)	48
				1000 (96 well)	48
PC-3	Prostate Adenocarcinoma Bone Metastasis	ATCC	1:10 twice weekly	150 000 (6 well)	48/72/96
				30 000 (24 well)	48/72
				500 (96 well)	72
RPE-1	Retinal Epithelial (hTERT)	ATCC	1:7 twice weekly	50 000 (6 well)	72
				15 000 (24 well)	48/72
				500 (96 well)	72
RPE-1 FUCCI	Retinal Epithelial (hTERT) with FUCCI system	Medema Lab	1:7 twice weekly	15 000 (24 well)	72
SH-EP1	Neuroblastoma Bone Marrow Metastasis	ATCC	1:5 twice weekly	400 000 (6 well)	48
				3000 (96 well)	48
SH-EPTet21N	Neuroblastoma Bone Marrow Metastasis (Tet-repressible MYC-N)	Bryant Lab	1:5 twice weekly	400 000* (6 well)	48
				1500* (96 well)	48
SW480	Colorectal Adenocarcinoma	ATCC	1:10 twice weekly	300 000 (6 well)	48
U2OS	Osteosarcoma	ATCC	1:7 twice weekly	100 000 (6 well)	48
				20 000 (24 well)	48
U2OS Cyclin E	Osteosarcoma (Tet-repressible Cyclin E)	Petermann Lab	1:10 twice weekly	100 000 (6 well)	48
				900* (96 well)	48

Table 2.1.2.1.1 Mammalian Cell Lines.
Asterisk (*) demonstrates the plating density unless stated otherwise

The HCT116 H-RAS and MRC-5 H-RAS cells required culturing in 1μg/ml Puromycin to ensure the cells maintained the RAS overexpression phenotype as the pCAG-FLOX vector, a kind gift from Professor M. Meuth, contains a Puromycin resistance gene.

Before transfection, the HeLa FLP and HEK 293 FLP cells required culturing in Blasticidin and Zeocin to prevent the reversion to a wild type phenotype. Once the cells had been transfected with a FRT Destination vector (2.2.2.17), the cells required culturing in Blasticidin and Hygromycin to select for the transfected vectors (Table 2.1.2.1.2). These vectors required the cells to be cultured in 1μg/ml Tetracycline to induce expression.

Cell Line	Transfection Status	Blasticidin (μg/ml)	Zeocin (μg/ml)	Hygromycin (μg/ml)
HeLa FLP	Pre-transfection	4	50	NA
	Post-transfection	4	NA	200
HEK 293 FLP	Pre-transfection	15	100	NA
	Post-transfection	15	NA	150

Table 2.1.2.1.2 FLP Cell Line Culture Conditions.

The Fluorescence Ubiquitination Cell Cycle Indicator (FUCCI) system allows the direct visualisation of the stage a cell is in within the cell cycle through the fluorescent labelling of the DNA replication factor Cdt1 and the DNA replication inhibitor Geminin. This system was incorporated into RPE-1 cells which were a kind gift from Professor R. Medema (Netherlands Cancer Institute) (Slaats et al, 2014).

The ShepTet21N cells overexpressed MYC-N in a Tetracycline-repressible manner. The cells were cultured in RPM1 1640 with Tetracycline free foetal calf serum (FCS) to induce MYC-N overexpression. The cells were passaged 48 hours prior to plating to create two populations, a MYC-N overexpressing population and a MYC-N normal population, where 1μg/ml Tetracycline was added to the cells.

The U2OS cells with Tetracycline-repressible Cyclin E overexpression, a gift from Dr E. Petermann (University of Birmingham), required culturing in 1μg/ml Puromycin, 2μg/ml Tetracycline and 400μg/ml G418 to prevent the loss of the Cyclin E overexpression phenotype. The cells were plated in DMEM containing 10% Tetracycline free FCS to induce Cyclin E overexpression. Four hours after plating, 2μg/ml Tetracycline was added to half the cells to repress Cyclin E overexpression to allow comparison between the two conditions. Cells were transfected 24 hours after plating.

2.1.2.2 siRNAs

siRNA	Source	Sequence
SMARTpool: ON-TARGETplus ATR siRNA	Eurofins	GAACAACACUGCUGGUUUGUU GGUCAGCUGUCUACUGUUAUU GCAACUCGCCUAACAGAUAUU ACUGAUGGCUGAUUAUUUAUU
CCDC15 siRNA 1	Eurofins	UGCCAGAAGCCCAGGAU
CCDC15 siRNA 2	Eurofins	GAUAAGAAAGAGCGUCA
CCDC15 siRNA 3	Eurofins	CCGAAAGAAACCUCGAA
CCDC15 siRNA 4	Eurofins	GAAACAAGUUAAAUACC
ON-TARGETplus Non-targeting Pool	Dharmacon, D-001810-10	
ON-TARGETplus Non-targeting siRNA #1	Dharmacon, D-001810-01	UGGUUACAUGUCGACUAA
ON-TARGETplus Non-targeting siRNA #2	Dharmacon, D-001810-02	
ON-TARGETplus Non-targeting siRNA #3	Dharmacon, D-001810-03	
ON-TARGETplus Non-targeting siRNA #4	Dharmacon, D-001810-04	
PMVK siRNA 1	Eurofins	CCAUCUGGCUGGUGAGUGA
PMVK siRNA 2	Eurofins	GGUGGACGAUGCUGAGUCA
PMVK siRNA 3	Eurofins	GCAGACGGUCCGCGUUGUA
PMVK siRNA 4	Eurofins	GGAAGGACAUGAUCCGCUG
SMARTpool: ON-TARGETplus CCDC15 siRNA	Dharmacon, L-014545-02	UGCCAGAAGCCCAGGAU GAUAAGAAAGAGCGUCA CCGAAAGAAACCUCGAA GAAACAAGUUAAAUACC
SMARTpool: ON-TARGETplus CHEK1 siRNA	Dharmacon, L-003255-00	CCAGAUGUGUGGUACUUUA GAGAAGGCAAUAUCCAAUA CCACAUGUCCUGAUCAUAU GAAGUUGGGCUAUCAAUGG
SMARTpool: ON-TARGETplus RPA2 siRNA	Dharmacon, L-017058-01	AACAUGAAGUUCUGCGGUA UGGAACAGUGGAUUCGAAA GAGCAGGACCAGGGCGUUA GGAAGUAGGUUUCAUCUAU
SMARTpool: ON-TARGETplus RRM1 siRNA	Dharmacon, L-004270-00	UAUGAGGGCUCUCCAGUUA UGAGAGAGGUGCUUUCAUU UGGAAGACCUCUAUAACUA CUACUAAGCACCCUGACUA
SNRK siRNA 1	Eurofins	GCUACAAAGUAUAACAUUC
SNRK siRNA 2	Eurofins	GGGAGCACCAAGUACAUUA
SNRK siRNA 3	Eurofins	GAAGUGAGAUGCAUGAAAC
SNRK siRNA 4	Eurofins	GCUCAGAUAGUUCAUGCUA

Table 2.1.2.2.1 siRNA for Mammalian Cell Line Transfection.

The siRNAs included in the Targeted Screen are listed in Appendix 1.

2.1.2.3 Primary Antibodies

Antibody	Species	Source	Dilution
53BP1	Rabbit	AbCam (ab368823)	1:1000
Chk1	Mouse	Sigma (C9358)	1:2000
Chk2	Rabbit	Cell Signalling (2662S)	1:1000
Cyclin E	Mouse	Santa Cruz (sc-247)	1:1000
FANCD2	Mouse	AbCam (ab12450)	1:250,
FANCD2	Rabbit	AbCam (ab2187)	1:250 (IF),1:1000 (Western)
FLAG M2	Mouse	Sigma (F3165)	1:1000
GFP	Rabbit	AbCam (ab290)	1:1000 (IF and Western)
MYC-N	Mouse	Santa Cruz (sc-53993)	1:250
p53	Rabbit	Cell Signalling (9289)	1:1000
pChk1 (Serine 317)	Rabbit	Cell Signalling (2344S)	1:1000
pChk2 (Threonine 68)	Rabbit	Cell Signalling (2197S)	1:1000
pRPA2 (Serine 33)	Rabbit	Bethyl (A300-246A)	1:1000
pRPA2 (Serine 4/8)	Rabbit	Bethyl (A300-245A)	1:250
pRPA2 (Threonine 21)	Rabbit	AbCam (ab61065)	1:250 (IF)*, 1:1000 (Western)
RAD51	Rabbit	Santa Cruz (sc-8349)	1:500
RPA2	Mouse	Calbiochem (NA19L)	1:1000 (IF), 1:2000 (Western)
RRM1	Rabbit	Cell Signalling (3388S)	1:1000
TopBP1	Rabbit	AbCam (ab2402)	1:500*
RAS	Rabbit	Cell Signalling (3339S)	1:1000
β-Actin	Mouse	AbCam (ab8226)	1:2000
β-Tubulin	Mouse	AbCam (ab7797)	1:2000
ϒ-H2AX (S139)	Mouse	Millipore (05-636)	1:1000
ϒ-H2AX (S139)	Rabbit	Cell Signalling (25755)	1:500

Table 2.1.2.3.1 Primary Antibodies for Immunofluorescence and Western Blotting

Asterisk (*) demonstrates the concentration unless stated otherwise.

2.1.2.4 Secondary Antibodies

Antibody	Source	Dilution
Alexa Fluor® 488 goat anti-rabbit IgG	Life Technologies (A-11034)	1:1000
Alexa Fluor® 488 goat anti-mouse IgG	Life Technologies (A-11001)	1:1000
Alexa Fluor® 594 goat anti-mouse IgG	Life Technologies (A-11032)	1:1000
Alexa Fluor® 594 goat anti-rabbit IgG	Life Technologies (A-11012)	1:1000
Polyclonal Goat Anti-mouse IgG/HRP	Dako (P0447)	1:2000
Polyclonal Swine Anti-rabbit IgG/HRP	Dako (P0399)	1:2000

Table 2.1.2.4.1 Secondary Antibodies for Immunofluorescence and Western Blotting

2.1.2.5 Primers and Probes

Primer	Source	Sequence
CCDC15 Forward	Sigma	ATGCTGGGAAGTATGGCCCG
CCDC15 Reverse	Sigma	TTATAGATTTTTCAAAGTCCG
CCDC15 Gateway Forward	Sigma	GGGGACAAGTTTGTACAAAAAAGCAGGCT TGCTGGGAAGTATGGCCCGAAAGAAA
CCDC15 Gateway Reverse	Sigma	GGGGACCACTTTGTACAAGAAAGCTGGGT TTATAGATTTTTCAAAGTCCGCCTGT
CCDC15 Gateway Short Forward	Sigma	GGGGACAAGTTTGTACAAAAAAGCAGGCT TGCTGGGAAGTATGGCCCG
CCDC15 Gateway Short Reverse	Sigma	GGGGACCACTTTGTACAAGAAAGCTGGGT TTATAGATTTTTCAAAGTC
CCDC15 Gateway Long Forward	Sigma	GGGGACAAGTTTGTACAAAAAAGCAGGCT TGCTGGGAAGTATGGCCCGAAAGAAACCTC
CCDC15 Gateway Long Reverse	Sigma	GGGGACCACTTTGTACAAGAAAGCTGGGT TTATAGATTTTTCAAAGTCCGCCTGTGTGC
CCDC15 Seq F1	Sigma	ACCTGCCTCACCAGGTAGTT
CCDC15 Seq R1	Sigma	AACTACCTGGTGAGGCAGGT
CCDC15 Seq F2	Sigma	CTCCATAGCC ATGCAGTCTT
CCDC15 Seq F3	Sigma	ATCTCTTGTAACTGATGAGA
CCDC15 Seq F4	Sigma	CACAAATCAGGCTCTTCTAA
CCDC15 Seq F5	Sigma	ATTTTCTACCCAGAGACCAA
CCDC15 Seq F6	Sigma	CAAGCATATCAAACTACCCT
CCDC15 Seq F7	Sigma	CGAGCCCAAATCCAGGAGAA
CMV Seq Forward	Sigma	CGCAAATGGGCGGTAGGCGTG
YFP Seq Forward	Sigma	AGCTCGCCGACCACTACCAG
M13 Seq Forward	Sigma	TGTAAAACGACGGCCAGT

Table 2.1.2.5.1 Primers for PCR and DNA Sequencing
Underlined letters in Gateway Primers represent the attB sites required for Gateway Cloning.

The Gateway primers were designed to include *attB* sites, so following PCR amplification, these sites would flank the CCDC15 coding sequence. As the aim was to N-terminally tag CCDC15, the start codon had to be modified (removal of the adenine) to keep the tag in frame with the gene. No alterations were made to the stop codon.

Probe	Source
GAPDH	ThermoFisher, Hs02758991_g1
18S	ThermoFisher, Hs3003631_g1
CCDC15	ThermoFischer, Hs00228050_m1
SNRK	ThermoFIsher, Hs00299395_m1
PMVK	ThermoFisher, Hs01014319_m1

Table 2.1.2.5.2 TaqMan Probes for Quantitative PCR

2.1.2.6 Vectors

CCDC15 pcDNA3.1+C-(K)-DYK Vector, GenScript

pDONR™221, LifeTechnologies, (12536-017)

pcDNA™5/FRT/TO N-Terminal FLAG, modified from vector by Invitrogen (V6520-20) to include an N-terminal FLAG tag and be gateway cloning compatible (Boulton lab)

pcDNA™5/FRT/TO N-Terminal YFP, modified from vector by Invitrogen (V6520-20) to include an N-terminal YPF tag and be gateway cloning compatible (Boulton lab)

pOG44 Flp-Recombinase Expression Vector, Thermo Fisher V600520

2.1.2.7 Software

CometScore™ v 1.5, TriTek

FlowJo™, LLC

Image J 1.48v, National Institutes of Health

MetaXpress®, Molecular Devices

Prism 7, GraphPad Software Inc.

SDS 2.4, ThermoFisher

Sequencher 4.7, Gene Codes Corporation

Volocity® 6.1.1, PerkinElmer

2.1.3 Standard Solutions

0.5% Triton X-100, 3% BSA: 2.5ml Triton X-100 and 15g BSA dissolved in 500ml PBS

0.75% Triton X-100, 3% BSA: 3.75ml Triton X-100 and 15g BSA dissolved in 500ml PBS

1% Agarose Gel: 1g Agarose and 2µl Ethidium Bromide in 100ml 1X TAE

1% SDS (w/v): 5g SDS dissolved in 500ml ddH_2O

1% Triton X-100: 5ml Triton X-100 dissolved in 500ml ddH_2O

10X TBS pH 7.6 24.2g Tris, 80g NaCl in 500ml ddH_2O

1M $CaCl_2$: 55.49g $CaCl_2$ dissolved in 500ml ddH_2O

1M Hydrochloric Acid (HCl): 8.3ml 37% HCL in 91.7ml ddH2O

1M KCl: 37.28g KCl dissolved in 500ml ddH_2O

1M $MgCl_2$: 47.6g $MgCl_2$ dissolved in 500ml ddH_2O

1M PIPES pH 6.8: 151.19g PIPES dissolved in 500ml ddH_2O

1M Sucrose: 171.15g Sucrose dissolved in 500ml ddH_2O

1M Tris-HCl pH 7.5: 157.6g Tris-HCl dissolved in 1 litre ddH_2O

1mM DTT: 154mg dissolved in 1l ddH_2O

1mM EDTA pH 8: 292mg dissolved in 1l ddH_2O

200mM NaCl: 5.84 g NaCl dissolved in 500ml ddH_2O

3% BSA in PBS: 15g BSA dissolved in 500ml PBS

5% Marvel Milk: 10g Marvel milk powder dissolved in 200ml PBSt

500mM EDTA pH 8: 146.12g EDTA dissolved in 1 litre ddH_2O

500µg/ml Propidium Iodide: 25mg Propidium Iodide in 50ml PBS

50mM Tris Base pH 8: 6.06g Tris Base dissolved in 800ml ddH_2O, pH adjusted to 8 with concentrated HCL – solution made up to 1l with ddH_2O

50X TAE: 242g Tris Base, 57.1ml Acetic Acid, 100ml 500mM EDTA in 1 litre ddH_2O

5M NaCl: 146.1g NaCl dissolved in 500ml ddH_2O

70% Ethanol: 700ml Ethanol, 300ml ddH2O

Acetone Blocking Buffer: 1.5g BSA, 88.2g Sodium Citrate, pH to 7 with HCl

Agar: 15g Granulated Agar, 25g LB in 1l ddH_2O

Alkali Unwinding Solution: 0.8g NaOH pellets, 500µl 200mM EDTA (from kit), 99.5ml ddH_2O

Cold Pre-extraction Buffer: 500ml 200mM NaCl, 300ml 1M sucrose, 3ml 1M $MgCl_2$, 10ml 1M PIPES pH 6.8, 5ml Triton X-100-100

COMET electrophoresis solution: 8g NaOH pellets, 1ml 500mM EDTA pH 8 dissolved in 1l ddH_2O

IP Wash Buffer: 100µl 50mM Tris Base, 80µl 200mM NaCl, 20µl 1% Triton X-100, 4µL 1mM EDTA, 200µl PIB, 20µl Phosphatase inhibitor dissolved in 1.6ml ddH_2O

KCM: 500ml 1M KCL, 150ml 1M $CaCl_2$, 250ml 1M $MgCl_2$ dissolved in 500ml ddH_2O

LB Broth: 25g LB in 1 litre ddH_2O

Lysis Buffer: 100µl 50mM Tris Base, 80µl 200mM NaCl, 20µl 1% Triton X-100, 2µl 1mM DDT, 4µL 1mM EDTA, 4µL 50U/µl Benzonase, 200µl PIB, 20µl Phosphatase inhibitor dissolved in 1.6ml ddH_2O

Methylene Blue (0.4%): 2g Methylene Blue dissolved in 500ml 70% methanol

NuPage MOPS SDS Running Buffer: 50ml NuPage MOPS SDS Running Buffer (20X), 950ml ddH2O

NuPage Transfer Buffer: 50ml NuPage Transfer Buffer (20X), 200ml Methanol, 750ml ddH20

PBS-Tween 20: 1ml Tween 20 dissolved in 500ml PBS

PBS2t: 1.25ml Tween 20 and 2.5g Bovine Serum Albumin (BSA) dissolved in 500ml PBS

PBSt: 500µl Tween 20 dissolved in 500ml PBS

Phosphate Buffered Saline (PBS): 1 Oxoid PBS tablet (Cat. No. BR0014) dissolved in 100ml deionised water before autoclave sterilisation

SYBR Gold Comet Stain: 1µl SYBR Gold (X 10 000) in 30ml TE Buffer

TE Buffer: 10 ml 10mM Tris-HCl pH 7.5, 2ml 1mM EDTA dissolved in 1 litre ddH_2O

2.2 Methods

2.2.1 Mammalian Cell Biology

2.2.1.1 Passaging Cells

All mammalian cell lines (Table 2.1.2.1.1) were cultured in T75 flasks at 37°C and 5% CO_2 in DMEM supplemented with 10% FCS. The exceptions were IMR-32, which were cultured in a 50:50 mix of DMEM and RPMI 1640 with 10% FCS, and ShepTet21N cells, which were cultured in RPM1 1640 supplemented with 10% Tetracycline Free FCS. The cells were allowed to reach 80-90% confluence before passaging. The flasks were rinsed with 10ml PBS before the addition of Trypsin and once the cells had detached from the flask they were re-suspended in fresh 10% FCS DMEM. This cell suspension was pelleted at 200 x *g* for 3 minutes and the pellet was re-suspended in fresh 10% FCS DMEM. These cells were transferred to new flasks containing fresh 10% FCS DMEM with a dilution as stated in Table 2.1.2.1.1. Cells were mycoplasma tested on a bi-monthly basis to ensure that the cells were free of contamination.

2.2.1.2 siRNA Transfection

Cells were transfected with siRNA to abolish the expression of a gene of interest through the steric hindrance of the mRNA. Cells were seeded at densities stated previously, with HCT116 and HCT116 p53 Null cells being passaged with 1:2 dilution the day before plating. Cells were forward transfected (cells plated and then transfected), unless specified otherwise, with non-targeting or gene targeting siRNAs with a final concentration of 30nM. Lipid transfection reagents were utilised to deliver the siRNA to the cell's interior with. Primarily, DharmaFECT 1 was the chosen transfection reagent, with the exception of the earliest Screening Development (Chapter 3) assays where RNAiMAX was used, at concentrations specified in Table 2.2.1.3.1. Cells were transfected for 48, 72 or 96 hours as stated in Table 2.1.2.1.1.

Reagent	Plate Type	Concentration (µl/well)
RNAiMAX	24 well	0.5
DharmaFECT 1	6 well	0.5
	24 well	0.2
	96 well	0.05
	384 well	0.01*

Table 2.2.1.3.1 Transfection Reagent Concentrations in Different Assay Formats.
Asterisk (*) demonstrates the concentration unless stated otherwise.

In the Screen Development assays (Chapter 3), the media was replaced in the 24 well plates or supplemented with fresh DMEM containing 10% FCS in the 384 well plates 24 hours post-transfection to reduce the toxicity of the transfection reagents.

2.2.1.3 Chemotherapy and Small Molecule Drug Treatments

Where specified, cells were treated with the cytotoxic drugs HU, to induce replication stress, or MMC, to induce DNA interstrand crosslinks. Cells were treated with 2mM HU or 80ng/ml MMC for 16 hours before fixing or media removal. Untreated cells were mock

treatment with the same volume of PBS or ddH_2O respectively as the volume of drug administered.

To prevent entry into S phase, cells were treated with 10μg/ml Roscovitine, a small molecule CDK inhibitor (CDK1, CDK2 and CDK5), 4 hours prior to fixing to prevent DNA replication (Collis et al, 2007).

Where specified, cells were treated 24 hours after plating with the small molecule p53 inhibitor Pifithrin-α (0 - 30μM) to mimic loss of p53 function (Li et al, 2015a). The cells were then transfected 5 hours following the treatment.

2.2.1.4 Immunofluorescence

Immunofluorescent staining of fixed cells relies upon the specificity of antibodies; the primary antibodies bind to their individual antigens whilst the fluorescently conjugated secondary antibodies detect the species of the primary antibody. Transfected cells were grown in 24 well plates (with the exception of SW480 cells) on 13mm glass coverslips, which were etched for the growth of PC-3 cells to aid cell adherence. To do so, the coverslips were rinsed in distilled water and then incubated for 30 minutes in 1M HCL solution. They were then rinsed again with distilled water before incubating overnight in 100% ethanol. Each coverslip was then dried individually before baking for 4 hours to sterilise.

In the 24 well Screen Development Assays (Chapter 3), the coverslips were fixed in 4% PFA for 10 minutes before incubation with 0.5% Triton X-100, 3% BSA in PBS for 5 minutes (unless otherwise stated). The primary and secondary antibodies (Tables 2.1.2.3.1-2) were diluted in PBS2t and the coverslips were washed 3 times following fixation, extraction and antibody incubation with PBS-Tween 20. DNA was stained with 1μM DAPI which was included in the secondary antibody incubation. The coverslips were mounted on glass slides using Immu-Mount. This protocol was subsequently adapted for use in the 384 well plate screening assays. Cells were added to the plates using a Thermo Scientific Multidrop Combi, and the plates were washed as previously but using a Thermo Multidrop 384 and a BioTek Elx405 Select CW Plate Washer rather than manually. The fixation time was extended to 20 minutes due to the automated aspiration protocol, which left a 10μl residue in each well and so reagent concentrations needed to be increased. Various extraction and DNA staining procedures were trialled in this plate type as stated in Chapter 3.

In all other immunofluorescence assays, the cells were pre-extracted with 0.5% Triton X-100, 3% BSA in PBS for 5 minutes before fixing as stated previously. The exceptions to this were the HCT116 based cells lines which were extracted after fixing. The primary and secondary antibodies were diluted in 3% BSA in PBS and the coverslips were washed with PBS and mounted as described previously.

The mounted coverslips were imaged using a Nikon Eclipse TE2000 inverted microscope with a 100X objective and the Volocity software. For each condition, at least 100 cells were imaged, the total number of cells were counted and then scored for the number of cells with positive nuclei. A nucleus was considered positive if it contained 10 bright foci with

the exception of RAD51 stained cells where the average number of foci per cell was calculated, or where stated otherwise. The images were processed in ImageJ and the scoring graphs were generated and Unpaired Student's T-tests were carried out using GraphPad Prism.

The 384 well plates were imaged using the Molecular Devices ImageXpress Micro High Content Microscope with a 20X or 40X objective as specified where 6 or 9 sites were captured respectively. The images were generated using MetaXpress and false coloured in ImageJ. A MetaXpress Custom Module that identified the nuclei within each image and the foci present in the nuclei by their size and intensity was used to calculate the average and total number of foci within each nucleus this was subsequently used to calculate the number of positive nuclei within each condition.

2.2.1.5 MTT Colorimetric Assay

Metabolising cells convert soluble MTT into insoluble formazan crystals which can be subsequently dissolved which was utilised to colorimetrically assess the number of viable cells in an assay. Cells were seeded in 96 well plates and where necessary, p53 was inhibited and Cyclin E overexpression was induced before the cells were transfected.

When investigating the effects of genotoxic drugs, cells were either mock treated or treated with MMC (0 - 80ng/ml), Cisplatin (0 - 10μM), Hydroxyurea (0 - 100μM), Gemcitabine Hydrochloride (0 - 20nM), 5-Flurouracil (0μM - 25μM), Olaparib (0μM - 10μM) or KU55933 (0 - 10μM) following the specified transfection time. The cells were incubated with the drugs for 5 days. When investigating the effects of oncogene and tumour suppressor activity on cell survival following gene knockdown, the cells were left to grow for 5 days following transfection. The cells were then incubated with MTT at 3mg/ml in PBS for 3 hours at 37°C. The media was then removed from the plates using a Welch 2515C-75 REV A aspirator and 200μl DMSO was added per well to dissolve the formazan crystals. The plate was then read at 540nm on a Thermo Multiskan FC. The optical density (OD) values were used to calculate the percentage survival of each population of cells compared to the Control 1 transfected cells. The survival graphs were plotted in GraphPad Prism which was also used to carry out two way ANOVA analyses and unpaired Student's T-tests to determine if the differences between the conditions were significant.

2.2.1.6 Clonogenic Survival Assay

Clonogenic assays measure the ability of cells to form colonies following gene knockdown and/or drug treatment. This allows for assessments to be made in how these conditions affect cellular survival. Cells were seeded and transfected in 6 well plates for the specified transfection time. The cells were then trypsinised, re-suspended in fresh 10% FCS DMEM and counted to allow plating of 200 or 2000 cells per well in NUNC 6 well plates. Where specified, the cells were treated with MMC (0 - 100nM) or irradiated with UV light (0 - 6J/m^2). The cells were allowed to grow for 11 days before the media was removed and the colonies were stained with Methylene Blue (0.4%) for 30 minutes. The Methylene Blue was aspirated and any excess stain was removed by submersion in lukewarm water. The

colonies were then manually counted and the plating efficiency was calculated for each siRNA by dividing the number of colonies present in an untreated well by the number of cells initially plated. The surviving fraction of cells for each treatment was then calculated by dividing the number of colonies present by the plating efficiency multiplied by the number of cells initially plated.

In the case of RPE-1 cells, clear colonies were not formed in 6 well plates and so an alternative analysis method had to be employed. Once the cells had been stained with Methylene Blue, the plates were photographed (Fig. 2.2.1.7.1) and then 1ml of a 1% SDS solution was added per well. The plates were agitated for 1 hour at room temperature to allow the Methylene Blue to dissolve (Scragg & Ferreira, 1991). This was then re-plated in a 96 well plate which was read at 620nm on a Thermo Multiskan FC. The OD values were used to calculate the percentage survival of the cells in each condition compared to the untreated cells.

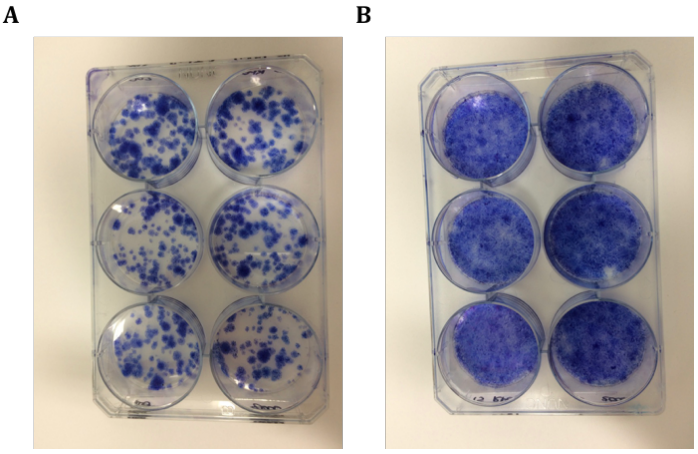

Figure 2.2.1.7.1 RPE-1 Clonogenic Survival Assay Plates.
Representative Images of RPE-1 Clonogenic Survival Assay plates. RPE-1 cells were transfected with Control 1, CCDC15 1 and CCDC15 3 (top row to bottom row), replated at (A) 200 cells or (B) 2000 cells per well and then treated with 6J/m² UV. The cells were grown for 11 days and then stained with 0.4% Methylene Blue to allow the colonies to be visualised.

2.2.1.7. Alkaline Comet Assay

The comet assay, or single cell gel electrophoresis, is a technique that directly measures DNA strand breaks. Single cells are suspended in agarose before they are lysed, their DNA unwound and they are subjected to electrophoresis. Any broken DNA migrates toward the anode creating a 'comet tail'. Cells were seeded and transfected in 6 well plates for the specified transfection time. The cells were then trypsinised, suspended in pre-warmed PBS and pelleted by centrifugation at 200 x *g* for 3 minutes. The cells were then re-suspended and diluted to give 10000 cell/ml solutions. For each sample, 25µl cells were added to 250µl low melt agarose and 100µl was then pipetted in duplicate onto a 2 well Comet slide. The slides were set for 30 minutes at 4°C before they were covered in lysis solution overnight at 4°C. This was removed and the slides were then incubated in the alkali unwinding solution for 1 hour at 4°C. The slides were then electrophoresed for 30

minutes at 300mA with a constant voltage of 21V. The slides were then washed twice in ddH_2O and 70% ethanol before drying at 25°C.

Each circle of agarose was incubated with 100µl SYBR Gold Comet Stain for 30 minutes before the excess stain was removed and the slides were allowed to dry. The cells were imaged within 48 hours of staining with the 20X objective of the Nikon Eclipse TE2000 inverted microscope and 100 cells were imaged per condition. The images were exported into CometScore for analysis and the Percentage DNA in the tail and Tail Moment were plotted for each condition.

2.2.1.8 Propidium Iodide Flow Cytometry

Propidium iodide (PI) is a fluorescent dye that intercalates into the DNA of fixed cells. It is routinely used to assess cell's DNA content by flow cytometry and so analyse the cell cycle distribution within a population of cells. Cells were seeded and transfected in 6 well plates for the specified transfection time. The media from each well was then placed in a 15ml tube which was used to collect the cells once they had been trypsinised. The cells were pelleted at 200 x *g* for 3 minutes before being washed twice in PBS and fixed in ice-cold 70% ethanol. The cells were then pelleted again and washed twice more in PBS before being incubated for 15 minutes with RNaseA as PI also binds RNA. The pellet was then incubated with 50µg/ml PI overnight at 4°C. The samples were then analysed using a BD FACSCalibur with 10000 cells analysed per sample. The single cells were gated and then the resultant histograms were used to calculate the percentage of cells in Sub G1, G1, S and G2-M phases of the cell cycle using FlowJo.

2.2.1.9 Cell Synchronisation

Cell synchronisation is commonly applied to generate a population of cells in the same phase of the cell cycle to allow how cells progress through the cell cycle to be studied. The RPE-1 FUCCI cells were plated and 24 hours post-plating, the cells were gently washed in PBS and the serum containing media was replaced with that lacking serum to synchronise the cell's cell cycles. The cells were then transfected for 72 hours with CCDC15 siRNA. The cells were released from serum starvation 12 hours prior to the completion of the designated transfection time. They were either fixed immediately or allowed to resume their cell cycles and fixed 12, 16 or 24 hours post-release. The number of green, yellow and red cells were then manually counted using the Nikon Eclipse TE2000 inverted microscope to and the proportion of cells within each stage of the cell cycle was calculated.

2.2.1.10 Micro-irradiation Induced Localisation of DNA Damage

Micro-irradiation of cells with lasers in combination with live cell imaging can allow for the observation of rapid and dynamic recruitment of repair proteins to sites of DNA damage. The HeLa FLP cells stably incorporating a CCDC15 containing pcDNA™5/FRT/TO N-Terminal YFP vector were plated in 35mm glass bottomed dishes and 24 hours post-plating, the cells were treated with 1µg/ml Tetracycline to induce CCDC15-YFP expression. Prior to imaging, the cells were pre-sensitised with 10µM BrdU for 24 hours. The live cells were imaged using the Perkin Elmer UltraView Vox Spinning Disk Confocal system via an Olympus IX81 Motorised Microscope. The YFP expressing cells were imaged

using a 40X objective before being irradiated with a 405nm UVA laser for 1 second. The cells were then subsequently imaged at 30 second intervals for a total of 10 minutes using the Volocity software. The images were then analysed and processed in ImageJ.

2.2.2 Molecular Biology

2.2.2.1 Western Blotting

Western blotting is used to detect the abundance and post translational modification of proteins. BSA was diluted in ddH_2O to produce a titration ranging from 0 - 0.1mg/ml BSA. Each concentration was added to a 96 well plate in triplicate and 200µl of the BioRad Protein Assay Dye Reagent Concentrate, diluted 1:5, was added per well. The plate was read on Thermo Multiskan FC plate reader at 570nm and the OD values were normalised to the 0mg/ml BSA background. These values were then used to generate a standard curve with the equation $y = 4.8871x + 0.0285$, where y is the absorbance and x is the concentration of protein (Fig. 2.2.2.1.1).

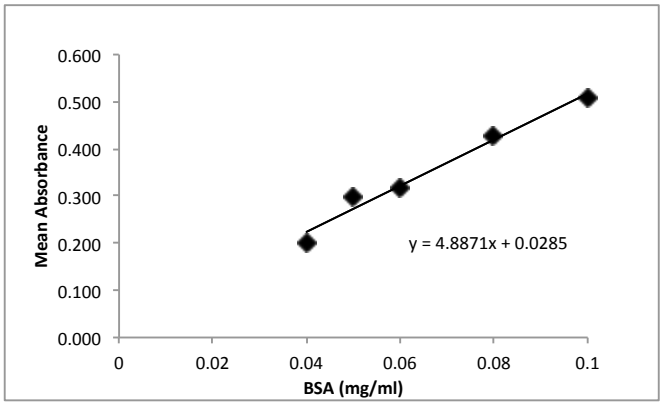

Figure 2.2.2.1.1 Standard Curve Generated from BSA Titration.
A BSA titration (0 - 0.1mg/ml) was plated in triplicate and a 1:5 dilution of the BioRad Protein Assay Dye Reagent was added to the plate. The OD_{570} values were read, normalised and plotted to generate an equation to calculate the concentration of a protein sample from its absorbance.

Cells were seeded and transfected in 6 well plates for the specified transfection time. The cell monolayer was washed in PBS before the addition of lysis buffer. This was scraped over the cells, collected and incubated on ice for 20 minutes with vortexing at 10 minute intervals. The samples were then pelleted at 15,000 x *g* for 15 minutes at 4°C and the supernatant was extracted. A 1:40 dilution of each sample was generated and this was plated in triplicate in a 96 well plate before the addition of a 1:5 dilution of the BioRad Protein Dye Reagent. The OD_{570} values of each sample were measured and the equation calculated above was used to determine their protein concentration. The lysates were then mixed with 4X NuPage Loading buffer supplemented with 5mM DTT and boiled on a hot block to prepare the samples for loading.

The protein samples (15µg) were loaded into 10 or 15 well NuPage 4-12% Bis-Tris Gels and the SeeBluePlus2 protein ladder was also loaded to determine the molecular weights of the bands observed. The proteins were electrophoresed in NuPage Running Buffer at 150V for 70 minutes and then transferred onto nitrocellulose membranes at 100V for 2 hours in NuPage Transfer Buffer. The membranes were blocked for 30 minutes in 5% Marvel Milk solution in PBS to prevent non-specific antibody binding. The primary and secondary antibodies (Table 2.1.2.3.1-2) were diluted in 5% milk solution and the membranes were washed in PBSt. The membranes were incubated with ECL (with the

exception of those stained with RRM1 which were incubated with the Visualiser detection kit) to allow the visualisation of the bands on Fuji Medical X-ray Film. The membranes were exposed to the film for 30 seconds, 1 minute, 5 minutes and overexposed before they were developed using a Konica Minolta SRX101A.

2.2.2.2 RNA Extraction

RNA was extracted from the cells either for use in qPCR analysis or the generation of cDNA libraries. Cells were seeded and transfected in 6 well plates for the specified transfection time before their Total RNA was extracted using the Qiagen RNeasy Mini Kit. The cells were washed in PBS before the addition of the RTL Buffer which was scraped over the cells, collected and transferred to QIA shredder columns. These were centrifuged for 2 minutes at 800 x *g* before 70% ethanol was added to the eluted solution. This was then transferred to Rneasy spin columns which were centrifuged for 15 seconds at 800 x *g*. RWI Buffer was then added to the columns, and centrifuged for 15 seconds after which the eluted solution was discarded. This step was repeated twice more using the RPE Buffer and on the second occasion the columns were centrifuged for 2 minutes. The columns were then transferred to fresh Eppendorfs and RNase free water was added to them to elute the RNA by centrifugation.

Total RNA was extracted from frozen cell pellets using the Perfect Pure RNA cultured cell kit. To each Eppendorf, the kit Lysis solution was added and vortexed vigorously to dislodge and homogenise the pellet. The Ependorffs were then centrifuged at 400 x *g* for 1 minute to remove any foam. The lysates were then transferred to purification columns, which were then centrifuged at 15000 x *g* for 1 minute. The columns were then washed once using Wash 1 solution and twice using Wash 2 solution with centrifugation for 1 minute following the addition of each solution. The columns were then transferred to collection tubes and Elution solution was added to each column before they were centrifuged for 1 minute to elute the RNA.

mRNA from cultured cells was extracted using the Qiagen Oligotex Direct mRNA Mini Kit. The cells were washed in PBS, trypsinised and $3x10^6$ cells were suspended in fresh 10% FCS DMEM. The cells were pelleted at 200 x *g* for 3 minutes, re-suspended in fresh 10% FCS DMEM and transferred into Eppendorfs. The cells were then centrifuged at 300 x *g* for 5 minutes and the supernatant was discarded. OL1 Buffer supplemented with β-Mercaptoethanol was added to the Eppendorfs which were vortexed for 10 seconds. The contents were transferred to QIAshredder tubes and centrifuged for 2 minutes at 13,000 x g. ODB Buffer was added to the supernatants and they were mixed thoroughly together before centrifuging for 3 minutes. The supernatants were then transferred to new Eppendorfs before the Oligotex suspension was added and incubated for 10 minutes at 25°C. These were then centrifuged for 5 minutes and the supernatants were mixed with OL1 Buffer and ODB Buffer. These were incubated at 70°C for 3 minutes and 25°C for a further 10 minutes. The Eppendorfs were then centrifuged for 5 minutes and the supernatants were mixed with OW1 Buffer before being transferred into small spin columns which were centrifuged for 1 minute at 13,000 x *g*. The columns were then transferred into new Eppendorfs and OW2 Buffer was added before centrifuging for 1

minute, this step was then repeated in the same Eppendorf. The columns were then transferred to new tubes and OEB buffer at 70°C was added to each column. These were then centrifuged for 1 minute, which was repeated to complete the elution of the mRNA.

2.2.2.3 Reverse Transcription

Extracted RNA had to be converted to cDNA before it could be amplified by qPCR or PCR. The Total RNA samples prepared above were reverse transcribed for qPCR using the Applied Biosystems High Capacity RNA-to-cDNA Kit and PCR using several kits (including the High Capacity RNA-to-cDNA Kit) as stated in Chapter 6. Total RNA levels were quantified using the NanoVue Plus or the Nanodrop ND 1000 Spectrophotometer.

For the High Capacity RNA-to-cDNA Kit, RNA samples were diluted to 1μg of total RNA per 9μl of sample. For each sample, a Mastermix containing the 2 X RT Buffer and 20X Enzyme mix was added to PCR tubes containing 1μg of the sample RNA. The tubes were vortexed to eliminate air bubbles and loaded onto the MJ Research PTC-200 Peltier Thermal Cycler programmed to the Kit Manufacturer's instructions.

For the Bioscript kit, 5μg of total RNA was added to 0.5μg Oligo(dT)18 made up to 12μl with nuclease free H_2O and incubated for 5 minutes at 70°C before chilling on ice. The Mastermix was made up according to kit instructions and mixed with the RNA mix before the addition of the BioScript (200u/μl) enzyme. This was incubated for 60 minutes at 37°C before heating to 70°C for 10 minutes to halt the reaction.

For the TaqMan Reverse Transcription Kit, the RNA primer mix was made up according to kit instructions with 1μg Total RNA. This was incubated for 5 minutes at 65°C then 2 minutes at 4°C. The Mastermix was then made following the kit instructions and mixed with the RNA/Primer mix. The reaction was then incubated at 37°C for 30 minutes followed by 5 minutes at 95°C to halt the reaction.

For the RT^2 First Strand Kit, GE Buffer was added to 5μg Total RNA to eliminate genomic DNA and made up to 10μl with nuclease free H_2O. This mix was then incubated at 42°C for 5 minutes and then placed on ice for 1 minute. The RT mix was made according to the kit instructions using Buffer BC3 and Control P2. This was added to the DNA elimination reaction and incubated for 60 minutes at 37°C followed by a 5 minute incubation at 95°C to halt the reaction. Finally 91μl Nuclease free water was added to the reaction.

2.2.2.4 Reverse-transcription PCR

Reverse transcription PCR (qPCR) quantifies the abundance of an mRNA of interest through its conversion to cDNA and subsequent amplification. It relies upon the use of primers conjugated to fluorescent tags, in this case FAM, that fluoresce as the cDNA of interest is amplified. The fluorescence is then measured to determine the abundance of the transcript within the sample.

Each cDNA sample was amplified with 2μl cDNA, 5μl TaqMan Universal PCR Mastermix, 2.5μl RNase free H_2O and 0.5μl probe (Table 2.1.2.5.2) per reaction. Each sample mix was

vortexed, then plated in triplicate in a 384 well PCR plate which was sealed using Polyolefin Film before loading onto an Applied Biosystems 7900 Real Time PCR machine.

Once the protocol was completed, the Ct values were used to assess gene expression and/or to calculate the percentage knockdown of achieved by siRNAs using the protocol below (Livak & Schmittgen, 2001).

For each sample calculate:

$$\Delta Ct = \text{Mean Control Probe Ct} - \text{Mean Gene Probe Ct}$$

$$\Delta Ct \text{ Expression} = 2^{-\Delta Ct}$$

For each gene knockdown sample calculate:

$$\Delta\Delta Ct = \frac{\Delta Ct \text{ Expression Knockdown Sample}}{\Delta Ct \text{ Expression Control Sample}}$$

$$\text{Percentage Knockdown} = (1 - \Delta\Delta Ct) \text{ X } 100$$

2.2.2.5 Polymerase Chain Reaction (PCR)

Several PCR kits were utilised in the attempts to amplify CCDC15 with the KOD Hot Start DNA Polymerase being the most commonly used. For each reaction 100ng of cDNA or plasmid was added to the KOD Mastermix made up according to kit instructions and gene specific primers (as stated in Chapter 6) with a total reaction volume of 25µl.

The KOD PCR protocol was performed as follows (unless otherwise stated):

94°C	3 mins	x1
94°C	1 min	x35
55-70°C	1.5 min	
68°C	3 min	
68°C	5 min	x1
4°C	∞	

Several additional PCR kits were trialled for the amplification of CCDC15 cDNA. The Platinum Hot Start PCR kit was carried out according to the kit instructions and 100ng of cDNA was added per reaction. The AccuPrime DNA Polymerase kit Mastermix was made up using Buffer 1 according to the kit instructions with 200ng of cDNA added per reaction. The AccuPrime GC Rich DNA Polymerase was also trialled using the kit instructions with either Buffer A or Buffer B as stated in Chapter 6 and 100ng of cDNA per reaction.

The same PCR protocol was carried out for all these additional kits (unless stated otherwise) as follows:

95°C	3 mins	x1
55-70°C	30 sec	┐
72°C	3 min	┘ x35
72°C	5 min	x1
4°C	∞	

2.2.2.6 Agarose Gel Electrophoresis

Agarose gel electrophorese allows for the separation of nucleic acids by size as longer transcrpts will migrate slower than those of a shorter length. The higher the concentration of the agarose, the slower the proteins will migrate as the pores within the gel will be smaller.

PCR products were electrophoresed on 1.5% agarose gels. Agarose was added to 1X TAE which was heated to dissolve the agarose. This was then allowed to cool before the addition of 0.2μg/ml ethidium bromide. The gel was poured and allowed to set before placing in the horizontal gel tank where Hyperladder 1 and PCR products mixed 4:1 with 5X Loading dye were loaded into the gel. This was then electrophoresed for 1 hour at 80V.

Relevant bands were excised from the gels using a UV Transilluminator, removing as little excess gel as possible. The PCR products were then extracted from the agarose gel using the QIAquick Gel Extraction Kit. The gel slice was weighed in an Eppendorf and QG Buffer was added at the volume specified by the kit for that weight of gel. The Eppendorf was incubated at 50°C for 10 minutes and was vortexed every 2 minutes to aid the dissolving of the gel. Isopropanol was then added to the tube at one gel volume. The sample was then added to a QAIquick spin column and centrifuged for 1 minute at 800 x *g* before discarding the flow through. QG Buffer was then added to the column which was centrifuged for a further minute. The column was then washed in PE Buffer and centrifuged for 1 minute twice to remove all of the buffer. The column was then placed in a microcentrifuge tube and 30μl of Buffer EB was added to the column, incubated for 1 minute and then centrifuged for 1 minute to elute the DNA.

2.2.2.7 Bacterial Transformation and Plasmid Isolation

Bacterial transformation is essential for the propagation of plasmids required for cloning studies. It requires the introduction of the plasmid into competent bacteria, culturing of the bacteria and then isolation of the plasmid using a membrane contained within a centrifugation column.

Ampicillin or Kanamycin were diluted to 100μg/ml or 50μg/ml respectively in agar before 20ml of agar was poured into sterile culture dishes under a flame. The plates were then allowed to set at room temperature before drying inverted at 37°C.

Plasmids were transformed into DH5α *E. coli* cells by adding 1μg of plasmid DNA to KCM and making up to 100μl in ddH_2O before mixing with the bacteria. A negative control was prepared that contained no plasmid DNA. These solutions were then incubated for 20

minutes on ice followed by 10 minutes at room temperature. Under a flame, 1ml of LB Broth was added to each sample before incubation for 1 hour at 37°C with shaking. The cells were then gently pelleted at 200 x *g* and 800µl of the supernatant was removed. The cells were then re-suspended in the remaining LB Broth which was spread on Ampicillin or Kanamycin Agar plates, depending on the resistance genes of the plasmid, and incubated at 37°C for 16 hours.

Ampicillin or Kanamycin were diluted to 100µg/ml or 50µg/ml respectively in LB Broth before 5ml was aliquoted into Universal Tubes. Bacterial colonies were looped from the Agar plates and a single colony was added to each tube which were then incubated at 37°C with shaking for 16 hours.

The QIAprep Spin Miniprep Kit was used to isolate the plasmids. The tubes were centrifuged at 6000 x *g* for 10 minutes and the resultant pellets were re-suspended in PI Buffer and P2 Buffer and transferred to Eppendorfs. After 5 minutes, N3 Buffer was added to the Eppendorfs which were centrifuged for 10 minutes at 17000 x *g*. The flow through was added to QIAprep 2.0 spin columns and centrifuged at 800 x *g* for 1 minute. The columns were then wash once with PB Buffer, centrifuged for 1 minute and then twice with PE Buffer before centrifuging twice to remove any residual buffer. The columns were then transferred into sterile Eppendorfs, and the plasmid DNA was eluted by the addition of EB Buffer and centrifugation.

2.2.2.8 Stable Cell Line Generation by Gateway Cloning

Gateway cloning (Invitrogen) relies upon the conservative recombination between *att* sites by the bacteriophage lambda. This system was used to create N-terminally tagged forms of the CCDC15 protein.

CCDC15 cDNA was amplified by PCR using the Gateway Primers (Table 2.1.2.5.1) resulting in a full length cDNA PCR product flanked by *attB* sites. These products were then recombined with a pDONR221 vector containing *attP* sites by BP Clonase II following the kit instructions to generate an Entry Clone containing *attL* sites. The resultant plasmids were then transformed into DH5α and isolated as described previously, using Kanamycin selection. The pDONR221 plasmid contained a death gene, *ccdB,* so products that had not recombined would not produce viable cells. The isolated DNA was then quantified and sent for sequencing.

Once the CCDC15 insert had been fully verified by sequencing in the pDONR221 vector, the plasmid was recombined with either an N-terminal FLAG tag or N-terminal YFP tag Destination Vector containing *attR* sites using the LR Clonase II kit. The reaction was transformed into DH5α, selected for using Ampicillin and isolated as described previously. The Destination Vectors also contained *ccdB* and so if recombination was not complete, cells containing those products would die. The isolated DNA was then sent for sequencing to determine if CCDC15 had entered the Destination Vectors and if it was in frame with the N-terminal tags (Fig. 2.2.2.8.1).

DNA was sequenced by the University of Sheffield Core Genomics Facility utilising an Applied Biosystems 3730 DNA analyser. For each reaction 10µl 10ng/µl template DNA

and 10µl of 1nM primer were provided. The resultant sequencing trace files were analysed using Sequencer 4.7 software.

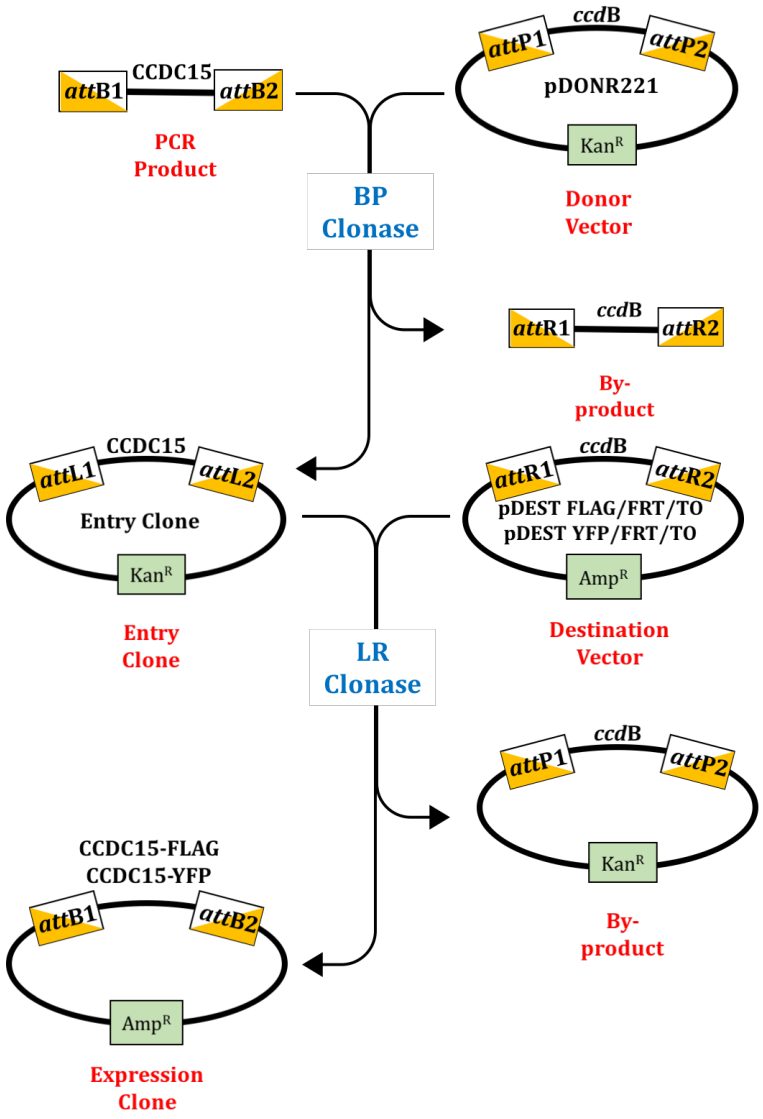

Figure 2.2.2.14.1 Gateway Cloning of CCDC15

CCDC15 was amplified using Gateway primers to yield a PCR product flanked by attB sites. These products were recombined into the Donor Vector pDONR221 which contained the ccdB death gene flanked by attP sites and a Kanamycin resistance gene using the BP Clonase. This yielded an Entry Clone containing CCDC15 flanked by attL sites and the Kanamycin resistance gene which was used to select transformed cells. The by-product of this reaction contained attR surrounding the ccdB death gene. Any bacteria that retained this by-product or Donor Vectors that had not successfully recombined were not viable due to the presence of the death gene. The resultant Entry Clones were then recombined with N-terminal FLAG tag or N-terminal YFP tag containing Destination vectors using LR Clonase. These also included an Ampicillin resistance gene and the ccdB death gene flanked by attR sites. This reaction yielded an Expression Clone containing the CCDC15 gene fused to the N-terminal tags flanked by attB sites and the Ampicillin resistance gene which was used for selection. The by-product of this reaction contained attP sites and the ccdB death gene. As previously any cells retaining the by-product or Destination Vectors that had not recombined would die.

To make stable cell lines, HeLa FLP and HEK 293 FLP cells were plated in 6 well plates. Once the cells were 80% confluent the N-terminal YFP tagged CCDC15 vector was transformed into the HeLa FLP cells and the N-terminal FLAG tagged CCDC15 vector was transformed into both the HeLa FLP and HEK 293 FLP cells. Cells were transfected with 1μg vector, 1μg pOG44 Flp-Recombinase and 4μl Lipo 2000 per well.

Twenty-four hours post-transfection the cells were trypsinised and the contents of each well were re-suspended in 10% FCS DMEM. The cells were added to a 10cm dish and treated with Blasticidin and Hygromycin as described in Table 2.1.2.1.2. The cells were left to grow in the dishes until colonies had formed and then trypsinised and transferred to 25cm^2 tissue culture flasks. Once confluent these cells were then cultured in 75cm^2 tissue culture flasks as described in Table 2.1.2.1.2.

2.2.2.9 Immunoprecipitation

Immunoprecipitation allows for the isolation of a protein of interest from a cell lysate by utilising antibodies that specifically bind to that protein. Attempts were made to isolate Flag-tagged CCDC15 from the HEK 293 FLP cells for use in mass spectrometry analyses.

The HEK 293 FLP cells stably transfected with a CCDC15 containing pcDNA™5/FRT/TO N-Terminal FLAG vector were plated in 10cm or 14cm dishes. The cells were then either mock treated with DMSO or treated with 1μg/ml Tetracycline to induce CCDC15-FLAG expression 24 hours after plating. The cells were grown for a total of 48 hours before the cells were washed twice in ice cold PBS.

In the small scale optimisation experiment, lysis buffer was added to the cells which were then mechanically disaggregated and aliquoted into Eppendorf tubes. In the scaled up experiment, the cells were disaggregated and aliquoted into falcon tubes before the addition of the lysis buffer without DTT. The lysates were then incubated on ice for 20 minutes with vortexing at 10 minute intervals. The samples were then pelleted at 15000G for 15 minutes at 4°C and the supernatant was collected and 50μl was saved as the Input for the FLAG Immunoprecipitation (IP) electrophoresis.

ANTI-FLAG M2 Affinity Gel was aliquoted into an Eppendorf per sample. The Eppendorfs were centrifuged for 30 seconds at 3000rpm then rotated 180° and centrifuged again. The supernatant was aspirated the gel was washed 3 times in IP buffer before the addition of the lysates in the small scale experiment. In the scaled up versions, the gel was washed with ice cold PBS before being transferred into a falcon tube where the lysates were added. Where stated, the gel was incubated with the FLAG M2 antibody before lysate addition. The lysates were incubated with the gel overnight at 4°C with rotation. The samples were then pelleted at 3000rpm and 200μl of the supernatant was removed and kept as the Unbound fraction. The gel was then washed three times in the IP Wash Buffer, with a 30 minute incubation with rotation between washes, before centrifugation and removal. Where stated, the first wash was retained for electrophoresis.

After the final wash in the small-scale optimisation experiments, the Bound fraction was eluted by adding 20μl of the 4X NuPage Loading buffer supplemented with 5mM DTT. In the scaled up experiments, the beads were washed in 1% TBS and the 3X FLAG Peptide

(diluted 1:30 in TBS) was added to the beads. This was incubated for 30 minutes with rotation before the samples were centrifuged and 110µl of the eluted supernatant was collected. Where stated, this incubation was repeated. In all experiments, the gel was then incubated with the FLAG peptide overnight at 4°C with rotation before supernatant removal. Loading buffer was also added to the retained Input, Unbound and Wash fractions as well as the Elutions and remaining gel for the scaled up experiments. The samples were then boiled for 5 minutes at 95°C. For both the small scale and scaled up assays, the samples were separated on NuPage 4-12% Bis-Tris Gel 1.5mm X 10 well gels which were transferred to membranes which were blotted with the FLAG M2 antibody.

Chapter Three:
Phospho-RPA2 RNAi Screen Development

TABLE OF FIGURES 92

3.1 INTRODUCTION 94

3.2 REPLICATION STRESS SUPPRESSOR KNOCKDOWN 95

3.3 PHOSPHO-RPA2 ANTIBODY SELECTION 96

3.3.1 Initial Staining Protocol for Phospho-RPA2 Foci Detection 96

3.3.2 Improved Protocol for Phospho-RPA2 Foci Detection 99

3.4 PHOSPHO-RPA2 REPLICATION STRESS DETECTION IN A CELL LINE PANEL 104

3.4.1 Phospho-RPA2 Replication Stress Detection in RPE-1 104

3.4.2 Phospho-RPA2 Replication Stress Detection in SW480 105

3.4.3 Phospho-RPA2 Replication Stress Detection in p53 Deficient HCT116 106

3.5 HIGH THROUGHPUT PHOSPHO-RPA2 REPLICATION STRESS DETECTION 108

3.5.1 Initial High Throughput Staining Protocol 108

3.5.2 Time Course to Determine Optimum Extraction Time 110

3.5.3 High Throughput Staining Protocol with Increased Extraction Time 112

3.5.4 High Throughput Staining Protocol with Cold Pre-Extraction 112

3.5.5 Triton X-100 Titration to Determine Optimum Concentration for Extraction 117

3.5.6 High Throughput Staining Protocol with Increased Triton X-100 Concentration 119

3.5.7 Assessment of Non-Targeting Controls in High Throughput Staining Protocol 120

3.5.8 Re-optimisation of High Throughput Assay Conditions 121

3.5.9 High Throughput Staining Protocol with Increased Cell Number 126

3.5.10 Trouble Shooting High Throughput Staining Protocol 131

3.6 ALTERNATIVE METHODS OF DETECTING REPLICATION STRESS 133

3.6.1 EGFP-RPA2 Expressing HeLa Cells for RPA2 Foci Detection 133

3.6.2 Total RPA2 Immunofluorescence 134

3.6.3 TopBP1 Immunofluorescence 136

3.7 DISCUSSION 140

Table of Figures

Figure 3.2.1. Gene Knockdown by Chk1 and RRM1 siRNA and induction of a replication stress response. 96

Figure 3.3.1.1 Comparison of pRPA2 Antibodies at 48 hour transfection time with initial protocol. 97

Figure 3.3.1.2 Comparison of pRPA2 Antibodies at 72 hour transfection time with initial protocol. 98

Figure 3.3.1.3 Percentage of HCT116 cells positive for T21 foci with initial protocol. 99

Figure 3.3.2.1 Comparison of pRPA2 Antibodies at 48 hour transfection time with improved protocol. 100

Figure 3.3.2.2 Comparison of pRPA2 Antibodies at 72 hour transfection time with improved protocol. 101

Figure 3.3.2.3 Percentage of HCT116 cells positive for T21 foci with improved protocol. 102

Figure 3.3.2.4 Percentage of Chk1 knocked down HCT116 cells positive for T21 foci. 102

Figure 3.3.2.5 RPA2 T21 staining in RRM1 knocked down HCT116 cells. 103

Figure 3.3.2.6 Percentage of RRM1 knocked down HCT116 cells positive for T21 foci. 103

Figure 3.4.1.1 RPA2 T21 staining in RPE-1 cells. 104

Figure 3.4.1.2 Percentage of RPE-1 cells positive for T21 foci. 105

Figure 3.4.2.1 RPA2 T21 staining in SW480 cells. 105

Figure 3.4.2.2 Percentage of SW480 cells positive for T21 foci. 106

Figure 3.4.3.1 RPA2 T21 staining in HCT116 p53 Null Cells. 106

Figure 3.4.3.2 Percentage of HCT116 p53 Null cells positive for T21 foci. 107

Figure 3.4.4.1 Comparison of the percentage of HCT116 wild type, RPE-1, SW480 and HCT116 p53 null cells positive for T21 foci. 107

Figure 3.5.1.1 RPA2 T21 staining with initial high throughput protocol 109

Figure 3.5.2.1 Extraction time course in 384 well plate at 48 hours. 110

Figure 3.5.2.2 Extraction time course in 384 well plate at 72 hours. 111

Figure 3.5.3.1 RPA2 T21 staining 10 minute extraction at 72 hours. 112

Figure 3.5.4.1 RPA2 staining T21 of Chk1 knocked down HCT116 with cold pre-extraction at 48 hours. 113

Figure 3.5.4.2 RPA2 staining T21 of Chk1 knocked down HCT116 with cold pre-extraction at 72 hours. 114

Figure 3.5.4.3 RPA2 T21 staining of RRM1 knocked down cells with cold pre-extraction at 48 hours. 115

Figure 3.5.4.4 RPA2 T21 staining of RRM1 knocked down cells with cold pre-extraction at 72 hours. 116

Figure 3.5.5.1 Triton X-100 Titration in RPA2 T21 stained cells imaged in the Cy5 channel 117

Figure 3.5.5.2 Triton X-100 Titration in RPA2 T21 stained cells imaged in the Texas Red channel. 118

Figure 3.5.6.1 RPA2 T21 staining of Chk1 or RRM1 knocked down cells with increased Triton X-100. 119

Figure 3.5.7.1 RPA2 T21 staining of Control Panel and Chk1 or RRM1 knocked down cells. 120

Figure 3.5.7.2 Comparison of average data and individual cell data generated by MetaXpress Custom Module Editor. 121

Figure 3.5.8.1 Re-optimisation of high throughput screening assay with 48 hour transfection. 123

Figure 3.5.8.2 Re-optimisation of high throughput screening assay with 72 hour transfection. 124

Figure 3.5.8.3 Automated scoring of re-optimised high throughput screening assay. 125

Figure 3.5.9.1 RPA2 T21 staining of Control Panel and Chk1 or RRM1 knocked down cells with increased plating density. 126

Figure 3.5.9.2 Automated scoring of Control Panel, and Chk1 or RRM1 knocked down cells with increased plating density. 127

Figure 3.5.9.3 RPA2 T21 staining of Control Panel, Chk1 or RRM1 knocked down cells to compare 20X and 40X objectives. 128

Figure 3.5.9.4 Comparison of Control Panel and Chk1 or RRM1 knocked down cells imaged with a 20X and a 40X objective. 129

Figure 3.5.9.5 RPA2 T21 staining of Control Panel, Chk1 or RRM1 knocked down cells at 20X objective 129

Figure 3.5.9.6 RPA2 T21 staining of Control Panel, Chk1 or RRM1 knocked down cells imaged using the InCell 2000 microscope 130

Figure 3.5.9.7 RPA2 T21 staining of RRM1 knocked down cells imaged using the InCell 2000 microscope 131

Figure 3.5.10.1 Comparison of Collis lab and SRSF protocols in 24 well and 384 well plate format. 132

Figure 3.6.1.1. Detection of pRPA foci in EGFP-RPA2 Expressing HeLa cells. 133

Figure 3.6.2.1. Total RPA2 staining in HCT116 cells at 48 hours. 134

Figure 3.6.2.2. Total RPA2 staining in HCT116 cells at 72 hours. 135

Figure 3.6.3.1. TopBP1 staining in HCT116 cells at 48 hours. 136

Figure 3.6.3.2 Percentage of HCT116 cells positive for TopBP1 foci. 137

Figure 3.6.3.3 TopBP1 staining in HCT116 cells in 384 well plate. 138

Figure 3.6.3.4 TopBP1 staining in Pre-extracted HCT116 cells in 384 well plate. 139

Figure 3.7.1 Phospo-RPA2 Screening Assay Development. 141

Figure 3.7.2. Difference in pixel coverage at 40X and 20X objectives. 147

3.1 Introduction

As mentioned previously, cancer cells display higher than normal levels of replication stress due to the chronic signalling of activated oncogenes. It has therefore been suggested that increasing these levels further could yield selective killing of tumour cells. The cancerous cells would be pushed over a threshold level of replication stress and forced into crisis whilst normal cells, with their lower basal stress levels, would remain below this limit and retain their viability. On this basis, it was predicted that screening cells for signs of increased replication stress after gene inhibition would reveal novel factors that regulate the replication stress response and could be therapeutically targeted to treat cancer. Therefore, it was proposed to develop a genome wide siRNA screen to identify novel suppressors of replication stress.

Currently, there is no well-defined cellular marker that can be used to identify cells undergoing replication stress as it is not a physical structure within the cell. One of the best ways to detect replication stress is a direct readout of DNA synthesis (Zeman & Cimprich, 2014), such as BrdU staining. This technique was used by Kavanaugh *et al.,* (2015) to assess endogenous levels of replication stress after gene knockdown by siRNA. An alternative method is to detect an event that is key in the response to replication stress. Abrogation of the phosphorylation of RPA2 at Threonine 21 (T21) and Serine 33 (S33) by ATR (Vassin et al, 2009) and Serine 4/8 (S4/8) by DNA-PK, prevents recovery from replication stress (Ashley et al, 2014). As phosphorylation of these sites is required for the resolution of replication stress, it can be considered an essential step in the cellular response to this phenomenon. Immunofluorescent staining has previously been shown to be capable of detecting phospho-RPA2 (pRPA2) foci (Collis et al, 2007; Collis et al, 2008) and so antibodies raised against these phosphosites can be utilised for replication stress detection. TopBP1 is also a crucial component of the replication stress response, as it is vital for the activation of ATR at stalled replication forks (Choi et al, 2010). Like pRPA2, it forms nuclear foci in stressed cells which can be detected by immunofluorescent staining (Kim et al, 2005) and so TopBP1 antibodies can similarly be used for the detection of replication stress.

To assess the ability of the pRPA2 antibodies to detect changes in replication stress levels, positive controls, whose knockdown has previously been established to induce replication slowing, were included in the screening development assays. Efficient DNA replication requires several components including a ready supply of nucleotides (Bester et al, 2011; Zeman & Cimprich, 2014). Ribonucleotide reductase catalyses the conversion of ribonucleotides (rNDPs) into deoxyribonucleotides (dNTPs) and its activity depends upon its catalytic subunit RRM1 (Mann et al, 1988). Knockdown of RRM1 results in a significant reduction in the dNTP pool resulting in slowed proliferation (Wang et al, 2013). Cell cycle checkpoints also play a role in the suppression of replication stress. The knockdown of Chk1 impairs the cell's ability to recover from replication stress (Kavanaugh et al, 2015) and in deficient cells, origin firing is deregulated (Syljuåsen et al, 2005). Knockdown of these two genes by siRNA were therefore used throughout the development of the screen

as positive controls for heightened replication stress. Additionally, hydroxyurea (HU) inactivates the enzyme ribonucleotide reductase (Yarbro, 1968) and results in replication fork stalling. HU was therefore used in these experiments as an additional transfection independent positive control.

It was hypothesised that novel suppressors of replication stress existed in the human genome. Therefore, attempts were made to develop a high throughput genome wide screening assay to assess endogenous levels of pRPA2 following gene knockdown, where an increase in phosphorylation indicated the loss of a suppressor of replication stress. Western blotting was initially used to detect a replication stress response after the knockdown of known replication stress suppressor genes. Three phospho-RPA2 antibodies were used to assess pRPA2 foci formation and the most successful was used to evaluate staining in a cell line panel containing both normal and cancerous cell lines. This assay was then re-optimised for use in a 384 well high throughput screening format. Alternative methods of replication stress detection were also trialled as screening approaches and for hit validation but unfortunately none proved successful in the high throughput format.

3.2 Replication Stress Suppressor Knockdown

Western blotting analysis was used to assess the efficiency of Chk1 or RRM1 knockdown by siRNA pools which would be used as positive controls in the pRPA2 screen. Cell populations treated with HU were used as an additional positive control for replication stress. HCT116 cells were reverse transfected for either 48 or 72 hours with Control 1 (non-targeting), Chk1 or RRM1 siRNA using DharmaFECT 1. Cells were then treated with 2mM HU or mock treated with PBS 16 hours before media removal. Total Chk1 and total RRM1 expression were determined to assess the efficiency of the knockdown. Levels of phospho-Chk1 (S317), total RPA2 and phospho-RPA2 (T21) were also determined to assess the levels of replication stress induced (Fig.3.2.1).

As shown in Figure 3.2.1, both Chk1 and RRM1 siRNA reduce target protein expression in HCT116 cells at both time points. A faint band is present in the Chk1 lane of the total Chk1 blot suggesting that the knockdown was not complete whilst the RRM1 knockdown appeared more effective. RRM1 knockdown induced Chk1 phosphorylation at S317 and knockdown of both proteins stimulated RPA2 phosphorylation, as shown using the specific phosphorylated T21 antibody and by the double band in the total RPA2 blot. At both time points RPA2 phosphorylation was more apparent in RRM1-depleted cells compared with Chk1-depleted cells, suggesting this produces a stronger replication stress response. As these bands are absent in the untreated Control 1 siRNA cells, it indicates that the replication stress response was the result of knockdown of RRM1 and Chk1. Similarly, treatment with HU promoted robust Chk1 and RPA2 phosphorylation in cells transfected with Control 1 siRNA and increased the level of phosphorylation seen in the Chk1 knockdown lanes but not RRM1. As the Chk1 and RRM1 siRNA transfection and HU treatment resulted in heightened levels RPA2 phosphorylation, they were considered appropriate positive controls for replication stress in the pRPA2 screening assays.

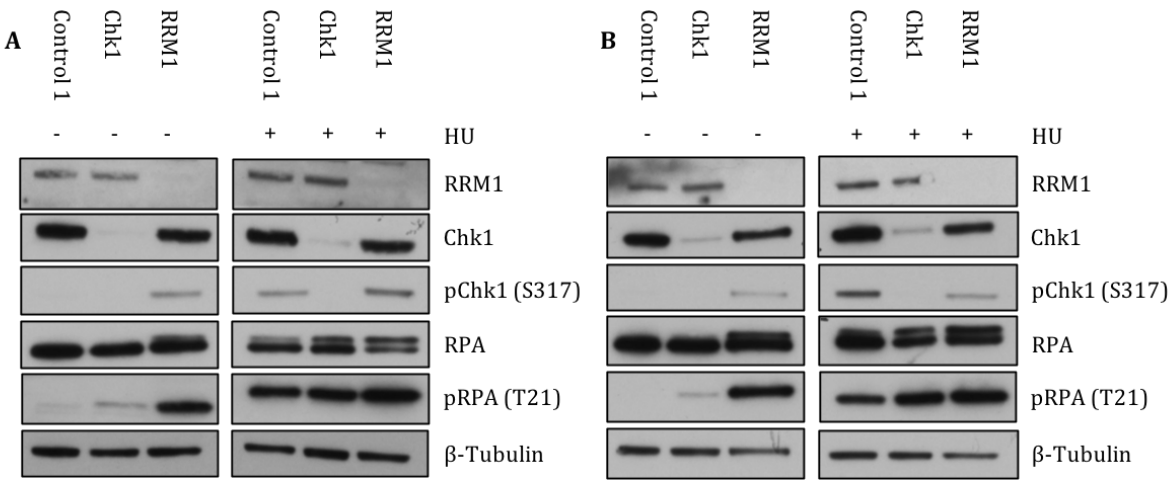

Figure 3.2.1. Gene Knockdown by Chk1 and RRM1 siRNA and induction of a replication stress response.

HCT116 cells were reverse transfected with Control 1, Chk1 or RRM1 siRNA for (A) 48 or (B) 72 hours. Cells were mock treated with PBS or treated with 2mM HU for 16 hours before media removal. The cells were lysed and 15μg of protein from each sample was loaded onto a NuPage 4-12% Bis-Tris Gel for separation. The gels were transferred to nitrocellulose membranes before blocking and blotting with total RRM1, total Chk1, pChk1 (S317), total RPA2, pRPA2 (T21) and β-Tubulin (loading control) primary antibodies. The primary antibodies were detected with HRP conjugated secondary antibodies.

3.3 Phospho-RPA2 Antibody Selection

Immunofluorescent identification of pRPA2 foci has previously been validated as a detection method for increased replication stress (Collis et al, 2007). RPA2 is phosphorylated at a number of sites in its N-terminus in response to cell cycle progression and cellular stress (Anantha et al, 2007). Three phospho-antibodies raised against the N-terminal sites S4/8, T21 and S33 were tested for their ability to detect replication stress in siRNA transfected HCT116 cells by immunofluorescence approaches to assess their suitability for use in a high throughput siRNA screen.

3.3.1 Initial Staining Protocol for Phospho-RPA2 Foci Detection

Initially, the cells were forward transfected with Control 1 or Chk1 siRNA using RNAiMAX for 48 or 72 hours. Once fixed, the cells were permeabilised by repeated washing of the coverslips with PBS-tween 20, blocked for 30 minutes with 0.5% BSA in PBS and stained with the three pRPA2 primary antibodies (Fig.3.3.1.1 and Fig. 3.3.1.2).

Of the three antibodies used to detect pRPA2 in this experiment, only the T21 antibody could identify discrete pRPA2 foci. The S4/8 antibody showed mostly cytoplasmic staining and where the antibody had entered the nucleus, it could not detect foci. The S33 antibody rarely appeared to enter the nucleus, so could not detect pRPA2 foci. Even with the addition of HU, this antibody could not detect replication stress under these staining conditions. In contrast, the T21 antibody detected clear foci in all conditions and the number of foci appeared to increase with the level of replication stress induced, with more foci appearing in the Chk1 knocked down and HU treated cells (Fig.3.1.1.1 and 3.3.1.2). As such, the T21 antibody images were scored for the number of pRPA2 foci they contained to determine whether it could detect discernible variation in the levels of replication

stress between the different conditions (Fig. 3.3.1.3). The S4/8 and S33 images could not be scored as these antibodies did not detect foci.

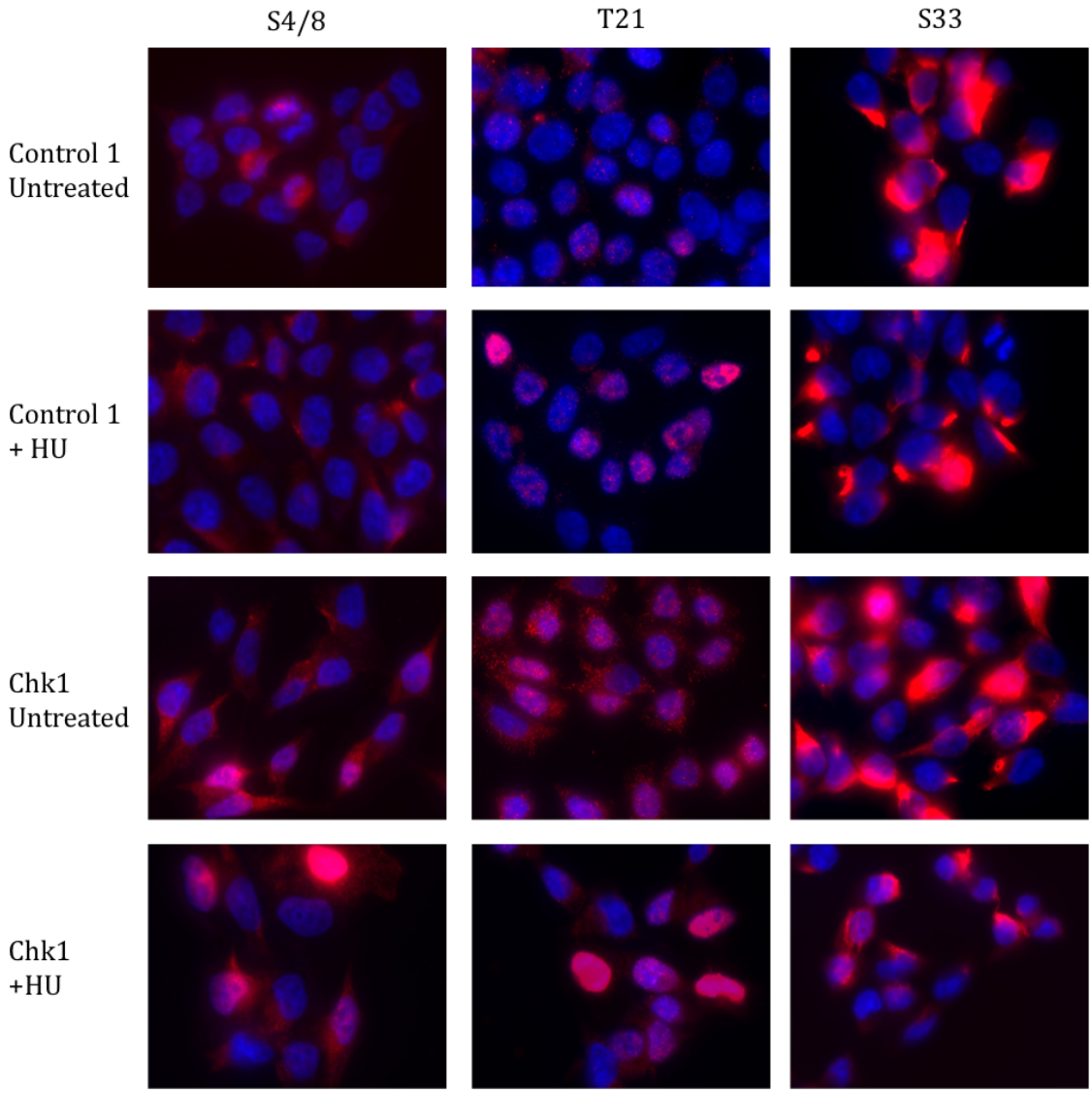

Figure 3.3.1.1 Comparison of pRPA2 Antibodies at 48 hour transfection time with initial protocol.

Representative images of HCT116 cells forward transfected with Control 1 or Chk1 siRNA and RNAiMAX and grown for 48 hours post-transfection. Cells were mock treated with PBS or treated with 2mM HU for 16 hours before fixing. Once fixed the cells were permeabilised with PBS-tween 20 in the washes. The cells were stained with antibodies raised against the S4/8, T21 and S33 phospho-sites within RPA2.

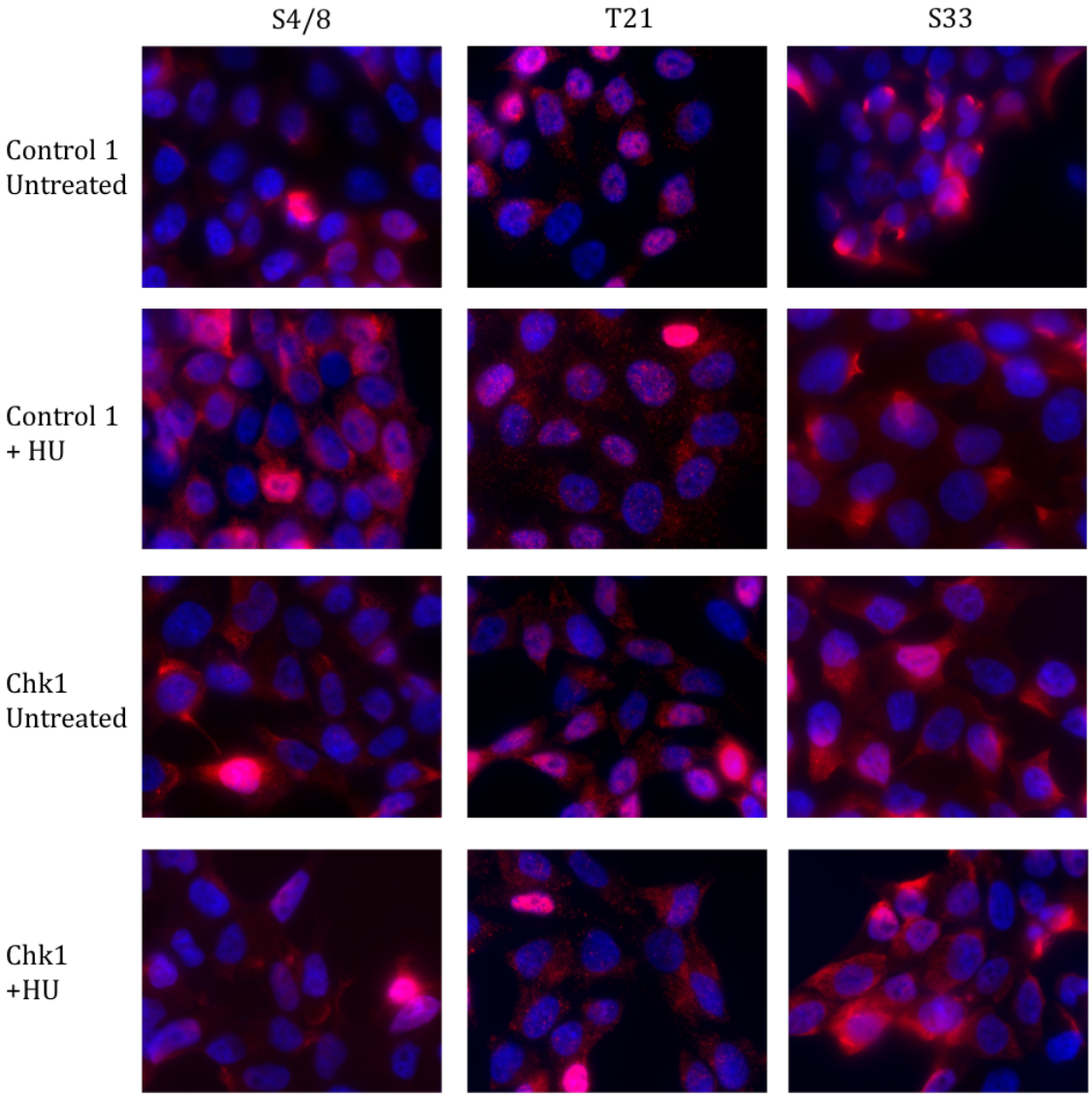

Figure 3.3.1.2 Comparison of pRPA2 Antibodies at 72 hour transfection time with initial protocol.

Representative images of HCT116 cells forward transfected with Control 1 or Chk1 siRNA and RNAiMAX and grown for 72 hours post-transfection. Cells were mock treated with PBS or treated with 2mM HU for 16 hours before fixing. Once fixed the cells were permeabilised with PBS-tween 20 in the washes. The cells were stained with antibodies raised against the S4/8, T21 and S33 phospho-sites within RPA2.

For the 48 hour samples, transfection with Chk1 siRNA or treatment with HU increased the percentage of nuclei positive for T21 foci when compared to Control 1 untreated cells (Figure 3.3.1.3). This is as expected as these cells would be experiencing an increased level of replication stress. No marked difference was seen between the Control 1 untreated cells and any other condition at 72 hours (Fig. 3.3.1.3). Unexpectedly, the combination of Chk1 knockdown and HU treatment did not increase the percentage of positive foci seen when compared to knockdown alone at either time point (Fig.3.3.1.3).

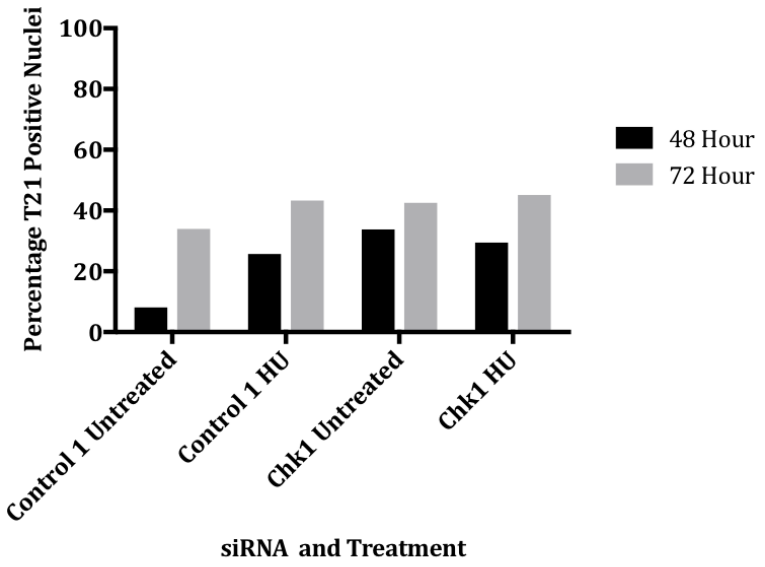

Figure 3.3.1.3 Percentage of HCT116 cells positive for T21 foci with initial protocol.
For each condition the number of cells were counted and the percentage of T21 positive nuclei was calculated. A nucleus was considered positive if it contained 10 or more bright T21 foci. Values derived from one experiment.

3.3.2 Improved Protocol for Phospho-RPA2 Foci Detection

The comparison of the three pRPA2 antibodies was repeated using a re-optimised protocol to improve the staining produced by the assay (see below), and to bring the protocol into line with the high throughput screening assays run at the Sheffield RNAi Screening Facility (SRSF). As such, HCT116 cells were reverse transfected with DharmaFECT 1 used as the transfection reagent. Additionally, a more stringent extraction step, where the cells were incubated with 0.5% Triton X-100 and 3% BSA in PBS for 5 minutes, was included post-fixation. This was incorporated to further permiabilise the membranes of the cell and allow the antibodies better access to the nucleus (Fig.3.3.2.1 and. 3.3.2.2).

With the improved extraction procedure, the S4/8 antibody demonstrated a higher level of nuclear staining, however there was still a high cytoplasmic background. Whilst some cells did display nuclear foci, this was only ever observed in the HU treated cells and not in the untreated Chk1 knocked down cells (Fig. 3.3.2.1 and 3.3.2.2). The alterations to the protocol also improved entry of the S33 antibody into the cells. However, the antibody now stained both the cytoplasm and the nucleus and no clear foci could be detected. It also showed very little change between the different conditions, especially at the 72 hour time

point (Fig. 3.3.2.1 and 3.3.2.2). The level of nuclear background staining observed in the T21 images was reduced using this amended protocol. The T21 antibody images were scored for the number of pRPA2 foci they contained to determine whether it could detect changes in the levels of replication stress between the different conditions (Fig. 3.3.2.3).

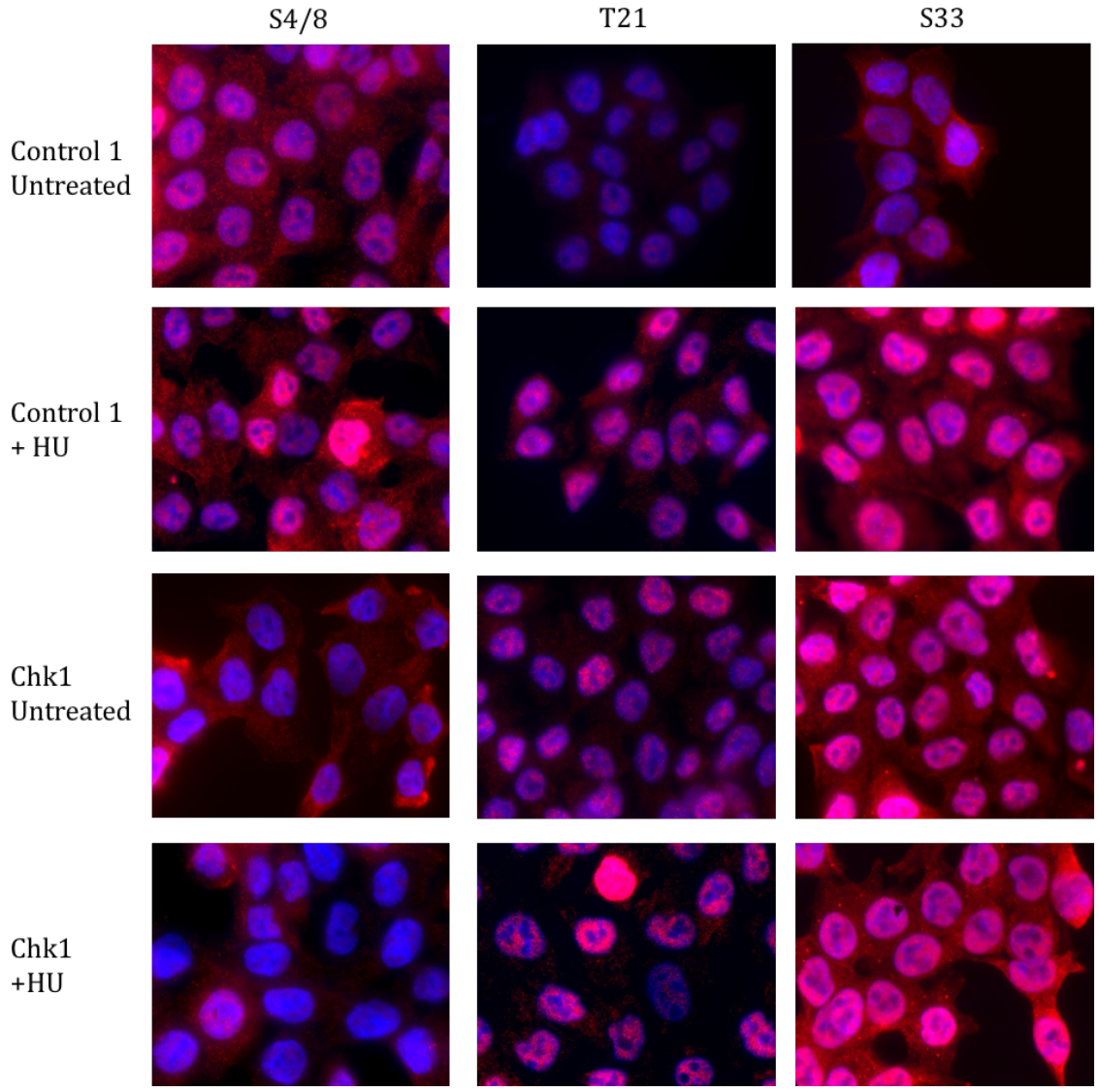

Figure 3.3.2.1 Comparison of pRPA2 Antibodies at 48 hour transfection time with improved protocol.

Representative images of HCT116 cells reverse transfected with Control 1 or Chk1 siRNA and DharmaFECT 1 and grown for 48 hours post-transfection. Cells were mock treated with PBS or treated with 2mM HU for 16 hours before fixing. Once fixed the cells were permeabilised with 0.5 % Triton X-100 and 3% BSA. The cells were stained with antibodies raised against the S4/8, T21 and S33 phospho-sites within RPA2.

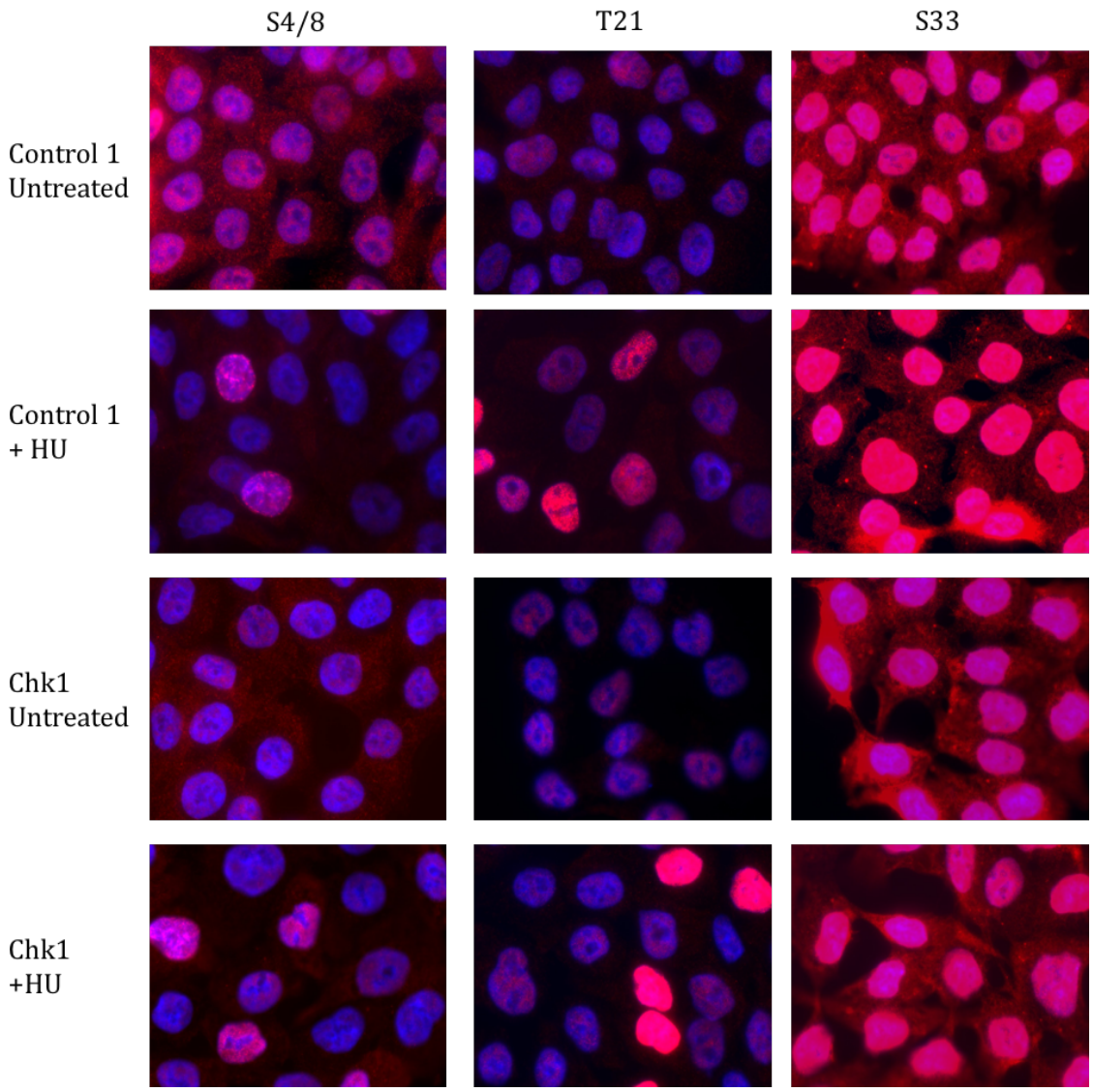

Figure 3.3.2.2 Comparison of pRPA2 Antibodies at 72 hour transfection time with improved protocol.

Representative images of HCT116 cells reverse transfected with Control 1 or Chk1 siRNA and DharmaFECT 1 and grown for 72 hours post-transfection Cells were mock treated with PBS or treated with 2mM HU for 16 hours before fixing. Once fixed the cells were permeabilised with 0.5 % Triton X-100 and 3% BSA. The cells were stained with antibodies raised against the S4/8, T21 and S33 phospho-sites within RPA2.

A higher percentage of T21 positive cells were detected in all conditions (Fig. 3.3.2.3) when reverse transfection and a stronger extraction procedure are used. In both the 48 hour and 72 hour experiments, Chk1 knockdown increased the percentage of T21 positive nuclei compared to Control 1 untreated cells. The signal window between these conditions was 47.35% at 48 hours and 23.55% at the 72 hour time point (Fig. 3.3.2.3). Unlike in the previous experiment, the combination of Chk1 knockdown and HU treatment increased the percentage of T21 positive cells observed at 72 hours but not 48 hours.

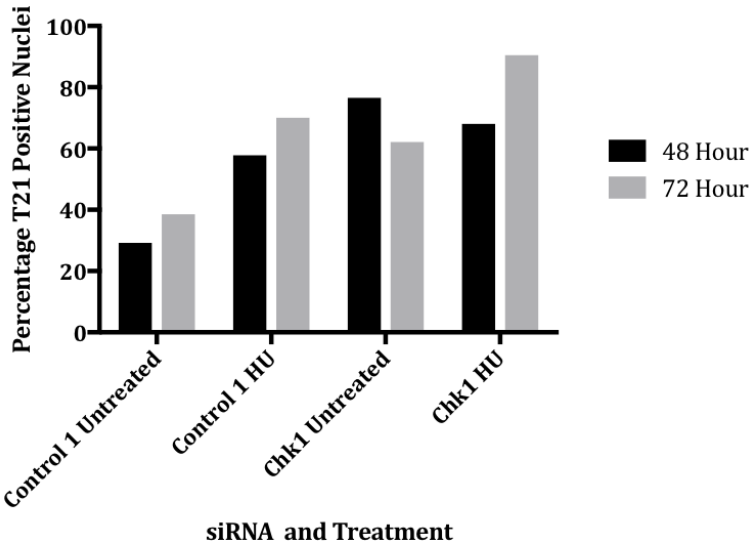

Figure 3.3.2.3 Percentage of HCT116 cells positive for T21 foci with improved protocol.
For each condition the number of cells were counted and the percentage of T21 positive nuclei was calculated. A nucleus was considered positive if it contained 10 or more bright T21 foci. Values derived from one experiment.

This experiment was repeated with a 48 hour transfection and without HU treatment to further investigate the staining of Chk1 knocked down cells by the T21 antibody. The scoring data from these additional two repeats was combined with the original data to assess the T21 antibodies ability to repeatedly detect replication stress (Fig. 3.3.2.4).

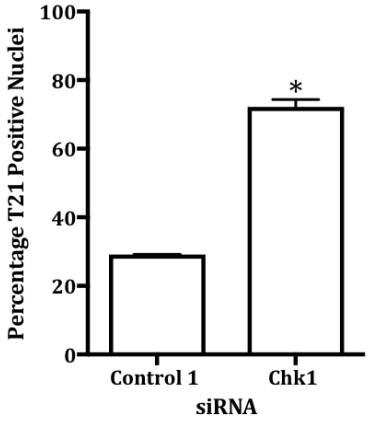

Figure 3.3.2.4 Percentage of Chk1 knocked down HCT116 cells positive for T21 foci.
For each condition the number of cells were counted and the percentage of T21 positive nuclei was calculated. A nucleus was considered positive if it contained 10 or more bright T21 foci. Asterisks indicate significant difference from Control 1, p value <0.05. Mean values derived from three independent experiments, with their respective SEMs.

The scoring data produced by the T21 antibody was reproducible in the three repeats. Chk1 knockdown significantly increased the percentage of T21 positive nuclei when compared to the Control 1 cells (p value of 0.0006) and produced a signal window of 43.4%.

Once the staining procedure was established it was repeated in cells transfected with RRM1 siRNA (Fig.3.2.1). The cells were reverse transfected with Control 1 or RRM1 siRNA and DharmaFECT 1 for 48 hours. The cells were then scored for T21 positive nuclei (Fig.3.3.2.5 and Fig. 3.3.2.6).

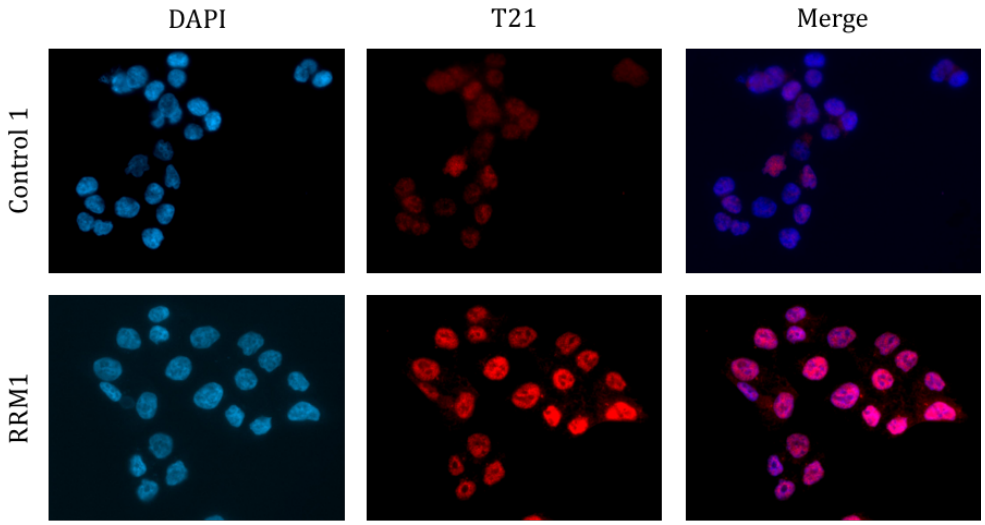

Figure 3.3.2.5 RPA2 T21 staining in RRM1 knocked down HCT116 cells.
Representative images of HCT116 cells reverse transfected with Control 1 or RRM1 siRNA and DharmaFECT 1. Cells were grown for 48 hours post-transfection before fixing. Once fixed, the cells were permeabilised with 0.5 % Triton X-100 and 3% BSA. The cells were stained with an antibody raised against the T21 phospho-site within RPA2.

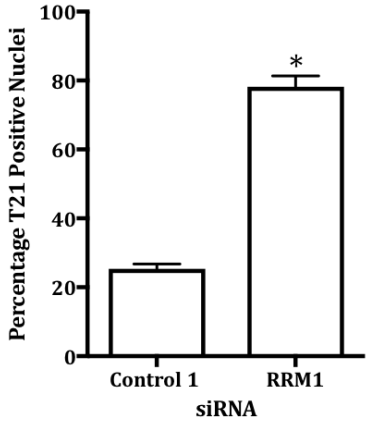

Figure 3.3.2.6 Percentage of RRM1 knocked down HCT116 cells positive for T21 foci.
For each condition the number of cells were counted and the percentage of T21 positive nuclei was calculated. A nucleus was considered positive if it contained 10 or more bright T21 foci. Asterisks indicate significant difference from Control 1, p value <0.05. Mean values derived from three independent experiments, with their respective SEMs

The staining pattern produced by the knockdown of RRM1 was distinct from that of the Chk1 knocked down cells. A number of cells displayed very bright staining and a highly positive nucleus, in some cases leading to the saturation of the image (Fig.3.3.2.5). The knockdown of RRM1 produced a significantly higher percentage of T21 positive cells than Control 1 siRNA cells (p value 0.0001) (Fig.3.3.2.6) and a slightly higher percentage than Chk1 knockdown (78.84% compared to 72.52%). The signal window of this assay, 53.33%, was also larger than that produced by Chk1 knockdown (47.35%). As Chk1 and RRM1 knockdown produced repeatable induction of replication stress and suitable signal windows, both were used for further development of the screening assay.

3.4 Phospho-RPA2 Replication Stress Detection in a Cell Line Panel

Once the T21 protocol had been established in HCT116 cells, it was tested in several different cell lines to ensure that the staining was not a cell line specific effect. The experiment was repeated in RPE-1, SW480 and p53 deficient HCT116 cell lines.

3.4.1 Phospho-RPA2 Replication Stress Detection in RPE-1

The hTERT immortalised normal cell line RPE-1 was used to assess the effect of replication stress suppressor knockdown in a normal, as opposed to a cancerous cell line (Fig.3.4.1.1, Table 3.4.1.1 and Fig 3.4.1.2). The staining pattern produced by the T21 antibody in RPE-1 cells was comparable to that seen in HCT116. When scored, a similar trend was seen in the levels of positive nuclei, with RRM1 inducing a slightly stronger response than Chk1 knockdown. RRM1 knockdown produced a higher percentage of cells that showed very bright staining and the cell morphology was also altered with the nuclei appearing much larger than in Control 1 cells (Fig.3.4.1.1). However, neither knockdown of Chk1 or RRM1 produced a statistically significant increase in T21 positive nuclei (p values 0.09 and 0.12 respectively; Fig 3.4.1.2).

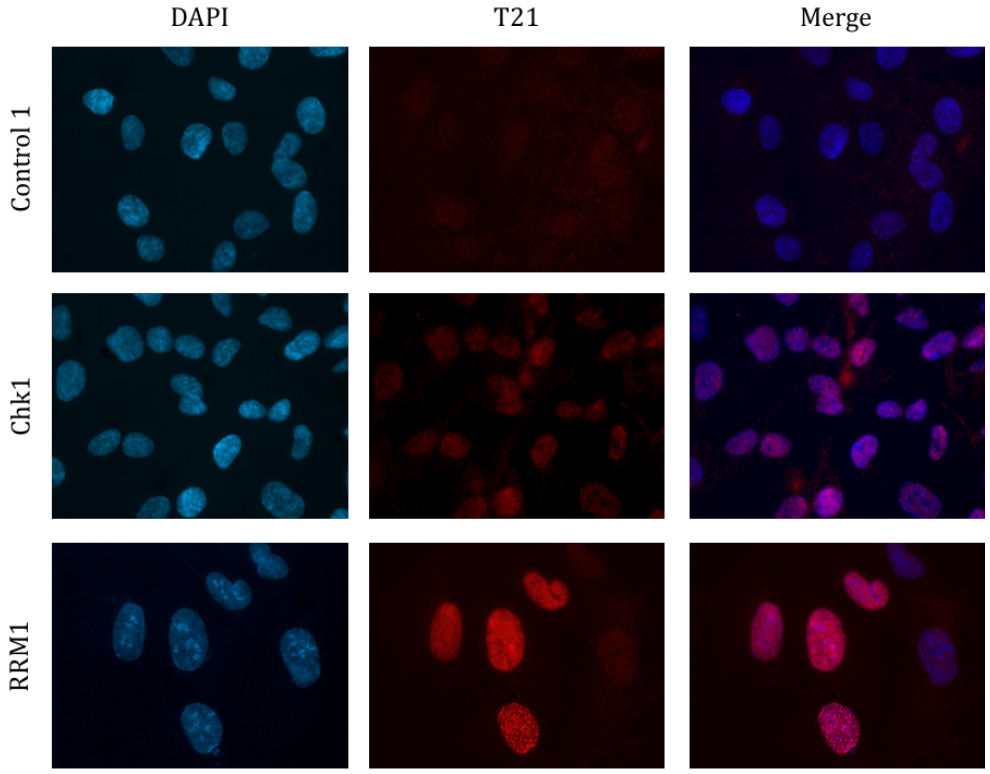

Figure 3.4.1.1 RPA2 T21 staining in RPE-1 cells.

Representative images of RPE-1 cells reverse transfected with Control 1, Chk1 or RRM1 siRNA and DharmaFECT 1. Cells were grown for 48 hours post-transfection before fixing. Once fixed, the cells were permeabilised with 0.5 % Triton X-100 and 3% BSA. The cells were stained with an antibody raised against the T21 phospho-site within RPA2.

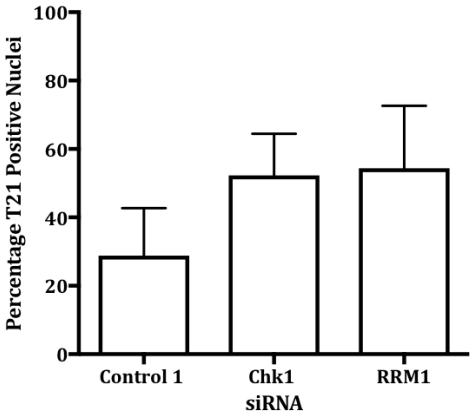

Figure 3.4.1.2 Percentage of RPE-1 cells positive for T21 foci.

For each condition the number of cells were counted and the percentage of T21 positive nuclei was calculated. A nucleus was considered positive if it contained 10 or more bright T21 foci. Asterisks indicate significant difference from Control 1, p value <0.05. Mean values derived from three independent experiments, with their respective SEMs.

3.4.2 Phospho-RPA2 Replication Stress Detection in SW480

The adenocarcinoma derived SW480 cell line and HCT116 differ in their MMR and p53 status. The T21 protocol was repeated in this cell line to assess the possible effects of MIN and p53 deficiency on the levels of replication stress detected (Fig. 3.4.2.1 and Fig. 3.4.2.2).

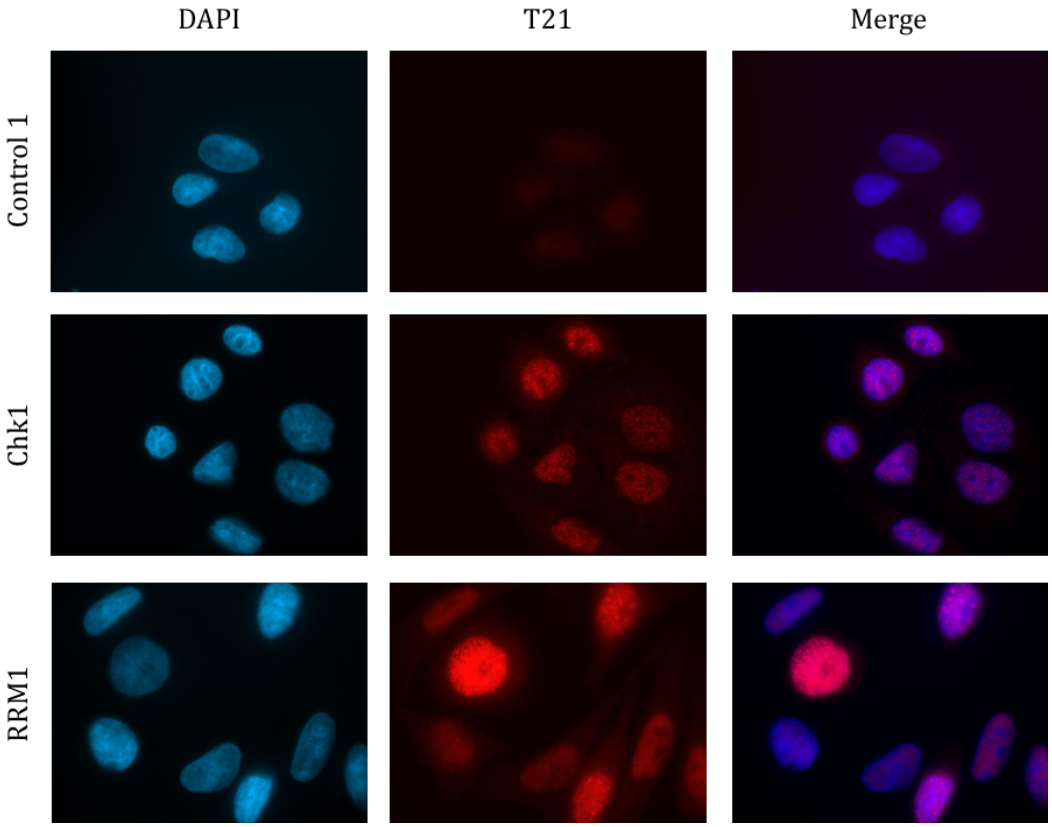

Figure 3.4.2.1 RPA2 T21 staining in SW480 cells.

Representative images of SW480 cells reverse transfected with Control 1, Chk1 or RRM1 siRNA and DharmaFECT 1. Cells were grown for 48 hours post-transfection before fixing. Once fixed, the cells were permeabilised with 0.5 % Triton X-100 and 3% BSA. The cells were stained with an antibody raised against the T21 phospho-site within RPA2.

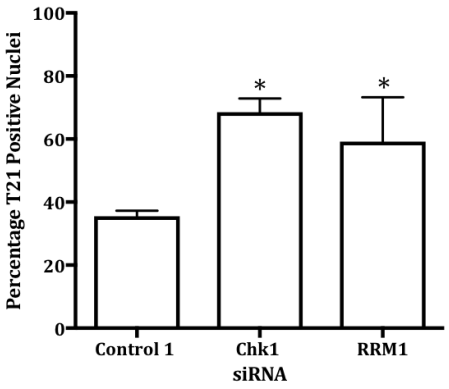

Figure 3.4.2.2 Percentage of SW480 cells positive for T21 foci.

For each condition the number of cells were counted and the percentage of T21 positive nuclei was calculated. A nucleus was considered positive if it contained 10 or more bright T21 foci. Asterisks indicate significant difference from Control 1, p value <0.05. Mean values derived from three independent experiments, with their respective SEMs.

As with RPE-1 cells, the staining pattern observed in the SW480 cells was similar to that seen in HCT116. However, in these cells, Chk1 knockdown produced a higher percentage of positive nuclei than loss of RRM1 (Fig.3.4.2.2). Nonetheless, the RRM1 knockdown again produced more cells with a very high number of foci (Fig.3.4.2.1). The knockdown of both genes produced a significant increase in the level of T21 positive nuclei observed with p values of 0.0003 and 0.043 respectively (Fig.3.4.2.2).

3.4.3 Phospho-RPA2 Replication Stress Detection in p53 Deficient HCT116

The T21 staining protocol was carried out in HCT116 with p53 function abolished by HR (Bunz et al, 1998), a kind gift from Professor M. Meuth. These were used to assess the effects of p53 disruption in an otherwise unchanged genetic background (Fig.3.4.3.1 and Fig 3.4.3.2). It was anticipated that these p53 deficient cells could be utilised to detect any replication stress suppressors that conferred a synthetic lethal relationship with p53 loss.

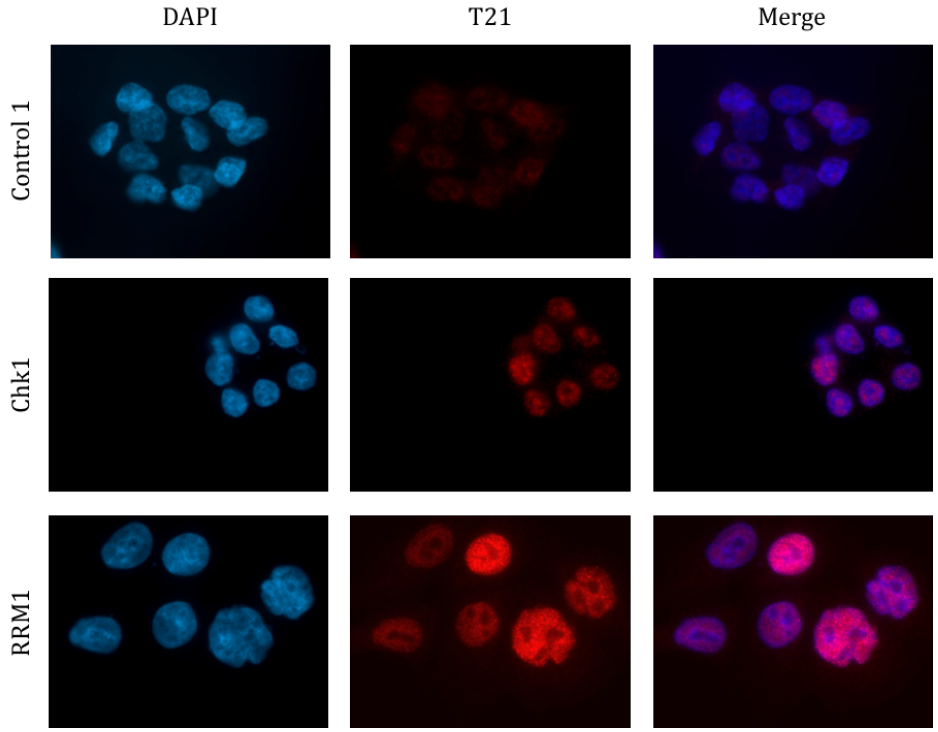

Figure 3.4.3.1 RPA2 T21 staining in HCT116 p53 Null Cells.

Representative images of HCT116 p53 Null cells reverse transfected with Control 1, Chk1 or RRM1 siRNA and DharmaFECT 1. Cells were grown for 48 hours post-transfection before fixing. Once fixed, the cells were permeabilised with 0.5 % Triton X-100 and 3% BSA. The cells were stained with an antibody raised against the T21 phospho-site within RPA2.

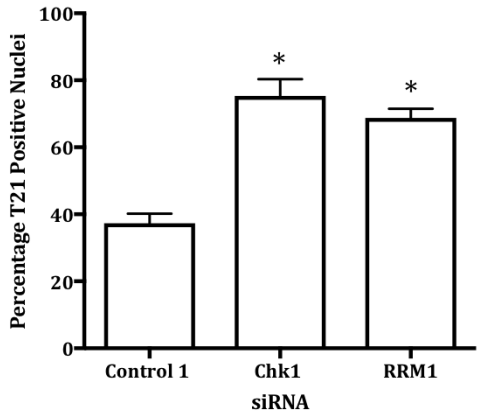

Figure 3.4.3.2 Percentage of HCT116 p53 Null cells positive for T21 foci.
For each condition the number of cells were counted and the percentage of T21 positive nuclei was calculated. A nucleus was considered positive if it contained 10 or more bright T21 foci. Asterisks indicate significant difference from Control, p value <0.05. Mean values derived from three independent experiments, with their respective SEMs.

The p53 deficient HCT116 cells produced the same scoring trend as the p53 deficient SW480 cell line, with a higher level of replication stress detected in the Chk1 knocked down cells than the RRM1. Chk1 and RRM1 knockdown resulted in a significant increase in the levels of replication stress detected when compared to Control 1 transfected cells with p values 0.0028 and 0.0013 respectively (Fig. 3.4.3.2).

3.4.4 Comparison of Phospho-RPA2 Detection in the Cell Line Panel

Comparison of the HCT116 wild type scoring data and that obtained from RPE-1 cells shows that the RPE-1 Control 1 transfected population displayed a higher proportion of cells positive for replication stress, which was unexpected (Fig 3.4.4.1). However, in both the Chk1 and RRM1 knocked down cells, the level of positive nuclei observed was lower in the RPE-1, suggesting that the loss of replication stress suppressors had less of an effect in this cell line.

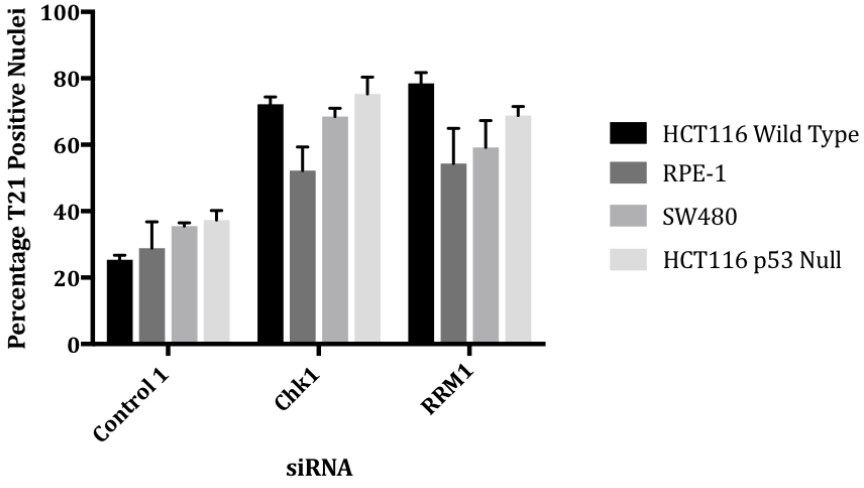

Figure 3.4.4.1 Comparison of the percentage of HCT116 wild type, RPE-1, SW480 and HCT116 p53 null cells positive for T21 foci.
For each condition the number of cells were counted and the percentage of T21 positive nuclei was calculated. A nucleus was considered positive if it contained 10 or more bright T21 foci. Mean values derived from three independent experiments with error bars representing the SEM.

Likewise, the SW480 Control 1 siRNA transfected cells showed a higher background level of replication stress compared to the HCT116 wild type cells. In this cell line, the loss of Chk1 also appeared to have a greater effect upon the levels of replication stress observed compared to the knockdown of RRM1 which was not observed in the HCT116 wild type cells. Very similar results were seen when comparing the HCT116 wild type and HCT116 p53 null cells. This suggests that the higher basal levels and greater dependence on Chk1 for suppressing replication stress were due to the loss of p53 in the SW480 cells.

3.5 High Throughput Phospho-RPA2 Replication Stress Detection

For the identification of heightened replication stress following gene knockdown on a genome-wide scale, a high throughput assay was required and was developed at the Sheffield RNAi Screening Facility (SRSF).

3.5.1 Initial High Throughput Staining Protocol

The protocol previously optimised in 24 well plates was scaled down into the 384 well format with some minor adjustments, as described in section 2.2.1.5 due to the nature of this plate type. The initial optimisation experiment aimed to determine which concentration of the T21 pRPA2 antibody to use in this assay. For this, HCT116 cells were reverse transfected for 48 or 72 hours with non-targeting Control 1 or Chk1 siRNA using DharmaFECT 1. The cells were fixed with 4% PFA containing a 1:500 dilution of Hoescht, permeabilised for 5 minutes with 0.5% Triton X-100 and 3% BSA and stained with a titration of the T21 pRPA primary antibody (1:250 - 1:1000). Images were captured with the 20X objective of the Molecular Devices ImageXpress Micro High Content Microscope (Fig. 3.5.1.1 and Fig 3.5.1.2).

In both assay plates, the T21 antibody appeared to have entered the cells but did not stain the nucleus strongly. In the 48 hour plate (Fig.3.5.1.1) very little difference was observed between the Control 1 and Chk1 knocked down cells. Whilst pRPA2 staining appeared stronger in the 72 hour plate (Fig.3.5.1.2) only a few Chk1 knocked down cells appeared brightly stained. The levels of background staining were high and no clear foci could be detected at any antibody concentration. Upon examination of the images, it was deemed that the staining was not suitable for analysis due to the lack of foci perceived.

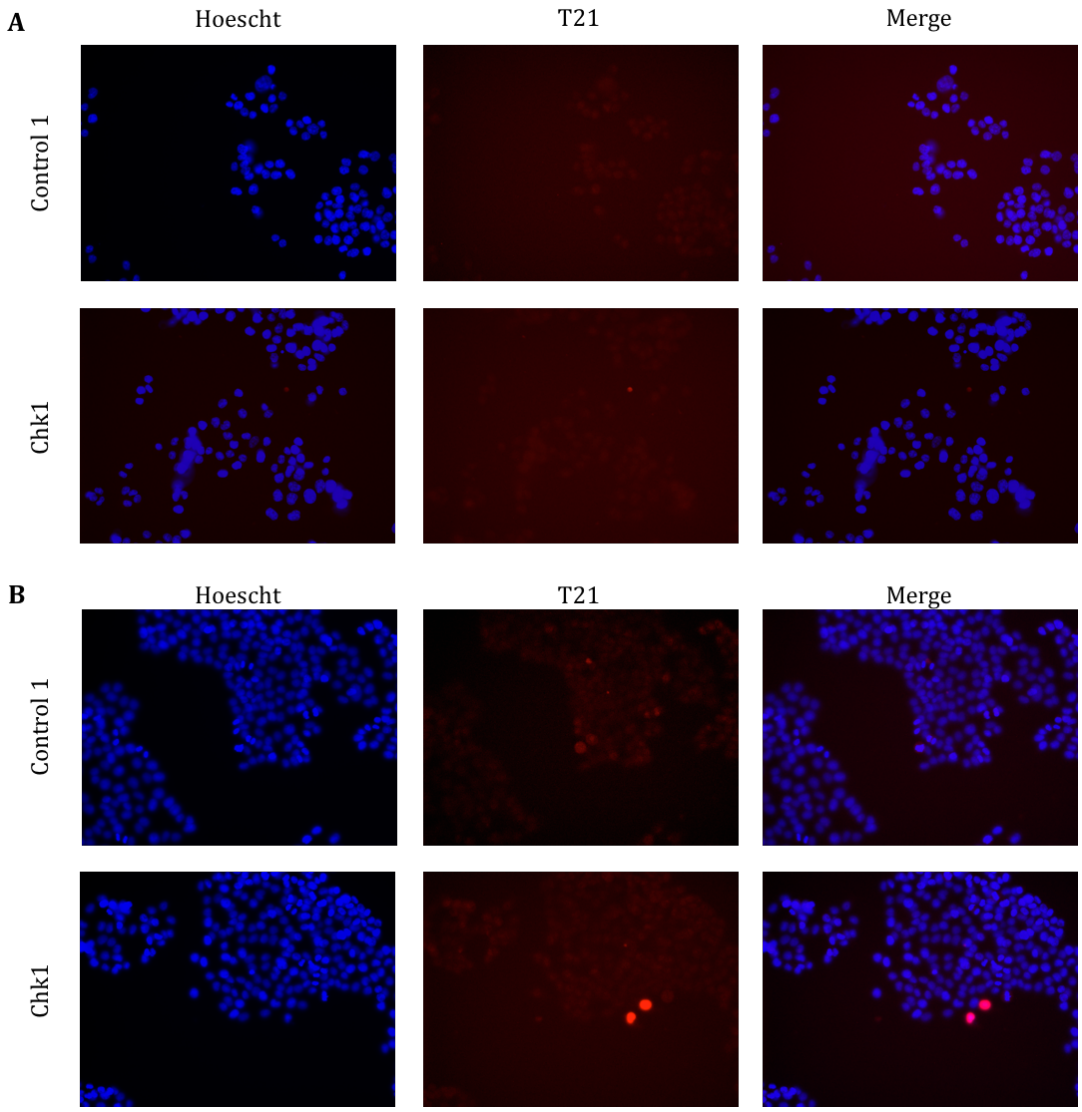

Figure 3.5.1.1 RPA2 T21 staining with initial high throughput protocol

Representative images of HCT116 cells reverse transfected with Control 1 or Chk1 siRNA and DharmaFECT 1 and grown for (A) 48 or (B) 72 hours post-transfection. Once fixed and permeabilised with 0.5% Triton X-100 and 3% BSA for 5 minutes, cells were stained with a 1:250 dilution of an antibody raised against the T21 site in RPA2.

3.5.2 Time Course to Determine Optimum Extraction Time

As the initial staining protocol was not successful, further optimisation was required to produce a staining pattern suitable for scoring in this plate type. Due to the dimensions of the plate and the use of automated aspiration, the incubation time with 4% PFA had to be increased to achieve optimal fixation of the cells. A similar approach was trialled with 0.5% Triton X-100 and 3% BSA to assess if increasing the extraction time would improve the levels of antibody entering the nucleus. The experiment was set up as previously described but with extraction times of 5, 7, 10 or 15 minutes and a single concentration of T21 primary antibody (1:250) (Fig.3.5.2.1 and Fig 3.5.2.2).

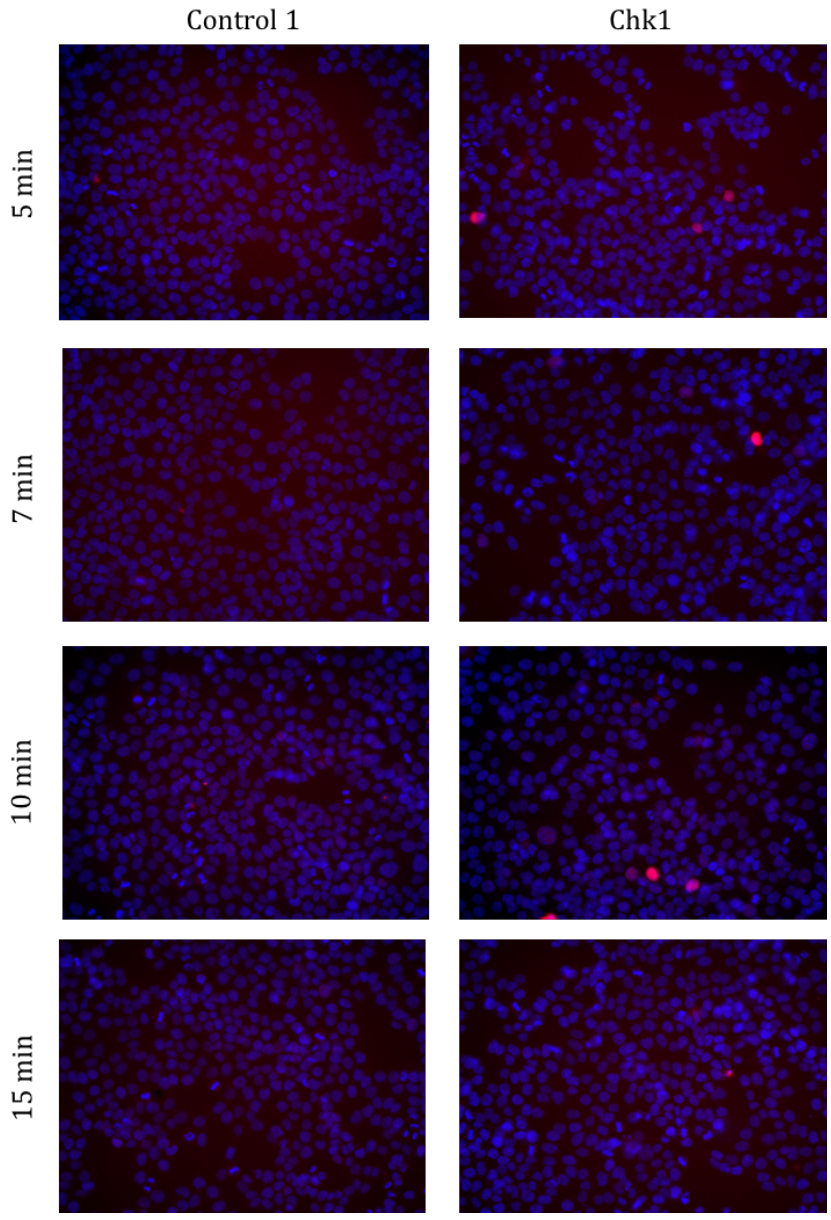

Figure 3.5.2.1 Extraction time course in 384 well plate at 48 hours.

Representative images of HCT116 cells reverse transfected with Control 1 or Chk1 siRNA and DharmaFECT 1 and grown for 48 hours post-transfection. Once fixed and permeabilised with 0.5% Triton X-100 and 3% BSA for 5, 7, 10 or 15 minutes, cells were stained with a 1:250 dilution of an antibody raised against the T21 site in RPA2.

In both assay plates, the staining with a 5 minute extraction was poor with little antibody entering the nucleus (Fig.3.5.2.1 and Fig. 3.5.2.2). As the extraction time increased to 10 minutes, the level of nuclear staining increased slightly. Conversely, at the 15 minute time point, the antibody signal appeared to have diffused out of the cells, probably due to over permeabilisation of the cytoplasmic membrane. The 10 minute time point was therefore chosen for all further high throughput screening experiments to improve the nuclear entry of the antibody.

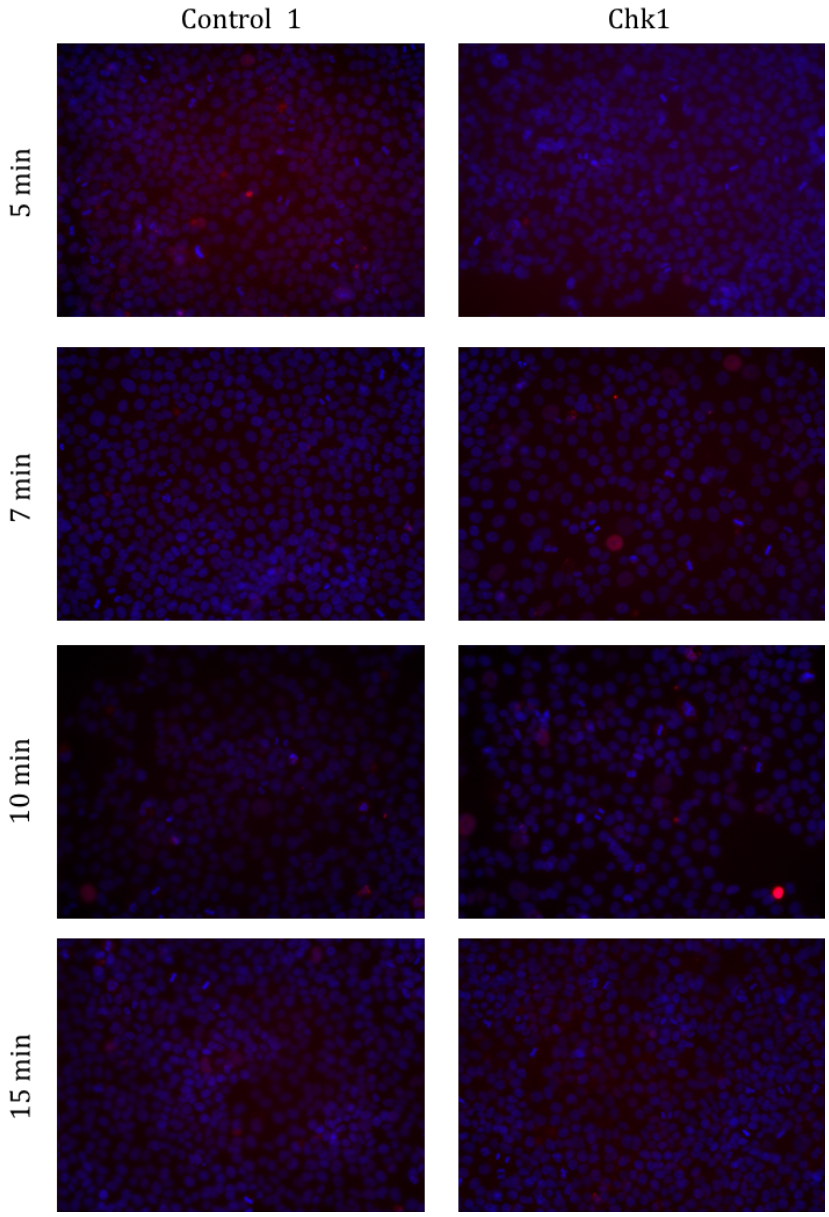

Figure 3.5.2.2 Extraction time course in 384 well plate at 72 hours.

Representative images of HCT116 cells reverse transfected with Control 1 or Chk1 siRNA and DharmaFECT 1 and grown for 72 hours post-transfection. Once fixed and permeabilised with 0.5% Triton X-100 and 3% BSA for 5, 7, 10 or 15 minutes, cells were stained with a 1:250 dilution of an antibody raised against the T21 site in RPA2.

3.5.3 High Throughput Staining Protocol with Increased Extraction Time

The T21 primary antibody titration (1:250 – 1:1000) was repeated with the optimal extraction time (10 minutes) identified previously to determine the concentration of primary antibody to be used in the final screening assay (Fig.3.5.3.1).

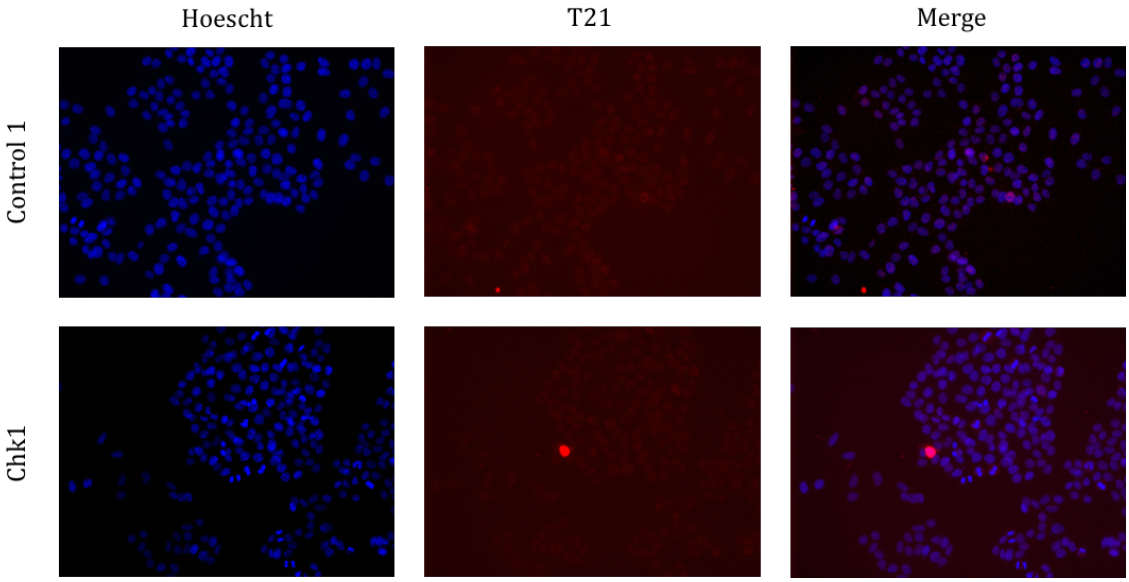

Figure 3.5.3.1 RPA2 T21 staining 10 minute extraction at 72 hours.
Representative images of HCT116 cells reverse transfected with Control 1 or Chk1 siRNA and DharmaFECT 1 and grown for 72 hours post-transfection. Once fixed and permeabilised with 0.5% Triton X-100 and 3% BSA for 10 minutes, cells were stained with a 1:250 dilution of an antibody raised against the T21 site in RPA2.

Antibody staining appeared to be increased when compared to the images obtained for the initial staining procedure, yet the antibody staining was still not sufficient for automated scoring. Very little difference in the proportions of highly stained nuclei were observed between the Control 1 and Chk1 knocked down cells. Unfortunately, images could not be obtained for the 48 hour plate due to a lack of cells present in the wells. This was due to an error made during the fixation of the plates, where Triton X-100 at 0.5% was added to the plates in the place of 4% PFA. As the increased extraction time proved insufficient to allow the differentiation between Control 1 and Chk1 knocked down cells, the 48 hour experiment was not repeated in favour of further optimisation.

3.5.4 High Throughput Staining Protocol with Cold Pre-Extraction

It was decided to add a pre-extraction step before the fixation of the cells to remove their cytoplasm as well as permeabilising the nuclear membrane. The rationale for its inclusion was that pre-extraction is commonly used to reduce non-specific antibody staining whilst improving access of the antibody to the nucleus. The decision was also made to include the Hoechst in the secondary antibody incubation, rather than in the fixative step to prevent any interactions with the binding of the primary antibody to chromatin associated RPA2. A 2mM overnight HU treatment was included as a transfection independent positive control. HCT116 cells were transfected as previously and were either treated or mock treated with HU 16 hours prior to fixing. A 5 minute incubation with the cold pre- extraction buffer at

4°C was included before the fixing of the cells in 4% PFA alone. The cells were then extracted and stained with 1:250 dilution of the T21 antibody and with the addition of the Hoechst in the secondary antibody incubation (Fig.3.5.4.1 and Fig. 3.5.4.2).

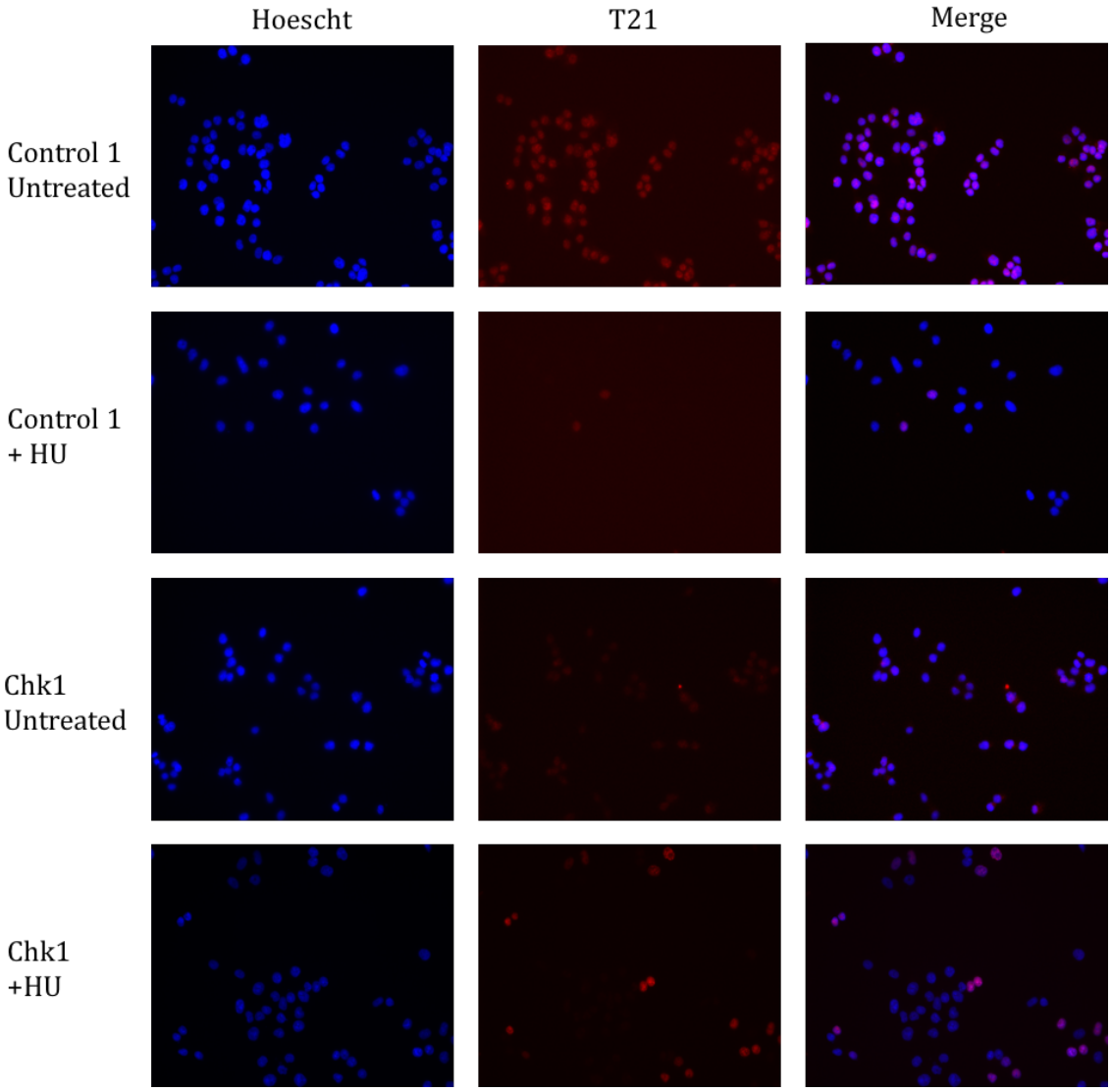

Figure 3.5.4.1 RPA2 staining T21 of Chk1 knocked down HCT116 with cold pre-extraction at 48 hours.

Representative images of HCT116 cells reverse transfected with Control 1 or Chk1 siRNA and DharmaFECT 1 and grown for 48 hours post-transfection. Cells were mock treated with PBS or treated with 2mM HU for 16 hours before fixing. Cells were incubated with cold pre-extraction buffer, fixed and then further permeabilised with 0.5% Triton X-100 and 3% BSA for 5 minutes. Cells were stained with a 1:250 dilution of an antibody raised against the T21 site in RPA2.

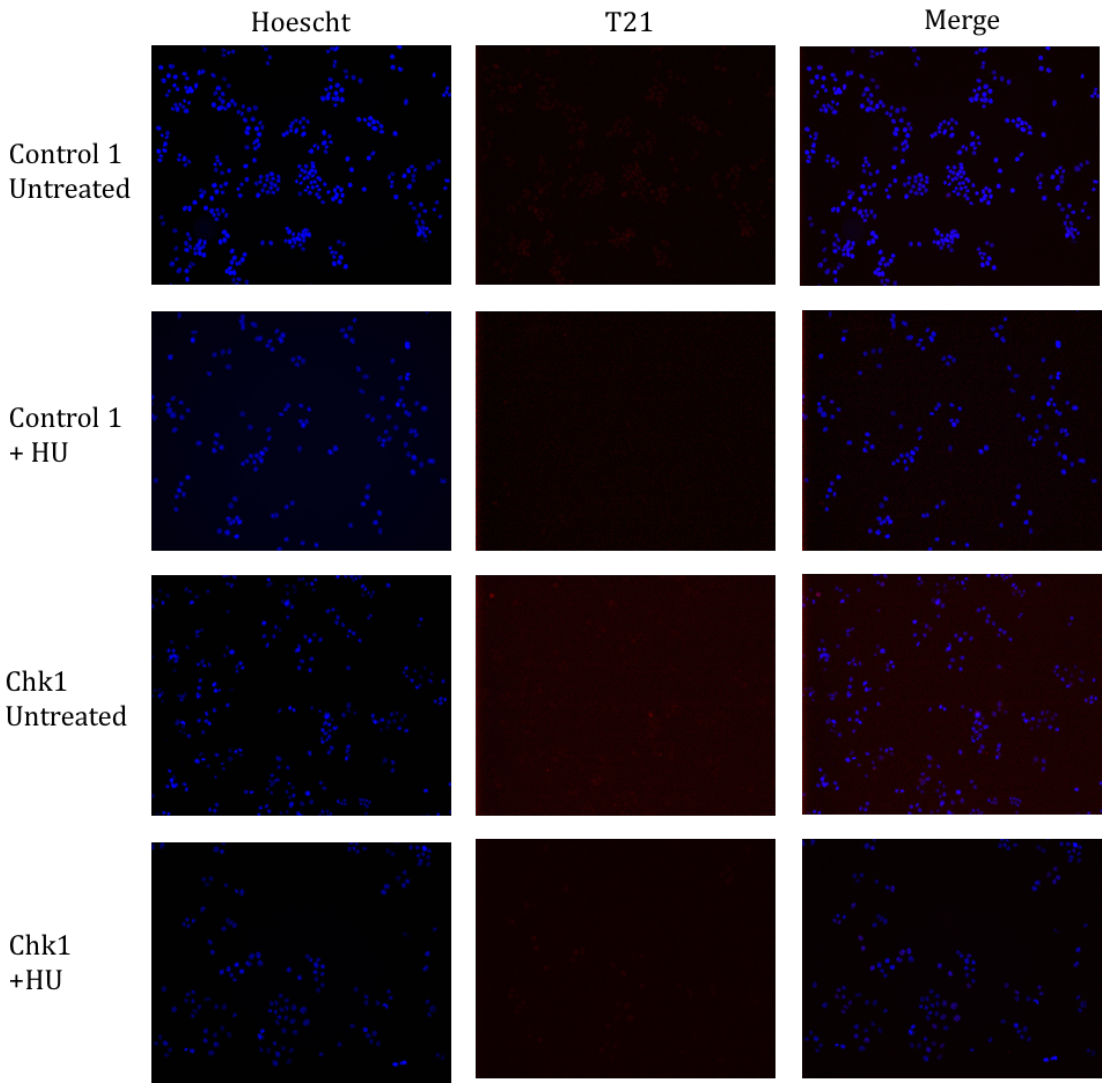

Figure 3.5.4.2 RPA2 staining T21 of Chk1 knocked down HCT116 with cold pre-extraction at 72 hours.

Representative images of HCT116 cells reverse transfected with Control 1 or Chk1 siRNA and DharmaFECT 1 and grown for 72 hours post-transfection. Cells were mock treated with PBS or treated with 2mM HU for 16 hours before fixing. Cells were incubated with cold pre-extraction buffer, fixed and then further permeabilised with 0.5% Triton X-100 and 3% BSA for 5 minutes. Cells were stained with a 1:250 dilution of an antibody raised against the T21 site in RPA2.

At both the 48 and 72 hour time points, very few cells remained in the wells once the cells were permeabilised and fixed. The 48 hour plate showed a very high level of background staining in the Control 1 siRNA transfected wells and discrete foci could not be observed. The addition of HU or the knockdown of Chk1 alone failed to raise the levels of T21 foci detected in this assay. However, when combined, the T21 stain appeared brighter and clear foci could be distinguished in some of the wells. The 72 hour plate showed a very low level of T21 staining making it very difficult to focus the microscope in the Cy5 channel. As a result of this, the plate had to be imaged using the 10X objective rather than the 20X to detect the T21 signal. No differences could be detected in the levels of staining between the different conditions.

As the Chk1 knockdown was not showing a detectable difference when compared to the Control 1 cells in this assay, the decision was made to test the RRM1 siRNA in this format. This siRNA had showed a stronger induction of T21 phosphorylation than Chk1 knockdown by western blotting (Fig. 3.2.1) and so it was thought that this siRNA may prove a more successful positive control in the high throughput assay. The experiment was repeated as previously described with the ice cold pre-extraction step, the only difference being the inclusion of RRM1 siRNA in the place of Chk1 (Fig.3.5.4.3 and Fig 3.5.4.4). As with the previous assay, insufficient cells were imaged due to a scarcity of cells remaining in the wells, even when the number of images taken per well was doubled.

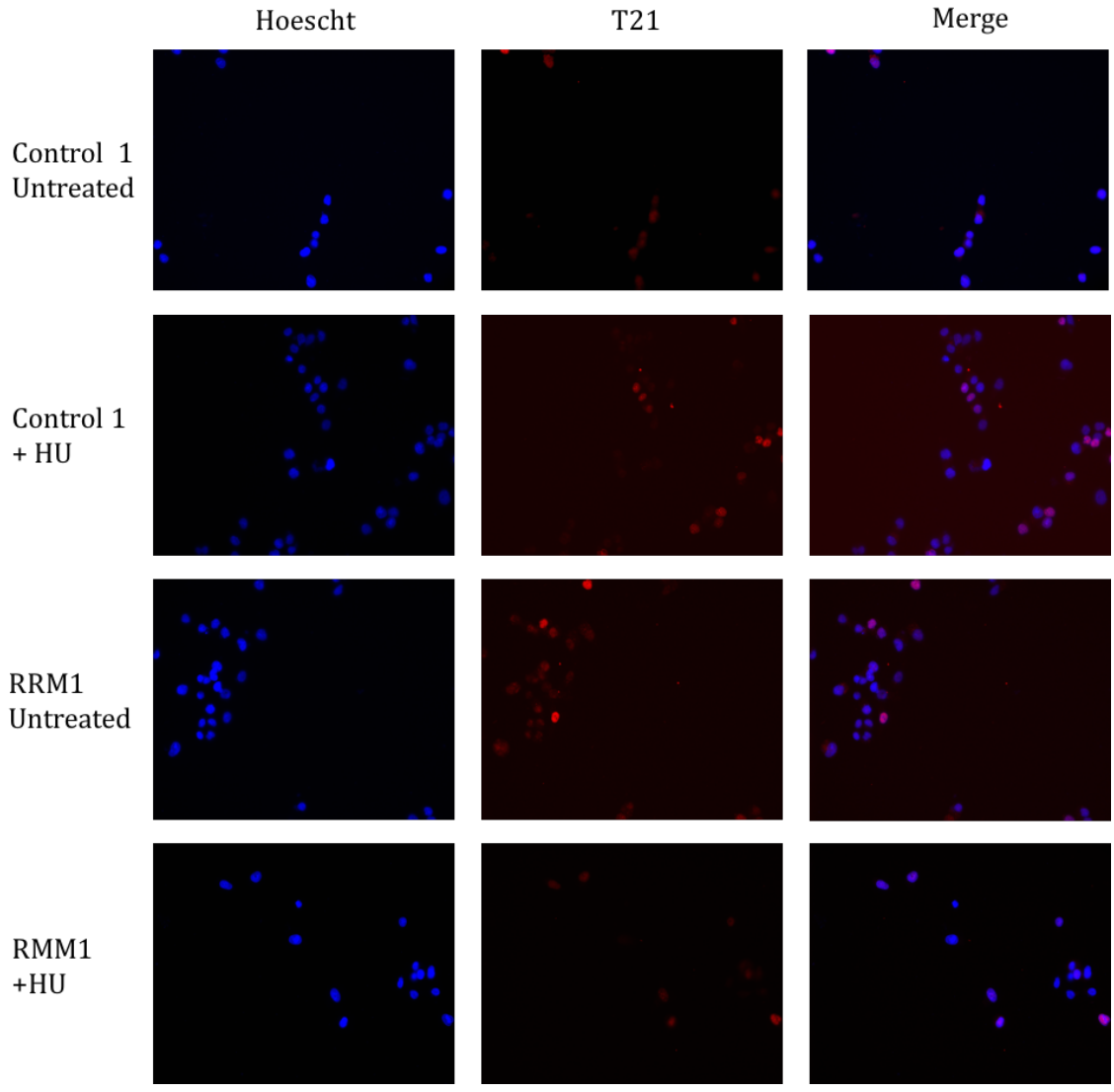

Figure 3.5.4.3 RPA2 T21 staining of RRM1 knocked down cells with cold pre-extraction at 48 hours.

Representative images of HCT116 cells reverse transfected with Control 1 or RRM1 siRNA and DharmaFECT 1 and grown for 48 hours post-transfection Cells were mock treated with PBS or treated with 2mM HU for 16 hours before fixing. Cells were incubated with cold pre-extraction buffer, fixed and then further permeabilised with 0.5% Triton X-100 and 3% BSA for 5 minutes. Cells were stained with a 1:250 dilution of an antibody raised against the T21 site in RPA2.

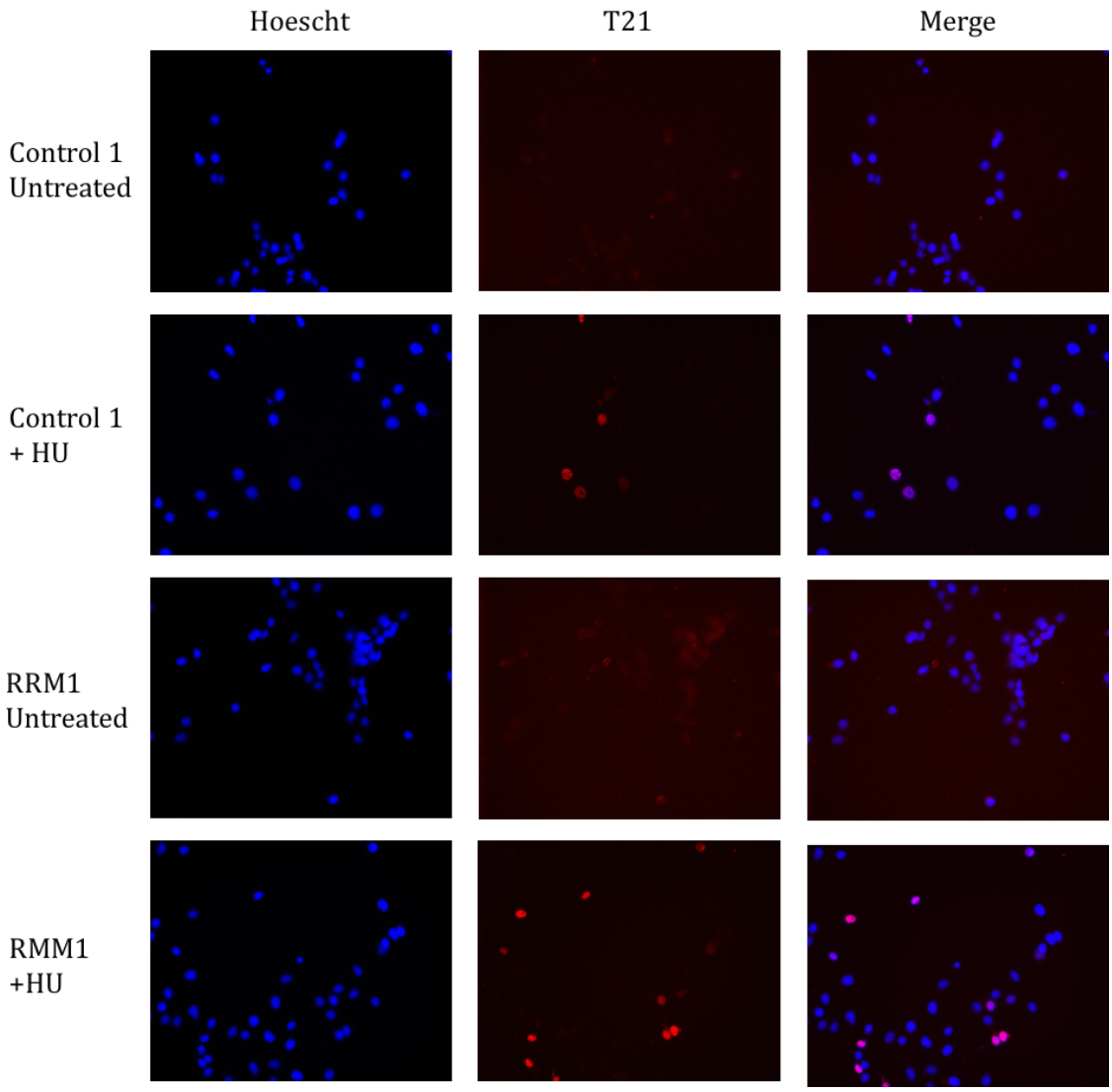

Figure 3.5.4.4 RPA2 T21 staining of RRM1 knocked down cells with cold pre-extraction at 72 hours.

Representative images of HCT116 cells reverse transfected with Control 1 or RRM1 siRNA and DharmaFECT 1 and grown for 72 hours post-transfection. Cells were mock treated with PBS or treated with 2mM HU for 16 hours before fixing. Cells were incubated with cold pre-extraction buffer, fixed and then further permeabilised with 0.5% Triton X-100 and 3% BSA for 5 minutes. Cells were stained with a 1:250 dilution of an antibody raised against the T21 site in RPA2.

In the 48 hour assay, RRM1 knockdown alone was sufficient to produce a difference in staining when compared to the untreated Control 1 cell populations. Clear foci could be detected in several cells in both the RMM1 knockdown and HU treated wells suggesting that the antibody was reaching the nucleus in sufficient quantities in this assay. On the 72 hour plate, RRM1 knockdown alone failed to produce foci, however bright cells could be seen in the images but they were not in sharp focus. Even though this assay seemed capable of producing cells containing bright foci, several factors prevented the continuation of cold pre-extraction as a viable method for preparing screening plates, including the lack of cells present at the end of the assay and logistical concerns regarding the cold incubation. A decision was therefore made to pursue other methods of improving the extraction of the cells to maintain the high throughput nature of the assay.

3.5.5 Triton X-100 Titration to Determine Optimum Concentration for Extraction

As the cold pre-extraction procedure was deemed impractical for high throughput screening, an alternative method of increasing the permeabilisation of the cell's nucleus was required. As a longer extraction time decreased the nuclear antibody signal detected, a titration of Triton X-100 was carried out to determine the optimum concentration for a 10 minute incubation. Solutions of 0.5%, 0.75% or 1.0% Triton X-100 with 3% BSA were used to extract Control 1 or RRM1 siRNA transfected cells. These were then stained with T21 antibody diluted at 1:250. The plate was imaged using the Cy5 channel and 20X objective and the Texas Red channel with both the 20X and 40X objectives to detect different wavelengths of light being emitted by the secondary antibody's fluorophore (Fig.3.5.5.1 and 3.5.5.2). The assay was not carried out at 72 hours as in previous experiments the extended transfection plates had shown increased levels of background staining.

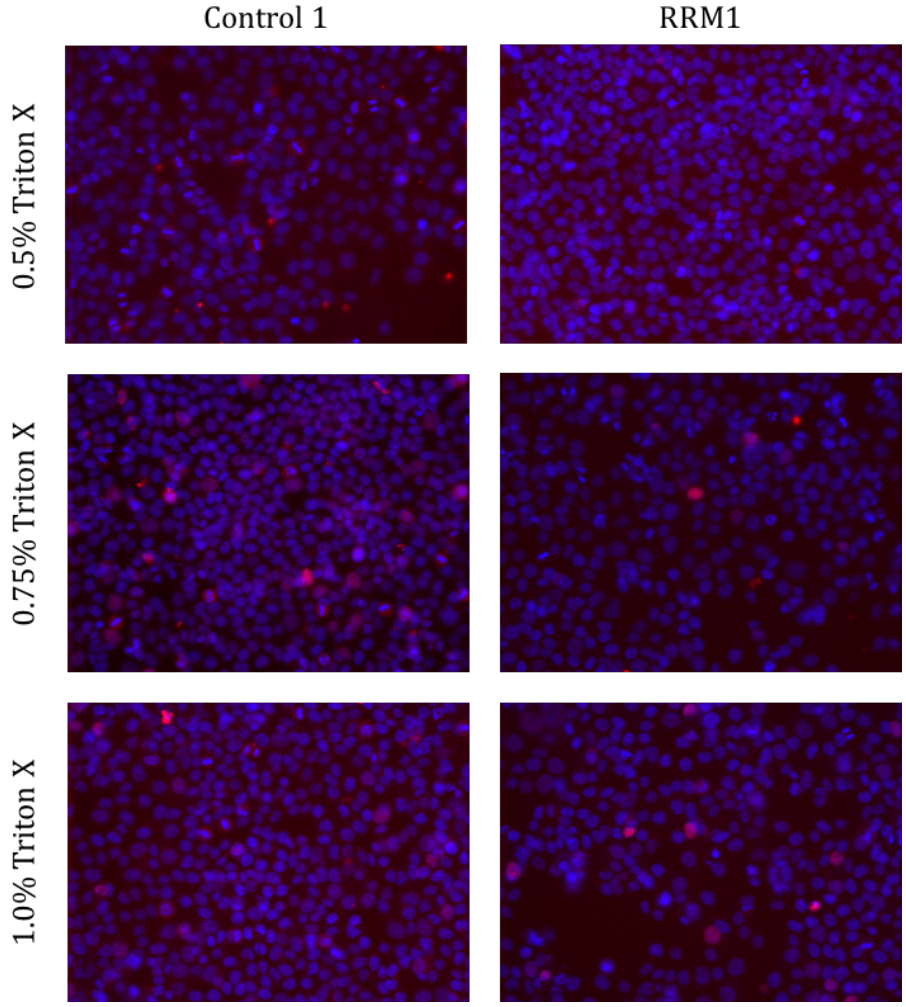

Figure 3.5.5.1 Triton X-100 Titration in RPA2 T21 stained cells imaged in the Cy5 channel
Representative images of HCT116 cells reverse transfected with Control 1 or RRM1 siRNA and DharmaFECT 1 and grown for 48 hours post-transfection. Once fixed the cells were permeabilised with 0.5%, 0.75% or 1.0% Triton X-100 and 3% BSA for 10 minutes. Cells were stained with a 1:250 dilution of an antibody raised against the T21 site in RPA2. Cells were imaged using the Cy5 channel of the Molecular Devices ImageXpress Micro High Content Microscope.

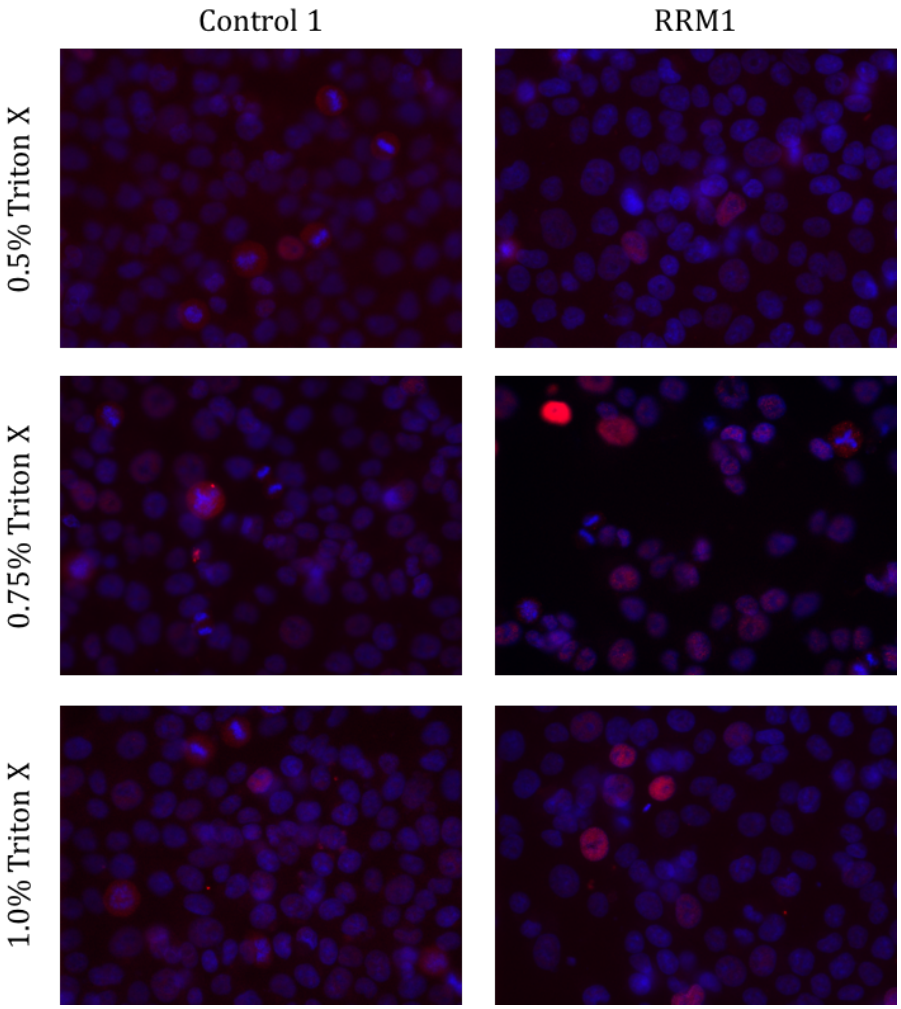

Figure 3.5.5.2 Triton X-100 Titration in RPA2 T21 stained cells imaged in the Texas Red channel.

Representative images of HCT116 cells reverse transfected with Control 1 or RRM1 siRNA and DharmaFECT 1 and grown for 48 hours post-transfection. Once fixed the cells were permeabilised with 0.5%, 0.75% or 1.0% Triton X-100 and 3% BSA for 10 minutes. Cells were stained with a 1:250 dilution of an antibody raised against the T21 site in RPA2. Cells were imaged using the Texas Red channel with a 40X objective on the Molecular Devices ImageXpress Micro High Content Microscope.

When the plate was imaged using the Cy5 channel, little differences could be detected between the Control 1 and RRM1 knocked down cells (Fig.3.5.5.1). Most of the brightly stained cells observed were mitotic and so of little interest in this assay. However, switching to the Texas Red channel greatly improved the detection of the secondary antibody signal (Fig.3.5.5.2); a reduced level of background staining was observed and clear foci could be detected in the RRM1 knocked down cells at 40X. Increasing the Triton X-100 concentration used to permeabilised the plates improved the levels of antibody entering the nucleus and aided in the clear detection of foci by reducing the non-specific staining, as seen in Figure 3.5.5.2. However, in some wells where a 1.0% Triton X-100 solution had been used, the antibody signal had started to diffuse out of the nucleus, suggesting the nuclear membrane had been over permeabilised. To prevent this from occurring in future experiments, a solution of 0.75% Triton X-100 and 3% BSA in PBS was chosen to permeabilise the cells.

3.5.6 High Throughput Staining Protocol with Increased Triton X-100 Concentration

The increased Triton X-100 concentration of 0.75% was next used to extract Chk1 or RRM1 knocked down cells in an attempt to determine the concentration of primary antibody to be used in the final screening assay. Cells were reverse transfected for 48 hours using DharmaFECT 1 and fixed and extracted as previously described. The cells were then stained with a titration of RPA2 T21 primary antibody from a 1:250 dilution to a 1:1000 dilution (Fig.3.5.6.1).

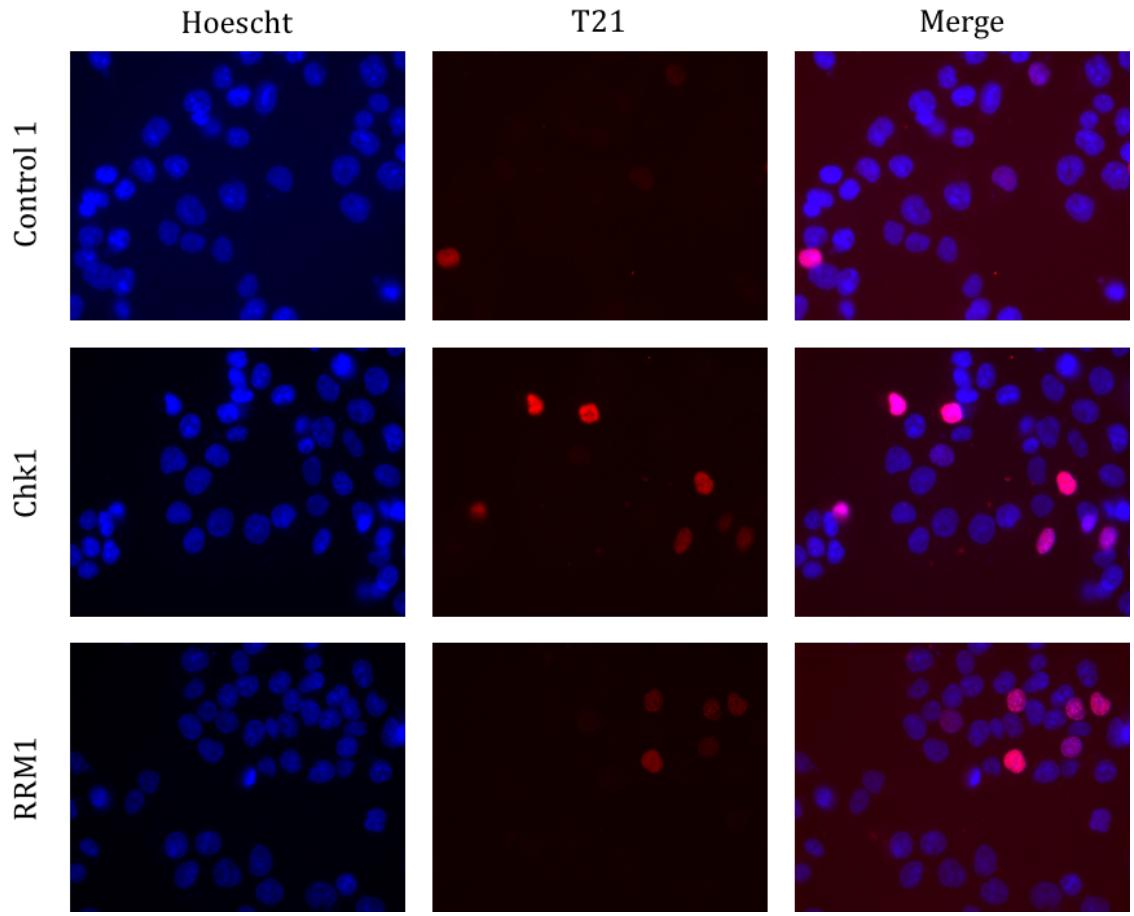

Figure 3.5.6.1 RPA2 T21 staining of Chk1 or RRM1 knocked down cells with increased Triton X-100.

Representative images of HCT116 cells reverse transfected with Control 1, Chk1 or RRM1 siRNA and DharmaFECT 1 and grown for 48 hours post-transfection. Once fixed the cells were permeabilised with 0.75% Triton X-100 and 3% BSA for 10 minutes. Cells were stained with a 1:250 dilution of an antibody raised against the T21 site in RPA2.

Increasing the Triton X-100 concentration and imaging the plate using the Texas Red channel allowed for differentiation between the Control 1 and Chk1 or RRM1 knocked down cells (Fig.3.5.6.1). The RRM1 knocked down wells contained fewer cells than the other conditions, suggesting that re-optimisation of cell number may be required. In some of the Control 1 transfected wells, a higher than expected proportion of cells stained brightly for T21 foci, which would reduce the screening window of the assay. This prevented the selection of an antibody concentration for screening as further optimisation of the non-targeting Controls was required.

3.5.7 Assessment of Non-Targeting Controls in High Throughput Staining Protocol

As the Control 1 siRNA used in previous experiments appeared to be producing a higher than expected proportion of brightly stained cells, the complete panel of ON-TARGETplus non-targeting Control siRNAs were tested in the assay. Cells were reverse transfected with Control 1, 2, 3, 4 and the non-targeting siRNA Control Pool (comprised of Control siRNA 1 to 4), as well as Chk1 and RRM1 as positive controls for replication stress. Cells were grown for 48 hours post transfection, fixed and extracted as previously described and then stained with a 1:250 dilution of the RPA2 T21 antibody (Fig.3.5.7.1).

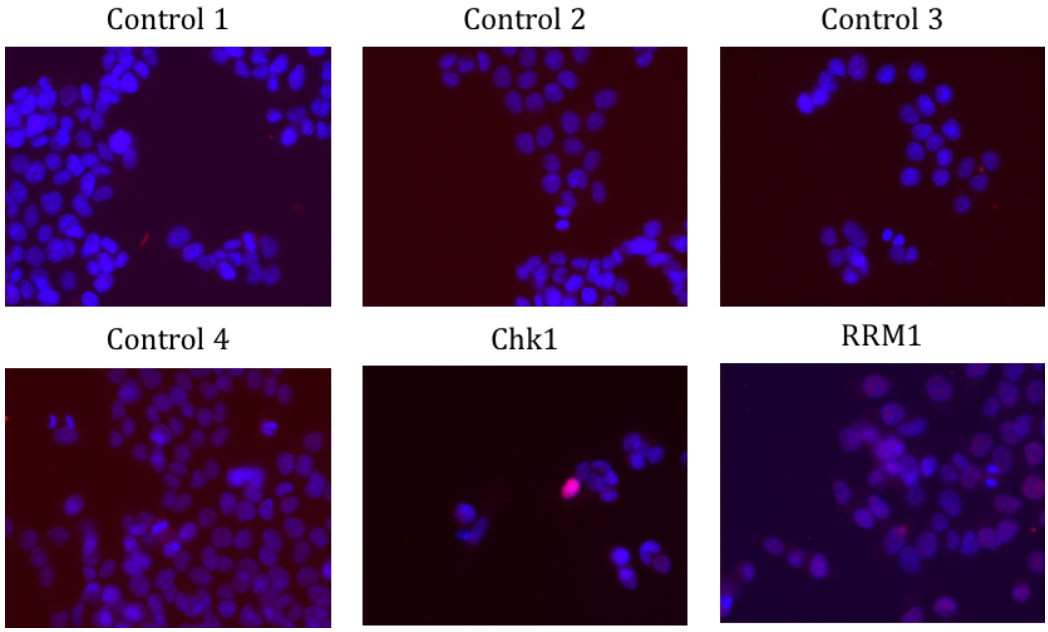

Figure 3.5.7.1 RPA2 T21 staining of Control Panel and Chk1 or RRM1 knocked down cells.
Representative images of HCT116 cells reverse transfected with Control 1, 2, 3, 4, Control Pool, Chk1 or RRM1 siRNA and DharmaFECT 1 and grown for 48 hours post-transfection. Once fixed the cells were permeabilised with 0.75% Triton X-100 and 3% BSA for 10 minutes. Cells were stained with a 1:250 dilution of an antibody raised against the T21 site in RPA2.

The images were deemed to be of high enough quality to assess using the MetaXpress Custom Module Editor. This was used to calculate the average number of foci per cell (Fig.3.5.7.2A) and the exact number of foci present within each cell imaged. This individual cell data was then used to determine how many cells were positive for T21 foci, with cells containing more than 10 foci being considered positive (Fig 3.5.7.2B).

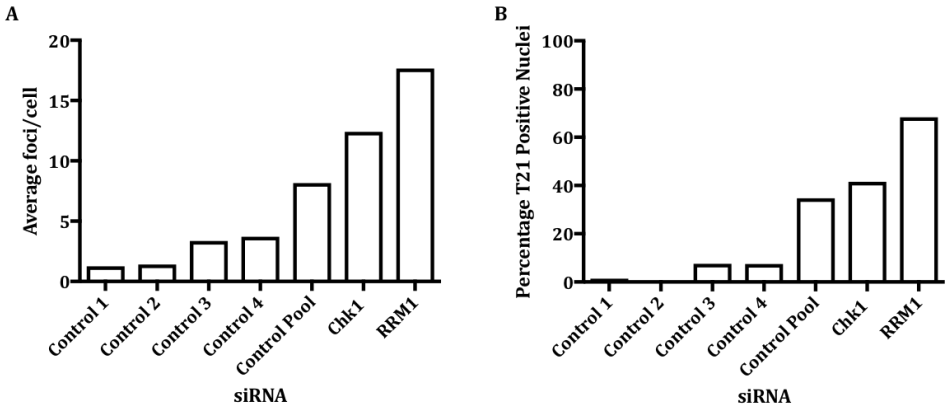

Figure 3.5.7.2 Comparison of average data and individual cell data generated by MetaXpress Custom Module Editor.

For each condition MetaXpress Custom Module Editor calculated the (A) average number of foci per cell and the number of foci in each individual cell. (B) The individual cell data was then used to calculate the number of positive nuclei. A nucleus was considered positive if it contained 10 or more bright T21 foci. Values derived from one experiment.

The most toxic non-targeting siRNA used in the assay was the Control Pool as it has the combined toxicity of all four individual siRNAs. Control 1 and Control 2 produced the lowest level of replication stress with Controls 3 and 4 producing a higher level of stressed cells. However, as this was still below 10% and produced a signal window of 33.95% (between Control 3 and Chk1), any of the four would be acceptable for use in the final screening assay.

Both the average data (Fig.3.5.7.2 A) and the individual cell data (Fig.3.5.7.2.B) produced a similar trend across the siRNAs and could differentiate between the non-targeting Controls and the positive controls. However, it was decided to analyse all further assays using the individual cell data as it gave more information about the frequency of positive cells in a well.

Again, the number of cells remaining in the wells at the end of the experiment were much lower than desired. The levels of replication stress being produced by the Chk1 and RRM1 knockdown were also lower than expected so further optimisation of the screening assay was carried out to try and improve this.

3.5.8 Re-optimisation of High Throughput Assay Conditions

As the cell numbers and transfection efficiency appeared to be sub-optimal in previous experiments, the screening assay was re-optimised to try to rectify this. Cells were plated at 1000, 1500 and 2000 cells per well to see if increased plating density resulted in more cells remaining at the end of the assay. An increased concentration of DharmaFECT 1 (0.04µl compared to 0.01µl per well) was trialled to try and improve the efficiency of transfection. The 72 hour time point was also re-introduced in an attempt to improve the efficiency of the gene knockdown.

The cells were transfected with Control 3 siRNA, as this produced the highest level of stress in the previous assay and Chk1 and RRM1 siRNA were used as positive controls for replication stress (Table 3.5.8.1, Fig 3.5.8.1, Fig 3.5.8.2 and Fig 3.5.8.3). The cells were fixed and stained as previously described with a 1:250 dilution of RPA2 T21.

siRNA	DharmaFECT1	Cells Plated	48 hour			72 hour		
			Total Cells	T21 Positive	% T21 Positive	Total Cells	T21 Positive	% T21 Positive
Control 3	0.01	1000	115	9	7.83	142	50	35.21
		1500	154	22	14.29	255	21	8.24
		2000	191	28	14.66	317	23	7.26
	0.04	1000	114	19	16.67	9	8	88.89
		1500	142	26	18.31	29	20	68.97
		2000	201	34	16.92	80	53	66.25
Chk1	0.01	1000	103	50	48.54	49	33	67.35
		1500	155	80	51.61	130	63	48.46
		2000	194	26	13.40	189	122	64.55
	0.04	1000	53	32	60.38	3	3	100.00
		1500	63	45	71.43	12	11	91.67
		2000	101	72	71.29	26	24	92.31
RRM1	0.01	1000	115	90	78.26	33	32	96.97
		1500	141	120	85.11	85	71	83.53
		2000	252	195	77.38	58	55	94.83
	0.04	1000	21	21	100.00	1	0	0.00
		1500	16	16	100.00	15	15	100.00
		2000	111	111	100.00	6	6	100.00

Table 3.5.8.1 Automated scoring of re-optimised high throughput screening assay.
For each condition the number of cells and foci were counted and the number of cells positive for T21 foci were calculated. A nucleus was considered positive if it contained 10 or more bright T21 foci. Two wells were assessed per condition.

Increasing the concentration of DharmaFECT 1 reduced the numbers of cells imaged in the gene knockdown wells of the 48 hour plate and drastically diminished the numbers of cells present in all conditions of the 72 hour plate (Table 3.5.8.1). It also increased the levels of replication stress reported, especially at the 72 hour time point (Fig.3.5.8.1, 3.5.8.2 and 3.5.8.3). The decision was made to remain at 0.01μl DharmaFECT 1 to allow 100 cells to be captured per well when nine sites were imaged.

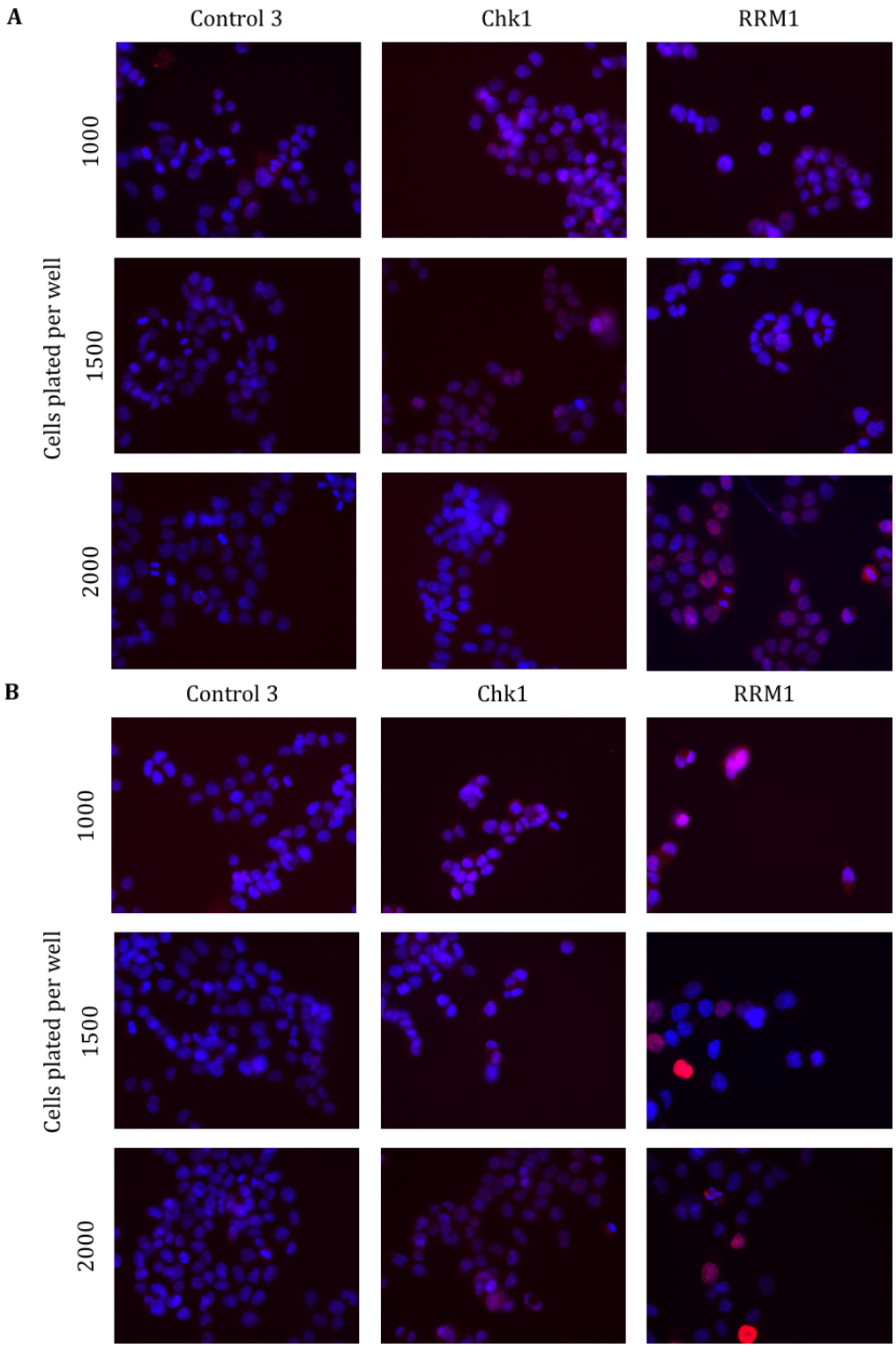

Figure 3.5.8.1 Re-optimisation of high throughput screening assay with 48 hour transfection. *Representative images of HCT116 cells, plated at 1000, 1500 or 2000 cells per well, reverse transfected with Control 3, Chk1 or RRM1 siRNA and (A) 0.01µl or (B) 0.04µl DharmaFECT 1 per well. Cells were grown for 48 hours post-transfection. Once fixed the cells were permeabilised with 0.75% Triton X-100 and 3% BSA for 10 minutes. Cells were stained with a 1:250 dilution of an antibody raised against the T21 site in RPA2.*

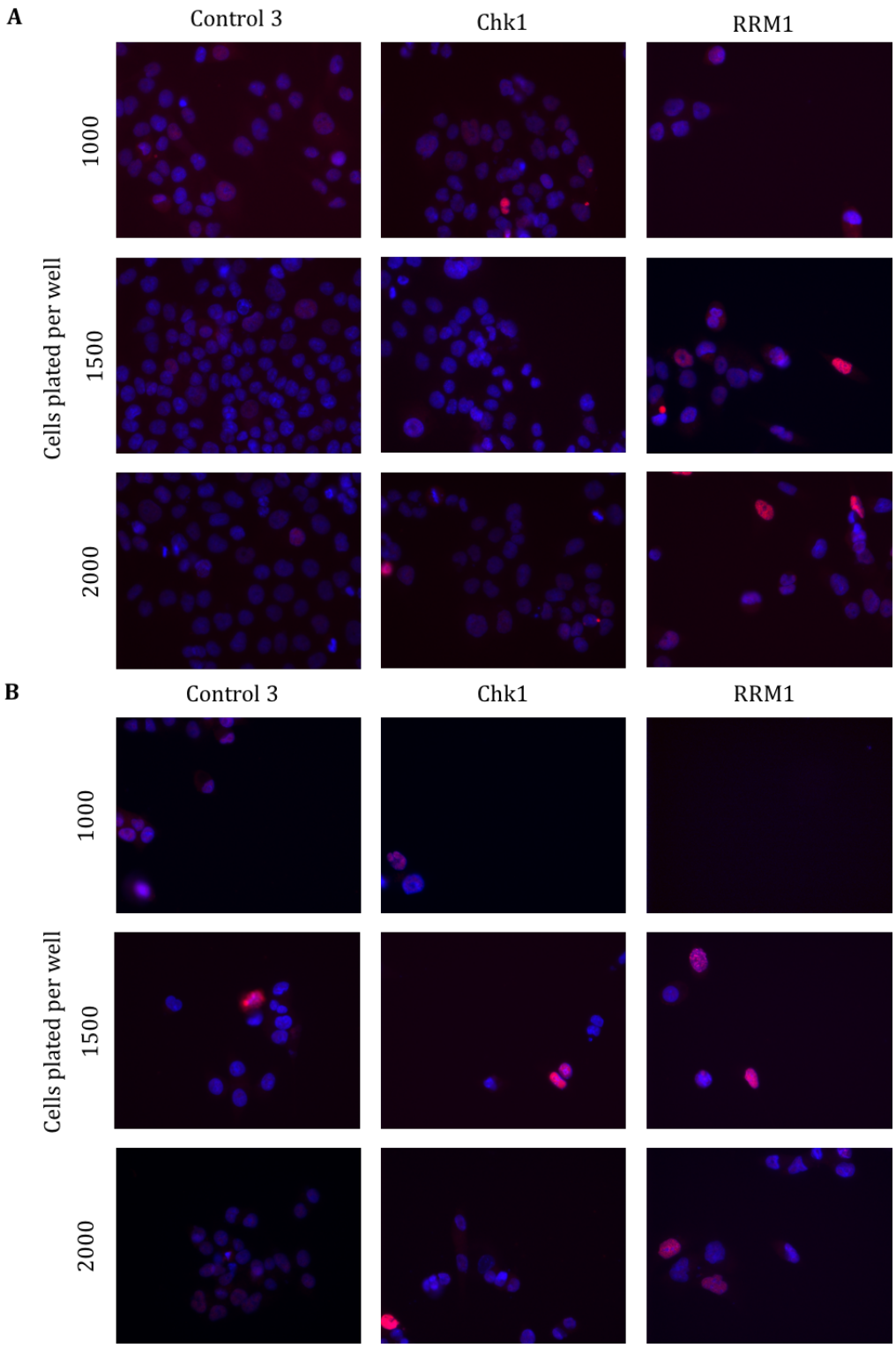

Figure 3.5.8.2 Re-optimisation of high throughput screening assay with 72 hour transfection. *Representative images of HCT116 cells, plated at 1000, 1500 or 2000 cells per well, reverse transfected with Control 3, Chk1 or RRM1 siRNA and (A) 0.01μl or (B) 0.04μl DharmaFECT 1 per well. Cells were grown for 72 hours post-transfection. Once fixed the cells were permeabilised with 0.75% Triton X-100 and 3% BSA for 10 minutes. Cells were stained with a 1:250 dilution of an antibody raised against the T21 site in RPA2.*

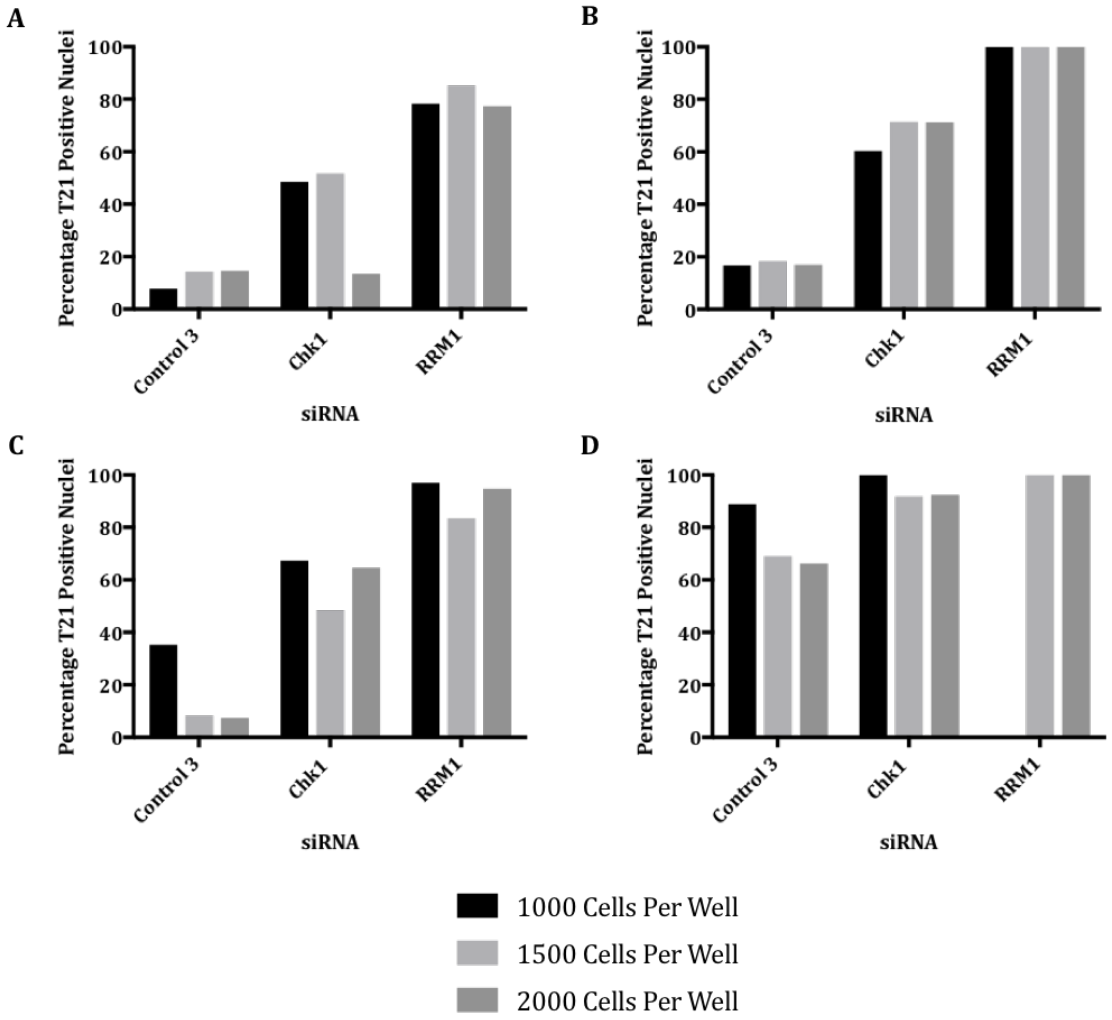

Figure 3.5.8.3 Automated scoring of re-optimised high throughput screening assay.
For each condition the number of cells and foci were counted. The number of cells positive for T21 foci were calculated. A nucleus was considered positive if it contained 10 or more bright T21 foci. (A) 0.01μL DharmaFECT 1, 48 hour transfection. (B) 0.04μL DharmaFECT 1, 48 hour transfection. (C) 0.01μL DharmaFECT 1, 72 hour transfection. (D) 0.04μL DharmaFECT 1, 72 hour transfection. No cells were present at 1000 cells per well with 0.04μL DharmaFECT1 and a 72 hour transfection. Values derived from one experiment.

Extending the transfection time from 48 to 72 hours increased the levels of replication stress observed in the assay (Fig.3.5.8.3), however even at 0.01μL DharmaFECT 1, there was a strong reduction in the number of cells imaged in the RRM1 knockdown wells (Table 3.5.8.1). As a result of this, the 48 hour time point was favoured over a 72 hour transfection time.

Increasing the plating density increased the number of cells that remained in the well at the end of the assay (Table 3.5.8.1). However, it did not have a dramatic effect on the levels of replication stress reported in the assay (Fig.3.5.8.3), so it could be increased without compromising the assay window. All future assays were carried out at 2000 cells per well as this plating density returned approximately 100 cells per well at 0.01μl per well DharmaFECT 1 with 48 hour transfection when nine sites were imaged (Table 3.5.8.1).

3.5.9 High Throughput Staining Protocol with Increased Cell Number

Following the previous re-optimisation experiment, the assessment of the Control Panel (excluding the Control Pool) was repeated with the increased cell plating density of 2000 cells per well to try and improve the number of cells imaged per condition.

When it came to imaging this plate, the microscope could not be focused appropriately in the Texas Red channel when using the 40X objective. However, when using the 20X objective the foci could be readily observed. The decision was made to image the plate at 20X and then write a scoring algorithm that could process the 20X images (Fig.3.5.9.1, Table 3.5.9.1 and Fig 3.5.9.2).

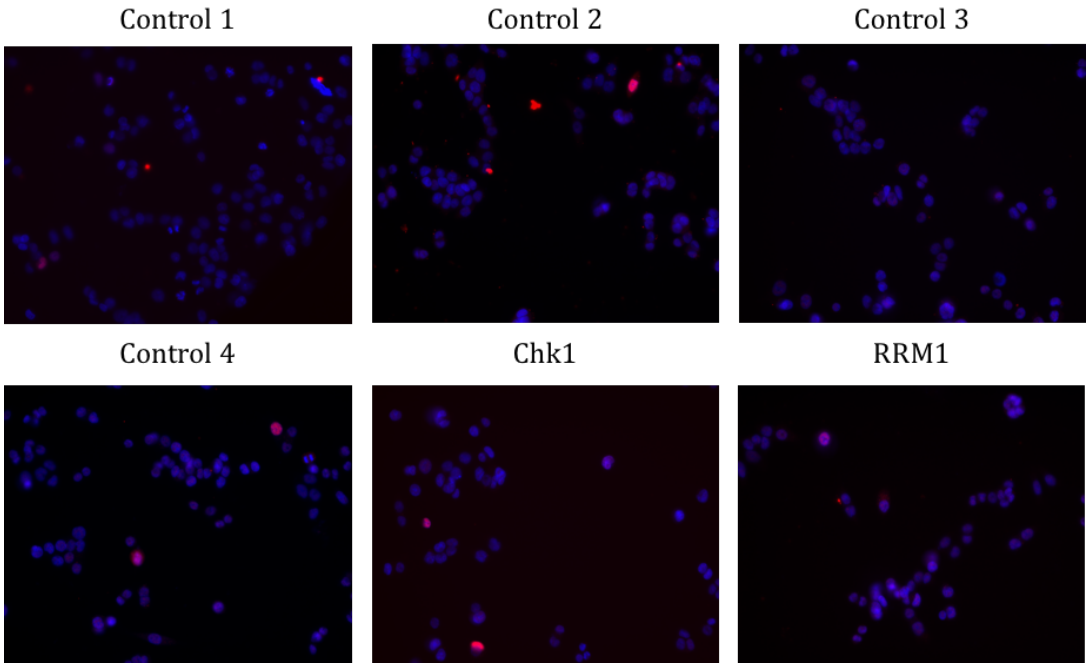

Figure 3.5.9.1 RPA2 T21 staining of Control Panel and Chk1 or RRM1 knocked down cells with increased plating density.

Representative images of HCT116 cells plated at 2000 cells per well and reverse transfected with Controls 1, 2, 3, 4, Chk1 or RRM1 siRNA and DharmaFECT 1. Cells were grown for 48 hours post-transfection. Once fixed the cells were permeabilised with 0.75% Triton X-100 and 3% BSA for 10 minutes. Cells were stained with a 1:250 dilution of an antibody raised against the T21 site in RPA2.

As the plate was imaged at 20X rather than 40X, no judgement could be made on whether the increased plating density would result in a sufficient number of cells being imaged at the end of the assay. It was also uncertain whether the 20X scoring algorithm was accurately detecting the number of foci present within the cells as all the Control siRNAs tested produced much higher proportions of positive cells than expected (Fig.3.5.9.2). A working 20X scoring algorithm would have been very useful as it would allow more cells to be counted per well and so further efforts were made to improve its functionality.

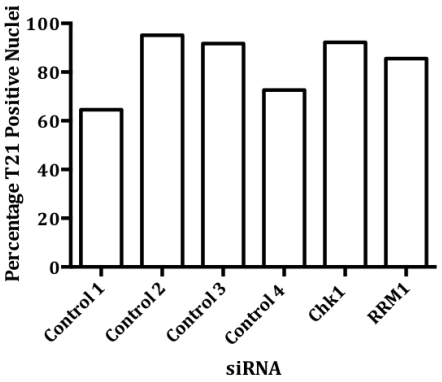

Figure 3.5.9.2 Automated scoring of Control Panel, and Chk1 or RRM1 knocked down cells with increased plating density.

For each condition the number of cells and foci were counted. The number of cells positive for T21 foci were calculated. A nucleus was considered positive if it contained 10 or more bright T21 foci. Values derived from one experiment.

The Control Panel assay with increased plating density was repeated with the aim of imaging the plate at both 20X and 40X and comparing the results generated by the respective algorithms. The 40X data could then be used to alter the 20X algorithm until they reported a similar trend. Cells were stained using the original T21 antibody lot (Fig.3.5.9.3 and 3.5.9.4A) and a new vial of the antibody (Fig.3.5.9.4B) to determine if the primary antibody was affecting the assay signal.

Comparison of the two scoring algorithms clearly shows that they were not identifying the same objects as T21 foci (Fig.3.5.9.4). The focusing was poor on the 40X images and the levels of replication stress detected did not correlate with previous assays or with the levels of replication stress expected following siRNA transfection. The 20X scoring algorithm appeared to be detecting much higher levels of foci in all conditions. The cells also appeared to be growing on top of one another, which may have prevented the accurate identification of individual cells.

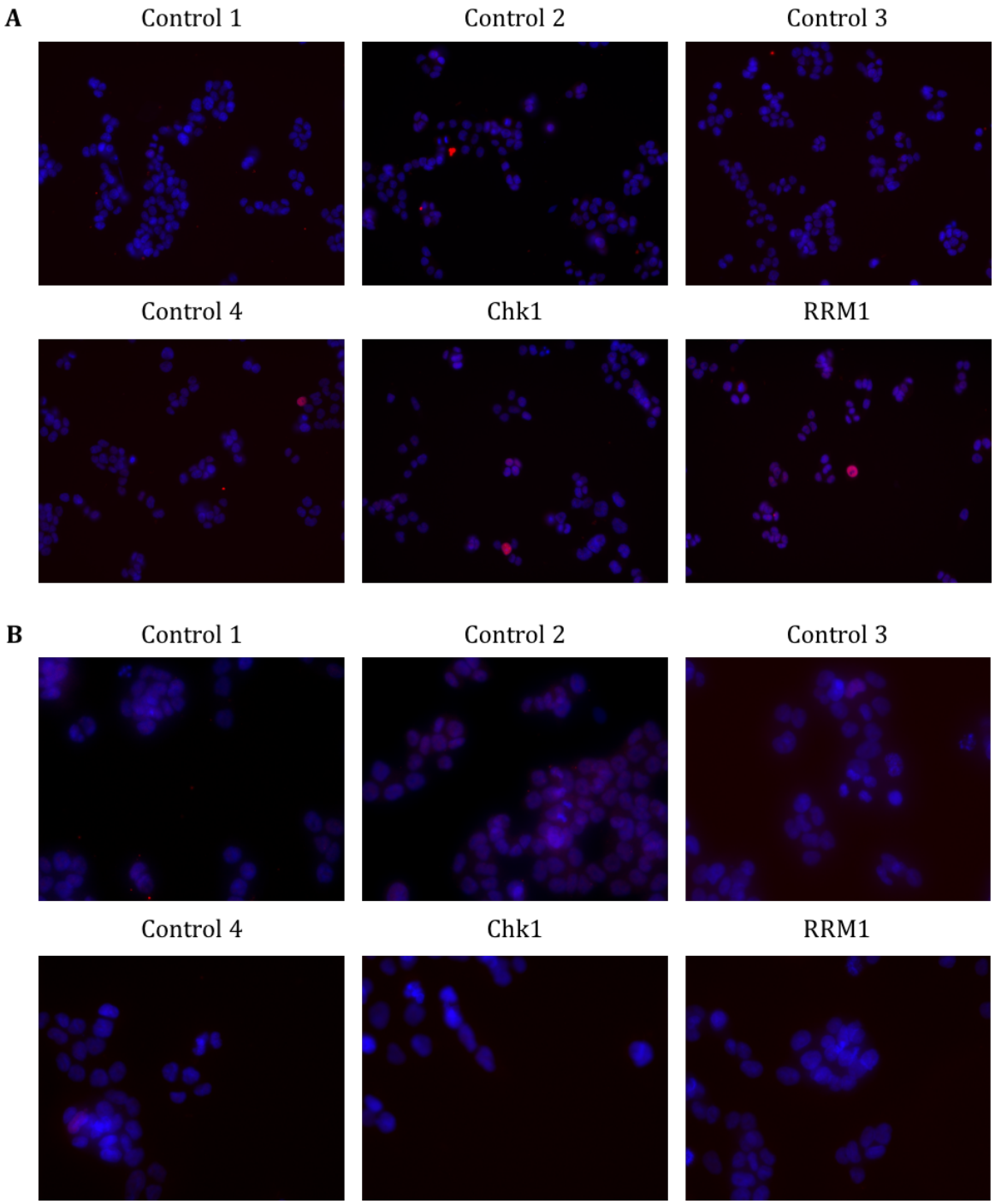

Figure 3.5.9.3 RPA2 T21 staining of Control Panel, Chk1 or RRM1 knocked down cells to compare 20X and 40X objectives.

Representative images of HCT116 cells plated at 2000 cells per well and reverse transfected with Controls 1, 2, 3, 4, Chk1 or RRM1 siRNA and DharmaFECT 1. Cells were grown for 48 hours post-transfection. Once fixed the cells were permeabilised with 0.75% Triton X-100 and 3% BSA for 10 minutes. Cells were stained with a 1:250 dilution of an antibody raised against the T21 site in RPA2. Cells were imaged using the (A) 20X and (B) 40X objectives of the Molecular Devices ImageXpress Micro High Content Microscope.

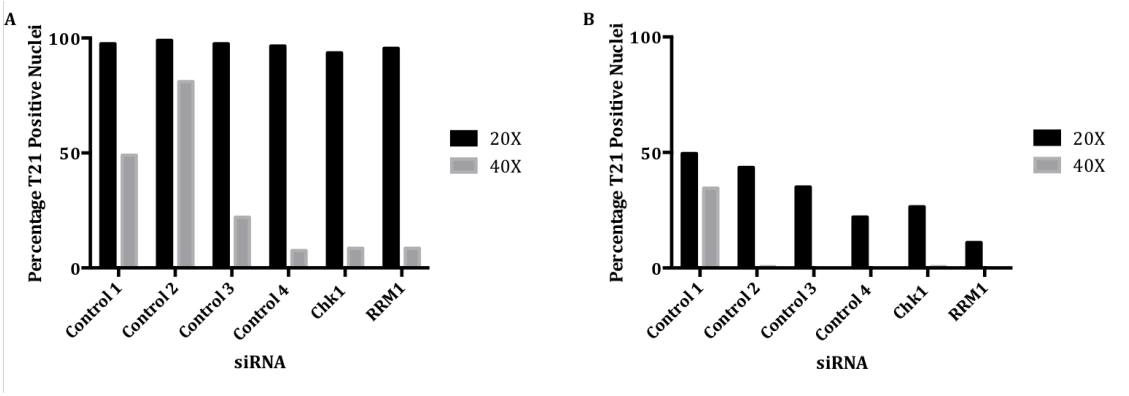

Figure 3.5.9.4 Comparison of Control Panel and Chk1 or RRM1 knocked down cells imaged with a 20X and a 40X objective.

For each condition the number of cells and foci were counted. The number of cells positive for T21 foci were calculated. A nucleus was considered positive if it contained 10 or more bright T21 foci. Values derived from one experiment. (A) Original T21 antibody lot. (B) New T21 antibody lot.

The 40X images and scoring data generated for both the original and new T21 antibody lots suggested that the staining of the plate has been sub-optimal so this experiment could not be used to alter the 20X scoring algorithm. The experiment was repeated, again, using only the original T21 antibody to maintain consistency throughout assay development (Fig.3.5.9.5).

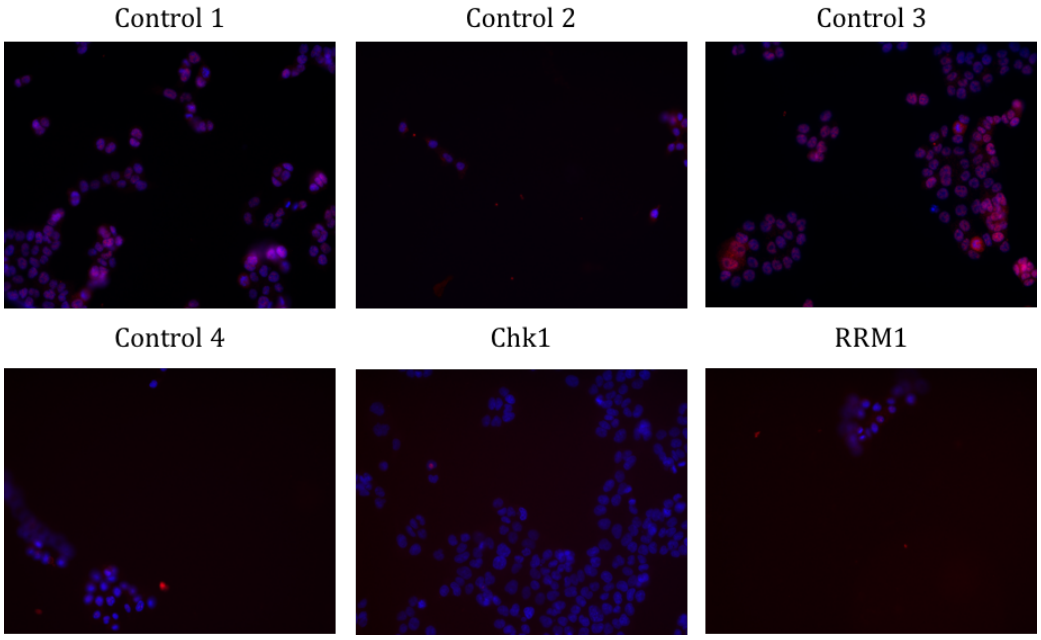

Figure 3.5.9.5 RPA2 T21 staining of Control Panel, Chk1 or RRM1 knocked down cells at 20X objective

Representative images of HCT116 cells plated at 2000 cells per well and reverse transfected with Controls 1, 2, 3, 4, Chk1 or RRM1 siRNA and DharmaFECT 1. Cells were grown for 48 hours post-transfection. Once fixed the cells were permeabilised with 0.75% Triton X-100 and 3% BSA for 10 minutes. Cells were stained with a 1:250 dilution of an antibody raised against the T21 site in RPA2. Cells were imaged using the 20X objective of the Molecular Devices ImageXpress Micro High Content Microscope.

When imaging the plate with the 20X objective it was revealed that not all of the wells were in focus and that Chk1 transfected cells did not appear to be permeabilised (Fig.3.5.9.5). When it came to imaging the plate at 40X, the signal could not be detected in the Texas Red channel, which prevented the microscope from being able to focus properly. To try and determine the strength of the staining, the plate was subsequently imaged using the InCell 2000 near confocal Microscope (Fig.3.5.9.6).

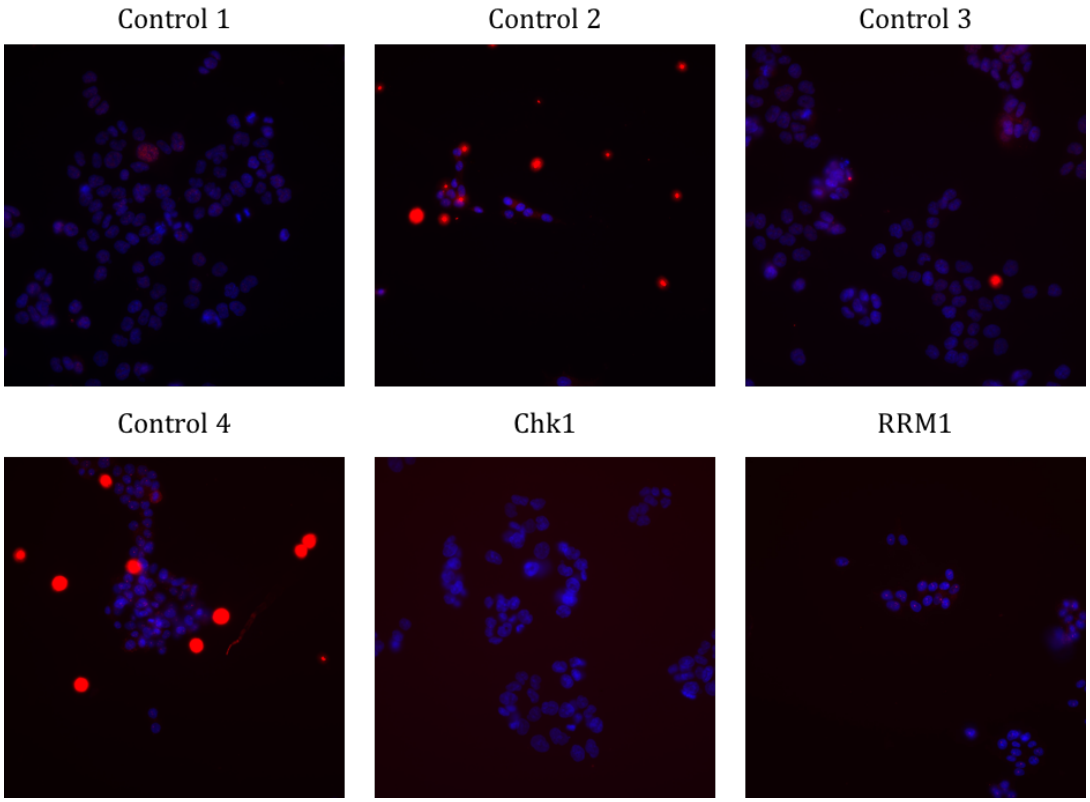

Figure 3.5.9.6 RPA2 T21 staining of Control Panel, Chk1 or RRM1 knocked down cells imaged using the InCell 2000 microscope

Representative images of HCT116 cells plated at 2000 cells per well and reverse transfected with Controls 1, 2, 3, 4, Chk1 or RRM1 siRNA and DharmaFECT 1. Cells were grown for 48 hours post-transfection. Once fixed the cells were permeabilised with 0.75% Triton X-100 and 3% BSA for 10 minutes. Cells were stained with a 1:250 dilution of an antibody raised against the T21 site in RPA2. Cells were imaged using the 100X objective of the InCell 2000 Microscope.

When examining the confocal images, it was noted that there were very few cells remaining on the plates, despite the increased plating density. A high level of non-specific staining was also observed outside of the cells in several images and as in the 20X images, the Chk1 knocked down cells did not appear to have been stained. There were a number of bright dots observed within the nuclei of the RRM1 knocked down cells (Fig.3.5.9.7), however these appeared too large to be RPA foci. This poor staining and apparent lack of true foci in the gene knocked down cells raised serious questions and concerns about the effectiveness and reproducibility of the assay in this format.

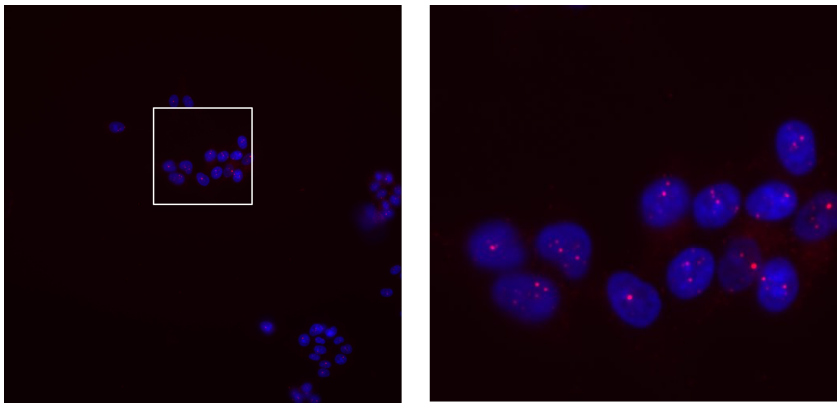

Figure 3.5.9.7 RPA2 T21 staining of RRM1 knocked down cells imaged using the InCell 2000 microscope

Representative images of HCT116 cells plated at 2000 cells per well and reverse transfected with RRM1 siRNA and DharmaFECT 1. Cells were grown for 48 hours post-transfection. Once fixed the cells were permeabilised with 0.75% Triton X-100 and 3% BSA for 10 minutes. Cells were stained with a 1:250 dilution of an antibody raised against the T21 site in RPA2. Cells were imaged using the 100X objective of the InCell 2000 Microscope.

3.5.10 Trouble Shooting High Throughput Staining Protocol

As the high throughput assay was still proving problematic, despite previously showing promising results, an attempt was made to pinpoint the cause of some of the recurrent issues. These experiments aimed to determine if there was some problem in the assay protocol being employed in the 384 well plates or if the complication was intrinsic to this plate type itself.

Three assay plates, two 384 well and one 24 well, were set up in the Collis lab using the same reagents as in the 24 well assays described previously. In each plate, cells were reverse transfected with Control 1, Chk1 or RRM1 siRNA and untransfected cells were treated with 2mM HU 16 hours prior to fixation. A shaking step was added to the protocol before cell plating to ensure the complexing of DharmaFECT 1 and siRNA to reduce toxicity to the cells. One of the 384 well plates and the 24 well plate were fixed and extracted using the extended incubations employed at the SRSF (Fig.3.5.10.1 A and B). The other 384 well plate was fixed and extracted using the Collis lab procedure utilised in the previous 24 well assays (Fig.3.5.10.1 C). The 384 well plates were manually fixed and stained due to the lack of a 384 well plate washer in the Collis lab.

The cell coverage observed in the 384 well plates was still very variable across the well, with some completely bald patches occurring. The only condition to produce bright foci in the 384 well format when using either protocol was the treatment with HU, there were no differences observed between the Control 1 transfected wells and the gene knockdown wells (Fig.3.5.10.1 B and C).

The SRSF protocol in 24 well plates produced very similar images to those produced previously in this plate type. Clear differences could be seen between the Control 1 transfected and the gene knockdown wells, which produced a similar, if less intense, staining pattern than that induced by HU treatment (Fig.3.5.10.1 A). This is in contrast to the lack

of foci observed in the 384 well plate assay, suggesting that it is something intrinsic in this 384 well plate format that is preventing the observation of pRPA2 foci, rather than the protocol in itself.

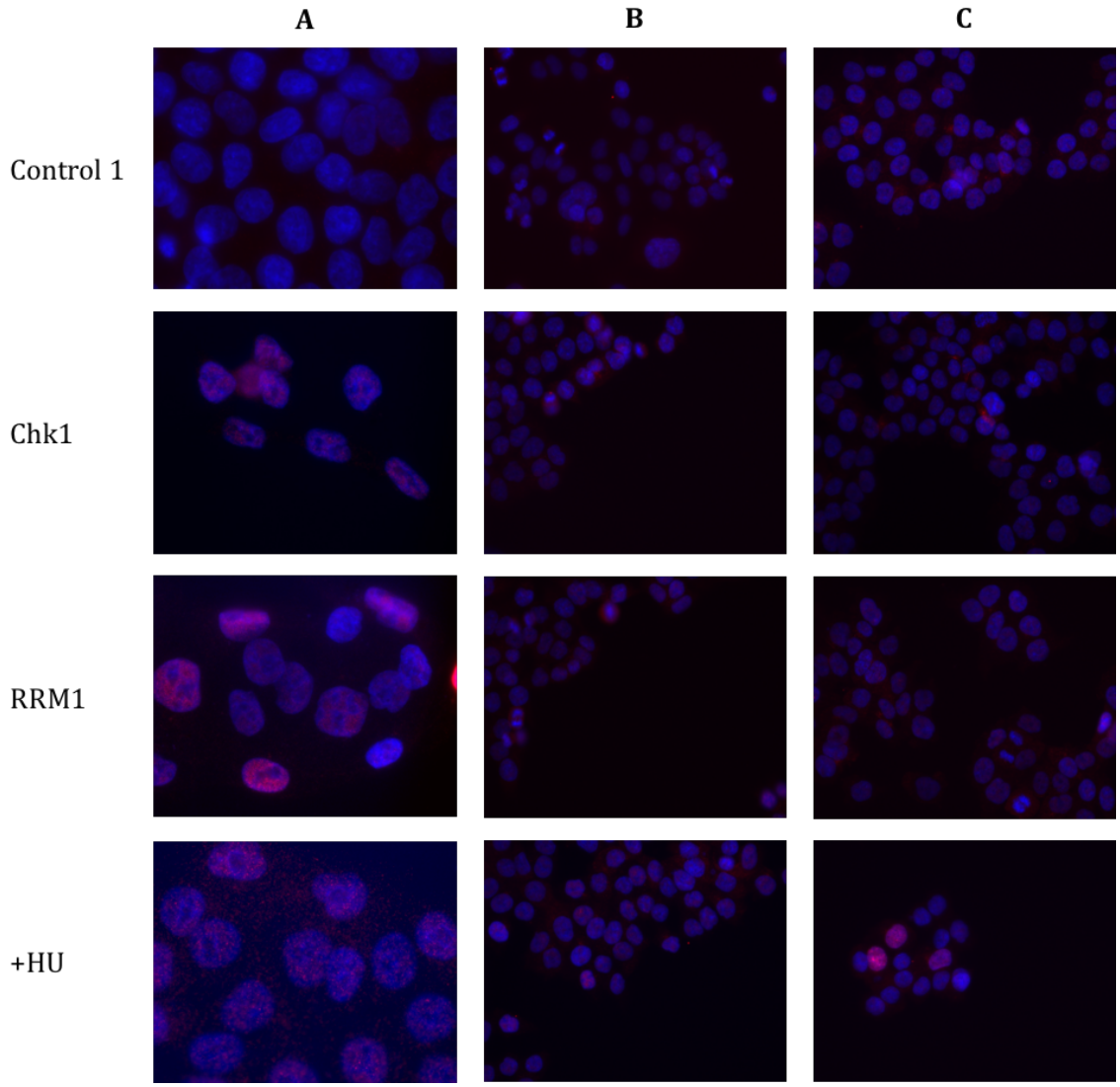

Figure 3.5.10.1 Comparison of Collis lab and SRSF protocols in 24 well and 384 well plate format.

Representative images of HCT116 cells plated at (A) 20 000 cells per well in a 24 well plate or (B & C) 2000 cells in a 384 well plate. Cells were either untransfected or reverse transfected with Control 1, Chk1 or RRM1 siRNA and DharmaFECT 1 and grown for 48 hours post-transfection. Transfected cells were mock treated with PBS whilst untransfected cells were treated with 2mM HU 16 hours before fixing. Cells were fixed for (C) 10 minutes and permeabilised with 0.5% Triton X-100 and 3% BSA for 5 minutes (Collis lab) or (A & B) fixed for 20 minutes and permeabilised with 0.75% Triton X-100 and 3% BSA for 10 minutes (SRSF). Cells were stained with a 1:250 dilution of an antibody raised against the T21 site in RPA2. Cells were imaged using the (A) Nikon Eclipse TE2000 Inverted Microscope or (B & C) the 40X objective of the Molecular Devices ImageXpress Micro High Content Microscope.

3.6 Alternative Methods of Detecting Replication Stress

3.6.1 EGFP-RPA2 Expressing HeLa Cells for RPA2 Foci Detection

The pRPA2 antibody selection immunofluorescence assay carried out in HCT116 cells was repeated in two clones (C1 and C3) of HeLa cells that stably expressed EGFP-RPA2. They were employed to see if the level of RPA2 foci that contained pRPA2 could be quantified (Fig.3.6.1.1). It was proposed that this technique could be used as an alternative screening method to the HCT116 assay or for hit validation.

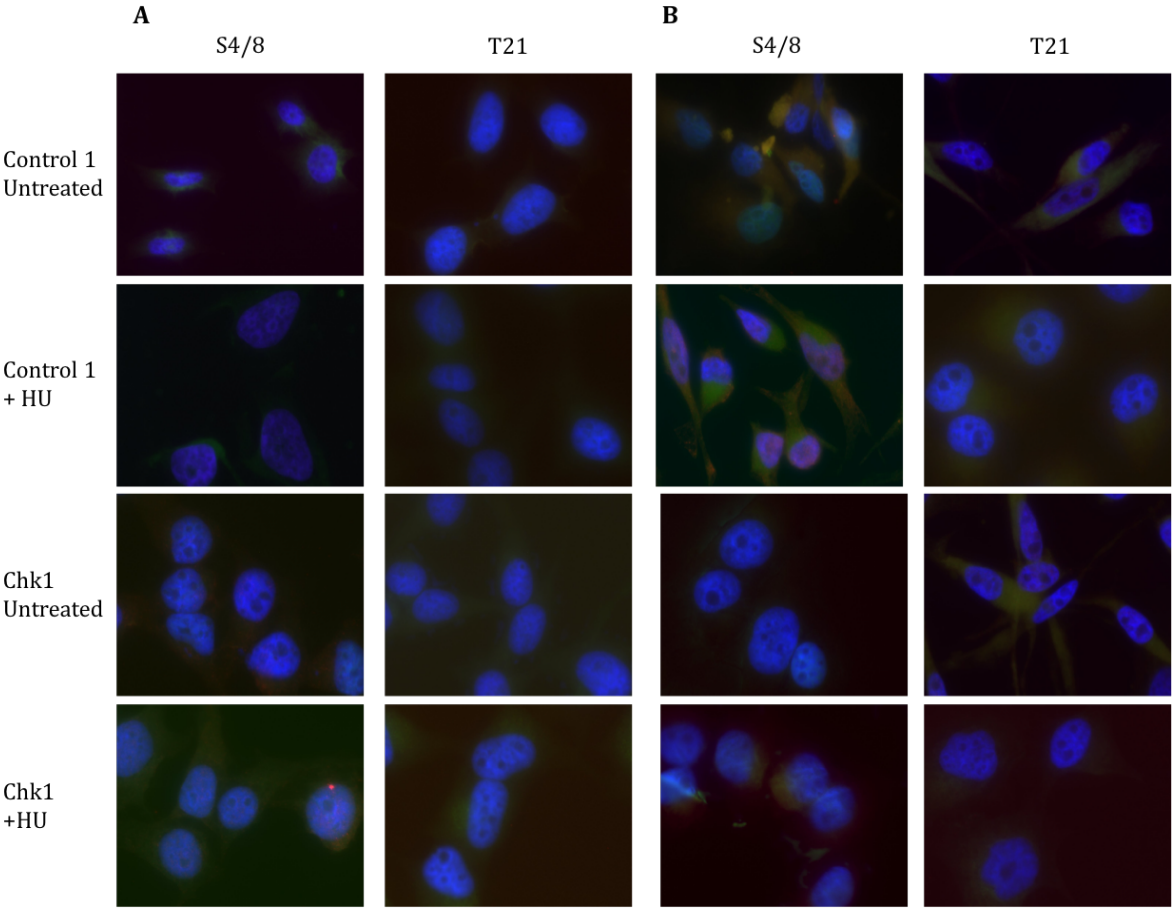

Figure 3.6.1.1. Detection of pRPA foci in EGFP-RPA2 Expressing HeLa cells.

Representative images of EGFP-RPA2 HeLa C1 (A) and C3 (B) cells forward transfected with Control 1 or Chk1 siRNA and RNAiMax. The cells were grown for 72 hours post-transfection. Cells were mock treated with PBS or treated with 2mM HU for 16 hours before fixing. Once fixed the cells were permeabilised with PBS-Tween 20 in the wash steps. The cells were stained with antibodies raised against the S4/8 and T21 phospho-sites within RPA2.

During the imaging of these coverslips it was observed that cells were only present at their edges where they grow most densely. Those that were still attached had stained poorly, expressed little to no EGFP-RPA2 (Fig.3.6.1.1) and photo-bleached quickly. This made it extremely difficult to focus on the cell and thus no images could be obtained for the S33 stained cells. All future work with this cell line was halted after the detection of mycoplasma contamination in the C3 clone and the lack of EGFP-RPA2 expression observed by fluorescent microscopy.

3.6.2 Total RPA2 Immunofluorescence

When the EGFP-RPA2 expressing HeLa cells showed poor autofluorescence, an alternative method for determining the level of foci containing pRPA2 within a cell was trialled. A total RPA2 antibody was used in this assay to stain HCT116 cells reverse transfected with Control or Chk1 siRNA and DharmaFECT 1 for 48 or 72 hours. The cells were treated with 2mM HU for 16 hours before fixing and permeabilised with 0.5% Triton X-100 and 3% BSA in PBS (Fig. 3.6.2.1 and Fig 3.6.2.2).

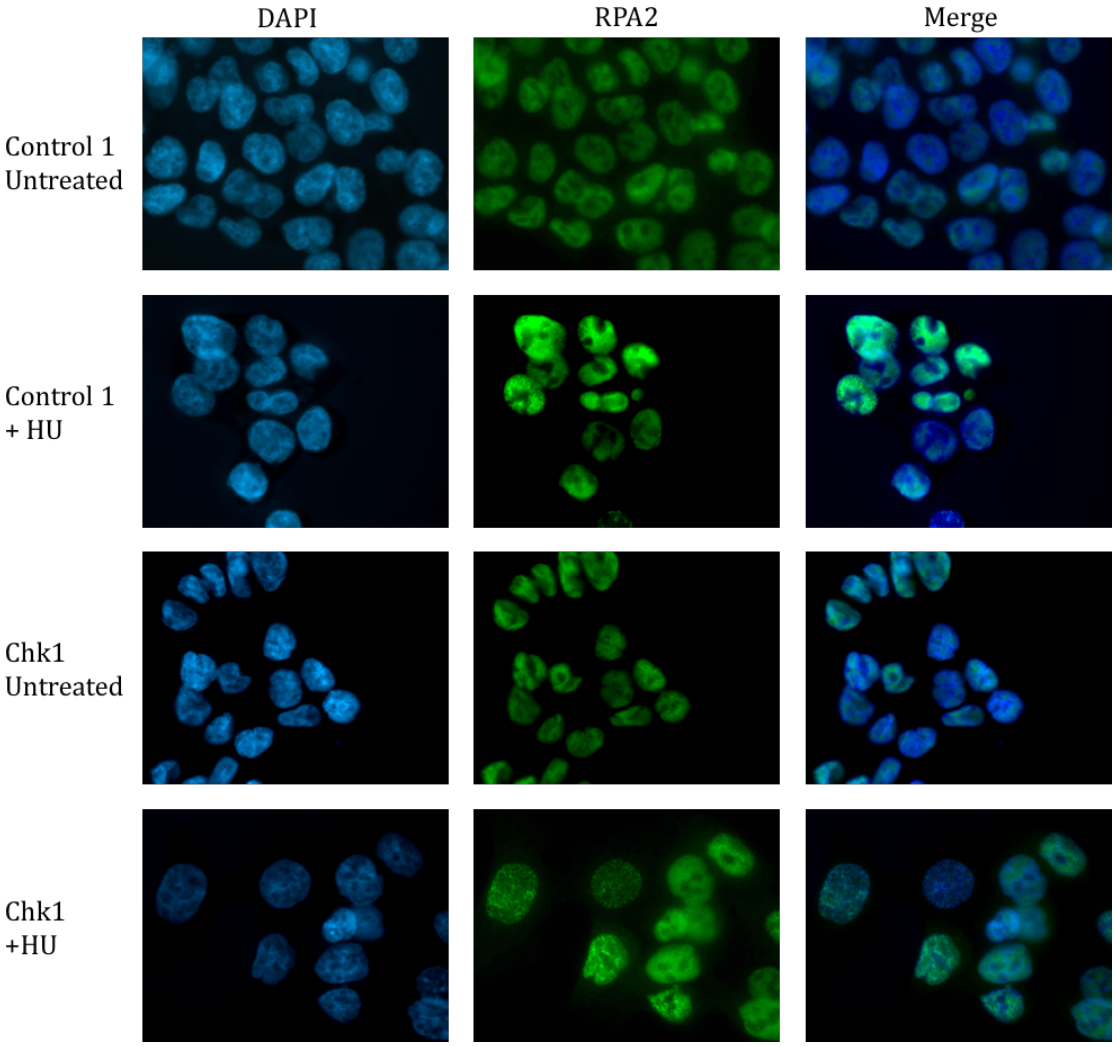

Figure 3.6.2.1. Total RPA2 staining in HCT116 cells at 48 hours.

Representative images of HCT116 cells reverse transfected with Control 1 or Chk1 siRNA and DharmaFECT 1. The cells were grown for 48 hours post-transfection. Cells were mock treated with PBS or treated with 2mM HU for 16 hours before fixing. Once fixed the cells were permeabilised with 0.5 % Triton X-100 and 3% BSA. The cells were stained with an antibody raised against total RPA2.

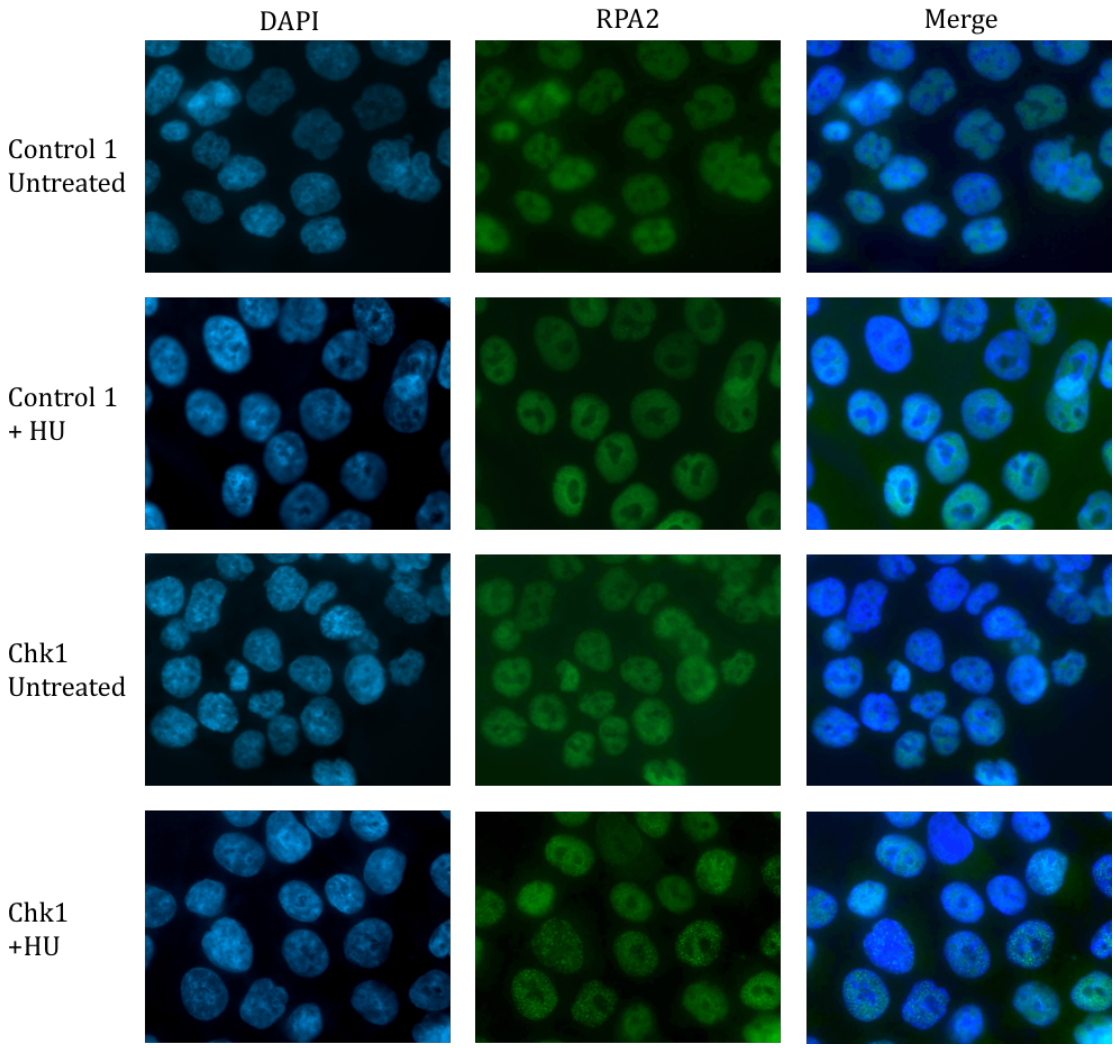

Figure 3.6.2.2. Total RPA2 staining in HCT116 cells at 72 hours.

Representative images of HCT116 cells reverse transfected with Control 1 or Chk1 siRNA and DharmaFECT 1. The cells were grown for 72 hours post-transfection. Cells were mock treated with PBS or treated with 2mM HU for 16 hours before fixing. Once fixed the cells were permeabilised with 0.5 % Triton X-100 and 3% BSA. The cells were stained with an antibody raised against total RPA2.

Little difference was observed between the RPA2 staining in the Control 1 and Chk1 knocked down untreated cells as both conditions display a pan nuclear stain (Fig.3.6.2.1 and Fig 3.6.2.2). A proportion of the cells treated with HU displayed foci which was clearer in the Chk1 knocked down cells. As this antibody failed to identify discrete foci in gene knockdown cells untreated with HU, it was not further investigated as this project aimed to identify genes that increased replication stress without the pressure of exogenous agents.

3.6.3 TopBP1 Immunofluorescence

An antibody raised against TopBP1 was also investigated as a potential alternative marker of replication stress that could be used for screening or hit validation. HCT116 cells were reverse transfected with Control 1 or Chk1 siRNA and DharmaFECT 1 for 48 hours and treated with 2mM HU for 16 hours prior to fixing. Once fixed, the cells were permeabilised by incubation with 0.5% Triton X-100 and 3% BSA in PBS for 5 minutes. The coverslips were then stained with a TopBP1 antibody (Fig.3.6.3.1).

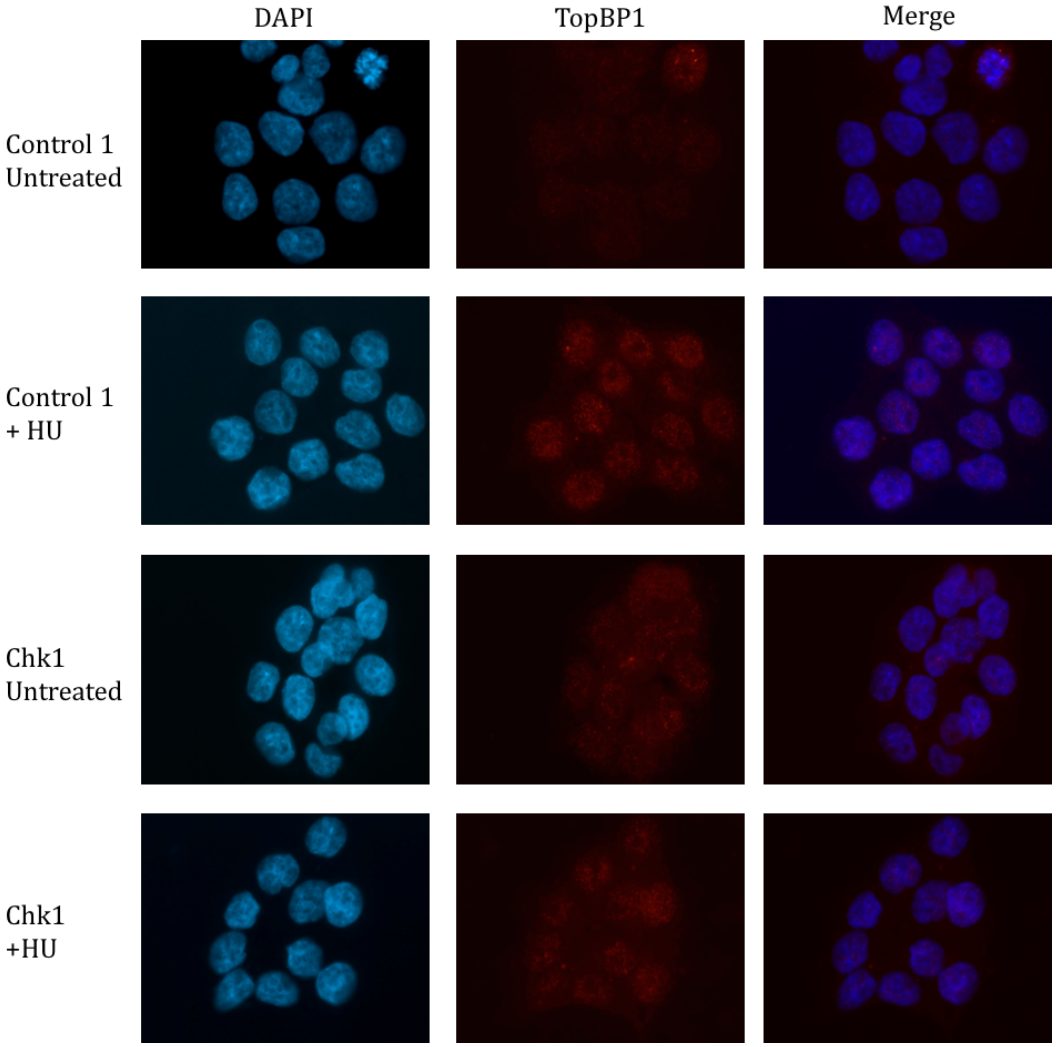

Figure 3.6.3.1. TopBP1 staining in HCT116 cells at 48 hours.

Representative images of HCT116 cells reverse transfected with Control 1 or Chk1 siRNA and DharmaFECT 1. The cells were grown for 48 hours post-transfection. Cells were mock treated with PBS or treated with 2mM HU for 16 hours before fixing. Once fixed the cells were permeabilised with 0.5 % Triton X-100 and 3% BSA. The cells were stained with an antibody raised against TopBP1.

The TopBP1 antibody images appeared to differ between the Control 1 and replication stress induced cells (Fig.3.6.3.1), however, there was some non-specific background staining observed. The images were scored for the presence of bright TopBP1 foci to see if the differences in signal detected were significant (Fig.3.6.3.2).

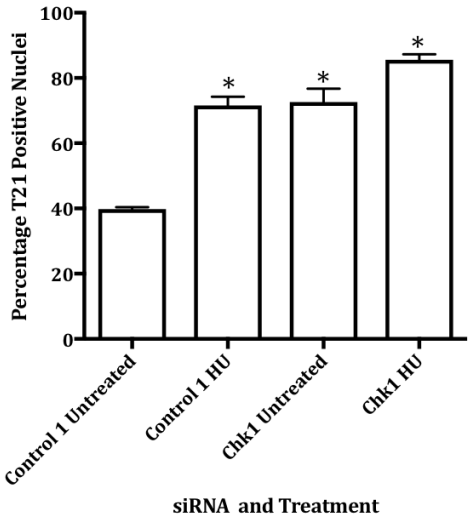

Figure 3.6.3.2 Percentage of HCT116 cells positive for TopBP1 foci.

For each condition the number of cells was counted and the percentage of TopBP1 positive nuclei was calculated. A nucleus was considered positive if it contained 10 ore more bright TopBP1 foci. Asterisks indicate significant difference from Control Untreated, p value <0.05. Mean values derived from two independent experiments, with their respective SEMs.

The scoring trend produced by this antibody was similar to that seen for the T21 antibody, with the cells expected to be experiencing higher levels of replication stress displaying more positive nuclei. Chk1 knockdown, treatment with HU and their combination each produced a significantly increased level of positive nuclei when compared to Control 1 untreated cells (p values 0.015, 0.007 and 0.001 respectively), although, this antibody produced a higher proportion of positive cells within Control 1 cell populations compared with the T21 antibody. However, as the TopBP1 antibody proved successful in detecting replication stress in the 24 well assay, it was scaled up to the 384 well format. HCT116 cells were reverse transfected with Control 1 or Chk1 siRNA with DharmaFECT 1 for 48 hours. The cells were fixed with 4% PFA and Hoescht for 20 minutes and permeabilised by incubation with 0.5% Triton X-100 and 3% BSA in PBS for 10 minutes. The cells were then stained with a titration of the TopBP1 antibody (1:500 – 1:1500). Cells were imaged using the 20X objective of the Molecular Devices ImageXpress Micro High Content Microscope (Fig.3.6.3.3).

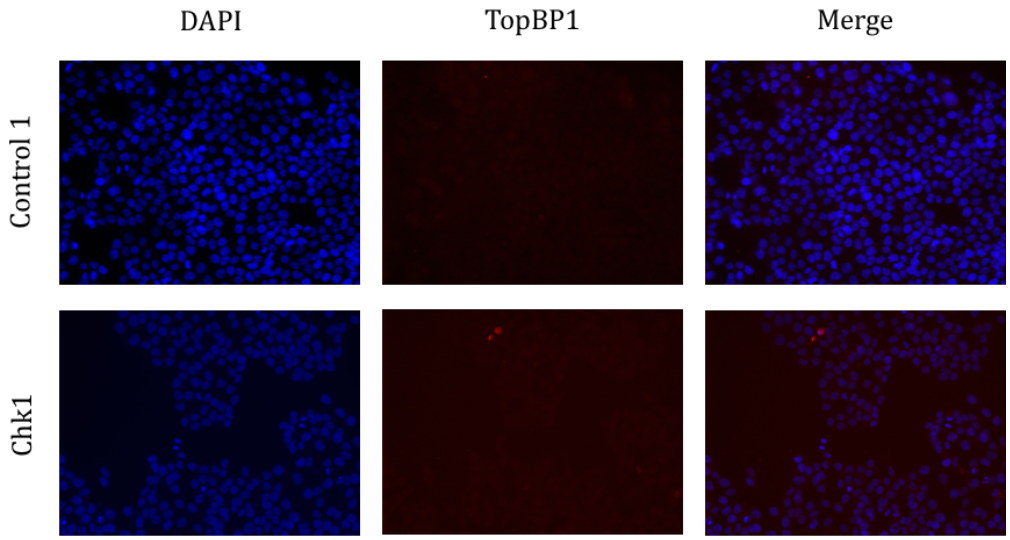

Figure 3.6.3.3 TopBP1 staining in HCT116 cells in 384 well plate.
Representative images of HCT116 cells reverse transfected with Control 1 or Chk1 siRNA and DharmaFECT 1. The cells were grown for 48 hours post-transfection. Once fixed the cells were permeabilised with 0.5 % Triton X-100 and 3% BSA. The cells were stained with a 1:500 dilution of an antibody raised against TopBP1.

The TopBP1 antibody did not appear to enter the nucleus at any concentration tested as there were no clear foci and no differences between the two conditions were observed (Fig.3.6.3.3), however, some non-specific staining of the assay plate was identified. No decisions could be made about which antibody concentration should be used in this plate format from these images, therefore further optimisation of the assay was required.

The assay was carried out with the inclusion of the cold pre-extraction procedure (described previously) and treatment of the cells with 2mM HU. The cells were stained with a 1:500 dilution of the TopBP1 antibody (Fig.3.6.3.4). The pre-extraction step reduced the non-specific staining observed in the initial experiment and increased the levels of antibody entering the nucleus. However, this did not allow the differentiation of Control 1 transfected and Chk1 knocked down cells with endogenous levels of replication stress. The minority of HU treated cells showed strong nuclear staining but demonstrated a pan-nuclear stain and no foci could be detected. Further optimisation of this antibody was halted in favour of further optimisation of the RPA2 T21 antibody.

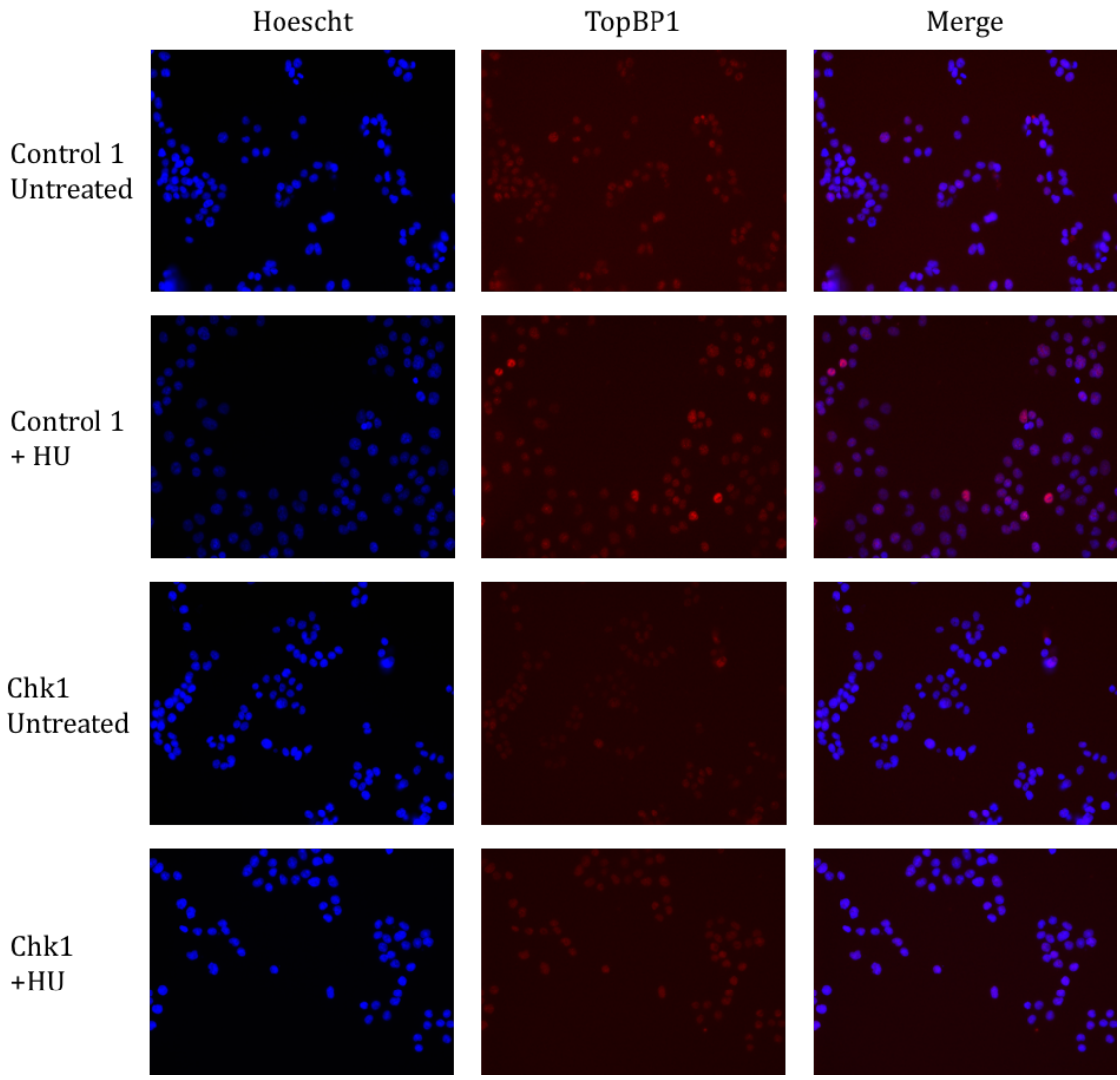

Figure 3.6.3.4 TopBP1 staining in Pre-extracted HCT116 cells in 384 well plate.

Representative images of HCT116 cells reverse transfected with Control 1 or Chk1 siRNA and DharmaFECT 1. The cells were grown for 48 hours post-transfection. Cells were mock treated with PBS or treated with 2mM HU for 16 hours before fixing Cells were incubated with cold pre-extraction buffer before fixing and further permeabilisation with 0.5 % Triton X-100 and 3% BSA. The cells were stained with a 1:500 dilution of antibody raised against TopBP1.

3.7 Discussion

As mentioned previously, replication stress is not a physical structure but a description of the state of a cell and its detection is hampered by the lack of a clearly defined cellular marker. The quantification of DNA synthesis, by techniques such as BrdU or EdU incorporation into nascent DNA, are regarded as the most effective methods for identifying replication stress (Zeman & Cimprich, 2014) and have recently been utilised in a genome wide screen to detect factors that impede replication restart (Kavanaugh et al, 2015).

Identification of downstream markers of replication stress had not previously been applied on a genome wide scale to assess the endogenous levels of replication stress following gene knockdown. Whilst this approach does not give a direct read out of replication stress, it is still a widely used and screens employing similar methods have previously proved successful including a γH2AX screen by Dr. S. Collis,(Barone et al, 2016; Myers et al, 2016; Staples et al, 2016; Staples et al, 2014; Staples et al, 2012).

RPA2 phosphorylation is a well characterised downstream event in the replication stress response and pRPA2 antibodies have been used previously within the Collis lab to identify stressed cells (Barone et al, 2016; Collis et al, 2007; Collis et al, 2008). As this technique was already employed within the lab, it was selected for the potential development for genome wide RNAi screen to identify novel regulators of replication stress.

As the screen completed by Dr. S. Collis and another completed within the lab of Professor M. Meuth at the SRSF had been carried out in HCT116 cells, this line was chosen to be used for the main body of this work. This was to allow comparisons between the three screens and also because it had proved successful in previous screens. As the Collis screen assessed γ-H2AX levels, it was thought that genes could be identified whose knockdown increased both replication stress and DNA damage, potentially through the collapse of stalled replication forks.

For the proper assessment of replication stress levels following gene knockdown, suitable positive controls needed to be identified. Efficient DNA replication is essential for the timely progression of replication forks and the knockdown of proteins that affect this process have been demonstrated to cause replication stress. One such protein is the ribonucleotide reductase subunit RRM1 which as mentioned previously is involved in the catalysis of dNTPs and whose loss results in slowed proliferation. Several components of the cell cycle checkpoints have also been characterised as suppressors of replication stress. The most notable example is Chk1 whose knockdown reduces the effectiveness of the Intra-S checkpoint (Kavanaugh et al, 2015). By maintaining replication stress, Chk1 loss allows for the formation and detection of pRPA2 foci. These two genes were therefore selected as siRNA positive controls for replication stress to be used throughout the development of the screening assay. Ribonucleotide reductase can also be inhibited by HU which provides similar effects to the loss of RRM1 with the advantage that its effects upon replication fork slowing are independent of transfection.

Western blotting revealed that the knockdown of both Chk1 and RRM1 by siRNA was sufficient at 48 and 72 hours for use as positive control siRNAs for future screening assays. The loss of either of these genes and treatment with HU induced Chk1 phosphorylation at Serine 137 and RPA2 at T21 (when present) which is indicative of a replication stress response (Vassin et al, 2004; Zhao & Piwnica-Worms, 2001). Of the two siRNAs, RRM1 produced the greater replication stress response. This may be a result of the more efficient knockdown of RRM1 compared to Chk1 or a difference in the phenotype produced by the knockdown. RRM1 inhibition hinders the initiation of DNA replication by reducing the pool of available nucleotides (Bester et al, 2011) whilst Chk1 loss increases replication initiation and then induces DNA strand breaks (Syljuåsen et al, 2005).

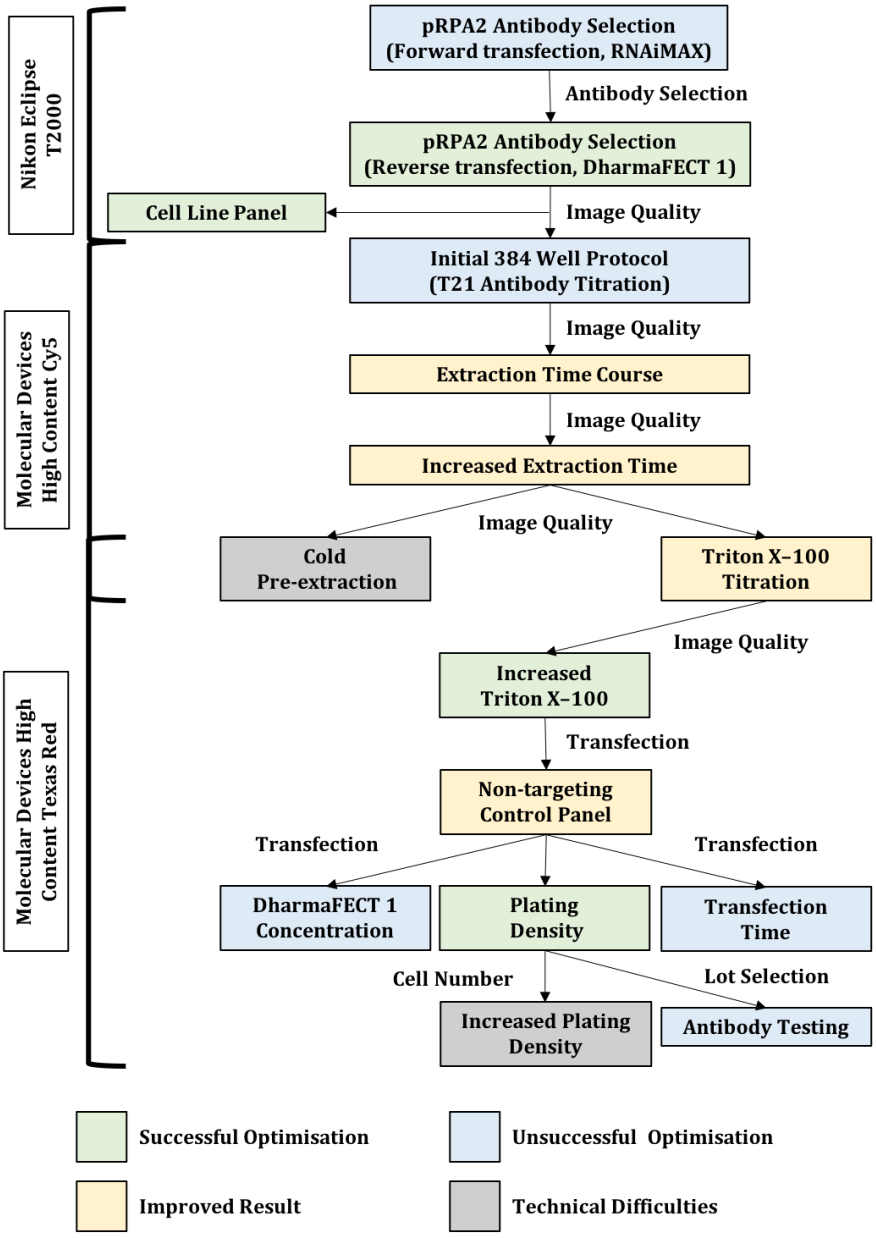

Figure 3.7.1 Phospo-RPA2 Screening Assay Development.

RPA2 is phosphorylated at several sites at its N-terminus, including S4/8, T21 and S33, by the PIKKs in response to cellular stress (Anantha et al, 2007). Antibodies raised against these three phospho-sites were assessed for their ability to detect RPA2 foci in an immunofluorescent protocol previously optimised within the Collis lab. Using this protocol, only the T21 antibody could detect the expected punctate pattern of pRPA foci. Despite being able to identify increases in the percentage of positive nuclei following Chk1 knockdown or HU treatment after 48 hours, the assay did not produce the expected results. Overall, the levels of foci produced were much lower than expected and the assay did not appear sensitive enough to differentiate between Chk1 knockdown alone or in combination with HU which produced a stronger replication stress response in the western blot. At the 72 hour time point, no increase in the levels of positive nuclei were observed as a result of the heightened levels of stress observed in the Control 1 untreated cells. This was most likely due to the prolonged incubation of the cells with the transfection reagents which induced additional toxicities.

In light of these results, several alterations were made to the transfection and staining procedure employed in this assay. At the advice of the SRSF, the media was replaced 24 hours post-transfection to reduce the harmful effects of prolonged transfection times and the switch was made to DharmaFECT 1 as this had produced limited toxicities in previous screens. The facility also required cells to be reverse transfected as the siRNAs are printed into the final assay plates and so forward transfection is not possible. To improve the sensitivity of the assay, efforts were made to improve the staining produced by the three antibodies. A stringent extraction protocol employed within the Collis lab to assess several chromatin bound damage markers was trialled for the pRPA2 antibodies. This employed a stronger detergent with a longer incubation than had been used previously. This was predicted to increase the permeabilisation of cellular membranes therefore improving nuclear entry of the antibody.

Whilst these alterations did modify the staining patterns produced for all three of the pRPA2 antibodies, both the S4/8 and S33 antibodies still failed to identify discrete foci following gene knockdown alone. For the T21 antibody, the changes reduced the levels of background staining observed and quantification of the images revealed that a higher proportion of nuclei appeared positive in all conditions. The sensitivity of the assay had also increased as a difference could now be observed between Chk1 knockdown alone and in combination with HU. As the 48 hour time point still produced the larger signal window, it was chosen for further investigation of Chk1 knockdown. The scoring data produced from these assays demonstrated that the knockdown of Chk1 significantly increased the number of cells positive for T21 foci (p-value of 0.0006). This suggests that there is a real increase in replication stress being induced by the loss of this gene.

When this assay was repeated in RRM1 knocked down cells, the staining pattern observed was subtly different to that observed in the cells lacking Chk1. More cells showed very bright staining and a proportion of nuclei were highly positive, containing many bright foci. As with the loss of Chk1, RRM1 knockdown significantly increased the level of cells experiencing replication stress (p-value 0.0001). It appeared to induce a greater stress

response than Chk1 loss, as was previously seen in the western blot. However, as both siRNA produced a detectable significant increase in replication stress it was decided that both should be included in further development of the screening assay.

To ensure that these observed effects were not cell line specific, these assays were repeated in several cell lines to further evaluate the effects of replication stress suppressor knockdown in differing genetic backgrounds.

When carried out in non-transformed RPE-1 cells, which are immortalised by human telomerase (h-TERT) expression (Bodnar et al, 1998; Jiang et al, 1999), a similar trend to HCT116 was observed. The levels of positive nuclei detected were lower than that seen in HCT116 cells, which was expected, as normal cells are predicted to be less effected by the disruption of replication than cancerous cells. However, the knockdown of neither Chk1 or RRM1 produced a significant difference in the levels of replication stress observed when compared to Control 1 siRNA transfected cells (p values 0.09 and 0.12 respectively). This was most likely due to the high levels of positive Control 1 transfected cells observed which was unanticipated as normal cells are predicted to have a lower basal level of replication stress. The RPE-1 cells were much more variable in the levels of replication stress reported in the assay, as evidenced by the size of the error bars in Figure 3.4.1.3, which may be why the Control cells appear to be more stressed in this cell line.

The assay was also carried out in the SW480 adenocarcinoma derived (Leibovitz et al, 1976) cell line which is MIN negative (Boland & Goel, 2010) and p53 deficient (Rochette et al, 2005) unlike HCT116. Whilst loss of both genes produced a significant increase in the levels of cells experiencing replication stress as seen previously, unlike in the other cell lines the knockdown of RRM1 did not produce a higher proportion of T21 positive nuclei than Chk1 knockdown. This change is thought to reflect the reliance of p53 deficient cells on the Intra-S and G2/M cell cycle checkpoints. Loss of these checkpoints through the knockdown of Chk1 would severely compromise these cell's ability to counter replication stress and DNA damage due to an inability to arrest the cell cycle and allow repair to occur. As further evidence for this, the Control 1 cells showed a higher background of replication stress than the HCT116 cells, which has been observed in other assays using this cell line (Collis lab, unpublished).

To further examine the effects of p53 deficiency on replication stress suppressor knockdown, the T21 assay was carried out in HCT116 cells where p53 function has been eradicated by targeted HR (Bunz et al, 1998) but they are otherwise genetically identical. As seen with the SW480 cell line, the loss of both genes significantly increased the levels of positive nuclei observed, the cells were more affected by the loss of Chk1 than RRM1 and high levels of background staining were observed in the Control 1 cells. As the SW480 and p53 deficient HCT116 cells produced such similar phenotypes, it suggests that p53 status plays a greater role in a cells response to replication suppressor knockdown than the presence of MIN.

The development of a high throughput screening assay was essential if the effects of gene knockdown on replication stress were to be assessed on a genome-wide scale (Fig.3.7.1,

Appendix 1). This involved attempts to automate the majority of the assay's set up, imaging and analysis to allow for data to be generated with a much higher throughput. While this automation removed some of the subjectivity from the data analysis it posed many problems including the adaptation of the assay to a high throughput format and the correct identification of the assay signal.

The nature of the 384 well plates and the automated techniques used at the SRSF demanded alterations be made to the transfection and staining protocol. The replacement of the media 24 hours post-transfection was replaced with addition of fresh media to the wells to dilute the transfection reagents. This had been found in previous screens to reduce the loss of cells from the plates. The use of plate washers meant that approximately 10μl of residue remained in the bottom of the wells following each aspiration so any reagents that were added were diluted by this residual buffer. This necessitated the extension of the incubation with the PFA fixative as this was bought at 4% and so could not be altered to account for the dilution. The SRSF protocols also commonly used Hoescht, rather than DAPI, to stain the DNA and included this in the fixative rather than the secondary antibody incubation. This allowed the assay plates to be checked for contamination and confluency before antibody staining as it can be very difficult to focus a light microscope on a 384 well plate. The 72 hour transfection time was re-introduced as it was unsure which time point would produce the better staining in this plate type.

Despite these alterations to the Collis lab method, the assay could not successfully detect T21 foci for any condition which necessitated the further optimisation of the staining protocol. To determine if it was a lack of membrane permeabilisation that was limiting the staining, a time course was carried out to determine if an increased incubation time improved access of the antibody to the nucleus. Up to the 10 minute time point the extended incubation improved antibody entry whilst beyond this time the antibody signal had begun to diffuse, suggesting that the nuclear membrane had become too degraded. In light of this, a 10 minute extraction time was chosen for further investigation. However, when this was subsequently trialled, the images produced were still inadequate for automated analysis as very little difference was observed between the Control 1 and Chk1 knocked down cells and so further optimisation was required to improve the signal window of the assay.

Another technique utilised within the Collis lab for the immunofluorescent detection of chromatin bound proteins is pre-extraction. In this technique, the cells are incubated with an extraction buffer to remove the cytoplasm and increase permeability before fixing (Staples et al, 2016). This method was trialled in the 384 well format with an ice cold pre-extraction buffer. HU treatment was included to determine if the poor signal window was due to insufficiency of transfection. The combination of Chk1 knockdown and HU was the only condition sufficient to induce high levels of staining suggesting that the assay was capable of detecting replication stress but was not sensitive enough to detect the lower levels caused by gene knockdown alone. When this assay was repeated with RRM1 siRNA the combination of RRM1 knockdown and HU treatment produced discrete foci but this was not seen for RRM1 alone.

It was thought further optimisation of this technique may have resulted in sufficient levels of staining to detect replication stress following gene knockdown alone. However, several factors prevented the continuation of cold pre-extraction as a viable method for preparing screening plates. A disturbing lack of cells was observed in the assay plates when applying this technique and so it would not have be possible to guarantee that enough cells would remain in the well to draw meaningful conclusions from the images. Additionally, the requirement to carry out the incubation with the pre-extraction buffer at 4°C would have hindered the high throughput capabilities of the assay. The Microlab Star Hamilton robot housed in the SRSF was capable of processing plates with short incubation times, however it could not be cooled to 4°C. To process the plates using the Multidrop and the plate washer would have been extremely time consuming, as few plates would be able to be extracted at one time to minimise the risk of over-permeabilisation.

As this technique proved unfeasible, a different method of further increasing the permeabilisation of the nuclear membrane was required. As increasing the incubation with the extraction buffer any further decreased the levels of antibody detected in the nucleus, it was decided to increase the detergent concentration in the buffer. When this plated was imaged using the Cy5 channel, little difference could be discerned between the Control 1 and RRM1 knocked down cells. However, images generated using the Texas Red channel showed improved detection of the secondary antibody. The Alexa Fluor® 594 dye is most commonly detected using a Texas Red filter set as both of these dyes emit in the red region of the spectrum (ThermoFisher, 2016) whilst the Cy5 channel is commonly used to detect far-red emission. However, the initial optimisation experiments were imaged using this channel due to a communication error with the SRSF during the development of the imaging protocol. As the Texas Red channel detected more signal, it was easier to focus the microscope and so improved the quality of the images being generated. Increasing the Triton X-100 concentration to 1% appeared to over permiabilise the cell's membranes whilst 0.75% allowed for the imaging of clear foci with the 40X objective.

The knockdown of Chk1 was re-introduced into the optimisation assays at this point as its loss produced a lower level of T21 phosphorylation than that of RRM1 in previous assays. . As it was unlikely that any novel replication stress suppressor would produce as strong a response as Chk1 knockdown, it was necessary to ensure that the assay could differentiate between Chk1 deficient and Control 1 cells as if it could not, it would not have been fit for purpose. Overall, the increased Triton X-100 concentration and the switch to the Texas Red channel had increased the sensitivity of the assay which was now capable of differentiating between Control 1 and Chk1 knocked down cells.

Some of the Control 1 wells displayed greater than anticipated levels of T21 positive nuclei, which reduced the signal window of the assay. Therefore, it was decided to assess alternative non-targeting controls for inclusion in the assay. The four individual non-targeting siRNAs in the ON-TARGETplus library and the pool combining all four were trialled alongside the Chk1 and RRM1 siRNAs. The MetaXpress Custom Module Editor software was used to develop an algorithm that could identify a nucleus and the foci

within it by assessing the size and intensity of the objects within the images. The average number of foci per cell was calculated for every well and the number of foci present per cell used to calculate the proportion of T21 positive cells. With the combined toxicities of the four individual siRNAs, the pool proved to be the most toxic and so was discarded. All four of the individual siRNA produced less than 10% positive nuclei and so would have been acceptable for inclusion in the final screening assay.

Comparison of the average data and the individual cell data showed that they both produced similar trends. However, for all further automated analysis, the individual cell data was used as it was less susceptible to biases. If a small number of highly positive cells occurred in a well, this would have skewed the average data and made it look like more replication stress is ensuing than is actually the case. The algorithm can miscount the number of cells in a well if the cells are growing in clumps and again this would affect the average data; this would be identified in the individual cell data and could be rectified. The average data also gives no indication of the variability of the staining within the well, which can be calculated from the cell data.

As with the previous assay, the number of cells imaged was a concern and the levels of replication stress being produced by Chk1 and RRM1 knockdown were lower than expected. Therefore, efforts were made to improve cell numbers by increasing the plating density and transfection by increasing the concentration of DharmaFECT 1 and transfection time. The increased level of DharmaFECT 1 reduced cell numbers in the gene knockdown wells, most likely due to increased non-specific toxicities. Similar results were seen for the 72 hour transfection with regards to RRM1 knocked down cells, possibly due the fact that cells can only survive for short periods of time with severely compromised nucleotide metabolism. These decreases in cell number offset any improvements in signal window observed with these conditions and so were not pursued further. Increasing the plating density resulted in more cells imaged per condition and had very little effect on the levels of replication stress reported, so the plating density was increased to 2000 cells as this gave approximately 100 cells per well for every condition.

Upon repeating the non-targeting control panel experiment with 2000 cells plated per well the antibody signal did not appear in the Texas Red channel when using the 40X objective. By reducing the magnification and using the 20X objective the signal was detected and foci could be identified. The differing abilities of the objectives to detect the signal is a result of how the microscope captures the images. In the 20X images the image of each cell comprises fewer pixels than in the 40X images. This means that in the 20X images, the intensity of the signal of the individual pixels in the 40X image are combined to form the smaller image (Fig. 3.7.2), resulting in a stronger antibody signal which can be detected by the microscope.

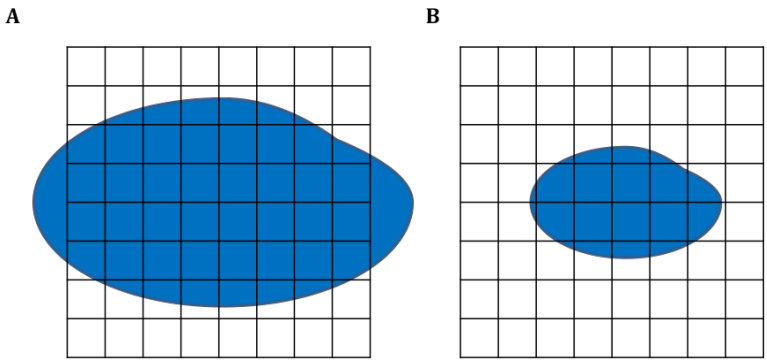

Figure 3.7.2. Difference in pixel coverage at 40X and 20X objectives.
Representative schematic of cell at a (A) 40X objective and a (B) 20X objective. Each square represents one pixel.

An algorithm was written to score the imaged obtained at the 20X objective however, this did not appear to correctly report the number of foci present accurately as all 4 non-targeting siRNAs produced higher replication stress levels than observed previously. Further attempts were made to optimise the 20X algorithm for automated scoring as more cells could be imaged at this objective whilst observing the same number of sites as the 40X foci, which would have improved the robustness of the scoring data. Several attempts were made to image a plate at both the 20X and the 40X objective and compare the result produced by the two respective algorithms and adjust the 20X to give a similar result to that produced for the 40X images.

The initial comparison revealed that the 20X algorithm was identifying much higher levels of foci than the 40X in every condition, indicating that either the criteria for identification of nuclei or foci required adjustment. In the 40X images, the levels of positive foci detected were surprising, with the non-targeting control transfected cells producing higher percentages of positive nuclei than the gene knocked down cells. This was observed for both antibody lots and so was not due to degradation of the original antibody. As the results appeared irregular the assay was repeated, however, the plate was not able to be imaged at the 40X objective due to a lack of T21 signal. In the 20X images the Chk1 cells appeared to be poorly stained and a high level of background staining was observed. Subsequent imaging of this plate on an InCell 2000 microscope to determine the strength of the antibody staining revealed that despite the efforts to increase cell density, the coverage of the wells was still sparse, with many images appearing completely devoid of cells. This inconsistent cell coverage was worrying as it had the potential to dramatically affect the robustness of the assay. The high levels of background staining were also concerning as this reduced the screening window of the assay and increased the likelihood of false positives being reported. The lack of staining in the Chk1 knocked down cells and the absence of true foci in the RMM1 knocked down cells was surprising as in the previous assays, transfection with these siRNAs had produced a clear staining pattern.

The next planned step in the optimisation of the assay was to trial a room temperature pre-extraction where cells are permeabilised with the 0.5% Triton X-100, 3% BSA buffer, fixed and then stained immediately. However, this was never completed in favour of the trouble shooting experiments.

As either the transfection or the staining did not appear repeatable between the assays, experiments were carried out to try and determine the cause of some of the recurrent issues. Their aim was to determine if there was an issue with the reagents or protocols being employed at the SRSF, or if the issues stemmed from the 384 well plate itself. Despite the protocol used to process the 384 well assay plates, the cell coverage was variable across the well, although this may have been an artefact of the manual washing. On HU treatment resulted in the induction of bright foci suggesting that the issues do not stem from the inability of the antibody to detect pRPA2. This suggests that it is either an issue with the reverse transfection within these wells or gene knockdown producing a weaker replication stress response than HU treatment. In contrast, when the SRSF procedure was carried out in a 24 well plate, clear differences could be distinguished between the Control 1, gene knocked down and HU treated cells. As this procedure is capable of producing foci in the 24 well format, it indicates that it is something implicit in the 384 well format that hindered the assay. One possibility is that the differing capabilities of the Nikon Eclipse and ImageXpress microscopes to detect the pRPA2 T21 signal may have caused the disconnect between the two assay formats. However, it was not possible to image 384 well plated on the Nikon or slides on the ImageXpress and so this could not be tested.

When looking back over the images produced during the optimisation of the high throughput assay it was observed that there were high levels of variability between the assays. Even when the images produced were of a decent quality, there was variability between the levels of foci observed for the same condition in the different assays. One source of this variability may have been the inconsistencies in how the assay plates were processed during the fixing and staining procedure. Due to the multi-user nature of the SRSF it was not always possible to guarantee the use of the same piece of equipment week on week and on several occasions the Multidrop and plate washer were not available due to technical difficulties. This may also have contributed to the irregularity of the cell coverage seen, as manual and automatic plate washing produce very different shearing forces and so may change the conditions faced by the cells during staining.

The background signal, irregularity of cell coverage and potential inconsistency of transfection efficiency all prevented the development of a robust assay suitable for genome wide RNAi screening. It was also highly concerning that the assay appeared to be very close to the detection limit of the 40X objective implied by the ability of the plate to be imaged using the 20X objective but not the 40X on several occasions. This was worrying as slight variability in the strength of the assay signal may have prevented the imaging of a plate and so wasted time and resources. This was not resolved by setting the assay up manually to eliminate the technical issues encountered at the SRSF with the Collis lab reagents.

Whilst a logical and methodical approach was taken to optimise this method, several factors prevented the development of a reliable screening assay. One major weakness of this study was the inconsistencies introduced by the technical difficulties encountered during the staining of the assay plates mentioned previously. These majorly undermined

the effectiveness of this optimisation and may have caused several of the problems, such as the variable cell coverage, that necessitated further optimisation of the assay. That said, it is likely that the choice of cell line also played a part in the failure of the development of this assay. Even in the 24 well assay, on several occasions, large bald patches were observed on the coverslips due to the cells lifting during staining. Most likely this is due to the propensity of this cell line to aggregate and so when they lift whole sheets are removed from the coverslips or well bottoms. Combined with the variability of the strength of signal produced either through inconsistent transfection, antibody binding or staining there was little confidence in this screening assay. Any one of these factors or a combination of them all may have resulted in the failure to produce a reliable and effective screening assay.

It was considered that the 384 well assay could be re-developed in 96 well assay plates or utilising a different cell line that would be less susceptible to aggregation or lifting. Ideally this cell line would have been of cancerous origin and previously been used in a SRSF antibody based screen. As either of these options could potentially have resulted in the re-optimisation of the entire assay, which would have been costly and time consuming, and still produced an assay unsuitable for screening, this was not attempted.

In parallel with the initial pRPA2 experiments in HCT116 cells, several complementary approaches were trialled as potential alternative screening methods or for hit validation. The first utilised HeLa cells expressing EGFP tagged RPA2 to determine if these cells formed EGFP foci following replication stress suppressor knockdown and if so, what proportion of the foci were stained by the pRPA2 antibodies. However, several issues arose with this assay including poor adherence to coverslips, poor staining and very low levels of EGFP expression. Repeating this experiment yielded no further results as without fail the plates became bacterially infected. Upon routine mycoplasma testing, the C3 clone returned a positive result which explained the issues with lifting cells and all further work was halted. The low levels of EGFP expression in the C1 clone also prevented further work. A very similar approach was attempted using a total RPA2 antibody which would have been assessed alongside the pRPA2 antibodies. However, this failed to yield foci following gene knockdown alone, suggesting this assay was not sensitive enough to detect endogenous levels of replication stress.

As previously mentioned, TopBP1 foci can also be used to assess replication stress levels (Kim et al, 2005) and was therefore investigated as an alternative screening approach. Although producing higher levels of non-specific staining, it did produce quantifiable images and could distinguish between Control 1 and Chk1 knocked down cells. As a result, this assay was miniaturised into a 384 well assay format. However, foci could not be readily detected, even with pre-extraction, and so the assay development was halted.

As neither the T21 pRPA2 foci detection assay or any of the alternative approaches investigated were suitable for use in a genome-wide screen, the development of this project had to be terminated. However, as the 24 well pRPA2 foci detection assay produced repeatable screening results, it was decided to utilise this protocol for screening purposes. It would have been too expensive and laborious to carry out an entire genome-

wide screen, or even a kinome screen using this protocol so a targeted kinase screen was proposed instead.

Chapter Four:
Phospho-RPA2 Targeted Screen

TABLE OF FIGURES 152

4.1 INTRODUCTION 153

4.2 PHOSPHO-RPA2 STAINING OPTIMISATION IN U2OS CELLS 154

4.3 PHOSPHO-RPA2 TARGETED SCREEN 156

4.4 HIT VALIDATION AND FURTHER KINASE SELECTION 159

4.4.1 TopBP1 Replication Stress Detection 159

4.4.2 Sensitisation to p53 Loss 161

4.4.3 Deconvolution of Hit siRNA Pools 162

4.5 FURTHER INVESTIGATION OF THE SENSITISATION TO P53 LOSS 166

4.5.1 Pharmacological Inhibition of p53 signalling 166

4.5.2 Sensitisation of p53 Deficient Cells 168

4.5.3 Assessment of DNA Damage in p53 Null Cells 169

4.5.4. Effect of SNRK on Cell Cycle Progression in p53 Null Cells 169

4.6 SNRK-MEDIATED LETHALITY TO ONCOGENE INDUCED REPLICATION STRESS 172

4.6.1 Sensitisation of Cyclin E Overexpressing Cells 172

4.6.2 Sensitisation of H-RAS Overexpressing Cells 173

4.6.3 Sensitisation of MYC-N Overexpressing Cells 175

4.7 SNRK-MEDIATED SENSITISATION TO REPLICATION STRESS CAUSING CHEMOTHERAPIES 178

4.7.1 Gemcitabine Sensitivity 178

4.7.2 PARP Inhibitor Sensitivity 179

4.7.3 5-Flurouracil Sensitivity 179

4.8 DISCUSSION 180

Table of Figures

Figure 4.2.1 Staining techniques trialled for the RPA2 staining of U2OS cells. 155
Figure 4.2.2 Optimisation of the RPA2 Staining Protocol in U2OS Cells. 156
Figure 4.3.1 Phospho-RPA2 Targeted Screen 157
Figure 4.3.2 Percentage of U2OS Cells positive for T21 foci in the Phospho-RPA2 Targeted Screen. 158
Figure 4.1.1.1 TopBP1 staining of selected Targeted Screen kinases 159
Figure 4.4.1.2 Percentage of U2OS cells positive for TopBP1 foci. 160
Figure 4.4.2.1 Expression of p53 in HCT116 and HCT116 p53 deficient cells. 161
Figure 4.4.2.2 Survival of HCT116 p53 Wild Type and p53 null cells following knockdown of selected Targeted Screen Kinases. 162
Figure 4.4.3.1 Percentage Knockdown of PMVK and SNRK following siRNA transfection with deconvoluted siRNA pools. 163
Figure 4.4.3.2 RPA2 staining of cells knocked down with PMVK or SNRK deconvoluted siRNA pools. 164
Figure 4.4.3.3 Percentage of PMVK and SNRK deconvoluted siRNA pool knocked down U2OS cells positive for T21 foci. 165
Figure 4.4.3.4 Survival of HCT116 p53 wild type and null cells following knockdown of PMVK or SNRK. 166
Figure 4.5.1.1 Sensitivity of SNRK and ATR knocked down cells to Pifithrin-α. 167
Figure 4.5.1.2 Sensitivity of SNRK and ATR knocked down cells to the KU55933. 168
Figure 4.5.2.1 Clonogenic survival of SNRK knocked down HCT116 p53 wild type and null cells. 168
Figure 4.5.3.1 γH2AX and 53BP1 staining of Roscovitine treated HCT116 p53 wild type and null cells. 169
Figure 4.5.3.2 Average number of γH2AX and 53BP1 foci in Roscovitine treated HCT116 wild type and p53 null cells. 170
Figure 4.5.4.1 Cell Cycle Distribution of SNRK knocked down p53 wild type and null HCT116 cells. 171
Figure 4.6.1.1 Tetracycline induced repression of Cyclin E overexpression 172
Figure 4.6.1.2 Survival of U2OS cells overexpressing Cyclin E following SNRK knockdown. 173
Figure 4.6.2.1 HCT116 and MRC-5 H-RAS overexpression. 174
Figure 4.6.2.2 Survival of HCT116 cells overexpressing H-RAS following SNRK knockdown. 174
Figure 4.6.2.3 Survival of MRC-5 cells overexpressing H-RAS following SNRK knockdown. 175
Figure 4.6.3.1 Neuroblastoma cell line MYC-N overexpression. 176
Figure 4.6.3.2 Survival of SH-EP1 and IMR-32 cells following SNRK knockdown. 176
Figure 4.6.3.3 Survival of SH-EPTet21N cells following SNRK knockdown 177
Figure 4.7.1.1 Survival of SNRK knocked down cells following treatment with Gemcitabine. 178
Figure 4.7.2.1 Survival of SNRK knocked down cells following treatment with Olaparib. 179
Figure 4.7.3.1 Survival of SNRK knocked down cells following treatment with 5-FU. 180

4.1 Introduction

Due to the failure of the high throughput screening methods to produce a feasible assay for the identification of novel replication stress suppressors, it was decided to adopt a more targeted approach. As the pRPA2 T21 24 well staining protocol had reproducibly generated a suitable screening window throughout assay development, this assay was further optimised and employed as a targeted kinase screen.

During the development of the high throughput screen, Kavanaugh and colleagues published a paper which detailed their identification of replication stress response genes using a genome wide screening approach (Kavanaugh et al, 2015). This genome wide screen utilised BrdU incorporation to quantify endogenous levels of replication stress following gene knockdown before treating the cells with HU to induce replication fork stalling. The cells were then incubated with EdU to measure the restart of replication forks before fixing and staining with γH2AX antibodies to determine the levels of unresolved damage. The EdU and γH2AX staining was quantified and used to calculate a replication restart score (RSS) which were then assigned robust Z-scores. The data published from this screen was used to generate a list of potential replication stress response genes to be assessed in the phospho-RPA2 Targeted Screen.

It was decided to specifically investigate kinases that suppressed replication stress, as these enzymes are considered 'druggable' (Hopkins & Groom, 2002). All of the kinases included in the ON-TARGETplus SMARTpool siRNA library were ranked by their average RSS Z-score, with hits with an average RSS Z-score of less than 3 being discarded.

These remaining kinases were shortlisted based on any cancer associated mutations, identified using cBioPortal (Cerami et al, 2012), or interesting phenotypes in the GenomeRNAi database (Schmidt et al, 2013) (Appendix 3) which resulted in a final list of 18 kinases (Table 4.1.1).

Kavanaugh Rank	Kinase Rank	Gene Symbol	Average RRS Z-score
61	4	CAMK1	11.09
110	6	DGKA	9.56
157	9	GAK	8.15
182	10	STK16 (TSF1)	7.83
234	14	STK36	7.15
355	15	MAP2K6	6.09
550	19	PIK4CA (PI4KA)	4.89
618	22	SRMS	4.60
623	23	DGKI	4.56
628	24	MAP4K1	4.54
671	25	PIK3R1	4.39
733	27	STK35	4.14
830	33	MAPKAPK5	3.88
871	35	PMVK	3.78
882	36	TTK (MPS1)	3.75
904	38	CDK10	3.72
910	39	PAK1	3.69
980	41	SNRK	3.54

Table 4.1.1. Kinases to be included in Phospho-RPA2 Targeted Screen.
The ON-TARGETplus SMARTpool kinases were ranked by their average RSS Z-score; those with an average Z-score less than 3 were discarded. These were then shortlisted based on associated cancer mutations and phenotypes reported in RNAi screens. The final list was compiled of kinases with no published replication stress suppressor activity in PubMed.

These kinases were also assigned their Z-scores from the Collis γH2AX RNAi screen (Barone et al, 2016; Myers et al, 2016; Staples et al, 2016; Staples et al, 2014; Staples et al, 2012) and a Caspase 3 activation and RPA2 Ser4/8 phosphorylation screen (Meuth lab, unpublished). However, it was found that there was little correlation between the Z-scores generated in the three screens and so these were not considered during target selection (Appendix 3).

It was hypothesised that as these kinases played a role in replication restart, they would also increase the levels of pRPA2 observed following gene knockdown and that these enzymes would make suitable candidates for targeted cancer therapies. Any gene that didn't confer an increase in pRPA2 foci formation following knockdown were discarded and the remaining hits were validated in a TopBP1 immunofluorescent screen. They were also assessed for their ability to preferentially decrease survival in p53 deficient cells and from this assay two hits, Phosphomevalonate Kinase (PMVK) and Sucrose Non-fermenting Related Kinase (SNRK), were selected for further assessment.

The siRNA pools used in these subsequent screens were deconvoluted and the individual siRNAs were assessed for their ability to reduce PMVK or SNRK expression, increase pRPA2 foci formation and sensitise p53 null cells. As the individual PMVK siRNA failed to decrease survival in the p53 deficient cells, work on this gene was halted. The SNRK deficient phenotype was characterised by immunofluorescence, MTT cytotoxicity and Clonogenic survival assays and flow cytometry to determine its status as a potential cancer drug target.

4.2 Phospho-RPA2 Staining Optimisation in U2OS Cells

When designing the Targeted Screening assay, it was decided to use U2OS cells as this was the cell line that had been used to carry out the Kavanaugh screen. As this assay would never be scaled down to a high throughput format, techniques that would have proved unfeasible could also now be employed to improve the quality of the immunofluorescent staining. Four staining methods were investigated to determine which produced the most specific staining pattern. Cells were forward transfected with Control 1, Chk1 or RRM1 siRNA and DharmaFECT 1. The cells were fixed 48 hours post-transfection with one set of coverslips pre-extracted with 0.5% Triton X-100, 3% BSA in PBS for 5 minutes before fixing. Two sets of coverslips were incubated with 0.5% Triton X-100, 3% BSA in PBS for 5 minutes after fixing, one of which was also blocked in 0.5% BSA in PBS 1 hour before staining. The final set of coverslips was extracted with acetone and blocked with Acetone Blocking Buffer before the cells were stained (Fig. 4.2.1 and Fig. 4.2.2).

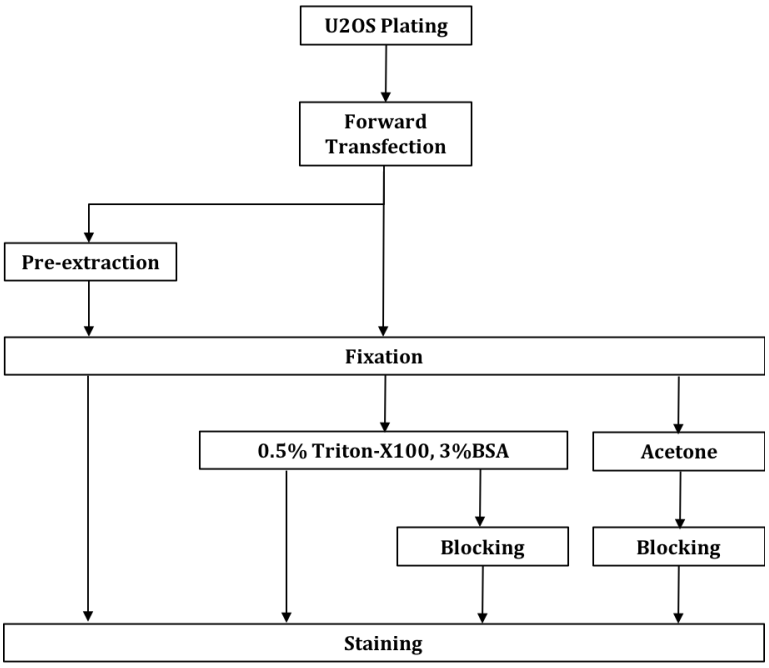

Figure 4.2.1 Staining techniques trialled for the pRPA2 staining of U2OS cells.

All of the four protocols trialled produced a very low level of T21 background staining in the Control 1 cells. Of the four techniques, the coverslips extracted with 0.5% Triton X-100, 3% BSA in PBS with no additional blocking produced the poorest quality images with the most non-specific staining of the nucleus (Fig. 4.2.2). This was particularly prominent in the Chk1 knocked down cells where less foci are present than in the RRM1 deficient cells. The coverslips that received the additional 0.5% BSA block also displayed higher than desirable levels of background staining in the Chk1 knocked down cells but the foci appeared clearer in the cells lacking RRM1. Extraction with acetone reduced the levels of background staining observed in Chk1 deficient cells but did not appear to improve the staining of RRM1 knocked down cells compared to the coverslips that received additional blocking (Fig. 4.2.2). The protocol that produced the least background staining was the pre-extraction of the cells. Very little background was observed in the Chk1 knocked down cells and the foci appeared more defined in the RRM1 deficient cells than for any other protocol. As a result of this, all further Immunofluorescent staining experiments were carried out using pre-extraction (unless otherwise stated).

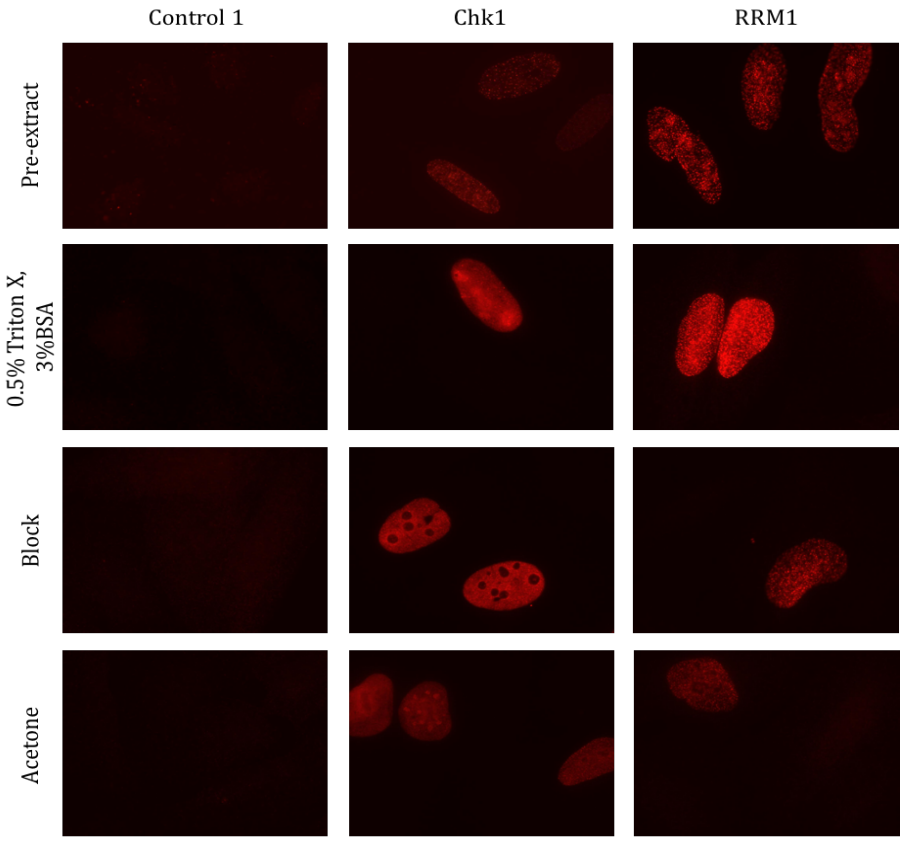

Figure 4.2.2 Optimisation of the RPA2 Staining Protocol in U2OS Cells.
Representative images of U2OS cells forward transfected with Control 1, Chk1 or RRM1 siRNA and DharmaFECT 1. The cells were grown for 48 hours post-transfection. Cells were either permeabilised with 0.5 % Triton X-100 and 3% BSA before fixing, permeabilised with 0.5 % Triton X-100 and 3% BSA after fixing (some of which were blocked in 0.5% BSA) or extracted with acetone. The cells were stained with a 1:250 dilution of antibody raised against the T21 site within RPA2.

4.3 Phospho-RPA2 Targeted Screen

Once the Phospho-RPA2 staining protocol had been selected, the Targeted Screen was carried out with five individual biological replicates (two carried out by Dr. K. Myers of the Collis lab). In addition to the Control 1 siRNA employed in the high throughput screen (Chapter 3), RPA2 siRNA was included as a further negative control to remove the primary antibody's target and so set a low level threshold of pRPA2 foci formation. As used previously, Chk1 and RRM1 siRNA were included as siRNA positive controls. Two untransfected wells were also included on each assay plate, one of which was subsequently treated with 2mM HU, as supplementary transfection independent controls. Each assay plate also included the 18 target kinases selected from the Kavanaugh data (Fig. 4.3.1). The kinases were numbered according to their location in a custom siRNA plate (A2-B9) to remove any potential bias from the scoring of the screen.

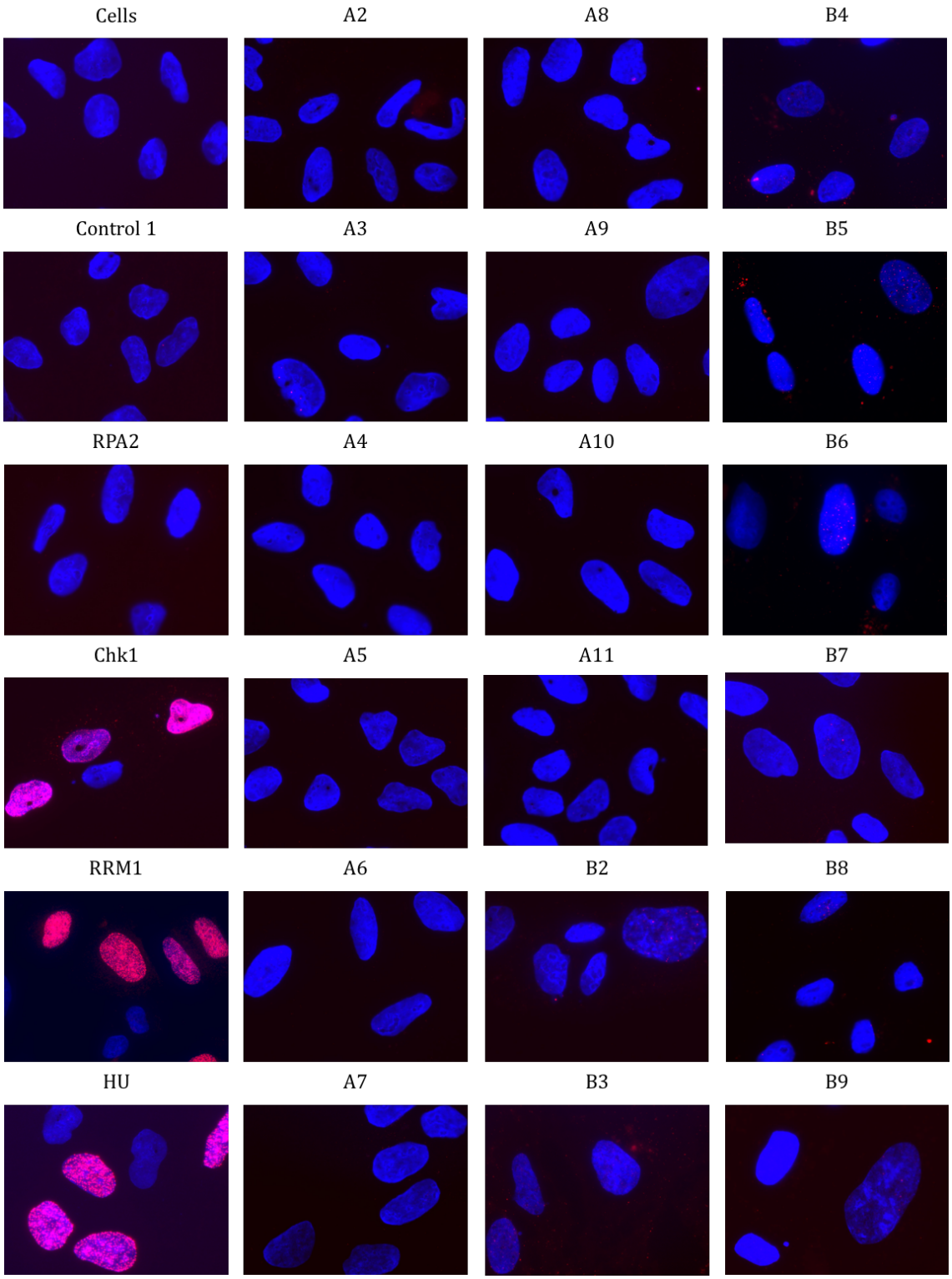

Figure 4.3.1 Phospho-RPA2 Targeted Screen

Representative images of U2OS cells forward transfected with Control 1, RPA2, Chk1, RRM1 or siRNA against the 18 selected kinases and DharmaFECT 1. Two wells remained untransfected, one of which was treated with 2mM HU for 16 hours pre-extraction. The cells were grown for 48 hours post-transfection then permeabilised with 0.5 % Triton X-100 and 3% BSA before fixing. The cells were stained with a 1:250 dilution of antibody raised against the T21 site within RPA2.

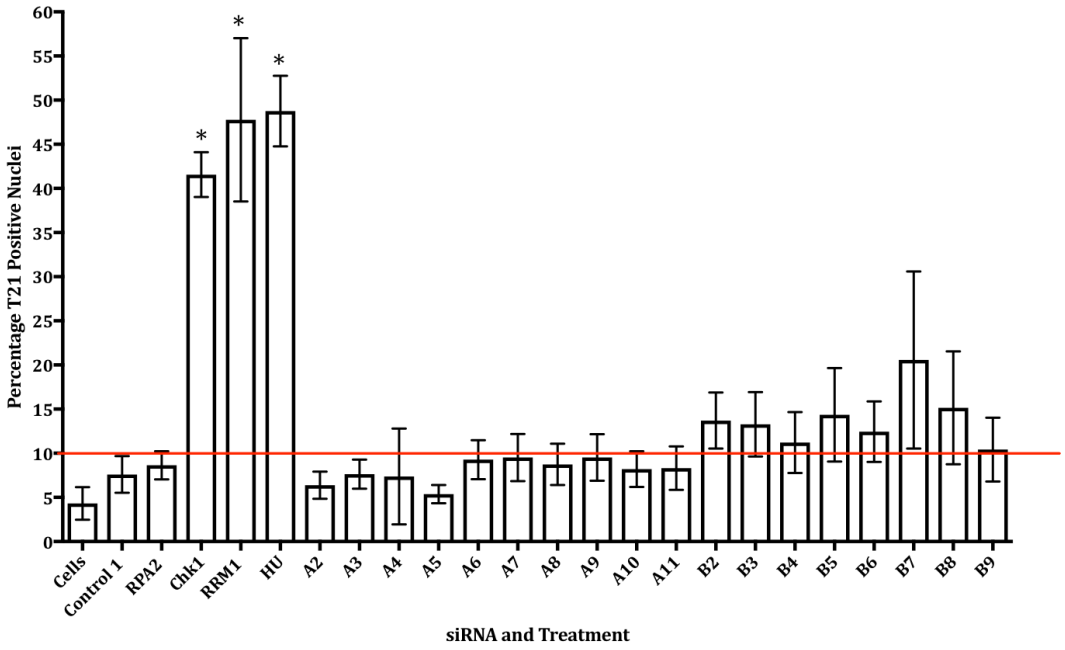

Figure 4.3.2 Percentage of U2OS Cells positive for T21 foci in the Phospho-RPA2 Targeted Screen.

For each condition the number of cells were counted and the percentage of T21 positive nuclei was calculated. A nucleus was considered positive if it contained 10 or more bright T21 foci. Asterisks indicate significant difference from untransfected Cells, p value <0.05. Mean values derived from five independent experiments, with their respective SEMs. Red line represents 10% T21 Positive Nuclei cut off for hit selection.

The untransfected cells (Cells), Control 1 and RPA2 knocked down cells showed very low levels of T21 staining. The Chk1 and RRM1 knocked down cells and the HU treated cells showed a very high level of staining as previously demonstrated in other cell lines. None of the selected kinases showed as high a level of staining as the positive controls, as was expected, as none of the kinases scored as highly in the Kavanaugh screen as Chk1. The images were subsequently scored for T21 foci to determine if differences could be distinguished between the target kinases and the negative controls (Fig. 4.3.2).

The knockdown of Chk1 or RRM1 and treatment with HU produced a significantly higher percentage of T21 positive cells when compared to the untransfected cells (p-values <0.0001, 0.0042 and <0.0001 respectively). However, none of the selected kinases produced a significant change in the levels of T21 phosphorylation (Fig. 4.3.2, Appendix 4). A statistically significant cut off of 10% T21 Positive Nuclei (p-value 0.0295) was chosen to allow the identification of kinases for further investigation; this resulted in the selection of kinases B2-B9.

4.4 Hit Validation and Further Kinase Selection

When the kinases for further investigation had been selected, several assays were carried to assess the validity of the hits as replication stress suppressors. These assays also served to further narrow down the list of remaining kinases to a number viable for more detailed analysis.

4.4.1 TopBP1 Replication Stress Detection

The alternative replication stress marker TopBP1 (as demonstrated in 3.6.3) was utilised to validate the selected hits as replication stress suppressors. Cells were transfected with Control 1 siRNA or siRNA targeting Chk1, RRM1 or one of the 8 selected kinases (B2-B9) with DharmaFECT 1. An untransfected (Cells) and a HU treated well was also included on each assay plate as transfection independent controls (Fig. 4.4.1.1).

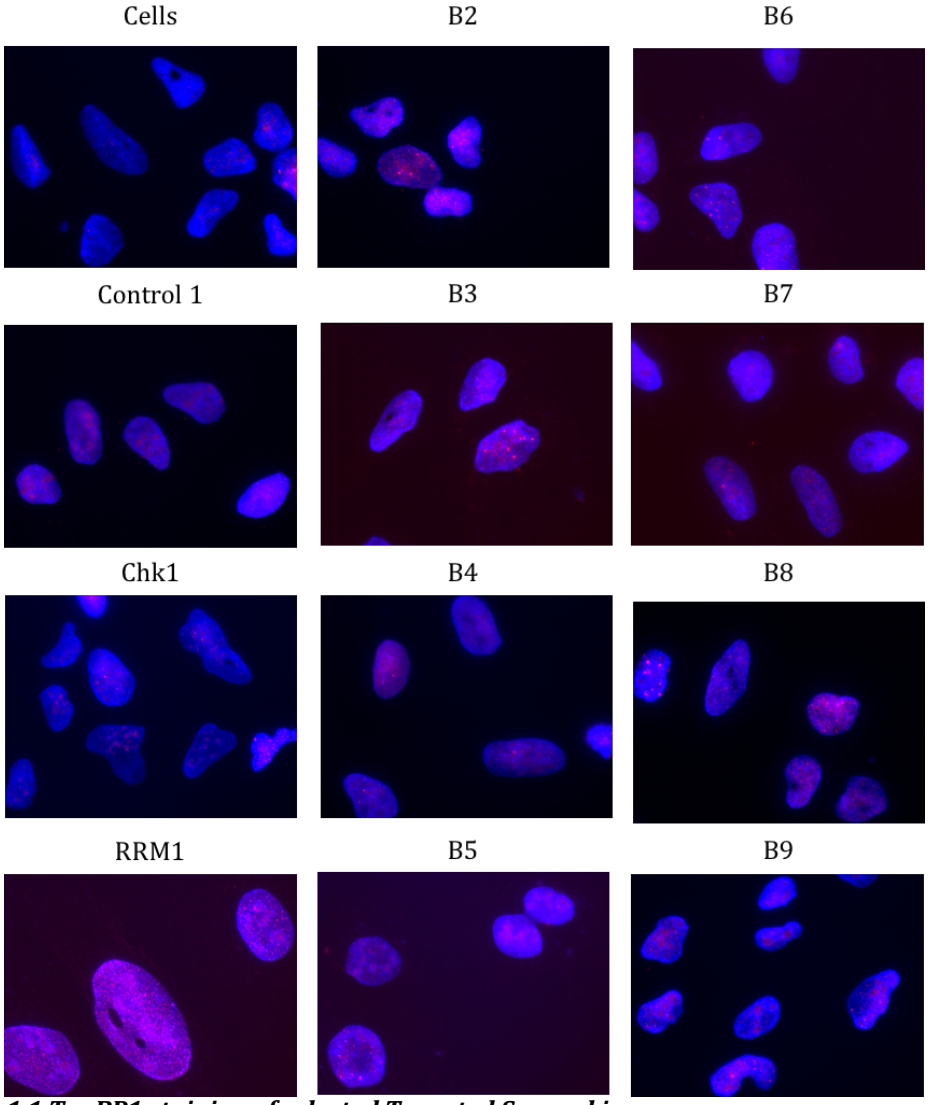

Figure 4.1.1.1 TopBP1 staining of selected Targeted Screen kinases

Representative images of U2OS cells forward transfected with Control 1, Chk1, RRM1 or siRNA against the 8 selected kinases and DharmaFECT 1. One well remained untransfected. The cells were grown for 48 hours post-transfection then permeabilised with 0.5 % Triton X-100 and 3% BSA before fixing. The cells were stained with a 1:500 dilution of antibody raised against TopBP1.

siRNA	Total Cells	TopBP1 Negative	% TopBP1 Negative	TopBP1 Positive	% TopBP1 Positive	p-value (Compared to Cells)
Cells	207	161	77.78	46	22.22	/
Control 1	307	239	77.85	68	22.15	/
Chk1	306	144	47.06	162	52.94	0.0126
RRM1	303	112	36.96	191	63.04	0.0005
HU	299	93	31.10	206	68.90	0.0013
B2	298	163	54.70	135	45.30	0.0469
B3	306	190	62.09	116	37.91	0.2016
B4	302	168	55.63	134	44.37	0.0264
B5	254	143	56.30	111	43.70	0.1047
B6	280	163	58.21	117	41.79	0.0564
B7	244	125	51.23	119	48.77	0.0197
B8	243	110	45.27	133	54.73	0.0042
B9	217	138	63.59	79	36.41	0.3092

Table 4.4.1.1 Scoring of selected Targeted Screen kinases for TopBP1 positive nuclei.
For each condition, the total number of cells were counted and the percentage of TopBP1 positive nuclei was calculated. A nucleus was considered positive if it contained 10 or more bright foci. Values derived from three independent experiments.

The untransfected cells and Control 1 cells produced a very low level of staining, which increased upon the knockdown of Chk1, RRM1 or treatment with HU (not shown). The TopBP1 images were subsequently scored to allow the quantification of the differences in replication stress induced by gene knockdown (Table 4.4.1.1 and Fig. 4.4.1.2). When compared to the untransfected cells, the knockdown of Chk1, RRM1 or HU treatment all produced a significant increase in the levels of TopBP1 positive cells (Table 4.4.1.1). Additionally, kinases B2, B4, B7 and B8 also all produced a significant increase in the levels of replication stress observed in this assay, whilst the remaining four kinases (B3, B5, B6 and B9) did not due the variability in staining produced by their knockdown.

Despite four kinases not producing a significant difference when compared to untransfected cells, as all of the kinases produced a similar increased level of replication stress in this assay compared with negative control cells, all 8 kinases were taken forward for further investigation.

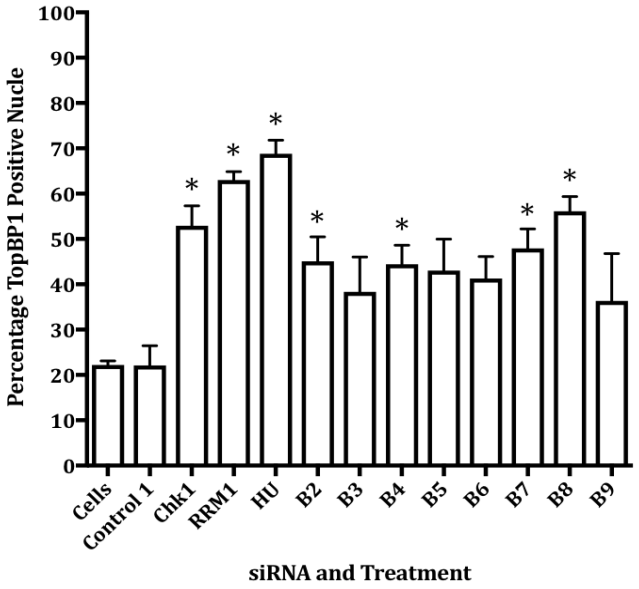

Figure 4.4.1.2 Percentage of U2OS cells positive for TopBP1 foci.
For each condition the number of cells were counted and the percentage of TopBP1 positive nuclei was calculated. A nucleus was considered positive if it contained 10 or more bright TopBP1 foci. Asterisks indicate significant difference from untransfected Cells, p value <0.05. Mean values derived from three independent experiments, with their respective SEMs.

4.4.2 Sensitisation to p53 Loss

One way in which drugs are being designed to target cancer cells more specifically is through the exploitation of synthetic lethal relationships with cancer associated mutations and/or cancer selective vulnerabilities such as gene addiction. Mutation of the tumour suppressor p53 is the most common genetic change that arises in cancer (Negrini et al, 2010). Therefore, the identification of any gene whose loss is more detrimental in cells lacking functional p53 may prove to be a promising cancer therapy target.

Two isogenic HCT116 cell lines that were wild type (WT) or null with regards to p53 (Bunz et al, 1999) were therefore used to investigate if any of the 8 selected kinases preferentially killed cells deficient for p53. To demonstrate that the HCT116 and HCT116 p53 null cell line did differ in their p53 expression status, western blotting analysis was used to determine the expression of p53 in each cell line. The cells were grown for 72 hours before being lysed to prepare samples for electrophoresis. The resultant membranes were blotted with p53 and β-Actin antibodies (Fig. 4.4.2.1).

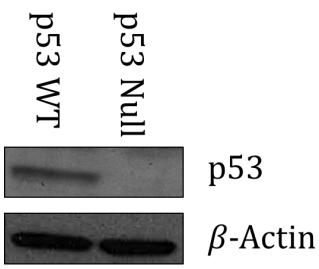

Figure 4.4.2.1 Expression of p53 in HCT116 wild type and HCT116 p53 null cells.

HCT116 wild type and HCT116 p53 null cells were grown for 72 hours before lysis. For each cell line, 15μg of protein was loaded onto a NuPage 4-12% Bis-Tris Gel for separation. The gels were transferred to nitrocellulose membranes before blocking and blotting with p53 and β-Actin primary antibodies which were detected by HRP conjugated secondary antibodies.

Once the disparity in p53 expression had been established, the existence of any potential sensitisation of p53 deficient cells was investigated. MTT cytotoxicity assays were carried out where each kinase was knocked down in p53 wild type and p53 null HCT116 cells. The cells were forward transfected with Control 1, kinase B2-8 or ATR siRNA and DharmaFECT 1. ATR was used as a positive control as it has previously been shown to exhibit a synthetic lethal relationship with p53 deficiency (Kwok et al, 2016). The assay plates were left for 120 hours post-transfection before the addition of MTT (Fig. 4.4.2.2).

For every kinase, the HCT116 p53 wild type cells grew better following gene knockdown when compared to the p53 null cells (Fig. 4.4.2.2A). Calculation of the fold change between the p53 null and wild type cells revealed that the kinases B5 and B9 were the only two kinases to produce a significant difference (p-values 0.017 and 0.024 respectively) in growth. As knockdown of these two kinases, PMVK (B5) and SNRK (B9), produced a significant decrease in the growth of p53 deficient cells they were taken forward for further investigation.

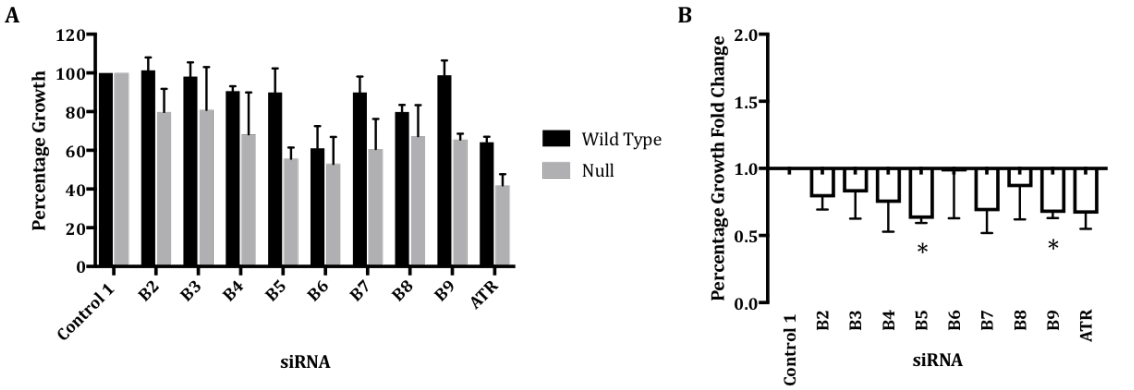

Figure 4.4.2.2 Growth of HCT116 p53 wild type and p53 null cells following knockdown of selected Targeted Screen Kinases.

HCT116 p53 wild type or p53 null cells were transfected with Control 1, ATR or siRNAs against the 8 selected Targeted Screen Kinases and DharmaFECT 1. The cells were grown for 120 hours post-transfection before the addition of MTT. Mean values were derived from 3 independent experiments, with their respective SEMs. (A) Percentage growth of each siRNA in HCT116 p53 wild type or p53 null cells. (B) Fold change in the percentage growth of p53 wild type compared to p53 null cells. Asterisks indicate significant difference from Control 1, p value <0.05

4.4.3 Deconvolution of Hit siRNA Pools

To validate the knockdown of PMVK and SNRK, the pool siRNAs that were used in the Phospho-RPA2, TopBP1 and sensitivity screens were deconvoluted to determine if the effects observed were due to specific gene knockdown or off target effects.

For both genes, the four individual siRNAs were assessed for their knockdown capabilities by qPCR. U2OS cells were forward transfected with Control 1, PMVK 1-4 or SNRK 1-4 siRNAs with DharmaFECT 1 and grown for 48 hours. The cells were then lysed, the RNA was extracted and subsequently reverse transcribed. The resultant cDNA was then amplified using TaqMan probes for 18S ribosomal RNA and PMVK or SNRK. The Ct values produced were then used to calculate the percentage gene knockdown (Table 4.4.3.1 and Fig 4.4.3.1). This experiment was carried out with four repeats with two repeats carried out by Miss L. Sinclair (Masters student).

siRNA	Average Percentage Knockdown
PMVK 1	96.17
PMVK 2	92.63
PMVK 3	93.45
PMVK 4	96.93
SNRK 1	86.51
SNRK 2	79.21
SNRK 3	80.83
SNRK 4	69.54

Table 4.4.3.1 Percentage Knockdown of PMVK and SNRK following siRNA transfection with deconvoluted siRNA pools.

U2OS were transfected with Control 1, PMVK 1-4 or SNRK 1-4 for 48 hours. RNA was extracted from the cells, reverse transcribed and the resultant cDNA was amplified using TaqMan primers against 18S ribosomal RNA, and PMVK or SNRK. The Ct values generated were used to calculate the percentage knockdown using the $2^{-\Delta\Delta C}$ method. Mean values derived from four independent experiments.

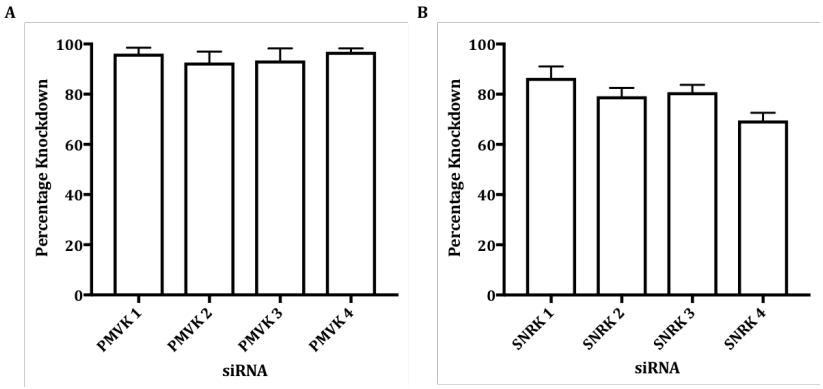

Figure 4.4.3.1 Percentage Knockdown of PMVK and SNRK following siRNA transfection with deconvoluted siRNA pools.

U2OS were transfected with Control 1, (A) PMVK 1-4 or (B) SNRK 1-4 for 48 hours. RNA was extracted from the cells, reverse transcribed and the resultant cDNA was amplified using TaqMan primers against 18S ribosomal RNA, and PMVK or SNRK. The Ct values generated were used to calculate the percentage knockdown using the $2^{-\Delta\Delta C}$ *method. Mean values derived from four independent experiments, with their respective SEMs.*

For both genes, all siRNAs produced a high percentage of gene knockdown with all four siRNA exceeding 90% knockdown for PMVK and siRNA 1-3 exceeding 75% knockdown for SNRK (Fig. 4.4.3.1).

The four individual siRNAs were also included in a RPA2 T21 immunofluorescence assay to determine how many produced comparable results to those observed in the initial

pooled siRNA screen. U2OS cells were forward transfected with Control 1, RPA2, Chk1, RRM1, PMVK 1-4 or SNRK 1-4 siRNAs with DharmaFECT 1 and grown for 48 hours post-transfection. An untransfected well (Cells) and a HU treated well were also included as transfection independent controls. The cells were then fixed and stained as described previously (Fig. 4.4.3.2). This experiment was carried out with four repeats with three repeats carried out by Miss L. Sinclair.

The images obtained show a very similar staining pattern to the initial T21 screen, with the negative controls producing a very low level of scoring whilst the positive controls showed a much higher level of positive nuclei. The PMVK and SNRK siRNAs produced a low level of T21 stained nuclei, again as previously, but they demonstrated a greater proportion of positive nuclei than the negative control cells. The images were scored for T21 positive nuclei to determine if the individual siRNAs produced a similar result to that seen in the initial screen (Fig 4.4.3.3).

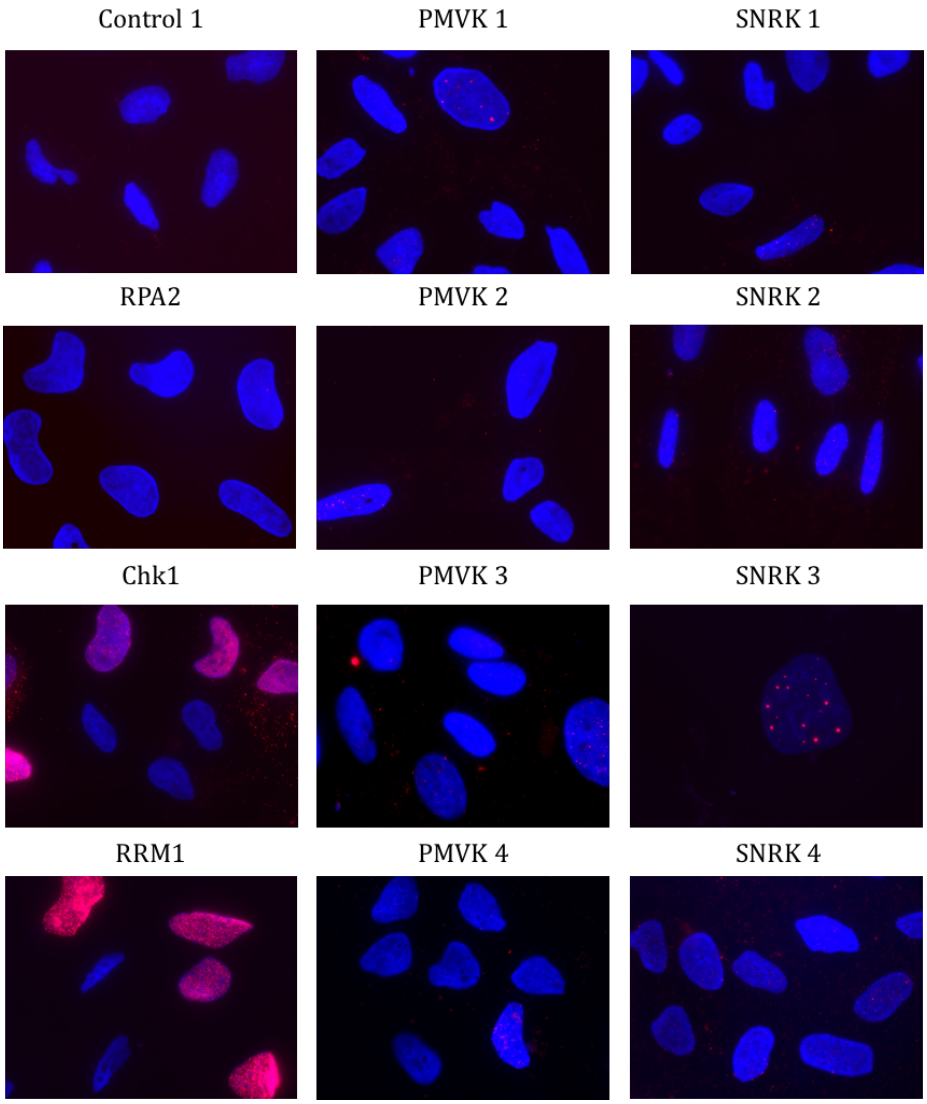

Figure 4.4.3.2 RPA2 staining of cells knocked down with PMVK or SNRK deconvoluted siRNA pools.

Representative images of U2OS cells forward transfected with Control 1, RPA2, Chk1, RRM1 PMVK 1-4 or SNRK 1-4 and DharmaFECT 1. The cells were grown for 48 hours post-transfection then permeabilised with 0.5 % Triton X-100 and 3% BSA before fixing. The cells were stained with a 1:250 dilution of antibody raised against the T21 site within RPA2 T21.

The three positive controls produced a significant difference in the percentage of T21 positive cells compared to that observed in the untransfected Cells (p-values of <0.0001 for Chk1, 0.0112 for RRM1 and <0.0001 for HU). Of the deconvoluted hit siRNAs, only PMVK 4 and SNRK 1 produced a significant increase in the levels of pRPA foci (p-values of 0.320 and 0.004 respectively), with most siRNA producing a non-significant increase, as was seen in the initial screen.

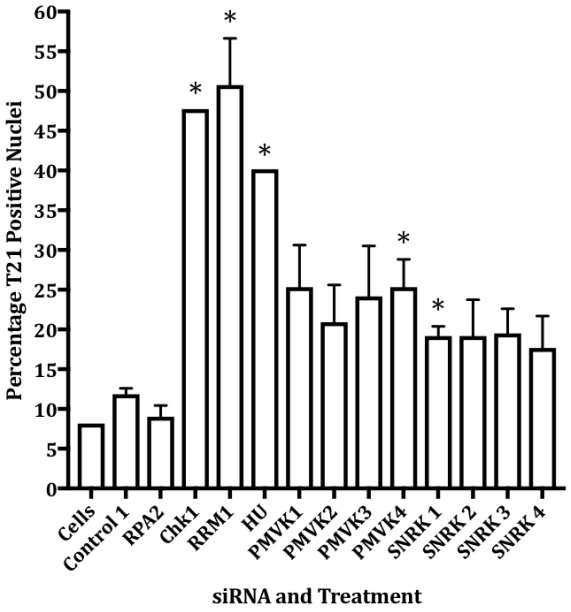

Figure 4.4.3.3 Percentage of PMVK and SNRK deconvoluted siRNA pool knocked down U2OS cells positive for T21 foci.

For each condition the number of cells were counted and the percentage of T21 positive nuclei was calculated. A nucleus was considered positive if it contained 10 or more bright T21 foci. Mean values derived from four independent experiments, with their respective SEMs.

As neither the qPCR or the T21 scoring could conclusively differentiate between the siRNAs, PMVK 1-4 and SNRK 1-3 siRNAs were taken forward to repeat the p53 sensitivity screen. The HCT116 p53 wild type and p53 null cells were forward transfected with Control 1, PMVK 1-4, SNRK 1-3 or ATR siRNA and DharmaFECT 1. The assay plates were left for 120 hours following transfection before the addition of MTT (Fig. 4.4.3.4). This experiment was carried out with five repeats with two repeats carried out by Miss L. Sinclair.

In both the PMVK and SNRK assays, the knockdown of ATR significantly decreased the growth of the p53 deficient HCT116 cells as expected. However, despite their significance, the differences in growth were not large and so may not have been biologically relevant. None of the PMVK siRNAs tested significantly reduced growth which was unexpected given that the siRNA pool did. For SNRK, siRNA 2 significantly decreased growth in the deficient cells and siRNA 3 did decrease growth to a similar level but this was not significant. These two siRNAs were used in further experiments to investigate the potential of this kinase as a cancer drug target. As none of the PMVK siRNA had made a repeatable impact on cellular growth, investigation into this kinase was halted in favour of the continued characterisation of SNRK.

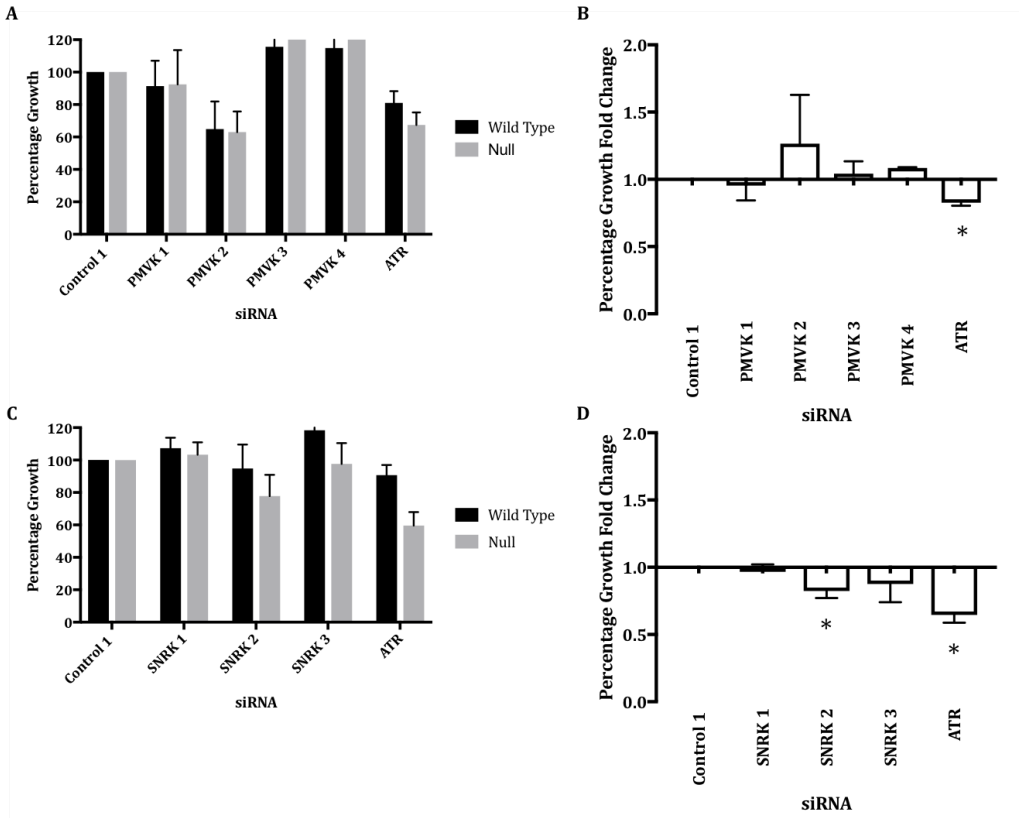

Figure 4.4.3.4 Growth of HCT116 p53 wild type and null cells following knockdown of PMVK or SNRK.

HCT116 p53 Wild Type or p53 null cells were transfected with Control 1, (A-B) PMVK 1-4, (C-D) SNRK 1-4 or ATR siRNAs and DharmaFECT 1. The cells were grown for 120 hours post-transfection before the addition of MTT. Mean values were derived from five independent experiments, with their respective SEMs. (A, C) Percentage growth of each siRNA in HCT116 p53 wild type or p53 null cells. (B, D) Fold change in the percentage growth of HCT116 p53 wild type compared to the p53 null cells. Asterisks indicate significant difference from Control 1, p value <0.05.

4.5 Further Investigation of the Sensitisation to p53 Loss

4.5.1 Pharmacological Inhibition of p53 signalling

Rather than relying solely on the results obtained using the p53 null HCT116 cell line, the sensitivity assays were repeated in wild type HCT116 cells that had their p53 signalling disrupted by Pifithrin-α (PTN-α). Whilst this p53 inhibitor has been shown to have off target effects (Sohn et al, 2009), it has previously been demonstrated that it protects cells and mice from genotoxic insults (Gudkov & Komarova, 2005; Komarov et al, 1999) and decreases the expression of p53 target genes (Culmsee et al, 2001). It was therefore deemed as an appropriate alternative chemical approach to complement the previously obtained genetic data. HCT116 wild type cells were plated and 24 hours post-plating the cells were treated with a 0 - 30μM titration of PTN-α. Five hours after the cells were treated they were transfected with Control 1, SNRK 2, SNRK 3 or ATR siRNAs with DharmaFECT 1 and grown for 120 hours before the addition of MTT (Fig. 4.5.1.1).

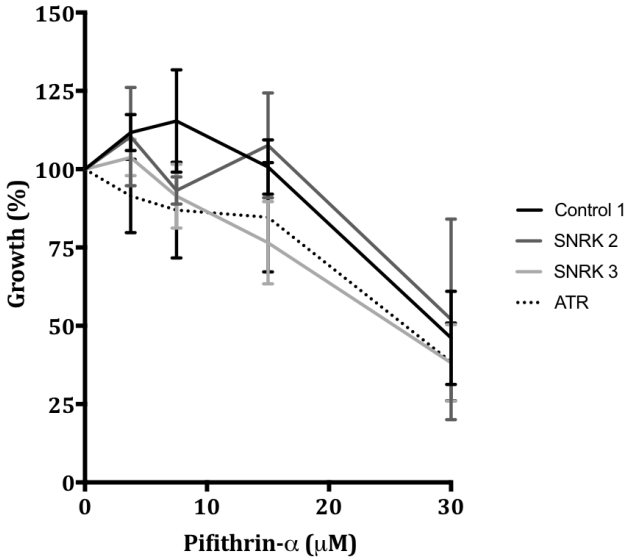

Figure 4.5.1.1 Sensitivity of SNRK and ATR knocked down cells to Pifithrin-α.
HCT116 cells were grown for 24 hours before treatment with 0, 3.75, 7.5, 15 or 30μM Pifithrin-α. The cells were then transfected with Control 1, SNRK 2, SNRK 3 or ATR siRNA and DharmaFECT 1 5 hours after treatment. The cells were grown for 120 hours post-transfection before the addition of MTT. Mean values were derived from three independent experiments, with their respective SEMs.

Knockdown of neither SNRK nor ATR significantly decreased the growth of PTN-α treated cells compared to cells transfected with Control 1 siRNA. However, at 7.5μM PTN-α, Control 1 transfected cells appeared to grow better than any of the gene knocked down cells, suggesting that drug is potentially capable of mimicking the results seen in the p53 null cells.

ATM lies upstream of p53 in the DNA damage response and its mutation in tumour cells can produce similar results as the loss of p53 (Bartkova et al, 2005). Therefore, it was decided to assess if SNRK knockdown could sensitise cells to inhibition of ATM by the ATM inhibitor KU55933. HCT116 cells were transfected with Control 1, SNRK 2, SNRK 3 or ATR siRNAs with DharmaFECT 1 for 48 hours. The cells were then treated with a 0 - 10μM titration of KU55933 and grown for 120 hours before the addition of MTT (Fig. 4.5.1.2).

The combination of ATR knockdown and KU55933 treatment did not result in cell killing although it has previously been reported that ATR inhibition selectively kills ATM deficient cells (Kwok et al, 2016; Min et al, 2017; Reaper et al, 2011). This calls into question the effectiveness of the KU55933/ATR siRNA combination in this assay and therefore judgements cannot be made as to whether SNRK knockdown sensitises cells to ATM inhibition.

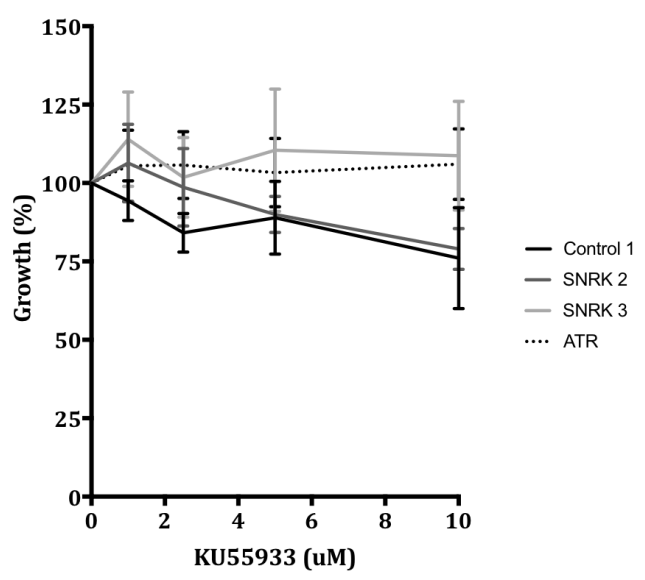

Figure 4.5.1.2 Sensitivity of SNRK and ATR knocked down cells to KU55933.
HCT116 cells were transfected with Control 1, SNRK 2, SNRK 3 or ATR siRNA and DharmaFECT 1 for 48 hours before treatment with 0, 1, 2.5, 5, 10μM KU55933 for 120 hours. Mean values were derived from three independent experiments, with their respective SEMs.

4.5.2 Sensitisation of p53 Deficient Cells

As the knockdown of SNRK preferentially killed p53 deficient cells in the MTT survival assay, a Clonogenic survival assay was carried to further assess the effects of SNRK loss on cell survival using this more sensitive technique. HCT116 wild type and p53 null cells were transfected with Control 1, SNRK 2, SNRK 3 or ATR siRNA for 48 hours. The cells were then trypsinised, counted and replated at either 200 or 2000 cells per well. The cells were grown for 11 days to allow colonies to form which were subsequently stained with Methylene Blue (0.4%) and manually counted (Fig. 4.5.2.1).

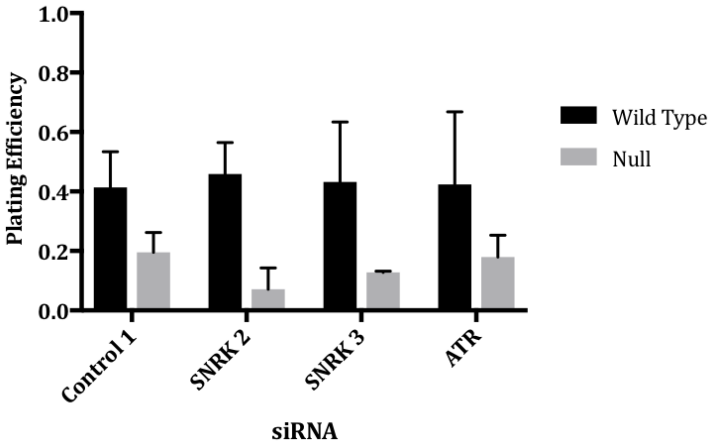

Figure 4.5.2.1 Clonogenic survival of SNRK knocked down HCT116 p53 wild type and null cells.
HCT116 p53 wild type and null cells were transfected with Control 1, SNRK 2, SNRK 3 or ATR siRNA and DharmaFECT 1 and grown for 48 hours before being trypsinised and replated at 200 or 2000 cells per well. The cells were then grown for 11 days to allow colonies to form which were then stained with 0.4% Methylene Blue. The colonies were counted and the plating efficiencies were calculated. Mean values derived from three independent experiments, with their respective SEMs.

In the wild type cells, the knockdown of SNRK or ATR did not significantly affect the survival of the cells. In the p53 null cells, knockdown of SNRK with either siRNA produced a trend towards decreased survival, but this was not significant due to the variability of the number of colonies produced. This suggests the possibility that the loss of SNRK may decrease survival in a p53 deficient background.

4.5.3 Assessment of DNA Damage in p53 Null Cells

It was hypothesised that the loss of SNRK may induced DNA damage through increased replication stress, which would be more severe in p53 deficient cells, leading to increased cell death. Therefore, the levels of γH2AX and 53BP1 foci were determined following SNRK siRNA-mediated knockdown in the p53 wild type and null HCT116 cells. Both cell lines were also treated with the CDK inhibitor Roscovitine to determine if DNA replication was required for the induction of the damage (Collis et al, 2007). The HCT116 p53 wild type and null cells were plated and transfected with Control 1, SNRK 2, SNRK 3 or ATR siRNAs with DharmaFECT 1 for 48 hours. Four hours prior to fixation, the cells were either treated with 10μg/ml Roscovitine or mock treated with DMSO. The cells were then fixed, extracted with 0.5% Triton X-100 and 3% BSA in PBS before co-staining for γH2AX and 53BP1 (Fig. 4.5.3.1). The cells were imaged and scored for the average number of γH2AX and 53BP1 per cell (Fig. 4.5.3.2).

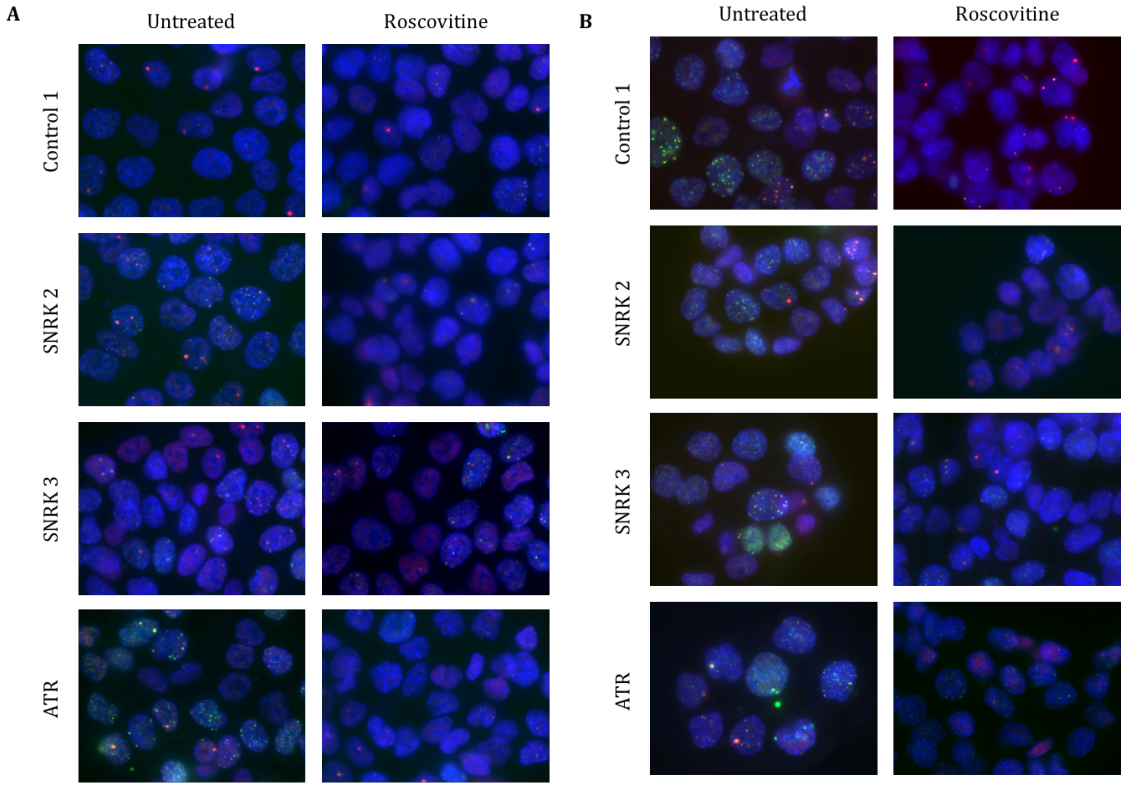

Figure 4.5.3.1 γH2AX and 53BP1 staining of Roscovitine treated HCT116 p53 wild type and null cells.

Representative images of (A) HCT116 wild type and (B) HCT116 p53 null cells forward transfected with Control 1, SNRK 2, SNRK 3 or ATR siRNA and DharmaFECT 1. The cells were grown for 48 hours post-transfection, mock treated with PBS or treated with 10μg/ml Roscovitine for 4 hours, fixed and then permeabilised with 0.5 % Triton X-100 and 3% BSA. The cells were stained with 1:1000 dilutions of antibodies raised against γH2AX (green) and 53BP1 (red).

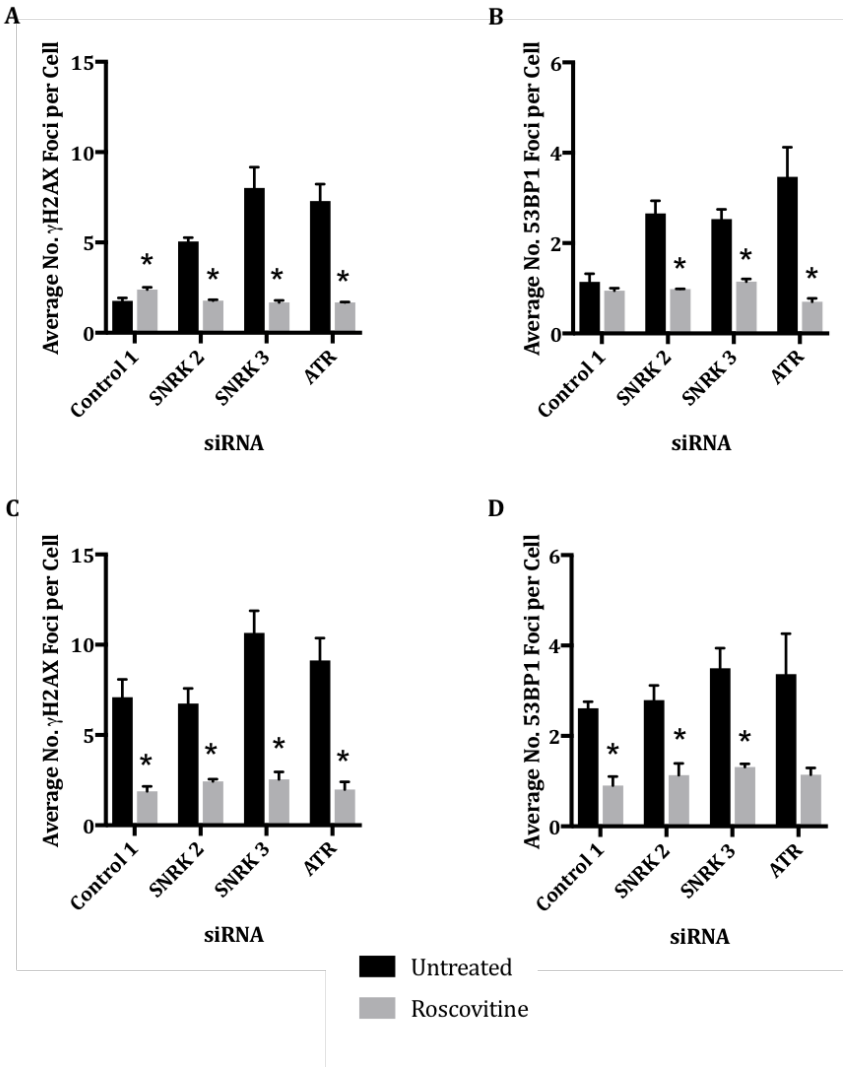

Figure 4.5.3.2 Average number of γH2AX and 53BP1 foci in Roscovitine treated HCT116 wild type and p53 null cells.

For each condition, the total number of cells were counted and the average number of γH2AX and 53BP1 foci per cell were calculated Mean values derived from three independent experiments, with their respective SEMs. Asterisks indicate significant difference from Untreated cells, p value <0.05. (A) HCT116 p53 Wild Type. (B) HCT116 p53 null.

In the untreated HCT116 wild type cells, the knockdown of either SNRK or ATR significantly increased the number of γH2AX and 53BP1 foci observed when compared to Control 1 transfected cells. In the HCT116 p53 null cells, the loss of neither SNRK nor ATR expression resulted in a significant increase in the numbers of foci observed for either damage marker, although there is a trend towards increased numbers for both.

The treatment with Roscovitine significantly decreased the number of foci present compared to the untreated cells in the majority of conditions (Fig 4.5.3.2). The loss of neither SNRK nor ATR resulted in an increase in the number of foci observed, suggesting that the damage resulting from their knockdown is dependent upon DNA replication. This suggests that such damage is likely occurring through the collapse of stalled replication forks. However, this was not observed for the wild type control cells where Roscovitine treatment increased γH2AX levels and had little effect upon the number of 53BP1 foci

present. It was also not observed in the ATR transfected p53 null cells due to the variability of numbers observed in the untreated cells.

For both γH2AX and 53BP1, more foci were observed in the p53 null Control 1 transfected cells than the wild type cells. As this was reversed by Roscovitine treatment, it appears that the increased damage occurring in these cells is dependent upon DNA replication. For γH2AX, the SNRK and ATR knocked down cells also displayed higher numbers of foci in the p53 null than the wild type cells. However, this was not seen to the same extent for 53BP1.

4.5.4. Effect of SNRK on Cell Cycle Progression in p53 Null Cells

To assess the potential effects of SNRK knockdown on cell cycle distribution, PI FACS analysis was carried out on both the wild type and p53 null HCT116 cells. Both cell lines were transfected with Control 1, SNRK 2, SNRK 3 or ATR siRNA for 48 hours. The cells were trypsinised and fixed in ice cold 70% ethanol before they were treated with RNase A and stained with 50μg/ml PI. The stained cells were then analysed by flow cytometry with 10000 cells counted per sample (Fig. 4.5.4.1).

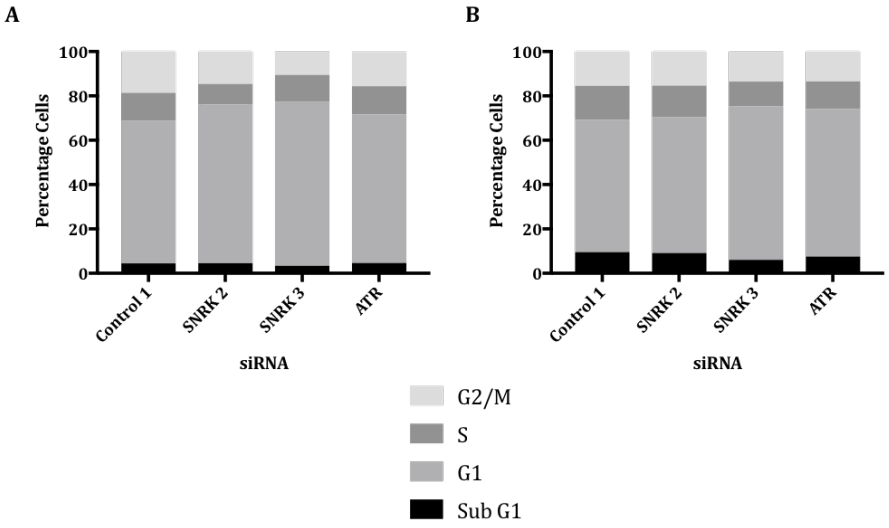

Figure 4.5.4.1 Cell cycle distribution of SNRK knocked down p53 wild type and null HCT116 cells.

(A) HCT116 p53 wild type and (B) p53 null cells were transfected with Control 1, SNRK 2, SNRK 3 or ATR siRNA and DharmaFECT 1 for 48 hours. Cells were fixed in ice cold 70% ethanol, treated with RNase A and stained with 50μg/ml propidium iodide. Cells were then analysed by flow cytometry, with 10000 cells analysed per sample, to determine the DNA content of the cells. Values derived from one experiment.

The knockdown of neither SNRK nor ATR in either of the cell lines drastically affected cell cycle distribution. In the wild type cells, gene knockdown slightly increased the percentage of cells in G1 and reduced the proportion in S or G2/M but these changes were only slight. The p53 null cells displayed a slightly higher proportion of cells in Sub G1 than the wild type cells but this was the same for all siRNA. The same trend was observed in these cells with increased G1 and decreased S and G2/M cells when SNRK or ATR were knocked down. No statistical analysis could be carried out on this data as the experiment was only carried out once due to time constraints.

4.6 SNRK-mediated Lethality to Oncogene Induced Replication Stress

4.6.1 Sensitisation of Cyclin E Overexpressing Cells

The overexpression of Cyclin E is associated with an increase in the firing of replication origins, deregulation of the initiation of S phase and increases the likelihood of DNA replication interfering with gene transcription. This ultimately results in DNA damage and genomic instability which aids the evolution of cancerous cells (Jones et al, 2013). Its overexpression has been identified in a large number of cancers, including breast, lung, cervix and gastrointestinal (Malumbres & Barbacid, 2001), and is commonly associated with poor disease free survival (Hwang & Clurman, 2005).

As it is frequently overexpressed in tumours and those tumours typically demonstrate poorer survival outcomes, it would be beneficial to identify cancer targets that specifically detrimentally affect Cyclin E overexpressing cells. Previous work has demonstrated that the overexpression of Cyclin E may be synthetic lethal with the loss of ATR (Toledo et al, 2011), which suggests that inhibition of replication stress suppressors may be unfavourable in Cyclin E overexpressing cells.

U2OS cells with Tetracycline repressible Cyclin E overexpression, a kind gift from Dr. E. Petermann, were therefore used to determine if the knockdown of SNRK was specifically detrimental to Cyclin E overexpressing cells. Western blotting analysis was used to verify the Tetracycline repressible nature of the Cyclin E overexpression. The U2OS Cyclin E cells were grown for 4 hours before the addition of 2μg/ml Tetracycline to repress Cyclin E overexpression or mock treated with DMSO. The cells were grown for a further 48 hours before they were lysed. A total Cyclin E antibody was used to assess the protein levels present within the cell lysates (Fig. 4.6.1.1).

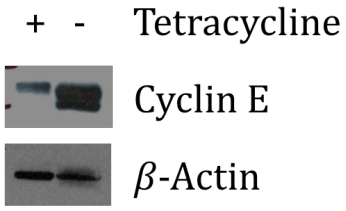

Figure 4.6.1.1 Tetracycline induced repression of Cyclin E overexpression

U2OS Cyclin E cells were plated for four hours before mock treatment with DMSO or treatment with 2μg/ml Tetracycline and grown for a further 48 hours. The cells were lysed and 15μg of protein from each sample was loaded onto a NuPage 4-12% Bis-Tris Gel for separation. The gels were transferred to nitrocellulose membranes before blocking and blotting with Total Cyclin E and β-Actin (loading control) primary antibodies. The primary antibodies were detected with HRP conjugated secondary antibodies.

A much lower level of Cyclin E is present in the Tetracycline treated cells compared to the mock treated cells which demonstrates that the Cyclin E overexpression in these cells is Tetracycline repressible. A double band can be seen in the mock treated cells but this has previously been reported in this cell line (Jones et al, 2013).

These cells were then used to assess whether the knockdown of SNRK was preferentially cytotoxic to Cyclin E overexpressing cells. The U2OS Cyclin E cells were plated and 4 hours later, the cells were either mock treated with DMSO or treated with 2μg/ml Tetracycline to repress Cyclin E overexpression. The cells were transfected with Control 1, SNRK 2,

SNKR 3 or ATR siRNA and DharmaFECT 1 24 hours after plating. The cells were grown for 120 hours before the addition of 3mg/ml MTT (Fig. 4.6.1.2).

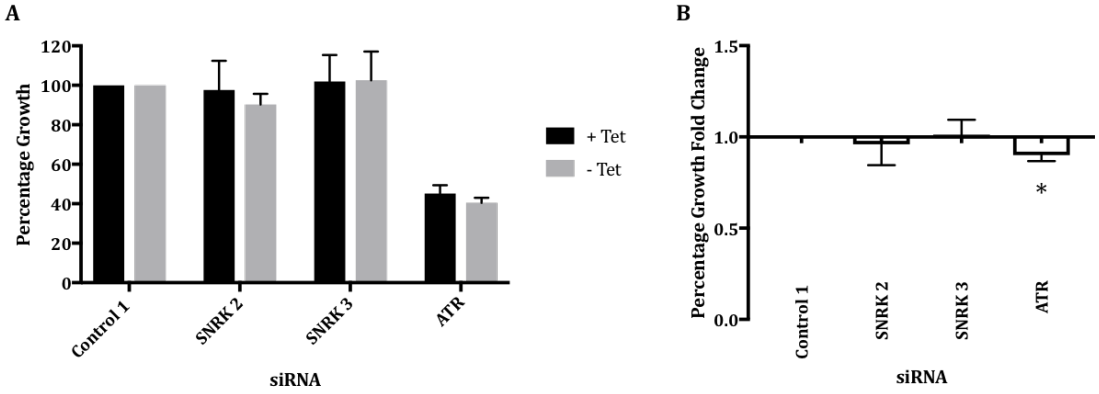

Figure 4.6.1.2 Growth of U2OS cells overexpressing Cyclin E following SNRK knockdown.
U2OS Cyclin E cells were plated for four hours before mock treatment with DMSO or treatment with 2μg/ml Tetracycline. The cells were transfected with Control 1, SNRK 2, SNRK 3 or ATR and DharmaFECT 1 24 hours post-plating. The cells were grown for 120 hours post-transfection before the addition of MTT. Mean values were derived from 3 independent experiments, with their respective SEMs. (A) Percentage growth of each siRNA in U2OS Cyclin E cells with or without Tetracycline. (B) Fold change in the percentage growth of U2OS Cyclin E cells with Tetracycline compared to cells without Tetracycline. Asterisks indicate significant difference from Control 1, p value <0.05.

The knockdown of SNRK by either siRNA did not impact on the growth of Cyclin E overexpressing cells when compared to the cells with repressed Cyclin E overexpression. Only the knockdown of ATR significantly decreased the growth of the Cyclin E overexpressing cells (p-value 0.0358), suggesting that the loss of SNRK is not detrimental in cells overexpressing this oncogene.

4.6.2 Sensitisation of H-RAS Overexpressing Cells

The canonical RAS genes, K-RAS, N-RAS and H-RAS are mutated in up to 30% of human tumours, making RAS mutations one of the most common incidents during cancer evolution (Pylayeva-Gupta et al, 2011). The mutations of these genes are often commonly found in cancers with poorer prognosis, including pancreatic ductal adenocarcinoma (Fernandez-Medarde & Santos, 2011). Previously, oncogenic RAS expression has been demonstrated to be synthetic lethal when the ATR pathway is significantly inhibited (Gilad et al, 2010), suggesting that the inhibition of replication suppression pathways may be preferentially detrimental to cells with mutated or overexpressed RAS.

The HCT116 and MRC-5 H-RAS^{G12V} overexpressing cell lines were generated by Miss C. Fellows (PhD student; Cox and Collis labs) using a pCAG-FLOX vector containing the H-RAS gene, a kind gift from Professor M. Meuth. H-RAS mutation is only found in 3% of human tumours compared to the 25-30% of tumours harbouring K-RAS (Fernandez-Medarde & Santos, 2011). However, as a vector containing this gene was readily available in the Sheffield Academic Unit of Molecular Oncology, and it had previously been demonstrated to alter replication kinetics (Gagou et al, 2014), H-RAS^{G12V} overexpressing cell lines were generated rather than using the more common K-RAS mutation.

The overexpression of H-RAS^{G12V} in these two cell lines, compared to the wild type parental cells was assessed by western blotting. HCT116 wild type, HCT116 H-RAS^{G12V}, MCR-5 wild type and MRC-5 H-RAS^{G12V} cells were grown for 72 hours before they were lysed. A total RAS antibody was used to assess the protein levels present within the cell lysates (Fig. 4.6.2.1).

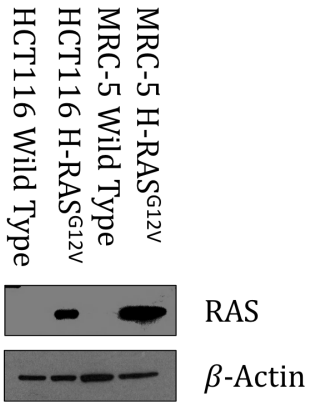

Figure 4.6.2.1 HCT116 and MRC-5 H-RAS overexpression.
HCT116 wild type, HCT116 H-RAS^{G12V}, MCR-5 wild type and MRC-5 H-RAS^{G12V} cells were grown for 72 hours. The cells were lysed and 15μg of protein from each sample was loaded onto a NuPage 4-12% Bis-Tris Gel for separation. The gels were transferred to nitrocellulose membranes before blocking and blotting with Total RAS and β- Actin (loading control) primary antibodies. The primary antibodies were detected with HRP conjugated secondary antibodies.

RAS bands were only detectable in the two vector containing cell lines and no bands were visible in either of the parental cell lines, demonstrating that these cells are overexpressing H-RAS^{G12V}.

The HCT116 wild type and HCT116 H-RAS^{G12V} cells were primarily used to assess if the knockdown of SNRK preferentially sensitised the RAS overexpressing cells. Both cell lines were transfected with Control 1, SNRK 2, SNKR 3 or ATR siRNA and DharmaFECT 1 24 hours after plating and the cells were grown for 120 hours before the addition of 3mg/ml MTT (Fig. 4.6.2.2).

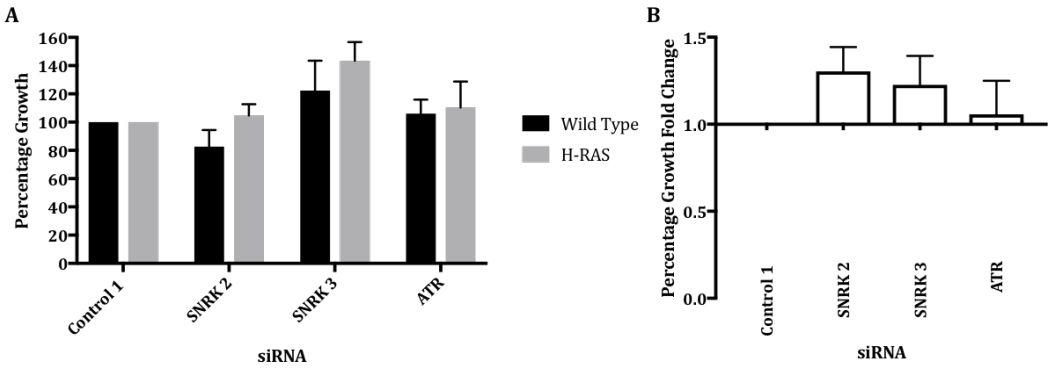

Figure 4.6.2.2 Growth of HCT116 cells overexpressing H-RAS following SNRK knockdown.
HCT116 wild type and HCT116 H-RAS^{G12V} cells were transfected with Control 1, SNRK 2, SNRK 3 or ATR and DharmaFECT 1 24 hours post-plating. The cells were grown for 120 hours post-transfection before the addition of MTT. Mean values were derived from 3 independent experiments, with their respective SEMs. (A) Percentage growth of each siRNA in HCT116 wild type or the HCT116 H-RAS^{G12V} cells. (B) Fold change in the percentage growth of HCT116 wild type compared to HCT116 H-RAS^{G12V} cells.

None of the siRNA produced a significant change in growth when compared to the Control 1 transfected cells due to the variability in the assay. Unexpectedly, all three siRNA produced a trend to increased growth in the H-RAS^{G12V} overexpressing cells, even ATR. However, it has been reported that partial knockdown of ATR in cells expressing

oncogenic K-RAS promoted tumour formation (Gilad et al, 2010), suggesting that the gene knockdown may not be optimal in this assay.

This experiment was repeated in the MRC-5 H-RAS^{G12V} cell line as MRC-5 cells are normal cells and the overexpression of H-RAS^{G12V} in this line is more reminiscent of early neoplastic lesions (Fig. 4.6.2.3).

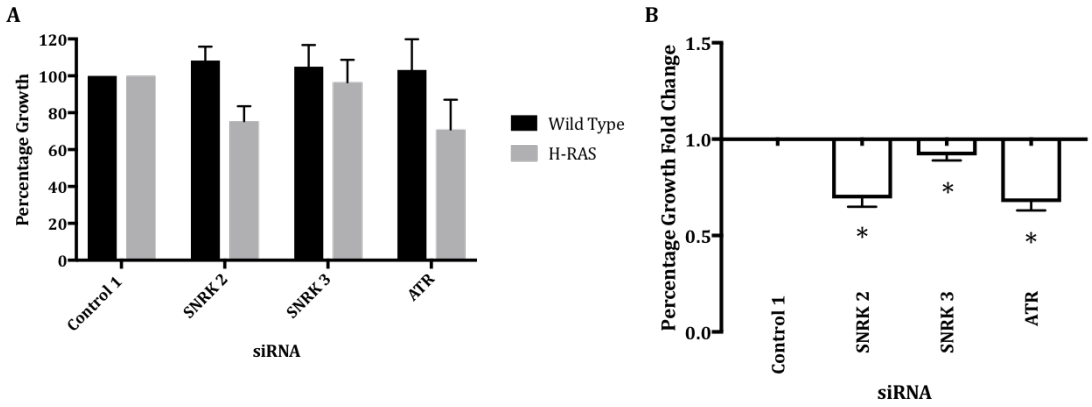

Figure 4.6.2.3 Growth of MRC-5 cells overexpressing H-RAS following SNRK knockdown.
MRC-5 wild type and MRC-5 H-RAS^{G12V} cells were transfected with Control 1, SNRK 2, SNRK 3 or ATR and DharmaFECT 1 24 hours post-plating. The cells were grown for 120 hours post-transfection before the addition of MTT. Mean values were derived from 3 independent experiments, with their respective SEMs. (A) Percentage growth of each siRNA in MRC-5 wild type or the MRC-5 H-RAS^{G12V} cells. (B) Fold change in the percentage growth of MRC-5 wild type compared to MRC-5 H-RAS^{G12V} cells.

The knockdown of SNRK, with both siRNA, and ATR significantly decreased the growth of H-RAS^{G12V} overexpressing cells (p-values of 0.0022, 0.0379 and 0.0017 respectively). This differs for results seen in the HCT116 H-RAS^{G12V} cells possibly due to the efficiency of gene knockdown in this cell line. It is also plausible that the genetic background of the parental cells has resulted in this discrepancy.

4.6.3 Sensitisation of MYC-N Overexpressing Cells

Overexpression of MYC-N, a member of the MYC family of transcription factors, can induce the transformation of rat embryonic fibroblasts (Huang & Weiss, 2013). This gene was identified due to its amplification in approximately 20% of neuroblastoma cases (Beltran, 2014) which is correlated with high grade, poor prognosis (Huang & Weiss, 2013) and is used to stratify at risk patients for more aggressive forms of treatment. The amplification of MYC-N has also been described in a number of other tumour types, including glioblastoma, retinoblastoma and prostate cancer, and is typically associated with poor prognosis (Beltran, 2014).

The amplification of MYC-N is thought to increase the levels of replication stress present when compared to normal cells, resulting in a dependence upon ATR/Chk1 signalling. It has previously been demonstrated that further enhancing this replication stress, by means of PCNA inhibition by R9-caPep, resulted in cell death (Gu et al, 2015). It was therefore decided to investigate whether the knockdown of SNRK would detrimentally affect survival in MYC-N overexpressing cells.

The overexpression of MYC-N in the SH-EP1 (no MYC-N), IMR-32 (MYC-N overexpressing) and SH-EPTet21N (Tetracycline repressible MYC-N overexpressing) (Lutz et al, 1996) neuroblastoma cells was assessed by western blotting. The SH-EP1, IMR-32 and SH-EPTet21N cells (in the presence and the absence of Tetracycline) were plated; in all assays twice as many cells were plated in the presence of Tetracycline due to the slower cycling of these cells. The cells were grown for 72 hours before lysis and sample preparation. A total MYC-N antibody was used to assess the protein levels present within the cell lysates (Fig. 4.6.3.1).

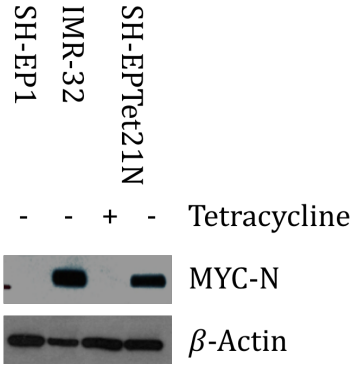

Figure 4.6.3.1 Neuroblastoma cell line MYC-N overexpression.
SH-EP1, IMR-32 and SH-EPtet21N (with and without Tetracycline) were grown for 72 hours. The cells were lysed and 15μg of protein from each sample was loaded onto a NuPage 4-12% Bis-Tris Gel for separation. The gels were transferred to nitrocellulose membranes before blocking and blotting with Total MYC-N and β- Actin (loading control) primary antibodies. The primary antibodies were detected with HRP conjugated secondary antibodies.

MYC-N expression was only detectable in the IMR-32 and SH-EPTet21N without Tetracycline lanes as expected and so these cell lines were used to assess the affected of SNRK loss in MYC-N overexpressing cells.

Initially, the SH-EP1 and IMR-32 cells were used to determine if loss of SNRK detrimentally affected MYC-N overexpressing cells more than cells with no MYC-N expression. Both cell lines were transfected with Control 1, SNRK 2, SNKR 3 or ATR siRNA and DharmaFECT 1 24 hours after plating and the cells were grown for 120 hours before the addition of 3mg/ml MTT (Fig. 4.6.3.2).

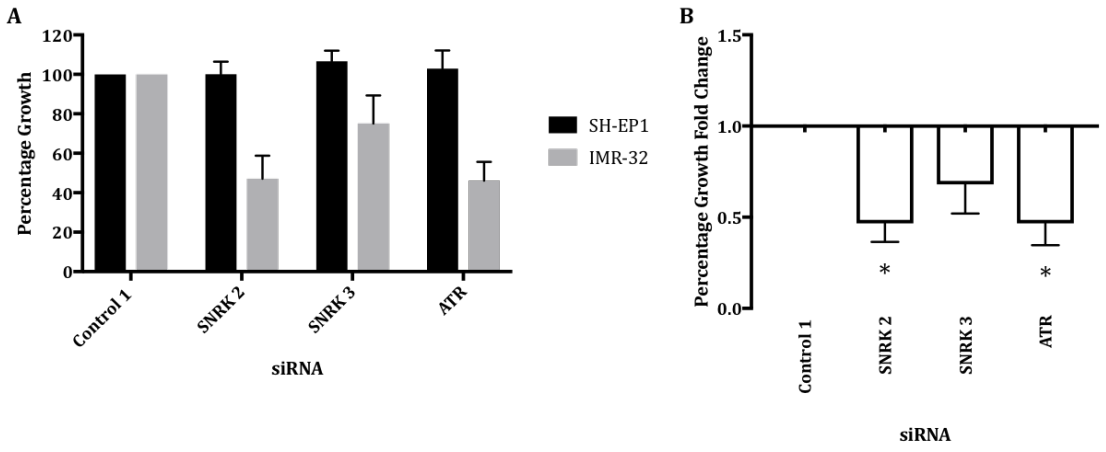

Figure 4.6.3.2 Growth of SH-EP1 and IMR-32 cells following SNRK knockdown.
SH-EP1 and IMR-32 cells were transfected with Control 1, SNRK 2, SNRK 3 or ATR and DharmaFECT 1 24 hours post-plating. The cells were grown for 120 hours post-transfection before the addition of MTT. Mean values were derived from 3 independent experiments, with their respective SEMs. (A) Percentage growth of each siRNA in SH-EP1 or the IMR-32 cells. (B) Fold change in the percentage growth of SH-EP1 compared to IMR-32 cells.

Transfection with both SNRK siRNA and ATR siRNA resulted in reduced growth in the MYC-N overexpressing IMR-32 cells. Both SNRK 2 and ATR produced a significant decrease in growth (p-values 0.0064 and 0.0113 respectively) but this was not seen for SNRK 3, most likely due to the variability in growth produced by this siRNA.

This assay was repeated using the SH-EPTet21N Tetracycline repressible MYC-N system. Cells in the presence and absence of Tetracycline were plated and then transfected with Control 1, SNRK 2, SNKR 3 or ATR siRNA and DharmaFECT 1 24 hours after plating and the cells were grown for 120 hours before the addition of 3mg/ml MTT (Fig. 4.6.3.3A). However, the Control 1 transfected cells cultured in the absence of Tetracycline did not grow well in this assay, which prevented the normalisation of the results. The assay was repeated with a different Control siRNA (Eurofins Control) (Fig. 4.6.3.3B) but again the cell growth and resulting OD values were very low for the Control transfected cells in the absence of Tetracycline. As this siRNA produced a similar result to the ATR positive control, there was a very small signal window for this assay and therefore it was not repeated.

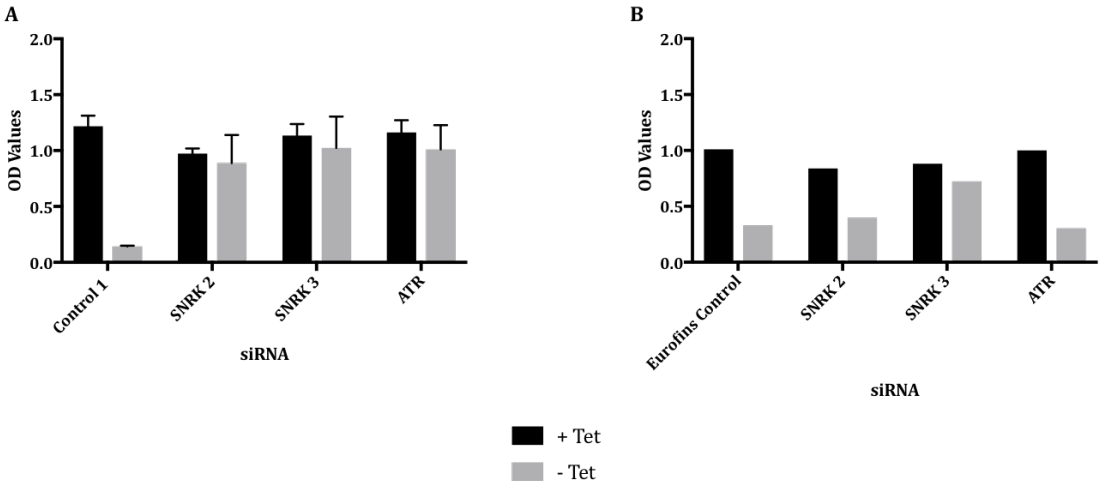

Figure 4.6.3.3 Growth of SH-EPTet21N cells following SNRK knockdown

SH-EPTet21N cells were plated in the presence or absence of Tetracycline. The cells were transfected with (A) Control 1 or (B) Eurofins Control siRNA along with SNRK 2, SNRK 3 or ATR with DharmaFECT 1. The cells were grown for 120 hours post-transfection before the addition of MTT. Mean values derived from (A) two independent with their respective SEMs or (B) one experiment.

4.7 SNRK-mediated Sensitisation to Potentially Replication Stress Inducing Chemotherapies

4.7.1 Gemcitabine Sensitivity

Gemcitabine is a deoxycytidine analogue that causes DNA replication stress in a number of ways (Plunkett et al, 1995). It can be incorporated into DNA where it results in strand termination and the halting of the DNA polymerases. This lesion cannot be removed by normal DNA repair mechanisms and so can result in prolonged fork stalling (Mini et al, 2006; Plunkett et al, 1995). It also acts as an inhibitor of DNA polymerases and ribonucleotide reductase, the later of which results in the depletion of nucleotide pools (Mini et al, 2006) in a similar manner to HU. In pre-clinical studies, the effects of Gemcitabine have been shown to be potentiated by Chk1 inhibition, in a number of cell lines (Matthews et al, 2007; Parsels et al, 2009; Venkatesha et al, 2012), and Wee1 inhibition, specifically in p53 deficient cells (Rajeshkumar et al, 2011). Both Chk1 inhibitors and Wee1 inhibitors in combination with Gemcitabine have been taken forward into clinical trials (ClinicalTrials.gov, 2017b; Thompson & Eastman, 2013).

As the effects of Gemcitabine have been potentiated by other replication stress suppressors, it was decided to investigate if the loss of SNRK acted synergistically with this drug. HCT116 cells were transfected with Control 1, SNRK 2, SNKR 3 or ATR siRNA and DharmaFECT 1 for 48 hours. The cells were then treated with a 0 - 20nM titration of Gemcitabine and grown for 120 hours before the addition of MTT (Fig. 4.7.1.1).

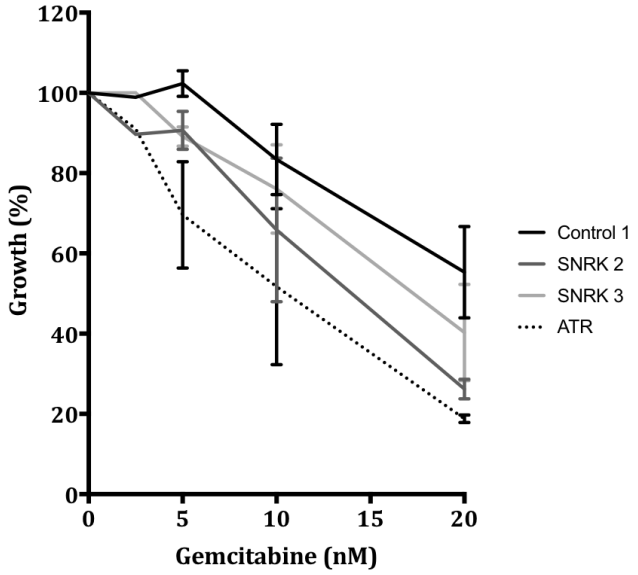

Figure 4.7.1.1 Sensitivity of SNRK and ATR knocked down cells to Gemcitabine.
HCT116 cells were transfected with Control 1, SNRK 2, SNRK 3 or ATR siRNA and DharmaFECT 1 for 48 hours before treatment with 0, 2.5, 5, 10, 20nM Gemcitabine for 120 hours. Mean values were derived from 3 independent experiments, with their respective SEMs.

Knockdown of SNRK, especially with siRNA 2, and ATR appears to increase the sensitivity of cells to Gemcitabine, however, this effect was not significant due to the variability of the values produced in this assay.

4.7.2 PARP Inhibitor Sensitivity

Poly (ADP-ribose) polymerase 1 (PARP1) is involved in the BER DNA damage repair pathway and has been shown to be essential for the survival of HR deficient cells (Bryant et al, 2005; Farmer et al, 2005). As replication stress relies on HR for its resolution and PARP has been shown to be required for its completion in response to replication stress (Bryant et al, 2009), the loss of PARP function results in prolonged DNA replication arrest. In pre-clinical work, PARP inhibition has been shown to be potentiated by Chk1 and ATR inhibition when compared to single agent therapy (Kim et al, 2017; Sen et al, 2017) and currently the Chk1 inhibitor Prexasertib is being trialled with the licensed PARP inhibitor Olaparib (ClinicalTrials.gov, 2017a).

As the combination of PARP inhibitors have previously shown promise with the loss of replication stress suppressors, it was decided to see if the loss of SNRK would augment their function. HCT116 cells were transfected with Control 1, SNRK 2, SNKR 3 or ATR siRNA and DharmaFECT 1 for 48 hours. The cells were then treated with a 0 - 10μM titration of Olaparib and grown for 120 hours before the addition of MTT (Fig. 4.7.2.1).

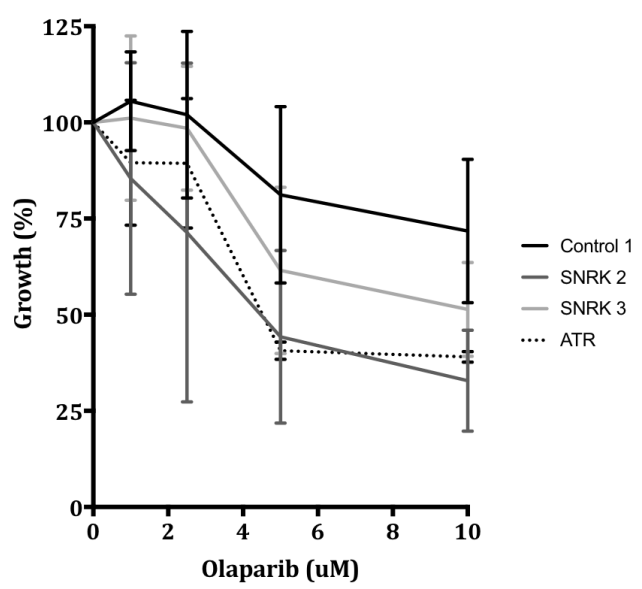

Figure 4.7.2.1 Sensitivity of SNRK and ATR knocked down cells to Olaparib.
HCT116 cells were transfected with Control 1, SNRK 2, SNRK 3 or ATR siRNA and DharmaFECT 1 for 48 hours before treatment with 0, 1, 2.5, 5, 10μM Olaparib for 120 hours. Mean values were derived from 3 independent experiments, with their respective SEMs.

Whilst the knockdown of SNRK with both siRNA and ATR produced a decrease in growth when compared to the Control 1 transfected cells, these differences were not significant due to the variability of the assay, however, this does suggest that the loss of SNRK may potentiate PARP inhibitors.

4.7.3 5-Flurouracil Sensitivity

5-Fluorouracil (5-FU) is an uracil analogue which is intracellularly converted into several metabolites which disrupt RNA synthesis, misincoporate into DNA and inhibit the enzyme thymidylate synthase. This enzyme is required for the *de novo* synthesis of thymidylate

and the maintenance of nucleotide pools, therefore the inhibition of this enzyme results in replication stress (Longley et al, 2003).

It has previously been determined that inhibition of Chk1 in colorectal cancer and Wee1 in p53 deficient cells sensitised them to 5-FU, therefore it was decided to investigate whether the loss of SNRK would also sensitise cells to this drug. HCT116 cells were transfected with Control 1, SNRK 2, SNKR 3 or ATR siRNA and DharmaFECT 1 for 48 hours. The cells were then treated with a 0 - 25μM titration of 5-FU and grown for 120 hours before the addition of MTT (Fig. 4.7.3.1).

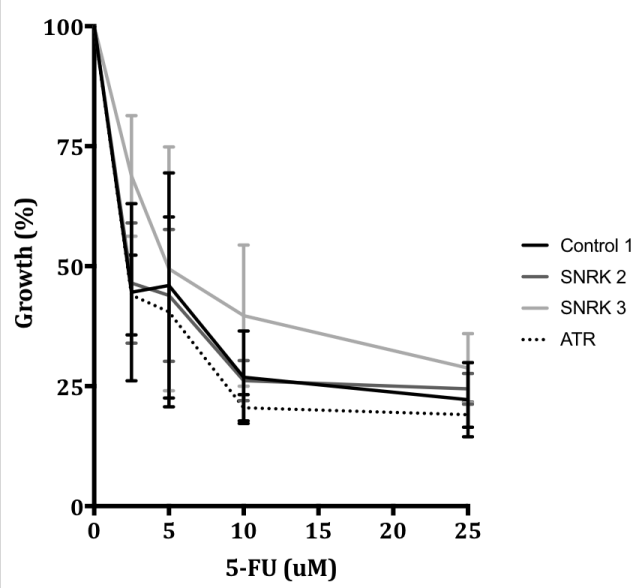

Figure 4.7.3.1 Sensitivity of SNRK and ATR knocked down cells to 5-Flurouracil.
HCT116 cells were transfected with Control 1, SNRK 2, SNRK 3 or ATR siRNA and DharmaFECT 1 for 48 hours before treatment with 0, 2.5, 5, 10, 25μM 5-Flurouracil for 120 hours. Mean values were derived from 3 independent experiments, with their respective SEMs.

The knockdown of neither SNRK nor ATR significantly sensitised HCT116 cells treated with 5-FU. Whilst ATR did produce a trend towards sensitisation, this was only slight. Transfection with SNRK 3 appeared to reduce the sensitivity of the cells to 5-FU but the results seen with this siRNA were highly variable in this assay and the difference was not significant.

4.8 Discussion

As the high throughput pRPA2 T21 screen did not prove viable, it was decided to utilise the 24 well format as a more targeted screening approach. This assay had been optimised in a number of cell lines and reproducibly produced a signal window that would be considered suitable for screening purposes. It was decided to focus on protein kinases, as these enzymes are considered druggable and so make attractive drug targets (Hopkins & Groom, 2002).

During the development of the high throughput screen, Kavanaugh *et al.* published a genome wide screen identifying modulators of the replication stress response. Following gene knockdown U2OS cells were labelled with BrdU to measure the endogenous levels of replication stress following gene knockdown. The cells were subsequently treated with HU

for 24 hours before labelling with EdU. The cells were then fixed and stained for BrdU, EdU and γH2AX. The rationale of this assay was that cells with compromised fork restart would not have recovered from the HU treatment and so would have low EdU incorporation and high levels of γH2AX present within their nuclei. Replication restart scores (RSS) were calculated by dividing the γH2AX intensity by that of EdU for each cell and then taking an average of every cell within the samples. These RSS scores were converted into Z-scores which were ranked to identify genes whose loss negatively affected replication restart.

Whilst this technique more directly measures DNA replication stress (Zeman & Cimprich, 2014) than identifying pRPA foci, the pRPA2 T21 screen aimed to identify genes whose knockdown increased replication stress under endogenous conditions. In the Kavanaugh screen, any gene whose knockdown alone significantly reduced BrdU incorporation were discounted from further analysis. Therefore, the genes whose loss endogenously increased replication stress were not studied further. As this paper only investigated the genes whose knockdown affected the restart of DNA replication following HU treatment, a number of factors involved in the initiation of DNA replication may have been overlooked.

Any kinase that generated an average Z-score of greater than 3 in this screen was considered as a potential gene of interest. The top three, Chk1, WEE1 and ATR, were discarded as they are already well established replication stress response genes. The cBioPortal and GenomeRNAi databases were utilised to cherry pick the interesting genes from the list of 42 remaining kinases. A gene was considered interesting if its knockdown resulted in phenotypes commonly associated with cells experiencing DNA replication stress, including decreased viability with replication stress causing drugs or oncogene overexpression, increased DNA content in S phase and increased γH2AX levels (Appendix 3).

It was also thought that the Kavanaugh Z-scores could be combined with those generated in the Collis γH2AX screen (Barone et al, 2016; Myers et al, 2016; Staples et al, 2016; Staples et al, 2014; Staples et al, 2012) and an unpublished screen conducted in the Meuth lab investigating Caspase 3 activation and RPA2 S4/8 phosphorylation following Chk1 inhibition and incubation with excess thymidine. However, it was found that there was very little correlation between the three screens. For example, CAMK1 was the fourth highest ranked kinase in the Kavanaugh screen but generated a negative Z-score in the Meuth pRPA2 S4/8 screen. The differences in conditions that the cells were exposed to may have played a role in these differences. In both the Kavanaugh and Meuth screens the cells were exposed to exogenous sources of stress, HU and excess thymidine with Chk1 inhibition respectively. In contrast, the Collis screen aimed to identify genes whose loss increased DNA damage following gene knockdown alone. It is therefore unsurprising there was little correlation between the three screens as in each the cells had different replication and cell cycle defects induced before gene knockdown.

Even screens investigating the same phenotype can generate different results as demonstrated by PMVK. This kinase was reported to increase γH2AX intensity in the

GenomeRNAi database (Paulsen et al, 2009) but this was not identified as a hit in the Collis screen as it generated a negative Z-score. This may be due to the different cell lines utilised for the screens (HeLa versus HCT116).

The targeted screen was carried out in U2OS cells, to maintain consistency with the Kavanaugh screen, and so the pRPA2 T21 staining protocol was re-optimised for this cell line. Once established, it was utilised to screen the 18 selected kinases of which kinases B2-B9 were selected for further screening. The loss of these genes increased the proportion of cells positive for pRPA2 foci above the 10% positive threshold. This cut off was chosen as it was a significant increase in T21 foci compared to the average of the negative control values. These 8 kinases were then validated in a TopBP1 screen where all 8 increased the levels of TopBP1 foci compared to the negative controls. However, the results were so similar that it was felt that this assay could not be used to narrow down the list of kinases. Therefore, all 8 were subsequently assessed to see if their loss preferentially sensitised p53 deficient cells. The loss of every kinase reduced the growth of the p53 null HCT116 compared to the wild type cells, which was unsurprising as in previous assays these cells had shown higher basal levels of replication stress (Fig. 3.4.4.1). Only two genes, B5 (PMVK) and B9 (SNRK) produced a significant difference in growth and were therefore taken forward for further investigation.

Gene knockdown was validated by assessing the deconvoluted siRNA pools by qPCR and all 4 PMVK and 3 of the SNRK siRNAs produced sufficient gene knockdown. These individual siRNA recapitulated the pRPA2 results observed with the siRNA pools, although they could not fully reproduce those seen in the p53 MTT assay. Only 1 out of the 4 PMVK siRNA tested mildly reduced growth in the p53 null cells, therefore the investigation of this hit was discontinued. However, 2 of the 3 SNRK siRNAs (SNRK 2 and SNRK 3) reduced growth in the p53 null cells, therefore this kinase was investigated further.

The effects of the p53 inhibitor Pifithrin-α (PTN-α) was predicted to mimic the mutation of p53 found in cancer cells more closely than a genetic knockout. As PTN-α is a crude drug and more than likely does not completely abrogate p53 signalling it was unsurprising that the loss of SNRK or ATR did not significantly decrease cell growth, as seen in the p53 null cells. However, at 7.5μM PTN-α, the loss of SNRK or ATR did appear to be sensitising the cells compared to the Control 1 transfected cells. Pharmacological inhibition of ATM by KU53933 was also assessed for its ability to preferentially kill SNRK deficient cells. However, the assay did not appear to be functioning correctly. It has previously been reported that the loss of ATR kills ATM deficient cells (Kwok et al, 2016; Min et al, 2017; Reaper et al, 2011), however ATR siRNA did not kill the KU55933 treated cells. It is uncertain if this arose due to lack of action of the drug or due to issues with cell confluency within the assay, but as the positive control did not induce cell killing, it called the assay's results into question. Whilst the ATR siRNA was not explicitly examined for gene knockdown in this project, the same siRNA had previously been reported by the Collis laboratory to induce significant knockdown (Beveridge et al, 2014; Staples et al, 2016).

Assessment of the survival of p53 deficient cells following SNRK knockdown in the Clonogenic assay demonstrated a strong trend but no statistically significant decrease in survival following siRNA transfection in either the p53 wild type or null cell line. The loss of ATR also did not significantly affect p53 null cell survival, despite apparently being in a synthetic lethal relationship (Kwok et al, 2016). Due to the differences in assay length and end point (growth or survival) this data does not necessarily contradict the results observed in the MTT assays. However, as both SNRK siRNA did show a trend to decreased survival in the p53 null cells, these results may have become significant if they had been repeated further.

Loss of SNRK or ATR resulted in significantly increased levels of γH2AX and 53BP1 foci in wild type p53 but not p53 null HCT116 cells, although there is a trend to increased damage following gene knockdown in the later cell line. This lack of significance was most likely due to the increased levels of damage observed in the Control 1 transfected cells. Treatment with Roscovitine abrogated these increases, suggesting that they were dependent upon DNA replication and that the damage is likely occurring due to the heightened replication stress within these cells. The loss of SNRK and ATR displayed higher numbers of γH2AX foci in the wild type than the null cells but this was not true for 53BP1. This most likely is due to the difference in the type of damage identified by these antibodies: γH2AX more generally identifies damage whilst 53BP1 is considered to be DSB specific.

The heightened levels of DNA damage observed in the p53 null cell line correlated with the results obtained for this cell line with the pRPA2 T21 antibody (Fig. 3.4.4.1). Levels of replication stress were also increased in the Control 1 transfected cells compared to those observed in the p53 wild type cell line. As Roscovitine treatment abrogated the increased foci numbers observed in the p53 null Control 1 transfected cells, it appears that the heightened levels of damage were a result of the previously observed increased replication stress. This is as expected as these cells lack a functional G1/S checkpoint and so their entry to S phase can occur in unfavourable conditions.

Despite the increased levels of damage and replication stress induced by the loss of SNRK, this does not appear to affect cell cycle distribution as demonstrated by PI FACS analysis. It may be that the loss of SNRK only affects replication at a local level rather than globally throughout the nucleus and so does not cause large perturbations in cell cycle progression. It is also possible that as this data is only taken from a single experiment, loss of SNRK may result in altered cell cycle distribution but were not observed.

The loss of SNRK in Cyclin E overexpressing cells appeared to have little impact on their growth when compared to cells with normal Cyclin E expression. However, in Jones *et al.* these cells had entered a senescent state within 4-6 days of the induction of Cyclin E overexpression. As this assay was ended 7 days after induction the cells may have already entered a senescent state and therefore not have been as affected by the loss of SNRK as the un-induced cells.

In the H-RAS^{G12V} overexpressing HCT116 cells the loss of ATR did not decrease growth as had been previously reported (Gilad et al, 2010) and therefore the assay was repeated in the MRC-5 H-RAS^{G12V} overexpressing cells. Unlike in the HCT116 cells, loss of SNRK significantly decreased the growth of the overexpressing MRC-5. It is most likely that the differing genetic backgrounds in this assay affected the results, as MRC-5 are a normal cell line they contain less replication stress and DNA damage (unpublished data). As a result of this, these cells may be more affected by the overexpression of H-RAS^{G12V} than the HCT116 cells. Also, they would likely have more stringent cell cycle control than the cancerous HCT116 cells and so an increase in replication stress may have been less well tolerated within this model of oncogene induced replication stress.

Whilst SNRK loss appeared to affect the growth of the MYC-N overexpressing IMR-32 cell line more than the MYC-N normal SH-EP1 cells, the two lines originate from different patients and therefore have differing genetic background. It was consequently decided to repeat this assay in the SH-EPTet21N cell line that overexpressed MYC-N in a Tetracycline repressible manner. However, when this assay was attempted the majority of the MYC-N overexpressing cells transfected with two different control siRNA died, making it impossible to calculate growth values for these cells. This assay was repeated using a different scrambled control siRNA (Eurofins Control) where more cells survived than previously. However, a similar proportion of cells survived when they were transfected with the ATR siRNA. As the negative and positive controls were producing similar survival, there was a very small assay window and so the experiment was not considered robust.

Overall, this suggests that the loss of SNRK may be detrimental in cells that have higher levels of replication stress due to the overexpression of certain oncogenes.

Three chemotherapies were chosen to assess whether loss of SNRK would sensitise cells to their mechanism of action. The first, Gemcitabine, is a well-established inducer of replication stress through DNA polymerase halting and ribonucleotide reductase inhibition. The second, Olaparib, induces replication stress by preventing its resolution by HR as well as trapping the PARP molecule on DNA which inhibits DNA polymerase progression. The knockdown of both SNRK and ATR sensitised cells to Gemcitabine and Olaparib when compared to Control 1 transfected cells, most likely by pushing the cells over a threshold of replication stress beyond which the cells could not remain viable. Nevertheless, these effects were not significant due to the variability of the assay. The third drug, 5-FU, has a very complicated metabolism and its effectiveness may not solely rely upon increased levels of replication stress. Whilst the inhibition of thymidylate synthetase by this enzyme does disrupt the nucleotide pool, it results in the incorporation of dUTP and FdUTP into DNA and the latter may not be able to be removed by post-replicative repair. It is therefore not completely surprising that SNRK and ATR loss did not significantly sensitise cells to the effects of this drug.

Whilst this study focused mostly on SNRK deficiency and how this affected various oncogene and drug induced replication stress models, it would have been advantageous to investigate other aspects of SNRK within the cellular responses to replication stress and also to further investigate PMVK.

The gene SNRK contains a protein kinase domain, a ubiquitin associated domain (UBA) (UniProt, 2017) and is predicted to contain a strong nuclear localisation sequence suggesting that it is localised within the nucleus (Kosugi et al, 2009). In AMPK related kinases, the UBA domain regulates kinase activity rather than actively binding to ubiquitin chains. A crystal structure of the SNRK UBA domain suggests that its binding inhibits the activity of the kinase domain by binding between the C and N terminal lobes of the domain (Wang et al, 2018). It may therefore be possible for inhibitors of SNRK to be developed that mimic the structure of its UBA domain or that specifically bind to the inactive form of the enzyme and prevent its activation by the removal of the UBA domain.

SNRK has been shown to play a role in the metastasis of ovarian cancers (Hopp et al, 2017) and its overexpression reduces proliferation of colon cancer cells. Increased levels of SNRK upregulate calcyclin binding protein which reduces proliferation through the degradation of non-phosphorylated β-catenin. Loss of SNRK increases the tumorigenicity of colon cancer cells (Rines et al, 2012), potentially through increased proliferation. Knockdown has also been previously reported to sensitise cells to Gemcitabine (Azorsa et al, 2009), further suggesting that loss of this gene increases proliferation and subsequently levels of replication stress.

Liver Kinase B1 (LKB1 also known as STK11) phosphorylates SNRK at residue T173, within its T-loop, which activates its kinase activity. This phosphorylation is absent in HeLa cells lacking LKB1 expression and SNRK is not active in these cells (Jaleel et al, 2005). As one mechanism of activation for SNRK has been elucidated, at least *in vitro*, it should have been possible to determine whether it is activated constituently in cells or if it becomes activated in response to DNA replication stress. No commercial antibody is available for the detection of SNRK phosphorylated at T173, but it could have been possible to utilise a pan pS/T antibody to detect activation.

LKB1 is a tumour suppressor mutated in the cancer susceptibility syndrome Peutz Jeghers Syndrome (PJS). It interacts with p53 to induce p21 expression and its loss increases the expression of Cyclin D, Cyclin E and Cyclin A. It may therefore have been useful to assess the replication stress suppressor phenotype of LKB1 to see if its loss produced a similar phenotype to that of SNRK. However, this approach most likely would have been complicated by the effects that the loss of LKB1 would have had on other cellular pathways. For example, via its phosphorylation of AMPK, LKB1 controls cell growth in response to nutrient fluctuations and the polarity of cells (Shackelford & Shaw, 2009).

Whilst mass spectrometry has predicted proteins that interact with SNRK (UniProt, 2017), only one project specifically set out to identify proteins that interacted with it (Al-Hakim et al, 2005) as it was included as one of the 12 AMPK related kinases investigated in this study. It may therefore have been advantageous to carry out mass spectrometry by generating a FLAG-tagged version of the protein, as attempted in Chapter 6.

One of the biggest weaknesses of this study was the lack of results demonstrating the effects of SNRK loss upon replication stress signalling. The phosphorylation of Chk1 (S317 and S345) by ATR results in its activation (Cimprich & Cortez, 2008) and can be identified

by western blotting, as demonstrated in Chapter 3. Whilst this was attempted for SNRK knocked down cells, it was never conclusively shown that SNRK loss induced Chk1 phosphorylation due to issues with the antibody.

A polyclonal antibody raised against SNRK is commercially available (abcam, 2017) and could have been used to confirm the localisation of SNRK within the nucleus of cells by immunofluorescence. This antibody could also have been used to assess gene knockdown by both immunofluorescence and western blotting. The immunofluorescent images provided for the antibody (abcam, 2017) suggest that SNRK is located throughout the nucleus but it would have been useful to see if it localised into foci following replication stress. It would also have been beneficial to carry out co-localisation experiments with the replication stress and DNA damage markers mentioned in this chapter.

Another potentially useful approach would have been to investigate if SNRK knockdown synergised with Aphidicolin. This drug is a potent inhibitor of the B family DNA polymerases (α, δ, ε and ζ) in eukaryotes and induces replication fork stalling in cells already in S phase. A low dose of Aphidicolin has also been shown to sensitise unresponsive cancer stem cells to Chk1 inhibition (Manic et al, 2017) and therefore it would have been extremely useful to see if this could be replicated with SNRK loss.

DNA fibre analysis allows for an in depth investigation of the replication dynamics within cells. It relies of the consecutive incorporation of the halogenated nucleotides IdU and CldU which can be detected and reveal a number of replication fork behaviours. These include their speed, direction of travel, firing, stalling, termination and re-start (Nieminuszczy et al, 2016). Use of this technique would have allowed for a further and more sensitive quantification of the levels of replication stress induced by the loss of SNRK and how this deficiency affects other replication fork dynamics such as fork stalling and dormant origin firing.

It would also have been valuable to ascertain if it was present at active or stalled DNA replication forks. It is possible to isolate proteins on nascent DNA, a technique referred to as iPOND, which allows the identification of proteins that accumulate at replication forks and newly synthesised DNA. In this procedure, nascent DNA is labelled by EdU which is subsequently conjugated to Biotin which allows the purification of the DNA:protein complexes using Streptavidin (Sirbu et al, 2012). This method could have been used to determine if SNRK localises to all replication forks, whether it is recruited following the initiation of replication stress or if the loss of SNRK affected the formation of the replisome.

PMVK is predicted to contain no nuclear localisation sequences (Kosugi et al, 2009) and is most likely located within the cytoplasm (Binder et al, 2017b). High expression has been shown to positively correlate with multi-drug response in ER positive breast cancers (Shen et al, 2012) and its knockdown increased γH2AX foci formation (Paulsen et al, 2009) and sensitised cells to PARP inhibition (Turner et al, 2008).

It is a peroxisomal enzyme involved in the mevalonate pathway (Chambliss et al, 1996) which is fundamental for the growth of tumour cells and has been shown to be modulated

by oncogenic signalling (Mullen et al, 2016). Mevalonate diphosphate decarboxylase (MVD) lies downstream of PMVK in the mevalonate pathway. Its inhibition by fluoromevalonate results in the depletion of dNTPs, S phase arrest and the induction H2AX and Chk1 phosphorylation which were reversed by exogenous dNTPs. The depletion of the dNTP pool was linked to an increase in mevalonate phosphate, the substrate of MVD, which was exhausting the cellular pool of ATP (Martín Sánchez et al, 2015). This may explain why PMVK knockdown resulted in increased levels of replication stress. It would therefore have been useful to assess if loss of PMVK affected cellular levels of ATP and dNTPs to see if a similar depletion occurred.

Mass spectrometry data suggests that it may interact with the RNA/DNA helicase Senataxin, (Huttlin et al, 2015) amongst other proteins, which is required for the resolution of R-loops that can impact on DNA replication and lead to genome instability (Garcia-Muse & Aguilera, 2016). Senataxin has been shown to prevent replication forks colliding with transcription complexes and loss of this protein results in abnormal DNA and DNA/RNA structures that hinder replication fork progression (Alzu et al, 2012). As this protein acts as a replication stress suppressor itself, it may have been valuable to have investigated whether its predicted association with PMVK was functional as this may have provided another explanation as to how PMVK acted to suppress replication stress. This could have been achieved by FLAG tagging PMVK to allow immunoprecipitation and mass spectrometry analysis of its interacting proteins. It may also have been beneficial to compare cells deficient of both Senataxin and PMVK to cells where only one gene was lost to determine if the combination increased levels of replication stress, suggesting that they were not acting in the same pathway.

Whilst the individual PMVK siRNA failed to sensitise p53 deficient cells, it would have been beneficial to further examine the replication stress suppressor phenotype of this gene. If time restrictions had not prevented this, it would have been investigated in the oncogene induced replication stress models and for its ability to sensitise cells to replication stress inducing chemotherapies. It would have been particularly interesting to investigate if the knockdown of this gene sensitised cells to PARP inhibition as this has been previously reported (Turner et al, 2008). It would also have been advantageous to have carried out γH2AX immunofluorescence, as its loss has been reported to increase the prevalence of this marker (Paulsen et al, 2009), and investigate if the damage caused relied upon DNA replication. The DNA fibre analysis described previously would also have confirmed its role as a replication stress suppressor and if it affected the restart of stalled DNA replication forks.

Chapter Five:
Characterisation of CCDC15 Deficient Cells

TABLE OF FIGURES 190

5.1 INTRODUCTION 192

5.2 VALIDATION OF GENE SET ENRICHMENT ANALYSIS 194

5.2.1 CCDC15 RNA EXPRESSION IN COMMON CELL LINES 194

5.2.2 CCDC15 KNOCKDOWN BY SIRNA 195

5.2.3 ASSESSMENT OF DNA DAMAGE IN CCDC15 DEPLETED CELLS 196

5.2.4 DNA DAMAGING AGENT SENSITIVITY 198

5.2.4.1 MITOMYCIN C SENSITIVITY 198

5.2.4.2 CISPLATIN SENSITIVITY 199

5.2.4.3 HYDROXYUREA SENSITIVITY 200

5.2.5. DECONVOLUTION OF THE CCDC15 SIRNA POOL 200

5.3 DNA DAMAGE RESPONSE PHENOTYPE 201

5.3.1 DNA DAMAGE RESPONSE ACTIVATION 201

5.3.1.1 DNA DAMAGE MARKER IMMUNOFLUORESCENCE 201

5.3.2.2 DIRECT MEASUREMENT OF DNA DAMAGE 204

5.3.2 SENSITISATION TO DNA CROSSLINKING AGENTS 205

5.3.2.1 CLONOGENIC SURVIVAL ASSAYS 205

5.3.2.2 ASSESSMENT OF DNA DAMAGE IN CCDC15-DEPLETED CELLS IN RESPONSE TO MMC AND UV 207

5.3.3 INVOLVEMENT IN THE FANCONI ANAEMIA/BRCA PATHWAY 213

5.3.3.1 FANCD2 UBIQUITINATION 213

5.3.3.2 FANCONI ANAEMIA/BRCA PATHWAY IMMUNOFLUORESCENCE 214

5.3.4 ASSOCIATION WITH DNA REPLICATION AND CELL CYCLE PROGRESSION 220

5.3.4.1 ACTIVATION OF THE DNA REPLICATION STRESS RESPONSE 220

5.3.4.2 REPLICATION ASSOCIATED DNA DAMAGE 222

5.3.4.3 EFFECTS UPON CELL CYCLE PROGRESSION 224

5.4 DISCUSSION 228

Table of Figures

Figure 5.1.1 Bioinformatics analysis of CCDC15. 193
Figure 5.2.2.1 Percentage knockdown of CCDC15 following siRNA transfection in PC-3. 195
Figure 5.2.3.1 DNA damage detection in CCDC15 knocked down PC-3 cells. 196
Figure 5.2.3.2 DNA damage detection in CCDC15 knocked down HeLa cells. 196
Figure 5.2.3.3 DNA damage detection in CCDC15 knocked down RPE-1 cells. 197
Figure 5.2.3.4 Percentage of PC-3, HeLa and RPE-1 cells positive for γH2AX and 53BP1 foci. 198
Figure 5.2.4.1.1 Sensitivity of CCDC15 knocked down cells to Mitomycin C. 199
Figure 5.2.4.2.1 Sensitivity of CCDC15 knocked down cells to Cisplatin. 199
Figure 5.2.4.3.1 Sensitivity of CCDC15 knocked down cells to Cisplatin. 200
Figure 5.2.5.1 Percentage knockdown of deconvoluted CCDC15 siRNA pool following siRNA transfection in PC-3 cells. 201
Figure 5.3.1.1.1 DNA damage detection in deconvoluted CCDC15 siRNA knocked down PC-3 cells. 201
Figure 5.3.1.1.2 DNA damage detection in deconvoluted CCDC15 siRNA knocked down HeLa cells. 202
Figure 5.3.1.1.3 DNA damage detection in deconvoluted CCDC15 siRNA knocked down RPE-1 cells. 202
Figure 5.3.1.1.4 Percentage of PC-3, HeLa and RPE-1 cells positive for γH2AX and 53BP1 foci following transfection with individual CCDC15 siRNAs. 203
Figure 5.3.1.2.1 Percentage DNA in Tail and Tail Moment of PC-3, HeLa and RPE-1 cells following CCDC15 knockdown. 204
Figure 5.3.2.1.1 Survival of CCDC15 knocked down cells in the presence of MMC. 205
Figure 5.3.2.1.2 Survival of CCDC15 knocked down RPE-1 in the presence of MMC. 206
5.3.2.1.2 Survival of CCDC15 knocked down RPE-1 after UV irradiation 207
Figure 5.3.2.2.1 DNA damage detection following DNA crosslinking in PC-3 cells. 208
Figure 5.3.2.2.2 DNA damage detection following DNA crosslinking in HeLa cells. 209
Figure 5.3.2.2.3 DNA damage detection following DNA crosslinking in RPE-1 cells. 210
Figure 5.3.2.2.4 Percentage of PC-3, HeLa and RPE-1 cells positive for γH2AX and 53BP1 foci following DNA crosslinking. 211
Figure 5.3.2.2.5 γH2AX foci in RPE-1 cells following recovery from UV irradiation. 212
Figure 5.3.2.2.6 Percentage of RPE-1 cells positive for γH2AX following recovery from UV irradiation. 213
Figure 5.3.3.1.1 Induction of FANCD2 Ubiquitination following CCDC15 knockdown and MMC treatment. 214
Figure 5.3.3.2.1 Fanconi Anaemia pathway activation following CCDC15 knockdown in PC-3 cells. 215
Figure 5.3.3.2.2 Fanconi Anaemia pathway activation following CCDC15 knockdown in HeLa cells. 215
Figure 5.3.3.2.3 Fanconi Anaemia pathway activation following CCDC15 knockdown in RPE-1 cells. 216

Figure 5.3.3.2.4 Percentage of PC-3, HeLa and RPE-1 cells positive for FANCD2 foci following DNA crosslinking. 216

Figure 5.3.2.2.5 FANCD2 foci in RPE-1 cells following recovery from UV irradiation. 217

Figure 5.3.3.2.6 Percentage of RPE-1 cells positive for FANCD2 foci following recovery from UV irradiation. 218

Figure 5.3.2.2.7 RAD51 foci in RPE-1 cells following recovery from UV irradiation. 219

Figure 5.3.3.2.8 Average number of RAD51 foci in RPE-1 cells following recovery from UV irradiation. 220

Figure 5.3.4.1.1 RPA2 T21 foci in HeLa cells following CCDC15 knockdown. 221

Figure 5.3.4.1.2 RPA2 T21 foci in RPE-1 cells following CCDC15 knockdown. 221

Figure 5.3.3.2.4 Percentage of HeLa and RPE-1 cells positive for pRPA2 T21 foci following CCDC15 knockdown and DNA crosslinking. 222

Figure 5.3.4.2.1 DNA Damage in RPE-1 cells following CCDC15 knockdown and Roscovitine treatment. 223

Figure 5.3.4.2.2 Percentage of PC-3, HeLa and RPE-1 cells positive for γH2AX and 53BP1 foci following transfection with individual CCDC15 siRNAs. 223

Figure 5.3.4.3.1 Cell cycle distribution of CCDC15 knocked down PC-3 and Hela cells 224

Figure 5.3.4.3.2 Cell cycle distribution of CCDC15 knocked down RPE-1 FUCCI cells following recovery from UV irradiation. 226

Figure 5.3.4.3.3 Cell cycle distribution of CCDC15 knocked down RPE-1 FUCCI cells. 227

Figure 5.3.4.3.4. Failure of cell synchronisation in RPE-1 FUCCI cells. 228

Figure 5.4.1 Interstrand crosslink repair by the Fanconi Anaemia pathway. 230

Figure 5.4.2 Nucleotide excision repair pathway 234

5.1 Introduction

Coiled-coil domain-containing protein 15 (CCDC15) is a 951 amino acid protein, located on chromosome 11 which contains 4 coiled coil domains but no other identifiable structures. It is reportedly present in the chordate common ancestor, but despite this, it has no known function (GeneCards, 2017a; UniProt, 2016). However, it was identified as a protein whose knockdown increased γH2AX levels in a genome wide RNAi screen (Barone et al, 2016; Myers et al, 2016; Staples et al, 2016; Staples et al, 2014), carried out by Dr. S. Collis, where it generated a modest Z score of 1.2.

All of the uncharacterised hits (proteins of unknown function) from this screen, including CCDC15, were assessed for functional associations with DNA repair genes by Dr. J Bradford. RNA Sequencing data (TCGA database) was used to determine if the expression of a gene of interest was correlated with that of all other genes in a given cancer type which produced a table of Pearson correlation coefficients (PCC). This was repeated across numerous cancer types and combined into a gene versus cancer matrix, where every gene had a PCC listed for each cancer type examined. These PCCs were then ranked, from high to low, to generate a ranked gene versus cancer matrix which was used as the input for the Robust Rank Aggregation (RRA) R package, which aggregated the ranked lists to generate significance probabilities for every gene (Kolde et al, 2012). These probabilities represented how likely that a given rank was to occur across the number of cancers investigated, with a low p-value representing consistent correlation with the gene of interest. The genes were then ranked by their P-values (significant to not significant) and this list was used as the input for Gene Set Enrichment Analysis (GSEA) (Subramanian et al, 2005) to identify enrichment of Reactome-defined DNA repair pathway genes at the top of the list to generate an enrichment score. If numerous DNA repair genes occurred at the top of the list, the enrichment score would be significant (Fig. 5.1.1).

Along with the uncharacterised hits, a list of random genes and a list of known DNA repair factors were subjected to GSEA as negative and positive controls respectively. All of the known DNA repair factors tested generated enrichment scores with significant p-values for DNA repair genes whilst only one of the nine random genes appeared correlated with DNA repair (Table 5.1.1).

A

Gene	Enrichment Score	p-value
RAD54L	0.84	0.000
ATR	0.71	0.001
PARP1	0.73	0.002
BRCA1	0.80	0.000
MRE11A	0.70	0.007
BRCA2	0.76	0.000
ATM	0.73	0.000
POLE	0.79	0.001
XRCC1	0.75	0.002

B

Gene	Enrichment Score	p-value
TIMP3	N/A	
ITGA10	N/A	
PCSK9	N/A	
MGC72080	0.82	0
TSTA3	N/A	
VEGFC	N/A	
ZNF143	N/A	
FCRL5	N/A	
BUD31	N/A	

Table 5.1.1 Enrichment Scores for the correlation of the expression of known DNA repair factors and random genes for Reactome-defined DNA repair genes.

(A) Known DNA repair genes and (B) random genes were subjected to Gene Set Enrichment Analysis to generate Enrichment Scores and their significance for their correlation with DNA repair genes.

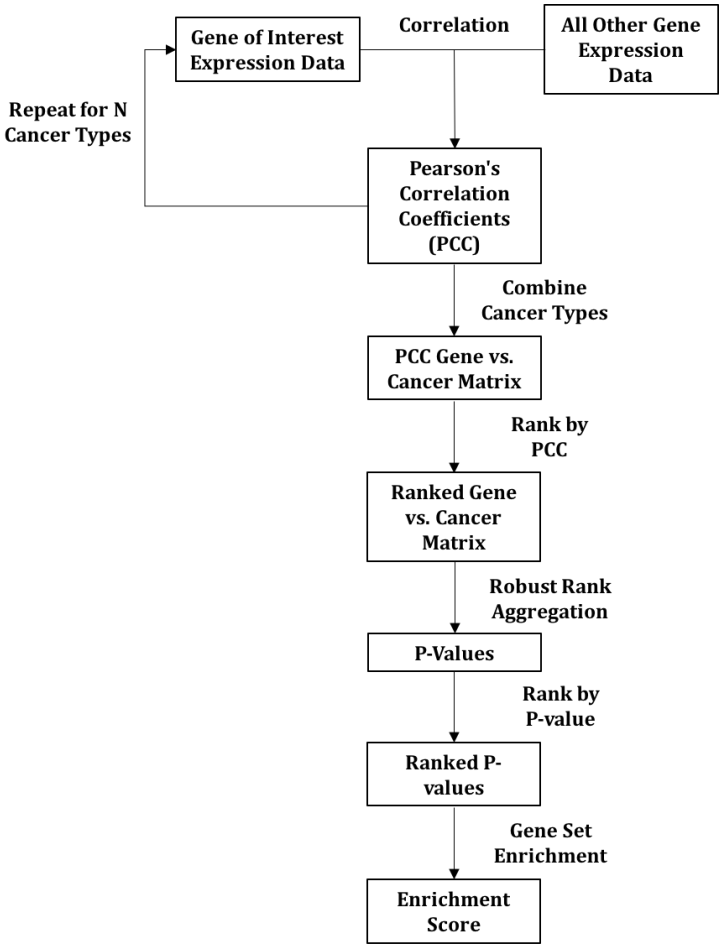

Figure 5.1.1 Bioinformatics analysis of CCDC15.
CCDC15 RNA expression data was correlated with that of all other genes in a given cancer type. This was repeated for a number of cancers and the resultant Pearson's correlation coefficients(PCCs) were combined to form a Gene vs. Caner Matrix. The PCC were then ranked and this ranked matrix was input into the Robust Rank Aggregation R package. This converted the matrix into a list of p-values, with a low value meaning the gene was consistently correlated with CCDC15 across the cancer types. These p-values were subsequently ranked from significant to not significant and used as the input for Gene Set Enrichment Analysis to generate an Enrichment Score.

C16orf75 generated a Z-score of 1.54 in the γH2AX screen and was included in the list of uncharacterised hits. Through the GSEA, this gene was predicted to correlate with the Fanconi Anemia (FA) pathway and MCM complex components (MCM2-8 and MCM10) were the top ranked DNA repair genes. This gene has since been reclassified RMI2, a BLM complex component that is required for the limitation of crossovers during DNA repair (Singh et al, 2008). It has experimentally been shown to interact with the FA pathway component FANCM (Deans & West, 2009) and has been predicted to interact with MCM10 (GeneCards, 2017b). Taken together, this suggested that GSEA can make accurate predictions about the function and interactions of proteins.

CCDC15 proved to be consistently correlated with DNA repair genes across all cancer types investigated, with an Enrichment Score of 0.74 (p-value 0.00) and Mre11A was reported as the top-ranking DNA repair gene (Table 5.1.2). Many of the top ranked genes were components of the Fanconi Anaemia(FA)/BRCA, Damage Tolerance and Nucleotide Excision Repair (NER) pathways, suggesting that CCDC15 may be involved in the repair of DNA crosslinks, or lesions that impede DNA replication.

It was therefore decided to investigate CCDC15 further to determine if it was a novel DNA repair factor, and in particular, if it was involved in the detection or repair of replication impeding lesions, as suggested by the top ranked genes from the GSEA.

Gene	Rank in Gene List
MRE11A	0
FANCM	7
POLD3	14
USP1	31
ERCC4	61
PALB2	78
BRIP1	98
ATM	146
BRCA2	177
GTF2H3	288
ERCC3	344
ATR	366
POLR2B	427
ERCC8	434
PRKDC	451

Gene	Rank in Gene List
RFC5	486
RFC3	579
TDP1	584
FANCB	586
RAD50	595
REV1	645
MDC1	777
XRCC5	808
LIG3	960
REV3L	1080
RPA1	1083
FANCD2	1111
ERCC6	1174
RFC4	1223
POLH	1338

Table 5.1.2 Top correlated Reactome-defined DNA repair genes for CCDC15.
Genes were ranked by p-value for correlated Enrichment Analysis to assess enrichment of Reactome-defined DNA repair genes.

To validate the findings of the GSEA, qPCR was used to validate CCDC15 siRNAs which were used to assess DNA damage in CCDC15-depleted cells and if its loss sensitised cells to chemotherapeutic agents. Once this was established, western blotting, immunofluorescence, Comet assays and flow cytometry were used to characterise the involvement CCDC15 in the DNA damage response. Clonogenic survival assays were also attempted to further define the sensitisation of CCDC15 knocked down cells to DNA crosslinking agents.

5.2 Validation of Gene Set Enrichment Analysis

5.2.1 CCDC15 RNA Expression in Common Cell Lines

Quantitative PCR (qPCR) was used to determine the RNA expression levels of CCDC15 in a number of cancer cell lines (PC-3, T47D, HCT116, H460, HeLa) used within the Sheffield Academic Unit of Molecular Oncology, and the normal immortalised cell line, RPE-1. PC-3 RNA was isolated from a frozen pellet, a kind gift from Professor J. Catto, and T47D, HCT116, H460 and HeLa RNA extracts were a kind gift from the Professor M. Meuth. The RPE-1 RNA was isolated directly from cultured cells. The RNA was reverse transcribed and the resultant cDNA was amplified by PCR using TaqMan probes for GAPDH and CCDC15 (Fig. 5.2.1.1).

Of all the cell lines tested, RPE-1 had the lowest Delta Ct value, meaning that it had the highest CCDC15 expression when normalised to the expression of GAPDH. The cell lines with the next lowest Delta Ct values were H460, T47D and PC-3 (Table 5.2.1.1), which were all very similar, whilst HeLa cells produced the highest Delta Ct value. Three cell lines were selected for further analysis of CCDC15: RPE-1 to determine the effects of CCDC15 in normal cells, PC-3 as it had previously been optimised within the Collis lab for clonogenic survival and MTT assays and HeLa to determine if low endogenous expression levels affected the knockdown phenotype.

Cell Line	Probe	Mean Ct Value	Delta Ct
RPE-1	GAPDH	24.07	9.30
	CCDC15	33.37	
H460	GAPDH	20.10	10.68
	CCDC15	30.78	
T47D	GAPDH	21.08	10.71
	CCDC15	31.79	
PC-3	GAPDH	16.94	10.82
	CCDC15	27.76	
HCT116	GAPDH	22.84	11.07
	CCDC15	33.91	
HeLa	GAPDH	18.12	19.87
	CCDC15	37.99	

Table 5.2.1.1 CCDC15 RNA expression in cancer cell line panel.
RNA extracts were reverse transcribed and the resultant cDNA was amplified using TaqMan probes against GAPDH and CCDC15. The resultant Ct values were used to calculate the Delta Ct values for each cell line.

5.2.2 CCDC15 Knockdown by siRNA

The effectiveness of CCDC15 knockdown by siRNA at various time points post-transfection was assessed by qPCR. PC-3 and HeLa cells were transfected with Control 1 and CCDC15 for 48, 72 or 96 hours. The cells were then lysed, shredded and had their RNA extracted before it was reverse transcribed. The resultant cDNA was amplified as described previously and the Ct values produced for GAPDH and CCDC15 were used to calculate the percentage gene knockdown (Fig. 5.2.2.1).

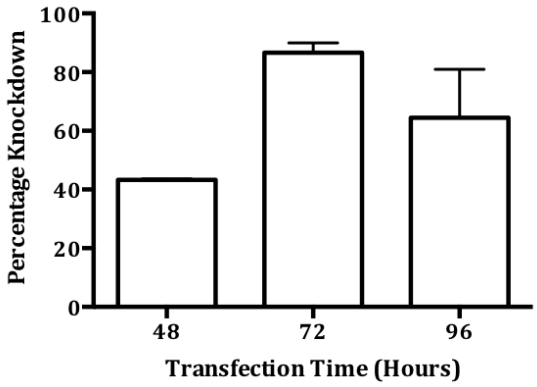

Figure 5.2.2.1 Percentage knockdown of CCDC15 following siRNA transfection in PC-3.
PC-3 were transfected with Control 1 or CCDC15 siRNA for 48, 72 or 96 hours. RNA was extracted from the cells, reverse transcribed and the resultant cDNA was amplified using TaqMan probes against GAPDH and CCDC15. The Ct values generated were used to calculate the percentage knockdown using the $2^{-\Delta\Delta Ct}$ method. Mean values derived from three independent experiments, with their respective SEMs.

Despite repeated attempts, this experiment did not produce meaningful results when RNA was extracted from HeLa cells; the qPCR analysis would produce an "undetermined" result in both the Control 1 and CCDC15 siRNA transfected extracts for the CCDC15 probe, most likely due to the low expression levels of CDC15 within this cell line.

In PC-3 cells, a 72 hour transfection produced the most effective knockdown of CCDC15 gene expression (Fig. 5.2.2.1), with an average knockdown of 89.89%. By 96 hours gene expression appeared to be recovering (68.50% knockdown), so a 72 hour transfection was chosen for future experiments (unless stated otherwise).

5.2.3 Assessment of DNA Damage in CCDC15 Depleted Cells

To determine if CCDC15 knockdown increased the levels of DNA damage experienced by unchallenged cells, CCDC15 siRNA transfected cells were stained with antibodies raised against the DNA damage markers γH2AX and 53BP1. PC-3, HeLa and RPE-1 cells were transfected with Control 1 and CCDC15 siRNA using DharmaFECT 1 for 48 hours. The cells were pre-extracted with 0.5% Triton X and 3% BSA in PBS before fixing and co-staining for γH2AX and 53BP1 (Fig. 5.2.3.1 - 3).

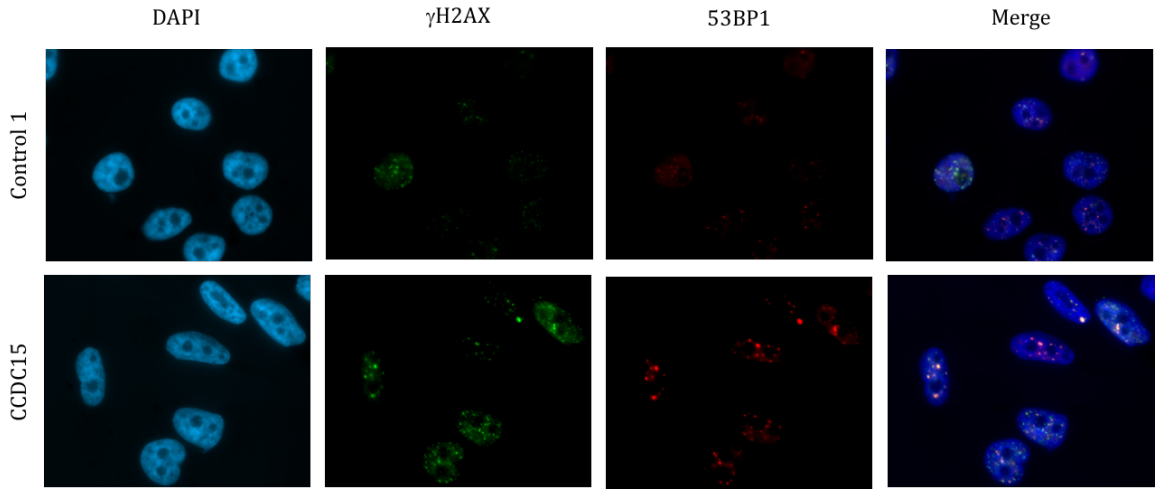

Figure 5.2.3.1 DNA damage detection in CCDC15 knocked down PC-3 cells.
Representative images of PC-3 cells transfected with Control 1 or CCDC15 siRNA and DharmaFECT 1 and grown for 48 hours post-transfection. Cells were incubated with 0.5% Triton X-100 and 3% BSA in PBS for 5 minutes before fixing and staining with antibodies raised against γH2AX and 53BP1.

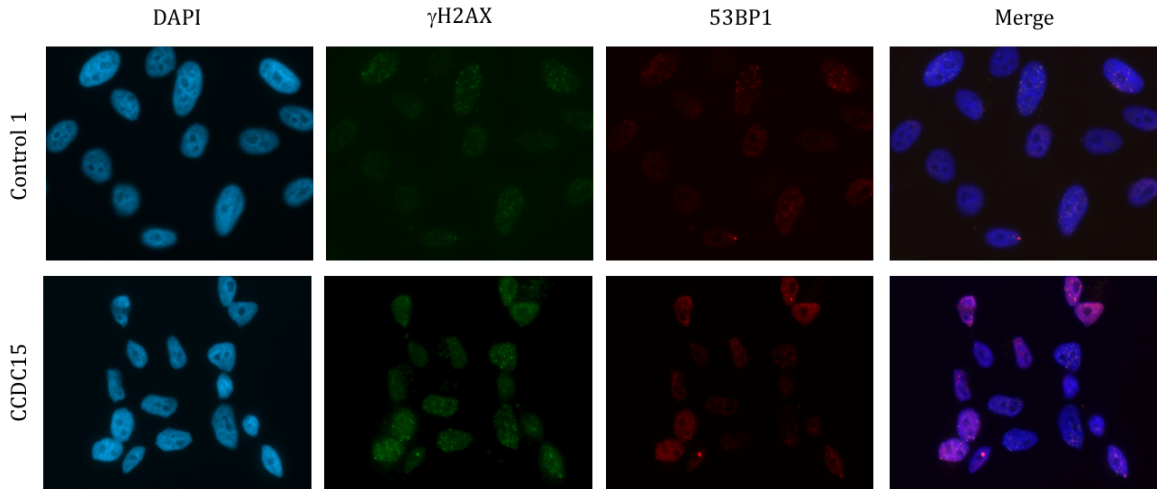

Figure 5.2.3.2 DNA damage detection in CCDC15 knocked down HeLa cells.
Representative images of HeLa cells transfected with Control 1 or CCDC15 siRNA and DharmaFECT 1 and grown for 48 hours post-transfection. Cells were incubated with 0.5% Triton X-100 and 3% BSA in PBS for 5 minutes before fixing and staining with antibodies raised against γH2AX and 53BP1.

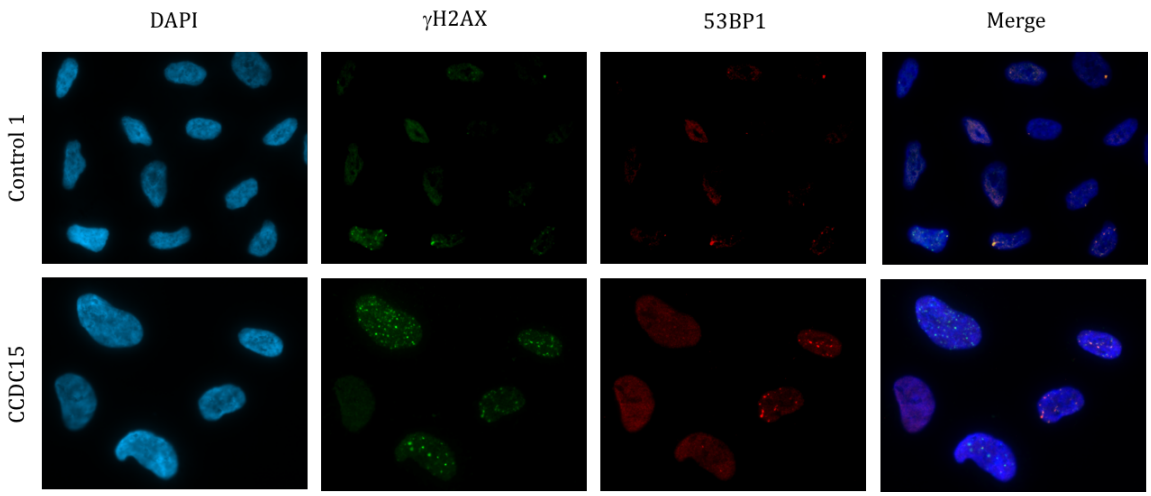

Figure 5.2.3.3 DNA damage detection in CCDC15 knocked down RPE-1 cells.
Representative images of RPE-1 cells transfected with Control 1 or CCDC15 siRNA and DharmaFECT 1 and grown for 48 hours post-transfection. Cells were incubated with 0.5% Triton X-100 and 3% BSA in PBS for 5 minutes before fixing and staining with antibodies raised against γH2AX and 53BP1.

The suboptimal transfection time of 48 hours was used for these experiments as the qPCR analysis was still ongoing, in an attempt to ascertain if CCDC15 was worth studying. In all three cell lines, CCDC15 knockdown increased the levels of γH2AX and 53BP1 foci observed. The images were scored for the number of foci they contained to allow the DNA damage response in the respective cell populations to be quantified (Fig 5.2.3.4).

In all three cell lines the knockdown of CCDC15 significantly increased the proportion of cells positive for γH2AX, when compared to Control 1 transfected cells, with p-values of 0.025, 0.026 and 0.009 in PC-3, HeLa and RPE-1 cells respectively. Loss of CCDC15 also resulted in the increase in the number of cells positive for 53BP1 foci, this difference was significant in PC-3 and RPE-1 cells (p-values 0.0009 and 0.017) but not in HeLa cells (p-value 0.129) due to the variability of the staining in this cell line. Collectively, this suggests that CCDC15 loss increases the levels of DNA damage experienced by unchallenged cells and that CCDC15 may play a role in the maintenance of genome stability.

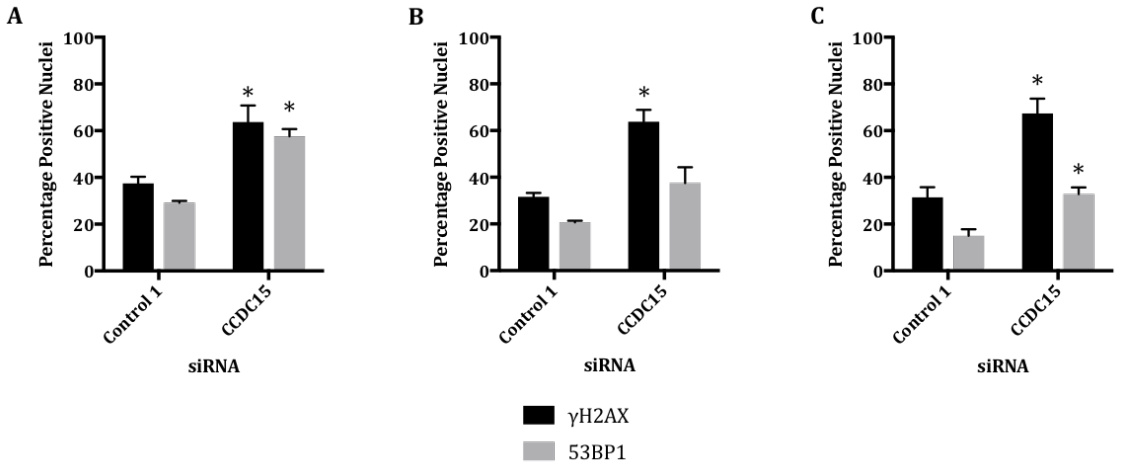

Figure 5.2.3.4 Percentage of PC-3, HeLa and RPE-1 cells positive for γH2AX and 53BP1 foci.
For each condition the number of (A) PC-3, (B) HeLa or (C) RPE-1 were counted and the percentage of γH2AX and 53BP1 positive nuclei was calculated. A nucleus was considered positive if it contained 10 or more bright foci. Asterisks indicate significant difference from Control 1, p value <0.05. Mean values derived from three independent experiments for PC-3 and RPE-1 and two for HeLa, with their respective SEMs.

5.2.4 DNA Damaging Agent Sensitivity

As the GSEA suggested that CCD15 expression correlated with a number genes associated with the resolution of DNA crosslinks and replication impeding damage, MTT cytotoxicity assays were carried out to determine whether CCDC15 knockdown sensitised cells to these lesions.

5.2.4.1 Mitomycin C Sensitivity

Mitomycin C (MMC), is a cytotoxic chemotherapeutic agent, that induces crosslinks in complementary DNA strands (interstrand crosslinks, ICLs). PC-3, HeLa and RPE-1 cells were transfected with Control 1 or CCDC15 siRNA using DharmaFECT 1 for 72 hours. The cells were then treated with MMC (0 - 80ng/ml) for 120 hours before the addition of MTT (Fig. 5.2.4.1.1).

In the RPE-1 cells, CCDC15 knockdown significantly sensitised cells to the effects of MMC, and a trend towards sensitisation was observed in PC-3 cells but this was not significant. No difference was seen at all in HeLa cells, suggesting that the role of CCDC15 in dealing with DNA crosslinks may depend upon expression level.

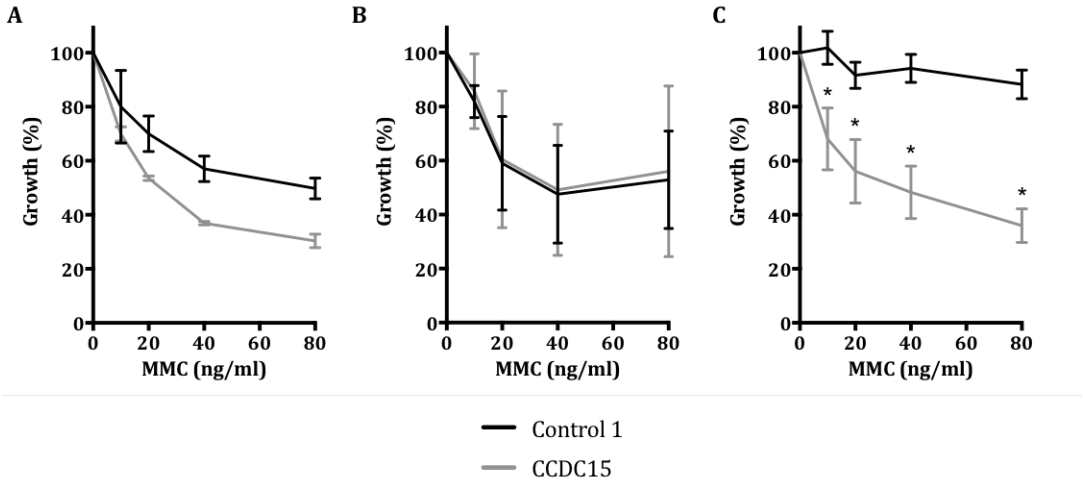

Figure 5.2.4.1.1 Sensitivity of CCDC15 knocked down cells to Mitomycin C.

(A) PC-3, (B) HeLa and (C) RPE-1 cells were transfected with Control 1 or CCDC15 siRNA and DharmaFECT 1 and grown for 72 hours before treatment with 0, 10, 20, 40 or 80ng/ml MMC for 120 hours. Asterisks indicate significant difference from Control 1, p value <0.05. Mean values were derived from 3 independent experiments, with their respective SEMs.

5.2.4.2 Cisplatin Sensitivity

Cisplatin is a platinum based chemotherapeutic that forms DNA ICLs and intrastrand crosslinks by the binding of purine bases, resulting in DNA damage and ultimately apoptosis (Dasari & Tchounwou, 2014). PC-3, HeLa and RPE-1 cells were transfected with Control 1 or CCDC15 siRNA using DharmaFECT 1 for 72 hours. The cells were then treated with Cisplatin (0 - 10μM) for 120 hours before the addition of MTT (Fig. 5.2.4.2.1).

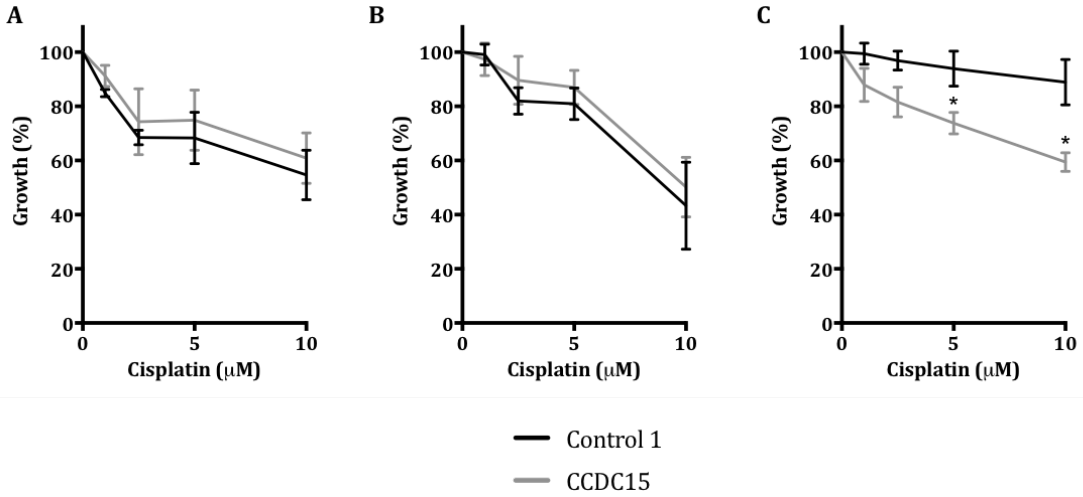

Figure 5.2.4.2.1 Sensitivity of CCDC15 knocked down cells to Cisplatin.

(A) PC-3, (B) HeLa and (C) RPE-1 cells were transfected with Control 1 or CCDC15 siRNA and DharmaFECT 1 and grown for 72 hours before treatment with 0, 1, 2.5, 5 or 10μM Cisplatin for 120 hours. Asterisks indicate significant difference from Control 1, p value <0.05. Mean values were derived from 3 independent experiments, with their respective SEMs.

Of the three cell lines, only the RPE-1 cells showed a significant increase in sensitivity to Cisplatin after the knockdown of CCDC15 but this sensitisation was less than that

observed for MMC treatment. This suggests that CCDC15 loss may be more detrimental in the presence of ICLs than intrastrand crosslinks. Unlike the MMC experiments, PC-3 cells did not appear to be sensitised to Cisplatin and HeLa cells again showed no sensitisation.

5.2.4.3 Hydroxyurea sensitivity

The enzyme ribonucleotide reductase is essential for the synthesis of deoxyribonucleotides and the efficient progression of DNA replication. It is inactivated by the drug hydroxyurea (HU) which results in the stalling of DNA replication forks (Yarbro, 1968). PC-3, RPE-1 and HeLa cells were transfected with Control 1 or CCDC15 siRNA using DharmaFECT 1 for 72 hours. The cells were then treated with HU (0 - 125μM) for 120 hours before the addition of MTT (Fig. 5.2.4.3.1). For all three cell lines, the knockdown of CCDC15 did not sensitise the cells to HU treatment; suggesting that CCDC15 is not required for the resolution of stalled replication forks *per se*.

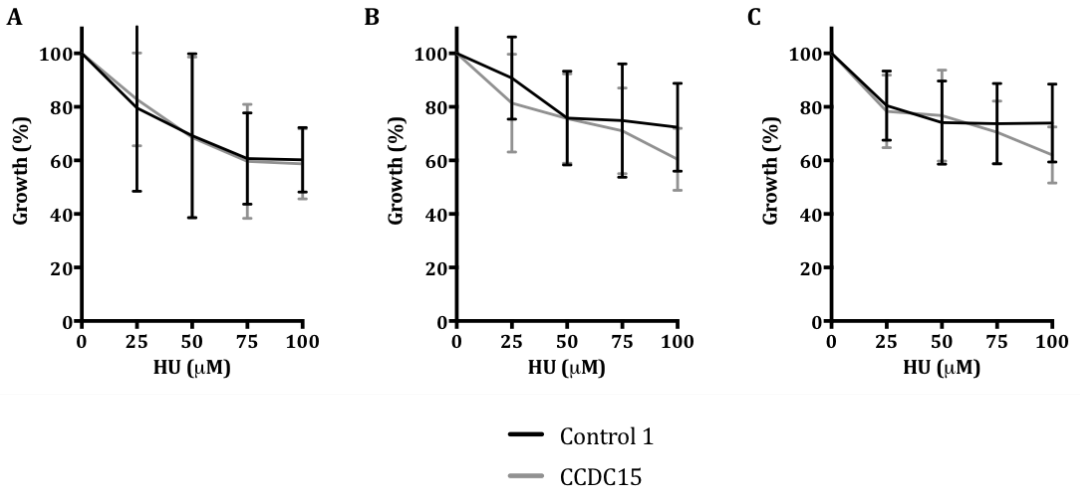

Figure 5.2.4.3.1 Sensitivity of CCDC15 knocked down cells to Hydroxyurea.
(A) PC-3, (B) HeLa and (C) RPE-1 cells were transfected with Control 1 or CCDC15 siRNA and DharmaFECT 1 and grown for 72 hours before treatment with 0, 25, 50, 75 or 100μM HU for 120 hours. Mean values were derived from 3 independent experiments, with their respective SEMs.

5.2.5. Deconvolution of the CCDC15 siRNA Pool

To ensure that the effects observed following the knockdown of CCDC15 were not off target effects, the siRNA pool was deconvoluted into the four individual siRNAs and qPCR analysis was used to assess their knockdown. PC-3 cells were transfected with Control 1 and CCDC15 1 - 4 for 72 hours. The cells were lysed, the RNA extracted and converted to cDNA which was subsequently amplified as described previously. The Ct values produced for GAPDH and CCDC15 were then used to calculate the percentage gene knockdown (Fig. 5.2.5.1).

Of the three individual siRNAs, CCDC15 1 and CCDC15 3, produced a greater than 80% knockdown of CCDC15 expression (80.17% and 83.51% respectively). These two siRNAs were chosen for all further work on this project. The remaining siRNAs were discarded as they did not produce a satisfactory knockdown (CCDC15 2 67.26% and CCDC15 4 54.59%).

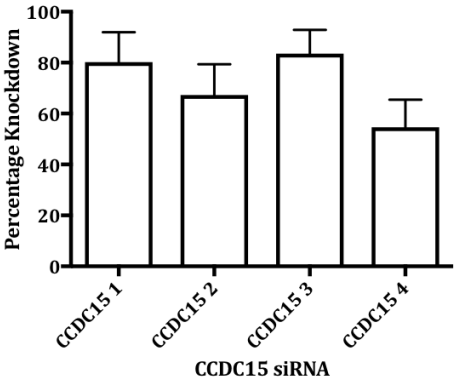

Figure 5.2.5.1 Percentage knockdown of deconvoluted CCDC15 siRNA pool following siRNA transfection in PC-3 cells.

PC-3 cells were transfected with Control 1 or CCDC15 1-4 siRNA for 72 hours. RNA was extracted from the cells, reverse transcribed and the resultant cDNA was amplified using TaqMan primers against GAPDH and CCDC15. The Ct values generated were used to calculate the percentage knockdown using the $2^{-\Delta\Delta Ct}$ method. Mean values derived from three independent experiments, with their respective SEMs.

5.3 DNA Damage Response Phenotype

Once it had been established that CCDC15 loss increased endogenous DNA damaged and in some cases sensitised cells to exogenous genotoxic stress; further analysis was carried out to ascertain the role it played in DNA damage repair using the validated individual siRNA.

5.3.1 DNA Damage Response Activation

5.3.1.1 DNA Damage Marker Immunofluorescence

The previous immunofluorescent analysis of the DNA damage markers γH2AX and 53BP1 was repeated with the individual CCDC15 siRNA and at the 72 hour time point. PC-3, HeLa and RPE-1 cells were transfected with Control 1, CCDC15 1 or CCDC15 3 siRNA using DharmaFECT 1 for 72 hours. The cells were pre-extracted with 0.5% Triton X and 3% BSA in PBS before fixing and co-staining for γH2AX and 53BP1 (Fig. 5.3.1.1.1 - 3).

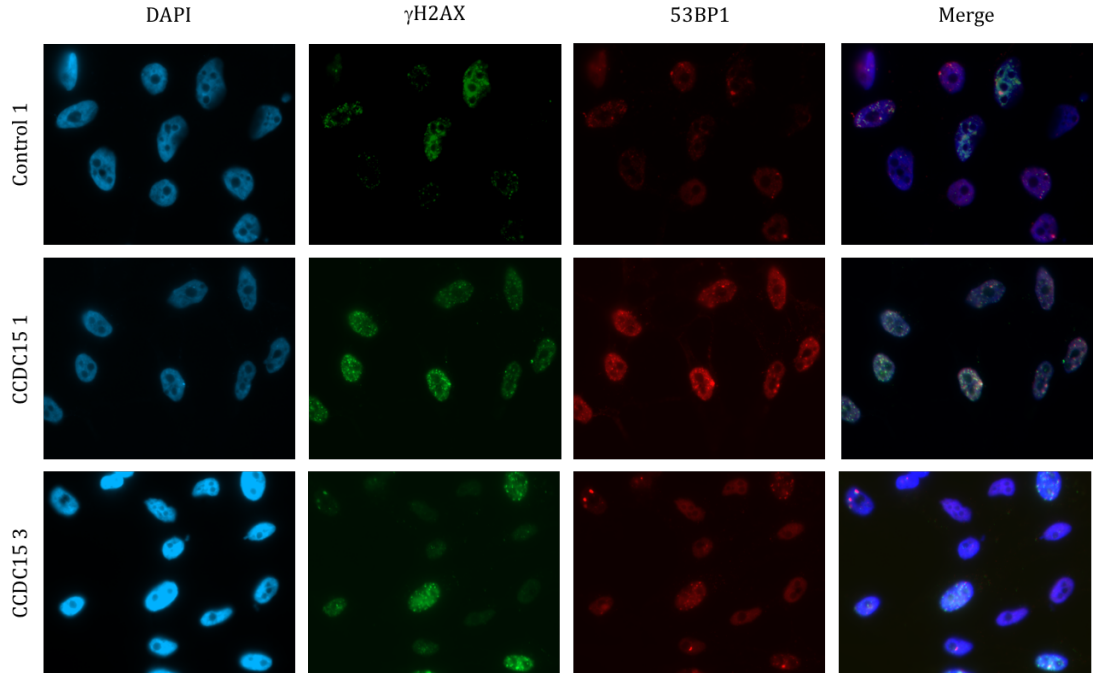

Figure 5.3.1.1.1 DNA damage detection in deconvoluted CCDC15 siRNA knocked down PC-3 cells.

Representative images of PC-3 cells transfected with Control 1, CCDC15 1 or CCDC15 3 siRNA and DharmaFECT 1 and grown for 72 hours post-transfection. Cells were incubated with 0.5% Triton X-100 and 3% BSA in PBS for 5 minutes before fixing and subsequent staining with antibodies raised against γH2AX and 53BP1.

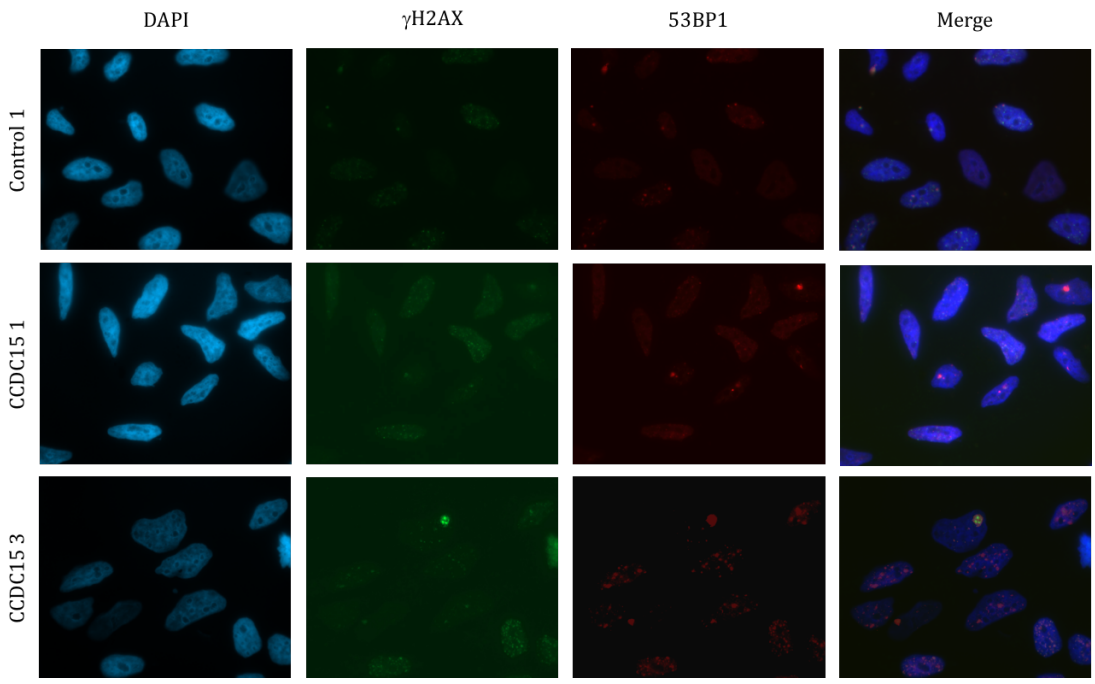

Figure 5.3.1.1.2 DNA damage detection in deconvoluted CCDC15 siRNA knocked down HeLa cells.

Representative images of HeLa cells transfected with Control 1, CCDC15 1 or CCDC15 3 siRNA and DharmaFECT 1 and grown for 72 hours post-transfection. Cells were incubated with 0.5% Triton X-100 and 3% BSA in PBS for 5 minutes before fixing and subsequent staining with antibodies raised against γH2AX and 53BP1.

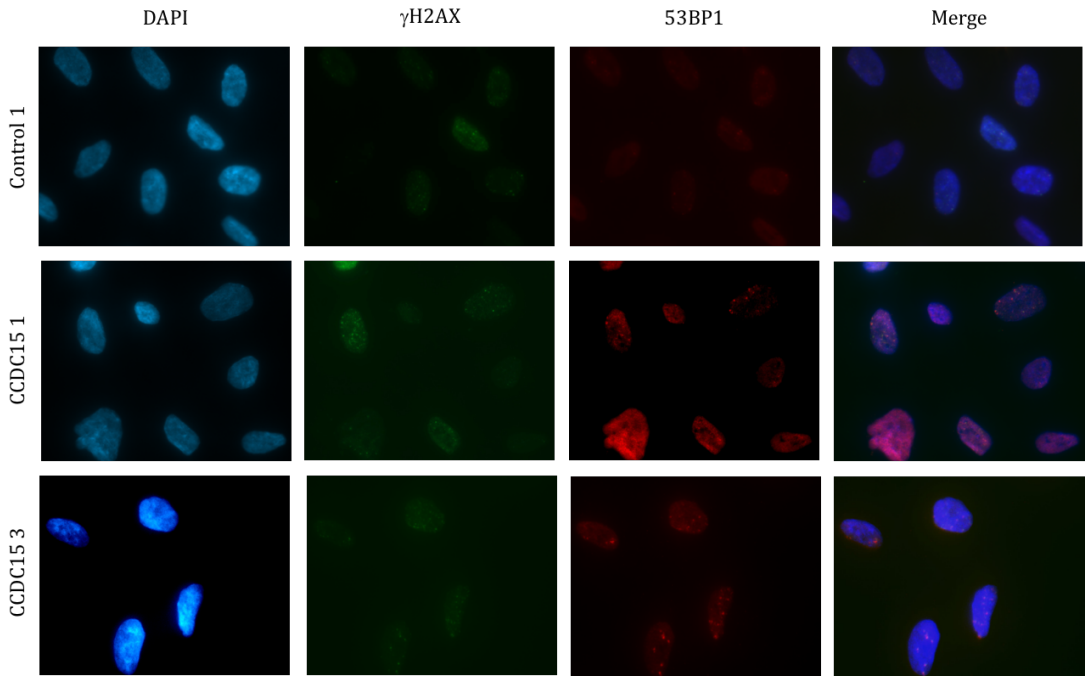

Figure 5.3.1.1.3 DNA damage detection in deconvoluted CCDC15 siRNA knocked down RPE-1 cells.

Representative images of RPE-1 cells transfected with Control 1, CCDC15 1 or CCDC15 3 siRNA and DharmaFECT 1 and grown for 72 hours post-transfection. Cells were incubated with 0.5% Triton X-100 and 3% BSA in PBS for 5 minutes before fixing and subsequent staining with antibodies raised against γH2AX and 53BP1.

As observed previously, knockdown of CCDC15 with either siRNA increased the levels of γH2AX and 53BP1 foci observed in all three cell lines. The images were subsequently scored for the number of positive nuclei they contained to allow the DNA damaged caused by gene knockdown to be quantified (Fig 5.3.1.1.4).

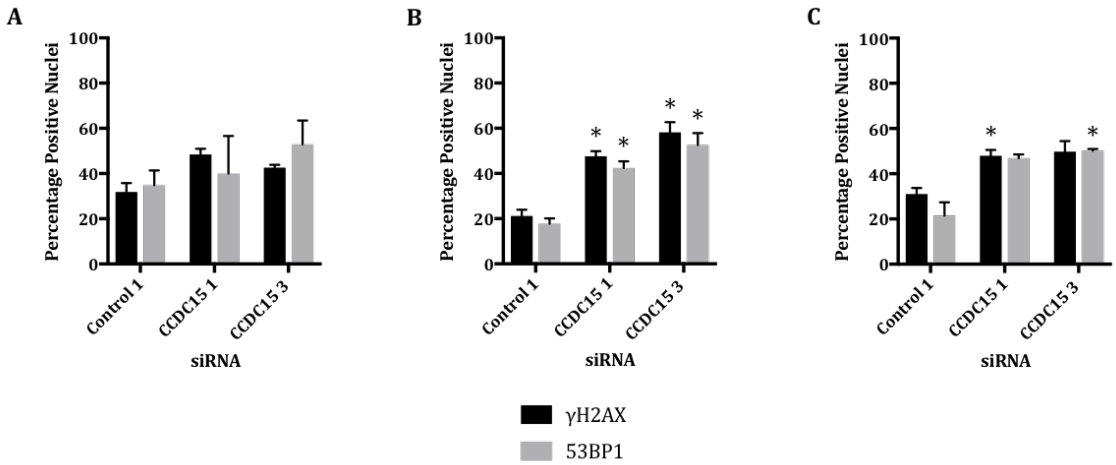

Figure 5.3.1.1.4 Percentage of PC-3, HeLa and RPE-1 cells positive for γH2AX and 53BP1 foci following transfection with individual CCDC15 siRNAs.

For each condition the number of (A) PC-3, (B) HeLa or (C) RPE-1 were counted and the percentage of γH2AX and 53BP1 positive nuclei was calculated. A nucleus was considered positive if it contained 10 or more bright foci. Asterisks indicate significant difference from Control 1, p value <0.05. Mean values derived from three independent experiments for HeLa cells and two for PC-3 and RPE-1 cells, with their respective SEMs.

In all three cell lines there was a general trend that the knockdown of CCDC15 with either siRNA increased the percentage of cells positive for γH2AX and 53BP1. In the PC-3 cells, the knockdown of CCDC15 with either siRNA failed to significantly increase the levels of γH2AX or 53BP1 foci detected, in contrast to the result seen when using the pool siRNA. However, in the HeLa cells, both siRNA significantly increase the levels of γH2AX (p values of 0.0018 and 0.0021) and 53BP1 (p-values of 0.0028 and 0.0037). For the RPE-1 cells CCDC15 1 significantly increased the levels of γH2AX (p-value 0.0443) but not 53BP1 (p-value 0.523). The opposite was seen for CCDC15 3 where γH2AX levels were not significantly increased (p-value 0.0720) but 53BP1 levels were (p-value 0.0396). Overall, this data suggests that CCDC15 loss does result in DNA damage and that the phenotype observed when using the pool siRNA was not due to off target effects.

5.3.2.2 Direct Measurement of DNA Damage

Comet assays (single-cell gel electrophoresis) were employed to directly measure the levels of DNA damage caused by CCDC15 knockdown, rather than relying solely on surrogate immunofluorescence markers. PC-3, HeLa and RPE-1 cells were transfected with Control 1, CCDC15 1 or CCDC15 3 siRNA using DharmaFECT 1 for 72 hours. The cells were then trypsinised and suspended in agarose on Comet slides before they were lysed and their DNA was unwound. These slides were the electrophoresed, stained with SYBR Gold, imaged and scored (Fig. 5.3.1.2.1).

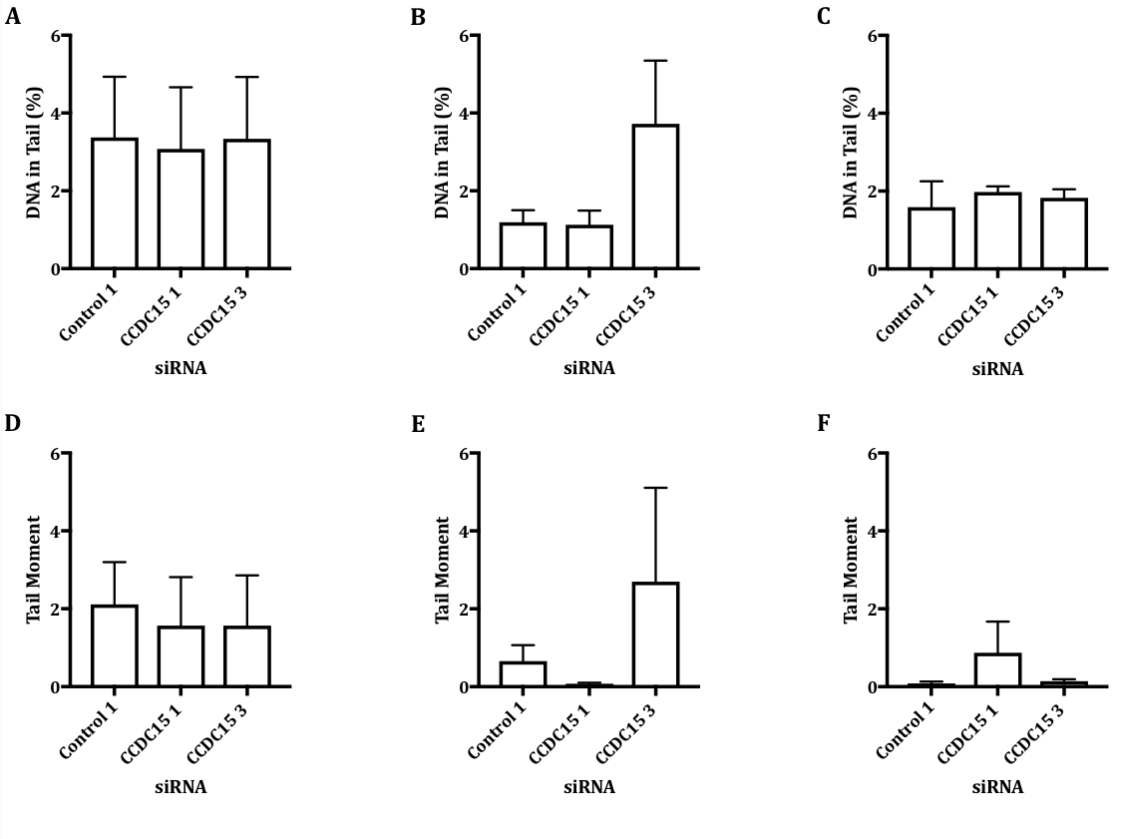

Figure 5.3.1.2.1 Percentage DNA in Tail and Tail Moment of PC-3, HeLa and RPE-1 cells following CCDC15 knockdown.

(A,D) PC-3, (B,E) HeLa and (C,F) RPE-1 cells were transfected with Control 1, CCDC15 1 or CCDC15 3 siRNA and DharmaFECT 1 and grown for 72 hours before being trypsinised and re-suspended in agarose. The cells were then lysed, their DNA unwound and electrophoresed. The cells were then stained with SYBR Gold, imaged, scored and the (A-C) Percentage DNA in their Comet Tails and their (D-F) Tail Moments were calculated. Mean values derived from three independent experiments for PC-3 and HeLa cells and two for RPE-1 cells, with their respective SEMs.

In all three cells lines, the knockdown of CCDC15 with either siRNA failed to significantly increase either the Percentage DNA in the Tail or the Tail Moment of the Comets (Fig. 5.3.1.2.1). In PC-3 cells this was probably due to the extreme variability of the assay and the high levels of damage observed in the Control 1 transfected cells. In the HeLa cells, CCDC15 1 did not appear to be having any effect as very few tails were produced which resulted in a Tail Moment lower than that of the Control 1 cells. In the RPE-1 cells, CCDC15 knockdown with both siRNA slightly increased the Percentage DNA in the Tail of the Comets but this was not significant as the variability of the Control 1 transfected cells

exceeded this increase. CCDC15 1 non-significantly increased the Tail Moment in these cells but again this was extremely variable and was not seen for CCDC15 3.

As the results in all three cells lines were extremely inconstant and a number of users within the Bryant and Collis labs were experiencing technical difficulties with this assay (see Discussion) it was decided not to pursue this assay in order to focus on further characterisation of the CCDC15 knockdown phenotype.

5.3.2 Sensitisation to DNA Crosslinking Agents

5.3.2.1 Clonogenic Survival Assays

Clonogenic assays typically demonstrate a greater decrease in cell survival as drug doses increase when compared to MTT assays. These assays were attempted as they may have allowed for some of the small differences seen in the MTT assays to be amplified and analysed in more detail. PC-3, HeLa and RPE-1 cells were transfected with Control 1, CCDC15 1 or CCDC15 3 siRNA for 72 hours. The cells were then trypsinised, counted and replated at either 200 or 2000 cells per well. Once the cells had settled they were drugged with a 0 – 100nM titration of MMC. The cells were grown for 11 days to allow colonies to form which were then stained with Methylene Blue (0.4%). In the case of PC-3 and HeLa cells the resultant colonies were then manually counted (Fig. 5.3.2.1.1).

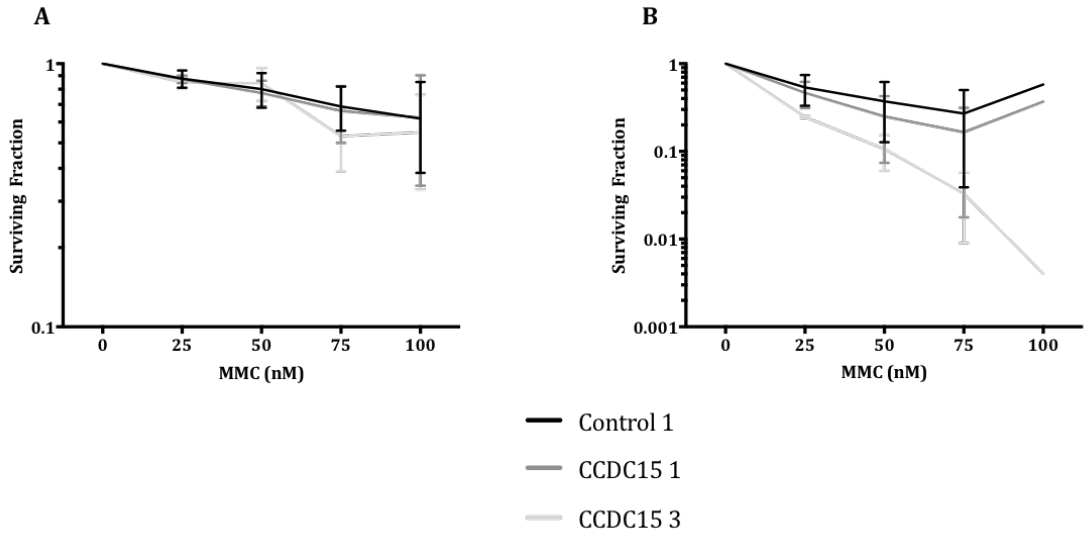

Figure 5.3.2.1.1 Survival of CCDC15 knocked down cells in the presence of MMC.
(A) PC-3 and (B) HeLa cells were transfected with Control 1, CCDC15 1 or CCDC15 3 siRNA and DharmaFECT 1 and grown for 72 hours before being trypsinised and replated at 200 or 2000 cells per well. The cells were then drugged with 0, 25, 50, 75 or 100nM MMC for 11 days to allow colonies to form. The cells were then stained with 0.4% Methylene Blue which were counted and the surviving fractions were calculated.

In the PC-3 cells, no difference at all could be observed between the surviving fractions of the Control 1, CCDC15 1 and CCDC15 3 transfected cells, despite a difference being observed in the previously described MTT assay with the pool siRNA. In the HeLa cells, the CCDC15 knocked down cells did appear more sensitised to MMC, but due to the variability seen in the Control 1 cells, the difference in survival were not significant. Unlike the PC-3 and HeLa cells, the RPE-1 cells did not form distinct individual colonies that were

countable in this assay, therefore an alternative quantification method was trailed to assess cell survival. Once the cells had been stained the Methylene Blue was dissolved with 1% SDS and assessed colorimetrically (Fig. 5.3.2.1.2).

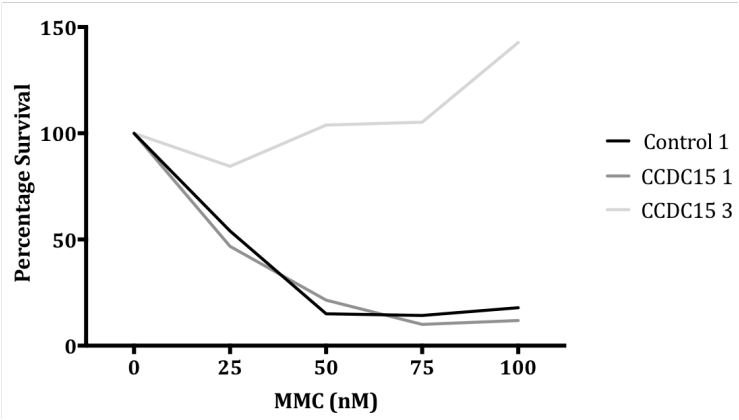

Figure 5.3.2.1.2 Survival of CCDC15 knocked down RPE-1 in the presence of MMC.
RPE-1 cells were transfected with Control 1, CCDC15 1 or CCDC15 3 siRNA and DharmaFECT 1 and grown for 72 hours before being trypsinised and replated at 200 cells per well. The cells were then drugged with 0, 25, 50, 75 or 100nM MMC for 11 days to allow colonies to form. The cells were then stained with 0.4% Methylene Blue which was dissolved with 1% SDS and analysed colorimetrically. Values derived from one experiment.

In this assay, no difference was seen in the survival of RPE-1 cells knocked down with CCDC15 1 siRNA compared to the control cells, unlike the results seen in the MTT assay. The cells transfected with CCDC15 3 appeared to survive better in the presence of MMC, which was most likely an artefact of the assay. For the 2000 cell per well plates, the wells had reached confluence and saturated the plate reader during the colorimetric analysis.

In parallel with the MMC assay, a UV sensitivity assay was carried out in the RPE-1 cells as they had shown sensitivity to both MMC and Cisplatin in the MTT assays. The cells were transfected and re-plated as in the MMC assay and then irradiated with 0 – 6J/m^2 UV light. The cells were then left for 11 days to form colonies before they were stained and analysed as described previously (Fig. 5.3.2.1.3).

For all three siRNA, the cells appeared to survive better after UV irradiation, despite there seeming to be less colonies on the plate at the higher doses. It appeared that the colonies were stained more darkly on the plates irradiated with the higher UV doses which most likely resulted in this unusual outcome. It was decided not to continue with this method of analysing clonogenic assays as it did not appear to accurately represent the number of cells surviving.

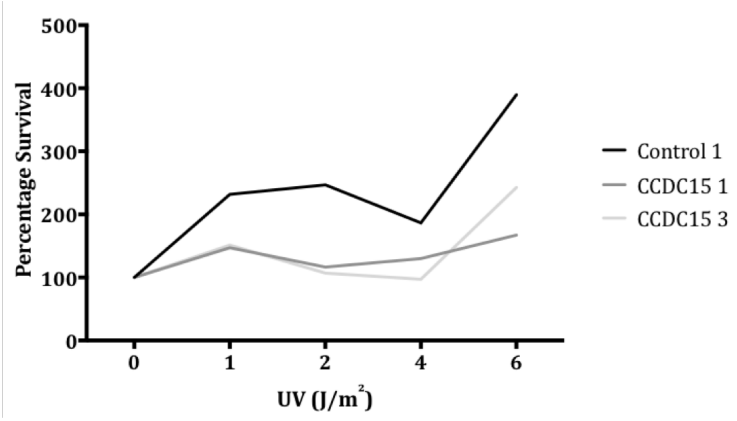

5.3.2.1.2 Survival of CCDC15 knocked down RPE-1 after UV irradiation

RPE-1 cells were transfected with Control 1, CCDC15 1 or CCDC15 3 siRNA and DharmaFECT 1 and grown for 72 hours before being trypsinised and replated at 200 cells per well. The cells were then irradiated with 0, 1, 2, 4 or 6J/m² UV then allowed to grow for 11 days so colonies formed. The cells were then stained with 0.4% Methylene Blue which was dissolved with 1% SDS and analysed colorimetrically. Values derived from one experiment.

5.3.2.2 Assessment of DNA Damage in CCDC15-depleted cells in response to MMC and UV

As the clonogenic survival assays had failed to identify any sensitisation to DNA crosslinking agents, it was decided to investigate if CCDC15's loss affected the levels of DNA damage experienced by cells following treatment with MMC or UV. PC-3, HeLa and RPE-1 cells were transfected with Control 1, CCDC15 1 or CCDC15 3 siRNA using DharmaFECT 1 for 72 hours. The cells were either treated with 80ng/ml MMC for 16 hours or irradiated with 60J/m² UV light 4 hours prior to pre-extraction. The cells were pre-extracted, fixed and co-stained for γH2AX and 53BP1 (Fig. 5.3.2.2.1-3). For all three cell lines, the images were scored for the number of positive nuclei they contained (Fig 5.3.2.2.4).

Treatment with MMC or irradiation with UV increased the levels of γH2AX and 53BP1 observed when compared to the untreated cells (Fig. 5.3.1.1.4) as expected. However, the knockdown of CCDC15 did not drastically alter the levels of DNA damage reported following treatment compared to the Control 1 transfected cells, with only the combinations of CCDC15 3 and MMC significantly increasing the levels of 53BP1 observed in RPE-1 cells and CCDC15 3 and UV significantly increasing the levels of γH2AX observed in HeLa cells.

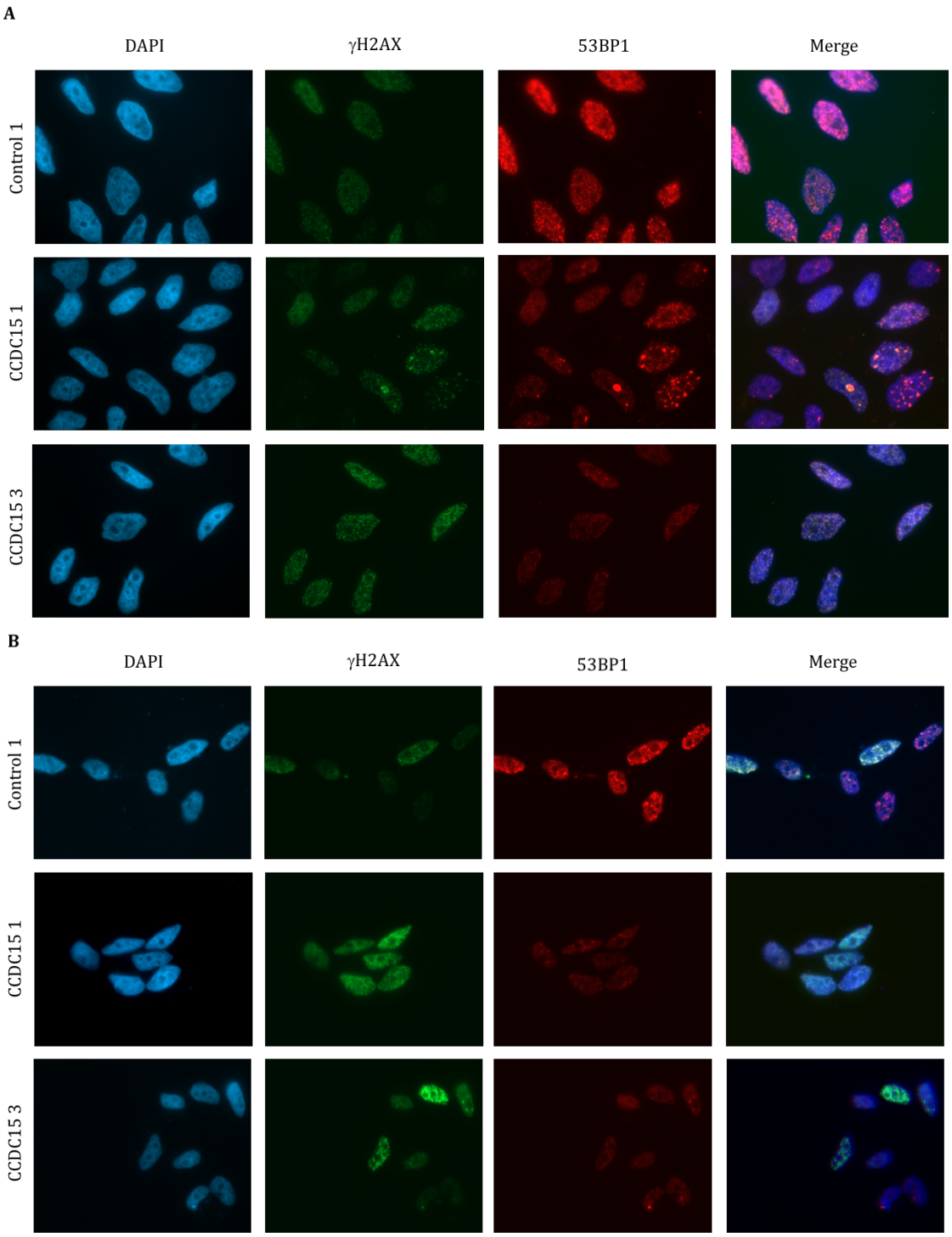

Figure 5.3.2.2.1 DNA damage detection following DNA crosslinking in PC-3 cells.

Representative images of PC-3 cells transfected with Control 1, CCDC15 1 or CCDC15 3 siRNA and DharmaFECT 1 and grown for 72 hours post-transfection. Cells were either treated with (A) 80ng/ml MMC for 16 hours or (B) irradiated with 60J/m² UV light 4 hours prior to pre-extraction. Cells were incubated with 0.5% Triton X-100 and 3% BSA in PBS for 5 minutes before fixing and staining with antibodies raised against γH2AX and 53BP1.

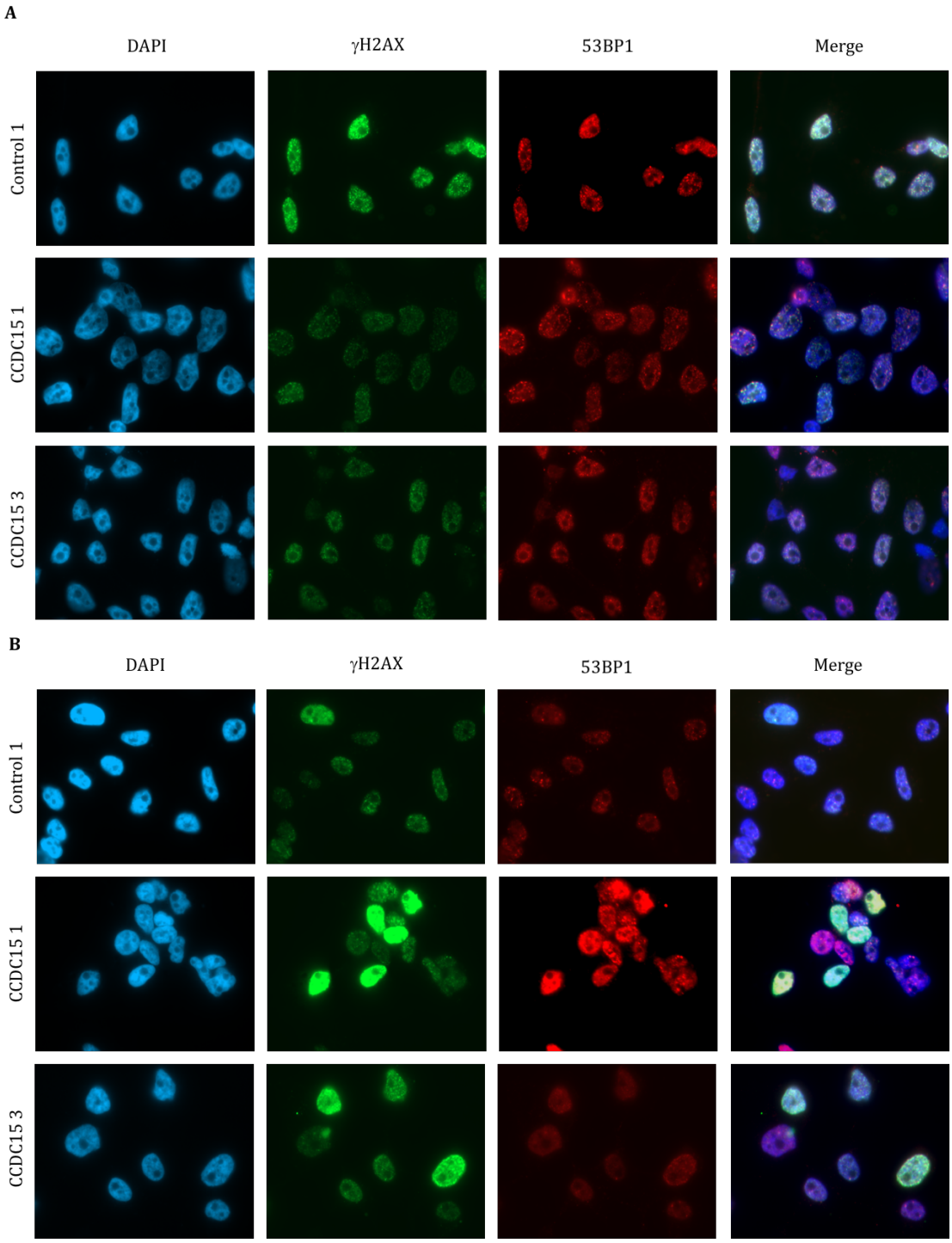

Figure 5.3.2.2.2 DNA damage detection following DNA crosslinking in HeLa cells.

Representative images of HeLa cells transfected with Control 1, CCDC15 1 or CCDC15 3 siRNA and DharmaFECT 1 and grown for 72 hours post-transfection. Cells were either treated with (A) 80ng/ml MMC for 16 hours or (B) irradiated with 60J/m² UV light 4 hours prior to pre-extraction. Cells were incubated with 0.5% Triton X-100 and 3% BSA in PBS for 5 minutes before fixing and staining with antibodies raised against γH2AX and 53BP1.

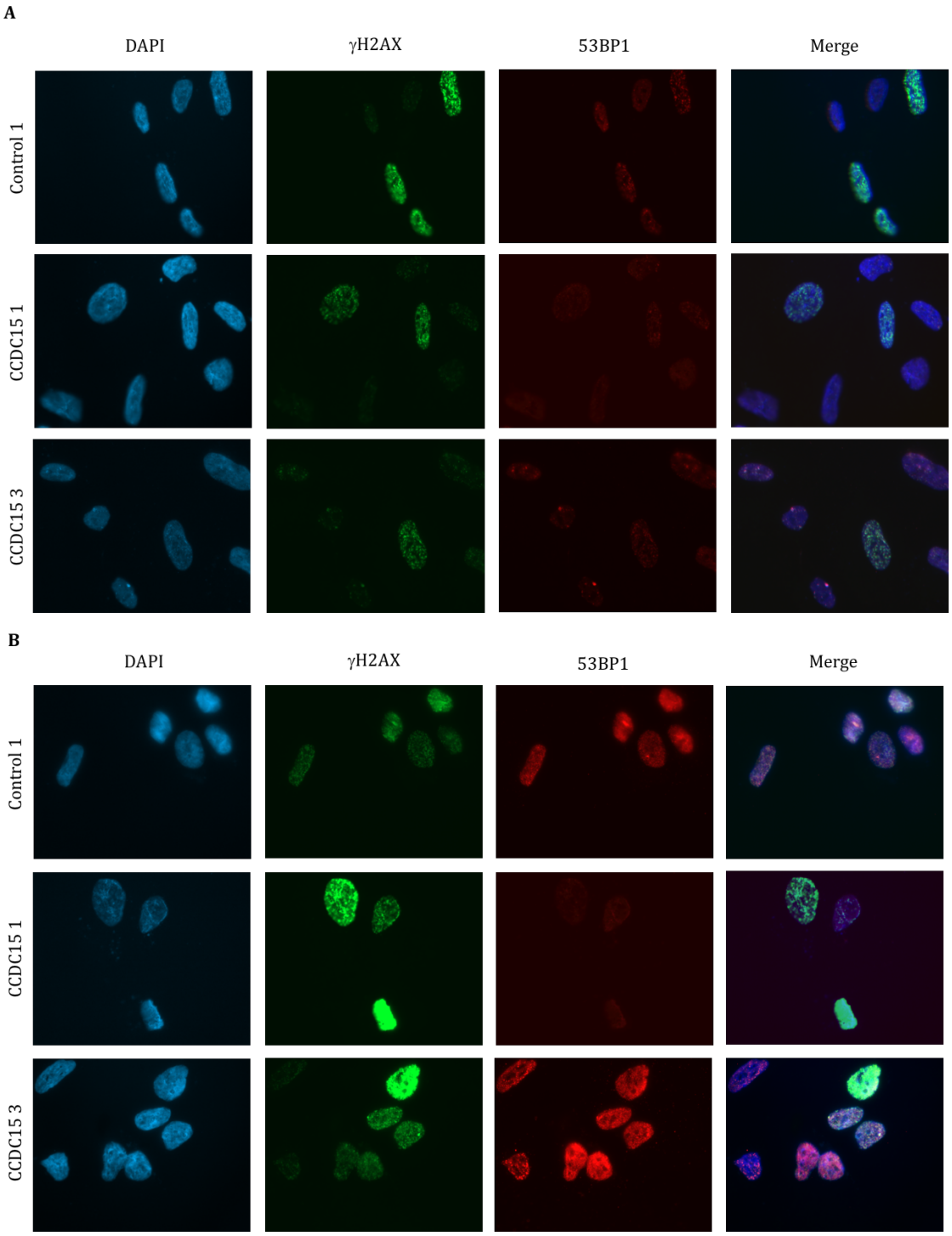

Figure 5.3.2.2.3 DNA damage detection following DNA crosslinking in RPE-1 cells.

Representative images of RPE-1 cells transfected with Control 1, CCDC15 1 or CCDC15 3 siRNA and DharmaFECT 1 and grown for 72 hours post-transfection. Cells were either treated with (A) 80ng/ml MMC for 16 hours or (B) irradiated with 60J/m² UV light 4 hours prior to pre-extraction. Cells were incubated with 0.5% Triton X-100 and 3% BSA in PBS for 5 minutes before fixing and staining with antibodies raised against γH2AX and 53BP1.

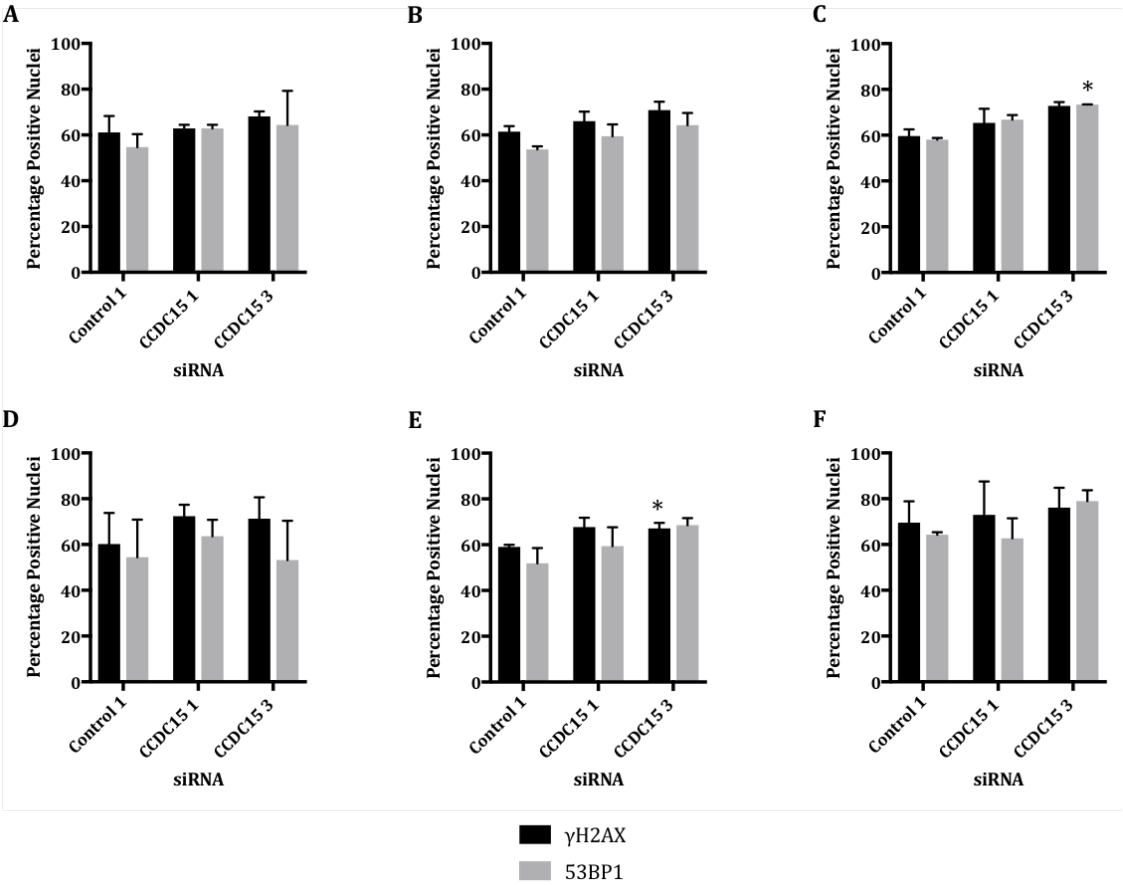

Figure 5.3.2.2.4 Percentage of PC-3, HeLa and RPE-1 cells positive for γH2AX and 53BP1 foci following DNA crosslinking.

For each condition the number of (A, D) PC-3, (B, E) HeLa or (C, F) RPE-1 cells that had been treated with (A-C) MMC or (D-F) UV irradiation were counted and the percentage of γH2AX and 53BP1 positive nuclei was calculated. A nucleus was considered positive if it contained 10 or more bright foci. Asterisks indicate significant difference from Control 1, p value <0.05. Mean values derived from three independent experiments for HeLa cells and two for PC-3 and RPE-1 cells, with their respective SEMs.

As crosslinking agents did not appear to be having an effect at these time points, it was decided to carry out a time course experiment to determine how CCDC15 deficient cells respond to UV induced damage over time and if the dynamics of the DNA damage response were altered in these cells. RPE-1 cells were transfected with Control 1, CCDC15 1 or CCDC15 3 siRNA using DharmaFECT 1 for 72 hours. Cells were either mock irradiated or irradiated with 60J/m^2 UV light 0, 4, 8 or 24 hours before pre-extraction and fixing. The cells were then stained for γH2AX (Fig. 5.3.2.2.5) imaged and then scored for γH2AX positive nuclei (Fig 5.3.2.2.6).

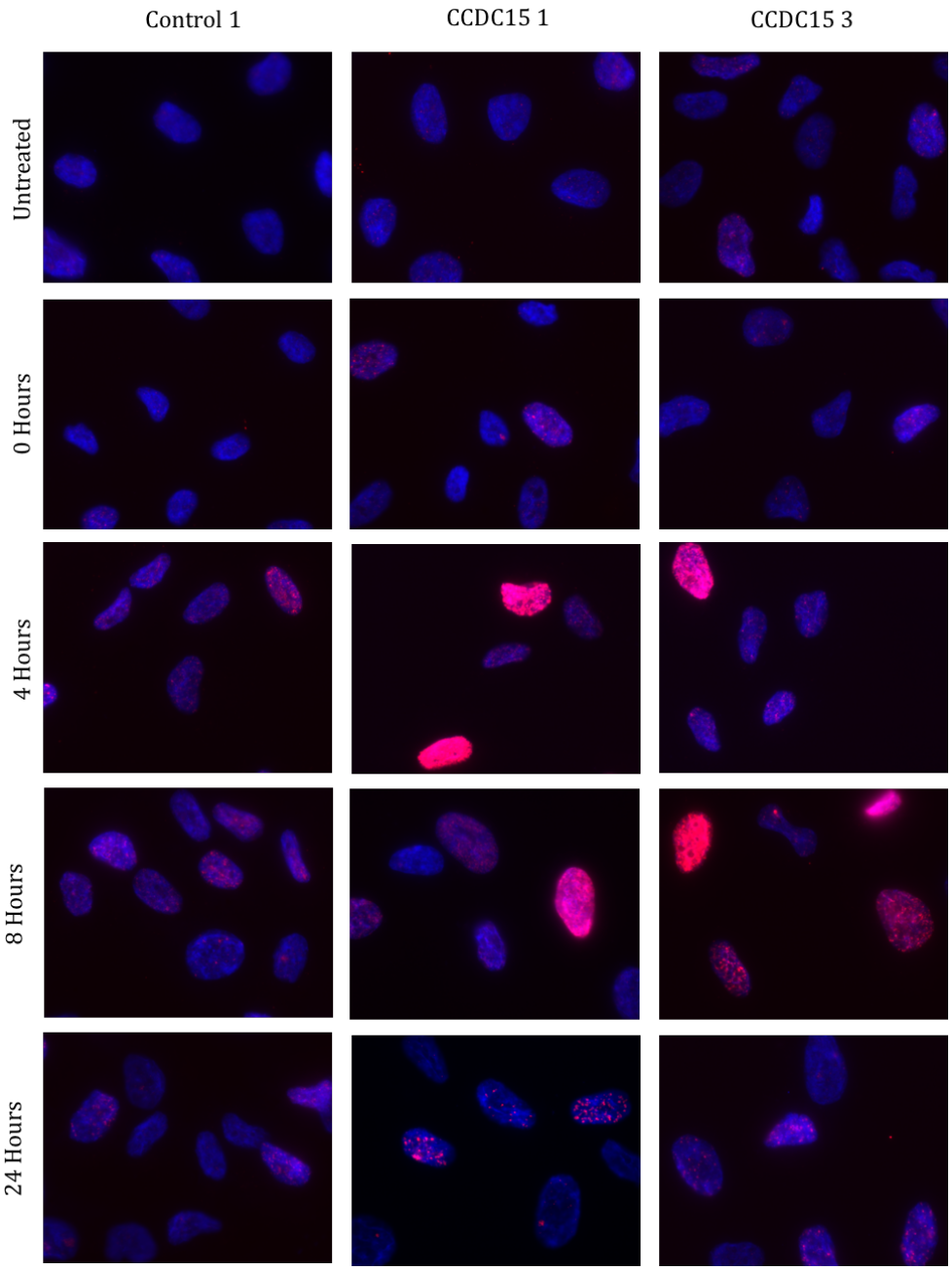

Figure 5.3.2.2.5 γH2AX foci in RPE-1 cells following recovery from UV irradiation.

Representative images of RPE-1 cells transfected with Control 1, CCDC15 1 or CCDC15 3 siRNA and DharmaFECT 1 and grown for 72 hours post-transfection. Cells were either mock irradiated or irradiated with 60J/m² UV light 0, 4, 8 or 24 hours prior to pre-extraction. Cells were incubated with 0.5% Triton X-100 and 3% BSA in PBS for 5 minutes before fixing and staining with an antibody raised against γH2AX.

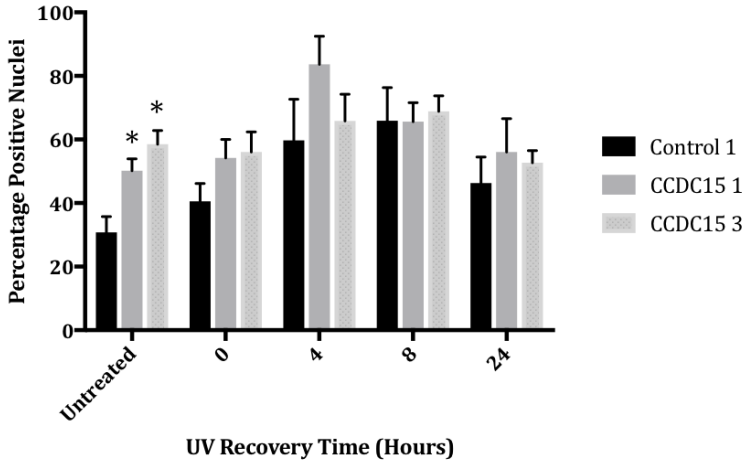

Figure 5.3.2.2.6 Percentage of RPE-1 cells positive for γH2AX following recovery from UV irradiation.

For each condition the number of RPE-1 cells were counted and the percentage of γH2AX positive nuclei was calculated. A nucleus was considered positive if it contained 10 or more bright foci. Asterisks indicate significant difference from Control 1, p value <0.05. Mean values derived from four independent experiments, with their respective SEMs.

As observed previously, the knockdown of CCDC15 in unchallenged cells significantly increased the levels of DNA damage observed with siRNA 1 and siRNA 3 (p-values of 0.0203 and 0.0055 respectively). The same increase was observed when the cells were fixed immediately after irradiation but the increases were not significant with either siRNA as the values were too variable; this trend was also observed at the 4 hour time point. However, by 8 hours, all three cell populations had a similar level of damage. A similar trend was observed at 24 hours with all 3 siRNAs producing levels of positive nuclei comparative to the CCDC15 knocked down cells at the 0 hour time point. This suggests that the knockdown of CCDC15 may have accelerated the formation of DNA damage in UV irradiated cells, however, they appeared to recover at a similar rate to cells with functional CCDC15.

5.3.3 Involvement in the Fanconi Anaemia/BRCA Pathway

5.3.3.1 FANCD2 Ubiquitination

A number of proteins involved in the Fanconi Anaemia (FA) and BRCA pathway appeared in the GSEA list of DNA repair genes whose expression correlated best with that of CCDC15. Furthermore, CCDC15-depleted cells exhibited an increased sensitivity to ICL inducing agents (Fig. 5.2.4.1.1 and 5.2.4.2.1). Therefore, it was decided to investigate its potential role within this pathway. Western blotting analysis was used to assess the post-translational modification status of FANCD2, which becomes ubiquitinated upon DNA damage and is critical for the repair of ICLs (Liang et al, 2016). PC-3, HeLa and RPE-1 cells were transfected with Control 1, CCDC15 1 or CCDC15 3 using DharmaFECT 1 for 72 hours. Cells were either mock treated with ddH_2O or treated with 80ng/ml MMC 16 hours before the cells were lysed. A total FANCD2 antibody, in which a band shift is observed upon ubiquitination, was used to assess protein levels and its post-translational modification (Fig. 5.3.3.1.1).

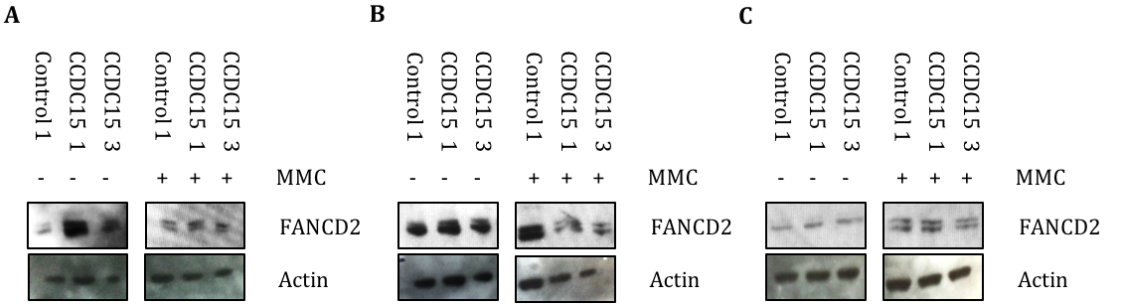

Figure 5.3.3.1.1 Induction of FANCD2 Ubiquitination following CCDC15 knockdown and MMC treatment.

PC-3, (B) HeLa or (C) RPE-1 cells were transfected with Control 1, CCDC15 1 or CCDC15 3 siRNA for 72 hours with DharmaFECT 1. Cells were mock treated with ddH_2O or treated with 80ng/ml MMC for 16 hours before media removal. The cells were lysed and 15μg of protein from each sample was loaded onto a NuPage 4-12% Bis-Tris Gel for separation. The gels were transferred to nitrocellulose membranes before blocking and blotting with a Total FANCD2 and Actin (loading control) primary antibodies. The primary antibodies were detected with HRP conjugated secondary antibodies.

In PC-3 cells, FANCD2 appeared to be ubiquitinated in the Control 1 untreated lane, which was unexpected as these cells had not been exposed to exogenous DNA crosslinking agents. The ubiquitination was not reduced by the knockdown of CCDC15 by either siRNA, suggesting that CCDC15 is not required for this event. In the HeLa cells, some ubiquitinated FANCD2 was present in the Control 1 untreated lane and this appeared to increase with CCDC15 knockdown. Unlike the other two cell lines, RPE-1 cells did not appear to have ubiquitinated FANCD2 in the untreated conditions but it was present in all the cells treated with MMC which suggests that CCDC15 is not essential for the activation of the FA pathway and this is not how the loss of CCDC15 results in DNA damage.

5.3.3.2 Fanconi Anaemia/BRCA Pathway Immunofluorescence

To validate the western blotting analysis, CCDC15 knocked down cells were assessed for the activation of the FA pathway by immunofluorescence. In the presence of DNA crosslinks, FANCD2 localises into foci within the nucleus (Liang et al, 2016) and can therefore be quantified to determine pathway activation. PC-3, HeLa and RPE-1 were transfected with Control 1, CCDC15 1 or CCDC15 3 using DharmaFECT 1 for 72 hours. The cells were either mock treated, treated with 80ng/ml MMC for 16 hours or irradiated with 60J/m^2 UV light 4 hours prior to pre-extraction. The cells were pre-extracted fixed, stained with a FANCD2 antibody (Fig. 5.3.3.2.1-3) and the resultant images were scored for FANCD2 positive nuclei (Fig 5.3.3.2.4).

Foci formation appeared to slightly increase with the loss of CCDC15 in the three cell lines, however this effect was not significant. PC-3 cells appeared to have a higher percentage of positive nuclei following gene knockdown and treatment with either MMC or UV but again this effect was not significant as this experiment was only carried out successfully once. Neither MMC or UV appeared to increase the number of HeLa cells or RPE-1 cells positive for FANCD2 foci following CCDC15 knockdown.

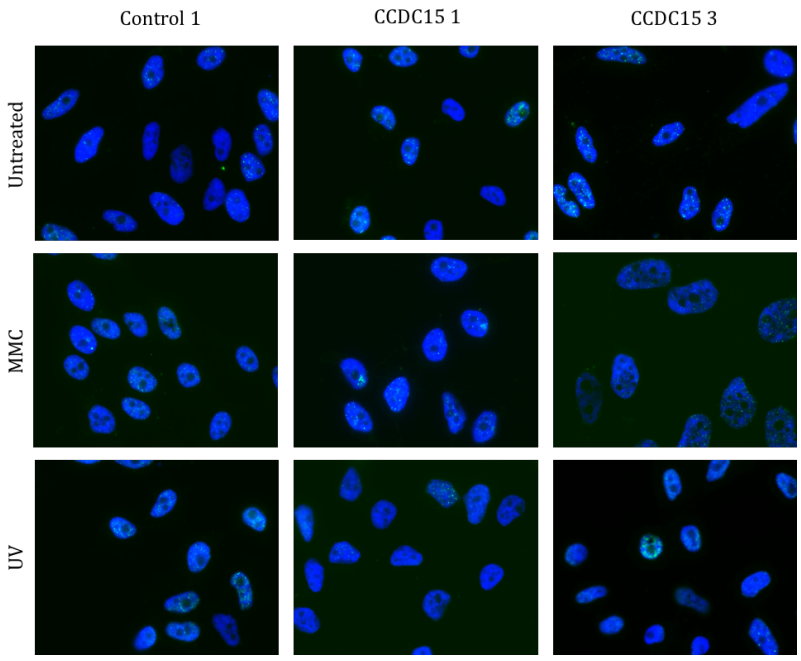

Figure 5.3.3.2.1 Fanconi Anaemia pathway activation following CCDC15 knockdown in PC-3 cells.

Representative images of PC-3 cells transfected with Control 1, CCDC15 1 or CCDC15 3 siRNA and DharmaFECT 1 and grown for 72 hours post-transfection. Cells were either mock treated, treated with 80ng/ml MMC for 16 hours or irradiated with 60J/m² UV light 4 hours prior to pre-extraction. Cells were incubated with 0.5% Triton X-100 and 3% BSA in PBS for 5 minutes before fixing and staining an antibody raised against FANCD2.

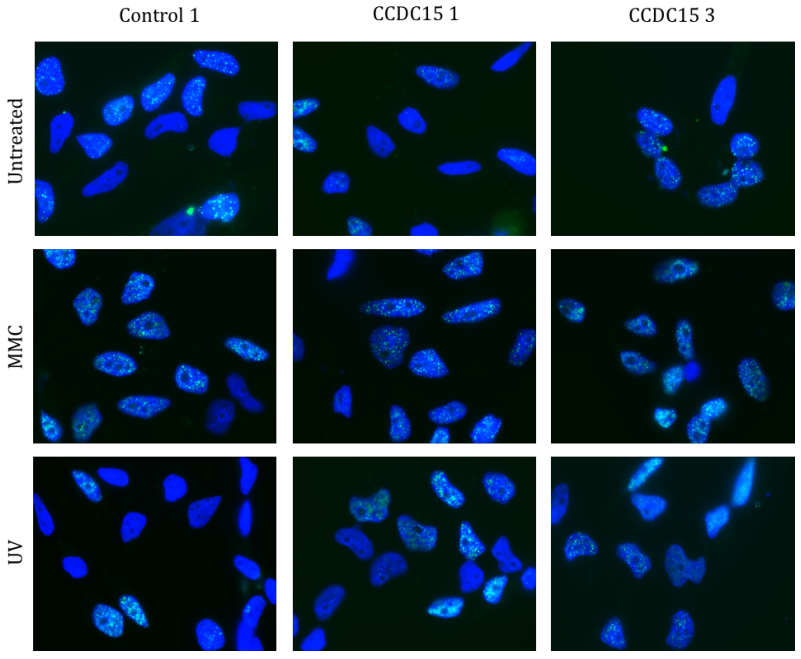

Figure 5.3.3.2.2 Fanconi Anaemia pathway activation following CCDC15 knockdown in HeLa cells.

Representative images of HeLa cells transfected with Control 1, CCDC15 1 or CCDC15 3 siRNA and DharmaFECT 1 and grown for 72 hours post-transfection. Cells were either mock treated, treated with 80ng/ml MMC for 16 hours or irradiated with 60J/m² UV light 4 hours prior to pre-extraction. Cells were incubated with 0.5% Triton X-100 and 3% BSA in PBS for 5 minutes before fixing and staining with an antibody raised against FANCD2.

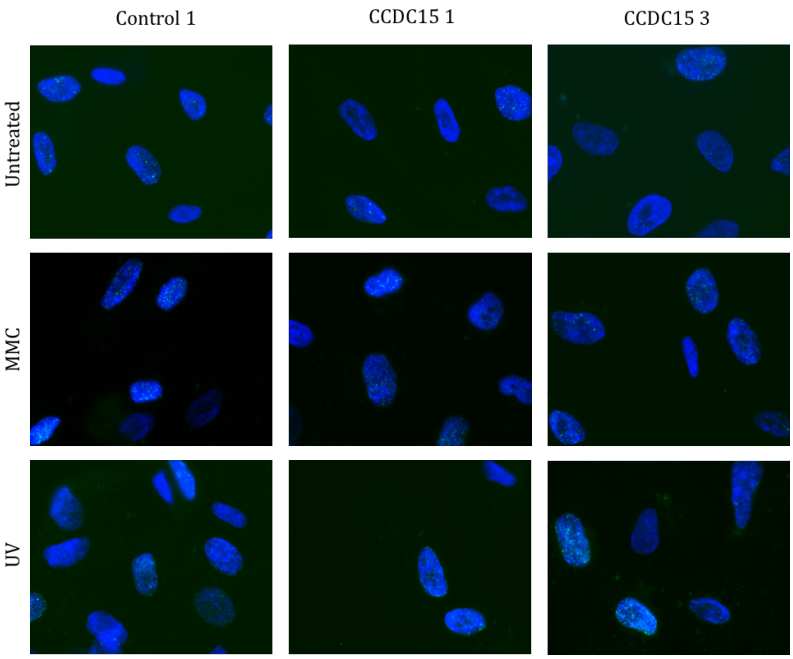

Figure 5.3.3.2.3 Fanconi Anaemia pathway activation following CCDC15 knockdown in RPE-1 cells.

Representative images of RPE-1 cells transfected with Control 1, CCDC15 1 or CCDC15 3 siRNA and DharmaFECT 1 and grown for 72 hours post-transfection. Cells were either mock treated, treated with 80ng/ml MMC for 16 hours or irradiated with 60J/m² UV light 4 hours prior to pre-extraction. Cells were incubated with 0.5% Triton X-100 and 3% BSA in PBS for 5 minutes before fixing and staining with an antibody raised against FANCD2.

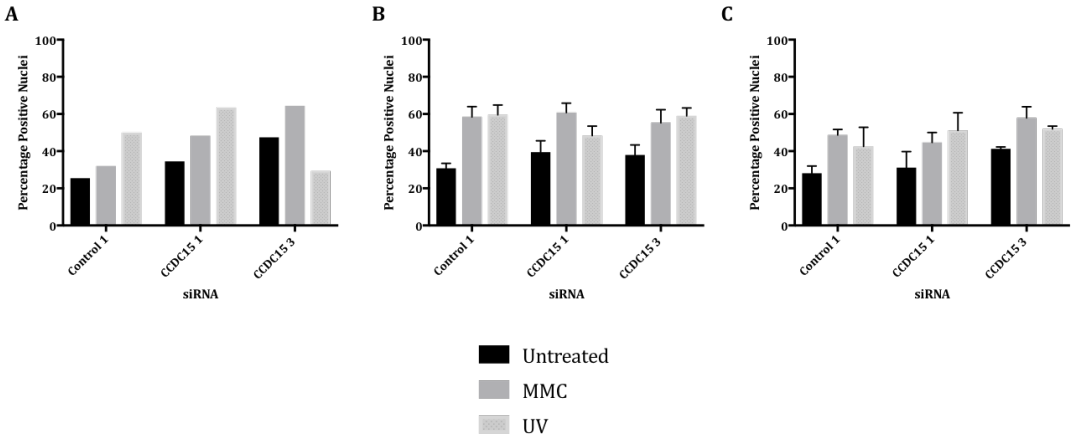

Figure 5.3.3.2.4 Percentage of PC-3, HeLa and RPE-1 cells positive for FANCD2 foci following DNA crosslinking.

(A) PC-3, (B) HeLa or (C) RPE-1 cells were either mock treated, treated with MMC or UV irradiation. For each condition the number of cells were counted and the percentage of FANCD2 positive nuclei was calculated. A nucleus was considered positive if it contained 10 or more bright foci. Mean values derived from three independent experiments for HeLa cells, two for RPE-1 cells and one for PC-3 cells, with their respective SEMs.

The cells in the previously described γH2AX UV recovery time course were co-stained for FANCD2 to determine if CCDC15 knockdown affected the resolution of FANCD2 foci after exposure to DNA crosslinks (Fig. 5.3.3.2.5). The cells were imaged and then scored for FANCD2 positive nuclei (Fig 5.3.3.2.6).

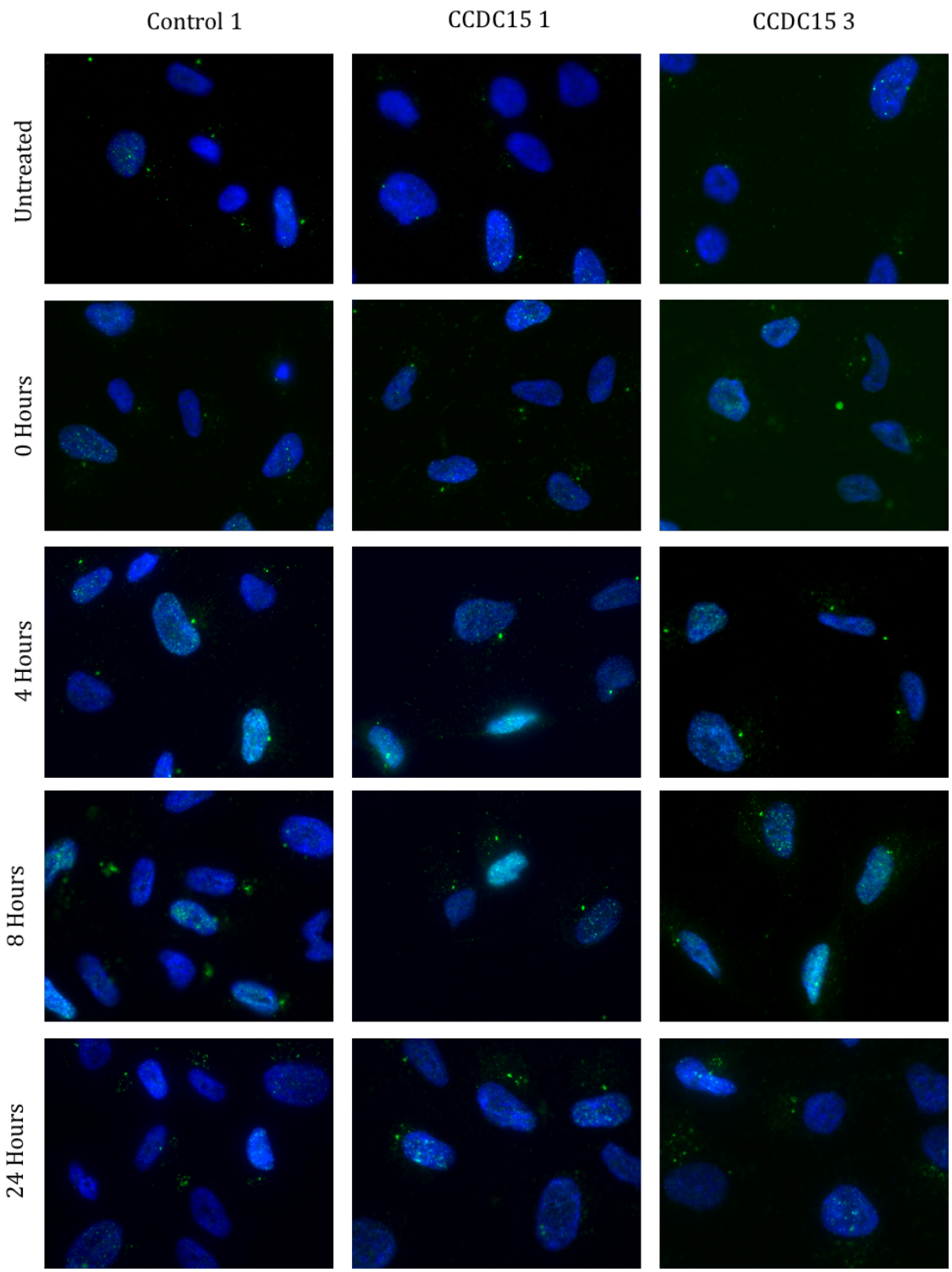

Figure 5.3.2.2.5 FANCD2 foci in RPE-1 cells following recovery from UV irradiation.
Representative images of RPE-1 cells transfected with Control 1, CCDC15 1 or CCDC15 3 siRNA and DharmaFECT 1 and grown for 72 hours post-transfection. Cells were either mock irradiated or irradiated with 60J/m² UV light 0, 4, 8 or 24 hours prior to pre-extraction. Cells were incubated with 0.5% Triton X-100 and 3% BSA in PBS for 5 minutes before fixing and staining with an antibody raised against FANCD2.

As observed in the single time point experiment, the knockdown of CCDC15 in untreated RPE-1 cells did not significantly alter the levels of FANCD2 foci detected and the same was seen when the cells were fixed immediately after irradiation. By 4 hours, the level of

FANCD2 foci had increased compared to the 0 hour time-point, but very little difference could be observed between the 3 siRNAs. The levels of positive nuclei remained stable until the 24 hour time point when the percentage of positive nuclei had decreased to that of untreated cells for all three cell populations. Collectively, these data suggest that the loss of CCDC15 has little effect upon the formation or resolution of FANCD2 foci after UV irradiation.

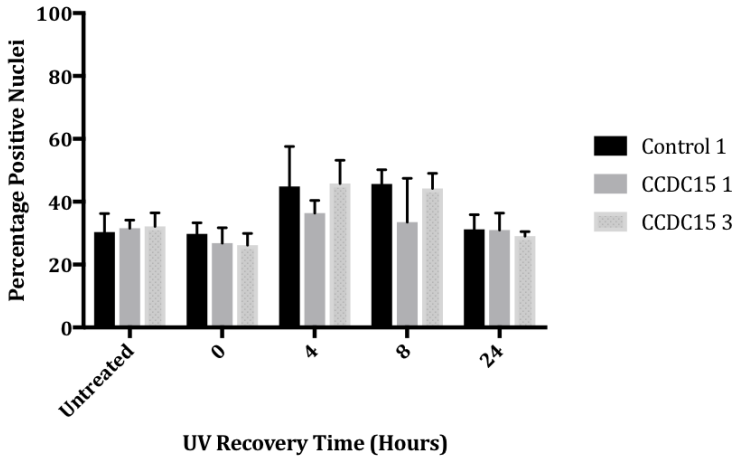

Figure 5.3.3.2.6 Percentage of RPE-1 cells positive for FANCD2 foci following recovery from UV irradiation.

For each condition the number of RPE-1 cells were counted and the percentage of FANCD2 positive nuclei was calculated. A nucleus was considered positive if it contained 10 or more bright foci. Mean values derived from four independent experiments, with their respective SEMs.

The FA protein BRCA2 (FANCD1) recruits the recombinase RAD51 (FANCR) to ssDNA, which is involved in homologous repair of DSB and mutations in this protein have been demonstrated to sensitise cells to DNA ICLs (Hashimoto et al, 2016). As it is believed to act downstream of FANCD2 ubiquitination (Walden & Deans, 2014), the UV recovery time course was repeated and the cells were stained for RAD51, which forms foci in the presence of DSB and ICLs (Gospodinov et al, 2009), to determine if CCDC15 knockdown affected these later events in ICL repair (Fig. 5.3.3.2.7). In these cells, the average number of foci per cell was calculated, as much fewer RAD51 foci form in damage cells compared to the other markers (Fig 5.3.3.2.6).

In the untreated cells and the cells fixed immediately following UV irradiation (0 hours), there was very little evidence of RAD51 foci formation in any of the conditions, with an average of 1 foci per cell. By 4 hours post-irradiation, the Control 1 transfected cells contained more RAD51 foci than the cells transfected with CCDC15 1 and CCDC15 3 but the differences were not significant. The trend was reversed by 8 hours, with both the CCDC15 1 and CCDC15 3 populations containing a higher average number of foci per cell, but again the differences were not significant. By 24 hours, the levels of foci produced by all three siRNA were reduced, with the Control 1 transfected cells showing a slightly lower average number of foci than the cells transfected with either of the CCDC15 siRNAs. This suggests that the formation of RAD51 foci is slightly delayed in the cells lacking CCDC15 as is their resolution compared to the Control 1 transfected cells.

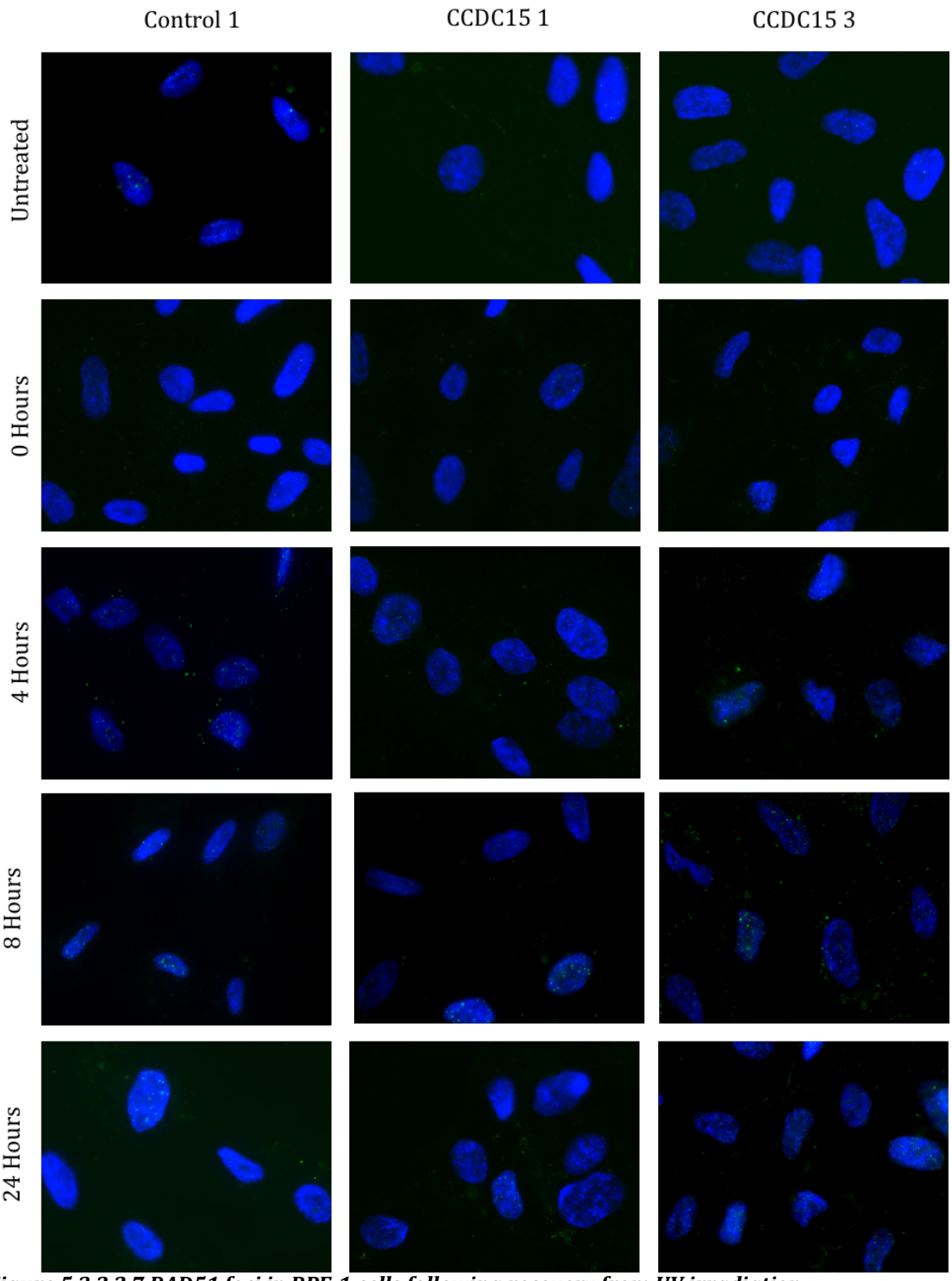

Figure 5.3.2.2.7 RAD51 foci in RPE-1 cells following recovery from UV irradiation.

Representative images of RPE-1 cells transfected with Control 1, CCDC15 1 or CCDC15 3 siRNA and DharmaFECT 1 and grown for 72 hours post-transfection. Cells were either mock irradiated or irradiated with 60J/m² UV light 0, 4, 8 or 24 hours prior to pre-extraction. Cells were incubated with 0.5% Triton X-100 and 3% BSA in PBS for 5 minutes before fixing and staining with an antibody raised against RAD51.

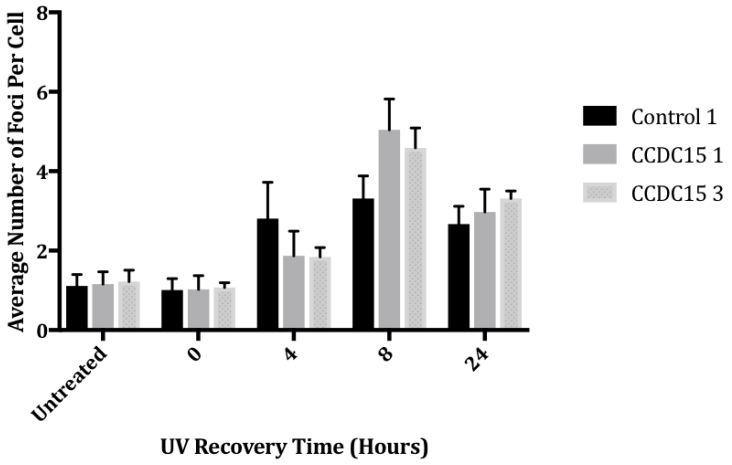

Figure 5.3.3.2.8 Average number of RAD51 foci in RPE-1 cells following recovery from UV irradiation.

For each condition, the total number of cells were counted and the average number of foci per cell was calculated. Mean values derived from four independent experiments, with their respective SEMs.

5.3.4 Association with DNA Replication and Cell Cycle Progression

5.3.4.1 Activation of the DNA Replication Stress Response

CCDC15 was hypothesised to be involved in the repair of replication impeding lesions due to the genes its expression correlated with in the GSEA. The phenotypes produced by the loss of this gene bear some similarity to those produced when the helicase HELQ is lost in mammalian cells; mainly the sensitivity to MMC and association with RAD51 paralogues apparently independent of the FA pathway (Adelman et al, 2013; Takata et al, 2013). As this protein appears to also be associated with ATR signalling and its loss results in reduced Chk1 phosphorylation (Takata et al, 2013), it was investigated if CCDC15 knockdown resulted in DNA replication stress.

Immunofluorescence analysis was used to determine if gene knockdown resulted in increased RPA2 phosphorylation (pRPA2) at Threonine 21 (T21). The HeLa and RPE-1 cells previously described in the FANCD2 immunofluorescent assay were co-stained for pRPA2 T21 (Fig. 5.3.4.1.1) and the images were then scored for pRPA2 T21 positive nuclei (Fig 5.3.4.1.3).

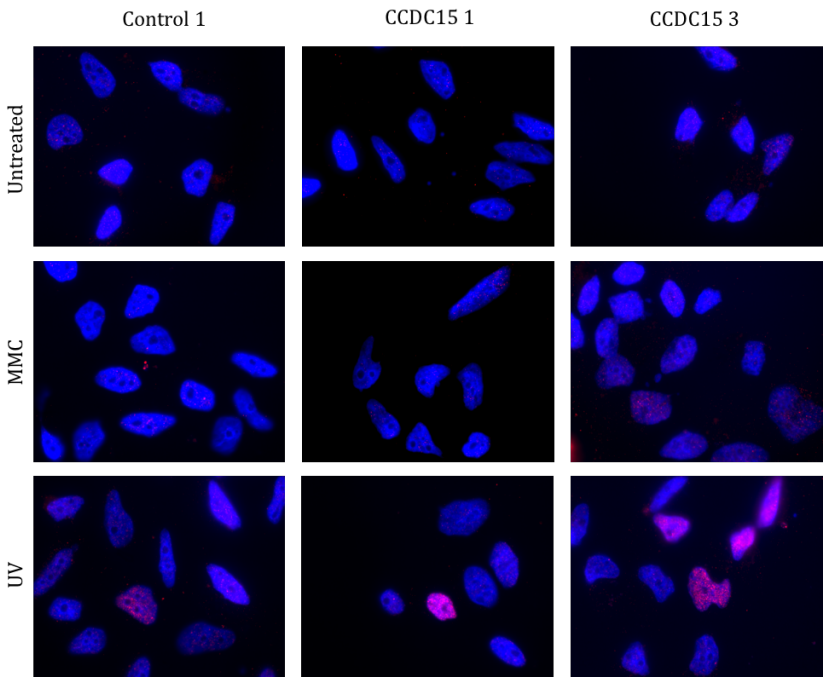

Figure 5.3.4.1.1 RPA2 T21 foci in HeLa cells following CCDC15 knockdown.

Representative images of HeLa cells transfected with Control 1, CCDC15 1 or CCDC15 3 siRNA and DharmaFECT 1 and grown for 72 hours post-transfection. Cells were either mock treated, treated with 80ng/ml MMC for 16 hours or irradiated with 60J/m² UV light 4 hours prior to pre-extraction. Cells were incubated with 0.5% Triton X-100 and 3% BSA in PBS for 5 minutes before fixing and staining with an antibody raised against T21 phosphorylated RPA2.

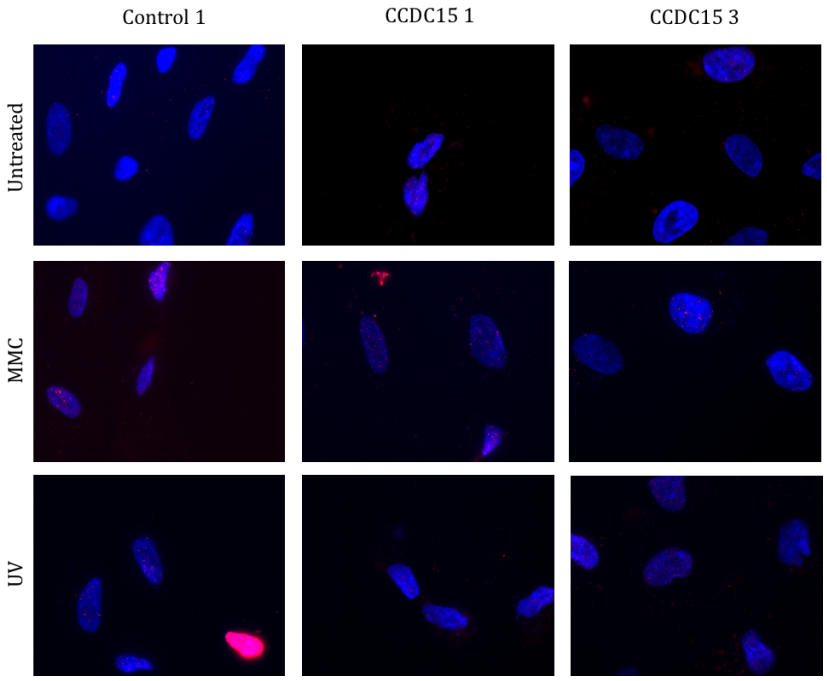

Figure 5.3.4.1.2 RPA2 T21 foci in RPE-1 cells following CCDC15 knockdown.

Representative images of RPE-1 cells transfected with Control 1, CCDC15 1 or CCDC15 3 siRNA and DharmaFECT 1 and grown for 72 hours post-transfection. Cells were either mock treated, treated with 80ng/ml MMC for 16 hours or irradiated with 60J/m² UV light 4 hours prior to pre-extraction. Cells were incubated with 0.5% Triton X-100 and 3% BSA in PBS for 5 minutes before fixing and staining with an antibody raised against T21 phosphorylated RPA2.

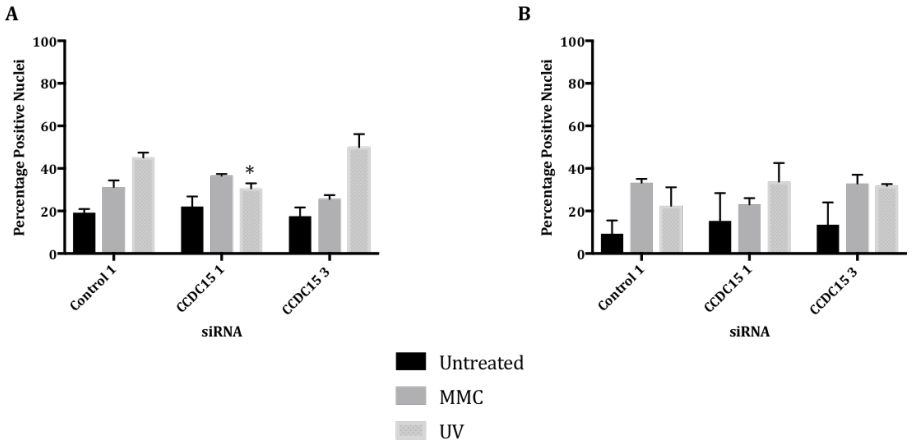

Figure 5.3.4.1.3 Percentage of HeLa and RPE-1 cells positive for pRPA2 T21 foci following CCDC15 knockdown and DNA crosslinking.

(A) HeLa or (B) RPE-1 cells were either mock treated, treated with MMC or UV irradiation. For each condition the number of cells were counted and the percentage of pRPA2 T21 positive nuclei was calculated. A nucleus was considered positive if it contained 10 or more bright foci. Asterisks indicate significant difference from Control 1, p value <0.05. Mean values derived from two independent experiments, with their respective SEMs.

In HeLa cells, the knockdown of CCDC15 alone did not result in an increase in the levels of T21 positive nuclei observed; a very slight trend was seen in RPE-1 cells but the increase was not significant for this set of data. Treating the cells with MMC or irradiating them with UV light also did not increase the levels of replication stress in CCDC15 knocked down cells further than that observed in the Control 1 transfected cells. All of this suggests that CCDC15 is not required for the suppression of replication stress from endogenous or exogenous sources, which implies that it is not essential for the repair of lesions that impeded DNA replication.

5.3.4.2 Replication Associated DNA damage

To determine if the DNA damage caused by the knockdown of CCDC15 was related to DNA replication, the CDK inhibitor Roscovitine was used to prevent S-phase entry (Collis et al, 2007). RPE-1 cells were transfected with Control 1, CCDC15 1 or CCDC15 3 siRNA using DharmaFECT 1 for 72 hours. Four hours prior to pre-extraction the cells were either treated with 10μg/ml Roscovitine or mock treated with DMSO. The cells were then pre-extracted and fixed before staining with γH2AX (Fig. 5.3.4.2.1) and the images were scored for γH2AX positive nuclei (Fig 5.3.4.2.2).

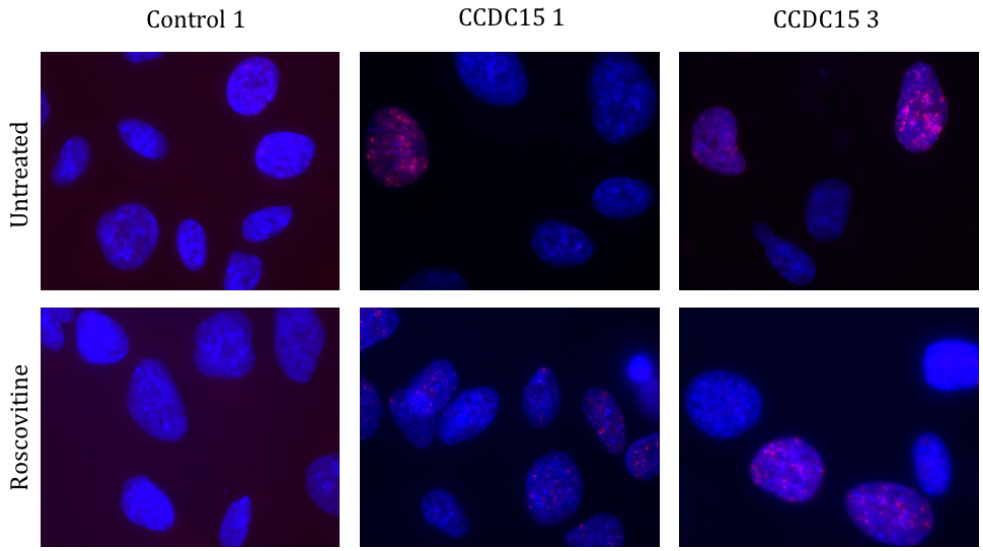

Figure 5.3.4.2.1 DNA Damage in RPE-1 cells following CCDC15 knockdown and Roscovitine treatment.

Representative images of RPE-1 cells transfected with Control 1, CCDC15 1 or CCDC15 3 siRNA and DharmaFECT 1 and grown for 72 hours post-transfection. Cells were either mock treated or treated with 10μg/ml Roscovitine 4 hours prior to pre-extraction. Cells were incubated with 0.5% Triton X-100 and 3% BSA in PBS for 5 minutes before fixing and staining with an antibody raised against γH2AX.

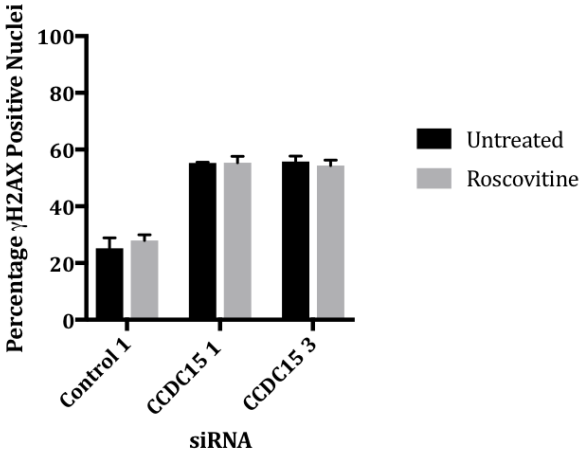

Figure 5.3.4.2.2 Percentage of RPE-1 cells positive for γH2AX foci following transfection with individual CCDC15 siRNAs.

For each condition the number of RPE-1 cells were counted and the percentage of γH2AX positive nuclei was calculated. A nucleus was considered positive if it contained 10 or more bright foci.

As seen previously, the knockdown of CCDC15 significantly increased the percentage of cells positive for γH2AX when compared to Control 1 transfected cells (significance not shown on graph; p-values 0.0081 for Untreated CCDC15 1, 0.0008 Roscovitine CCDC15 1, 0.0018 Untreated CCDC15 3 and 0.0007 Roscovitine CCDC15 3). However, the treatment with Roscovitine did not significantly alter the proportion of cells that displayed γH2AX positive nuclei when compared to the Untreated cells for any siRNA. This suggests that the damage caused by CCDC15 knockdown is not replication associated as it occurs to the same extent in the presence of CDK inhibitors at an incubation time demonstrated to inhibit entry into S phase.

5.3.4.3 Effects Upon Cell Cycle Progression

As part of the characterisation of CCDC15 in potential DNA damage response mechanisms, FACS analysis of propidium iodide (PI) stained cells was used to resolve if the loss of this gene affected cell cycle progression. PC-3, HeLa and RPE-1 cells were transfected with Control 1, CCDC15 1 or CCDC15 3 siRNA using DharmaFECT 1 for 72 hours. Sixteen hours prior to fixation the cells were either treated with 80ng/ml MMC or mock treated with ddH_2O. The cells were trypsinised and fixed in ice cold 70% ethanol before being treated with RNase A and stained with 50μg/ml PI. The stained cells were then analysed by flow cytometry with 10000 cells counted per sample (Fig. 5.3.4.3.1).

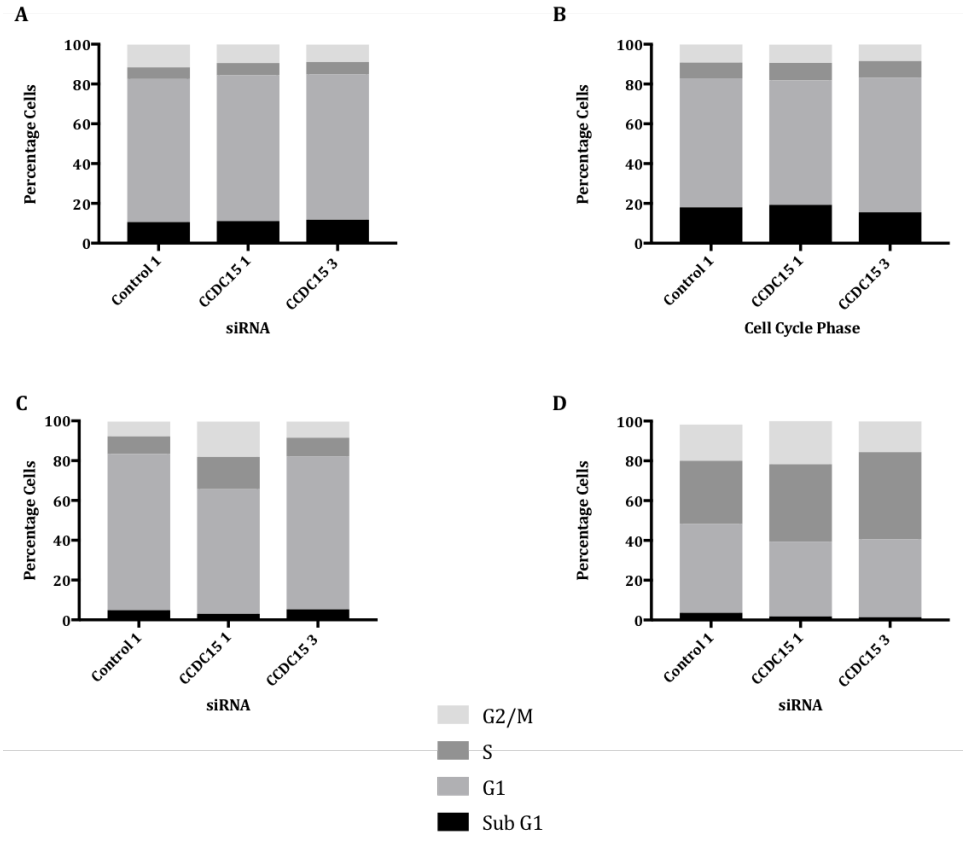

Figure 5.3.4.3.1 Cell cycle distribution of CCDC15 knocked down PC-3 and Hela cells
(A,B) PC-3 and (C,D) HeLa cells transfected with Control 1, CCDC15 1 or CCDC15 3 siRNA and DharmaFECT 1 and grown for 72 hours post-transfection. Cells were either (A,C) mock treated with ddH_2O or (B,D) treated with 80ng/ml MMC 16 hours prior to fixation. Cells were fixed in ice cold 70% ethanol, treated with RNase A and stained with 50μg/ml propidium iodide. Cells were then analysed by flow cytometry, with 10000 cells analysed per sample, to determine the DNA content of the cells.

For the RPE-1 cells, not enough cells were repeatedly present in the samples, so the cell cycle profiles generated were not accurate. In the untreated PC-3 cells, the knockdown of CCDC15 had no effect upon the progression of the cells through the cell cycle. In the MMC treated populations, there was an increase in cells in the Sub G1 population, a decrease in the proportion of cells present in G1 and an increase in the percentage of cells in S phase, however, these differences were seen in all MMC treated cells, regardless of the siRNA they had been transfected with, suggesting that CCDC15 loss has little effect on cell cycle progression in the presence of DNA crosslinking agents. In the Untreated HeLa cells, the

loss of CCDC15 also appeared to have little impact on cell cycle progression, with minor differences observed in cells transfected with CCDC15 1 but not CCDC15 3. In the MMC treated populations, there was an increase in the percentage of cells in S and G2/M but again the loss of CCDC15 did not drastically alter the proportions of cells in each phase compared to the Control 1 transfected cells.

The Fluorescence Ubiquitination Cell Cycle Indicator (FUCCI) system allows the direct visualisation of the stage a cell is in within the cell cycle through the fluorescent labelling of the DNA replication factor Cdt1 and the DNA replication inhibitor Geminin. This system was used to further investigate the effects of CCDC15 knockdown on cell cycle progression.

One theory as to why the formation of RAD51 foci formation was delayed in the CCDC15 knocked down cells was that it altered the kinetics of the cell cycle following UV irradiation. It was thought that CCDC15-depleted cells could be entering S phase at a slower rate than the Control 1 siRNA transfected cells and therefore initiating HR later. This was investigated using the RPE-1 FUCCI cells, a kind gift from Professor R. Medema (Netherlands Cancer Institute), to assess if the cell cycle distributions were altered following UV irradiation. The cells were plated and transfected with Control 1, CCDC15 1 or CCDC15 3 siRNA using DharmaFECT 1 for 72 hours. Cells were either mock irradiated or irradiated with 60J/m^2 UV light 0, 4, 8 or 24 hours before fixing. The number of G1 (green), G1/S (yellow) and S/G2/early-M (red) cells were then manually counted on using the Nikon Eclipse TE2000 inverted microscope and the proportion of cells within each stage of the cell cycle was calculated (Fig. 5.3.4.3.2).

The loss of CCDC15 did not appear to affect the progression of the cells through the cell cycle following UV irradiation as at all time points, the distribution was very similar to that observed in the Control 1 transfected cells. This implies that is not a postponed entry into S phase that delays the formation of RAD51 foci in the deficient cells following UV irradiation.

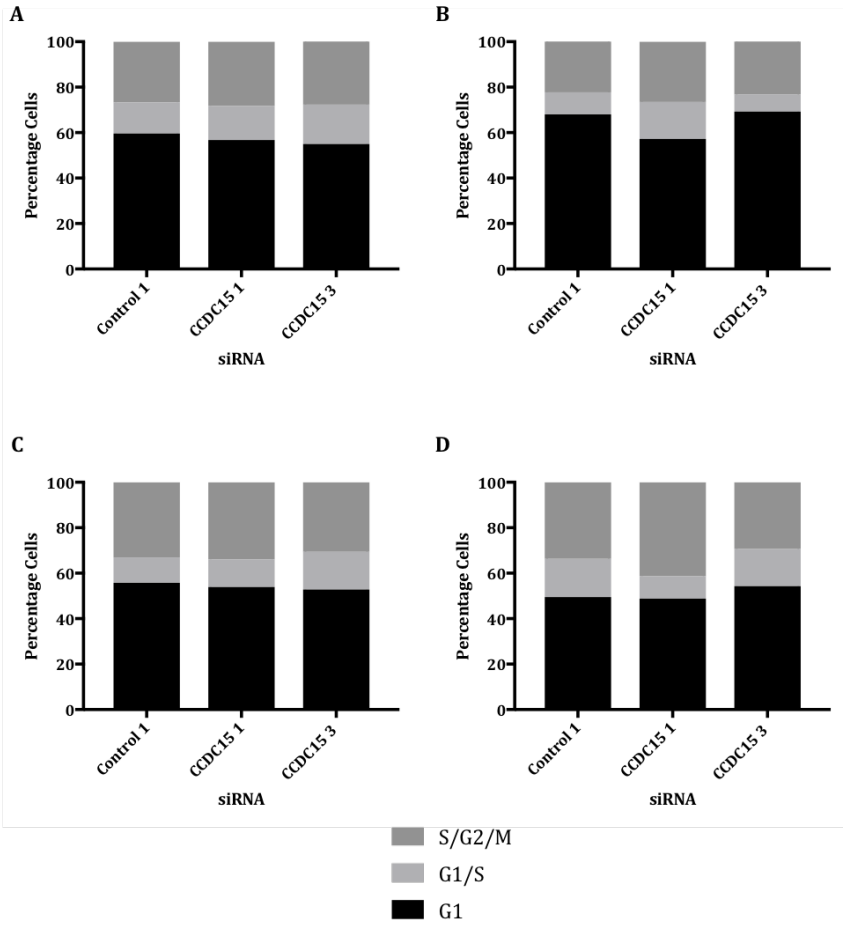

Figure 5.3.4.3.2 Cell cycle distribution of CCDC15 knocked down RPE-1 FUCCI cells following recovery from UV irradiation.

RPE-1 FUCCI cells were trans transfected with Control 1, CCDC15 1 or CCDC15 3 siRNA and DharmaFECT 1 and grown for 72 hours post-transfection. Cells were irradiated with 60J/m² UV light (A) 0, (B) 4, (C) 8 or (D) 24 hours prior to fixation.

The RPE-1 FUCCI cells were also utilised to determine how CCDC15 knockdown affects the re-entry of cells into the cell cycle following reversible cell cycle exit. The cells were plated and 24 hours post-plating, the serum containing media was replaced with that lacking serum to synchronise the cell's cell cycles. The cells were then transfected with Control 1, CCDC15 1 or CCDC15 3 siRNA using DharmaFECT 1. After 60 hours of serum starvation, the cells were released back into serum and fixed immediately or allowed to resume their cell cycles and fixed 12, 16 or 24 hours post-release. The cells were then manually counted as previously and the proportion of cells within each stage of the cell cycle was calculated (Fig. 5.3.4.3.3).

The CCDC15 knocked down cells appeared to re-enter the cell cycle at a slower rate than the Control 1 transfected cells as 12 hours post-release the majority remained in G1. However, by 16 hours post-release the cell cycle distribution of the knocked down cells showed little difference from the Control 1 cells.

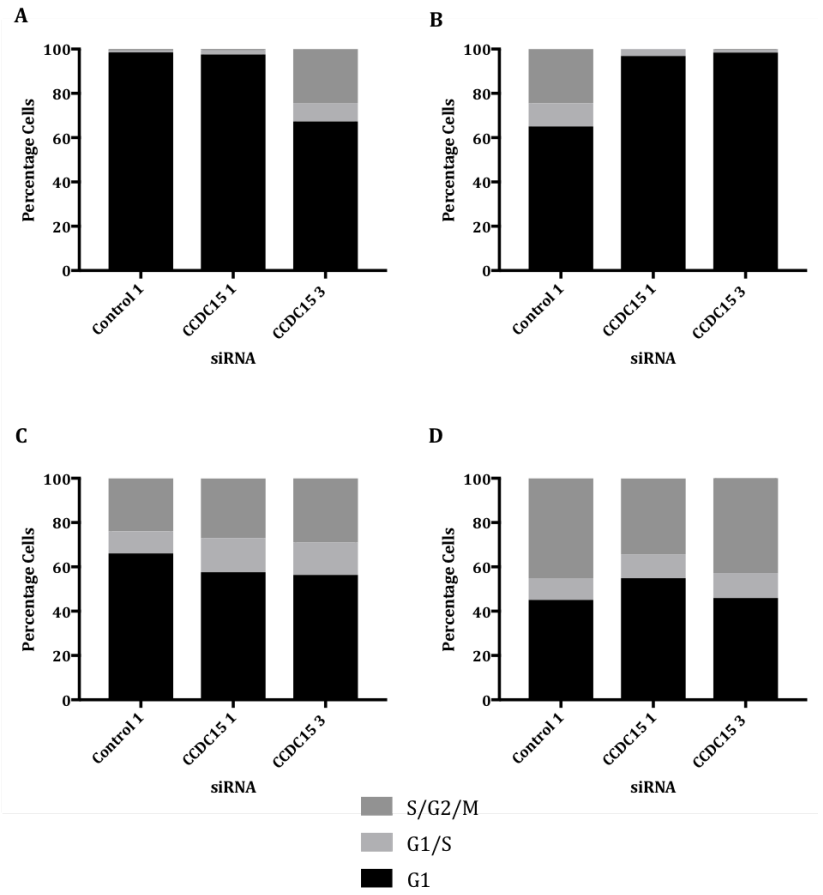

Figure 5.3.4.3.3 Cell cycle distribution of CCDC15 knocked down RPE-1 FUCCI cells.
RPE-1 FUCCI cells were plated and 24 hours post-plating the cell culture media was replaced with fresh media lacking serum. The cells were then transfected with Control 1, CCDC15 1 or CCDC15 3 siRNA and DharmaFECT 1. The cells were grown in the serum free media for 60 hours before release back into serum. The cells were then fixed (A) immediately, (B) 12, (C) 16 or (D) 24 hours following release.

Unfortunately, when this experiment was repeated, the cells did not respond to the serum starvation and so their cell cycle profiles were not synchronised (Fig. 5.3.4.3.4). In the first experiment, the CCDC15 3 transfected cells fixed immediately following release also did not show synchronisation but this was not observed at the 12 hour time point. It is thought that possibly the serum was not all removed from the wells which prevented the synchronisation, however as the experiment was carried out with the same protocol for each replicate, this was considered unlikely. This prevented the further analysis of the delayed re-entry of the cell cycle by CCDC15 knocked down cells as time constraints prevented the repeating of the experiment.

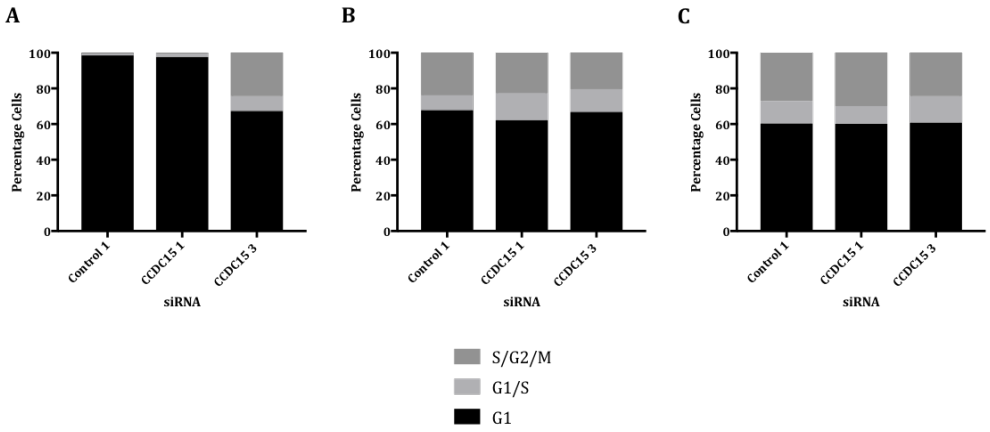

Figure 5.3.4.3.3. Failure of cell synchronisation in RPE-1 FUCCI cells.
(A) Initially the RPE-1 FUCCI cells transfected with Control 1 and CCDC15 1 were almost all in G1 immediately following release from serum starvation. (B,C) However, when this experiment was repeated, the cells failed to synchronise in G1.

5.4 Discussion

A coiled coil is a superhelical domain containing multiple (2-7) α-helices (UniProt, 2016) and proteins containing these domains are involved in gene transcription (Guo et al, 2015), vesicle transport, cytoskeletal formation and motility (Burkhard et al, 2001). They are also involved in the repair of DNA damage as BRCA1 interacts with PALB2 via coiled coil domains (Zhang et al, 2009) and several coiled coil domain containing (CCDC) proteins were identified in a RNAi screen searching for genes whose knockdown increased γH2AX formation (Collis, unpublished). This included the then uncharacterised CCDC13, which has since been classified as a centriolar satellite protein that is required for the maintenance of genome stability during mitosis (Staples et al, 2014). The list of remaining uncharacterised proteins (which included a number of CCDC proteins) identified as hits within this screen were assessed by GSEA for functional associations with DNA repair genes.

To validate this approach, the GSEA were carried out using a list of known DNA repair genes and a list of arbitrary genes not previously identified as involved in DNA repair as positive and negative controls, respectively. All of the known DNA repair genes included in the analysis returned significant enrichment scores. Of the negative control list, only one out of the nine random genes, MGC72080, returned a significant enrichment score. MGC72080 is a read-through transcript of two pseudogenes; CCZIP, a vacuolar trafficking protein homolog and OR7E38P, an olfactory receptor pseudogene (National Centre for Biotechnology Information, 2017) so it is uncertain why expression of this gene would be correlated with that of DNA repair genes. The gene C16orf75 was included in the list of uncharacterised hits, as it was uncharacterised in 2009 when the screen data was generated. Its expression significantly correlated with that of FA pathway components. This gene has since been re-classified as RMI2, a BLM component complex, which has been shown by co-purification to interact with FANCM (Deans & West, 2009; Singh et al, 2008).

As this analysis had correctly identified the test DNA damage repair genes and known DNA repair genes included in the list of uncharacterised hits, it was decided to investigate a number of the proteins predicted by the analysis to be involved in DNA repair. This included the gene CCDC15, whose expression consistently correlated with that of DNA repair genes, suggesting that it may be involved in the maintenance of genome stability. The list of genes whose expression most significantly correlated with CCDC15 contained several components of the FA/BRCA (Fig. 5.4.1), NER (Fig. 5.4.2) and Damage Tolerance pathways as well as proteins involved in DNA replication. Therefore, it was hypothesised that this protein was involved in the detection or repair of replication impeding DNA lesion.

Out of the panel of cell lines examined in this study, CCDC15 shows high levels of mRNA expression in RPE-1 and PC-3 cells and low levels in HeLa cells. These three cell lines were utilised to assess the CCDC15 knockdown phenotype and if this was altered by gene expression level.

The qPCR analysis to determine the optimal transfection time for CCDC15 siRNA was only successfully carried out in PC-3 cells. Despite repeated attempts to determine expression following transfection in HeLa cells, the assay kept returning an "undetermined" result. This was thought to be due to the low endogenous expression level as it takes 37.99 cycles for CCDC15 to be detected in untransfected cells and as the protocol only cycles 40 times, this is very close to the limit of detection. This technique was used to assess gene expression and knockdown, rather than by determining protein expression by western blotting as although there are commercial antibodies available for CCDC15, no satisfactory evidence has been generated that they can detect this protein.

As siRNAs can have off target effects, it is widely accepted that if a phenotype can be generated by several siRNAs targeting different regions of a gene of interest's mRNA, it is considered more likely due to target mRNA knockdown rather than off-target effects. As the initial experiments in this study had been carried out using siRNA pools, it was decided to deconvolute this into its four constituent siRNAs and validate the phenotypes observed.

Another technique to ensure that an observed phenotype is due to the knockdown of the target gene is to carry out rescue experiments (Morita et al, 2012). Knockdown of the endogenous gene is achieved through siRNA targeting the 3' or 5' UTR of the gene of interest in cells exogenously overexpressing said gene. These siRNA do not affect the exogenous gene and so it can be determined if this overexpression can reverse the phenotype induced by the siRNA. The CCDC15 N-terminally tagged vectors generated in Chapter 6 could have been used for these studies, however the siRNA discussed here could not as they did not target the UTR regions of the gene. The lack of these rescue experiments are considered to be one of the main weaknesses of this study.

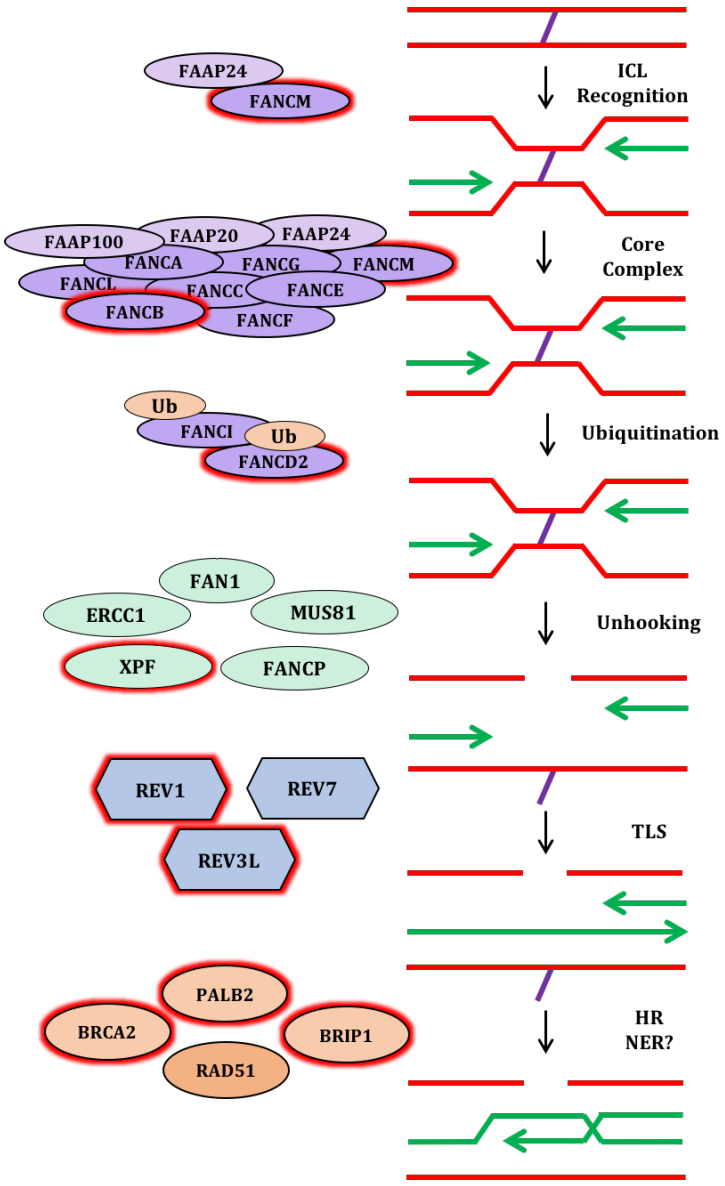

Figure 5.4.1 Interstrand crosslink repair by the Fanconi Anaemia pathway.
Interstrand cross links (ICL- purple) link the two strands of the DNA and prevent them from separating during replication and gene transcription. When two replication forks (green arrows) converge on a ICL, they stall and the ICL is recognised by FANCM and FAAP24. This results in the recruitment of the FA core complex (FANCA/B/C/E/F/G/L and FAAP20/100) which monoubiquitinates FANCD2 and FANCI. These proteins recruit nucleases such as FAN1, MUS81, ERCC1, XPF and FANCP to incise the DNA and unhook the ICL. The lesion can then be bypassed by the translesion synthesis polymerases REV1, REV7 or REV3L and it is possible that the ICL is removed by nucleotide excision repair (NER). The double strand break in the opposite strand is then repaired by homologous recombination (HR) mediated by RAD51, BRCA2, PALB2 and BRIP1. Genes located in the list of top 30 genes whose expression correlated with that of CCDC15 are highlighted red.

Knockdown of CCDC15 increased the levels of nuclei positive for the DNA damage marker γH2AX and 53BP1 in all three cell lines under endogenous conditions with both pooled and individual siRNAs. This was encouraging, as it suggested that CCDC15 was really involved in the DNA damage response and it was not a cell line or siRNA specific effect.

However, its loss did not increase the levels of foci observed following MMC treatment or UV irradiation when compared to proficient cells. This is despite the fact that the same

dose of MMC (80ng/ml) showed significant sensitisation of RPE-1 cells and decreased growth of PC-3 cells in the MTT assay. The immunofluorescence results following MMC and UV are not necessarily incompatible with those reported in the MTT assays, as even though DNA crosslinking agents failed to dramatically increase the levels of DNA damage observed at these time points, the cells in the MTT assay were in contact with the crosslinking agents for a much longer time period. The MTT assays were also measuring the percentage of cells that grew in the presence of the agents, which cannot be achieved using γH2AX and 53BP1 immunofluorescence, as it is not possible to know how many cells have been lost over the course of the experiment.

Alkaline Comet assays were employed to more directly measure the levels of DNA damage induced by CCDC15 knockdown rather than solely relying on downstream markers. However, despite repeated attempts in all three cell lines, no increase in damage could be observed with either siRNA repeatedly. It was thought that changes in the pH of the EDTA used to generate the unwinding and electrophoresis buffers were resulting in very low levels of Tail induction within the assays. Similar issues were experienced by other members of the Collis lab during this time.

Comparison to previous data produced within the lab highlighted that the assays were not behaving as expected. The Control 1 transfected cells produced much lower Percentage DNA in the Tail and Tail Moment values than in this previous work (Barone et al, 2016; Myers et al, 2016; Staples et al, 2016). When compared to the results produced for EBLN1, whose knockdown induces comparable levels of γH2AX and 53BP1 to CCDC15, the results were much lower (1.2% DNA in the tail compared to 5%) (Myers et al, 2016). An alternative reason as to why the results differed between the CCDC15 and EBLN deficient cells is the type of damage induced by the loss of these genes. As ICLs join strands of DNA together which prevents their separation, this may result in reduced migration of damaged DNA during the electrophoresis stage of the Comet assay. As CCDC15 is believed to be involved in the repair of DNA crosslinks, its loss may result in their accumulation whilst EBLN1 has not been implicated in cross link repair.

As alkali conditions were used in these assays, both single strand breaks and DSBs would have been detected. It would have been beneficial to have repeated the assay using neutral conditions, as these assays only detect DSBs and CCDC15 knockdown increased the percentage of cells positive for 53BP1, which only occurs at DSBs. However, time constraints prevented this. It would also have been beneficial, given the sensitisation of deficient cells to cross linking agents, to assess the effects of CCDC15 loss in a Comet assay modified for the purpose of detecting ICLs. In this assay, a defined dose of IR that induces SSB is utilised following lysis to break the DNA strands allowing the DNA to migrate through the gel, with the presence of ICL retarding the movement through the gel (Wu & Jones, 2012).

Despite the apparent sensitivity of PC-3 cells to MMC in the MMT assay, this was not seen in the Clonogenic survival assay. The plating efficiencies calculated for this cell line were really low (16% for CCDC15 and 9% for CCDC15 3) suggesting that the majority of the replated cells had not formed colonies. It is thought that this remaining population of cells

represented an untransfected population which is why the result is so similar to that seen in the Control 1 transfected cells.

The difficult in re-suspending the RPE-1 cells may have been mitigated by plating a lower number of cells, thus allowing distinct colonies to have formed. However, this was not attempted and instead a different approach to analysing the data was trialled. A 1% solution of SDS was used to dissolve the Methylene Blue stain which was then measured colorimetrically (Scragg & Ferreira, 1991). This method was used to assess MMC and UV sensitivity following CCDC15 knockdown in this cell line. However, knockdown did not appear to sensitise cells to MMC as seen in the MTT assay and increasing the dose of UV irradiation appeared to increase the survival of all three cell populations. It is thought that possibly the size of the colonies was affecting the assay, as large colonies stained more darkly than small colonies. Therefore a few large colonies could produce a similar result to a greater number of small colonies. As there was little confidence in this technique, the assay was not repeated. As a result, it would have been beneficial to repeat the MMC MTT assays with individual siRNAs to see if they produced the same results as the pool but time constraints prevented this.

In the MMC MTT assays, a top concentration of 80ng/ml was used which equates to 239μM MMC. This is much higher than the highest dose used in the MMC Clonogenic assay of 100nM. However, when doses higher than 100nM were trialled, very few CCDC15 knocked down cells survived at either plating density, therefore the top dose had to be limited in this format. It is possible that no effect was seen in the Clonogenic assays as the drug doses were not high enough to see the sensitising effect of CCDC15 knockdown observed in the MTT assays. It may have been possible to use higher drug doses by plating more cells for these doses, as this would have been accounted for during the calculation of the surviving fraction, but this was not attempted.

Loss of CCDC15 did not affect the ubiquitination of FANCD2 nor did it have a dramatic effect upon the levels of FANCD2 foci formed in untreated, MMC treated or UV irradiated cells. It also had little effect on the formation and resolution of foci following UV irradiation suggesting that its loss does not dramatically effect crosslink formation. In contrast, it appeared to delay the formation and the resolution of RAD51 foci during the recovery from UV treatment. This suggests that it may be involved upstream of the loading of RAD51 onto DNA following UV irradiation and therefore may be interacting with the HR machinery downstream of FANCD2.

The delay in the binding of RAD51 to DNA may have been caused by the prolonged binding of RPA, which competes with RAD51 to bind to single stranded DNA (Stauffer & Chazin, 2010). The co-staining of the RAD51 UV recovery cells with the pRPA2 T21 antibody or a total RPA2 antibody was considered but previous difficulties with the RAD51 antibody in the past within the Collis lab prevented these analyses. The UV recovery assay could have been repeated with either the pRPA2 or Total RPA2 antibodies, possibly with some earlier time points, as this protein typically binds more quickly to ssDNA than RAD51. Another possibility was that DNA resection at the DSB ends was delayed, which could have been

investigated through BrdU immunofluorescence or the ER-*Asi*SI system combined with qPCR (Zhou et al, 2014).

As RAD51 binding was perturbed, this may have affected the ability of CCDC15 deficient cells to successfully carry out HR. Several assays are available that directly measure a cells ability to repair DSB by a variety of repair pathways including HR and MMEJ. One such assay is the Traffic Light Reporter (TLR) assay where transfection with the I-SceI endonuclease results in the formation of a functional GFP gene in cells carrying out HR (Schmidt et al, 2015). The TLR assay was kindly sourced from Professor Steve Jackson, but unfortunately, time constraints prevented any of these avenues from being explored.

A lack of RPA phosphorylation following CCDC15 loss and the presence of DNA damage marker foci after treatment with Roscovitine indicates that CCDC15 is not a replication stress suppressor, despite the indication that it is involved in the repair of replication halting lesions. Loss of this gene also had little effect upon cell cycle progression under endogenous conditions, following treatment with MMC or UV irradiation. It did however, appear to delay re-entry into the cell cycle following serum starvation. Cellular mechanisms that govern the exit from a quiescent state are understood poorly but it is thought to be controlled by the Rb-E2F network (Kwon et al, 2017; Wang et al, 2017). Modulation of this pathway has been shown to determine how deep the quiescent state of a cell is and so how easily they re-enter the cell cycle (Kwon et al, 2017; Wang et al, 2017). As very few interactions are known for CCDC15 it is unsure whether it may be involved in this pathway in some way and if this is how its loss delays re-entry into the cell cycle. Nevertheless, the effects upon cell cycle re-entry were only observed once and so little judgement can be made about the significance of CCDC15's role in quiescence.

Whilst this work focuses mainly on the involvement of CCDC15 in FA/BRCA pathway and its association with DNA replication, the GSEA highlighted other mechanisms by which its loss may result in genome instability.

Of the top 30 DNA repair genes whose expression correlated well with that of CCDC15, 6 were involved in NER (ERCC4/XPF, GTF2H3, ERRC3/XPB, ERCC8/CSA, LIG3 and ERCC6/CSB). NER is split into two sub-pathways, global genome (gg)-NER and transcription coupled (TC)-NER, that recognise different types of DNA lesions but ultimately result in the recruitment of the same DNA damage repair factors in a core reaction. ERCC8 and ERCC6 are involved in the early stages of TC-NER whilst the remaining 4 genes are involved in the core NER reaction shared by both sub-pathways (Marteijn et al, 2014).

Mutations in NER genes result in three diseases: Cockayne Syndrome (CS) characterised by neurological and developmental abnormalities, Trichothiodystrophy (TTD) characterised by brittle hair/nails and some neurological defects and the cancer susceptibility syndrome Xeroderma Pigmentosum (XP). Most XP patients display sensitivity to crosslinking agents (Murray et al, 2002), compromised repair of UV induced DNA damage and an increased incidence of skin cancers (Kleijer et al, 2008). As CCDC15

has shown some evidence of being involved in the repair/formation of UV induced DNA damage, it is possible that it may interact with components of the NER pathways.

The most commonly used tool to diagnose XP patients it to measure their cell's ability to repair DNA damage following UV irradiation; during this process nascent DNA is synthesised to replace the damaged DNA which is referred to as unscheduled DNA synthesis (USD). Classically, this would have been measured by the incorporation of radiolabelled nucleotides (Lehmann et al, 2011) but this technique has been superceded by the incorporation of EdU and its subsequent fluorescent labelling (Limsirichaikul et al, 2009). This protocol has been adapted to confirm the involvement of candidate DNA repair genes in NER by knocking them down with RNAi and determining their ability to carry out USD (Jia et al, 2015). This modified technique could have been used to resolve if CCDC15 has any involvement in the NER pathway.

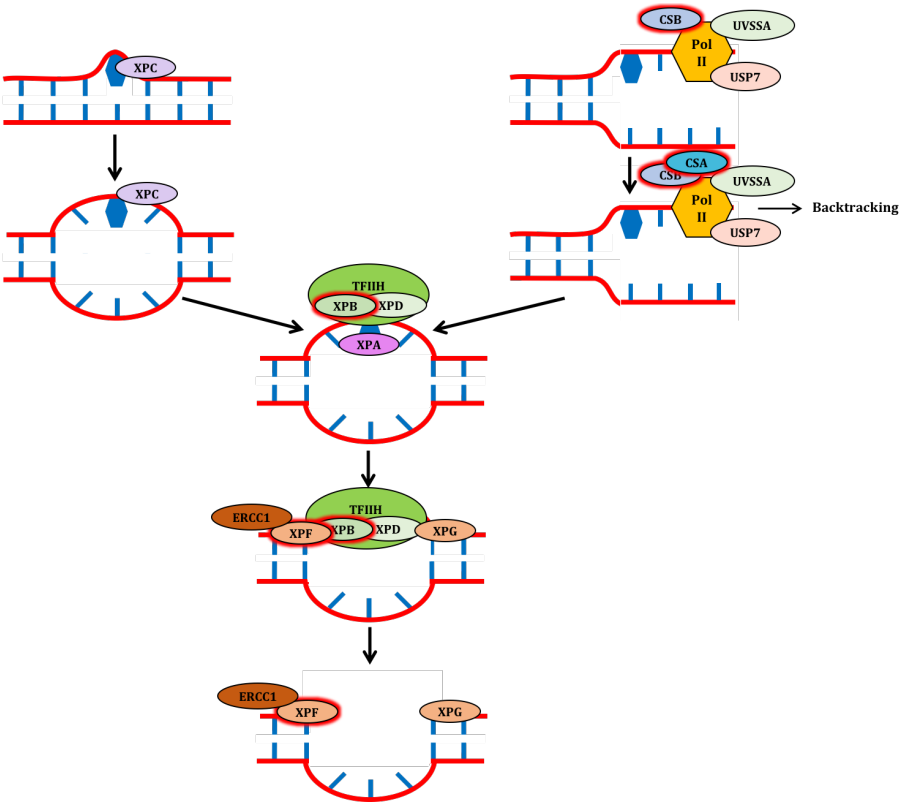

Figure 5.4.2 Nucleotide excision repair pathway

Nucleotide excision repair (NER) removes modified bases that distort the structure of the DNA helix. Global genome NER (left hand pathway) occurs when modified bases are detected by XPC. The binding of this protein to DNA induces local opening which allows for the binding of further NER factors. In transcription coupled repair (right hand pathway) lesions prevent RNA Polymerase II (Pol II) from progressing which results in the binding of CSB, UVSSA and USP7. CSB is bound by CSA and this complex results in the backtracking of the polymerase which facilitates the binding of further NER component. Once the DNA is opened it is bound to by the TFIIH complex, containing the XPB and XPD helicases, which further open the DNA (not depicted). This facilitates the binding of XPG and the XPF/ERCC1 complex which act as the 3' and the 5' endonucleases respectively. These proteins incise the DNA to remove the strand containing the altered base. Genes located in the list of top 30 genes whose expression correlated with that of CCDC15 are highlighted red.

The expression levels of a number of genes involved in Translesion synthesis (TLS) also correlated well with that of CCDC15. These included POLH (DNA Polη), REV1, REV3L (catalytic subunit of DNA Polζ) and POLD3 (accessory subunit of Pol ζ). Both Polη and REV1 belong to the Y family of DNA polymerases, the most copious family of damage tolerance DNA polymerases (Sale et al, 2012) whilst Polζ is a B family DNA polymerase (Waters et al, 2009).

REV1 is only capable of inserting a cytosine opposite an abasic site (Nelson et al, 1996) although its role in TLS is believed to be as a scaffold protein rather than through its catalytic activity (Ross et al, 2005; Waters et al, 2009). In contrast, Polη's catalytic activity is required for the bypassing of UV induced DNA crosslinks (Kannouche et al, 2003) and those induced by Cisplatin treatment (Alt et al, 2007). It has also been shown to accumulate at stalled replication forks (Kannouche et al, 2001) and co-localises with phosphorylated ATM at γH2AX where it is required for efficient phosphorylation of ATM's

substrates, including Chk2 and p53 (Liu & Chen, 2006). Deficiency of Polη results in the variant form of XP (XP-V), which is characterised by defective post-replicative DNA repair (Kannouche et al, 2001) and its loss also results in a decrease in DSB induced HR (Kawamoto et al, 2005). Polζ has been implicated in the development of Cisplatin resistance (Lin et al, 2006), the repair of DSBs via HR in combination with REV1 (Sharma et al, 2012b) and it is proposed to be involved in the repair of DNA crosslinks induced by MMC (Gan et al, 2008).

If CCDC15 was interacting with Polη or Polζ it may explain why its loss resulted in an increase in DNA damage, sensitisation to DNA crosslinks and altered HR dynamics. As Polη forms nuclear foci following UV induced DNA damage (Kannouche et al, 2001), it may have been possible to repeat the UV recovery experiment using an antibody raised against this protein, to see if its recruitment was hindered in CCDC15 knocked down cells. Although Polζ is predicted to localise to the nucleus, no suitable antibody is available for immunofluorescent analysis and so this assay would not be possible. However, co-immunoprecipitation (Chapter 6) would reveal if this protein interacted with CCDC15.

It may also have been beneficial to ascertain how the loss of CCDC15 would affect development which would have allowed comparison to the phenotypes generated by the loss of other DDR genes. This work could have been carried out in Zebrafish, which contain a CCDC15 ortholog (GeneCards, 2017a), by modifying CCDC15 expression with morpholinos. RAD51 mutant Zebrafish have recently been reported to display FA like symptoms after treatment with DNA crosslinking agents (Botthof et al, 2017) and as loss of CCDC15 appeared to affect RAD51 kinetics, it would be interesting to observe if loss of this gene produced a similar phenotype. These models could also be used to compare CCDC15 and NER mutants as the NER pathway is conserved in Zebrafish (Li et al, 2015a; Zeng et al, 2009).

Chapter Six:
CCDC15 Localisation and Interaction Studies

TABLE OF FIGURES 238

6.1 INTRODUCTION 239

6.2 CCDC15 CLONING AND STABLE CELL LINE GENERATION 240

6.2.1 CCDC15 PCR 240

6.2.1.1 ISOLATION OF CCDC15 CDNA FROM CELL LINES 240

6.2.1.2 CCDC15 VECTOR PCR AMPLIFICATION 246

6.2.2 STABLE CELL LINE GENERATION 247

6.2.2.1 TRANSFECTION INTO FLP CELL LINES 247

6.2.2.2 YPF AND FLAG EXPRESSION 247

6.3 CCDC15 SUBCELLULAR LOCALISATION 249

6.3.1 TRANSIENT CCDC15-YFP TRANSFECTION 249

6.3.2 TET INDUCIBLE CCDC15-YPF LOCALISATION 250

6.3.2.1 LOCALISATION IN UNDAMAGED CELLS 250

6.3.2.2. LOCALISATION FOLLOWING DNA DAMAGE 251

6.4 CCDC15 INTERACTION STUDIES 253

6.4.1 CCDC15 IMMUNOPRECIPITATION 253

6.5 DISCUSSION 256

Table of Figures

Figure 6.2.1.1.1 PC-3 cDNA amplified by Gateway Primers using the KOD Hot Start DNA Polymerase kit. 240

Figure 6.2.1.1.2 PC-3 cDNA amplified using less stringent DNA Polymerase kits. 241

Figure 6.2.1.1.3 PC-3 cDNA amplified using the AccuPrime DNA Polymerase kit. 241

Figure 6.2.1.1.4 PC-3 cDNA amplified using the AccuPrime DNA Polymerase Kit with Altered PCR Conditions. 242

Figure 6.2.1.1.5 PC-3 cDNA produced by alternative reverse transcription kits. 243

Figure 6.2.1.1.6 Messenger RNA amplification. 243

Figure 6.2.1.1.7 MDA-231 cDNA amplification. 244

Figure 6.2.1.1.8 MDA-231 and PC-3 RNA amplification. 245

Figure 6.2.1.1.8 MDA-231 and PC-3 RNA amplification with annealing temperature gradient. 245

Figure 6.2.1.2.1 CCDC15 vector DNA amplification 246

Figure 6.2.2.2.1 YFP expression in transfected HeLa FLP Cells 248

Figure 6.2.2.2.2 FLAG Expression in transfected HeLa-FLP and HEK 293-FLP cell lines 248

Figure 6.3.1.1 Transient transfection of CCDC15-YFP into HeLa Cells. 249

Figure 6.3.2.1.1 CCDC15-YFP localisation in HeLa FLP CCDC15 YFP cells following treatment with DNA crosslinking agents. 250

Figure 6.3.2.2.2 Micro-irradiation induced localisation of CCDC15-YFP in HeLa FLP CCDC15-YFP. 252

Figure 6.4.1.1 Small Scale FLAG Immunoprecipitation of HEK 293 FLP CCDC15-FLAG Cells. 253

Figure 6.4.1.2 FLAG Immunoprecipitation of HEK 293 FLP CCDC15-FLAG Cells. 254

Figure 6.4.1.3 FLAG Immunoprecipitation of HEK 293 FLP CCDC15-FLAG Cells with saturated affinity gel. 254

Figure 6.4.1.4 FLAG Immunoprecipitation of HEK 293 FLP CCDC15-FLAG Cells with additional elution. 255

6.1 Introduction

As described previously (Section 5.1), expression of Coiled-coil domain-containing 15 (CCDC15) has been shown to be associated with DNA repair factors using Gene Set Enrichment Analysis (GSEA), in particular those associated with the FA/BRCA, NER and Damage Tolerance pathways. As such, it has been hypothesised to be a novel DNA repair factor involved in the resolution of replication impeding DNA lesions.

The accurate subcellular localisation of CCDC15 has not been clearly defined. Gene Ontology analysis appears to indicate that it is located at centrosomes (UniProt, 2016), however examination of the quoted paper reveals that CCDC15 is not mentioned as one of the predicted novel centrosomal components (Jakobsen et al, 2011). The subcellular localisation database Compartments (Binder et al, 2014) suggests that the cytoskeleton (including the centrosomes) is its most likely location with the plasma membrane and the nucleus being rated as the most unlikely (Binder et al, 2017a). However, it does contain a predicted nuclear localisation sequence, suggesting that it localises to both the nucleus and the cytoplasm (Kosugi et al, 2009).

A number of potential interactors have been reported for CCDC15 in high throughput interaction studies (Table 6.1.1) (GeneCards, 2017a). The resultant STRING network for these shows no interactions between any interactors included in the network (BioGRID, 2017).

Gene Name	Experimental Evidence	Citation
APP	Reconstituted Complex	(Olah et al, 2011)
KIAA0753	Proximity Labelled Mass Spectrometry	(Firat-Karalar et al, 2014)
MEF2A	Affinity Capture Mass Spectrometry	(Li et al, 2015b)
PLK4	Proximity Labelled Mass Spectrometry	(Firat-Karalar et al, 2014)
TRIM44	Affinity Capture Mass Spectrometry	(Huttlin et al, 2015)

Table 6.1.1 Reported Interactors of CCDC15
Interactors of CCDC15 as reported by the BioGrid Interaction Database (BioGRID, 2017).

It was therefore decided to investigate the localisation and interactions of CCDC15 in more detail to determine if any of the interactions predicted by the GSEA were biologically relevant and if it was potentially involved in any DNA damage repair pathways. To achieve this, we generated two N-terminally tagged versions of the CCDC15 protein by Gateway Cloning; one fused with YFP and the other FLAG. These were used to generate stable cell lines with Tetracycline inducible expression of the CCDC15 fusion proteins which were then utilised for subcellular localisation (YFP) and immunoprecipitation (FLAG) with the aim of carrying out mass spectrometry analyses.

6.2 CCDC15 Cloning and Stable Cell Line Generation

6.2.1 CCDC15 PCR

6.2.1.1 Isolation of CCDC15 cDNA from Cell Lines

Initially, attempts were made to isolate CCDC15 cDNA by extracting RNA from PC-3 cells, reverse transcribing this and then amplifying the CCDC15 cDNA by PCR. The Qiagen RNeasy Mini Kit was utilised to extract the RNA from PC-3 cells and this was subsequently reverse transcribed to cDNA using the Applied Biosystems High Capacity RNA-to-cDNA Kit. The CCDC15 Gateway Forward and Reverse primers were used to amplify the cDNA using the KOD Hot Start DNA Polymerase kit, with 200ng cDNA template per reaction, an annealing temperature gradient of 55 - 70°C and a 3 minute extension time. The resultant PCR products were loaded onto a 1% Agarose gel and electrophoresed for 1 hour to separate the products (Fig. 6.2.1.1.1).

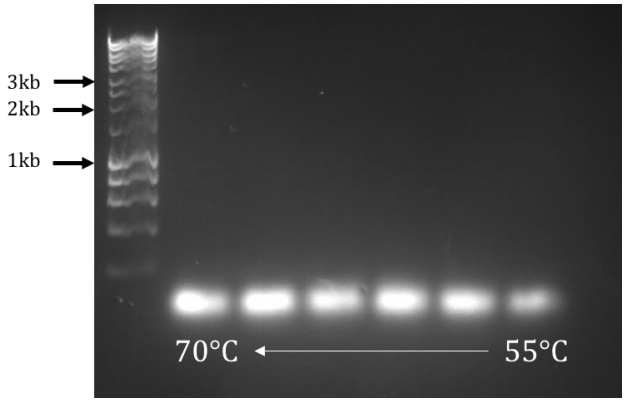

Figure 6.2.1.1.1 PC-3 cDNA amplified by Gateway Primers using the KOD Hot Start DNA Polymerase kit.
PC-3 RNA was extracted using the Qiagen RNeasy Mini Kit and reverse transcribed to cDNA using the Applied Biosystems High Capacity RNA-to-cDNA Kit. This was then amplified using the CCDC15 Gateway Forward and Reverse primers and the KOD Hot Start DNA polymerase kit with a 55 - 70°C annealing temperature gradient and a 3 minute extension time. The PCR products were electrophoresed on a 1% agarose gel. Only primer dimers are visible (predicted CCDC15 cDNA ~3Kb)

At every annealing temperature, only primer dimers could be detected on the agarose gel suggesting that these conditions were not optimal for the amplification of CCDC15 cDNA using these primers. Two new sets of Gateway primers were designed, one set shorter than the original primers and the other longer. The initial amplification experiment was then repeated using the original gateway primers, the short primers, the long primers or the combination of short and long primers (short forward and long reverse or long forward and short reverse). As seen previously, these PCR conditions only produced primer dimers for all primer combinations (data not shown).

In a further attempt to amplify CCDC15 cDNA, normal primers that did not contain the *attB* sites required for Gateway Cloning were used in combination with several less stringent PCR kits; these included the Platinum Hot Start PCR kit, the AccuPrime DNA Polymerase kit and the AccuPrime GC Rich DNA Polymerase kit with Buffer B (cDNA) (Fig. 6.2.1.1.2). The previously isolated PC-3 cDNA was included in these PCR reactions.

In both the Platinum Hot Start and AccuPrime DNA Polymerase reactions only primer dimers were observed on the gel. However, in the AccuPrime GC Rich reactions with the higher annealing temperatures, some product was formed. Nevertheless, these products

were too small to be full length CCDC15 (approximately 3kb). The experiment with this kit was repeated but Buffer A (genomic DNA) was used in the place of Buffer B. (Figure 6.2.1.1.3).

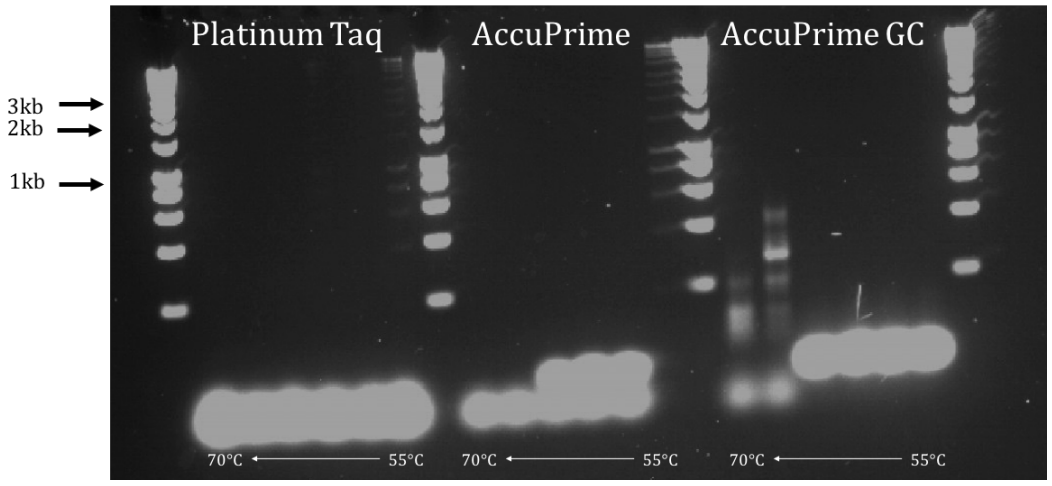

Figure 6.2.1.1.2 PC-3 cDNA amplified using less stringent DNA Polymerase kits.
PC-3 RNA was extracted using the Qiagen RNeasy Mini Kit and reverse transcribed to cDNA using the Applied Biosystems High Capacity RNA-to-cDNA Kit. This was then amplified using the CCDC15 Forward and Reverse primers and either Platinum Hot Start PCR kit, the AccuPrime DNA Polymerase kit or the AccuPrime GC Rich DNA Polymerase kit with Buffer B. A 55 - 70°C annealing temperature gradient and a 3 minute extension time were used. The PCR products were electrophoresed on a 1% agarose gel.

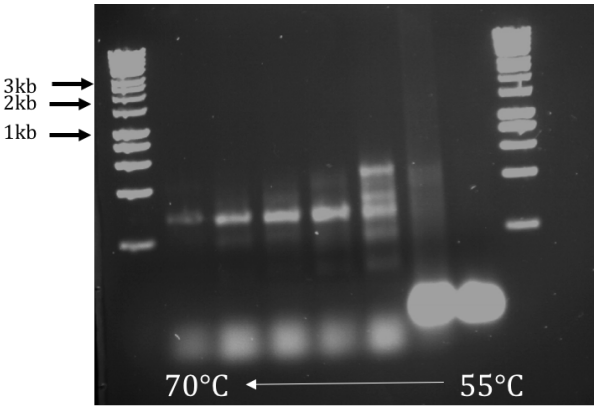

Figure 6.2.1.1.3 PC-3 cDNA amplified using the AccuPrime DNA Polymerase kit.
PC-3 RNA was extracted using the Qiagen RNeasy Mini Kit and reverse transcribed to cDNA using the Applied Biosystems High Capacity RNA-to-cDNA Kit. This was then amplified using the CCDC15 Forward and Reverse primers and the AccuPrime GC Rich DNA Polymerase kit with Buffer A. A 55 - 70°C annealing temperature gradient and a 3 minute extension time were used. The PCR products were electrophoresed on a 1% agarose gel.

With Buffer A, PCR products were seen at all but the lowest annealing temperature, however they were still too small to be full length CCDC15. The decision was made to repeat this experiment but alter the conditions of the PCR reaction; one set of reactions used a 4 minute extension time, whilst another set cycled through the protocol 40 times rather than 35 (Fig. 6.2.1.1.4).

The increased extension time appeared to decrease the levels of PCR product formed whilst the increase in the number of cycle did not increase the size of the products formed when compared to 35 cycles.

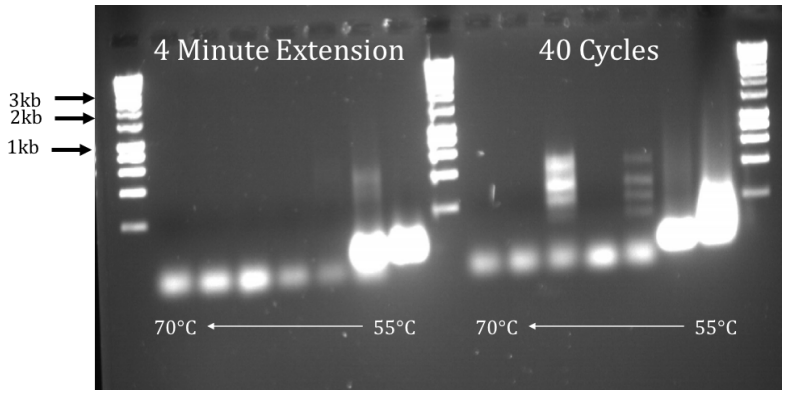

Figure 6.2.1.1.4 PC-3 cDNA amplified using the AccuPrime DNA Polymerase Kit with Altered PCR Conditions.

PC-3 RNA was extracted using the Qiagen RNeasy Mini Kit and reverse transcribed to cDNA using the Applied Biosystems High Capacity RNA-to-cDNA Kit. This was then amplified using the CCDC15 Forward and Reverse primers and the AccuPrime GC Rich DNA Polymerase kit with Buffer A. A 55 - 70°C annealing temperature gradient, a 3 or 4 minute extension time and a 35 or 40 cycle protocol were used. The PCR products were electrophoresed on a 1% agarose gel.

CCDC15 amplification was also attempted using the primers lacking the *attB* sites and the KOD Hot Start DNA Polymerase Kit with a fresh vial of the polymerase. As with the Gateway primers, this kit only produced primer dimers and failed to amplify CCDC15 (not shown).

As a range of different PCR kits and primers had failed to result in the amplification of CCDC15 cDNA other alternative approaches were explored in an attempt to produce a full-length PCR product. As mentioned previously, CCDC15 expression is comparatively low in mammalian cell lines and so it was thought that by altering the reverse transcription or the RNA extraction it may increase the levels of CCDC15 cDNA in the library and thus allow the amplification of the gene.

Three alternative reverse transcription kits, the Bioscript, TaqMan Reverse Transcription Reagents and the RT^2 First Strand kits, were trialled to produce and improved cDNA library. All three of these kits claimed to be able to produce cDNA transcripts longer than CCDC15's approximate 3kb length. The cDNA produced by each kit was amplified by the KOD Hot Start DNA Polymerase with an extension time of 3 minutes and a 55 - 70°C annealing temperature gradient (Fig. 6.2.1.1.5).

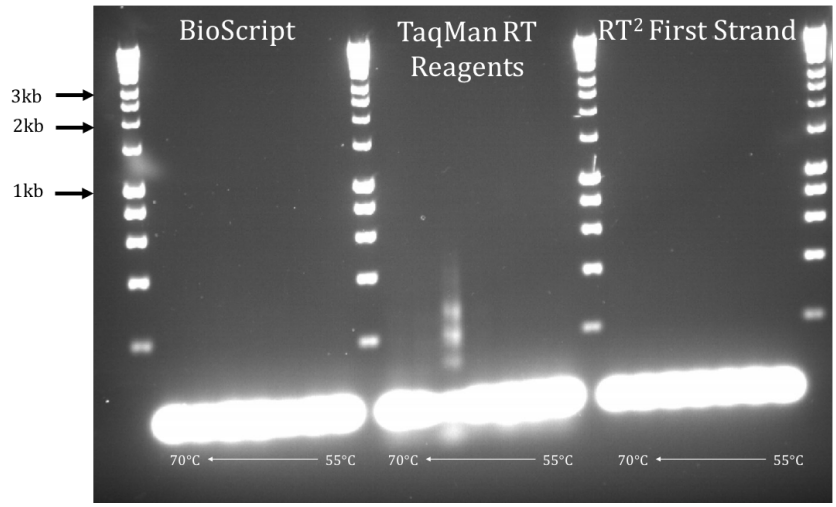

Figure 6.2.1.1.5 PC-3 cDNA produced by alternative reverse transcription kits.
PC-3 RNA was extracted using the Qiagen RNeasy Mini Kit and reverse transcribed to cDNA using either the Bioscript, TaqMan Reverse Transcription Reagents or the RT² First Strand kit. This was then amplified using the CCDC15 Forward and Reverse primers and the KOD Hot Start Polymerase kit. A 55 - 70°C annealing temperature gradient and a 3 minute extension time were used. The PCR products were electrophoresed on a 1% agarose gel.

The alternative reverse transcription kits did not improve the amplification of CCDC15 as only primer dimers were observed on the gel. As a result of this, it was decided to try and extract the mRNA from PC-3 cells. As only the mRNA would be added to the reverse transcription reaction, rather than total RNA, it was thought that this would increase the relative level of CCDC15 mRNA being added to the reaction and therefore increased the levels of cDNA being produced. The mRNA extraction was carried out using the Oligotex Direct mRNA Mini Kit with the resultant cDNA reverse transcribed using the BioScript kit as other users in the lab had successfully used this kit to produce cDNA for PCR. The cDNA was then amplified using the KOD Hot Start DNA Polymerase kit as described previously (Fig. 6.2.1.1.6).

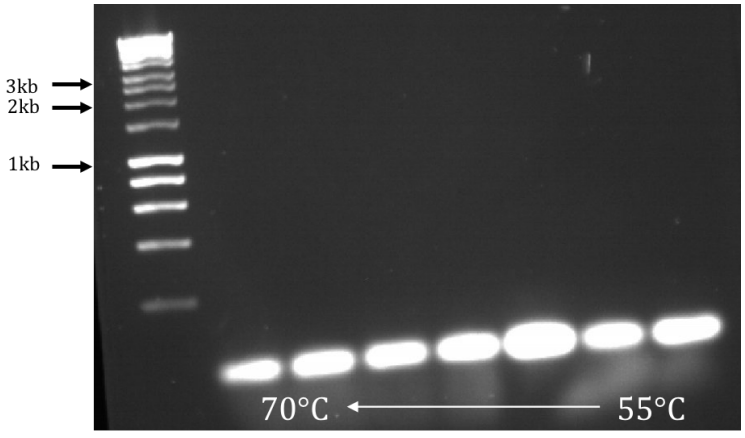

Figure 6.2.1.1.6 Messenger RNA amplification.
PC-3 RNA was extracted using the Oligotex Direct mRNA Mini Kit and reverse transcribed to cDNA using the BioScript Kit. This was then amplified using the CCDC15 Forward and Reverse primers and the KOD Hot Start Polymerase kit. A 55 - 70°C annealing temperature gradient and a 3 minute extension time were used. The PCR products were electrophoresed on a 1% agarose gel.

The mRNA extraction also did not result in the amplification of CCDC15 cDNA as only primers were observed on the gel. As PC-3 cells were failing to yield full length CCDC15, an alternative cell line, MDA-MB-231, was trialled as a source of mRNA. The cells were grown and the RNA was extracted using the Qiagen RNeasy Mini Kit by Mr. A Ganesh. The RNA was reverse transcribed using the BioScript kit and amplified using the KOD Hot Start DNA Polymerase kit by Dr. K. Myers using both the normal and Gateway primers and an annealing gradient of 48 - 72°C (Fig. 6.2.1.1.7).

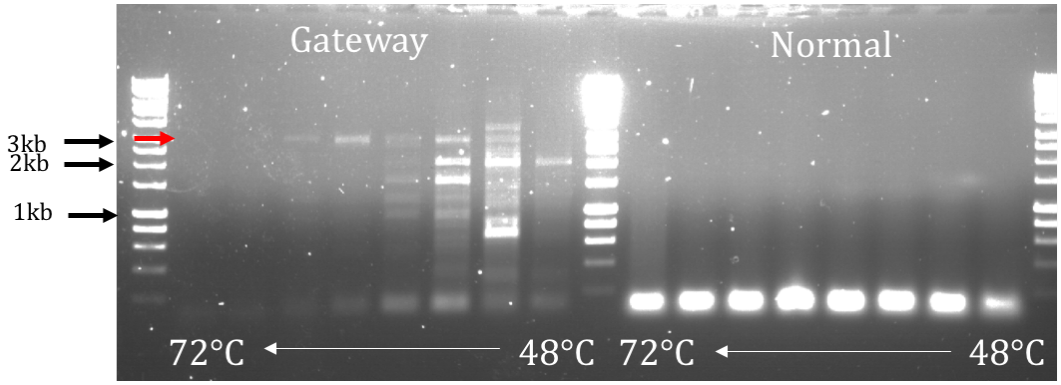

Figure 6.2.1.1.7 MDA-MB-231 cDNA amplification.

MDA-231 RNA was extracted using the Qiagen RNeasy Mini Kit and reverse transcribed to cDNA using the BioScript Kit. This was then amplified using the CCDC15 Normal and Gateway Forward and Reverse primers and the KOD Hot Start Polymerase kit. A 48 - 72°C annealing temperature gradient and a 3 minute extension time were used. The PCR products were electrophoresed on a 1% agarose gel. Red arrow represents 3kb band presumed to be amplified CCDC15 cDNA.

As shown on the gel, the intermediate annealing temperatures produced a 3kb band, presumed to be amplified CCDC15. The 3kb region of the gel was excised by Dr. K. Myers and the DNA was extracted using the QIAquick PCR Purification Kit. This experiment was repeated using the same MDA-MB-231 RNA and a fresh preparation of PC-3 RNA with an annealing temperature of 65°C as this resulted in amplification in Dr. K. Myers' experiment. However, this did not yield any amplification, only primer dimers. The PCR was repeated and as well as the MDA-MB-231 and PC-3 cDNA, the DNA purified from the gel fragment by Dr. K. Myers was also included (Fig. 6.2.1.1.8).

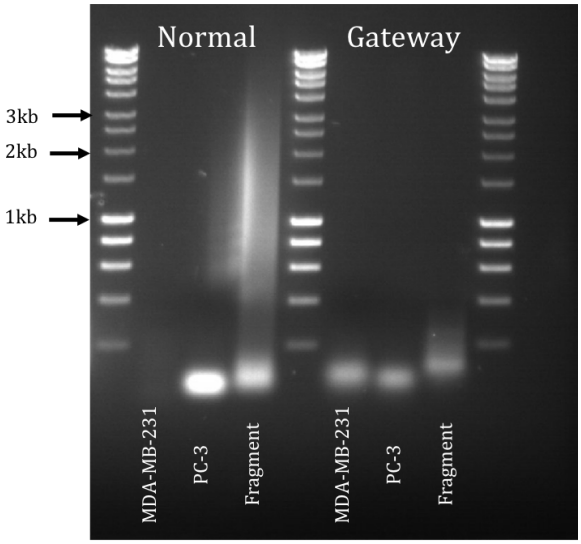

Figure 6.2.1.1.8 MDA-MB-231 and PC-3 RNA amplification.

MDA-231 and PC-3 RNA was extracted using the Qiagen RNeasy Mini Kit and reverse transcribed to cDNA using the BioScript Kit. This, and an MDA-MB-231 cDNA extracted from a previous gel, was then amplified using the CCDC15 Normal and Gateway Forward and Reverse primers and the KOD Hot Start Polymerase kit. A 65°C annealing temperature and a 3 minute extension time were used. The PCR products were electrophoresed on a 1% agarose gel.

Again, the result produced by Dr. K. Myers could not be reproduced in either cell line or with either set of primers. The DNA that had been isolated from the previous gel (Fig. 6.2.1.1.7) could not be re-amplified at this annealing temperature. This prompted a repeat of the experiment but only using the Gateway primers and with an annealing temperature gradient of 65 - 67°C (Fig. 6.2.1.1.9) as these were the two temperatures that produced the clearest 3kb band on Dr. K. Myers' gel.

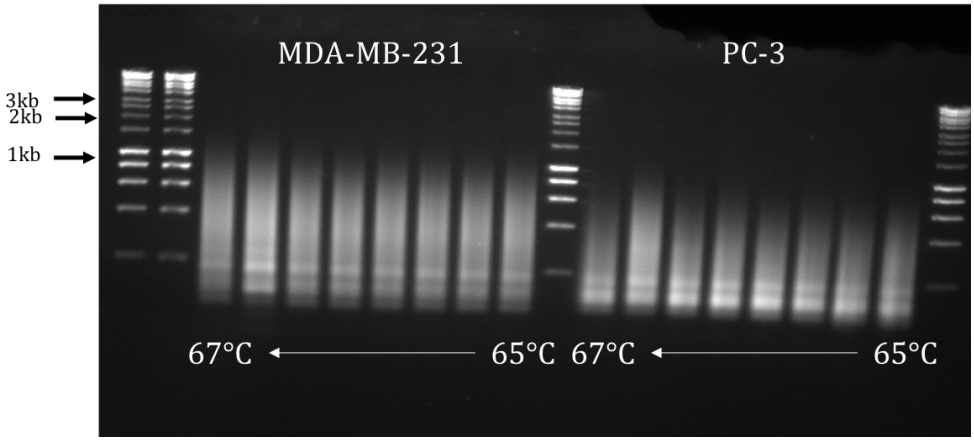

Figure 6.2.1.1.9 MDA-MB-231 and PC-3 RNA amplification with annealing temperature gradient.

MDA-MB-231 and PC-3 RNA was extracted using the Qiagen RNeasy Mini Kit and reverse transcribed to cDNA using the BioScript Kit. This was then amplified using the CCDC15 Normal and Gateway Forward and Reverse primers and the KOD Hot Start Polymerase kit. A 65 - 67°C annealing temperature gradient and a 3 minute extension time were used. The PCR products were electrophoresed on a 1% agarose gel.

None of the annealing temperatures trialled produced amplification of CCDC15 so the PCR was repeated with a wider range of annealing temperatures (48 - 72°C), but as before, no amplification was observed (data not shown).

6.2.1.2 CCDC15 Vector PCR Amplification

As amplification of CCDC15 from cell line derived cDNA libraries had not been possible, a pcDNA3.1+/C-(K)-DYK vector containing CCDC15 cDNA was purchased from GenScript. This vector contained a FLAG-tagged version of CCDC15 and an Ampicillin resistance gene to allow the selection of transformed bacteria. This vector was transformed into DH5α which were subsequently grown on Ampicillin containing agar plates for 16 hours at 37°C. Individual colonies were isolated and added to LB broth containing Ampicillin and incubated at 37°C for a further 16 hours with shaking. A negative control sample, where no vector DNA was included in the transformation reaction, was also plated and no bacterial colonies were formed on the plate. Once the bacteria had been incubated in the LB for 16 hours, the plasmid DNA was isolated using the QIAprep Spin Miniprep Kit which yielded 801ng/µl plasmid DNA.

The plasmid DNA was then amplified using the KOD Hot Start DNA Polymerase kit, with the CCDC15 Gateway primers, an annealing temperature gradient of 60 - 70°C and an extension time of 3 minutes. The PCR products were then separated on a 1% agarose gel (Fig. 6.2.1.2.1).

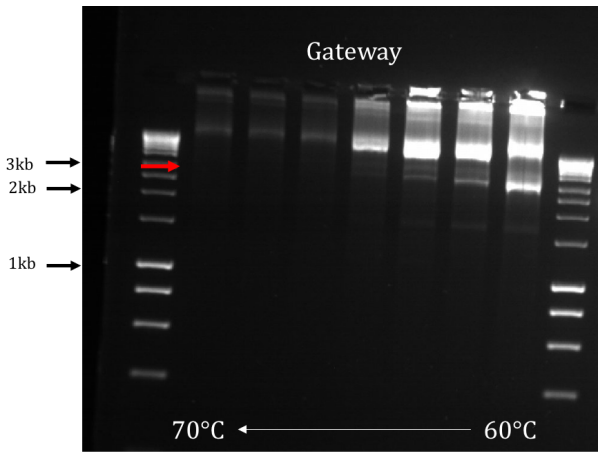

Figure 6.2.1.2.1 CCDC15 vector DNA amplification

CCDC15 Vector was transformed into DH5α and then isolated using the QIAprep Spin Miniprep Kit. The resultant plasmid DNA was then amplified using the CCDC15 Gateway Forward and Reverse primers and the KOD Hot Start Polymerase kit. A 60 - 70°C annealing temperature gradient and a 3 minute extension time were used. The PCR products were electrophoresed on a 1% agarose gel Red arrow represents 3kb band presumed to be amplified CCDC15 cDNA

The highest four annealing temperatures produced no band at 3kb, however, a band was present in the three lowest temperatures (64.8°C, 62.8°C and 60°C). These three bright bands were excised and gel purified using the QIAquick PCR Purification Kit which yielded 62.5ng/µl DNA.

6.2.2 Stable Cell Line Generation

The Gateway cloning method (described 2.2.2.14) was employed to generate N-terminally FLAG tagged and an N-terminally YFP tagged CCDC15 fusion proteins. To carry out the proposed localisation and interaction studies, it was decided to utilise two cell lines, HeLa FLP and HEK 293 FLP, to allow the stable expression of the CCDC15 fusion proteins in a Tetracycline dependent manner. During the generation of these cell lines, the Entry clones generated in the BP reaction were fully sequenced verified to ensure that they did contain CCDC15. Likewise, the Expression clones were sequenced to confirm that the CCDC15 cDNA was in frame with their respective N-terminal tags.

6.2.2.1 Transfection into FLP Cell Lines

The HeLa FLP and HEK 293 cells were plated in 6 well plates for 24 hours before they were transfected with either the CCDC15-YFP or CCDC15-FLAG Expression clone (HEK 293 FLP cells were only transfected with CCDC15-FLAG). These cells were then grown for 24 hours post-transfection before they were transferred into 10cm dished and treated as described in Table 2.1.2.1.2. The cells were then grown for 3 weeks to allow colonies to form before they were transferred into 25cm^2 flasks. Once these had reached confluence, the cells were transferred into 75cm^2 flasks for culturing.

6.2.2.2 YPF and FLAG Expression

Western blotting analysis was used to determine if the transfected cell lines expressed YFP or FLAG at the correct molecular weight to suggest its fusion to CCDC15. CCDC15 has a molecular weight of 110kDa, YFP of 27kDa and FLAG of 1kDa, therefore CCDC15-YFP should be observable at around 137kDa and CCDC15-FLAG at 111kDa. HeLa, HeLa FLP CCDC15-YFP, HeLa FLP CCDC15-FLAG and the HEK 293 FLP CCDC15-FLAG cells were plated in 10cm dishes for 24 hours before the addition of 1μg/ml Tetracycline to induce gene expression (negative control dishes were mock treated with DMSO). The cells were grown for 48 hours in total before media removal and cell lysis. The expression of YFP (Fig. 6.2.2.2.1) and FLAG (Fig. 6.2.2.2.2) was determined in the respective cell lines to ascertain if a band correlating to that of tagged CCDC15 could be observed and if the formation of the band was Tetracycline inducible.

In the untreated HeLa cells, Tetracycline treated HeLa cells or the untreated HeLa FLP CCDC15-YFP cells there was no GFP band that corresponded with the expression of CCDC15-YFP (Fig. 6.2.2.2.1). However, when Tetracycline had been added to the HeLa FLP CCDC15-YPF cells, a GFP band was clearly visible (Fig. 6.2.2.2.1). As with the GFP blot, the addition of Tetracycline did not induce a FLAG band that corresponded with CCDC15-FLAG in the HeLa cells. The same was true in the HeLa FLP CCDC15-FLAG cells suggesting that this cell line did not actually contain CCDC15-FLAG and so work with this cell line was discontinued. In the HEK 293 FLP cells, no FLAG band was present in the untreated population, however, in the cells treated with Tetracycline a band was visible at 110kDa (Fig. 6.2.2.2.2).

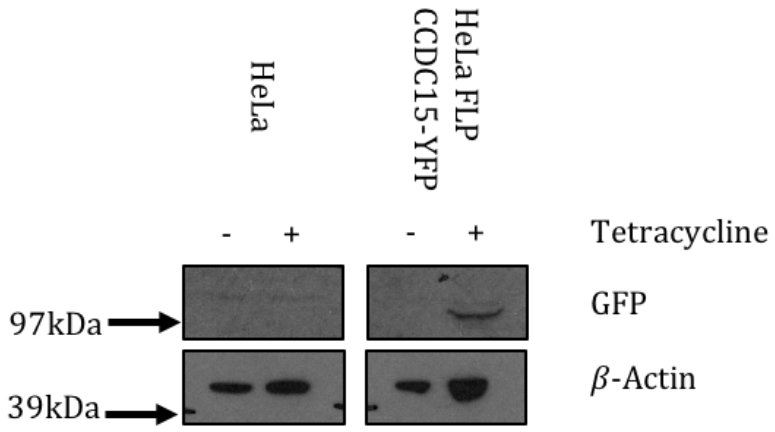

Figure 6.2.2.2.1 YFP expression in transfected HeLa FLP Cells

HeLa and HeLa FLP CCDC15-YFP, cells were plated for 24 hours before either mock treatment with DMSO or treatment with 1μg/ml Tetracycline to induce CCDC15 fusion protein expression. The cells were grown for a further 24 hours before media removal. The cells were lysed and 15μg of protein from each sample was loaded onto a NuPage 4-12% Bis-Tris Gel for separation. The gels were transferred to nitrocellulose membranes before blocking and blotting with GFP and β-Actin primary antibodies. The primary antibodies were detected with HRP conjugated secondary antibodies.

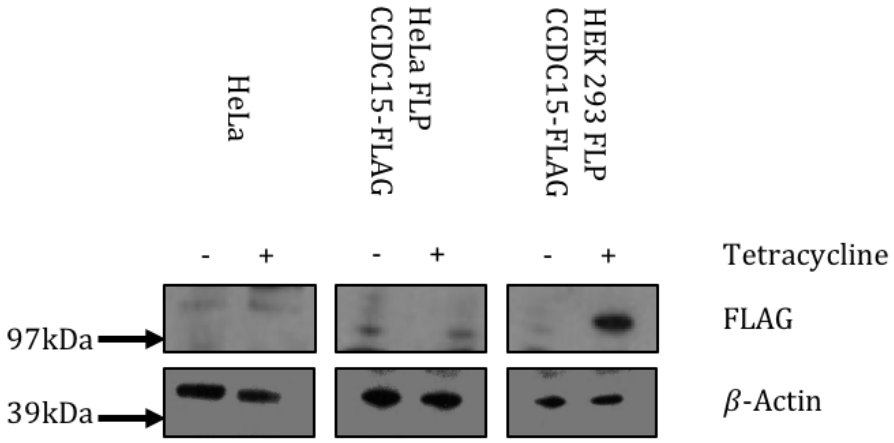

Figure 6.2.2.2.2 FLAG Expression in transfected HeLa-FLP and HEK 293-FLP cell lines

HeLa, HeLa FLP CCDC15-FLAG and HEK 293 FLP CCDC15-FLAG cells were plated for 24 hours before either mock treatment with DMSO or treatment with 1μg/ml Tetracycline to induce CCDC15 fusion protein expression. The cells were grown for a further 24 hours before media removal. The cells were lysed and 15μg of protein from each sample was loaded onto a NuPage 4-12% Bis-Tris Gel for separation. The gels were transferred to nitrocellulose membranes before blocking and blotting with FLAG and β-Actin primary antibodies. The primary antibodies were detected with HRP conjugated secondary antibodies.

6.3 CCDC15 Subcellular Localisation

6.3.1 Transient CCDC15-YFP Transfection

Whilst waiting for the generation of the HeLa FLP cells containing CCDC15-FLAG, HeLa cells were transiently transfected with the CCDC15-YFP Expression clone to observe the subcellular localisation of CCDC15. The cells were either transiently transfected with 1µg of the CCDC15-YFP Expression clone and Lipo 2000 or mock transfected with Lipo 2000 alone. The cells were grown for 48 hours post-transfection before they were pre-extracted and fixed. The coverslips were then stained with anti-GFP antibodies (Fig. 6.3.1.1).

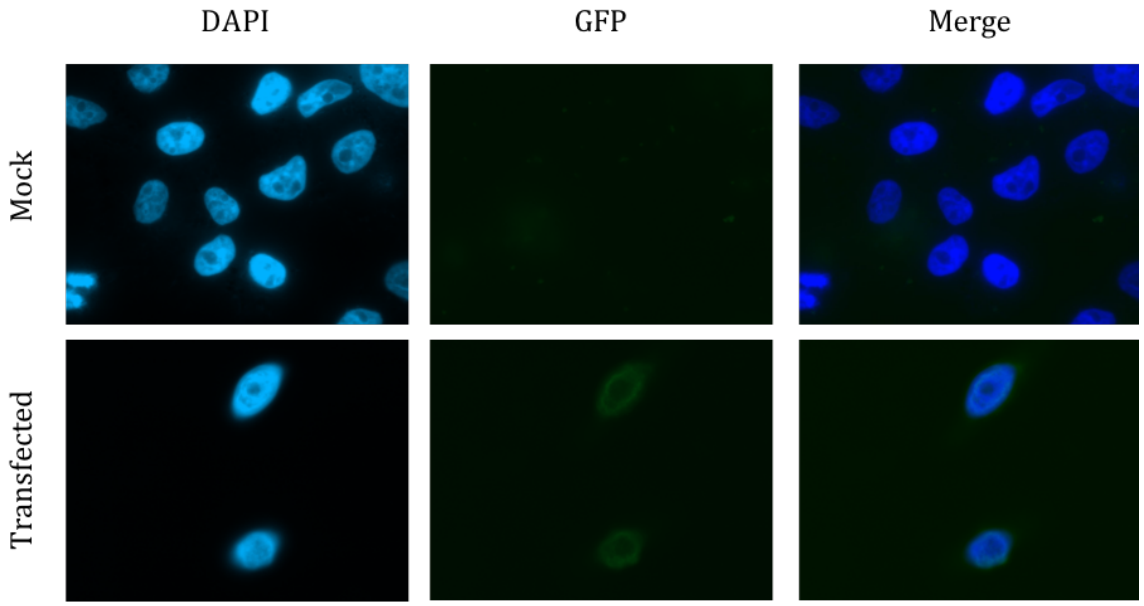

Figure 6.3.1.1 Transient transfection of CCDC15-YFP into HeLa Cells.

Representative images of HeLa cells either transiently transfected with 1µg of the CCDC15-YFP Expression Vector and Lipo 2000 or mock transfected with Lipo 2000 alone. The cells were grown for 48 hours post-transfection before they were pre-extracted, fixed and stained with a primary antibody raised against GFP.

No fluorescent cells could be observed in the mock transfected population whilst cells were observed that contained YFP within the transfected population. However, the transfection efficiency was very low as the majority of the cells did not fluoresce. The cells also looked unhealthy and far fewer remained on these coverslips compared to the untransfected cells. These images were of too poor a quality to determine the subcellular localisation of CCDC15 so the experiment was repeated with the HeLa FLP CCDC15-YFP cells.

6.3.2 Tet Inducible CCDC15-YPF Localisation

6.3.2.1 Localisation in Undamaged Cells

The HeLa FLP CCDC15-YFP cells were plated and 24 hours later the cells were either treated with 1μg/ml Tetracycline or mock treated with DMSO. The cells were grown for 48 hours post-treatment before they were fixed and stained with a GFP antibody (Fig. 6.3.2.1.1).

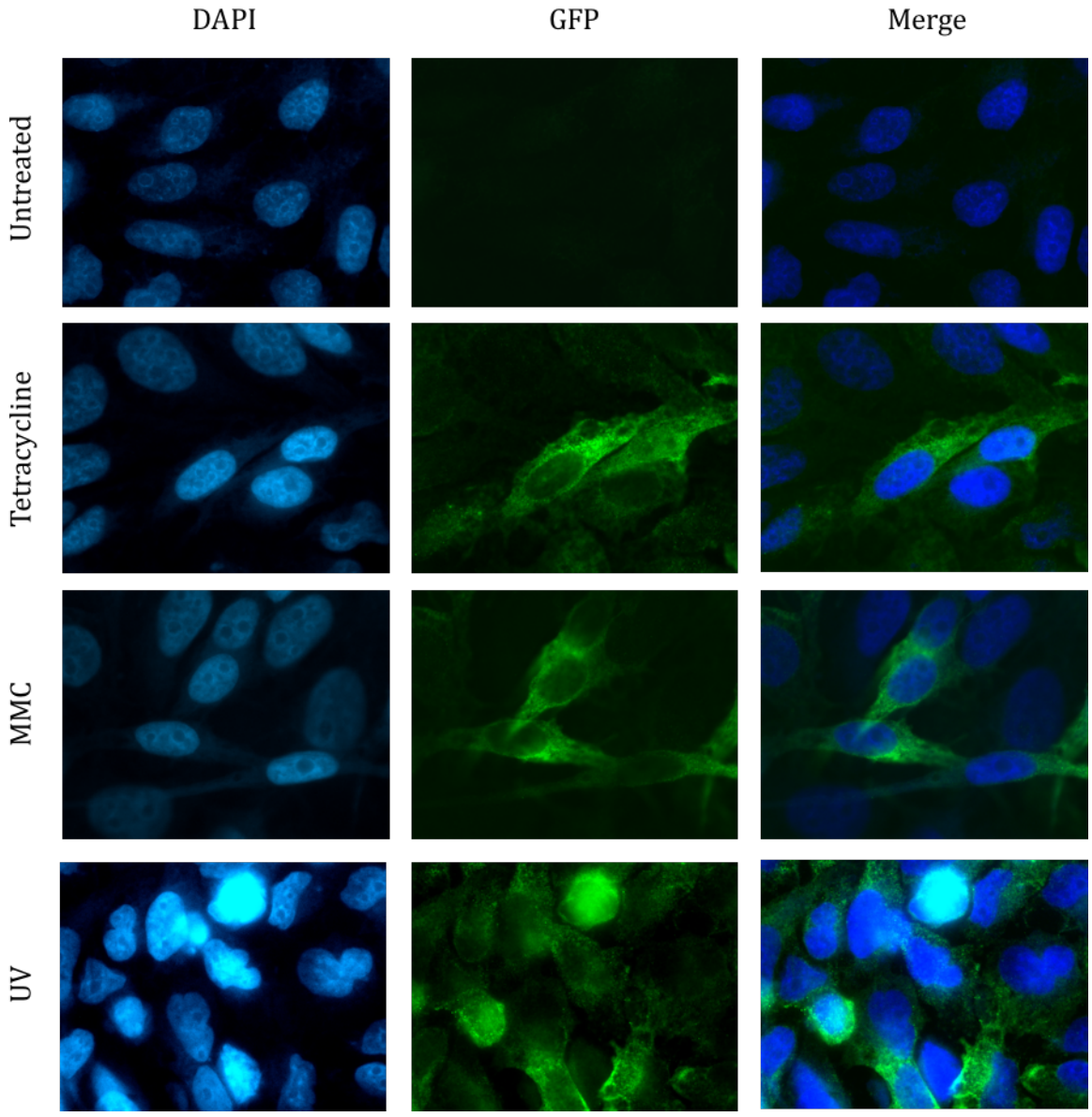

Figure 6.3.2.1.1 CCDC15-YFP localisation in HeLa FLP CCDC15 YFP cells following treatment with DNA crosslinking agents.

Representative images of HeLa FLP CCDC15-YFP cells either treated with 1μg/ml Tetracycline or mock treated with DMSO. The Tetracycline treated cells either received no further treatment or were treated for 16 hours with 80ng/ml MMC or 60J/m² UV for 4 hours prior to pre-extraction. The cells were grown for 48 hours post Tetracycline treatment before they were pre-extracted, fixed and stained with a primary antibody raised against GFP.

As expected, in the cells not treated with Tetracycline there was almost negligible YFP detected. In the Tetracycline treated cells, most cells demonstrated some level of YFP expression with a few cells expressing it highly (Fig. 6.3.2.1.1). The cells appeared to express YFP in the cytoplasm of the cells with very little expression in the nucleus.

6.3.2.2. Localisation Following DNA Damage

To determine if the induction of DNA crosslinks result in a change in the localisation of CCDC15-YFP, the HeLa FLP CCDC15-YFP cells were plated as previously and then the Tetracycline treated cells were either treated with 80ng/ml MMC for 16 hours or 60J/m^2 UV 4 hours prior to fixing (Fig. 6.3.2.1.1). The treatment with MMC or irradiation with UV did not result in a marked change in the localisation of CCDC15-YFP as the majority of the signal was still observed within the cytoplasm.

As MMC and UV had no effect upon the localisation at these time points, it was decided to use a UVA laser to induce DNA damage in live cells and then monitor the localisation of CCDC15-YFP. This technique is used to identify rapid re-localisation of fluorescently tagged proteins and is considered more sensitive than immunofluorescence. The HeLa CCDC15-YFP cells were plated and 24 hours later were treated with 1μg/ml Tetracycline. The cells were pre-sensitised by treating with 10μM BrdU 24 hours before imaging. The cells were imaged before they were irradiated and for 10 minutes following irradiation at 30 second intervals (Fig. 6.3.2.2.2).

Following the induction of DNA damage with the UVA laser, CCDC15-YFP did not appear to re-localise immediately following irradiation or in the 10 minutes post-irradiation. Taken together with the MMC and UV data, this suggests that CCDC15 is located within the cytoplasm and does not exhibit any sub-cellular re-localisation following the induction of DNA damage.

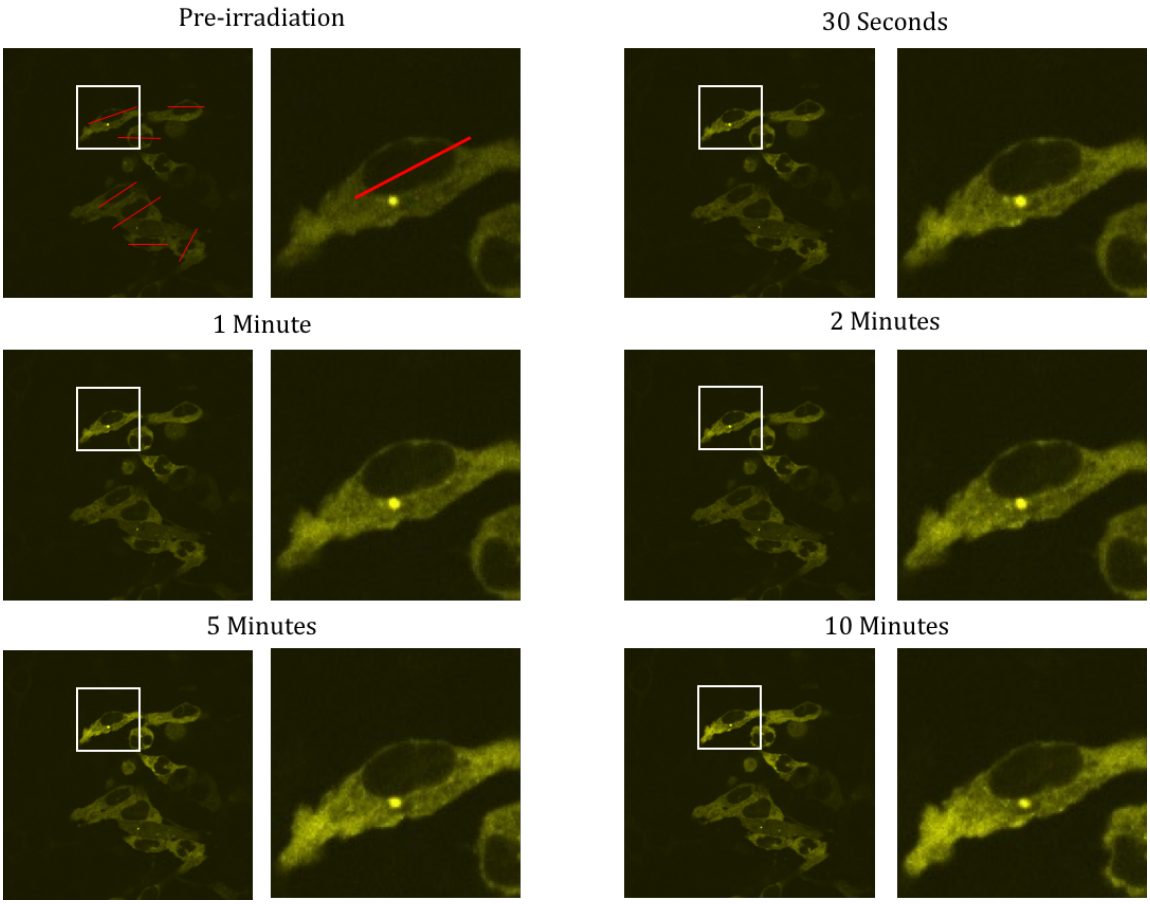

Figure 6.3.2.2.2 Micro-irradiation induced localisation of CCDC15-YFP in HeLa FLP CCDC15-YFP.

Representative images of HeLa FLP CCDC15-YFP cells treated with 1μg/ml Tetracycline, pre-sensitised with BrdU and micro-irradiated with a 405nm UVA laser for 1 second. The cells were imaged prior to irradiation, and for 10 minutes after at 30 second intervals. The red lines in the Pre-irradiation image represent the laser's path through the nucleus.

6.4 CCDC15 Interaction Studies

6.4.1 CCDC15 Immunoprecipitation

The HEK 293 FLP CCDC15-FLAG cells were utilised for the immunoprecipitation of CCDC15. The cells were plated and treated with 1μg/ml Tetracycline or mock treated with DMSO 24 hours after plating. After a total of 48 hours the cells were lysed and the resultant lysates were incubated with ANTI-FLAG M2 Affinity Gel for 16 hours. The samples were then eluted by boiling with the NuPage Loading buffer supplemented with 5mM DTT. The Input (5% total lysate), Unbound and Bound fractions were then separated by electrophoresis and the resultant membrane was blotted with the FLAG M2 antibody (Fig. 6.4.1.1)

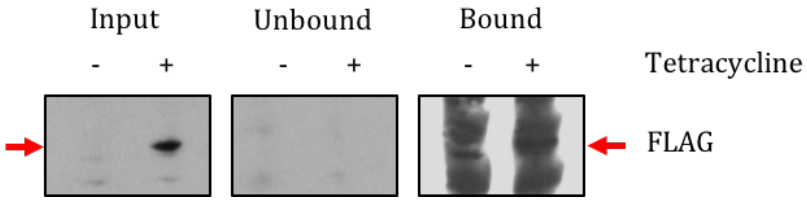

Figure 6.4.1.1 Small Scale FLAG Immunoprecipitation of HEK 293 FLP CCDC15-FLAG Cells.
HEK 293 FLP CCDC15-FLAG cells were plated for 24 hours before being either mock treatment with DMSO or treated with 1μg/ml Tetracycline to induce CCDC15-FLAG expression. The cells were grown for a further 24 hours before lysis. The lysates were incubated with ANTI-FLAG M2 Affinity Gel for 16 hours before elution by boiling with the NuPage Loading buffer supplemented with 5mM DTT. The Input, Unbound and Bound fractions were loaded onto a NuPage 4-12% Bis-Tris Gel for separation. The gels were transferred to nitrocellulose membranes before blocking and blotting with FLAG M2 primary antibodies which were detected with HRP conjugated secondary antibodies. Red arrows represent CCDC15-FLAG molecular weight.

In the Input lanes, a band corresponding to the molecular weight of CCDC15-FLAG was only present in the cells treated with Tetracycline. No bands at this molecular weight were present in the Unbound lanes, suggesting that the CCDC15-FLAG had bound to the gel. As a band at the correct molecular weight could be observed in the Tetracycline treated Bound lane and not in the mock treated lane (Fig. 6.4.1.1) it was decided to scale this experiment up in an attempt to prepare samples for mass spectrometry (Fig. 6.4.1.2).

As seen in the small scale experiment, CCDC15-FLAG was only present in the Input sample treated with Tetracycline. There was a non-specific band just below the CCDC15-FLAG band that was present in both lanes. This was also present in the Unbound fractions but there did not appear to be any CCDC15-FLAG present or remaining bound to the Affinity Gel, suggesting that the protein had been eluted. Whilst a faint band was present at the correct molecular weight in Tetracycline treated 30 minute Elution fraction, the mock treated lane was very dark and so it was not possible to determine whether the band had been induced by Tetracycline. It was therefore decided to repeat the experiment to attempt to elucidate if the band was CCDC15-FLAG. In this experiment, the gel was pre-incubated with the FLAG M2 antibody for 1 hour on ice to saturate it before the lysates were added (Fig. 6.4.1.3).

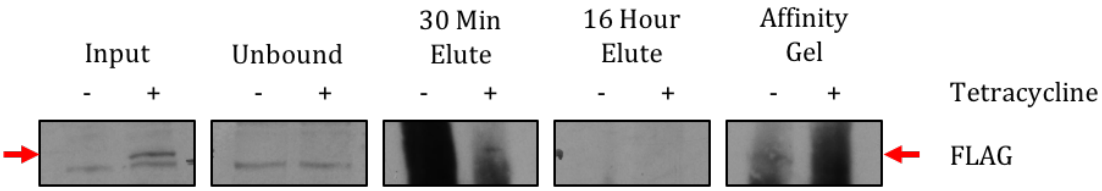

Figure 6.4.1.2 FLAG Immunoprecipitation of HEK 293 FLP CCDC15-FLAG Cells.

HEK 293 FLP CCDC15-FLAG cells were plated for 24 hours before being either mock treated with DMSO or treated with 1μg/ml Tetracycline to induce CCDC15-FLAG expression. The cells were grown for a further 24 hours before lysis. The lysates were incubated with ANTI-FLAG M2 Affinity Gel for 16 hours before elution by incubation with the 3X FLAG Peptide for 30 minutes or 16 hours. The Input, Unbound, remaining Affinity Gel and two eluted supernatant samples were loaded onto a NuPage 4-12% Bis-Tris Gel for separation. The gels were transferred to nitrocellulose membranes before blocking and blotting with FLAG M2 primary antibodies which were detected with HRP conjugated secondary antibodies. Red arrows represent CCDC15-FLAG molecular weight

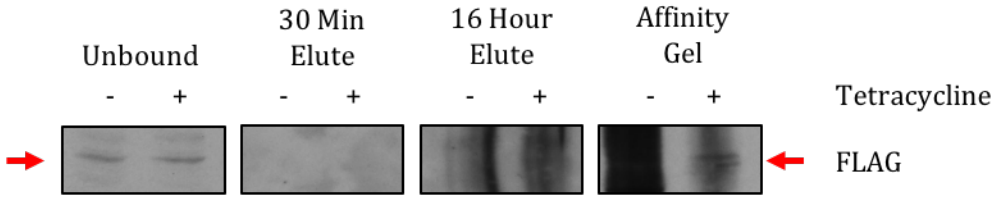

Figure 6.4.1.3 FLAG Immunoprecipitation of HEK 293 FLP CCDC15-FLAG Cells with saturated affinity gel.

HEK 293 FLP CCDC15-FLAG cells were plated for 24 hours before being either mock treated with DMSO or treated with 1μg/ml Tetracycline to induce CCDC15-FLAG expression. The cells were grown for a further 24 hours before lysis. The ANTI-FLAG M2 Affinity Gel was pre-incubated with the FLAG M2 primary antibody for one hour on ice before the addition of the lysates. The lysates were incubated with ANTI-FLAG M2 Affinity Gel for 16 hours before elution by incubation with the 3X FLAG Peptide for 30 minutes or 16 hours. The Input, Unbound, remaining Affinity Gel and two eluted supernatant samples were loaded onto a NuPage 4-12% Bis-Tris Gel for separation. The gels were transferred to nitrocellulose membranes before blocking and blotting with FLAG M2 primary antibodies which were detected with HRP conjugated secondary antibodies. Red arrows represent CCDC15-FLAG molecular weight.

In this experiment, the original lysate was unfortunately not retained as an Input sample, therefore it is uncertain if the addition of Tetracycline induced CCDC15-FLAG expression. There were no bands corresponding with the molecular weight of CCDC15-FLAG present in the Unbound lanes but the non-specific band below the CCDC15-FLAG band was present. There were also no bands visible in either of the two sets of Elution lanes but a faint band was present in the Tetracycline treated affinity gel lane. However, this band was much fainter than would be expected if all of the protein had been retained on the gel.

As the protein was still not present in the Elutates, the experiment was repeated without the pre-incubation of the gel but with an additional half hour incubation with the FLAG peptide between the initial and overnight incubations. The first wash of the gel following lysate incubation was also retained for electrophoresis (Fig. 6.4.1.4).

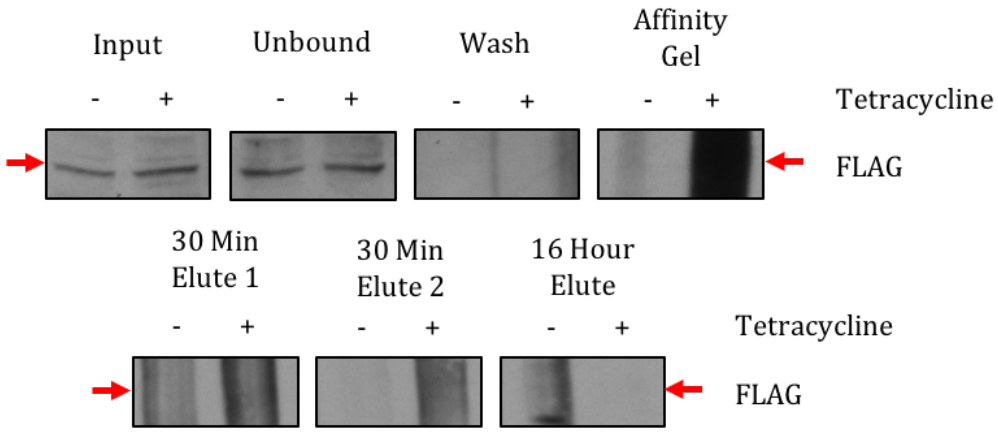

Figure 6.4.1.4 FLAG Immunoprecipitation of HEK 293 FLP CCDC15-FLAG Cells with additional elution.

HEK 293 FLP CCDC15-FLAG cells were plated for 24 hours before being either mock treated with DMSO or treated with 1μg/ml Tetracycline to induce CCDC15-FLAG expression. The cells were grown for a further 24 hours before lysis.. The lysates were incubated with ANTI-FLAG M2 Affinity Gel for 16 hours before elution by incubation with the 3X FLAG Peptide for 30 minutes (carried out twice) or 16 hours. The Input, Unbound, first wash, remaining Affinity Gel and three eluted supernatant samples were loaded onto a NuPage 4-12% Bis-Tris Gel for separation. The gels were transferred to nitrocellulose membranes before blocking and blotting with FLAG M2 primary antibodies which were detected with HRP conjugated secondary antibodies. Red arrows represent CCDC15-FLAG molecular weight.

In this experiment, CCDC15-FLAG was not induced by Tetracycline, despite a new preparation of the drug being used for this experiment. It was therefore, not surprising that no bands corresponding to the protein appeared in the Unbound, Wash, Affinity Gel or Eluted fractions (Fig. 6.4.1.4).

It was decided to determine if the HEK 293 FLP CCDC15-FLAG were still expressing the CCDC15-FLAG fusion gene by repeating the experiment carried out in section 6.2.3.2. However, the current vial of the FLAG M2 primary antibody had been expended. An old vial of the antibody was used but this produced a very faint blot and no bands corresponding to CCDC15-FLAG were observed (data not shown). It was decided to validate this blot by carrying out qPCR analysis to determine if the expression of CCDC15 changed following Tetracycline addition. The HEK 293 FLP CCDC15-FLAG cells were plated and 24 hours later 1μg/ml Tetracycline was added. After a further 24 hours the cells were then lysed, shredded and had their RNA extracted before it was reverse transcribed. The resultant cDNA was amplified by PCR using TaqMan probes for GAPDH and CCDC15 (Table 6.4.1.1).

Treatment	Probe	Mean Ct Value	Delta Ct
Untreated	GAPDH	12.87	15.68
	CCDC15	28.55	
Tetracycline	GAPDH	13.04	15.66
	CCDC15	28.70	

Table 6.4.1.1 CCDC15 RNA expression in HEK 293 FLP CCDC15-FLAG cells.
HEK 293 FLP CCDC15-FLAG cells were plated and 24 hours later treated with Tetracycline or mock treated with DMSO. After a further 24 hours the cells were lysed and their RNA was extracted. The RNA extracts were reverse transcribed and the resultant cDNA was amplified using TaqMan probes against GAPDH and CCDC15. The resultant Ct values were used to calculate the Delta Ct values for each cell line.

As demonstrated by the Delta Ct values, no difference in the expression of CCDC15 could be detected between the two populations. If the cells were still expressing CCDC15-FLAG in a Tetracycline inducible manner, the Ct value for CCDC15 should have decreased as should have the Delta Ct value for the Tetracycline treated cells. However, this was not the case and so it was concluded that the cells were unfortunately no longer expressing this fusion protein.

6.5 Discussion

Little work has been carried out regarding the localisation and interactors of CCDC15, which is suggested to be involved in the DNA damage response. It has been reported to be localised to the centrosomes (UniProt, 2016), however further investigation of the cited paper reveals that it is not the case (Jakobsen et al, 2011). The nucleus is rated as one of the most unlikely regions of the cell for CCDC15 to localise to by the database Compartments (Binder et al, 2017a), however it does contain a strongly predicted nuclear localisation sequence (Kosugi et al, 2009). Several interactors have also been identified in high throughput studies, however none of these proteins share a function or interact with each other (BioGRID, 2017; GeneCards, 2017a). Efforts were therefore made to elucidate the subcellular localisation and interactors of this protein through the generation of N-terminally tagged fusion proteins.

Initial attempts were made to isolate CCDC15 cDNA from the PC-3 and MDA-MB-231 cell lines using several PCR kits. These two cell lines were chosen as they were reported to have high expression levels of CCDC15 in The Human Protein Atlas (Uhlén et al, 2015). However, this proved unsuccessful, most likely due to the low levels at which this gene is expressed even in these comparatively highly expressing cell lines. Instead, a pcDNA3.1^{+}/C-(K)-DYK vector containing CCDC15 cDNA was acquired and this cDNA was amplified using the Gateway primers. This *attB* flanked DNA was then used to produce CCDC15-YFP and CCDC15-FLAG Expression Clones via the Gateway cloning method.

These vectors were stably incorporated into the HeLa FLP and HEK 293 FLP cell lines. At the first attempt, the stable cell line generation was unsuccessful for the HEK 293 FLP cells and had to be repeated. In the HeLa FLP cells, CCDC15-YFP incorporation could be detected but not that of CCDC15-FLAG. It is thought that because all of the colonies that had formed following the stable cell line generation were pooled and grown collectively, a heterogeneous population of cells were created. Some colonies may have originated from

cells that managed to incorporate the Hygromycin resistance gene without the CCDC15-FLAG gene, or epigenetically silenced CCDC15 expression, and these could have outcompeted those that had incorporated the gene correctly. Unlike the HeLa FLP cells, the HEK 293 FLP cells did express CCDC15-FLAG and so these cells were maintained.

Before the stable cell lines were generated, the CCDC15-YFP Expression clone was transiently transfected into HeLa cells. However, the transfection efficiency was very low and expression of the gene detrimentally affected the cells, most likely due to the large size of the fusion gene. No fluorescent cells were observed in the mock transfected population whilst a few of the cells remaining in the transfected population faintly fluoresced. Due to the poor levels of transfection and the faintness of the fluorescence, these images could not be used to judge the subcellular localisation of the fusion gene.

In the HeLa FLP CCDC15-YPF expressing cells YFP was undetectable in untreated cells whilst Tetracycline induced CCDC15-YFP expression throughout the cytoplasm. No bright dots or structures could be determined that suggested it was localising to the cytoskeleton or the centrosomes. MMC and UV treatment produced little redistribution of the YFP signal, although a few cells did appear to have nuclear YFP following UV. However, as these images were not taken on a confocal microscope it is not entirely clear if the YFP signal was within the nucleus or located above the nucleus in the cytoplasm. As these images were taken several hours after the induction of DNA damage it was decided to irradiate the cells with a UV laser and monitor CCDC15-YFP localisation immediately following DNA damage. However, CCDC15-YFP did not re-localise in the 10 minutes immediately following damage suggesting that CCDC15 remains in the cytoplasm.

One possibility is that overexpression of this fusion gene resulted in its mis-localisation within the cell and its accumulation in the cytoplasm or that the protein products formed aggregates in the cytoplasm. However, the latter is considered unlikely as the fluorescence appears to be distributed evenly throughout the cytoplasm in the majority of the cells. If the HeLa FLAG-CCDC15 cells had formed correctly, it could have been possible to determine the localisation of CCDC15 using an anti-FLAG antibody for immunofluorescence. This could not be carried out in the HEK 293 FLP cells as this cell line is not amenable for this procedure. This would have determined if the YFP tag was affecting CCDC15 localisation. Another possibility is that the N-terminal location of the tag was affecting its localisation, possibly due to disruption of its secondary structure or its binding to an interacting protein. To rule out this possibility, a C-terminally tagged version of the protein could have been generated.

To determine that the YFP expression induced by Tetracycline addition was due to CCDC15-YFP expression, the cells could have been transfected with the CCDC15 siRNA investigated in Chapter 5. As these siRNA targeted the main body of the gene they would also have knocked down the overexpressed version.

However, if CCDC15 truly does reside in the cytoplasm, it is not alone as several other genes that affect DNA repair have also been located there. Several repair factors and checkpoint genes localise to the centrosomes throughout the course of the cell cycle

including ATM, ATR, Chk2, Chk1, BRCA1 and Centrin 2. The role that ATM, ATR, and Chk2 play at the centrosomes has not yet been elucidated (Mullee & Morrison, 2016). Centrosomal Chk1 is thought to regulate the activation of CDK1/Cyclin B at the centrosomes through the modulation of CDC25B (Kramer et al, 2004) whilst BRCA1 loss results in centrosomal duplication (Xu et al, 1999). Centrin 2, which is predominantly located at the centrosomes, has been shown to interact with XPC to stimulate NER (Nishi et al, 2005). As these genes may influence DNA damage repair and cell cycle progression whilst remaining outside the nucleus, it is not infeasible that CCDC15 may do the same. It is possible that it may be influencing DNA damage repair from the cytoplasm by regulating the actions of certain proteins through cellular trafficking. Its loss may mean that their actions are de-regulated which subsequently results in the DNA damage or prevents its efficient repair. As BRCA1 is located at centrosomes it is plausible that an interaction with CCDC15 outside of the nucleus may modulate its effects upon PALB2 and subsequently the loading of RAD51 by BRCA2.

Immunoprecipitation of CCDC15-FLAG was attempted using the HEK 293 FLP CCDC15-FLAG cells. In the initial small scale experiment, CCDC15 FLAG was successfully eluted from the Affinity Gel so the experiment was scaled up in an attempt to generate samples for use in mass spectrometry analysis. In the first attempt, a faint band at the correct molecular weight was identified in the Tetracycline treated 30 minute Elution. However, as the untreated lane was so dark it was impossible to determine if this was a nonspecific band and so the experiment was repeated. In this experiment, it is uncertain if the cells were expressing the fusion gene as no Input sample was retained. No evidence of CCDC15-FLAG was detected in either of the Eluates but it appears that some remained bound to the Affinity Gel. This is most likely due to the saturation of the gel with the M2 FLAG primary antibody prior to incubation with the lysates. The final repeat of this experiment yielded no evidence of CCDC15-FLAG in any of the fractions, including the Tetracycline treated Inputs.

Lysates were prepared for western blotting analysis to determine if the cells were still expressing the fusion gene but the previously used vial of the M2 FLAG primary antibody was empty and an older vial produced a faint blot with no bands corresponding to CCDC15-FLAG. To validate this blot, qPCR analysis was carried out on Tetracycline treated and mock treated cells. No change in CCDC15 RNA expression was observed between the two populations of cells, suggesting that the cells were no longer expressing the fusion gene.

As stated previously, as all the clones were pooled during the generation of the stable cell lines it is possible that some cells did not incorporate the entire plasmid and so could survive the antibiotic selection without expressing the fusion gene, or silenced CCDC15 expression through epigenetic mechanisms. It is thought that these cells may have out competed the correctly expressing cells at some point during their culturing as these cells had previously repeatedly demonstrated CCDC15-FLAG expression. Though vials had been frozen down whilst the cells were still expressing the fusion gene, all the vials had been thawed. Between the small scale and larger scale immunoprecipitation experiments, the

cells had died and new cells had to be defrosted. However, the cells had not frozen well and it took the pooling of 10 vials to produce a viable population. This problem had previously been encountered with the HEK 293 FLP cells within the Collis lab. These cells displayed CCDC15-FLAG expression in western blots and so were used for the large-scale immunoprecipitation assays. By the time the cells had been mycoplasma tested and frozen down the cells had ceased expressing the fusion gene.

If we had not been constrained by time pressures, the HEK 293 FLP cells would have been re-transfected with the CCDC15-FLAG Expression Clone. Rather than pooling all of the colonies, individual colonies would have been grown separately and assessed for their expression of the fusion gene. Hopefully, this would have eliminated the issues surrounding the continued expression of this gene.

As there had also been issues with the immunoprecipitation before the cells stopped expressing the gene, it may also have been beneficial to produce a CCDC15-MYC tagged protein. An Affinity Gel for the immunoprecipitation of MYC-tagged proteins is also available and so the assay could be carried out under similar conditions. This may have yielded the successful elution of the protein and the MYC antibody may have produced less non-specific bands than the M2 FLAG antibody. However, FLAG immunoprecipitation has been used previously within the Collis lab to produce samples for mass spectrometry (Myers et al, 2016; Staples et al, 2016; Staples et al, 2014; Staples et al, 2012) and so cross-referencing with the data produced in these projects may have allowed for the elimination of some false positives. If the immunoprecipitation assay had proved feasible, the eluted samples would have been prepared for mass spectrometry analysis by the Sheffield University Biological Mass Spectrometry Facility. This data would have been compared to the list of genes produced by the GSEA to determine if any were true interactors. Such analyses may also have determined the role that CCDC15 appears to play in genome maintenance and the cell cycle by determining which pathways it may be involved in, and how to further interrogate these hypotheses.

Chapter Seven:
Conclusions

7.1 IDENTIFICATION OF REPLICATION STRESS SUPPRESSORS 262

7.1.1 GENOME WIDE RNAI SCREEN DEVELOPMENT 262

7.1.2 TARGETED SCREENING, VALIDATION AND CLASSIFICATION 263

7.1.3 SCREENING CONCLUSIONS 264

7.2 CHARACTERISATION OF CCDC15 264

7.2.1 CHARACTERISATION OF THE CCDC15 DEFICIENT PHENOTYPE 265

7.2.2 LOCALISATION AND INTERACTION OF CCDC15 266

7.2.3 CCDC15 CONCLUSIONS 266

7.1 Identification of Replication Stress Suppressors

Targeting the increased levels of replication stress observed in cancerous cells has been proposed as a method of specifically inducing cancer cell death. It is hypothesised that increasing this level further would drive these cells over a threshold beyond which they could not maintain their viability. Normal cells, with their reduced basal levels of stress, would remain below this level and survive the therapy. Consequently, the identification of genes whose loss increases DNA replication stress is of therapeutic relevance.

RNAi screening has previously been successfully utilised for the identification of genome maintenance factors and specifically, replication stress response genes. No previous screen identifying the latter has relied solely upon immunofluorescent detection or quantified the endogenous levels of replication stress. Therefore, a screening assay was developed that assessed the levels of RPA2 phosphorylation following gene knockdown.

7.1.1 Genome Wide RNAi Screen Development

The known replication stress suppressors Chk1 and RRM1 were chosen as positive controls in this assay as their knockdown induced a DNA replication stress response. The drug hydroxyurea (HU) was also included as a transfection independent positive control. Assessment of three antibodies raised against several phospho-sites within RPA2 (pRPA2) resulted in the selection of the pRPA2 Threonine 21 (T21) antibody for use in the assay. It could detect increases in replication stress in HCT116 cells following Chk1 or RRM1 knockdown. This assay was repeated in a cell line panel to ensure that the staining was not cell line specific. Whilst the staining pattern was reproducible between the three cell lines, those without functional p53 showed a greater reliance on the function of Chk1 for suppressing replication stress.

Once it was determined that the pRPA2 T21 antibody could detect increases in replication stress, this protocol was used to develop a high throughput screening assay. Several variables within the assay were extensively optimised, including the extraction method, primary antibody concentration, cell number, transfection time and the transfection reagent concentration.

Despite the logical approach taken to optimise the protocol, the assay proved unreliable; the number of cells remaining in the wells at the end of the assay was highly variable and the intensity of the antibody staining appeared inconsistent. These issues may have been a result of the technical difficulties encountered during assay set up at the SRSF. Neither increasing the cell number nor preparing the plates manually in the Collis lab improved the cell coverage or assay signal. The high throughput screening method was trialled in the original small scale format assay plates where it could identify changes in the levels of endogenous replication stress. This suggested that it was an intrinsic property of the high throughput format, potentially the ImageXpress microscope, that was limiting its feasibility, therefore further optimisation of the assay was halted.

Several other methods of replication stress were trialled including Total RPA2 and TopBP1 detection but these also proved unfeasible for the detection of endogenous replication stress in a high throughput format.

7.1.2 Targeted Screening, Validation and Classification

Due to the impracticalities encountered in the development of the high throughput screen, the pRPA2 T21 assay was instead utilised as a targeted kinase screen. This was used to assess the replication stress suppression of several of the kinases identified as hits in the U2OS-based Kavanaugh screen (Kavanaugh et al, 2015), which was published during the optimisation of the whole genome wide screen. The pRPA2 T21 assay was therefore re-optimised for small scale screening in U2OS cells before the list of 18 selected kinases was included for screening.

Of these kinases, 8 were identified as potential suppressors of endogenous replication stress within this assay and carried forward as initial hits. These were then included in a TopBP1 validation screen which confirmed that their loss increased endogenous levels of replication stress. To determine which kinases were worth further study, the hits were included in a cytotoxicity assay to determine if their knockdown preferentially affected the growth of p53 deficient cells. This revealed that the depletion of PMVK or SNRK is particularly detrimental to the survival of cells lacking p53. The siRNA pools targeting these kinases were deconvoluted and the individual siRNAs were assessed by qPCR, pRPA2 T21 immunofluorescence and a p53 sensitivity. Only the individual siRNAs targeting SNRK resulted in preferential sensitisation of the p53 null HCT116 cells so further investigation of PMVK was ceased.

In clonogenic assays, SNRK knockdown appeared to sensitise the p53 null cells but did not affect wild type cells, although this was not significant. Loss of SNRK in both cell lines increased the levels of the DNA damage markers γH2AX and 53BP1. This was abrogated by treatment with the CDK inhibitor Roscovitine, suggesting that damage formation depended upon DNA replication. The loss of SNRK was also assessed for its ability to affect the survival of cells whose p53 signalling had been pharmacologically disrupted. It did decrease the survival of cells treated with the p53 inhibitor Pifithrin-α at 7.5μM, although this was not significant. This was not surprising given the crude nature of the drug. It did not affect cells treated with the ATM inhibitor KU55933, however, neither did loss of ATR, which is reportedly synthetic lethal with ATM deficiency, so called the validity of this assay into question.

SNRK loss was also examined for its effects upon the survival of cells overexpressing several clinically relevant oncogenes. It had no detrimental effects on the survival of U2OS with induced Cyclin E overexpression, although these cells may have entered senescence and so were less affected by the knockdown than the un-induced cells. A disconnect was observed between the effects of SNRK loss in HCT116 and MRC-5 cells overexpressing H-RAS^{G12V}. In the HCT116 cells its loss did not affect growth but it did in the MRC-5 cells, most likely due to the differing genetic backgrounds of the two lines. Likewise, knockdown of SNRK sensitised the MYC-N overexpressing IMR-32 cells when compared to the MYN-N normal SH-EP1 cells. This implies that SNRK loss is preferentially unfavourable in cells with high levels of replication stress due to oncogene overexpression.

The loss of SNRK was also shown to sensitise cells to the effects of the replication stress inducing drugs Gemcitabine and Olaparib but not that of 5-FU whose main mechanism of action is not thought to involve replication stress.

7.1.3 Screening Conclusions

RNAi screening is a valid approach for the identification of replication stress suppressors through monitoring the formation of pRPA2 T21 foci. Whilst the high throughput genome wide approach proved unreliable, the developed assay proved effective as a small scale targeted screen. This yielded the identification of several potential novel replication suppressors, including SNRK. Given its ability to target p53 deficient cells and those overexpressing certain oncogenes, SNRK appears to be a promising candidate for targeted cancer therapies. As it is a kinase it is considered a druggable protein and the identification of its UBA domain as a potential natural inhibitor of its function makes it an appealing drug candidate. Its ability to enhance the efficacy of clinically available therapies also enhances its desirability as a potential novel therapeutic target. It is therefore considered further investigation into its cellular function and the effects of its loss are justified. Although not investigated in detail within this project, PMVK also appears to merit further study as it has a defined role within a cancer relevant pathway and a highly plausible mechanism for causing replication stress through nucleotide depletion.

7.2 Characterisation of CCDC15

Gene set enrichment analysis (GSEA) has previously been shown to be capable of predicting biologically relevant interactions based on gene expression data, as is seen in the case of C19orf75/RMI2 (Deans & West, 2009; Singh et al, 2008). Therefore, it was decided to characterise the putative genome maintenance factor CCDC15, which had been predicted by GSEA to be involved in DNA damage repair. In particular, its expression correlated well with several genes involved in the Fanconi Anaemia (FA), nucleotide excision repair and translesion synthesis pathways, all of which remove replication impeding lesions from the genome. It was hypothesised that CCDC15 may be involved in the repair of these lesions and consequently potentially be a suppressor of DNA replication stress.

Whilst CCDC15 has been reported to localise to centrosomes by Gene Ontology analysis, this is due to a mis-annotation (Jakobsen et al, 2011). However, further information suggests that it may localise to the cytoskeleton or the nucleus due to a predicted nuclear localisation sequence (Kosugi et al, 2009). No experimental evidence outside of high throughput interaction studies have identified any interactors of CCDC15.

In several projects within the Collis lab, characterisation of a protein's function by assessing the knockdown phenotype has yielded positive results (Barone et al, 2016; Myers et al, 2016; Staples et al, 2016; Staples et al, 2014; Staples et al, 2012). In several of these projects, tagged fusion proteins have also been generated to allow for the subcellular localisation and interactions to be established.

7.2.1 Characterisation of the CCDC15 Deficient Phenotype

The expression of CCDC15 was validated in a cell line panel by qPCR which was subsequently used to assess its knockdown by siRNA. Transfected cells were then assessed for DNA damage markers and sensitivity to several DNA damaging agents in a cell line panel that ranged in their levels of CCDC15 RNA expression. Depletion of CCDC15 increased damage accumulation in all cell lines but only sensitised the highly expressing RPE-1 cells to the effects of MMC and Cisplatin. CCDC15 siRNA had little effects upon the sensitivity of PC-3 and HeLa cells to these drugs and no effect upon the efficacy of HU in any cell line.

The siRNA pool was then deconvoluted and the DNA damage immunofluorescence experiments were replicated, producing similar increased levels of endogenous DNA damage to those observed for the pooled siRNA. The DNA damage marker assays were repeated following MMC treatment or UV irradiation, however the loss of CCDC15 did not increase the damage seen when compared to Control 1 transfected cells. The difference in the apparent sensitivity of the cells between the MTT and immunofluorescence assays is most likely due to the difference in the length of time that the cells were exposed to the drug. In Clonogenic survival assays, its loss had little effects upon the sensitivity of both PC-3 and HeLa cells to MMC. In the former cell line, this was thought to be due to lack of CCDC15 knocked down cells surviving following re-plating as it showed some MMC sensitivity in the MTT assay. Clonogenic assays proved unfeasible in the RPE-1 cells as they did not form distinct colonies at the plating densities chosen and colorimetric quantification of the Methylene Blue did not appear to represent the number of cells present in the assay plates.

As it was predicted to interact with several FA genes, the effects of CCDC15 knockdown on the FA pathway were investigated. Depletion of CCDC15 did not prevent the ubiquitination of FANCD2 (a marker of FA pathway activation) and only slightly increased the levels of foci formed in untreated but not MMC or UV treated cells. Similarly, no overt effects on the kinetics of FANCD2 foci following UV irradiation were observed in CCDC15-depleted cells, although these cells did exhibit delayed formation of RAD51 foci and resolution following UV irradiation. This change was not due to altered cell cycle dynamics affecting the induction of HR and so was most likely thought to be due to competition with RPA for ssDNA binding or delayed resection.

It was hypothesised that CCDC15 was involved in the removal of replication impeding lesions and predicted that its loss would result in the induction of replication stress. However, knockdown of CCDC15 did not alter the formation of pRPA2 T21 foci and Roscovitine treatment did not alter the levels of damage reported, suggesting that this occurs independently of DNA replication. Knockdown of CCDC15 also had little effect upon cell cycle progression in untreated or MMC treated PC-3 and HeLa cells. When RPE-1 cells were synchronised in G1 by serum starvation, the loss of CCDC15 appeared to delay re-entry into the cell cycle through a currently unknown mechanism, although it must be noted that this experiment was only successfully carried out once. It is possible that this

may be due to as yet undiscovered link between CCDC15 and the Rb-E2F network which is known to regulate quiescent exit.

7.2.2 Localisation and Interaction of CCDC15

Initial attempts were made to isolate RNA from PC-3 and MDA-MB-231 cells to act as a template for the production of cDNA for use in the Gateway cloning system. However, this proved unattainable, most likely due to the low levels of RNA expressed for this gene. A plasmid containing CCDC15 cDNA was therefore sourced and this was successfully amplified using the Gateway primers, which were subsequently used to generate CCDC15-YFP and CCDC15-FLAG expression vectors. These clones were stably incorporated into HeLa FLP (YFP and FLAG) and HEK 293 FLP cell lines (FLAG only). Western blotting analysis revealed that the HeLa FLP cells were expressing CCDC15-YFP but not CCDC15-FLAG, whilst the HEK 293 FLP cells were initially expressing the CCDC15-FLAG construct.

Transient transfection of CCDC15-YFP into HeLa cells was inefficient and detrimentally affected the viability of the cells and so could not be used to assess subcellular localisation. The HeLa FLP cells stably expressing CCDC15-YFP revealed that it was expressed in the cytoplasm and did not re-localise following MMC treatment or UV irradiation (initial 10 minutes following irradiation or 4 hours later). Small scale immunoprecipitation was carried out successfully using the HEK 293 FLP CCDC15-FLAG expressing cells. However, when this experiment was scaled up to produce samples for mass spectrometry analysis, the fusion protein could not be successfully purified. Further optimisation of this technique was halted when it was discovered that the cells had stopped expressing FLAG-tagged CCDC15.

7.2.3 CCDC15 Conclusions

CCDC15 is a putative genome maintenance factor that appears to affect the sensitivity of cells to DNA cross linking agents in an expression dependent manner, potentially due to an increased rate in the formation of DNA damage. The loss of CCDC15 slightly increases the formation of FANCD2 foci in untreated cells but not following treatment with crosslinking agents. It also delays the formation and resolution of RAD51 foci which is not due to postponed entry into S phase and is therefore more likely due to alterations in the availability of ssDNA or the loading machinery. Its loss does not result in the induction of a replication stress response and the damage that accumulates forms independently of DNA replication. It also appears not to be involved in determining the cell cycle distribution of cycling cells, but may promote the restart of cells paused in G1, although the mechanism for this is unknown. It appears to localise in the cytoplasm and does not redistribute in response to DNA damage, however, through interaction with cytoplasmic and centrosomal DNA repair and cell cycle proteins it may regulate DNA damage repair.

As it appears to influence the formation of DNA damage foci and potentially the onset of homologous recombination mediated repair, further elucidation of this gene's function is warranted. Particularly, investigation into whether this gene interacts with BRCA1 or some other component of the HR machinery outside of the nucleus may reveal its mechanism of action. Within this work, no investigation of its role within nucleotide

excision repair or translesion synthesis was attempted. Alongside this work, mass spectrometry analysis may also be key in elucidating its interactors and subsequently understanding how it results in the formation of DNA damage and potentially delayed exit from a quiescent state when depleted from cells.

7.3 Overall Conclusions

This work presents the optimisation and completion of a RNAi screen aiming to identify novel suppressors of replication stress as well as the investigation of a putative genome maintenance factor. In this study it has been demonstrated that siRNA screens are capable of identifying replication stress suppressors by indirect immunofluorescence, although this was not achieved at the genome wide scale. However, even at the small scale it resulted in the identification of a potential drug target in SNRK and an interesting novel replication stress suppressor in PMVK. The use of siRNA and immunofluorescence also identified a potential novel regulator of HR and quiescence exit in CCDC15 which warrants further investigation.

Whilst this work demonstrates that siRNA knockdown is capable of elucidating certain aspect of a protein of interests function, it also highlights that reliance on RNAi alone is not enough to fully characterise a protein. One of the greatest weaknesses in this work is that no rescue experiments were carried out and so it cannot be stated with certainty that all of the phenotypes observed are due to the knockdown of the gene of interest. Another flaw was the reliance on downstream markers for detecting DNA damage and replication stress. Whilst attempts were made to directly assess the former, none were made to measure replication stress more directly, such as DNA fibre analysis or BrdU incorporation. Addition of these techniques to this body of work would have increased confidence in the conclusions drawn.

Bibliography

Aarts, M., Sharpe, R., Garcia-Murillas, I., Gevensleben, H., Hurd, M. S., Shumway, S. D., Toniatti, C., Ashworth, A. & Turner, N. C. (2012) Forced Mitotic Entry of S-Phase Cells as a Therapeutic Strategy Induced by Inhibition of WEE1. *Cancer Discovery*, 2(6), 524-539.

abcam (2017) *Anti-SNRK antibody (ab96762)*, 2017. Available online: http://www.abcam.com/snrk-antibody-ab96762.html#description_images_1 [Accessed.

Abe, S., Nagasaka, K., Hirayama, Y., Kozuka-Hata, H., Oyama, M., Aoyagi, Y., Obuse, C. & Hirota, T. (2011) The initial phase of chromosome condensation requires Cdk1-mediated phosphorylation of the CAP-D3 subunit of condensin II. *Genes & Development*, 25(8), 863-874.

Addington, J. & Freimer, M. (2016) Chemotherapy- induced peripheral neuropathy: an update on the current understanding. *F1000Research*, 5.

Adelman, C. A., Lolo, R. L., Birkbak, N. J., Murina, O., Matsuzaki, K., Horejsi, Z., Parmar, K., Borel, V., Skehel, J. M., Stamp, G., D'Andrea, A., Sartori, A. A., Swanton, C. & Boulton, S. J. (2013) HELQ promotes RAD51 paralogue-dependent repair to avert germ cell loss and tumorigenesis. *Nature*, 502(7471), 381-384.

Aguilera, A. & Gomez-Gonzalez, B. (2008) Genome instability: a mechanistic view of its causes and consequences. *Nature Reviews Genetics*, 9(3), 204-217.

Al-Hakim, A. K., Göransson, O., Deak, M., Toth, R., Campbell, D. G., Morrice, N. A., Prescott, A. R. & Alessi, D. R. (2005) 14- 3- 3 cooperates with LKB1 to regulate the activity and localization of QSK and SIK. *Journal Of Cell Science*, 118(Pt 23), 5661-5673.

Alt, A., Lammens, K., Chiocchini, C., Lammens, A., Pieck, J. C., Kuch, D., Hopfner, K.-P. & Carell, T. (2007) Bypass of DNA lesions generated during anticancer treatment with cisplatin by DNA polymerase eta. *Science*, 318(5852), 967-970.

Alvarez-Fernandez, M. & Malumbres, M. (2014) Preparing a cell for nuclear envelope breakdown: Spatio-temporal control of phosphorylation during mitotic entry. *Bioessays*, 36(8), 757-765.

Alzu, A., Bermejo, R., Begnis, M., Lucca, C., Piccini, D., Carotenuto, W., Saponaro, M., Brambati, A., Cocito, A., Foiani, M. & Liberi, G. (2012) Senataxin associates with replication forks to protect fork integrity across RNA- polymerase- II- transcribed genes. *Cell*, 151(4), 835-846.

American Cancer Society (2015) *Global Cancer Facts & Figures 3rd Edition*, 2015. Available online: [Accessed.

Ammazzalorso, F., Pirzio, L. M., Bignami, M., Franchitto, A. & Pichierri, P. (2010) ATR and ATM differently regulate WRN to prevent DSBs at stalled replication forks and promote replication fork recovery. *EMBO J*, 29(18), 3156-3169.

An, R., Jia, Y., Wan, B., Zhang, Y., Dong, P., Li, J. & Liang, X. (2014) Non- Enzymatic Depurination of Nucleic Acids: Factors and Mechanisms. *PLOS One*, 9(12).

Anantha, R. W., Vassin, V. M. & Borowiec, J. A. (2007) Sequential and synergistic modification of human RPA stimulates chromosomal DNA repair. *Journal of Biological Chemistry*, 282(49), 35910-35923.

Araújo, S. J., Nigg, E. A. & Wood, R. D. (2001) Strong functional interactions of TFIIH with XPC and XPG in human DNA nucleotide excision repair, without a preassembled repairosome. *Molecular and Cellular Biology*, 21(7), 2281-2291.

Arias, E. E. & Walter, J. (2005) Replication- dependent destruction of Cdt1 limits DNA replication to a single round per cell cycle in Xenopus egg extracts. *Faseb J.*, 19(5), 114-126.

Arora, S., Kothandapani, A., Tillison, K., Kalman-Maltese, V. & Patrick, S. M. (2010) Downregulation of XPF– ERCC1 enhances cisplatin efficacy in cancer cells. *DNA Repair*, 9(7), 745-753.

Ashley, A. K., Shrivastav, M., Nie, J., Amerin, C., Troksa, K., Glanzer, J. G., Liu, S., Opiyo, S. O., Dimitrova, D. D., Le, P., Sishc, B., Bailey, S. M., Oakley, G. G. & Nickoloff, J. A. (2014) DNA- PK phosphorylation of RPA32 Ser4/ Ser8 regulates replication stress checkpoint activation, fork restart, homologous recombination and mitotic catastrophe. *DNA Repair*, 21, 131 - 139.

Auerbach, A. D. & Smogorzewska, A. (2017) *Fanconi Anemia Mutation Database*. (10 October 2017. New York: The Rockefeller University. Available online: http://www2.rockefeller.edu/fanconi/.

Azorsa, D. O., Gonzales, I. M., Basu, G. D., Choudhary, A., Arora, S., Bisanz, K. M., Kiefer, J. A., Henderson, M. C., Trent, J. M., Von Hoff, D. D. & Mousses, S. (2009) Synthetic lethal RNAi screening identifies sensitizing targets for gemcitabine therapy in pancreatic cancer. *Journal of Translational Medicine*, 7(43).

Azzam, E. I., Jay-Gerin, J.-P. & Pain, D. (2012) Ionizing radiation- induced metabolic oxidative stress and prolonged cell injury. *Cancer Letters*, 327(1-2), 48-60.

Bae, S., Bae, K., Kim, J. & Seo, Y. (2001) RPA governs endonuclease switching during processing of Okazaki fragments in eukaryotes. *Nature*, 412(6845), 456 - 461.

Bakkenist, C. J. & Kastan, M. B. (2003) DNA damage activates ATM through intermolecular autophosphorylation and dimer dissociation. *Nature*, 421(6922), 499-506.

Banasik, M., Komura, H., Shimoyama, M. & Ueda, K. (1992) Specific inhibitors of poly(ADP- ribose) synthetase and mono(ADP- ribosyl) transferase. *Journal of Biological Chemistry*, 267(3), 1569-1575.

Bansbach, C. E., Bétous, R., Lovejoy, C. A., Glick, G. G. & Cortez, D. (2009) The annealing helicase SMARCAL1 maintains genome integrity at stalled replication forks. *Genes and Development*, 23(20), 2405-2414.

Barber, L. J., Sandhu, S., Chen, L., Campbell, J., Kozarewa, I., Fenwick, K., Assiotis, I., Rodrigues, D. N., Reis - Filho, J. S., Moreno, V., Mateo, J., Molife, L. R., De Bono, J., Kaye, S., Lord, C. J. & Ashworth, A. (2013) Secondary mutations in BRCA2 associated with clinical resistance to a PARP inhibitor. *Journal of Pathology*, 229(3), 422-429.

Barlow, J. & Nussenzweig, A. (2014) Replication initiation and genome instability: a crossroads for DNA and RNA synthesis. *Cellular and Molecular Life Sciences*, 71(23), 4545-4559.

Barnum, K. J. & O'Connell, M. J. (2014) Cell Cycle Regulation by Checkpoints, in Noguchi, E. & Gadaleta, M. C. (eds), *Cell Cycle Control: Mechanisms and Protocols*. New York, NY: Springer New York, 29-40.

Barone, G., Staples, C. J., Ganesh, A., Patterson, K. W., Bryne, D. P., Myers, K. N., Patil, A. A., Eyers, C. E., Maslen, S., Skehel, J. M., Eyers, P. A. & Collis, S. J. (2016) Human CDK18 promotes replication stress signaling and genome stability. *Nucleic Acids Research*, 44(18), 8772-8785.

Bartek, J. & Lukas, J. (2001) Pathways governing G1/S transition and their response to DNA damage. *FEBS Letters*, 490(3), 117-122.

Bartkova, J., Horejsi, Z., Koed, K., Kramer, A., Tort, F., Zieger, K., Guldberg, P., Sehested, M., Nesland, J. M., Lukas, C., Orntoft, T., Lukas, J. & Bartek, J. (2005) DNA damage response as a candidate anti-cancer barrier in early human tumorigenesis. *Nature*, 434(7035), 864-870.

Bartkova, J., Rezaei, N., Liontos, M., Karakaidos, P., Kletsas, D., Issaeva, N., Vassiliou, L.-V. F., Kolettas, E., Niforou, K., Zoumpourlis, V. C., Takaoka, M., Nakagawa, H., Tort, F., Fugger, K., Johansson, F.,

Sehested, M., Andersen, C. L., Dyrskjot, L., Orntoft, T., Lukas, J., Kittas, C., Helleday, T., Halazonetis, T. D., Bartek, J. & Gorgoulis, V. G. (2006) Oncogene-induced senescence is part of the tumorigenesis barrier imposed by DNA damage checkpoints. *Nature*, 444(7119), 633-637.

Bartosova, Z. & Krejci, L. (2014) Nucleases in homologous recombination as targets for cancer therapy. *FEBS Letters*, 588(15), 2446 - 2456.

Baumann, M., Krause, M., Overgaard, J., Debus, J., Bentzen, S. M., Daartz, J., Richter, C., Zips, D. & Bortfeld, T. (2016) Radiation oncology in the era of precision medicine. *Nature Reviews Cancer*, 16(4), 234-249.

Baylin, S. B. & Ohm, J. E. (2006) Epigenetic gene silencing in cancer - a mechanism for early oncogenic pathway addiction? *Nature Reviews Cancer*, 6(2), 107-116.

Bebenek, K., Pedersen, L. C. & Kunkel, T. A. (2014) Structure- function studies of DNA polymerase λ. *Biochemistry*, 53(17), 2781 - 2792.

Bebenek, K., Tissier, A., Frank, E. G., McDonald, J. P., Prasad, R., Wilson, S. H., Woodgate, R. & Kunkel, T. A. (2001) 5′ - deoxyribose phosphate lyase activity of human DNA polymerase ι in vitro. *Science*, 291(5511), 2156-2159.

Beck, H., Nähse-Kumpf, V., Larsen, M. S. Y., Hanlon, K. A., Patzke, S., Holmberg, C., Mejlvang, J., Groth, A., Nielsen, O., Syljuåsen, R. G. & Sørensen, C. S. (2012) Cyclin- dependent kinase suppression by WEE1 kinase protects the genome through control of replication initiation and nucleotide consumption. *Molecular and Cellular Biology*, 32(20), 4226-4236.

Beltran, H. (2014) The N-myc Oncogene: Maximizing its Targets, Regulation, and Therapeutic Potential. *Molecular Cancer Research*, 12(6), 815-822.

Ben-Neriah, Y., Daley, G. Q., Mes-Masson, A. M., Witte, O. N. & Baltimore, D. (1986) The chronic myelogenous leukemia- specific P210 protein is the product of the bcr/ abl hybrid gene. *Science*, 233(4760), 212-214.

Bendris, N., Lemmers, B., Blanchard, J.-M. & Arsic, N. (2011) Cyclin A2 Mutagenesis Analysis: A New Insight into CDK Activation and Cellular Localization Requirements. *PLOS One*, 6(7).

Benjamin, D. J. (2014) The efficacy of surgical treatment of cancer-20 years later. *Medical Hypotheses*, 82(4), 412-420.

Bennardo, N., Cheng, A., Huang, N., Stark, J. M. & Haber, J. E. (2008) Alternative- NHEJ Is a Mechanistically Distinct Pathway of Mammalian Chromosome Break Repair. *PLOS Genetics*, 4(6).

Berkovich, E., Monnat, R. & Kastan, M. B. (2007) Roles of ATM and NBS1 in chromatin structure modulation and DNA double- strand break repair. *Nat. Cell Biol.*, 9(6), 683-690.

Berns, K., Horlings, H. M., Hennessy, B. T., Madiredjo, M., Hijmans, E. M., Beelen, K., Linn, S. C., Gonzalez-Angulo, A. M., Stemke-Hale, K., Hauptmann, M., Beijersbergen, R. L., Mills, G. B., van de Vijver, M. J. & Bernards, R. (2007) A Functional Genetic Approach Identifies the PI3K Pathway as a Major Determinant of Trastuzumab Resistance in Breast Cancer. *Cancer Cell*, 12(4), 395-402.

Bernstein, N. K., Williams, R. S., Rakovszky, M. L., Cui, D., Green, R., Karimi-Busheri, F., Mani, R. S., Galicia, S., Koch, C. A., Cass, C. E., Durocher, D., Weinfeld, M. & Glover, J. N. M. (2005) The Molecular Architecture of the Mammalian DNA Repair Enzyme, Polynucleotide Kinase. *Molecular Cell*, 17(5), 657-670.

Berti, M., Chaudhuri, A., Thangavel, S., Gomathinayagam, S., Kenig, S., Vujanovic, M., Odreman, F., Glatter, T., Graziano, S., Mendoza-Maldonado, R., Marino, F., Lucic, B., Biasin, V., Gstaiger, M., Aebersold, R., Sidorova, J., Monnat, R., Lopes, M. & Vindigni, A. (2013) Human RECQ1 promotes restart of replication forks reversed by DNA topoisomerase I inhibition. *Nat. Struct. Mol. Biol.*, 20(3), 347-354.

Berti, M. & Vindigni, A. (2016) Replication stress: getting back on track. *Nature Structural & Molecular Biology*, 23(2), 103 - 109.

Bester, A. C., Roniger, M., Oren, Y. S., Im, M. M., Sarni, D., Chaoat, M., Bensimon, A., Zamir, G., Shewach, D. S. & Kerem, B. (2011) Nucleotide Deficiency Promotes Genomic Instability in Early Stages of Cancer Development. *Cell*, 145(3), 435-446.

Beveridge, R. D., Staples, C. J., Patil, A. A., Myers, K. N., Maslen, S., Skehel, J. M., Boulton, S. J. & Collis, S. J. (2014) The leukemia-associated Rho guanine nucleotide exchange factor LARG is required for efficient replication stress signaling. *Cell Cycle*, 13(21), 3450-3459.

Bhargava, R., Onyango, D. O. & Stark, J. M. (2016) Regulation of Single- Strand Annealing and its Role in Genome Maintenance. *Trends in Genetics*, 32(9), 566-575.

Bianchi, J., Rudd, Sean g., Jozwiakowski, Stanislaw k., Bailey, Laura j., Soura, V., Taylor, E., Stevanovic, I., Green, Andrew j., Stracker, Travis h., Lindsay, Howard d. & Doherty, Aidan j. (2013) PrimPol Bypasses UV Photoproducts during Eukaryotic Chromosomal DNA Replication. *Molecular Cell*, 52(4), 566-573.

Biddlestone-Thorpe, L., Sajjad, M., Rosenberg, E., Beckta, J. M., Valerie, N. C. K., Tokarz, M., Adams, B. R., Wagner, A. F., Khalil, A., Gilfor, D., Golding, S. E., Deb, S., Temesi, D. G., Lau, A., Connor, M. J., Choe, K. S., Parada, L. F., Lim, S. K., Mukhopadhyay, N. D. & Valerie, K. (2013) ATM kinase inhibition preferentially sensitizes p53- mutant glioma to ionizing radiation. *Clinical Cancer Research*, 19(12), 3189-3200.

Binder , J., Frankild , S., Tsafou, K., Stolte , C., O'Donoghue , S., Schneider , R. & Jensen, L. (2017a) *COMPARTMENTS - CCDC15 localisations*, 2017a. Available online: http://compartments.jensenlab.org/Entity?figures=subcell_cell_%%&knowledge=10&textmining=10&predictions=10&type1=9606&type2=-22&id1=ENSP00000341684 [Accessed.

Binder , J., Frankild , S., Tsafou, K., Stolte , C., O'Donoghue , S., Schneider , R. & Jensen, L. (2017b) *COMPARTMENTS - PMVK localisations*, 2017b. Available online: http://compartments.jensenlab.org/Entity?figures=subcell_cell_%%&knowledge=10&textmining=10&predictions=10&type1=9606&type2=-22&id1=ENSP00000357452 [Accessed.

Binder, J. X., Pletscher-Frankild, S., Tsafou, K., Stolte, C., O'Donoghue, S. I., Schneider, R. & Jensen, L. J. (2014) COMPARTMENTS: unification and visualization of protein subcellular localization evidence. *Database-the Journal of Biological Databases and Curation*, bau012.

BioGRID (2017) *CCDC15 Results Summary*, 2017. Available online: https://thebiogrid.org/123101 [Accessed.

Blagosklonny, M. V. & Pardee, A. B. (2002) The Restriction Point of the Cell Cycle. *Cell Cycle*, 1(2), 103-110.

Blain, S. W., Montalvo, E. & Massagué, J. (1997) Differential Interaction of the Cyclin-dependent Kinase (Cdk) Inhibitor p27Kip1 with Cyclin A-Cdk2 and Cyclin D2-Cdk4. *Journal of Biological Chemistry*, 272(41), 25863-25872.

Blasina, A., Hallin, J., Chen, E., Arango, M. E., Kraynov, E., Register, J., Grant, S., Ninkovic, S., Chen, P., Nichols, T., Connor, P. & Anderes, K. (2008) Breaching the DNA damage checkpoint via PF-00477736, a novel small- molecule inhibitor of checkpoint kinase 1. *Molecular cancer therapeutics*, 7(8), 2394 - 2404.

Blier, P. R., Griffith, A. J., Craft, J. & Hardin, J. A. (1993) Binding of Ku protein to DNA. Measurement of affinity for ends and demonstration of binding to nicks. *The Journal of biological chemistry*, 268(10), 7594 - 7601.

Blow, J. J. & Gillespie, P. J. (2008) Replication licensing and cancer - A fatal entanglement? *Nat Rev Cancer*, 8(10), 799-806.

Blow, J. J. & Hodgson, B. (2002) Replication licensing — Origin licensing: defining the proliferative state? *Trends in Cell Biology*, 12(2), 72-78.

Blow, J. J. & Laskey, R. A. (1988) A role for the nuclear-envelope in controlling DNA-replication within the cell-cycle. *Nature*, 332(6164), 546-548.

Bodnar, A. G., Ouellette, M., Frolkis, M., Holt, S. E., Chiu, C. P., Morin, G. B., Harley, C. B., Shay, J. W., Lichtsteiner, S. & Wright, W. E. (1998) Extension of life-span by introduction of telomerase into normal human cells. *Science*, 279(5349), 349-352.

Boland, C. R. & Goel, A. (2010) Microsatellite Instability in Colorectal Cancer. *Gastroenterology*, 138(6), 2073-2087.

Botthof, J. G., Bielczyk-Maczynska, E., Ferreira, L. & Cvejic, A. (2017) Loss of the homologous recombination gene rad51 leads to Fanconi anemia-like symptoms in zebrafish. *Proceedings of the National Academy of Sciences of the United States of America*, 114(22), E4452-E4461.

Bowman, G. D., Donnell, M. & Kuriyan, J. (2006) Structural analysis of a eukaryotic sliding DNA clamp- clamp loader complex. *Nature*, 429, 724 - 730.

Brandt, A., Bermejo, J., Sundquist, K. & Hemminki, K. (2008) Age of onset in familial cancer. *Annals of Oncology*, 19(12), 2084-2088.

Brunet, A., Kanai, F., Stehn, J., Xu, J., Sarbassova, D., Frangioni, J. V., Dalal, S. N., Decaprio, J. A., Greenberg, M. E. & Yaffe, M. B. (2002) 14- 3- 3 transits to the nucleus and participates in dynamic nucleocytoplasmic transport. *Journal of Cell Biology*, 156(5), 817-828.

Bryant, H. E., Petermann, E., Schultz, N., Jemth, A. S., Loseva, O., Issaeva, N., Johansson, F., Fernandez, S., McGlynn, P. & Helleday, T. (2009) PARP is activated at stalled forks to mediate Mre11‐dependent replication restart and recombination. *EMBO Journal*, 28(17), 2601-2615.

Bryant, H. E., Schultz, N., Thomas, H. D., Parker, K. M., Flower, D., Lopez, E., Kyle, S., Meuth, M., Curtin, N. J. & Helleday, T. (2005) Specific killing of BRCA2- deficient tumours with inhibitors of poly(ADP-ribose) polymerase. *Nature*, 434(7035), 913-917.

Bulavin, D. V., Higashimoto, Y., Popoff, I. J., Gaarde, W. A., Basrur, V., Potapova, O., Appella, E. & Fornace, A. J. (2001) Initiation of a G2/ M checkpoint after ultraviolet radiation requires p38 kinase. *Nature*, 411(6833), 102 - 107.

Bunz, F., Dutriaux, A., Lengauer, C., Waldman, T., Zhou, S., Brown, J. P., Sedivy, J. M., Kinzler, K. W. & Vogelstein, B. (1998) Requirement for p53 and p21 to Sustain G$_2$ Arrest After DNA Damage. *Science*, 282(5393), 1497-1501.

Bunz, F., Hwang, P. M., Torrance, C., Waldman, T., Zhang, Y. G., Dillehay, L., Williams, J., Lengauer, C., Kinzler, K. W. & Vogelstein, B. (1999) Disruption of p53 in human cancer cells alters the responses to therapeutic agents. *Journal of Clinical Investigation*, 104(3), 263-269.

Burhans, W. C. & Weinberger, M. (2007) DNA replication stress, genome instability and aging. *Nucleic Acids Research*, 35(22), 7545-7556.

Burkhard, P., Stetefeld, J. & Strelkov, S. V. (2001) Coiled coils: a highly versatile protein folding motif. *Trends in Cell Biology*, 11(2), 82-88.

Burma, S., Chen, B. P., Murphy, M., Kurimasa, A. & Chen, D. J. (2001) ATM phosphorylates histone H2AX in response to DNA double- strand breaks. *Journal of Biological Chemistry*, 276(45), 42462 - 42467.

Burrell, R. A., McClelland, S. E., Endesfelder, D., Groth, P., Weller, M.-C., Shaikh, N., Domingo, E., Kanu, N., Dewhurst, S. M., Gronroos, E., Chew, S. K., Rowan, A. J., Schenk, A., Sheffer, M., Howell, M., Kschischo, M., Behrens, A., Helleday, T., Bartek, J., Tomlinson, I. R. & Swanton, C. (2013) Replication stress links structural and numerical cancer chromosomal instability. *Nature*, 494(7438), 492-496.

Burren, R., Scaletta, C., Frenk, E., Panizzon, R. G. & Lee Applegate, A. (1998) Sunlight and carcinogenesis: Expression of p53 and pyrimidine dimers in human skin following UVA I, UVA I + II and solar simulating radiations. *International Journal of Cancer*, 76(2), 201-206.

Buschta-Hedayat, N., Buterin, T., Hess, M. T., Missura, M. & Naegeli, H. (1999) Recognition of nonhybridizing base pairs during nucleotide excision repair of DNA. *Proceedings of the National Academy of Sciences of the United States of America*, 96(11), 6090-6095.

Bykov, V. J. N., Issaeva, N., Shilov, A., Hultcrantz, M., Pugacheva, E., Chumakov, P., Bergman, J., Wiman, K. G. & Selivanova, G. (2002) Restoration of the tumor suppressor function to mutant p53 by a low-molecular-weight compound. *Nature Medicine*, 8(3), 282-288.

Bykov, V. J. N., Issaeva, N., Zache, N., Shilov, A., Hultcrantz, M., Bergman, J., Selivanova, G. & Wiman, K. G. (2005) Reactivation of mutant p53 and induction of apoptosis in human tumor cells by maleimide analogs. *Journal of Biological Chemistry*, 280(34), 30384-30391.

Cancer Research UK (2015) *Ovarian cancer drug wins NICE approval*, 2015. Available online: http://www.cancerresearchuk.org/about-us/cancer-news/news-report/2015-12-11-ovarian-cancer-drug-wins-nice-approval?_ga=2.194515117.165681934.1508152267-410760155.1508152267 [Accessed.

Cancer Research UK (2017) *Cancer Statistics for the UK*, 2017. Available online: http://www.cancerresearchuk.org/health-professional/cancer-statistics#heading-Two [Accessed 8 July 2017].

Cappelli, E., Taylor, R., Cevasco, M., Abbondandolo, A., Caldecott, K. & Frosina, G. (1997) Involvement of XRCC1 and DNA ligase III gene products in DNA base excision repair. *Journal of Biological Chemistry*, 272(38), 23970-23975.

Cappuzzo, F., Jänne, P., Skokan, M., Finocchiaro, G., Rossi, E., Ligorio, C., Zucali, P., Terracciano, L., Toschi, L., Roncalli, M., Destro, A., Incarbone, M., Alloisio, M., Santoro, A. & Varella-Garcia, M. (2009) MET increased gene copy number and primary resistance to gefitinib therapy in non- small- cell lung cancer patients. *Annals of Oncology*, 20(2), 298-304.

Carrassa, L., Broggini, M., Erba, E. & Damia, G. (2004) Chk1, but not Chk2, is involved in the cellular response to DNA damaging agents: differential activity in cells expressing or not p53. *Cell cycle*, 3(9), 1177-1181.

Caswell, D. R. & Swanton, C. (2017) The role of tumour heterogeneity and clonal cooperativity in metastasis, immune evasion and clinical outcome. *BMC medicine*, 15(1), 133.

Cerami, E., Gao, J., Dogrusoz, U., Gross, B. E., Sumer, S. O. & Aksoy, B. A. (2012) The cBio Cancer Genomics Portal: An Open Platform for Exploring Multidimensional Cancer Genomics Data (vol 2, pg 401, 2012). *Cancer Discovery*, 2(10), 960-960.

Chabner, B. A. & Roberts, T. G. (2005) Timeline - Chemotherapy and the war on cancer. *Nature Reviews Cancer*, 5(1), 65-72.

Chambliss, K. L., Slaughter, C. A., Schreiner, R., Hoffmann, G. F. & Gibson, K. M. (1996) Molecular cloning of human phosphomevalonate kinase and identification of a consensus peroxisomal targeting sequence. *Journal of Biological Chemistry*, 271(29), 17330-17334.

Chan, T., Hermeking, H., Lengauer, C., Kinzler, K. & Vogelstein, B. (1999) 14- 3- 3sigma is required to prevent mitotic catastrophe after DNA damage. *Nature*, 401(6753), 616-620.

Chang, D. C., Xu, N. H. & Luo, K. Q. (2003) Degradation of cyclin B is required for the onset of anaphase in mammalian cells. *Journal of Biological Chemistry*, 278(39), 37865-37873.

Chang, H. H. Y., Pannunzio, N. R., Adachi, N. & Lieber, M. R. (2017) Non- homologous DNA end joining and alternative pathways to double- strand break repair. *Nature reviews. Molecular cell biology*, 18, 495 - 506.

Chen, T., Stephens, P. A., Middleton, F. K. & Curtin, N. J. (2012) Targeting the S and G2 checkpoint to treat cancer. *Drug Discovery Today*, 17(5-6), 194-202.

Chen, Z., Yang, H. & Pavletich, N. P. (2008) Mechanism of homologous recombination from the RecA– ssDNA/ dsDNA structures. *Nature*, 453, 489 - 494.

Cheng, Q., Cross, B., Li, B. Z., Chen, L. H., Li, Z. Y. & Chen, J. D. (2011) Regulation of MDM2 E3 Ligase Activity by Phosphorylation after DNA Damage. *Molecular and Cellular Biology*, 31(24), 4951-4963.

Chibazakura, T., Kamachi, K., Ohara, M., Tane, S., Yoshikawa, H. & Roberts, J. M. (2011) Cyclin A promotes S- phase entry via interaction with the replication licensing factor Mcm7. *Molecular and cellular biology*, 31(2), 248 - 255.

Choi, J. H., Lindsey-Boltz, L. A., Kemp, M., Mason, A. C., Wold, M. S. & Sancar, A. (2010) Reconstitution of RPA- covered single- stranded DNA- activated ATR- Chk1 signaling. *Proceedings of the National Academy of Sciences of the United States of America*, 107(31), 13660-13665.

Chong, J. P. J., M., M. H., Chong-Yee, K. & Julian, B. J. (1995) Purification of an MCM-containing complex as a component of the DNA replication licensing system. *Nature.*, 375(6530), 418 - 421.

Ciccia, A., Bredemeyer, A. L., Elledge, S. J., Sowa, M. E., Harper, J. W., Terret, M.-E. & Jallepalli, P. V. (2009) The SIOD disorder protein SMARCAL1 is an RPA- interacting protein involved in replication fork restart. *Genes and Development*, 23(20), 2415-2425.

Ciccia, A., Ling, C., Coulthard, R., Yan, Z., Xue, Y., Meetei, A. R., Laghmani, E. H., Joenje, H., McDonald, N., de Winter, J. P., Wang, W. & West, S. C. (2007) Identification of FAAP24, a Fanconi anemia core complex protein that interacts with FANCM. *Molecular Cell*, 25(3), 331-343.

Ciccia, A., McDonald, N. & West, S. (2008) Structural and Functional Relationships of the XPF/ MUS81 Family of Proteins. *Annual Review of Biochemistry*, 77, 259 - 287.

Cimprich, K. A. & Cortez, D. (2008) ATR: an essential regulator of genome integrity. *Nature Reviews Molecular Cell Biology*, 9(8), 616-627.

Ciszewski, W., Tavecchio, M., Dastych, J. & Curtin, N. (2014) DNA- PK inhibition by NU7441 sensitizes breast cancer cells to ionizing radiation and doxorubicin. *Breast Cancer Research and Treatment*, 143(1), 47-55.

ClinicalTrials.gov (2017a) *Combination Study of Prexasertib and Olaparib in Patients With Advanced Solid Tumors*, 2017a. Available online: https://clinicaltrials.gov/ct2/show/NCT03057145 [Accessed.

ClinicalTrials.gov (2017b) *Gemcitabine Hydrochloride With or Without WEE1 Inhibitor MK-1775 in Treating Patients With Recurrent Ovarian, Primary Peritoneal, or Fallopian Tube Cancer*, 2017b. Available online: https://clinicaltrials.gov/ct2/show/NCT02101775 [Accessed.

Coleman, T. R., Carpenter, P. B. & Dunphy, W. G. (1996) The Xenopus Cdc6 Protein Is Essential for the Initiation of a Single Round of DNA Replication in Cell- Free Extracts. *Cell*, 87(1), 53-63.

Collis, S. J., Barber, L. J., Clark, A. J., Martin, J. S., Ward, J. D. & Boulton, S. J. (2007) HCLK2 is essential for the mammalian S-phase checkpoint and impacts on Chk1 stability. *Nature Cell Biology*, 9(4), 391-401.

Collis, S. J., Ciccia, A., Deans, A. J., Horejsi, Z., Martin, J. S., Maslen, S. L., Skehel, J. M., Elledge, S. J., West, S. C. & Boulton, S. J. (2008) FANCM and FAAP24 Function in ATR-Mediated Checkpoint Signaling Independently of the Fanconi Anemia Core Complex. *Molecular Cell*, 32(3), 313-324.

Cooke, M. S., Evans, M. D., Dizdaroglu, M. & Lunec, J. (2003) Oxidative DNA damage: mechanisms, mutation, and disease. *Faseb J.*, 17(10), 1195-1214.

Costantino, L., Sotiriou, S. K., Rantala, J. K., Magin, S., Mladenov, E., Helleday, T., Haber, J. E., Iliakis, G., Kallioniemi, O. P. & Halazonetis, T. D. (2014) Break-Induced Replication Repair of Damaged Forks Induces Genomic Duplications in Human Cells. *Science*, 343(6166), 88-91.

Couch, F., Bansbach, C. E., Driscoll, R., Luzwick, J., Glick, G., Betous, R., Carroll, C., Jung, S., Qin, J., Cimprich, K. & Cortez, D. (2013) ATR phosphorylates SMARCAL1 to prevent replication fork collapse. *Genes & Development*, 27(14), 1610-1623.

Coverley, D., Laman, D. & Laskey, R. A. (2002) Distinct roles for cyclins E and A during DNA replication complex assembly and activation. *Nature Cell Biology*, 4(7), 523 - 528.

Culmsee, C., Zhu, X. X., Yu, Q. S., Chan, S. L., Camandola, S., Guo, Z. H., Greig, N. H. & Mattson, M. P. (2001) A synthetic inhibitor of p53 protects neurons against death induced by ischemic and excitotoxic insults, and amyloid beta-peptide. *Journal of Neurochemistry*, 77(1), 220-228.

Curtin, N. J. (2013) Inhibiting the DNA damage response as a therapeutic manoeuvre in cancer. *B J Pharmacol*, 169(8), 1745-1765.

Curtin, N. J., Wang, L.-Z., Yiakouvaki, A., Kyle, S., Arris, C. A., Canan-Koch, S., Webber, S. E., Durkacz, B. W., Calvert, H. A., Hostomsky, Z. & Newell, D. R. (2004) Novel poly(ADP- ribose) polymerase- 1 inhibitor, AG14361, restores sensitivity to temozolomide in mismatch repair-deficient cells. *Clinical cancer research : an official journal of the American Association for Cancer Research*, 10(3), 881-889.

Dai, Y. & Grant, S. (2010) New insights into checkpoint kinase 1 in the DNA damage response signaling network. *Clinical Cancer Research*, 16(2), 376-383.

Dasari, S. & Tchounwou, P. B. (2014) Cisplatin in cancer therapy: Molecular mechanisms of action. *European Journal of Pharmacology*, 740, 364-378.

Davies, A. A., Huttner, D., Daigaku, Y., Chen, S. & Ulrich, H. D. (2008) Activation of ubiquitin-dependent DNA damage bypass is mediated by replication protein A. *Molecular Cell*, 29(5), 625-636.

Davies, K. D. & Doebele, R. C. (2013) Molecular pathways: ROS1 fusion proteins in cancer. *Clinical cancer research : an official journal of the American Association for Cancer Research*, 19(15), 4040 - 4045.

Davies, S. L., North, P. S. & Hickson, I. D. (2007) Role for BLM in replication- fork restart and suppression of origin firing after replicative stress. *Nature Structural & Molecular Biology*, 14(7), 677 - 679.

De Boer, L., Oakes, V., Beamish, H., Giles, N., Stevens, F., Somodevilla-Torres, M., DeSouza, C. & Gabrielli, B. (2008) Cyclin A/cdk2 coordinates centrosomal and nuclear mitotic events. *Oncogene*, 27(31), 4261-4268.

De Bont, R. & van Larebeke, N. (2004) Endogenous DNA damage in humans: a review of quantitative data. *Mutagenesis*, 19(3), 169-185.

De Piccoli, G., Labib, K., Katou, Y., Itoh, T., Nakato, R. & Shirahige, K. (2012) Replisome Stability at Defective DNA Replication Forks Is Independent of S Phase Checkpoint Kinases. *Molecular Cell*, 45(5), 696-704.

Deans, A. J. & West, S. C. (2009) FANCM Connects the Genome Instability Disorders Bloom's Syndrome and Fanconi Anemia. *Molecular Cell*, 36(6), 943-953.

Deans, A. J. & West, S. C. (2011) DNA interstrand crosslink repair and cancer. *Nature Reviews Cancer*, 11(7), 467-480.

Deckbar, D., Stiff, T., Koch, B., Reis, C., Löbrich, M. & Jeggo, P. A. (2010) The limitations of the G1- S checkpoint. *Cancer research*, 70(11), 4412-4421.

Deininger, M. W. N., Vieira, S., Mendiola, R., Schultheis, B., Goldman, J. M. & Melo, J. V. (2000) BCR-ABL tyrosine kinase activity regulates the expression of multiple genes implicated in the pathogenesis of chronic myeloid leukemia. *Cancer Research*, 60(7), 2049-2055.

Delacroix, S., Wagner, J. M., Kobayashi, M., Yamamoto, K. & Karnitz, L. M. (2007) The Rad9-Hus1-Rad1 (9-1-1) clamp activates checkpoint signaling via TopBP1. *Genes & Development*, 21(12), 1472-1477.

Di Micco, R., Fumagalli, M., Cicalese, A., Piccinin, S., Gasparini, P., Luise, C., Schurra, C., Garre, M., Nuciforo, P. G., Bensimon, A., Maestro, R., Pelicci, P. G. & di Fagagna, F. d. A. (2006) Oncogene-induced senescence is a DNA damage response triggered by DNA hyper-replication. *Nature*, 444(7119), 638-642.

Dianov, G., Price, A. & Lindahl, T. (1992) Generation of single- nucleotide repair patches following excision of uracil residues from DNA. *Molecular and Cellular Biology*, 12(4), 1605-1612.

Diaz, M., Watson, N. B., Turkington, G., Verkoczy, L. K., Klinman, N. R. & McGregor, W. G. (2003) Decreased frequency and highly aberrant spectrum of ultraviolet- induced mutations in the hprt gene of mouse fibroblasts expressing antisense RNA to DNA polymerase zeta. *Molecular cancer research*, 1(11), 836 - 847.

Do, K., Doroshow, J. & Kummar, S. (2013) Wee1 kinase as a target for cancer therapy. *Cell Cycle*, 12(19), 3159-3164.

Dong, H., Nebert, D., Bruford, E., Thompson, D. C., Joenje, H. & Vasiliou, V. (2015) Update of the human and mouse Fanconi anemia genes. *Hum. Genomics*, 9(32).

Douglas, M. E. & Diffley, J. F. X. (2016) Recruitment of Mcm10 to Sites of Replication Initiation Requires Direct Binding to the Minichromosome Maintenance (MCM) Complex. *The Journal of biological chemistry*, 291(11), 5879 - 5888.

Douki, T., Perdiz, D., Grof, P., Kuluncsics, Z., Moustacchi, E., Cadet, J. & Sage, E. (1999) Oxidation of Guanine in Cellular DNA by Solar UV Radiation: Biological Role†. *Photochemistry and Photobiology*, 70(2), 184-190.

Druker, B. J., Talpaz, M., Resta, D. J., Peng, B., Buchdunger, E., Ford, J. M., Lydon, N. B., Kantarjian, H., Capdeville, R., Ohno-Jones, S. & Sawyers, C. L. (2001) Efficacy and safety of a specific inhibitor of the BCR-ABL tyrosine kinase in chronic myeloid leukemia. *New England Journal of Medicine*, 344(14), 1031-1037.

Durkin, S. G. & Glover, T. W. (2007) Chromosome fragile sites. *Annual Review of Genetics*, 41, 169-192.

Elliott, S. L., Crawford, C., Mulligan, E., Summerfield, G., Newton, P., Wallis, J., Mainou-Fowler, T., Evans, P., Bedwell, C., Durkacz, B. W. & Willmore, E. (2011) Mitoxantrone in combination with an inhibitor of DNA- dependent protein kinase: A potential therapy for high risk B- cell chronic lymphocytic leukaemia. *British Journal of Haematology*, 152(1), 61-71.

Ellison, V. & Stillman, B. (2003) Biochemical Characterization of DNA Damage Checkpoint Complexes: Clamp Loader and Clamp Complexes with Specificity for 5′ Recessed DNA (Checkpoint Clamp Loading In Vitro). *PLOS Biology*, 1(2), e33.

Elvers, I., Johansson, F., Groth, P., Erixon, K. & Helleday, T. (2011) UV stalled replication forks restart by re- priming in human fibroblasts. *Nucleic acids research*, 39(16), 7049-7057.

Evers, B., Drost, R., Schut, E., de Bruin, M., van Der Burg, E., Derksen, P. W. B., Holstege, H., Liu, X., van Drunen, E., Beverloo, H. B., Smith, G. C. M., Martin, N. M. B., Lau, A., Connor, M. J. & Jonkers, J. (2008) Selective inhibition of BRCA2- deficient mammary tumor cell growth by AZD2281 and cisplatin. *Clinical cancer research : an official journal of the American Association for Cancer Research*, 14(12), 3916 - 3925.

Falck, J., Coates, J. & Jackson, S. P. (2005) Conserved modes of recruitment of ATM, ATR and DNA-PKcs to sites of DNA damage. *Nature*, 434(7033), 605-611.

Falck, J., Mailand, N., Syljuåsen, R. G., Bartek, J. & Lukas, J. (2001) The ATM- Chk2- Cdc25A checkpoint pathway guards against radioresistant DNA synthesis. *Nature*, 410(6830), 842-847.

Fang, F. & Newport, J. (1993) Distinct roles of cdk2 and cdc2 in RPA phosphorylation during the cell cycle. *Journal of cell science. London, New York NY*, 106(3), 983-994.

Farmer, H., McCabe, N., Lord, C. J., Tutt, A. N. J., Johnson, D. A., Richardson, T. B., Santarosa, M., Dillon, K. J., Hickson, I., Knights, C., Martin, N. M. B., Jackson, S. P., Smith, G. C. M. & Ashworth, A. (2005) Targeting the DNA repair defect in BRCA mutant cells as a therapeutic strategy. *Nature*, 434(7035), 917-921.

Ferguson, L. R., Chen, H., Collins, A. R., Connell, M., Damia, G., Dasgupta, S., Malhotra, M., Meeker, A. K., Amedei, A., Amin, A., Ashraf, S. S., Aquilano, K., Azmi, A. S., Bhakta, D., Bilsland, A., Boosani, C. S., Chen, S., Ciriolo, M. R., Fujii, H., Guha, G., Halicka, D., Helferich, W. G., Keith, W. N., Mohammed, S. I., Niccolai, E., Yang, X. J., Honoki, K., Parslow, V. R., Prakash, S., Rezazadeh, S., Shackelford, R. E., Sidransky, D., Tran, P. T., Yang, E. S. & Maxwell, C. A. (2015) Genomic instability in human cancer: Molecular insights and opportunities for therapeutic attack and prevention through diet and nutrition. *Seminars in Cancer Biology*, 35, S5-S24.

Fernandez-Medarde, A. & Santos, E. (2011) Ras in cancer and developmental diseases. *Genes & cancer*, 2(3), 344-58.

Ferrao, P., Bukczynska, E., Johnstone, R. & McArthur, G. (2012) Efficacy of CHK inhibitors as single agents in MYC- driven lymphoma cells. *Oncogene*, 31(13), 1661-1672.

Fien, K., Cho, Y. S., Lee, J. K., Raychaudhuri, S., Tappin, I. & Hurwitz, J. (2004) Primer Utilization by DNA Polymerase alpha - Primase Is Influenced by Its Interaction with Mcm10p. *Journal of Biological Chemistry*, 279(16), 16144-16153.

Filippo, J. S., Chi, P., Sehorn, M. G., Etchin, J., Krejci, L. & Sung, P. (2006) Recombination mediator and Rad51 targeting activities of a human BRCA2 polypeptide. *Journal of Biological Chemistry*, 281(17), 11649-11657.

Firat-Karalar, E. N., Rauniyar, N., Yates, J. R., III & Stearns, T. (2014) Proximity Interactions among Centrosome Components Identify Regulators of Centriole Duplication. *Current Biology*, 24(6), 664-670.

Fishel, R., Lescoe, M. K., Rao, M. R., Copeland, N. G., Jenkins, N. A., Garber, J., Kane, M. & Kolodner, R. (1993) The human mutator gene homolog MSH2 and its association with hereditary nonpolyposis colon cancer. *Cell*, 75(5), 1027 - 1038.

Fisher, R. P. & Morgan, D. O. (1994) A novel cyclin associates with M015/CDK7 to form the CDK-activating kinase. *Cell*, 78(4), 713-724.

Fousteri, M., Vermeulen, W., van Zeeland, A. A. & Mullenders, L. H. F. (2006) Cockayne Syndrome A and B Proteins Differentially Regulate Recruitment of Chromatin Remodeling and Repair Factors to Stalled RNA Polymerase II In Vivo. *Molecular Cell*, 23(4), 471-482.

Fragkos, M., Ganier, O., Coulombe, P. & Mechali, M. (2015) DNA replication origin activation in space and time. *Nat. Rev. Mol. Cell Biol.*, 16(6), 360-374.

Freschauf, G. K., Karimi-Busheri, F., Ulaczyk-Lesanko, A., Mereniuk, T. R., Ahrens, A., Koshy, J. M., Rasouli-Nia, A., Pasarj, P., Holmes, C. F. B., Rininsland, F., Hall, D. G. & Weinfeld, M. (2009) Identification of a small molecule inhibitor of the human DNA repair enzyme polynucleotide kinase/ phosphatase. *Cancer research*, 69(19), 7739-7746.

Fukada, S. I., Uezumi, A., Ikemoto, M., Masuda, S., Segawa, M., Tanimura, N., Yamamoto, H., Miyagoe‐Suzuki, Y., Takeda, S. & Ichi (2007) Molecular Signature of Quiescent Satellite Cells in Adult Skeletal Muscle. *Stem Cells*, 25(10), 2448-2459.

Fukami-Kobayashi, J. & Mitsui, Y. (1999) Cyclin D1 inhibits cell proliferation through binding to PCNA and Cdk2. *Experimental Cell Research*, 246(2), 338-347.

Gagou, M. E., Ganesh, A., Phear, G., Robinson, D., Petermann, E., Cox, A. & Meuth, M. (2014) Human PIF1 helicase supports DNA replication and cell growth under oncogenic-stress. *Oncotarget*, 5(22), 11381-11398.

Gan, G. N., Wittschieben, J. P., Wittschieben, B. Ø. & Wood, R. D. (2008) DNA polymerase zeta (pol zeta) in higher eukaryotes. *Cell research*, 18(1), 174 - 183.

Ganzinelli, M., Carrassa, L., Crippa, F., Broggini, M., Damia, G. & Tavecchio, M. (2008) Checkpoint kinase 1 down- regulation by an inducible small interfering RNA expression system sensitized in vivo tumors to treatment with 5- fluorouracil. *Clinical Cancer Research*, 14(16), 5131-5141.

Garcia-Higuera, I., Taniguchi, T., Ganesan, S., Meyn, M. S., Timmers, C., Hejna, J., Grompe, M., amp, Amp, Apos & Andrea, A. D. (2001) Interaction of the Fanconi Anemia Proteins and BRCA1 in a Common Pathway. *Molecular Cell*, 7(2), 249-262.

Garcia-Muse, T. & Aguilera, A. (2016) Transcription-replication conflicts: how they occur and how they are resolved. *Nature Reviews Molecular Cell Biology*, 17(9), 553-563.

García-Gómez, S., Reyes, A., Martínez-Jiménez, María i., Chocrón, E. s., Mourón, S., Terrados, G., Powell, C., Salido, E., Méndez, J., Holt, Ian j. & Blanco, L. (2013) PrimPol, an Archaic Primase/ Polymerase Operating in Human Cells. *Molecular Cell*, 52(4), 541-553.

Garg, P., Stith, C. M., Sabouri, N., Johansson, E. & Burgers, P. M. (2004) Idling by DNA polymerase δ maintains a ligatable nick during lagging-strand DNA replication. *Genes and Development*, 18(22), 2764-2773.

Gari, K., Décaillet, C., Delannoy, M., Wu, L. & Constantinou, A. (2008) Remodeling of DNA replication structures by the branch point translocase FANCM. *Proceedings of the National Academy of Sciences of the United States of America*, 105(42), 16107-16112.

Gavande, N. S., Vandervere-Carozza, P. S., Hinshaw, H. D., Jalal, S. I., Sears, C. R., Pawelczak, K. S. & Turchi, J. J. (2016) DNA repair targeted therapy: The past or future of cancer treatment? *Pharmacology and Therapeutics*, 160, 65-83.

Ge, X. Q. & Blow, J. J. (2010) Chk1 inhibits replication factory activation but allows dormant origin firing in existing factories. *Journal of Cell Biology*, 191(7), 1285-1297.

Ge, X. Q., Jackson, D. A. & Blow, J. J. (2007) Dormant origins licensed by excess Mcm2- 7 are required for human cells to survive replicative stress. *Genes & development*, 21(24), 3331-3341.

Gell, D. & Jackson, S. P. (1999) Mapping of protein-protein interactions within the DNA-dependent protein kinase complex. *Nucleic Acids Research*, 27(17), 3494-3502.

GeneCards (2017a) *CCDC15 Gene (Protein Coding)*, 2017a. Available online: [Accessed.

GeneCards (2017b) *RMI2 Gene (Protein Coding)*, 2017b. Available online: http://www.genecards.org/cgi-bin/carddisp.pl?gene=RMI2 [Accessed.

Gilad, O., Nabet, B. Y., Ragland, R. L., Schoppy, D. W., Smith, K. D., Durham, A. C. & Brown, E. J. (2010) Combining ATR suppression with oncogenic ras synergistically increases genomic instability, causing synthetic lethality or tumorigenesis in a dosage-dependent manner. *Cancer Research*, 70(23), 9693-9702.

Gilman, A. & Philips, F. S. (1946) The biological actions and therapeutic applications of the B-Chloroethyl amines and sulfides. *Science*, 103(2675), 409-415.

Glanzer, J. G., Liu, S., Wang, L., Mosel, A., Peng, A. & Oakley, G. G. (2014) RPA Inhibition Increases Replication Stress and Suppresses Tumor Growth. *Cancer research*, 74(18), 5165.

Gligorov, J. & Lotz, J. P. (2004) Preclinical pharmacology of the taxanes: Implications of the differences. *Oncologist*, 9(2), 3-8.

Golding, S. E., Rosenberg, E., Adams, B. R., Wignarajah, S., Beckta, J. M., O'connor, M. J. & Valerie, K. (2012) Dynamic inhibition of ATM kinase provides a strategy for glioblastoma multiforme radiosensitization and growth control. *Cell Cycle*, 11(6), 1167-1173.

Golding, S. E., Rosenberg, E., Valerie, N., Hussaini, I., Frigerio, M., Cockcroft, X. F., Chong, W. Y., Hummersone, M., Rigoreau, L., Menear, K. A., Connor, M. J., Povirk, L. F., van Meter, T. & Valerie, K. (2009) Improved ATM kinase inhibitor KU- 60019 radiosensitizes glioma cells, compromises insulin, AKT and ERK prosurvival signaling, and inhibits migration and invasion. *Molecular cancer therapeutics*, 8(10), 2894-2902.

Goodarzi, A. A., Yu, Y., Riballo, E., Douglas, P., Walker, S. A., Ye, R., Harer, C., Marchetti, C., Morrice, N., Jeggo, P. A. & Lees-Miller, S. P. (2006) DNA-PK autophosphorylation facilitates Artemis endonuclease activity. *EMBO Journal*, 25(16), 3880-3889.

Goodwin, J. & Knudsen, K. (2014) Beyond DNA Repair: DNA- PK Function in Cancer. *Cancer Discov.*, 4(10), 1126-1139.

Gorgoulis, V. G., Vassiliou, L. V. F., Karakaidos, P., Zacharatos, P., Kotsinas, A., Liloglou, T., Venere, M., DiTullio, R. A., Kastrinakis, N. G., Levy, B., Kletsas, D., Yoneta, A., Herlyn, M., Kittas, C. & Halazonetis, T. D. (2005) Activation of the DNA damage checkpoint and genomic instability in human precancerous lesions. *Nature*, 434(7035), 907-913.

Gospodinov, A., Tsaneva, I. & Anachkova, B. (2009) RAD51 foci formation in response to DNA damage is modulated by TIP49. *International Journal of Biochemistry and Cell Biology*, 41(4), 925-933.

Gotwals, P., Cameron, S., Cipolletta, D., Cremasco, V., Crystal, A., Hewes, B., Mueller, B., Quaratino, S., Sabatos-Peyton, C., Petruzzelli, L., Engelman, J. A. & Dranoff, G. (2017) Prospects for combining targeted and conventional cancer therapy with immunotherapy. *Nature Reviews Cancer*, 17(5), 286-301.

Graf, N., Ang, W. H., Zhu, G., Myint, M. & Lippard, S. J. (2011) Role of Endonucleases XPF and XPG in Nucleotide Excision Repair of Platinated DNA and Cisplatin/ Oxaliplatin Cytotoxicity. *ChemBioChem*, 12(7), 1115-1123.

Gravel, S., Chapman, J. R., Magill, C. & Jackson, S. P. (2008) DNA helicases Sgs1 and BLM promote DNA double- strand break resection. *Genes and Development*, 22(20), 2767-2772.

Gravells, P., Hoh, L., Canovas, D., Rennie, I. G., Sisley, K. & Bryant, H. E. (2011) Resistance of uveal melanoma to the interstrand cross-linking agent mitomycin C is associated with reduced expression of CYP450R. *British Journal of Cancer*, 104(7), 1098-1105.

Grawunder, U., Wilm, M., Wu, X. & Kulesza, P. (1997) Activity of DNA ligase IV stimulated by complex formation with XRCC4 protein in mammalian cells. *Nature*, 388(6641), 492-495.

Greaves, M. & Maley, C. C. (2012) Clonal evolution in cancer. *Nature*, 481(7381), 306-313.

Grinkevich, V. V., Nikulenkov, F., Shi, Y., Enge, M., Bao, W. J., Maljukova, A., Gluch, A., Kel, A., Sangfelt, O. & Selivanova, G. (2009) Ablation of Key Oncogenic Pathways by RITA-Reactivated p53 Is Required for Efficient Apoptosis. *Cancer Cell*, 15(5), 441-453.

Gu, L., Chu, P. G., Lingeman, R., McDaniel, H., Kechichian, S., Hickey, R. J., Liu, Z., Yuan, Y. C., Sandoval, J. A., Fields, G. B. & Malkas, L. H. (2015) The Mechanism by Which MYCN Amplification Confers an Enhanced Sensitivity to a PCNA-Derived Cell Permeable Peptide in Neuroblastoma Cells. *Ebiomedicine*, 2(12), 1923-1931.

Guan, R., Tapang, P., Leverson, J., Albert, D., Giranda, V. & Luo, Y. (2005) Small Interfering RNA-Mediated Polo- Like Kinase 1 Depletion Preferentially Reduces the Survival of p53- Defective, Oncogenic Transformed Cells and Inhibits Tumor Growth in Animals. *Cancer Research*, 65(7), 2698-2704.

Guan, Y., Hu, H., Peng, Y., Gong, Y., Yi, Y., Shao, L., Liu, T., Li, G., Wang, R., Dai, P., Bignon, Y.-J., Xiao, Z., Yang, L., Mu, F., Xiao, L., Xie, Z., Yan, W., Xu, N., Zhou, D. & Yi, X. (2015) Detection of inherited mutations for hereditary cancer using target enrichment and next generation sequencing. *Familial Cancer*, 14(1), 9-18.

Gudjonsson, T., Altmeyer, M., Savic, V., Toledo, L., Dinant, C., Grofte, M., Bartkova, J., Poulsen, M., Oka, Y., Bekker-Jensen, S., Mailand, N., Neumann, B., Heriche, J.-K., Shearer, R., Saunders, D., Bartek, J., Lukas, J. & Lukas, C. (2012) TRIP12 and UBR5 Suppress Spreading of Chromatin Ubiquitylation at Damaged Chromosomes. *Cell*, 150(4), 697-709.

Gudkov, A. V. & Komarova, E. A. (2005) Prospective therapeutic applications of p53 inhibitors. *Biochemical and Biophysical Research Communications*, 331(3), 726-736.

Guo, C., Fischhaber, P. L., Luk‐Paszyc, M. J., Masuda, Y., Zhou, J., Kamiya, K., Kisker, C. & Friedberg, E. C. (2003) Mouse Rev1 protein interacts with multiple DNA polymerases involved in translesion DNA synthesis. *EMBO Journal*, 22(24), 6621-6630.

Guo, C., Sonoda, E., Tang, T.-S., Parker, J. L., Bielen, A. B., Takeda, S., Ulrich, H. D. & Friedberg, E. C. (2006) REV1 Protein Interacts with PCNA: Significance of the REV1 BRCT Domain In Vitro and In Vivo. *Molecular Cell*, 23(2), 265-271.

Guo, Y. R., Scheuermann, T. H., Partch, C. L., Tomchick, D. R. & Gardner, K. H. (2015) Coiled-coil Coactivators Play a Structural Role Mediating Interactions in Hypoxia-inducible Factor Heterodimerization. *Journal of Biological Chemistry*, 290(12), 7707-7721.

Haeusler, A. R., Donnelly, C. J. & Rothstein, J. D. (2016) The expanding biology of the C9orf72 nucleotide repeat expansion in neurodegenerative disease. *Nature Reviews Neuroscience*, 17(6), 383-395.

Halazonetis, T. D., Gorgoulis, V. G. & Bartek, J. (2008) An oncogene- induced DNA damage model for cancer development. *Science*, 319(5868), 1352-1355.

Hanahan, D. & Weinberg, R. A. (2000) The Hallmarks of Cancer. *Cell*, 100(1), 57-70.

Hanahan, D. & Weinberg, Robert a. (2011) Hallmarks of Cancer: The Next Generation. *Cell*, 144(5), 646-674.

Hashimoto, S., Anai, H. & Hanada, K. (2016) Mechanisms of interstrand DNA crosslink repair and human disorders. *Genes and Environment*, 38(9).

He, G. G., Siddik, Z. H., Huang, Z. F., Wang, R. N., Koomen, J., Kobayashi, R., Khokhar, A. R. & Kuang, J. (2005) Induction of p21 by p53 following DNA damage inhibits both Cdk4 and Cdk2 activities. *Oncogene*, 24(18), 2929-2943.

He, J. X., Kang, X., Yin, Y. X., Chao, K. S. C. & Shen, W. H. (2015) PTEN regulates DNA replication progression and stalled fork recovery. *Nature Communications*, 6.

Heller, Ryan c., Kang, S., Lam, Wendy m., Chen, S., Chan, Clara s. & Bell, Stephen p. (2011) Eukaryotic Origin- Dependent DNA Replication In Vitro Reveals Sequential Action of DDK and S- CDK Kinases. *Cell*, 146(1), 80-91.

Helmrich, A., Ballarino, M., Nudler, E. & Tora, L. (2013) Transcription-replication encounters, consequences and genomic instability. *Nature Structural & Molecular Biology*, 20(4), 412-418.

Heyer, W.-D., Ehmsen, K. T. & Liu, J. (2010) Regulation of Homologous Recombination in Eukaryotes. *Annual Review of Genetics*, 44, 113-139.

Hickson, I., Zhao, Y., Richardson, C. J., Green, S. J., Martin, N. M. B., Orr, A. I., Reaper, P. M., Jackson, S. P., Curtin, N. J. & Smith, G. C. M. (2004) Identification and characterization of a novel and specific inhibitor of the ataxia- telangiectasia mutated kinase ATM. *Cancer research*, 64(24), 9152-9159.

Hills, S. A. & Diffley, J. F. X. (2014) DNA Replication and Oncogene-Induced Replicative Stress. *Current Biology*, 24(10), R435-R444.

Hinchcliffe, E. H., Li, C., Thompson, E. A., Maller, J. L. & Sluder, G. (1999) Requirement of Cdk2- Cyclin E Activity for Repeated Centrosome Reproduction in Xenopus Egg Extracts. *Science*, 283(5403), 851-854.

Hirai, H., Arai, T., Okada, M., Nishibata, T., Kobayashi, M., Sakai, N., Imagaki, K., Ohtani, J., Sakai, T., Yoshizumi, T., Mizuarai, S., Iwasawa, Y. & Kotani, H. (2010) MK- 1775, a small molecule Wee1 inhibitor, enhances antitumor efficacy of various DNA- damaging agents, including 5- fluorouracil. *Cancer Biology and Therapy*, 9(7), 514-522.

Hirai, H., Iwasawa, Y., Okada, M., Arai, T., Nishibata, T., Kobayashi, M., Kimura, T., Kaneko, N., Ohtani, J., Yamanaka, K., Itadani, H., Takahashi-Suzuki, I., Fukasawa, K., Oki, H., Nambu, T., Jiang, J., Sakai, T., Arakawa, H., Sakamoto, T., Sagara, T., Yoshizumi, T., Mizuarai, S. & Kotani, H. (2009) Small- molecule inhibition of Wee1 kinase by MK- 1775 selectively sensitizes p53- deficient tumor cells to DNA-damaging agents. *Molecular cancer therapeutics*, 8(11), 2992-3000.

Hoeijmakers, J. H. J. (2001) Genome maintenance mechanisms for preventing cancer. *Nature*, 411(6835), 366-374.

Hopkins, A. L. & Groom, C. R. (2002) The druggable genome. *Nature Reviews Drug Discovery*, 1(9), 727-730.

Hopp, E. E., Cossette, S. M., Kumar, S. N., Eastwood, D., Ramchandran, R. & Bishop, E. (2017) Sucrose nonfermenting 1-related kinase (SNRK) expression in ovarian cancer and correlation with clinical features. *Cancer Invest.*, 35(7), 456-462.

Horton, J. K., Stefanick, D. F., Prasad, R., Gassman, N. R., Kedar, P. S. & Wilson, S. H. (2014) Base excision repair defects invoke hypersensitivity to PARP inhibition. *Molecular Cancer Research*, 12(8), 1128-1139.

Huang, M. & Weiss, W. A. (2013) Neuroblastoma and MYCN. *Cold Spring Harbor perspectives in medicine*, 3(10), a014415.

Huang, Y. & Li, L. (2013) DNA crosslinking damage and cancer - a tale of friend and foe. *Translational Cancer Research*, 2(3), 144-154.

Huttlin, E. L., Ting, L., Bruckner, R. J., Gebreab, F., Gygi, M. P., Szpyt, J., Tam, S., Zarraga, G., Colby, G., Baltier, K., Dong, R., Guarani, V., Vaites, L. P., Ordureau, A., Rad, R., Erickson, B. K., Wuehr, M., Chick, J., Zhai, B., Kolippakkam, D., Mintseris, J., Obar, R. A., Harris, T., Artavanis-Tsakonas, S., Sowa, M. E., De Camilli, P., Paulo, J. A., Harper, J. W. & Gygi, S. P. (2015) The BioPlex Network: A Systematic Exploration of the Human Interactome. *Cell*, 162(2), 425-440.

Hwang, H. C. & Clurman, B. E. (2005) Cyclin E in normal and neoplastic cell cycles. *Oncogene*, 24(17), 2776-2786.

Hwang, L. H., Lau, L. F., Smith, D. L., Mistrot, C. A., Hardwick, K. G., Hwang, E. S., Amon, A. & Murray, A. W. (1998) Budding yeast Cdc20: A target of the spindle checkpoint. *Science*, 279(5353), 1041-1044.

Höglund, A., Nilsson, L. M., Muralidharan, S. V., Nilsson, J. A., Nikolova, V., Keller, U., Rudelius, M., Hasvold, L. A. & Merta, P. (2011) Therapeutic implications for the induced levels of Chk1 in Myc-expressing cancer cells. *Clinical Cancer Research*, 17(22), 7067-7079.

Ianzini, F. & Mackey, M. A. (1997) Spontaneous premature chromosome condensation and mitotic catastrophe following irradiation of HeLa S3 cells. *International Journal of Radiation Biology*, 72(4), 409-421.

Ilves, I., Petojevic, T., Pesavento, J. J. & Botchan, M. R. (2010) Activation of the MCM2- 7 Helicase by Association with Cdc45 and GINS Proteins. *Molecular Cell*, 37(2), 247-258.

Im, J.-S., Ki, S.-H., Jung, D.-S., Lee, J.-K., Farina, A. & Hurwitz, J. (2009) Assembly of the Cdc45- Mcm2-7- GINS complex in human cells requires the Ctf4/And- 1, RecQL4, and Mcm10 proteins. *Proceedings of the National Academy of Sciences of the United States of America*, 106(37), 15628-15632.

Ishimi, Y. (1997) A DNA helicase activity is associated with an MCM4, -6, and -7 protein complex. *The Journal of biological chemistry*, 272(39), 24508-24513.

Issaeva, N., Bozko, P., Enge, M., Protopopova, M., Verhoef, L., Masucci, M., Pramanik, A. & Selivanova, G. (2004) Small molecule RITA binds to p53, blocks p53-HDM-2 interaction and activates p53 function in tumors. *Nature Medicine*, 10(12), 1321-1328.

Iyer, R. R., Pluciennik, A., Burdett, V. & Modrich, P. L. (2006) DNA mismatch repair: Functions and mechanisms. *Chem. Rev.*, 106(2), 302-323.

Izhar, L., Ziv, O., Cohen, I. S., Geacintov, N. E. & Livneh, Z. (2013) Genomic assay reveals tolerance of DNA damage by both translesion DNA synthesis and homology-dependent repair in mammalian cells. *Proceedings of the National Academy of Sciences of the United States of America*, 110(16), E1462-E1469.

Jaeckle, K. A., Eyre, H. J., Townsend, J. J., Schulman, S., Knudson, H. M., Belanich, M., Yarosh, D. B., Bearman, S. I., Giroux, D. J. & Schold, S. C. (1998) Correlation of tumor O-6 methylguanine-DNA methyltransferase levels with survival of malignant astrocytoma patients treated with bis-chloroethylnitrosourea: A Southwest Oncology Group study. *Journal of Clinical Oncology*, 16(10), 3310-3315.

Jain, M., Arvanitis, C., Chu, K., Dewey, W., Leonhardt, E., Trinh, M., Sundberg, C. D., Bishop, J. M. & Felsher, D. W. (2002) Sustained loss of a neoplastic phenotype by brief inactivation of MYC. *Science*, 297(5578), 102-104.

Jakobsen, L., Vanselow, K., Skogs, M., Toyoda, Y., Lundberg, E., Poser, I., Falkenby, L. G., Bennetzen, M., Westendorf, J., Nigg, E. A., Uhlen, M., Hyman, A. A. & Andersen, J. S. (2011) Novel asymmetrically localizing components of human centrosomes identified by complementary proteomics methods. *EMBO Journal*, 30(8), 1520-1535.

Jaleel, M., McBride, A., Lizcano, J. M., Deak, M., Toth, R., Morrice, N. A. & Alessi, D. R. (2005) Identification of the sucrose non-fermenting related kinase SNRK, as a novel LKB1 substrate. *FEBS Letters*, 579(6), 1417-1423.

Jia, N., Nakazawa, Y., Guo, C. W., Shimada, M., Sethi, M., Takahashi, Y., Ueda, H., Nagayama, Y. & Ogi, T. (2015) A rapid, comprehensive system for assaying DNA repair activity and cytotoxic effects of DNA- damaging reagents. *Nat. Protoc.*, 10(1), 12-24.

Jiang, X., R,, Jimenez, G., Chang, E., Frolkis, M., Kusler, B., Sage, M., Beeche, M., Bodnar, A., G,, Wahl, G., M,, Tlsty, T., D & Chiu, C., P, (1999) Telomerase expression in human somatic cells does not induce changes associated with a transformed phenotype. *Nature Genetics*, 21(1), 111-114.

Jin, B. L. & Robertson, K. D. (2013) DNA Methyltransferases, DNA Damage Repair, and Cancer. *Epigenetic Alterations in Oncogenesis*, 754, 3-29.

Jin, Q., Fleming, A. M., Johnson, R. P., Ding, Y., Burrows, C. J. & White, H. S. (2013) Base- excision repair activity of uracil- DNA glycosylase monitored using the latch zone of α- hemolysin. *Journal of the American Chemical Society*, 135(51), 19347-19353.

Jones, M. J. K. & Jallepalli, P. V. (2012) Chromothripsis: Chromosomes in Crisis. *Developmental Cell*, 23(5), 908-917.

Jones, R. M., Mortusewicz, O., Afzal, I., Lorvellec, M., Garcia, P., Helleday, T. & Petermann, E. (2013) Increased replication initiation and conflicts with transcription underlie Cyclin E-induced replication stress. *Oncogene*, 32(32), 3744-3753.

Jung‐Suk, S. & Demple, B. (2006) Roles of base excision repair subpathways in correcting oxidized abasic sites in DNA. *FEBS*, 273(8), 1620-1629.

Kadyrov, F. A., Dzantiev, L., Constantin, N. & Modrich, P. (2006) Endonucleolytic Function of MutLα in Human Mismatch Repair. *Cell*, 126(2), 297-308.

Kaelin Jr, W. G. (2005) The concept of synthetic lethality in the context of anticancer therapy. *Nat Rev Cancer*, 5(9), 689-698.

Kannouche, P., Broughton, B., Volker, M., Hanaoka, F., Mullenders, L. & Lehmann, A. (2001) Domain structure, localization, and function of DNA polymerase eta , defective in xeroderma pigmentosum variant cells. *Genes & Development*, 15(2), 158-172.

Kannouche, P., de Henestrosa, A. R. F., Coull, B., Vidal, A. E., Gray, C., Zicha, D., Woodgate, R. & Lehmann, A. R. (2003) Localization of DNA polymerases eta and iota to the replication machinery is tightly co-ordinated in human cells. *EMBO Journal*, 22(5), 1223-1233.

Karakaidos, P., Taraviras, S., Vassiliou, L. V., Zacharatos, P., Kastrinakis, N. G., Kougiou, D., Kouloukoussa, M., Nishitani, H., Papavassiliou, A. G., Lygerou, Z. & Gorgoulis, V. G. (2004) Overexpression of the replication licensing regulators hCdt1 and hCdc6 characterizes a subset of non-small-cell lung carcinomas - Synergistic effect with mutant p53 on tumor growth and chromosomal instability - Evidence of E2F-1 transcriptional control over hCdt1. *American Journal of Pathology*, 165(4), 1351-1365.

Kavanaugh, G., Ye, F., Mohni, K., Luzwick, J. W., Glick, G. & Cortez, D. (2015) A whole genome RNAi screen identifies replication stress response genes. *Dna Repair*, 35, 55-62.

Kawamoto, T., Araki, K., Sonoda, E., Yamashita, Y. M., Harada, K., Kikuchi, K., Masutani, C., Hanaoka, F., Nozaki, K., Hashimoto, N. & Takeda, S. (2005) Dual Roles for DNA Polymerase η in Homologous DNA Recombination and Translesion DNA Synthesis. *Molecular Cell*, 20(5), 793-799.

Kelman, Z. (1997) PCNA: structure, functions and interactions. *Oncogene*, 14(6), 629-640.

Kennedy, R., Chen, C., Stuckert, P. & Archila, E. (2007) Fanconi anemia pathway- deficient tumor cells are hypersensitive to inhibition of ataxia telangiectasia mutated. *Journal of Clinical Investigation*, 117(5), 1440-1449.

Kent, T., Chandramouly, G., McDevitt, S. M., Ozdemir, A. Y. & Pomerantz, R. T. (2015) Mechanism of Microhomology- Mediated End- Joining Promoted by Human DNA Polymerase Theta. *Nature structural & molecular biology*, 22(3), 230-237.

Khosravi, R., Maya, R., Gottlieb, T., Oren, M., Shiloh, Y. & Shkedy, D. (1999) Rapid ATM-dependent phosphorylation of MDM2 precedes p53 accumulation in response to DNA damage. *Proceedings of the National Academy of Sciences of the United States of America*, 96(26), 14973-14977.

Kilkenny, M. L., Longo, M. A., Perera, R. L. & Pellegrini, L. (2013) Structures of human primase reveal design of nucleotide elongation site and mode of Pol α tethering. *Proceedings of the National Academy of Sciences*, 110(40), 15961-15966.

Kim, H. & D'Andrea, A. D. (2012) Regulation of DNA cross-link repair by the Fanconi anemia/BRCA pathway. *Genes & Development*, 26(13), 1393-1408.

Kim, H., George, E., Ragland, R. L., Rafail, S., Zhang, R. G., Krepler, C., Morgan, M. A., Herlyn, M., Brown, E. J. & Simpkins, F. (2017) Targeting the ATR/CHK1 Axis with PARP Inhibition Results in Tumor Regression in BRCA-Mutant Ovarian Cancer Models. *Clinical Cancer Research*, 23(12), 3097-3108.

Kim, J.-E., McAvoy, S. A., Smith, D. I. & Chen, J. (2005) Human TopBP1 Ensures Genome Integrity during Normal S Phase. *Molecular and Cellular Biology*, 25(24), 10907-10915.

Kleijer, W. J., Laugel, V., Berneburg, M., Nardo, T., Fawcett, H., Gratchev, A., Jaspers, N. G. J., Sarasin, A., Stefanini, M. & Lehmann, A. R. (2008) Incidence of DNA repair deficiency disorders in western Europe: Xeroderma pigmentosum, Cockayne syndrome and trichothiodystrophy. *DNA Repair*, 7(5), 744-750.

Klein Douwel, D., Boonen, Rick A. C. M., Long, David T., Szypowska, Anna A., Räschle, M., Walter, Johannes C. & Knipscheer, P. (2014) XPF- ERCC1 Acts in Unhooking DNA Interstrand Crosslinks in Cooperation with FANCD2 and FANCP/ SLX4. *Molecular Cell*, 54(3), 460-471.

Kobayashi, S., Boggon, T. J., Dayaram, T., Jänne, P. A., Kocher, O., Meyerson, M., Johnson, B. E., Eck, M. J., Tenen, D. G. & Halmos, B. (2005) EGFR Mutation and Resistance of Non– Small- Cell Lung Cancer to Gefitinib. *The New England Journal of Medicine*, 352(8), 786-792.

Kolde, R., Laur, S., Adler, P. & Vilo, J. (2012) Robust rank aggregation for gene list integration and meta-analysis. *Bioinformatics*, 28(4), 573-580.

Komarov, P. G., Komarova, E. A., Kondratov, R. V., Christov-Tselkov, K., Coon, J. S., Chernov, M. V. & Gudkov, A. V. (1999) A chemical inhibitor of p53 that protects mice from the side effects of cancer therapy. *Science*, 285(5434), 1733-1737.

Kosugi, S., Hasebe, M., Tomita, M. & Yanagawa, H. (2009) Systematic identification of cell cycle-dependent yeast nucleocytoplasmic shuttling proteins by prediction of composite motifs (vol 106, pg 10171, 2009). *Proceedings of the National Academy of Sciences of the United States of America*, 106(31), 13142-13142.

Kotov, I. N., Siebring-van Olst, E., Knobel, P. A., van der Meulen-Muileman, I. H., Felley-Bosco, E., van Beusechem, V. W., Smit, E. F., Stahel, R. A. & Marti, T. M. (2014) Whole genome RNAi screens reveal a critical role of REV3 in coping with replication stress. *Molecular oncology*, 8(8), 1747-59.

Kozlov, S. V., Graham, M. E., Peng, C., Chen, P., Robinson, P. J. & Lavin, M. F. (2006) Involvement of novel autophosphorylation sites in ATM activation. *EMBO Journal*, 25(15), 3504-3514.

Kramer, A., Mailand, N., Lukas, C., Syljuasen, R. G., Wilkinson, C. J., Nigg, E. A., Bartek, J. & Lukas, J. (2004) Centrosome-associated Chk1 prevents premature activation of cyclin-B-Cdk1 kinase. *Nature Cell Biology*, 6(9), 884-891.

Krejci, L., Altmannova, V., Spirek, M. & Zhao, X. (2012) Homologous recombination and its regulation. *Nucleic acids research*, 40(13), 5795-5818.

Kroemer, G., Galluzzi, L., Vandenabeele, P., Abrams, J., Alnemri, E. S., Baehrecke, E. H., Blagosklonny, M. V., El-Deiry, W. S., Golstein, P., Green, D. R., Hengartner, M., Knight, R. A., Kumar, S., Lipton, S. A., Malorni, W., Nunez, G., Peter, M. E., Tschopp, J., Yuan, J., Piacentini, M., Zhivotovsky, B. & Melino, G. (2009) Classification of cell death: recommendations of the Nomenclature Committee on Cell Death 2009. *Cell Death and Differentiation*, 16(1), 3-11.

Krokan, H. E. & Bjørås, M. (2013) Base excision repair. *Cold Spring Harbor perspectives in biology*, 5(4), a012583.

Kumagai, A., Shevchenko, A., Shevchenko, A. & Dunphy, W. G. (2010) Treslin Collaborates with TopBP1 in Triggering the Initiation of DNA Replication. *Cell*, 140(3), 349-359.

Kunkel, T. A. (1988) Exonucleolytic proofreading. *Cell*, 53(6), 837-840.

Kunkel, T. A. & Burgers, P. M. (2008) Dividing the workload at a eukaryotic replication fork. *Trends in Cell Biology*, 18(11), 521-527.

Kunkel, T. A. & Erie, D. A. (2015) Eukaryotic Mismatch Repair in Relation to DNA Replication. *Annu. Rev. Genet.*, 49, 291-313.

Kwok, M., Davies, N. & Agathanggelou, A. (2016) ATR inhibition induces synthetic lethality and overcomes chemoresistance in TP53- or ATM-defective chronic lymphocytic leukemia cells (vol 127, pg 582, 2016). *Blood*, 127(21), 2647-2647.

Kwon, J. S., Everetts, N. J., Wang, X., Wang, W., Della Croce, K., Xing, J. & Yao, G. (2017) Controlling Depth of Cellular Quiescence by an Rb- E2F Network Switch. *Cell Reports*, 20(13), 3223-3235.

Le Tallec, B., Dutrillaux, B., Lachages, A. M., Millot, G. A., Brison, O. & Debatisse, M. (2011) Molecular profiling of common fragile sites in human fibroblasts. *Nature Structural & Molecular Biology*, 18(12), 1421-1423.

Lee, A. J. X., Endesfelder, D., Rowan, A. J., Walther, A., Birkbak, N. J., Futreal, P. A., Downward, J., Szallasi, Z., Tomlinson, I. P. M., Howell, M., Kschischo, M. & Swanton, C. (2011) Chromosomal Instability Confers Intrinsic Multidrug Resistance. *Cancer Research*, 71(5), 1858-1870.

Lee, J., Kumagai, A. & Dunphy, W. G. (2007a) The Rad9- Hus1- Rad1 checkpoint clamp regulates interaction of TopBP1 with ATR. *The Journal of biological chemistry*, 282(38), 28036-28044.

Lee, J.-B., Cho, W.-K., Park, J., Jeon, Y., Kim, D., Lee, S. H. & Fishel, R. (2014) Single- molecule views of MutS on mismatched DNA. *DNA Repair*, 20, 82-93.

Lee, J.-H. & Paull, T. T. (2005) ATM activation by DNA double- strand breaks through the Mre11-Rad50- Nbs1 complex. *Science (New York, N.Y.)*, 308(5721), 551-554.

Lee, J. A., Carvalho, C. M. B. & Lupski, J. R. (2007b) A DNA replication mechanism for generating nonrecurrent rearrangements associated with genomic disorders. *Cell*, 131(7), 1235-1247.

Lee, J. H. & Paull, T. T. (2004) Direct activation of the ATM protein kinase by the Mre11/Rad50/Nbs1 complex. *Science*, 304(5667), 93-96.

Lehmann, A., McGibbon, D. & Stefanini, M. (2011) Xeroderma pigmentosum. *Orphanet Journal of Rare Diseases*, 6(1), 70.

Leibovitz, A., Stinson, J. C., McCombs, W. B., McCoy, C. E., Mazur, K. C. & Mabry, N. D. (1976) Classification of human colorectal adenocarcinoma cell lines. *Cancer Research*, 36(12), 4562-4569.

Li, A. & Blow, J. J. (2005) Cdt1 downregulation by proteolysis and geminin inhibition prevents DNA re‐replication in Xenopus. *EMBO Journal*, 24(2), 395-404.

Li, J., Meyer, A. N. & Donoghue, D. J. (1997) Nuclear localization of cyclin B1 mediates its biological activity and is regulated by phosphorylation. *Proceedings of the National Academy of Sciences of the United States of America*, 94(2), 502-507.

Li, J., Xiong, J., Yang, B., Zhou, Q., Wu, Y., Luo, H., Zhou, H., Liu, N., Li, Y., Song, Z. & Zheng, Q. (2015a) Endothelial Cell Apoptosis Induces TGF-beta Signaling-Dependent Host Endothelial-Mesenchymal Transition to Promote Transplant Arteriosclerosis. *American Journal of Transplantation*, 15(12), 3095-3111.

Li, L., Murphy, K. M., Kanevets, U. & Reha-Krantz, L. J. (2005) Sensitivity to phosphonoacetic acid: A new phenotype to probe DNA polymerase δ in Saccharomyces cerevisiae. *Genetics*, 170(2), 569-580.

Li, X., Wang, W., Wang, J., Malovannaya, A., Xi, Y., Li, W., Guerra, R., Hawke, D. H., Qin, J. & Chen, J. (2015b) Proteomic analyses reveal distinct chromatin-associated and soluble transcription factor complexes. *Molecular systems biology*, 11(1), 775-775.

Li, X., Zhao, Q., Liao, R., Sun, P. & Wu, X. (2003) The SCFSkp2 ubiquitin ligase complex interacts with the human replication licensing factor Cdt1 and regulates Cdt1 degradation. *J. Biol. Chem.*, 278(33), 30854-30858.

Liang, C. C., Li, Z. L., Lopez-Martinez, D., Nicholson, W. V., Venien-Bryan, C. & Cohn, M. A. (2016) The FANCD2-FANCI complex is recruited to DNA interstrand crosslinks before monoubiquitination of FANCD2. *Nature Communications*, 7, 12124.

Lieber, M. R. (2010) The Mechanism of Double- Strand DNA Break Repair by the Nonhomologous DNA End- Joining Pathway. *Annu. Rev. Biochem.*, 79, 181-211.

Limsirichaikul, S., Niimi, A., Fawcett, H., Lehmann, A., Yamashita, S. & Ogi, T. (2009) A rapid non-radioactive technique for measurement of repair synthesis in primary human fibroblasts by incorporation of ethynyl deoxyuridine (EdU). *Nucleic acids research*, 37(4), e31.

Lin, X., Trang, J., Okuda, T. & Howell, S. (2006) DNA Polymerase zeta Accounts for the Reduced Cytotoxicity and Enhanced Mutagenicity of Cisplatin in Human Colon Carcinoma Cells That Have Lost DNA Mismatch Repair. *Clinical Cancer Research*, 12(2), 563-568.

Lindahl, T. (1993) Instability and decay of the primary structure of DNA. *Nature*, 362(6422), 709-715.

Lindqvist, A., van Zon, W., Rosenthal, C. K. & Wolthuis, R. M. F. (2007) Cyclin B1-Cdk1 activation continues after centrosome separation to control mitotic progression. *PLOS Biology*, 5(5), 1127-1137.

Liu, G. & Chen, X. (2006) DNA polymerase eta, the product of the xeroderma pigmentosum variant gene and a target of p53, modulates the DNA damage checkpoint and p53 activation. *Molecular and cellular biology*, 26(4), 1398-1413.

Liu, L., Markowitz, S. & Gerson, S. L. (1996) Mismatch repair mutations override alkyltransferase in conferring resistance to temozolomide but not to 1,3- bis(2- chloroethyl) nitrosourea. *Cancer research*, 56(23), 5375-5379.

Liu, Q., Guntuku, S., Cui, X. S., Matsuoka, S., Cortez, D., Tamai, K., Luo, G., Carattini-Rivera, S., Demayo, F., Bradley, A., Donehower, L. A. & Elledge, S. J. (2000) Chk1 is an essential kinase that is regulated by ATR and required for the G(2)/ M DNA damage checkpoint. *Genes & development*, 14(12), 1448-1459.

Liu, S., Opiyo, S. O., Manthey, K., Glanzer, J. G., Ashley, A. K., Amerin, C., Troksa, K., Shrivastav, M., Nickoloff, J. A. & Oakley, G. G. (2012) Distinct roles for DNA- PK, ATM and ATR in RPA phosphorylation and checkpoint activation in response to replication stress. *Nucleic Acids Research*, 40(21), 10780-10794.

Livak, K. J. & Schmittgen, T. D. (2001) Analysis of Relative Gene Expression Data Using Real- Time Quantitative PCR and the 2−ΔΔCT Method. *Methods*, 25(4), 402-408.

London, N. & Biggins, S. (2014) Signalling dynamics in the spindle checkpoint response. *Nat. Rev. Mol. Cell Biol.*, 15(11), 735-747.

Longley, D. B., Harkin, D. P. & Johnston, P. G. (2003) 5-Fluorouracil: Mechanisms of action and clinical strategies. *Nature Reviews Cancer*, 3(5), 330-338.

Lord, C. J. & Ashworth, A. (2012) The DNA damage response and cancer therapy. *Nature*, 481, 287-294.

Lukas, J., Bartkova, J. & Bartek, J. (1996) Convergence of mitogenic signalling cascades from diverse classes of receptors at the cyclin D- cyclin- dependent kinase- pRb- controlled G(1) checkpoint. *Mol. Cell. Biol.*, 16(12), 6917-6925.

Lundberg, A. S. & Weinberg, R. A. (1998) Functional inactivation of the retinoblastoma protein requires sequential modification by at least two distinct cyclin-cdk complexes. *Molecular and Cellular Biology*, 18(2), 753-761.

Luo, J., Emanuele, M. J., Li, D., Creighton, C. J., Schlabach, M. R., Westbrook, T. F., Wong, K.-K. & Elledge, S. J. (2009) A Genome- wide RNAi Screen Identifies Multiple Synthetic Lethal Interactions with the Ras Oncogene. *Cell*, 137(5), 835-848.

Lutz, W., Stohr, M., Schurmann, J., Wenzel, A., Lohr, A. & Schwab, M. (1996) Conditional expression of N-myc in human neuroblastoma cells increases expression of alpha-prothymosin and ornithine decarboxylase and accelerates progression into S-phase early after mitogenic stimulation of quiescent cells. *Oncogene*, 13(4), 803-812.

Lydeard, J. R., Jain, S., Yamaguchi, M. & Haber, J. E. (2007) Break- induced replication and telomerase- independent telomere maintenance require Pol32. *Nature*, 448(7155), 820-823.

Löbrich, M. & Jeggo, P. (2007) The impact of a negligent G2/ M checkpoint on genomic instability and cancer induction. *Nature Reviews. Cancer*, 7(11), 861-869.

Ma, Y., Lu, H., Tippin, B., Goodman, M. F., Shimazaki, N., Koiwai, O., Hsieh, C.-L., Schwarz, K. & Lieber, M. R. (2004) A Biochemically Defined System for Mammalian Nonhomologous DNA End Joining. *Molecular Cell*, 16(5), 701-713.

Ma, Y., Pannicke, U., Schwarz, K. & Lieber, M. R. (2002) Hairpin opening and overhang processing by an Artemis/ DNA- dependent protein kinase complex in nonhomologous end joining and V(D) J recombination. *Cell*, 108(6), 781-794.

MacNeill, S., Prakash, A. & Borgstahl, G. O. (2012) The Structure and Function of Replication Protein A in DNA Replication, *The Eukaryotic Replisome: a Guide to Protein Structure and Function*. Subcellular BiochemistrySpringer Netherlands, 171-196.

Maga, G., Stucki, M., Spadari, S. & Hübscher, U. (2000) DNA polymerase switching: I. Replication factor C displaces DNA polymerase α prior to PCNA loading. *Journal of Molecular Biology*, 295(4), 791-801.

Mahaney, B., Meek, K. & Lees-Miller, S. (2009) Repair of ionizing radiation- induced DNA double-strand breaks by non- homologous end- joining. *Biochem. J.*, 417, 639-650.

Mailand, N., Jacob, C., Falck, R., Lukas, N. & Syljuasen, N. (2000) Rapid destruction of human Cdc25A in response to DNA damage. *Science (Washington)*, 288(5470), 1425-1429.

Malumbres, M. & Barbacid, M. (2001) To cycle or not to cycle: A critical decision in cancer. *Nat Rev Cancer*, 1(3), 222-231.

Malumbres, M. & de Castro, I. P. (2014) Aurora kinase A inhibitors: promising agents in antitumoral therapy. *Expert Opinion on Therapeutic Targets*, 18(12), 1377-1393.

Manic, G., Signore, M., Sistigu, A., Russo, G., Corradi, F., Siteni, S., Musella, M., Vitale, S., De Angelis, M. L., Pallocca, M., Amoreo, C. A., Sperati, F., Di Franco, S., Barresi, S., Policicchio, E., De Luca, G., De Nicola, F., Mottolese, M., Zeuner, A., Fanciulli, M., Stassi, G., Maugeri-Saccà, M., Baiocchi, M., Tartaglia, M., Vitale, I. & De Maria, R. (2017) CHK1- targeted therapy to deplete DNA replication- stressed, p53- deficient, hyperdiploid colorectal cancer stem cells. *Gut*.

Mann, G. J., Musgrove, E. A., Fox, R. M. & Thelander, L. (1988) Ribonucleotide reductase-M1 subunit in cellular proliferation, quiescence and differentiation. *Cancer Research*, 48(18), 5151-5156.

Marteijn, J. A., Bekker-Jensen, S., Mailand, N., Lans, H., Schwertman, P., Gourdin, A. M., Dantuma, N. P., Lukas, J. & Vermeulen, W. (2009) Nucleotide excision repair- induced H2A ubiquitination is dependent on MDC1 and RNF8 and reveals a universal DNA damage response. *Journal of Cell Biology*, 186(6), 835-847.

Marteijn, J. A., Lans, H., Vermeulen, W. & Hoeijmakers, J. H. J. (2014) Understanding nucleotide excision repair and its roles in cancer and ageing. *Nat Rev Mol Cell Biol*, 15(7), 465-481.

Martincorena, I., Raine, K. M., Gerstung, M., Dawson, K. J., Haase, K., Van Loo, P., Davies, H., Stratton, M. R. & Campbell, P. J. (2017) Universal Patterns of Selection in Cancer and Somatic Tissues. *Cell*, 171, 1-13.

Martín Sánchez, C., Pérez Martín, J. M., Jin, J.-S., Dávalos, A., Zhang, W., de La Peña, G., Martínez-Botas, J., Rodríguez-Acebes, S., Suárez, Y., Hazen, M. J., Gómez-Coronado, D., Busto, R., Cheng, Y.-C. & Lasunción, M. A. (2015) Disruption of the mevalonate pathway induces dNTP depletion and DNA damage. *BBA - Molecular and Cell Biology of Lipids*, 1851(9), 1240-1253.

Maréchal, A. & Zou, L. (2014) RPA- coated single- stranded DNA as a platform for post- translational modifications in the DNA damage response. *Cell Research*, 25(1), 9-23.

Massey, A. J., Stephens, P., Rawlinson, R., McGurk, L., Plummer, R. & Curtin, N. J. (2016) mTORC1 and DNA- PKcs as novel molecular determinants of sensitivity to Chk1 inhibition. *Molecular Oncology*, 10(1), 101-112.

Masuda, Y., Kanao, R., Kaji, K., Ohmori, H., Hanaoka, F. & Masutani, C. (2015) Different types of interaction between PCNA and PIP boxes contribute to distinct cellular functions of Y-family DNA polymerases. *Nucleic acids research*, 43(16), 7898-7910.

Matthews, D. J., Yakes, F. M., Chen, J., Tadano, M., Bornheim, L., Clary, D. O., Tai, A., Wagner, J. M., Miller, N., Kim, Y. D., Robertson, S., Murray, L. & Karnitz, L. M. (2007) Pharmacological abrogation of S-phase checkpoint enhances the anti-tumor activity of gemcitabine in vivo. *Cell Cycle*, 6(1), 104-110.

Mc Gee, M. M. (2015) Targeting the Mitotic Catastrophe Signaling Pathway in Cancer. *Mediators of Inflammation*.

McCormick, A., Donoghue, P., Dixon, M., Sullivan, R., Donnell, R. L., Murray, J., Kaufmann, A., Curtin, N. J. & Edmondson, R. J. (2017) Ovarian Cancers Harbor Defects in Nonhomologous End Joining Resulting in Resistance to Rucaparib. *Clinical cancer research : an official journal of the American Association for Cancer Research*, 23(8), 2050-2060.

McElhinny, S. A. N., Havener, J. M., Garcia-Diaz, M., Juarez, R., Bebenek, K., Kee, B. L., Blanco, L., Kunkel, T. A. & Ramsden, D. A. (2005) A gradient of template dependence defines distinct biological roles for family X polymerases in nonhomologous end joining. *Molecular Cell*, 19(3), 357-366.

McGranahan, N. & Swanton, C. (2015) Biological and Therapeutic Impact of Intratumor Heterogeneity in Cancer Evolution. *Cancer Cell*, 27(1), 15-26.

McGrath, R. A. & Williams, R. W. (1966) Reconstruction *in vivo* of irradiated *Escherichia coli* deoxyribonucelic acid rejoining of broken pieces. *Nature*, 212(5061), 534-535.

McKinnon, P. J. (2004) ATM and ataxia telangiectasia. *EMBO Reports*, 5(8), 772-776.

McMahill, M. S., Sham, C. W. & Bishop, D. K. (2007) Synthesis- dependent strand annealing in meiosis. *PLOS. Biol.*, 5(11), 2589-2601.

McMillin, D., Negri, J. & Mitsiades, C. S. (2013) The role of tumour- stromal interactions in modifying drug response: challenges and opportunities. *Nat. Rev. Drug Discov.*, 12, 217-228.

McNeely, S., Conti, C., Sheikh, T., Patel, H., Zabludoff, S., Pommier, Y., Schwartz, G. & Tse, A. (2010) Chk1 inhibition after replicative stress activates a double strand break response mediated by ATM and DNA- dependent protein kinase. *Cell cycle (Georgetown, Tex.)*, 9(5), 995-1004.

Middleton, F., Patterson, M., Elstob, C. J., Fordham, S., Herriott, A., Wade, M. A., McCormick, A., Edmondson, R., May, F., Allan, J., Pollard, Jr. & Curtin, N. (2015) Common cancer- associated imbalances in the DNA damage response confer sensitivity to single agent ATR inhibition. *Oncotarget*, 6(32), 32396-32409.

Milholland, B., Dong, X., Zhang, L., Hao, X., Suh, Y. & Vijg, J. (2017) Differences between germline and somatic mutation rates in humans and mice. *Nature Communications*, 8.

Min, A., Im, S. A., Jang, H., Kim, S., Lee, M., Kim, D. K., Yang, Y., Kim, H. J., Lee, K. H., Kim, J. W., Kim, T. Y., Oh, D. Y., Brown, J., Lau, A., O'Connor, M. J. & Bang, Y. J. (2017) AZD6738, A Novel Oral Inhibitor of ATR, Induces Synthetic Lethality with ATM Deficiency in Gastric Cancer Cells. *Molecular Cancer Therapeutics*, 16(4), 566-577.

Mini, E., Nobili, S., Caciagli, B., Landini, I. & Mazzei, T. (2006) Cellular pharmacology of gemcitabine. *Annals of Oncology*, 17, V7-V12.

Mishmar, D., Rahat, A., Scherer, S. W., Nyakatura, G., Hinzmann, B., Kohwi, Y., Mandel-Gutfroind, Y., Lee, J. R., Drescher, B., Sas, D. E., Margalit, H., Platzer, M., Weiss, A., Tsui, L. C., Rosenthal, A. & Kerem, B. (1998) Molecular characterization of a common fragile site (FRA7H) on human chromosome 7 by the cloning of a simian virus 40 integration site. *Proceedings of the National Academy of Sciences of the United States of America*, 95(14), 8141-8146.

Mitchell, C., Park, M., Eulitt, P., Yang, C., Yacoub, A. & Dent, P. (2010a) Poly(ADP- Ribose) polymerase 1 modulates the lethality of CHK1 inhibitors in carcinoma cells. *Molecular Pharmacology*, 78(5), 909-917.

Mitchell, J. B., Choudhuri, R., Fabre, K., Sowers, A. L., Citrin, D., Zabludoff, S. D. & Cook, J. A. (2010b) In vitro and in vivo radiation sensitization of human tumor cells by a novel checkpoint kinase inhibitor, AZD7762. *Clinical Cancer Research*, 16(7), 2076-2084.

Moldovan, G.-L. & Andrea, A. D. (2009) How the fanconi anemia pathway guards the genome. *Annual review of genetics*, 43, 223-249.

Moon, A. F., Pryor, J. M., Ramsden, D. A., Kunkel, T. A., Bebenek, K. & Pedersen, L. C. (2014) Sustained active site rigidity during synthesis by human DNA polymerase μ. *Nature structural & molecular biology*, 21(3), 253-260.

Morgan, D. O. (1997) Cyclin-dependent kinases: Engines, Clocks, and Microprocessors. *Annu. Rev. Cell Dev. Biol.*, 13, 261-291.

Morita, E., Arii, J., Christensen, D., Votteler, J. & Sundquist, W. I. (2012) Attenuated protein expression vectors for use in siRNA rescue experiments. *BioTechniques*, 0(0), 1-5.

Mourón, S., Rodriguez-Acebes, S., Martínez-Jiménez, M. I., García-Gómez, S., Chocrón, S., Blanco, L. & Méndez, J. (2013) Repriming of DNA synthesis at stalled replication forks by human PrimPol. *Nature Structural & Molecular Biology*, 20(12), 1383-1389.

Moyer, S. E., Lewis, P. W. & Botchan, M. R. (2006) Isolation of the Cdc45/ Mcm2– 7/ GINS (CMG) complex, a candidate for the eukaryotic DNA replication fork helicase. *Proceedings of the National Academy of Sciences*, 103(27), 10236-10241.

Mullee, L. I. & Morrison, C. G. (2016) Centrosomes in the DNA damage response-the hub outside the centre. *Chromosome Research*, 24(1), 35-51.

Mullen, P. J., Yu, R., Longo, J., Archer, M. C. & Penn, L. Z. (2016) The interplay between cell signalling and the mevalonate pathway in cancer. *Nature Reviews Cancer*, 16(11), 718-731.

Murga, M., Bunting, S., Montana, M., Soria, R., Mulero, F., Canamero, M., Lee, Y., McKinnon, P., Nussenzweig, A. & Fernandez-Capetillo, O. (2009) A mouse model of ATR- Seckel shows embryonic replicative stress and accelerated aging. *Nature Genet.*, 41(8), 891-898.

Murray, A. (1994) Cell cycle checkpoints. *Current opinion in cell biology*, 6(6), 872-876.

Murray, A. W. (2004) Recycling the cell cycle: Cyclins revisited. *Cell*, 116(2), 221-234.

Murray, D., Vallee-Lucic, L., Rosenberg, E. & Andersson, B. (2002) Sensitivity of nucleotide excision repair-deficient human cells to ionizing radiation and cyclophosphamide. *Anticancer Research*, 22(1A), 21-26.

Musacchio, A. (2015) The Molecular Biology of Spindle Assembly Checkpoint Signaling Dynamics. *Current Biology*, 25(20), R1002-R1018.

Myers, K., Gagou, M. E., Zuazua-Villar, P., Rodriguez, R. & Meuth, M. (2009) ATR and Chk1 Suppress a Caspase-3-Dependent Apoptotic Response Following DNA Replication Stress. *PLOS Genetics*, 5(1), e1000324.

Myers, K. N., Barone, G., Ganesh, A., Staples, C. J., Howard, A. E., Beveridge, R. D., Maslen, S., Skehel, J. M. & Collis, S. J. (2016) The bornavirus-derived human protein EBLN1 promotes efficient cell cycle transit, microtubule organisation and genome stability. *Scientific Reports*, 6.

Nagy, R., Sweet, K. & Eng, C. (2004) Highly penetrant hereditary cancer syndromes, 23(38), 6445-6470.

Nassif, N., Engels, W. R., Gloor, G. B., Penney, J. & Pal, S. (1994) Efficient copying of nonhomologous sequences from ectopic sites via P- element- induced gap repair. *Molecular and Cellular Biology*, 14(3), 1613-1625.

National Centre for Biotechnology Information (2017) *CCZIP-OR7E38P Readthrough*, 2017. Available online: https://www.ncbi.nlm.nih.gov/gene/?term=389538 [Accessed.

Neelsen, K. J. & Lopes, M. (2015) Replication fork reversal in eukaryotes: From dead end to dynamic response. *Nature Reviews Molecular Cell Biology*, 16(4), 207-220.

Negrini, S., Gorgoulis, V. G. & Halazonetis, T. D. (2010) Genomic instability - an evolving hallmark of cancer. *Nature Reviews Molecular Cell Biology*, 11(3), 220-228.

Neher, T. M., Shuck, S. C., Liu, J.-Y., Zhang, J.-T. & Turchi, J. J. (2010) Identification of novel small molecule inhibitors of the XPA protein using in silico based screening. *ACS chemical biology*, 5(10), 953-965.

Nelson, J. R., Lawrence, C. W. & Hinkle, D. C. (1996) Deoxycytidyl transferase activity of yeast REV1 protein. *Nature*, 382(6593), 729-731.

Nguyen, V. Q., Co, C. & Li, J. L. (2001) Cyclin- dependent kinases prevent DNA re- replication through multiple mechanisms. *Nature*, 411(6841), 1068-1073.

Nicolette, M., Lee, K., Guo, Z., Rani, M., Chow, J., Lee, S. & Paull, T. (2010) Mre11- Rad50- Xrs2 and Sae2 promote 5 ' strand resection of DNA double- strand breaks. *Nat. Struct. Mol. Biol.*, 17(12), 1478-1485.

Nieminuszczy, J., Schwab, R. A. & Niedzwiedz, W. (2016) The DNA fibre technique – tracking helicases at work. *Methods*, 108, 92-98.

Niimi, A., Limsirichaikul, S., Yoshida, S., Iwai, S., Masutani, C., Hanaoka, F., Kool, E. T., Nishiyama, Y. & Suzuki, M. (2004) Palm mutants in DNA polymerases alpha and eta alter DNA replication fidelity and translesion activity. *Molecular and cellular biology*, 24(7), 2734-2746.

Nishi, R., Okuda, Y., Watanabe, E., Mori, T., Iwai, S., Masutani, C., Sugasawa, K. & Hanaoka, F. (2005) Centrin 2 stimulates nucleotide excision repair by interacting with xeroderma pigmentosum group C protein. *Molecular and Cellular Biology*, 25(13), 5664-5674.

Nishitani, H. & Lygerou, Z. (2002) Control of DNA replication licensing in a cell cycle. *Genes Cells*, 7, 523-534.

Niu, H., Manfredi, M. & Ecsedy, J. A. (2015) Scientific Rationale Supporting the Clinical Development Strategy for the Investigational Aurora A Kinase Inhibitor Alisertib in Cancer. *Frontiers in oncology*, 5, 189.

Nurse, P. (2000) A long twentieth century of the cell cycle and beyond. *Cell*, 100(1), 71-78.

Ohashi, K., Sequist, L. V., Arcila, M. E., Moran, T., Chmielecki, J., Lin, Y., Pan, Y., Wang, L., de Stanchina, E., Shien, K., Aoe, K., Toyooka, S., Kiura, K., Fernandez-Cuesta, L., Fidias, P., Yang, J., Miller, V. A., Riely, G., Kris, M. G., Engelman, J., Vnencak-Jones, C., Dias-Santagata, D., Ladanyi, M. & Pao, W. (2012) Lung cancers with acquired resistance to EGFR inhibitors occasionally harbor BRAF gene mutations but lack mutations in KRAS, NRAS, or MEK1. *Proc. Natl. Acad. Sci. U. S. A.*, 109(31), E2127-E2133.

Okita, N., Minato, S., Ohmi, E., Tanuma, S. & Higami, Y. (2012) DNA damage-induced CHK1 autophosphorylation at Ser296 is regulated by an intramolecular mechanism. *FEBS Letters*, 586(22), 3974-3979.

Olah, J., Vincze, O., Virok, D., Simon, D., Bozso, Z., Tokesi, N., Horvath, I., Hlavanda, E., Kovacs, J., Magyar, A., Szucs, M., Orosz, F., Penke, B. & Ovadi, J. (2011) Interactions of Pathological Hallmark Proteins Tubulin Polymerisation Promoting Protien/p25, beta-amyloid and alpha-synuclein. *Journal of Biological Chemistry*, 286(39), 34088-34100.

Olson, E., Nievera, C. J., Wu, X., Klimovich, V. & Fanning, E. (2006) RPA2 is a direct downstream target for ATR to regulate the S-phase checkpoint. *Journal of Biological Chemistry*, 281(51), 39517-39533.

Paige, A. J. W. (2003) Redefining tumour suppressor genes: exceptions to the two-hit hypothesis. *Cellular and Molecular Life Sciences*, 60(10), 2147-2163.

Pannunzio, N. R., Li, S., Watanabe, G. & Lieber, M. R. (2014) Non-homologous end joining often uses microhomology: Implications for alternative end joining. *DNA Repair*, 17, 74-80.

Parsels, L. A., Morgan, M. A., Tanska, D. M., Parsels, J. D., Palmer, B. D., Booth, R. J., Denny, W. A., Canman, C. E., Kraker, A. J., Lawrence, T. S. & Maybaum, J. (2009) Gemcitabine sensitization by checkpoint kinase 1 inhibition correlates with inhibition of a Rad51 DNA damage response in pancreatic cancer cells. *Mol. Cancer Ther.*, 8(1), 45-54.

Parsons, J. L., Dianova, I. I., Allinson, S. L. & Dianov, G. L. (2005) Poly(ADP‐ribose) polymerase‐1 protects excessive DNA strand breaks from deterioration during repair in human cell extracts. *FEBS Journal*, 272(8), 2012-2021.

Pascucci, B., Stucki, M., Jónsson, Z. O., Dogliotti, E. & Hübscher, U. (1999) Long patch base excision repair with purified human proteins. DNA ligase I as patch size mediator for DNA polymerases delta and epsilon. *The Journal of biological chemistry*, 274(47), 33696-33702.

Paull, T. T., Rogakou, E. P., Yamazaki, V., Kirchgessner, C. U., Gellert, M. & Bonner, W. M. (2000) A critical role for histone H2AX in recruitment of repair factors to nuclear foci after DNA damage. *Current Biology*, 10(15), 886-895.

Paulsen, R. D., Soni, D. V., Wollman, R., Hahn, A. T., Yee, M. C., Guan, A., Hesley, J. A., Miller, S. C., Cromwell, E. F., Solow-Cordero, D. E., Meyer, T. & Cimprich, K. A. (2009) A Genome-wide siRNA Screen Reveals Diverse Cellular Processes and Pathways that Mediate Genome Stability. *Molecular Cell*, 35(2), 228-239.

Pavletich, N. P. (1999) Mechanisms of cyclin-dependent kinase regulation: Structures of Cdks, their cyclin activators, and Cip and INK4 inhibitors. *Journal of Molecular Biology*, 287(5), 821-828.

Pegg, A. E. (2000) Repair of O-6-alkylguanine by alkyltransferases. *Mutation Research-Reviews in Mutation Research*, 462(2-3), 83-100.

Peng, C. Y., Graves, P. R., Thoma, R. S., Wu, Z., Shaw, A. S. & Piwnica-Worms, H. (1997) Mitotic and G 2 checkpoint control: Regulation of 14- 3- 3 protein binding by phosphorylation of Cdc25c on serine- 216. *Science*, 277(5331), 1501-1505.

Perlow-Poehnelt, R. A., Likhterov, I., Scicchitano, D. A., Geacintov, N. E. & Broyde, S. (2004) The spacious active site of a Y-family DNA polymerase facilitates promiscuous nucleotide incorporation opposite a bulky carcinogen-DNA adduct - Elucidating the structure-function relationship through experimental and computational approaches. *Journal of Biological Chemistry*, 279(35), 36951-36961.

Perry, J. & Kornbluth, S. (2007) Cdc25 and Wee1: analogous opposites? *Cell Div.*, 2(12).

Petermann, E. & Helleday, T. (2010) Pathways of mammalian replication fork restart. *Nature Reviews Molecular Cell Biology*, 11(10), 683-687.

Petermann, E., Helleday, T. & Caldecott, K. W. (2008) Claspin promotes normal replication fork rates in human cells. *Molecular Biology of the Cell*, 19(6), 2373-2378.

Petermann, E., Woodcock, M. & Helleday, T. (2010) Chk1 promotes replication fork progression by controlling replication initiation. *Proceedings of the National Academy of Sciences of the United States of America*, 107(37), 16090-16095.

Petruseva, I., Evdokimov, A. & Lavrik, O. I. (2014) Molecular Mechanism of Global Genome Nucleotide Excision Repair. *Acta Naturae*, 6(1), 23-34.

Plunkett, W., Huang, P., Xu, Y. Z., Heinemann, V., Grunewald, R. & Gandhi, V. (1995) Gemcitabine - metabolism, mechanisms of action and self-potentiation. *Seminars in Oncology*, 22(4), 3-10.

Podlutsky, A. J., Dianova, I. I., Podust, V. N., Bohr, V. A. & Dianov, G. L. (2001) Human DNA polymerase β initiates DNA synthesis during long - patch repair of reduced AP sites in DNA. *EMBO Journal*, 20(6), 1477-1482.

Powell, S. N., DeFrank, J. S., Connell, P., Eogan, M., Preffer, F., Dombkowski, D., Tang, W. & Friend, S. (1995) Differential Sensitivity of p53(-) and p53(+) Cells to Caffeine- induced Radiosensitization and Override of G2 Delay. *Cancer Research*, 55(8), 1643-1648.

Pursell, Z. F., Isoz, I., Lundström, E.-B., Johansson, E. & Kunkel, T. A. (2007) Yeast DNA polymerase epsilon participates in leading- strand DNA replication. *Science (New York, N.Y.)*, 317(5834), 127-130.

Pylayeva-Gupta, Y., Grabocka, E. & Bar-Sagi, D. (2011) RAS oncogenes: weaving a tumorigenic web. *Nature Reviews Cancer*, 11(11), 761-774.

Quinn, J. A., Jiang, S. X., Reardon, D. A., Desjardins, A., Vredenburgh, J. J., Rich, J. N., Gururangan, S., Friedman, A. H., Signer, D. D., Sampson, J. H., McLendon, R. E., Herndon Ii, J. E., Walker, A. & Friedman, H. S. (2009) Phase II Trial of Temozolomide Plus O 6 - Benzylguanine in Adults with Recurrent, Temozolomide-Resistant Malignant Glioma. *Journal of Clinical Oncology*, 27(8), 1262-1267.

Raab, M., Kramer, A., Hehlgans, S., Sanhaji, M., Kurunci-Csacsko, E., Dotsch, C., Bug, G., Ottmann, O., Becker, S., Pachl, F., Kuster, B. & Strebhardt, K. (2015) Mitotic arrest and slippage induced by pharmacological inhibition of Polo-like kinase 1. *Molecular Oncology*, 9(1), 140-154.

Rajeshkumar, N. V., De Oliveira, E., Ottenhof, N., Watters, J., Brooks, D., Demuth, T., Shumway, S. D., Mizuarai, S., Hirai, H., Maitra, A. & Hidalgo, M. (2011) MK-1775, a Potent Wee1 Inhibitor, Synergizes

with Gemcitabine to Achieve Tumor Regressions, Selectively in p53-Deficient Pancreatic Cancer Xenografts. *Clinical Cancer Research*, 17(9), 2799-2806.

Reaper, P. M., Griffiths, M. R., Long, J. M., Charrier, J. D., MacCormick, S., Charlton, P. A., Golec, J. M. C. & Pollard, J. R. (2011) Selective killing of ATM- or p53-deficient cancer cells through inhibition of ATR. *Nature Chemical Biology*, 7(7), 428-430.

Reha-Krantz, L. J. (2010) DNA polymerase proofreading: Multiple roles maintain genome stability. *Biochim Biophys Acta*, 1804(5), 1049-1063.

Reinhardt, H. C., Aslanian, A. S., Lees, J. A. & Yaffe, M. B. (2007) p53-Deficient Cells Rely on ATM- and ATR- Mediated Checkpoint Signaling through the p38MAPK/ MK2 Pathway for Survival after DNA Damage. *Cancer Cell*, 11(2), 175-189.

Rideout, W., Coetzee, G., Olumi, A. & Jones, P. (1990) 5- Methylcytosine as an Endogenous Mutagen in the Human LDL Receptor and p53 Genes. *Science*, 249(4974), 1288-1290.

Rieder, C. L., Cole, R. W., Khodjakov, A. & Sluder, G. (1995) The checkpoint delaying anaphase in response to chromosome monoorientation is mediated by an inhibitory signal produced by unattached kinetochores. *Journal of Cell Biology*, 130(4), 941-948.

Rines, A. K., Burke, M. A., Fernandez, R. P., Volpert, O. V. & Ardehali, H. (2012) Snf1-related kinase inhibits colon cancer cell proliferation through calcyclin-binding protein-dependent reduction of beta-catenin. *Faseb Journal*, 26(11), 4685-4695.

Rivera-Calzada, A., Lopez-Perrote, A., Melero, R., Boskovic, J., Munoz-Hernandez, H., Martino, F. & Llorca, O. (2015) Structure and Assembly of the PI3K-like Protein Kinases (PIKKs) Revealed by Electron Microscopy. *Aims Biophysics*, 2(2), 36-57.

Rochette, P. J., Bastien, N., Lavoie, J., Guerin, S. L. & Drouin, R. (2005) SW480, a p53 double-mutant cell line retains proficiency for some p53 functions. *Journal of Molecular Biology*, 352(1), 44-57.

Rogstad, D., Liu, P., Burdzy, A., Lin, S. & Sowers, L. (2002) Endogenous DNA Lesions Can Inhibit the Binding of the AP- 1 (c- Jun) Transcription Factor. *Biochemistry (Washington)*, 41(25), 8093-8102.

Ross, A.-L., Simpson, L. J. & Sale, J. E. (2005) Vertebrate DNA damage tolerance requires the C-terminus but not BRCT or transferase domains of REV1. *Nucleic acids research*, 33(4), 1280-1289.

Rowles, A., Chong, J. P. J., Brown, L., Howell, M., Evan, G. I. & Blow, J. J. (1996) Interaction between the Origin Recognition Complex and the Replication Licensing Systemin Xenopus. *Cell*, 87(2), 287-296.

Rundle, S., Bradbury, A., Drew, Y. & Curtin, N. J. (2017) Targeting the ATR- CHK1 Axis in Cancer Therapy. *Cancers*, 9(5), E41.

Rydberg, B. & Lindahl, T. (1982) Nonenzymatic methylation of DNA by the intracellular methyl group donor S- adenosyl- L- methionine is a potentially mutagenic reaction. *EMBO Journal*, 1(2), 211-216.

Sale, J., Lehmann, A. & Woodgate, R. (2012) Y- family DNA polymerases and their role in tolerance of cellular DNA damage. *Nature Reviews. Molecular Cell Biology*, 13(3), 141-52.

Saleh-Gohari, N., Bryant, H. E., Parker, K. M., Cassel, T. N., Helleday, T. & Schultz, N. (2005) Spontaneous homologous recombination is induced by collapsed replication forks that are caused by endogenous DNA single-strand breaks. *Molecular and Cellular Biology*, 25(16), 7158-7169.

Sarkaria, J. N., Busby, E. C., Tibbetts, R. S., Roos, P., Taya, Y., Karnitz, L. M. & Abraham, R. T. (1999) Inhibition of ATM and ATR kinase activities by the radiosensitizing agent, caffeine. *Cancer Research*, 59(17), 4375-4382.

Savitsky, K., Barshira, A., Gilad, S., Rotman, G., Ziv, Y., Vanagaite, L., Tagle, D. A., Smith, S., Uziel, T., Sfez, S., Ashkenazi, M., Pecker, I., Frydman, M., Harnik, R., Patanjali, S. R., Simmons, A., Clines, G. A., Sartiel, A., Gatti, R. A., Chessa, L., Sanal, O., Lavin, M. F., Jaspers, N. G. J., Malcolm, A., Taylor, R., Arlett, C. F., Miki, T., Weissman, S. M., Lovett, M., Collins, F. S. & Shiloh, Y. (1995) A single ataxia-telangiectasia gene with a product similar to PI-3 kinase. *Science*, 268(5218), 1749-1753.

Sawyers, C. (2004) Targeted cancer therapy. *Nature*, 432, 294-297.

Schmidt, C. K., Galanty, Y., Sczaniecka-Clift, M., Coates, J., Jhujh, S., Demir, M., Cornwell, M., Beli, P. & Jackson, S. P. (2015) Systematic E2 screening reveals a UBE2D-RNF138-CtIP axis promoting DNA repair. *Nature Cell Biology*, 17(11), 1458-1470.

Schmidt, E. E., Pelz, O., Buhlmann, S., Kerr, G., Horn, T. & Boutros, M. (2013) GenomeRNAi: a database for cell-based and in vivo RNAi phenotypes, 2013 update. *Nucleic Acids Research*, 41(D1), D1021-D1026.

Schulze, A., Zerfass, K., Spitkovsky, D., Middendorp, S., Berges, J., Helin, K., Jansendurr, P. & Henglein, B. (1995) Cell-cycle regulation of the the cyclin-A gene promoter is mediated by a variant E2F site. *Proceedings of the National Academy of Sciences of the United States of America*, 92(24), 11264-11268.

Schwertman, P., Lagarou, A., Dekkers, D., Raams, A., Laffeber, C., Hoeijmakers, J., Demmers, J., Fousteri, M., Vermeulen, W. & Marteijn, J. (2012) UV- sensitive syndrome protein UVSSA recruits USP7 to regulate transcription- coupled repair. *Nature Genetics*, 44(5), 598-602.

Scorah, J. & McGowan, C. H. (2009) Claspin and Chk1 regulate replication fork stability by different mechanisms. *Cell Cycle*, 8(7), 1036-1043.

Scragg, M. A. & Ferreira, L. R. (1991) Evaluation of different staining procedures for the quantification of fibroblast cultured in 96-well plates. *Analytical Biochemistry*, 198(1), 80-85.

Sen, T., Tong, P., Stewart, C. A., Cristea, S., Valliani, A., Shames, D. S., Redwood, A. B., Fan, Y. H., Li, L. R., Glisson, B. S., Minna, J. D., Sage, J., Gibbons, D. L., Piwnica-Worms, H., Heymach, J. V., Wang, J. & Byers, L. A. (2017) CHK1 Inhibition in Small-Cell Lung Cancer Produces Single-Agent Activity in Biomarker-Defined Disease Subsets and Combination Activity with Cisplatin or Olaparib. *Cancer Research*, 77(14), 3870-3884.

Shackelford, D. & Shaw, R. (2009) The LKB1- AMPK pathway: metabolism and growth control in tumour suppression. *Nature Reviews. Cancer*, 9(8), 563-75.

Shah, M. A. & Schwartz, G. (2001) Cell cycle- mediated drug resistance: An emerging concept in cancer therapy. *Clin. Cancer Res.*, 7, 2168-2181.

Sharma, A., Singh, K. & Almasan, A. (2012a) Histone H2AX phosphorylation: A marker for DNA damage. *Methods in Molecular Biology*, 920, 613-626.

Sharma, S., Hicks, J. K., Chute, C. L., Brennan, J. R., Ahn, J.-Y., Glover, T. W. & Canman, C. E. (2012b) REV1 and polymerase ζ facilitate homologous recombination repair. *Nucleic acids research*, 40(2), 682-691.

Sharma, S. V. & Settleman, J. (2007) Oncogene addiction: setting the stage for molecularly targeted cancer therapy. *Genes & Development*, 21(24), 3214-3231.

Shen, K., Rice, S. D., Gingrich, D. A., Wang, D. K., Mi, Z. B., Tian, C. Q., Ding, Z. Y., Brower, S. L., Ervin, P. R., Gabrin, M. J., Tseng, G. & Song, N. (2012) Distinct Genes Related to Drug Response Identified in ER Positive and ER Negative Breast Cancer Cell Lines. *PLOS One*, 7(7), e40900.

Shen, Z. (2011) Genomic instability and cancer: an introduction. *Journal of Molecular Cell Biology*, 3(1), 1-3.

Shen, Z., Wu, W. & Hazen, S. (2000) Activated leukocytes oxidatively damage DNA, RNA, and the nucleotide pool through halide- dependent formation of hydroxyl radical. *Biochemistry*, 39(18), 5474-5482.

Shibata, A., Conrad, S., Birraux, J., Geuting, V., Barton, O., Ismail, A., Kakarougkas, A., Meek, K., Taucher‐Scholz, G., Löbrich, M. & Jeggo, P. A. (2011) Factors determining DNA double‐strand break repair pathway choice in G2 phase. *EMBO Journal*, 30(6), 1079-1092.

Shimoda, R., Nagashima, M., Sakamoto, M., Yamaguchi, N., Hirohashi, S., Yokota, J. & Kasai, H. (1994) Increased formation of oxidative DNA damage, 8- hydroxydeoxyguanosine, in human livers with chronic hepatitis. *Cancer research*, 54(12), 3171-3172.

Sidi, S., Sanda, T., Kennedy, R. D., Hagen, A. T., Jette, C. A., Hoffmans, R., Pascual, J., Imamura, S., Kishi, S., Amatruda, J. F., Kanki, J. P., Green, D. R., amp, Amp, Apos, Andrea, A. A. & Look, A. T. (2008) Chk1 Suppresses a Caspase- 2 Apoptotic Response to DNA Damage that Bypasses p53, Bcl- 2, and Caspase- 3. *Cell*, 133(5), 864-877.

Sidorova, J. M., Li, N., Folch, A. & Monnat, R. J. (2008) The RecQ helicase WRN is required for normal replication fork progression after DNA damage or replication fork arrest. *Cell cycle (Georgetown, Tex.)*, 7(6), 796-807.

Sigurdsson, S., Dirac-Svejstrup, A. B. & Svejstrup, J. Q. (2010) Evidence that Transcript Cleavage Is Essential for RNA Polymerase II Transcription and Cell Viability. *Molecular Cell*, 38(2), 202-210.

Singh, T. R., Ali, A. M., Busygina, V., Raynard, S., Fan, Q., Du, C. H., Andreassen, P. R., Sung, P. & Meetei, A. R. (2008) BLAP18/RMI2, a novel OB-fold-containing protein, is an essential component of the Bloom helicase-double Holliday junction dissolvasome. *Genes & Development*, 22(20), 2856-2868.

Sirbu, B. M., Couch, F. B. & Cortez, D. (2012) Monitoring the spatiotemporal dynamics of proteins at replication forks and in assembled chromatin using isolation of proteins on nascent DNA. *Nature Protocols*, 7(3), 594-605.

Siu, K. T., Rosner, M. R. & Minella, A. C. (2012) An integrated view of cyclin E function and regulation. *Cell cycle (Georgetown, Tex.)*, 11(1), 57-64.

Slaats, G. G., Ghosh, A. K., Falke, L. L., Le Corre, S., Shaltiel, I. A., van de Hoek, G., Klasson, T. D., Stokman, M. F., Logister, I., Verhaar, M. C., Goldschmeding, R., Nguyen, T. Q., Drummond, I. A., Hildebrandt, F. & Giles, R. H. (2014) Nephronophthisis-Associated CEP164 Regulates Cell Cycle Progression, Apoptosis and Epithelial-to-Mesenchymal Transition. *PLOS Genetics*, 10(10), e1004594.

Sleeth, K. M., Dianov, G. L. & Robson, R. L. (2004) Exchangeability of mammalian DNA ligases between base excision repair pathways. *Biochemistry*, 43(40), 12924-12930.

Smeaton, M. B., Hlavin, E. M., McGregor Mason, T., Noronha, A. M., Wilds, C. J. & Miller, P. S. (2008) Distortion- dependent unhooking of interstrand cross- links in mammalian cell extracts. *Biochemistry*, 47(37), 9920-9930.

Smith, L. M., Willmore, E., Austin, C. A. & Curtin, N. J. (2005) The novel poly(ADP-ribose) polymerase inhibitor, AG14361, sensitizes cells to topoisomerase I poisons by increasing the persistence of DNA strand breaks. *Clinical Cancer Research*, 11(23), 8449-8457.

Smith, S. C., Petrova, A. V., Madden, M. Z., Wang, H., Pan, Y., Warren, M. D., Hardy, C. W., Liang, D., Liu, E. A., Robinson, M. H., Rudra, S., Wang, J., Ehdaivand, S., Torres, M. A., Wang, Y. & Yu, D. S. (2015) A gemcitabine sensitivity screen identifies a role for NEK9 in the replication stress response. *Nucleic acids research*, 42(18), 11517-11527.

Smits, V. A. J., Reaper, P. M. & Jackson, S. P. (2006) Rapid PIKK-dependent release of Chk1 from chromatin promotes the DNA-damage checkpoint response. *Current Biology*, 16(2), 150-159.

Smogorzewska, A., Desetty, R., Saito, T. T., Schlabach, M., Lach, F. P., Sowa, M. E., Clark, A. B., Kunkel, T. A., Harper, J. W., Colaiácovo, M. P. & Elledge, S. J. (2010) A Genetic Screen Identifies FAN1, a Fanconi Anemia- Associated Nuclease Necessary for DNA Interstrand Crosslink Repair. *Molecular Cell*, 39(1), 36-47.

Smogorzewska, A., Matsuoka, S., Vinciguerra, P., McDonald, E. R., III, Hurov, K. E., Luo, J., Ballif, B. A., Gygi, S. P., Hofmann, K., D'Andrea, A. D. & Elledge, S. J. (2007) Identification of the FANCI protein, a monoubiquitinated FANCD2 paralog required for DNA repair. *Cell*, 129(2), 289-301.

Sohn, D., Graupner, V., Neise, D., Essmann, F., Schulze-Osthoff, K. & Janicke, R. U. (2009) Pifithrin-alpha protects against DNA damage-induced apoptosis downstream of mitochondria independent of p53. *Cell Death and Differentiation*, 16(6), 869-878.

Srivastava, M., Nambiar, M., Sharma, S., Karki, Subhas s., Goldsmith, G., Hegde, M., Kumar, S., Pandey, M., Singh, Ram k., Ray, P., Natarajan, R., Kelkar, M., De, A., Choudhary, B. & Raghavan, Sathees c. (2012) An Inhibitor of Nonhomologous End- Joining Abrogates Double- Strand Break Repair and Impedes Cancer Progression. *Cell*, 151(7), 1474-1487.

Stack, D., Byun, J., Gross, M., Rogan, E. & Cavalieri, E. (1996) Molecular characteristics of catechol estrogen quinones in reactions with deoxyribonucleosides. *Chemical Research in Toxicology*, 9(5), 851-859.

Stallons, L. J. & McGregor, W. G. (2010) Translesion Synthesis Polymerases in the Prevention and Promotion of Carcinogenesis. *Journal of Nucleic Acids*, 2010.

Staples, C. J., Barone, G., Myers, K. N., Ganesh, A., Gibbs-Seymour, I., Patil, A. A., Beveridge, R. D., Daye, C., Beniston, R., Maslen, S., Ahel, I., Skehel, J. M. & Collis, S. J. (2016) MRNIP/C5orf45 Interacts with the MRN Complex and Contributes to the DNA Damage Response. *Cell Reports*, 16(10), 2565-2575.

Staples, C. J., Myers, K. N., Beveridge, R. D. D., Patil, A. A., Howard, A. E., Barone, G., Lee, A. J. X., Swanton, C., Howell, M., Maslen, S., Skehel, J. M., Boulton, S. J. & Collis, S. J. (2014) Ccdc13 is a novel human centriolar satellite protein required for ciliogenesis and genome stability. *Journal of Cell Science*, 127(13), 2910-2919.

Staples, C. J., Myers, K. N., Beveridge, R. D. D., Patil, A. A., Lee, A. J. X., Swanton, C., Howell, M., Boulton, S. J. & Collis, S. J. (2012) The centriolar satellite protein Cep131 is important for genome stability. *Journal of Cell Science*, 125(20), 4770-4779.

Stauffer, M. & Chazin, W. (2010) Physical Interaction between Replication Protein A and Rad51 Promotes Exchange on Single-stranded DNA. *J Biol Chem*, 279(24), 25638 - 25645.

Stratton, M. R., Campbell, P. J. & Futreal, P. A. (2009) The cancer genome. *Nature*, 458(7239), 719-724.

Strumberg, D., Pilon, A. A., Smith, M., Hickey, R., Malkas, L. & Pommier, Y. (2000) Conversion of topoisomerase 1 cleavage complexes on the leading strand of ribosomal DNA into 5 '-phosphorylated DNA double-strand breaks by replication runoff. *Molecular and Cellular Biology*, 20(11), 3977-3987.

Subramanian, A., Tamayo, P., Mootha, V. K., Mukherjee, S., Ebert, B. L., Gillette, M. A., Paulovich, A., Pomeroy, S. L., Golub, T. R., Lander, E. S. & Mesirov, J. P. (2005) Gene set enrichment analysis: A knowledge-based approach for interpreting genome-wide expression profiles. *Proceedings of the National Academy of Sciences of the United States of America*, 102(43), 15545-15550.

Sudakin, V., Chan, G. K. T. & Yen, T. J. (2001) Checkpoint inhibition of the APC/ C in HeLa cells is mediated by a complex of BUBR1, BUB3, CDC20, and MAD2. *Journal of Cell Biology*, 154(5), 925-936.

Sugasawa, K., Ng, J. M. Y., Masutani, C., Iwai, S., van der Spek, P. J., Eker, A. P. M., Hanaoka, F., Bootsma, D. & Hoeijmakers, J. H. J. (1998) Xeroderma pigmentosum group C protein complex is the initiator of global genome nucleotide excision repair. *Mol. Cell*, 2(2), 223-232.

Sugawara, N., Wang, X. & Haber, J. E. (2003) In Vivo Roles of Rad52, Rad54, and Rad55 Proteins in Rad51-Mediated Recombination. *Molecular Cell*, 12(1), 209-219.

Sung, P. & Robberson, D. L. (1995) DNA strand exchange mediated by a RAD51- ssDNA nucleoprotein filament with polarity opposite to that of RecA. *Cell*, 82(3), 453-461.

Suzuki, N., Grollman, A. P., Shibutani, S., Ohashi, E., Ohmori, H., Kolbanovskiy, A. & Geacintov, N. E. (2002) Translesion synthesis by human DNA polymerase κ on a DNA template containing a single stereoisomer of dG-(+)- or dG-(-)-anti-N 2 -BPDE (7,8-dihydroxy-anti-9,10-epoxy-7,8,9,10-tetrahydrobenzo[a]pyrene). *Biochemistry*, 41(19), 6100-6106.

Svendsen, J. M., Smogorzewska, A., Sowa, M. E., amp, Amp, Apos, Connell, B. C., Gygi, S. P., Elledge, S. J. & Harper, J. W. (2009) Mammalian BTBD12/ SLX4 Assembles A Holliday Junction Resolvase and Is Required for DNA Repair. *Cell*, 138(1), 63-77.

Syljuåsen , R. G., Sørensen , C. S., Hansen, L. T., Fugger, K., Lundin, C., Johansson, F., Helleday, T., Sehested, M., Lukas, J. & Bartek, J. (2005) Inhibition of human Chk1 causes increased initiation of DNA replication, phosphorylation of ATR targets, and DNA breakage. *Molecular and Cellular Biology*, 25(9), 3553-3562.

Szostak, J. W., Orr-Weaver, T. L., Rothstein, R. J. & Stahl, F. W. (1983) The double- strand- break repair model for recombination. *Cell*, 33(1), 25-35.

Sørensen , C. S., Hansen, L. T., Dziegielewski, J., Syljuåsen , R. G., Lundin, C., Bartek, J. & Helleday, T. (2005) The cell-cycle checkpoint kinase Chk1 is required for mammalian homologous recombination repair. *Nature Cell Biology*, 7(2), 195-201.

Sørensen, C. S. & Syljuåsen, R. G. (2012) Safeguarding genome integrity: the checkpoint kinases ATR, CHK1 and WEE1 restrain CDK activity during normal DNA replication. *Nucleic Acids Research*, 40(2), 477-486.

Takata, K., Reh, S., Tomida, J., Person, M. D. & Wood, R. D. (2013) Human DNA helicase HELQ participates in DNA interstrand crosslink tolerance with ATR and RAD51 paralogs. *Nature Communications*, 4, 2338.

Tanaka, S., Cao, K., Niimi, A., Limsirichaikul, S., Miao, H. Q., Nakamura, N., Murate, T., Hasegawa, Y., Takahashi, T. & Suzuki, M. (2010) Functions of base selection step in human DNA polymerase α. *DNA Repair*, 9(5), 534-541.

Tanaka, S., Komeda, Y., Umemori, T., Kubota, Y., Takisawa, H. & Araki, H. (2013) Efficient initiation of DNA replication in eukaryotes requires Dpb11/ TopBP1- GINS interaction. *Molecular and cellular biology*, 33(13), 2614-2622.

Tapias, A., Auriol, J., Forget, D., Enzlin, J. H., Schärer, O. D., Coin, F., Coulombe, B. & Egly, J. M. (2004) Ordered Conformational Changes in Damaged DNA Induced by Nucleotide Excision Repair Factors. *Journal of Biological Chemistry*, 279(18), 19074-19083.

Taylor, A. M. R., Harcourt, S. A., Lehmann, A. R., Stevens, S. & Bridges, B. A. (1975) Ataxia telangiectasia - human mutation with abnormal radiation sensitivity. *Nature*, 258(5534), 427-429.

Taylor, S. S., Hussein, D., Wang, Y., Elderkin, S. & Morrow, C. J. (2001) Kinetochore localisation and phosphorylation of the mitotic checkpoint components Bub1 and BubR1 are differentially regulated by spindle events in human cells. *Journal of cell science*, 114(24), 4385-4395.

Tell, G., Quadrifoglio, F., Tiribelli, C. & Kelley, M. R. (2009) The many functions of APE1/ Ref- 1: not only a DNA repair enzyme. *Antioxidants & redox signaling*, 11(3), 601-619.

Tercero, J. & Diffley, J. (2001) Regulation of DNA replication fork progression through damaged DNA by the Mec1/ Rad53 checkpoint. *Nature*, 412(6846), 553-557.

Terzi, M., Izmirli, M. & Gogebakan, B. (2016) The cell fate: senescence or quiescence. *An International Journal on Molecular and Cellular Biology*, 43(11), 1213-1220.

Thangavel, S., Berti, M., Levikova, M., Pinto, C., Gomathinayagam, S., Vujanovic, M., Zellweger, R., Moore, H., Lee, E. H., Hendrickson, E. A., Cejka, P., Stewart, S., Lopes, M. & Vindigni, A. (2015) DNA2 drives processing and restart of reversed replication forks in human cells. *The Journal of cell biology*, 208(5), 545-562.

ThermoFisher (2016) *Alexa Fluor 594 dye*, 2016. Available online: [Accessed.

Thomas, H. & Coley, H. M. (2003) Overcoming multidrug resistance in cancer: an update on the clinical strategy of inhibiting p-glycoprotein. *Cancer control : journal of the Moffitt Cancer Center*, 10(2), 159-65.

Thompson, R. & Eastman, A. (2013) The cancer therapeutic potential of Chk1 inhibitors: how mechanistic studies impact on clinical trial design. *British Journal of Clinical Pharmacology*, 76(3), 358-369.

Toledo, L. I., Murga, M., Zur, R., Soria, R., Rodriguez, A., Martinez, S., Oyarzabal, J., Pastor, J., Bischoff, J. R. & Fernandez-Capetillo, O. (2011) A cell-based screen identifies ATR inhibitors with synthetic lethal properties for cancer-associated mutations. *Nature Structural & Molecular Biology*, 18(6), 721-727.

Tomoo, O. & Alan, R. L. (2006) The Y- family DNA polymerase κ (pol κ) functions in mammalian nucleotide- excision repair. *Nature Cell Biology*, 8(6), 640-642.

Tran, H. T., Gordenin, D. A. & Resnick, M. A. (1999) The 3'-5' exonucleases of DNA polymerases delta and epsilon and the 5'-3' exonuclease Exo1 have major roles in postreplication mutation avoidance in Saccharomyces cerevisiae. *Molecular and cellular biology*, 19(3), 2000-2007.

Trego, K. S. & Turchi, J. J. (2006) Pre- steady- state binding of damaged DNA by XPC- hHR23B reveals a kinetic mechanism for damage discrimination. *Biochemistry*, 45(6), 1961-1969.

Trenz, K., Errico, A. & Costanzo, V. (2008) Plx1 is required for chromosomal DNA replication under stressful conditions. *EMBO Journal*, 27(6), 876-885.

Trenz, K., Smith, E., Smith, S. & Costanzo, V. (2006) ATM and ATR promote Mre11 dependent restart of collapsed replication forks and prevent accumulation of DNA breaks. *EMBO Journal*, 25(8), 1764-1774.

Tsodikov, O. V., Ivanov, D., Orelli, B., Staresincic, L., Shoshani, I., Oberman, R., Schärer, O. D., Wagner, G. & Ellenberger, T. (2007) Structural basis for the recruitment of ERCC1‐XPF to nucleotide excision repair complexes by XPA. *EMBO Journal*, 26(22), 4768-4776.

Tsuyama, T., Tada, S., Watanabe, S., Seki, M. & Enomoto, T. (2005) Licensing for DNA replication requires a strict sequential assembly of Cdc6 and Cdt1 onto chromatin in Xenopus egg extracts. *Nucleic acids research*, 33(2), 765-775.

Turner, N., Tutt, A. & Ashworth, A. (2004) Hallmarks of 'BRCAness' in sporadic cancers. *Nature Reviews Cancer*, 4(10), 814-819.

Turner, N. C., Lord, C. J., Iorns, E., Brough, R., Swift, S., Elliott, R., Rayter, S., Tutt, A. N. & Ashworth, A. (2008) A synthetic lethal siRNA screen identifying genes mediating sensitivity to a PARP inhibitor. *EMBO Journal*, 27(9), 1368-1377.

Uhlén, M., Fagerberg, L., Hallström, B. M., Lindskog, C., Oksvold, P., Mardinoglu, A., Sivertsson, Å., Kampf, C., Sjöstedt, E., Asplund, A., Olsson, I., Edlund, K., Lundberg, E., Navani, S., Szigyarto, C. A.-K., Odeberg, J., Djureinovic, D., Takanen, J. O., Hober, S., Alm, T., Edqvist, P.-H., Berling, H., Tegel, H., Mulder, J., Rockberg, J., Nilsson, P., Schwenk, J. M., Hamsten, M., Von Feilitzen, K., Forsberg, M., Persson, L., Johansson, F., Zwahlen, M., Von Heijne, G., Nielsen, J. & Pontén, F. (2015) Proteomics. Tissue- based map of the human proteome. *Science (New York, N.Y.)*, 347(6220), 1260419.

UniProt (2016) *Coiled-coil domain-containing protein 15*, 2016. Available online: http://www.uniprot.org/uniprot/Q0P6D6 [Accessed.

UniProt (2017) *SNF-related serine/threonine-protein kinase*, 2017. Available online: http://www.uniprot.org/uniprot/Q9NRH2 [Accessed.

Uto, K., Inoue, D., Shimuta, K., Nakajo, N. & Sagata, N. (2004) Chk1, but not Chk2, inhibits Cdc25 phosphatases by a novel common mechanism. *EMBO Journal*, 23(16), 3386-3396.

Vaisman, A. & Woodgate, R. (2017) Translesion DNA polymerases in eukaryotes: what makes them tick? *Crit. Rev. Biochem. Mol. Biol.*, 52, 274-303.

Vakifahmetoglu, H., Olsson, M. & Zhivotovsky, B. (2008) Death through a tragedy: mitotic catastrophe. *Cell Death and Differentiation*, 15(7), 1153-1162.

Valabrega, G., Montemurro, F. & Aglietta, M. (2007) Trastuzumab: mechanism of action, resistance and future perspectives in HER2- overexpressing breast cancer. *Ann. Oncol.*, 18, 977-984.

Vassin, V. M., Anantha, R. W., Sokolova, E., Kanner, S. & Borowiec, J. A. (2009) Human RPA phosphorylation by ATR stimulates DNA synthesis and prevents ssDNA accumulation during DNA-replication stress. *Journal of Cell Science*, 122(22), 4070-4080.

Vassin, V. M., Wold, M. S. & Borowiec, J. A. (2004) Replication protein A (RPA) phosphorylation prevents RPA association with replication centers. *Molecular and Cellular Biology*, 24(5), 1930-1943.

Venkatesan, R. N., Hsu, J. J., Lawrence, N. A., Preston, B. D. & Loeb, L. A. (2006) Mutator phenotypes caused by substitution at a conserved motif A residue in eukaryotic DNA polymerase delta. *The Journal of biological chemistry*, 281(7), 4486-4494.

Venkatesha, V. A., Parsels, L. A., Parsels, J. D., Zabludoff, S. D., Maybaum, J., Lawrence, T. S. & Morgan, M. A. (2012) Sensitization of pancreatic cancer stem cells to gemcitabine by Chk1 inhibition. *Neoplasia*, 14(6), 519-525.

Vidal-Eychenié, S., Décaillet, C., Basbous, J. & Constantinou, A. (2013) DNA structure-specific priming of ATR activation by DNA-PKcs. *Journal of Cell Biology*, 202(3), 421-429.

Vijg, J. & Suh, Y. (2013) Genome Instability and Aging. *Annual Review of Physiology, Vol 75*, 75, 645-668.

Vitale, I., Galluzzi, L., Castedo, M. & Kroemer, G. (2011) Mitotic catastrophe: a mechanism for avoiding genomic instability. *Nature Reviews. Molecular Cell Biology*, 12(6), 385-92.

Walden, H. & Deans, A. J. (2014) The Fanconi Anemia DNA Repair Pathway: Structural and Functional Insights into a Complex Disorder. *Annu. Rev. Biophys.*, 43, 257-278.

Wang, Q., Liu, X., Zhou, J., Huang, Y., Zhang, S., Shen, J., Loera, S., Yuan, X., Chen, W., Jin, M., Shibata, S., Liu, Y., Chu, P., Wang, L. & Yen, Y. (2013) Ribonucleotide Reductase Large Subunit M1 Predicts Poor Survival Due to Modulation of Proliferative and Invasive Ability of Gastric Cancer. *PLOS One*, 8(7), e70191.

Wang, X., Andreassen, P. R. & Andrea, A. D. (2004a) Functional interaction of monoubiquitinated FANCD2 and BRCA2/ FANCD1 in chromatin. *Molecular and Cellular Biology*, 24(13), 5850-5862.

Wang, X., Fujimaki, K., Mitchell, G., Kwon, J. S., Della Croce, K., Langsdorf, C., Zhang, H. H. & Yao, G. (2017) Exit from quiescence displays a memory of cell growth and division. *Nat Commun*, 8(1), 321-321.

Wang, Y., Decker, S. J. & Sebolt-Leopold, J. (2004b) Knockdown of Chk1, Wee1 and Myt1 by RNA interference abrogates G 2 checkpoint and induces apoptosis. *Cancer Biology and Therapy*, 3(3), 305-313.

Wang, Y., Probin, V. & Zhou, D. (2006) Cancer therapy-induced residual bone marrow injury-Mechanisms of induction and implication for therapy. *Current cancer therapy reviews*, 2(3), 271-279.

Wang, Y., Woodgate, R., McManus, T., Mead, S., McCormick, J. & Maher, V. (2007) Evidence that in Xeroderma Pigmentosum Variant Cells, which Lack DNA Polymerase eta , DNA Polymerase [iota] Causes the Very High Frequency and Unique Spectrum of UV- Induced Mutations. *Cancer Research*, 67(7), 3018-3026.

Wang, Y.-L., Wang, J., Chen, X., Wang, Z.-X. & Wu, J.-W. (2018) Crystal structure of the kinase and UBA domains of SNRK reveals a distinct UBA binding mode in the AMPK family. *Biochemical and Biophysical Research Communications*, 495(1), 1-6.

Ward, I. M., Wu, X. L. & Chen, J. J. (2001) Threonine 68 of Chk2 is phosphorylated at sites of DNA strand breaks. *Journal of Biological Chemistry*, 276(51), 47755-47758.

Waters, J. C., Salmon, R.-H., Chen, A. W., Murray, R.-H. & Chen, R.-H. (1998) Localization of Mad2 to kinetochores depends on microtubule attachment, not tension. *Journal of Cell Biology*, 141(5), 1181-1191.

Waters, L., Minesinger, B., Wiltrout, M., Souza, S., Woodruff, R. & Walker, G. (2009) Eukaryotic Translesion Polymerases and Their Roles and Regulation in DNA Damage Tolerance. *Microbiology and Molecular Biology Reviews*, 73(1), 134-154.

Welburn, J. P. I., Tucker, J. A., Johnson, T., Lindert, L., Morgan, M., Willis, A., Noble, M. E. M. & Endicott, J. A. (2007) How Tyrosine 15 Phosphorylation Inhibits the Activity of Cyclin-dependent Kinase 2-Cyclin A. *Journal of Biological Chemistry*, 282(5), 3173-3181.

Weller, M., Stupp, R., Reifenberger, G., Brandes, A. A., van den Bent, M. J., Wick, W. & Hegi, M. E. (2010) MGMT promoter methylation in malignant gliomas: ready for personalized medicine? *Nature Reviews Neurology*, 6(1), 39-51.

Whalley, H. J., Porter, A. P., Diamantopoulou, Z., White, G. R. M., Castaneda-Saucedo, E. & Malliri, A. (2015) Cdk1 phosphorylates the Rac activator Tiam1 to activate centrosomal Pak and promote mitotic spindle formation. *Nature Communications*, 6.

Wilsker, D., Petermann, E., Helleday, T. & Bunz, F. (2008) Essential function of Chk1 can be uncoupled from DNA damage checkpoint and replication control. *Proceedings of the National Academy of Sciences of the United States of America*, 105(52), 20752-20757.

Woodward, A., Göhler, T., Luciani, M. & Oehlmann, M. (2006) Excess Mcm2- 7 license dormant origins d replication that can be used under conditions of replicative stress. *The Journal of Cell Biology*, 173(5), 673-683.

Wu, J. H. & Jones, N. J. (2012) Assessment of DNA interstrand crosslinks using the modified alkaline comet assay. *Methods in Molecular Biology*, 817, 165-181.

Wu, L. & Hickson, I. D. (2003) The Bloom's syndrome helicase suppresses crossing over during homologous recombination. *Nature*, 426(6968), 870-874.

Wu, Y., Kantake, N., Sugiyama, T. & Kowalczykowski, S. C. (2008) Rad51 protein controls Rad52-mediated DNA annealing. *Journal of Biological Chemistry*, 283(21), 14883-14892.

Xu, X. L., Weaver, Z., Linke, S. P., Li, C. L., Gotay, J., Wang, X. W., Harris, C. C., Ried, T. & Deng, C. X. (1999) Centrosome amplification and a defective G(2)-M cell cycle checkpoint induce genetic instability in BRCA1 exon 11 isoform-deficient cells. *Molecular Cell*, 3(3), 389-395.

Yabroff, K., Lund, J., Kepka, D. & Mariotto, A. (2011) Economic Burden of Cancer in the United States: Estimates, Projections, and Future Research. *Cancer Epidemiol. Biomarkers Prev.*, 20(10), 2006-2014.

Yao, G. (2014) Modelling mammalian cellular quiescence. *Interface focus*, 4(3), 20130074.

Yao, Y. & Dai, W. (2014) Genomic Instability and Cancer. *Journal of carcinogenesis & mutagenesis*, 5, 1000165.

Yarbro, J. W. (1968) Further studies on the mechanism of action of hydroxyurea. *Cancer research*, 28(6), 1082-1087.

Yeeles, J. T. P., Poli, J., Marians, K. J. & Pasero, P. (2013) Rescuing stalled or damaged replication forks. *Cold Spring Harbor perspectives in biology*, 5(5), a012815.

Yi, C. & He, C. (2014) DNA Repair by Reversal of DNA Damage (vol 5, a012575, 2013). *Cold Spring Harbor Perspectives in Biology*, 5(1), a012575.

Yoon, D., Wang, Y., Stapleford, K., Wiesmüller, L. & Chen, J. (2004) p53 Inhibits Strand Exchange and Replication Fork Regression Promoted by Human Rad51. *Journal of Molecular Biology*, 336(3), 639-654.

You, Z. Z., Kong, L. & Newport, J. (2002) The role of single-stranded DNA and polymerase alpha in establishing the ATR, Hus1 DNA replication checkpoint. *Journal of Biological Chemistry*, 277(30), 27088-27093.

Yu, D. S., Zhao, R., Hsu, E. L., Cayer, J., Ye, F., Guo, Y., Shyr, Y. & Cortez, D. (2010) Cyclin‐dependent kinase 9‐cyclin K functions in the replication stress response. *EMBO reports*, 11(11), 876-882.

Zabludoff, S. D., Deng, C., Grondine, M. R., Sheehy, A. M., Ashwell, S., Caleb, B. L., Green, S., Haye, H. R., Horn, C. L., Janetka, J. W., Liu, D., Mouchet, E., Ready, S., Rosenthal, J. L., Queva, C., Schwartz, G. K., Taylor, K. J., Tse, A. N., Walker, G. E. & White, A. M. (2008) AZD7762, a novel checkpoint kinase inhibitor, drives checkpoint abrogation and potentiates DNA- targeted therapies. *Molecular Cancer Therapeutics*, 7(9), 2955-2966.

Zachariae, W., Schwab, M., Nasmyth, K. & Seufert, W. (1998) Control of cyclin ubiquitination by CDK-regulated binding of Hct1 to the anaphase promoting complex. *Science*, 282(5394), 1721-1724.

Zachos, G., Black, E. J., Walker, M., Scott, M. T., Vagnarelli, P., Earnshaw, W. C. & Gillespie, D. A. F. (2007) Chk1 Is Required for Spindle Checkpoint Function. *Developmental Cell*, 12(2), 247-260.

Zeman, M. K. & Cimprich, K. A. (2014) Causes and consequences of replication stress. *Nature Cell Biology*, 16(1), 2-9.

Zeng, Z., Richardson, J., Verduzco, D., Mitchell, D. & Patton, E. E. (2009) Zebrafish Have a Competent p53- Dependent Nucleotide Excision Repair Pathway to Resolve Ultraviolet B- Induced DNA Damage in the Skin. *Zebrafish*, 6(4), 405-415.

Zernik-Kobak, M., Vasunia, K., Connelly, M., Anderson, C. W. & Dixon, K. (1997) Sites of UV- induced phosphorylation of the p34 subunit of replication protein A from HeLa cells. *The Journal of biological chemistry*, 272(38), 23896-23904.

Zhai, Y., Li, N., Jiang, H., Huang, X., Gao, N. & Tye, B. K. (2017) Unique Roles of the Non- identical MCM Subunits in DNA Replication Licensing. *Molecular Cell*, 67(2), 168-179.

Zhang, F., Ma, J., Wu, J., Ye, L., Cai, H., Xia, B. & Yu, X. (2009) PALB2 Links BRCA1 and BRCA2 in the DNA-Damage Response. *Current Biology*, 19(6), 524-529.

Zhang, Y.-W., Regairaz, M., Seiler, J. A., Agama, K. K., Doroshow, J. H. & Pommier, Y. (2011) Poly(ADP- ribose) polymerase and XPF- ERCC1 participate in distinct pathways for the repair of topoisomerase I-induced DNA damage in mammalian cells. *Nucleic acids research*, 39(9), 3607-3620.

Zhao, H. & Piwnica-Worms, H. (2001) ATR-mediated checkpoint pathways regulate phosphorylation and activation of human Chk1. *Molecular and Cellular Biology*, 21(13), 4129-4139.

Zhao, Y., Thomas, H. D., Batey, M. A., Cowell, I. G., Richardson, C. J., Griffin, R. J., Calvert, A. H., Newell, D. R., Smith, G. C. M. & Curtin, N. J. (2006) Preclinical evaluation of a potent novel DNA- dependent protein kinase inhibitor NU7441. *Cancer research*, 66(10), 5354-5362.

Zheng, L. & Shen, B. (2011) Okazaki fragment maturation: nucleases take centre stage. *Journal of Molecular Cell Biology*, 3(1), 23-30.

Zhou, Y., Caron, P., Legube, G. & Paull, T. T. (2014) Quantitation of DNA double- strand break resection intermediates in human cells. *Nucleic acids research*, 42(3), e19.

Zhu, Z., Chung, W.-H., Shim, E. Y., Lee, S. E. & Ira, G. (2008) Sgs1 Helicase and Two Nucleases Dna2 and Exo1 Resect DNA Double- Strand Break Ends. *Cell*, 134(6), 981-994.

Zotter, A., Ibrahim, S., Hoeijmakers, J. H. J., Vermeulen, W., Luijsterburg, M. S., Warmerdam, D. O., Van Driel, R., Nigg, A., Houtsmuller, A. B. & Van Cappellen, W. A. (2006) Recruitment of the nucleotide excision repair endonuclease XPG to sites of UV- induced DNA damage depends on functional TFIIH. *Molecular and Cellular Biology*, 26(23), 8868-8879.

Zou, L. & Elledge, S. J. (2003) Sensing DNA damage through ATRIP recognition of RPA- ssDNA complexes. *Science*, 300(5625), 1542-1548.

Appendices

APPENDIX 1 TARGETED SCREEN SIRNA SEQUENCES 306
APPENDIX 2 HIGH THROUGHPUT SCREEN DEVELOPMENT 309
APPENDIX 3 TARGETED SCREEN HIT SELECTION 310
APPENDIX 4 TARGETED SCREEN STATISTICS 312

Appendix 1 Targeted Screen siRNA sequences

Well	siRNA	Source	Sequence
A02	**CAMK1**	J-004940-05	AGAUACAGCUCUAGAUAAG
		J-004940-06	GAAGAUAAGAGGACGCAGA
		J-004940-07	UGAAAUACCUGCAUGACCU
		J-004940-08	GAAUGAUGCCAAACUCUUU
A03	**DGKA**	J-006711-07	GAGAUAGGGCUCCGAUUAU
		J-006711-08	CAAUCAAGAUCACCCACAA
		J-006711-09	CGACCAGUGUGCCAUGAAA
		J-006711-10	ACAGUAGGCUGGAUUCUAG
A04	**GAK**	J-005005-06	GCAGAGAGUAUGCAUUAAA
		J-005005-07	CACCAGAAAUCAUAGACUU
		J-005005-08	GCGACACGGUUCUGAAGAU
		J-005005-09	GGACGCGUGUGACAUUCAA
A05	**STK16**	J-004054-05	CGACAUGCAUCGCCUCUUC
		J-004054-06	AAUAAGCGCUACCUCUUCA
		J-004054-07	GGUACGCUGUGGAAUGAGA
		J-004054-08	CCAUUCAUGCCAAGGGUUA
A06	**STK36**	J-005039-09	GGUAAUCAGUCUCGCAUCU
		J-005039-10	GAGCAGGUCUGUUGGCAUU
		J-005039-11	GUACAAGGGUCGAAGAAAA
		J-005039-12	GAAGCUAGGCAGUGACGUU
A07	**MAP2K6**	J-003967-05	CCAAAGAACGGCCUACAUA
		J-003967-06	CGUCAAGCCUUCUAAUGUA
		J-003967-07	GAUAAAGGCCAGACAAUUC
		J-003967-08	GAUCCGAGCCACAGUAAAU
A08	**PI4KA**	J-006776-13	GCUAUGUGCGGGAGUAUAU
		J-006776-14	GAUCGAGCGUCUCAUCACA
		J-006776-15	GUGGCCAACUGGAGAUCUA
		J-006776-16	GGAACGAAGUGACCCGUCU

Well	siRNA	Source	Sequence
A09	**SRMS**	J-005376-05	UCACGGAACUCAUGCGCAA
		J-005376-06	GGGAGAAGCUGCACGCCAU
		J-005376-07	GAUCAAGGUCAUCAAGUCA
		J-005376-08	GCAGAAGGGACGGCUCUUU
A10	**DGKI**	J-006717-07	AAGCAGGCGUUUCACAAUA
		J-006717-08	GGGAGAUUGUGAAAUAUAU
		J-006717-09	AAGAUGCGCUUGAAUUGUA
		J-006717-10	GAACUAGUGCAGUCAUUUG
A11	**MAP4K1**	J-003586-07	GAUACAAUGAGCUGUGUGA
		J-003586-08	CAACAACGUUCUCAUGUCU
		J-003586-09	GGAGUUAUCUCUGGUUGCA
		J-003586-10	GAAAGGACCCUCCAUUGGG
B02	**PIK3R1**	J-003020-14	AGUAAAGCAUUGUGUCAUA
		J-003020-15	CCAACAACGGUAUGAAUAA
		J-003020-16	GACGAGAGACCAAUACUUG
		J-003020-17	UAUUGAAGCUGUAGGGAAA
B03	**STK35**	J-005384-05	GCUACGGCGUGGUUUAUGA
		J-005384-06	GCAAAGAGGGCAAUCAAGA
		J-005384-07	GGUCACAUGUGCUGCUUAA
		J-005384-08	CAACAAAAGUUUCAUGCUA
B04	**MAPKAPK5**	J-005015-05	GAUAAAGUAGAUCGACUAA
		J-005015-06	GGAAUUAGUGGUCCAGUUA
		J-005015-07	GCGCAAAGAAGGCAUCAGA
		J-005015-08	UGCAAACUCCUAAGAGAUA
B05	**PMVK**	J-006782-05	CCAUCUGGCUGGUGAGUGA
		J-006782-06	GGUGGACGAUGCUGAGUCA
		J-006782-07	GCAGACGGUCCGCGUUGUA
		J-006782-08	GGAAGGACAUGAUCCGCUG
B06	**TTK**	J-004105-09	GAUAAGAUCAUCCGACUUU
		J-004105-10	GCAAUACCUUGGAUGAUUA
		J-004105-11	CCAGUUAACCUUCUAAAUA
		J-004105-12	GAUAGUUGAUGGAAUGCUA

Well	siRNA	Source	Sequence
B07	**CDK10**	J-003235-14	GGCCUAUGGUGUCCCAGUA
		J-003235-15	GGAAGCAGCCCUACAACAA
		J-003235-16	CCAACUUGCUCAUGACCGA
		J-003235-17	GCACAGGAACUUCAUUAUC
B08	**PAK1**	J-003521-09	ACCCAAACAUUGUGAAUUA
		J-003521-10	GGAGAAAUUACGAAGCAUA
		J-003521-11	UCAAAUAACGGCCUAGACA
		J-003521-12	CAUCAAAUAUCACUAAGUC
B09	**SNRK**	J-004322-19	GCUACAAAGUAUAACAUUC
		J-004322-20	GGGAGCACCAAGUACAUUA
		J-004322-21	GAAGUGAGAUGCAUGAAAC
		J-004322-22	GCUCAGAUAGUUCAUGCUA

Appendix 2 High Throughput Screen Development

	Plate Type	Plating Density	Transfection	Transfection Time (hours)	Fixation	Extraction	Primary Antibody	Secondary Antibody	DNA Stain	Microscope
pRPA Antibody Selection	24 well	20000	Forward RNAiMAX	48/72	4% PFA, 10 minutes	Tween 20 in washes	Ser 4/8 1:250 T21 1:250 S33 1:1000	Alexa Fluor® 594 goat anti-rabbit IgG	DAPI	Nikon Eclipse T2000
Initial T21 Titration	384 well	1000	Reverse DharmaFECT 1	48/72	4% PFA, 20 minutes	0.5% Triton X-100 3% BSA, 5 minutes	T21 (1:250 - 1:1000)		Hoescht (in Fix)	Molecular Devices High Content (Cy5)
Extraction Time Course						0.5% Triton X-100 3% BSA, Time Course	T21 1:250			
Increased Extraction Time				72		0.5% Triton X-100 3% BSA, 10 minutes	T21 (1:250 - 1:1000)			
Cold Pre-extraction				48/72		Pre-extraction, 0.5% Triton X-100 3% BSA, 10 minutes	T21 1:250		Hoescht (in Secondary)	
Triton X-100 Titration				48		Triton X-100 Titration 3% BSA, 10 minutes				Molecular Devices High Content (Cy5 and Texas Red)
Increased Triton X-100							T21 (1:250 - 1:1000)			
Non-targeting Control Panel							T21 1:250			Molecular Devices High Content (Texas Red)
Re-optimisation				48/72						
Increased Plating Density		2000		48						
Antibody Testing										

Appendix 3 Targeted Screen Hit Selection

Rank	Kinase Rank	Gene Symbol	Average RRS Z-score	γH2AX Z-Score	Casp3 Z-Score	RPA S4/8 Z-Score	cBioPortal	RNAi Database
61	4	CAMK1	11.09	-0.7	0.94	-0.4	Deletion in Kindney, increases survival (months)	Cell division defects, Decreased viability in combination with K-RAS, Synthetic lethal with gemcitabine
110	6	DGKA	9.56	-0.7	1.9	0.94		Increased apoptosis, Increased cell number in G1, Decreased viability after Gemcitabine, Decreased viability with K-RAS, Synthetic lethal with Gemcitabine
157	9	GAK	8.15	0.4	0.89	-0.45		Increased mitotic delay, Increased cell death, Increase in G2/M cells and polyploid cells, Decreased viability with K-RAS, Increased IR sensitivity, Decreased HR repair frequency
182	10	STK16 (TSF1)	7.83	0.2	-0.51	-1.29		Paclitxel sensitising effect, Increased S DNA content, Increased number of mitotic cells, Increased cell death, Increased gamma-H2AX phosphorylation, Decreased HR repair frequency
234	14	STK36	7.15	0.04	0.79	-0.6		Decreased viability with PARPi
355	15	MAP2K6	6.09	0.3	-0.55	-1.09	Amplified in 27% neuroendocrine prostate	Decreased viability with Cisplatin, Decreased HR repair frequency
550	19	PIK4CA (PI4KA)	4.89	-0.2	-0.73	-0.59		Decreased proliferation, Increased cell death, Decreased viability after Gemcitabine
618	22	SRMS	4.60	0.3	-1.77	-0.96	Amplification significantly alters survival (months) in ovarian cystadenocarcinoma)	Increased S and G2/M DNA content, Decreased HR repair frequency, Synthetic lethal with Ras

Rank	Kinase Rank	Gene Symbol	Average RRS Z-score	γH2AX Z-Score	Casp3 Z-Score	RPA S4/8 Z-Score	cBioPortal	RNAi Database
623	23	DGKI	4.56	1.2	-1.11	-0.3		Increased sensitivity to IR, Synthetic lethal with Ras
628	24	MAP4K1	4.54	1.9	-1.21	-1.47	Amplification in ovarian, altered survival	Decreased viability in combination with K-RAS
671	25	PIK3R1	4.39	0.8	-0.3	-0.03		Decreased viability after Gemcitabine, Increased HR repair frequency,
733	27	STK35	4.14	1.2	-13.2	-0.45		Decreased viability with KRAS, Decreased viability with PARPi, Decreased HR repair frequency
830	33	MAPKAPK5	3.88	-0.5	-0.59	-0.85		Decreased viability with K-RAS, Synthetic lethal with c-Myc after tamoxifen, Synthetic lethal with Ras
871	35	PMVK	3.78	-0.2	-0.29	-0.59	Amplification significantly decreases survival (months) in Liver hepatocellular carcinoma	Decreased viability with PARPi, Increased gamma H2AX phosphorylation
882	36	TTK (MPS1)	3.75	0.6	-0.45	-0.62		Decreased viability after Gemcitabine, Decreased HR repair frequency
904	38	CDK10	3.72	0.3	1.25	1.04		Paclitaxel antagonistic effect
910	39	PAK1	3.69	0.9	1.81	0.55		Decreased viability with K-RAS, Synthetic lethal with Gemcitabine
980	41	SNRK	3.54	1.3	-0.37	0.26		Synthetically lethal with Gemcitabine, Decreased HR frequency

Appendix 4 Targeted Screen Statistics

siRNA	p-value
Chk1	0.0001
RRM1	0.0042
HU	0.0001
A2	0.6979
A3	0.4022
A4	0.7660
A5	0.9929
A6	0.2397
A7	0.2725
A8	0.3222
A9	0.2673
A10	0.3574
A11	0.3993
B2	0.0744
B3	0.1208
B4	0.2133
B5	0.1940
B6	0.1399
B7	0.2283
B8	0.2318
B9	0.2947